ENHANCED HEAVY OIL RECOVERY BY WATER AND CARBON DIOXIDE FLOOD

By

Alireza Emadi

BSc., Msc.

Submitted for the Degree of Doctoral of Philosophy

In Petroleum Engineering

Institute of Petroleum Engineering

Heriot-Watt University

Riccarton, Edinburgh

February 2012

ABSTRACT

The world's dependence on heavy oil production is on the rise as the existing conventional oil reservoirs mature and their production decline. Compared to conventional oil, heavy oil is much more viscous and hence its production is more challenging. Various thermal methods have been applied in the field to heat up the oil and to help with its flow and production. However, the thermal recovery methods are very energy intensive with significant negative environmental impact including the production of large quantities of CO2. Alternative non-thermal recovery methods are therefore needed to allow heavy oil production by more environmentally acceptable methods. An attractive solution for meeting the increasing demand for oil and at the same time addressing the environmental concerns in relation to thermal heavy oil production would be to inject the CO2 produced from the steam generation process or other sources into the reservoir. Compared to light oil, application of CO2 injection in heavy oil reservoirs has received much less attention and hence mechanisms of heavy oil recovery by CO2 injection are not fully understood. One major difference is that in heavy oil reservoirs CO2 would not develop miscibility with the oil, however; there are various mechanisms operating during immiscible displacement of oil by CO2 that can lead to improved oil recovery.

The purpose of this study was to investigate the recovery mechanisms and develop efficient techniques of improved heavy oil recovery by utilizing various combinations of CO2, water and chemicals for two specific crude samples. The experimental work included fluid characterization, flow visualization and coreflood experiments. The fluid characterization experiments were mainly focused on the effect of CO2 dissolution on

modification of crude properties especially viscosity. The visualization tests were conducted using transparent micromodels to investigate the pore scale recovery mechanisms and displacement efficiency. Based on these observations, the coreflood tests were designed and carried out to quantitatively investigate the recovery performance of CO2 in different injection strategies and compare to that of water.

In the micromodel tests the effect of different strategies of CO2 and water injection as well as the impact of mobility control by CO2-foam (and/or emulsion) was investigated. The results showed that the contributing displacement mechanisms during heavy oil waterflood can be significantly different from the prevailing mechanisms in the case of light oils. During the period of CO2 injection, the colour of the heavy crude oil was changed from black to light brown as a result of CO2 dissolution. The diluted oil was either recovered by gravity forces or readily mobilised during subsequent water injection which resulted in a very high oil recovery. This recovery improvement was more pronounced in the tests where CO2 was injected at higher pressures (super critical or liquid CO2) resulting in higher viscosity reduction and oil production through extraction mechanism. Formation of the new phase in the oil blobs which were not in contact with the injected high pressure CO2 was observed and reported here for the first time which helped oil recovery during the period of CO2 injection and during the subsequent period of water injection. In another series of micromodel tests, the pore scale displacement mechanisms during CO2-foam (and/or emulsion) injection were studied and reported in detail for the first time in the literature.

The coreflood tests were performed subsequently to quantify the observations made during the micromodel tests which revealed a high potential of CO2 for enhanced heavy oil recovery. In the case of the less viscous heavy crude oil (viscosity of 674 cp at the test conditions) the oil recovery reached a value of around 70 %OOIP which was twice as much as the recovery during plain waterflood. In the case of extra-heavy crude oil (viscosity of 8700 cp at the test conditions), the improvement in oil recovery was less significant due to a low reservoir pressure. However, when the CO2 flood process was boosted by mobility control techniques through formation of foam/emulsion a recovery of 75 %OOIP was achieved which was as much as four times higher than the recovery during waterflooding in this crude oil. The co-injection of CO2 and surfactant resulted in formation of strong foam/emulsion in the core which significantly improved the mobility ratio and displacement efficiency of the recovery process.

DEDICATION

To my parents, my wife and my lovely daughter for their patient and continuous support throughout my study.

ACKNOWLEDGMENTS

I would like to express my sincere gratitude to my supervisors, Prof. Sohrabi and Dr. Jamiolahmady, who provided the opportunity, financial support and technical support. It would have been impossible to complete this thesis without their expertise, understanding and encouragement.

I would also like to thank Mr. Shaun Ireland for his help in setting up the experimental apparatus and his valuable advice. I wish to extend special appreciation to my colleagues Dr. Masoud Riazi, Hamidreza Shahverdi and Amir Farzaneh for helpful discussions and suggestions regarding this work.

Finally, I would like to express my sincere gratitude to my loving wife and my parents for their unconditional support, understanding and encouragement and my daughter, Asal, who was born in Edinburgh during my PhD studies.

ACADEMIC REGISTRY
Research Thesis Submission

Name*:*	Alireza Emadi		
School/PGI:	Institute of Petroleum Engineering		
Version: *(i.e. First, Resubmission, Final)*	First	Degree Sought (Award **and** Subject area)	Doctor of Philosophy in Petroleum Engineering

Declaration

In accordance with the appropriate regulations I hereby submit my thesis and I declare that:

1) the thesis embodies the results of my own work and has been composed by myself
2) where appropriate, I have made acknowledgement of the work of others and have made reference to work carried out in collaboration with other persons
3) the thesis is the correct version of the thesis for submission and is the same version as any electronic versions submitted*.
4) my thesis for the award referred to, deposited in the Heriot-Watt University Library, should be made available for loan or photocopying and be available via the Institutional Repository, subject to such conditions as the Librarian may require.
5) I understand that as a student of the University I am required to abide by the Regulations of the University and to conform to its discipline.

* *Please note that it is the responsibility of the candidate to ensure that the correct version of the thesis is submitted.*

Signature of Candidate*:*		Date:	

Submission

Submitted By *(name in capitals):*	
Signature of Individual Submitting:	
Date Submitted:	

For Completion in the Student Service Centre (SSC)

Received in the SSC by *(Name in capitals):*			
Method of Submission *(Handed in to SSC; posted through internal/external mail):*			
E-thesis Submitted *(Mandatory for final theses)*			
Signature:		Date:	

TABLE OF CONTENTS

VOLUME I

VOLUME II

LIST OF SYMBIOLS

σ	Interfacial tension (IFT)
ρ	Density
k	Permeability
μ	Viscosity
v	Front velocity
BT	Breakthrough
ccOil/ccInj	Volume of produced oil in cc per volume of injected fluid in cc at lab conditions (unit for oil production rate)
ccCO2/ccOil	Volume of produced CO2 in cc per volume of produced oil in cc at lab conditions (unit for gas/oil ratio)
ccWater/ccTot	Volume of produced water in cc per total volume of produced effluent in cc at lab conditions (unit for water cut)
DW	Distilled Water
GOR	Gas/Oil ratio
IFT	Interfacial Tension
MM PV	Micromodel pore volume
OOIP	Original oil in place
PV	Pore volume
SWAG	Simultaneous water alternating CO2 injection
Swi	Connate water saturation
Sorw	Waterflood residual oil saturation

LIST OF TABLES

LIST OF FIGURES

LIST OF PUBLICATIONS

- Sohrabi, M., Emadi, A., Jamiolahmady, M., Ireland, S. and Brown, C., "Mechanisms of Extra-Heavy Oil Recovery by Gravity-Stable CO2 Injection", proceedings of the International Symposium of the Society of Core Analysts, Abu Dhabi, UAH, 29 Oct- 2 Nov 2008, SCA2008-20.

- Emadi, A., Sohrabi, M., Hamon, G. and Jami, M, "Mechanistic Study of Improved Heavy Oil Recovery By Alkaline Flood And Effect Of Wettability", proceedings of the International Symposium of the Society of Core Analysts, Halifax, Nova Scotia, Canada, 4-7 October, 2010, SCA2010-13.

- Emadi, A., Sohrabi, M., Jamiolahmady, M., Ireland, S. and Robertson, G. (2010). "Reducing heavy oil carbon footprint and enhancing production through CO2 injection." Chemical Engineering Research and Design, Elsevier B.V. Vol 89, No 9, pp 1783-1793, DOI: 10.1016/j.cherd.2010.08.008

- Emadi, A., Sohrabi, M., Jami, M., Ireland, S. and Robertson, G., "Visual Investigation of Extra Heavy Oil Recovery by CO2/N2 Foam Injection", EAGE 16th European Symposium on Improved Oil Recovery (IOR), Cambridge, UK, 12-14 April 2011.

- Emadi, A., Sohrabi, M., Jamiolahmady, M, Ireland, S. and Robertson G. "Mechanistic Study of Improved Heavy Oil Recovery by CO2-Foam Injection",

SPE Enhanced Oil Recovery Conference, Kuala lumpur, Malaysia, 19-21 July, 2011, SPE 143013.

- Emadi, A., Sohrabi, M., Farzaneh, A., Jamiolahmady and, Ireland, S. (2012) "CO2 EOR and Storage in Heavy Oil Reservoirs Underlying Permafrost", to be presented in 3rd EAGE CO2 Geological Storage Workshop, Edinburgh, United Kingdom, 27 March, 2012.

- Emadi, A. and Sohrabi, M "Novel Insights into the Pore-Scale Mechanisms of Enhanced Oil Recovery by CO2 Injection", to be presented in SPE EUROPEC Conference, Copenhagen, Denmark, 4-7 June, 2012, SPE 154529.

- Emadi, A., Sohrabi, M., Jamiolahmady, M. and, Ireland, S. (2012) "Visual Investigation Of Heavy Oil Recovery by CO2 Foam Injection; Effect of Gas Type and Oil Viscosity", to be presented in SPE Symposium on Improved Oil Recovery, Tulsa, USA, April, 2012, SPE 152996.

- Emadi, A. and Sohrabi, M. " Visual Investigation of Low Salinity Effect; Formation of Micro-Emulsions and Wettability Alteration", to be presented in SPE Symposium on Improved Oil Recovery, Tulsa, USA, April, 2012, SPE 154362.

CHAPTER 1 INTRODUCTION

Heavy oil hydrocarbon resources are making important and ever-increasing contribution to the energy supply of the world. Worldwide there are huge quantities of heavy oils including medium-heavy oil, extra-heavy oil, and bitumen resources. The International Energy Agency (OECD/IEA, 2005) estimates that there are 6 trillion barrels of heavy oil in place which is twice as much as conventional oil resources. Although currently the volume of heavy oil production is much smaller than the production from conventional (light) oil but the world's dependence on heavy oil production is on the rise mainly due to the projected massive increase in demand in near future. As the heavy oil market is expanding around the world, an increasing number of oil companies are either becoming involved or increasing their activities around heavy oil production.

Unlike conventional (light) oil, heavy oil is very viscous, semi-solid, or even solid. Therefore, the exploitation of heavy oils by natural recovery mechanisms is very low and inefficient. Various thermal methods have been developed and applied in the field for improving heavy oil recovery mainly by reducing the oil viscosity. These methods include various forms of steam injection and in-situ combustion. Thermal heavy oil recovery methods are generally very capital intensive ventures and have significant environmental impact and carbon footprint. In addition to these concerns, many heavy oil reservoirs are not suitable for thermal methods and hence thermal oil recovery cannot be effectively and economically applied to these reservoirs. There is therefore a need for developing effective and efficient non-thermal heavy oil recovery methods.

Despite the unfavourable viscosity ratio, water is generally injected in heavy oil reservoirs for both voidage replacement and oil displacement purposes. The main advantages of waterflooding compared to the other techniques of heavy oil recovery are availability of water, low cost of utilizing and existence of significant experience in managing field application. Nevertheless, the unfavourable viscosity (mobility) ratio between the oil and water induces undesirable effects such as viscous fingering leading to high residual oil saturation. Therefore, waterflood on its own is not regarded as a very efficient technique for displacing viscous heavy oils.

CO2 injection is a well-researched and established oil recovery method but it has been mainly applied to conventional (light) oil reservoirs where the main focus is on the miscible displacement of the oil by CO2. This is very different from the immiscible application of CO2 in heavy oil reservoirs where the main benefit of CO2 injection comes from the substantial drop in the viscosity of heavy oil as a result of mixing with CO2. Viscosity reduction of two orders of magnitude is reported in the literature as a result of diluting heavy oil by CO2. However there are certain drawbacks regarding injection of CO2 in heavy oil reservoirs. One major issue is that the process of CO2 dissolution in heavy oils is slow and hence it may not happen effectively in the time scale required for field applications. Another important issue is the adverse viscosity ratio between CO2 and heavy oils which results in poor sweep efficiency and premature CO2 breakthrough requiring excessive volume of CO2 recycling.

Combining water and CO2 injection under various injection strategies and modifications can offer effective and viable solutions for improving oil recovery from heavy oil reservoirs. In its simplest form, injecting CO2 reduces the viscosity of heavy oil in a manner similar to steam injection. Water injected subsequent to CO2 would then be able to drive the CO2-diluted oil out of the reservoir and increase oil recovery. Various chemicals can be used in conjunction with water and CO2 injection to promote formation of foam and emulsion phases and increase displacement and sweep efficiencies. Furthermore, heavy oils are known for their natural surface active components that can potentially be used as surfactants or co surfactants if the governing mechanisms are identified and understood.

This thesis reports some of the experimental works of the Enhanced Heavy Oil Recovery Joint Industry Project (JIP). *The broad objective of this project at Heriot-*

Watt University is to investigate and develop non-thermal methods for improving heavy oil recovery by utilising various combinations of water, solvents and chemicals. The research objectives are achieved by conducting a comprehensive set of flow visualisation tests, conventional displacement tests, mathematical modelling and numerical simulation. The approach is to conduct flow visualization studies in the transparent micromodels to investigate pore scale displacement mechanisms and efficiency. The ability to see the movement of fluid interfaces, in micromodels, makes it possible to distinguish between varieties of mechanisms that may all lead to a similar production behavior at larger scales. The micromodel observations are then used to develop a model to explain the pore level displacement events and design appropriate displacement tests in slim tube, sandpack or consolidated core samples from original reservoirs. The slim-tests essentially simulate one dimensional flow conditions and their main use is to evaluate the effectiveness of the phase behavioral aspects of the displacement process. Sandpack and core floods, on the other hand, can be useful in evaluation of a wide range of displacement phenomena e.g., recovery mechanisms and efficiency, relative permeabilities, rock/fluid interactions and etc. The quantitative results from displacement tests will be used in the commercial simulators to examine if the conventional simulators can successfully simulate the experimental results. The results obtained from pore scale modeling studies can be used at this stage to help definition and tuning of the parameters and correlations in the numerical simulators. Eventually the tuned simulator will be used for scaling-up purposes and prediction of process performance at larger scales. Figure 1-1 schematically shows the work flow algorithm of the "Enhanced Heavy Oil Recovery JIP".

The focus of the work reported in this thesis was to develop efficient methods of heavy oil recovery by combinations of CO2 and water injection. Two specific heavy crude oils were assigned to this work with noticeably different thermodynamic properties and reservoir conditions. The first oil sample was crude "C", an extra-heavy crude oil with a viscosity of 8700 cp at reservoir pressure and temperature of 600 psia and 50 °C. The, second oil sample was crude "J" a (medium-) heavy crude oil with a viscosity of 674 cp at reservoir pressure and temperature of 1500 psia and 28 °C. CO2 is in vapor form at the relatively low reservoir pressure and temperature of the crude "C" and in liquid form at high reservoir pressure and exceptionally low reservoir temperature of crude "J". Hence, separate sets of experiments were required for each crude oil. The experimental work was structured in two parts:

1) Micromodel Experiments: The first part consisted of flow visualization studies in the transparent micromodels to reveal the underlying pore scale mechanisms during water, CO2, and foam/emulsion flood in the two heavy oil samples. During the past four years more than 100 micromodel experiments have been conducted in high-pressure glass micromodels. Table 1-1 summarises 16 of these micromodel experiments which are reported in c*hapters 4, 5 and 6*.

2) Coreflood Experiments: Based on the micromodel observations, the coreflood experiments in the second part of this work were designed to evaluate and quantify the potential of different recovery processes for improved recovery of these heavy crude oils. Table 1-2 summarises 8 of these coreflood experiments which are reported in c*hapters 7 and 8*. The first 3 tests were performed using a sandpack which was later replaced by a consolidated core that was more suitable for heavy oil displacement tests. This was to avoid the difficulties and uncertainties due to migrations of the sand particles which is a common issue in sandpacks.

This work introduces CO2 as an efficient agent for enhanced heavy oil recovery and includes some novel observations and results in both micromodel and coreflood experiments. In the micromodel experiments, the pore scale events during water and CO2 injection are studied for different experimental conditions. Vivid micromodel images show that the pore scale displacement and entrapment mechanisms during waterflood in heavy oils are different from those of light oils and capillary forces play an important role in recovery process especially after water breakthrough. This results in better displacement efficiency in water-wet systems compared to intermediate- and oil-wet systems. A new interaction between oil and high pressure CO2 is reported for the first time which contributes to oil recovery at the pore scale. Similarly, the pore scale displacement mechanisms of oil by (CO2-) foam are presented through vivid micro-scale images in this thesis which (some of them) have not been reported by other authors before. The coreflood results show that the performance of CO2 is to a large extent dependent on the reservoir conditions and physical properties of the heavy crude oil. In the case of the less viscous oil sample (crude "J") injection of CO2 at the reservoir conditions dramatically increased oil recovery to twice as much as recovery during plain waterflood. In the case of the highly viscous oil sample (crude "C"); while significant additional recovery was achieved during CO2 injection, an extended period

of injection was required. Further tests, revealed that if the CO2 flood process is boosted by mobility control techniques (e.g. formation of foam) the displacement process takes place in a much shorter time period and more efficiently.

In this thesis a literature review is presented in c*hapter 2*. The literature review gives a broad overview of the theoretical aspects of heavy oil recovery and the thermal and non-thermal recovery techniques. The focus of this chapter is on waterflood, CO2 flood and foam flood recovery processes. While these recovery processes have been extensively studied in light oils their application in heavy crude oils has received much less attention where the physics of the micro- and macro-scale event might be totally different due to high viscosity of these crudes. The pore scale displacement mechanisms, the trapping mechanisms and the recovery efficiency of these recovery processes are discussed in details in this chapter.

Chapter 3 describes the experimental facilities and the fluids used in this work. The first part of this chapter includes explanation of the micromodel and coreflood rigs, their important components and the working systems. The fluids which have been used for this study and results of the fluid characterization tests are all presented in the second part of this chapter. The Fluid characterization tests include viscosity measurement, rheology determination, compositional analysis and, CO2 saturation tests.

Chapter 4 describes the results of a comprehensive set of micromodel experiments to investigate the pore scale events during waterflood of heavy oils. Due to the high oil/water viscosity ratio, the physics of the displacement process in heavy oil is different from that of conventional oil which cannot be explained by conventional waterflood theories. The effect of oil viscosity and wettability of the system are studied in 7 micromodel tests and the differences with the case of conventional oil waterflood are highlighted through vivid images. The novel findings from these series of experiments reveal the unique role of capillary forces in displacement of heavy oils at the pore scale.

Chapter 5 presents the micromodel observations of the CO2 and CO2-foam displacement process in crude “C”. A total number of 5 micromodel tests are presented in this chapter in which the effect of CO2 injection on the recovery improvement and

the contributing recovery mechanisms are investigated. During the period of CO2 injection, the colour of the heavy crude oil was observed to change gradually but drastically from black to light brown as a result of the dilution of heavy oil with CO2. The discoloured diluted oil was readily mobilised and recovered during water injection carried out subsequent to CO2 injection and resulted in a very high oil recovery. The displacement process was significantly promoted as the viscosity of the injected CO2 was increased by formation of CO2-foam. The pore scale displacement mechanisms of foam flood have been extensively investigated in this section.

Chapter 6 presents the micromodel observations during CO2 and CO2-foam injection in crude "J". Having very low temperature and high pressure, CO2 is present in liquid state under reservoir conditions of crude "J". As a result, the oil recovery through CO2 dissolution and viscosity reduction was much more efficient in this crude oil which was followed with a period of oil production through extraction mechanism. A total number of 4 micromodel tests are presented in this chapter in which the effects of injection strategy, state of CO2 (vapour or liquid) and, CO2-foam injection on the oil recovery are investigated.

Chapter 7 presents the results of the coreflood experiments using crude "C". Different injection strategies including secondary (pre –waterflood) and tertiary (post-waterflood) injection of CO2 and CO2-SWAG injection and the effect of CO2-foam injection were investigated in 5 coreflood experiments. The results showed that despite the low reservoir pressure, the injection of CO2 enhances the recovery of this crude oil, however; due to the high oil viscosity, an extended period of CO2 injection is required. When the CO2 flood process was boosted by formation of foam the oil recovery accelerated and the ultimate oil recovery increased by a factor of three compared to the recovery during tertiary CO2 injection in this crude oil.

Chapter 8 presents the results of the coreflood experiments using crude "J". Different injection strategies and the effects of CO2-emulsion injection were investigated in 3 coreflood experiments. The liquid CO2 successfully displaced the heavy crude oil and doubled the oil recovery by waterflood in both secondary and tertiary mode of CO2 injection. However, at the early times of injection higher recovery was achieved when CO2 was injected in secondary mode. Co-injection of CO2 and surfactant solution

resulted in formation of a very strong CO2-emulsion and dramatically reduced the mobility of injected CO2.

A summary of the results is presented in Chapter 9 followed by conclusions and recommendations drawn from the work presented in this thesis.

Appendix A discusses repeatability of the micromodel experiments and Appendix B presents the relative permeability calculations from core flood experiments.

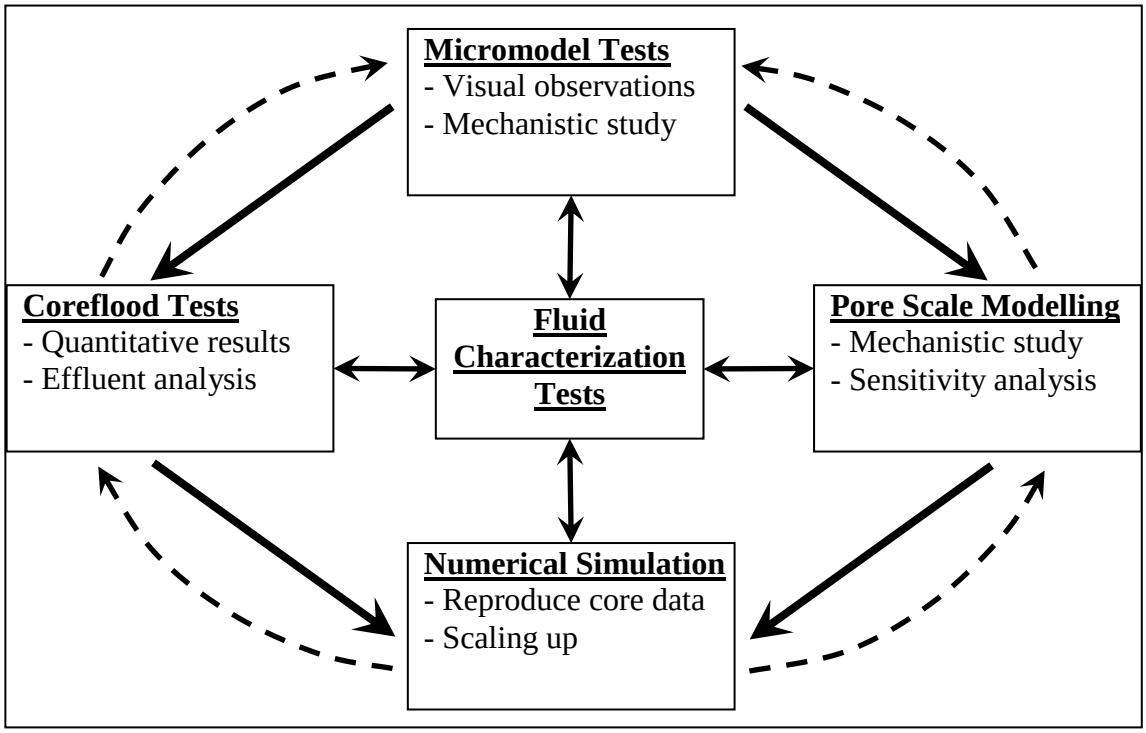

Figure 1-1: The work flow of the Enhanced Heavy Oil Recovery JIP.

Table 1-1: Summary of the micromodel experiments.

Exp No	**Experiment Name and Category**	**Crude**	**Chapter**
MM Exp 1	Effect of Oil Viscosity on Waterflood; Light Oil	Crude "A"	Chapter 4
MM Exp 2	Effect of Oil Viscosity on Waterflood; Medium-Heavy Oil	Crude "J"	Chapter 4
MM Exp 3	Effect of Oil Viscosity on Waterflood; Extra-Heavy Oil	Crude "C"	Chapter 4
MM Exp 4	Effect of Wettability on Waterflood; Strongly Water-Wet	Crude "C"	Chapter 4
MM Exp 5	Effect of Wettability on Waterflood; Slightly Water-Wet	Crude "C"	Chapter 4
MM Exp 6	Effect of Wettability on Waterflood; Slightly Oil-Wet	Crude "C"	Chapter 4
MM Exp 7	Effect of Wettability on Waterflood; Strongly Oil-Wet	Crude "C"	Chapter 4
MM Exp 8	Effect of Strategy of CO2 Injection; Tertiary CO2 Inj	Crude "C"	Chapter 5
MM Exp 9	Effect of Strategy of CO2 Injection; Secondary CO2 Inj	Crude "C"	Chapter 5
MM Exp 10	Effect of Strategy of CO2 Injection; CO2-SWAG Inj	Crude "C"	Chapter 5
MM Exp 11	Mobility Control; CO2-Foam Flood	Crude "C"	Chapter 5
MM Exp 12	Mobility Control; N2-Foam Flood	Crude "C"	Chapter 5
MM Exp 13	Effect of Pressure; Tertiary Low-Pressure CO2 Inj	Crude "J"	Chapter 6
MM Exp 14	Effect of Strategy of CO2 Injection; Tertiary CO2 Inj	Crude "J"	Chapter 6
MM Exp 15	Effect of Strategy of CO2 Injection; Secondary CO2 Inj	Crude "J"	Chapter 6
MM Exp 16	Mobility Control; CO2-Emulsion Flood	Crude "J"	Chapter 6

Table 1-2: Summary of the coreflood experiments.

Exp No	**Experiment Name and Category**	**Crude**	**Chapter**
Core Exp 1	Effect of Strategy of CO2 Injection; Tertiary CO2 Inj	Crude "C"	Chapter 7
Core Exp 2	Effect of Strategy of CO2 Injection; Secondary CO2 Inj	Crude "C"	Chapter 7
Core Exp 3	Effect of Strategy of CO2 Injection; CO2-SWAG Inj	Crude "C"	Chapter 7
Core Exp 4	Mobility Control; Tertiary CO2 Inj (consolidated Core)	Crude "C"	Chapter 7
Core Exp 5	Mobility Control; CO2-Foam Flood	Crude "C"	Chapter 7
Core Exp 6	Effect of Strategy of CO2 Injection; Tertiary CO2 Inj	Crude "J"	Chapter 8
Core Exp 7	Effect of Strategy of CO2 Injection; Secondary CO2 Inj	Crude "J"	Chapter 8
Core Exp 8	Mobility Control; CO2-Emulsion Flood	Crude "J"	Chapter 8

CHAPTER 2 LITERATURE REVIEW

2.1 INTRODUCTION

There are huge quantities of heavy oils worldwide, including medium-heavy oil, extra-heavy oil, and bitumen resources. The International Energy Agency (IEA) estimates that there are globally 6 trillion barrels of heavy oil in place (OECD/IEA, 2005). This is more than twice as much as conventional oil resources (Figure 2-1). Hence, heavy oil has the potential to be a major energy source for the 21st century. Although currently the volume of heavy oil production is much smaller than the production from conventional (light) oil, the world's dependence on heavy oil production is on the rise, mainly due to the projected massive increase in demand in the near future. As the heavy oil market is expanding around the world, an increasing number of oil companies are either becoming involved or increasing their activities around heavy oil production.

Heavy crude oils have been classified and denominated in various ways by different organizations involved in the petroleum industry (Cupcic, 2003; Martinez et al., 1987; Richard F. Meyer and Attanasi, 2003). The definition which is used in this text is the version defined by World Petroleum Congress (Martinez et al., 1987). This classification is based on the gas free properties of oil e.g. API gravity and viscosity at reservoir temperature. A crude oil is called “light oil” (or “conventional oil”) if it has an API gravity of at least 22.3° and a viscosity of less than 100 cp. “Heavy oil” is defined as a crude oil having a dead oil viscosity between 100 centipoises to 10000 centipoises with API gravity between 10° to 22.3°. “Extra-heavy oil” is that portion of heavy crudes having an API gravity of less than 10°. When reservoir viscosity measurements are not available, extra-heavy oil is considered to have a lower limit of 4°

API. Natural bitumen (also called "tar sands" or "oil sands") shares the attributes of extra-heavy oil but is yet more dense and viscous. Natural bitumen is oil having a viscosity greater than 10,000 centipoises

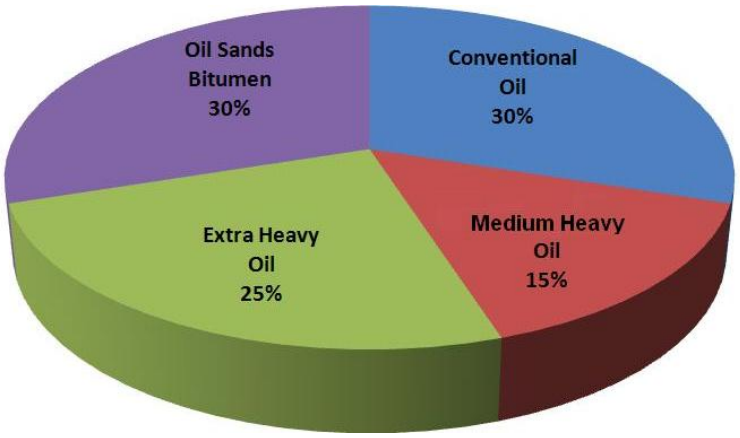

Figure 2-1: Total world oil resources. Medium-heavy, extra-heavy and bitumen make up to 70% of the world's total oil resources (Alboudwarej et al., 2006).

While some of the heavy oil reservoirs have shown favourable behaviour under solution-gas drive process, generally, the exploitation of heavy oil reservoirs by natural reservoir energy (primary recovery) yields a low ultimate recovery. Secondary recovery by pressure maintenance techniques is also not effective mainly due to the high viscosity of the resident oil that makes displacement and recovery of these heavy crudes difficult. The unfavourable viscosity (mobility) ratio between oil and displacing fluids induces undesirable effects, such as viscous fingering, leading to high residual oil saturation. Therefore it is necessary to implement EOR techniques early in the production life of heavy oil reservoirs. The most favourable solution to enhance recovery from heavy oil reservoirs is to reduce the mobility ratio between heavy oil and displacing fluid towards more favourable conditions. This can be achieved by either increasing viscosity of displacing fluid or by reducing the viscosity of heavy oil.

Thermal oil recovery techniques are the most common methods of heavy oil recovery and have been developed and applied in the field to alleviate the problem of poor sweep efficiency by reducing oil viscosity (Goyal and Kumar, 1989). These techniques include conventional steam floods with injectors and producers drilled in tight spacing patterns; cyclic production where the steam is injected and allowed to "soak" and, then produced out of the same well; steam assisted gravity drainage (SAGD) where steam is

injected in one horizontal well and produced from another lower horizontal well; and rarely used in-situ combustion projects.

However, thermal recovery techniques face their own set of obstacles and constraints with respect to technical, economic and, environmental issues. From a technical point of view, the heavy oil reservoirs with a thickness of less than 10 meters and depth of more than 1000 meters are considered to be poor candidates for thermal processes, as a consequence of heat loss to surrounding formations (Burger et al., 1985; Taber et al., 1997a). The limit for the reservoir depth and thickness is related to heat losses to the surrounding formation in the wellbore and reservoir (Boberg, 1988; Burger et al., 1985). Other specialized techniques present other challenges. The in-situ combustion projects require special equipment to deal with corrosion of sub-surface and surface equipment (similar corrosion issues exist in CO2 injection processes) and also require careful processing of the produced combustion gas (Thomas, 2007).

The economic constraints are related to the cost of steam generation and preparation of surface facilities. In such projects, upfront capital costs are considerable; with wells drilled on 2 acre spacing, expensive steam generation and production facilities and insulated lines. Furthermore, for environmental reasons, most steam generators are fired with natural gas which makes the operating expenses considerably higher than conventional production (Clark et al., 2007).

The negative environmental impacts also place serious limitations on the application of thermal recovery techniques. Exploitation of heavy oil reservoirs by thermal recovery techniques can generate as much as two to ten times more CO2 emissions compared to conventional production depending on the project and heavy oil recovery technique employed (Century, 2008; Plouchard, 2001; Romm, 2006). The other concerns are related to surface use and water resources. With tight spacing and considerable steam generator, producing facilities and flow lines, there is little else that the surface can be used for. Also, for steam preparation some or all of the water will be supplied by municipalities, competing with human use for quantities (Clark et al., 2007). Furthermore, specific fields have their own limitations and cannot be exploited by thermal recovery techniques. For instance, in Alaska, while production techniques are technically capable of developing thermal projects, new approaches are required to

allow production of shallow North Slope resources while protecting the permafrost (DOE, 2006).

Therefore, alternative non-thermal recovery methods are needed to improve recovery from heavy oil reservoirs. Compared to thermal methods, non-thermal methods offer advantages on capital cost, energy consumption, environmental pollution, safety and in-situ upgrading. They also provide a solution for recovery from heavy oil reservoirs in which thermal methods are impractical or uneconomical.

2.2 NON-THERMAL METHODS OF HEAVY OIL RECOVERY

Various non-thermal recovery techniques have been applied in heavy oil reservoirs to address the issue of poor mobility ratio and recovery efficiency. These methods can be divided into two groups. The first group are "viscosity reduction" techniques, which intend to reduce viscosity of heavy crude oils by gas and solvent injection e.g. CO2 and natural gas liquids (NGL). These recovery processes are assisted by gas assisted gravity drainage (GOGD) mechanisms in reservoirs with sufficient thickness. The second group of recovery processes are the mobility control processes, which intend to increase viscosity of the displacing phase by injection of chemicals. The most widely applied mobility control processes are the thickening of water with polymer and reducing gas mobility by foam. However if the heavy oil viscosity exceed certain values neither of these techniques can be efficient on their own and a combination of both is required.

This study is focused on the application of water as a base case and looks into the employment of CO2 and foam to improve heavy oil recovery. The following sections briefly review the existing literature on water, CO2 and foam flood processes.

2.3 WATERFLOOD

Water injection is the oldest assisted oil recovery method in the petroleum industry. In addition to pressure maintenance purposes, water is normally injected in the oil reservoirs to drive the resident oil (tertiary oil recovery) or to dispose produced brine (Craig, 1971; Latil, 1980; Willhite, 1986). Pore scale displacement mechanisms of waterflood in conventional oil reservoirs have been studied comprehensively and the impact of different parameters like pore structure, wettability and IFT has been investigated by many researchers. At the field scale, a well-documented body of

literature exists on the design, performance prediction, and operation of light oil waterflooding. However, waterflooding of heavy oil reservoirs has received much less attention. The major issue with regards to the waterflood of heavy oil reservoirs is the huge contrast in viscosity that exists between injected water (the displacing phase) and resident oil (the displaced phase), which may cause high waterflood residual oil saturation, front instabilities, and fingering. Despite this unfavourable viscosity ratio, water is normally injected in heavy oil reservoirs for both pressure maintenance and oil displacement purposes. The main advantages of waterflooding, compared to other techniques of heavy oil recovery are: availability of water, low cost of utilization, and existence of significant experience in managing field application.

The published data on heavy oil waterflooding are limited in the literature, and the results are sometimes conflicting (Ahmadloo et al., 2010; Beliveau, 2009; Brice and Renouf, 2008; Jenning, 1965; Kumar et al., 2008; Mai and Kantzas, 2009a; Mai and Kantzas, 2009b; Mai and Kantzas, 2010; Miller, 2006; Renouf, 2007; Sutton, 1968; Vittoratos, 2010). While some of the field applications have been reported to be successful, with promising incremental recoveries as high as 40%, there are numerous cases of unsuccessful waterflooding in heavy oil reservoirs (Ahmadloo et al., 2010; Kumar et al., 2008). Furthermore, the production performance, sensitive operational parameters and efficient techniques of recovery improvement are not the same as the case of light oil waterflood; and they cannot be fully explained and simulated by the existing theories developed, based on the physics of light oils (Miller, 2006; Renouf, 2007; Vittoratos, 2010). Therefore, it's believed that the current understanding of the active recovery mechanisms in heavy oil waterflood and how it differs from waterflood of light oils is limited and inadequate, despite its vital importance and wide use in industry (Kumar et al., 2008; Mai and Kantzas, 2008; Vittoratos, 2010). It's obvious that without this understanding, design and optimization of such projects is hardly practical.

The performance of waterflooding depends to a large extent on the interplay and competition between viscous (shear) and capillary forces. The viscous forces act as a resistance that must be overcome by the driving force before oil can be displaced and moved towards the production port. However, capillary forces either oppose or add to the driving force in effecting oil recovery (Moore and Slobod, 1956; Rose and Witherspoon, 1956). By definition, the viscous forces are proportional to viscosity and

frontal velocity and capillary forces vary with the interfacial tension and contact angle (Green and Willhite, 1986). Thus in the cases of light oils, heavy oils and extra-heavy oils with different magnitude of oil viscosity, there will be different equilibrium conditions between the driving force and the opposing viscous and capillary forces. This results in different displacement and trapping mechanisms, oil/water distribution pattern and recovery performance.

2.3.1 Parameters Controlling the Waterflood Performance

In reservoir conditions (conventional oils) the displacement process is usually assumed to be governed by capillary forces. In a capillary dominant displacement process however, what initiates the displacement is in fact the externally imposed force. The capillary forces rule the event at the pore scale (Moore and Slobod, 1956; Morrow, 1991; Rose and Witherspoon, 1956). Wettability and interfacial tension (IFT) are the principal factors controlling the displacement process at pore scale. Interfacial tension for water-oil interfaces during waterflooding, generally is in the range of 15 to 30 mN/m, and these relatively small variations are not thought to significantly affect the oil displacement process. This is of course different from the cases of interfacial tension lowering of orders of magnitude e.g. during surfactant flood, which might have important affects on the oil mobilization process, due to elimination of capillary forces in relation to viscous and gravity forces (Wardlaw, 1996b).

The oil/water viscosity ratio (μ_o/μ_w) is another important parameter; however, only when the displacement efficiency is considered at multi-pore level (Wardlaw, 1982; Willhite, 1986). An increase in the oil/water viscosity ratio causes strengthening of the resistance by viscous forces, which results in a higher saturation of trapped oil. Theoretically, velocity also has a large effect on viscous forces; however, the extent to which this is the case for the relatively small range of velocity variations (possible under field conditions of waterflooding) is likely to be small (Wardlaw, 1996b).

Therefore in reservoir conditions, performance of waterflood and recovery efficiency before and after breakthrough, are primarily controlled by wettability and viscosity ratio. Jenning's experiments demonstrated that highly unfavourable viscosity ratios cause early water breakthrough and an extended period of simultaneous oil and water production for both water- and oil-wet cores (Jenning, 1965). Conversely, when the oil/water viscosity ratio is very favourable (e.g. gas and water), there will be little oil

production after breakthrough at any wettability (Anderson, 1987). In waterflood, at moderate oil/water viscosity ratio (light oils and water), wettability is the principal parameter in determining flood behaviour (Moore and Slobod, 1956). In such a system with moderate oil/water viscosity ratio (depending on the state of the wettability) pore scale mechanisms of displacement and trapping will be distinctly different, which results in different oil and water distribution and displacement efficiency. In the following sections, the effect of wetting state of the system on displacement and entrapment mechanisms and recovery efficiency mechanisms will be reviewed.

2.3.2 Pore Scale Displacement Mechanisms

In the case of waterflooding of light oils, a moderate mobility ratio of 1.0 or less usually exists between the resident oil and injected water, which indicates that oil and water are moving at the same relative rate in the porous media (Willhite, 1986). In such a system, while the viscous forces are in our favour, the capillary forces remain the main trapping forces. As the water front progresses in porous media, the outcome of interface movement at pore scale (displacement mechanism) is a determinative parameter to oil entrapment and efficiency of the displacement process. Based on the state of wettability, the pore scale displacement process might take place through various mechanisms.

1. Water-Wet Systems: In a water-wet system, water occupies the smaller pores and forms a thin layer over all rock surfaces. The oil rests on a film of water spread over the rock surface and occupies the centres of larger pores. During waterflood of such a water-wet system, with respect to capillary pressures, injected water tends to invade small- or medium-sized pores before larger pores (Anderson, 1987). The displacement of resident oil takes place through existing films of water on pore walls in the form of "corner filament flow" (Sohrabi et al., 2000b), followed by either "snap-off" mechanism in pores with large pore-to-throat aspect ratio or by "piston type" motion in pores with smaller pore-to-throat aspect ratio (Chatzis et al., 1983; Li and Wardlaw, 1985b). During a low capillary number displacement process in porous media, only the continuous fluid phases (wet or non-wet) can flow (Li and Wardlaw, 1985a). As the water front passes, the remainder of the oil is trapped in the form of discontinuous oil blobs; therefore, almost all remaining oil will be immobile. Because of such immobility in the water-wet case, there is little or no production of oil after the

water breakthrough (Anderson, 1987). Figure 2-2(a) schematically demonstrates the process of oil displacement by corner filament flow and snap-off in a strongly water-wet pore/throat pair.

2. Oil-Wet Systems: In an oil-wet system, oil is generally located in smaller pores and as a thin film on rock surfaces, while water is present in the centres of larger pores (Anderson, 1987; Donaldson and Thomas, 1971). When waterflood is started, water "channels" through the centres of the largest pores leaving residual oil as a continuous film over pore surfaces and in smaller cervices and pores. As the water injection continues, successively smaller pores are invaded and join to form continuous channels. Additionally, "oil film drainage" over oil-wet paths along pore surfaces makes a significant contribution to displacement process in the previously flooded pores (Salathiel, 1973). Water invades smaller pores to form additional continuous channels. When sufficient water-filled flow channels form to permit nearly unrestricted water flow, oil flow falls to a very low rate or stops (Anderson, 1987). Figure 2-2(c) schematically demonstrates the process of oil displacement by water channelling mechanism in a strongly oil-wet system.

3. Intermediate-Wet Systems: If no preference is shown by the rock to either fluid, the system is said to exhibit intermediate wettability (contact angle of 90°). As capillary pressure is proportional to the cosine of the contact angle, capillary forces will be reduced in such wettability conditions. Systems with intermediate wettability, range from slightly water-wet to slightly oil-wet. In a slightly water-wet system, water still occupies most small pores; however, oil is definitely attached to some of the rock surfaces. As the system becomes more oil wet, oil occupies more of the small pores. When systems of intermediate-wetness are waterflooded, displacement at the pore scale is through a "piston type" motion (Figure 2-2b). The remaining oil after water breakthrough is frequently connected to oil in pores ahead by very thin filaments of oil. This oil is drained through these filaments until filament rupture occurs, leaving the oil completely surrounded by water (Donaldson and Thomas, 1971).

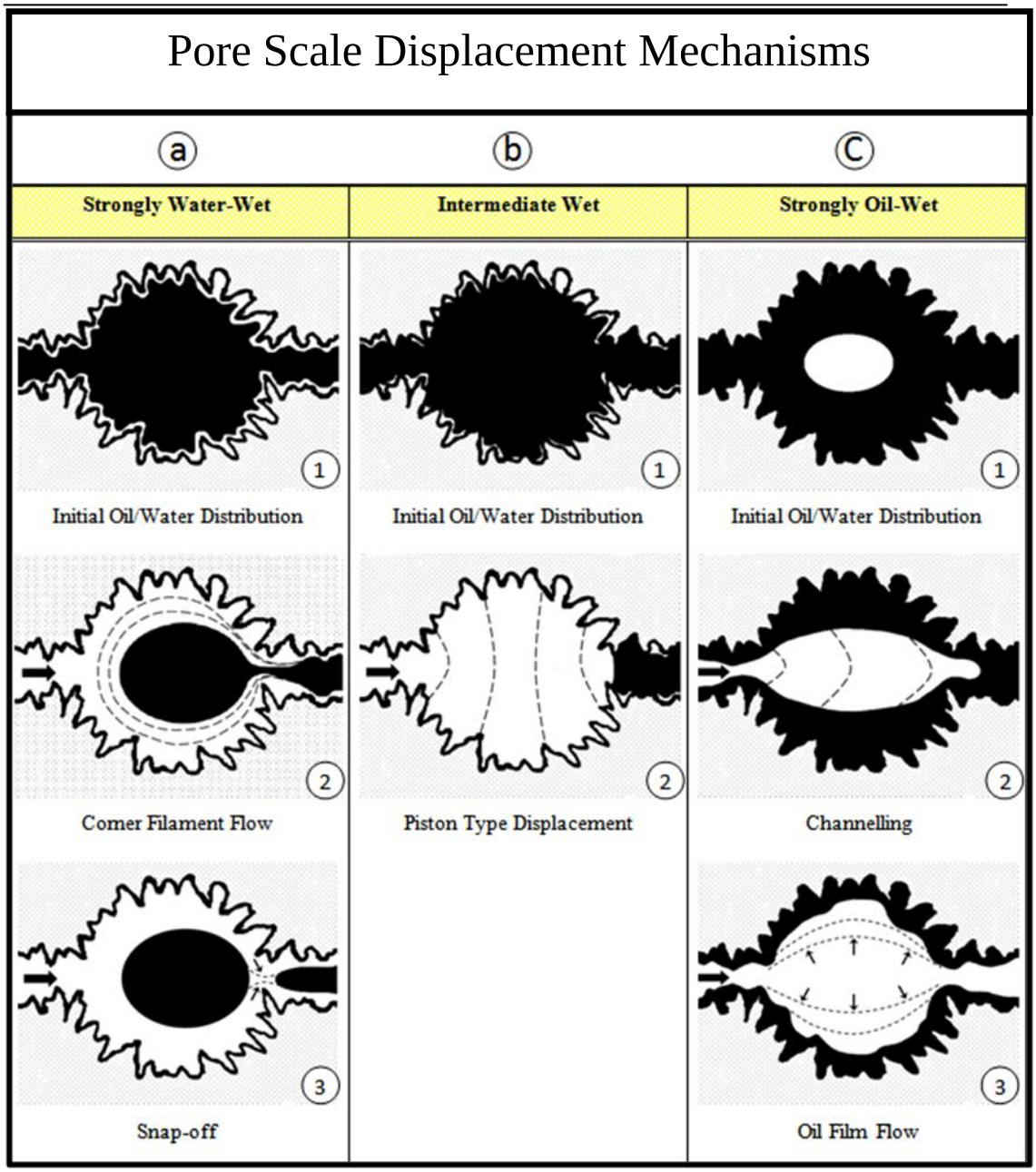

Figure 2-2: Schematic diagram of oil displacement process in a pore-throat pair through (a) corner filament flow and snap off in a strongly water-wet system, (b) piston type displacement in intermediate wet system, and (c) channelling and oil film flow in an oil wet system.

2.3.3 Entrapment Mechanisms

As water displaces oil by the recovery mechanisms explained above, a fraction of oil remains unswept and immobilized in the porous media. This residual oil exists in two basic forms: (1) trapped oil in a single pore either in the form of spherical globules at the centre of the pore or attached to the pore wall, (2) larger oil patches continuous over many pores that are surrounded by water (Anderson, 1987; Craig, 1971). The properties of the rock-pore system, properties and interaction of the fluids with pore

walls, are all important and determinative to the saturation and distribution of residual oil (Wardlaw, 1996a). Wardlaw (Wardlaw, 1996a) introduced four mechanisms of oil trapping in water-swept reservoir rocks (see Figure 2-3):

(1) Viscous fingering is believed to be caused by instabilities at the displacement front, whenever the viscosity of the displacing fluid is much less than that of displaced fluid. In such a system, water will finger through the oil phase and breakthrough will occur relatively early (Craig, 1971; Willhite, 1986). It should be noted that viscous fingering is not dependent on pore structure, as it occurs between parallel plates in the absence of structure (Wardlaw, 1996b).

(2) Capillary instability at the oil-water interface, may result in disconnection of the non-wet phase in pores or at pore throat junctions (Li and Wardlaw, 1985b). The simplest form of trapping by capillary instability is "snap-off" of oil in a simple model pore (Figure 2-2a), whereby an oil bridge in a pore throat becomes unstable and ruptures (Roof, 1970), resulting in trapping of oil in the pore body. Strongly water-wet conditions and a large pore-to-throat aspect ratio has been shown to increase oil trapping by a snap-off mechanism. (Chatzis et al., 1983; Li and Wardlaw, 1985a)

(3) Bypassing of oil is "final separation of an isolated oil blob by filling of a pore body." (Morrow and Heller, 1985). This entrapment mechanism is related to differential travel paths of water-oil interfaces, caused by heterogeneities in pore structures (Chatzis et al., 1983; Wardlaw, 1996b). The bypassed oil blobs might be located in a single pore or extended over a network of pores and throats.

(4) Surface trapping occurs in preferentially oil-wet systems where the matrix retains oil by capillarity. Surface trapping is likely to be particularly important in rocks with highly irregular pore surfaces and large surface areas (Hirasaki and Zhang, 2004; Wardlaw, 1996b).

Of the four mechanisms of oil entrapment, all occur at the pore scale during waterflooding and mechanisms 1 and 3 also occur at larger scales. This results in formation of larger patches of residual oil extending over many pores, which are completely surrounded by water.

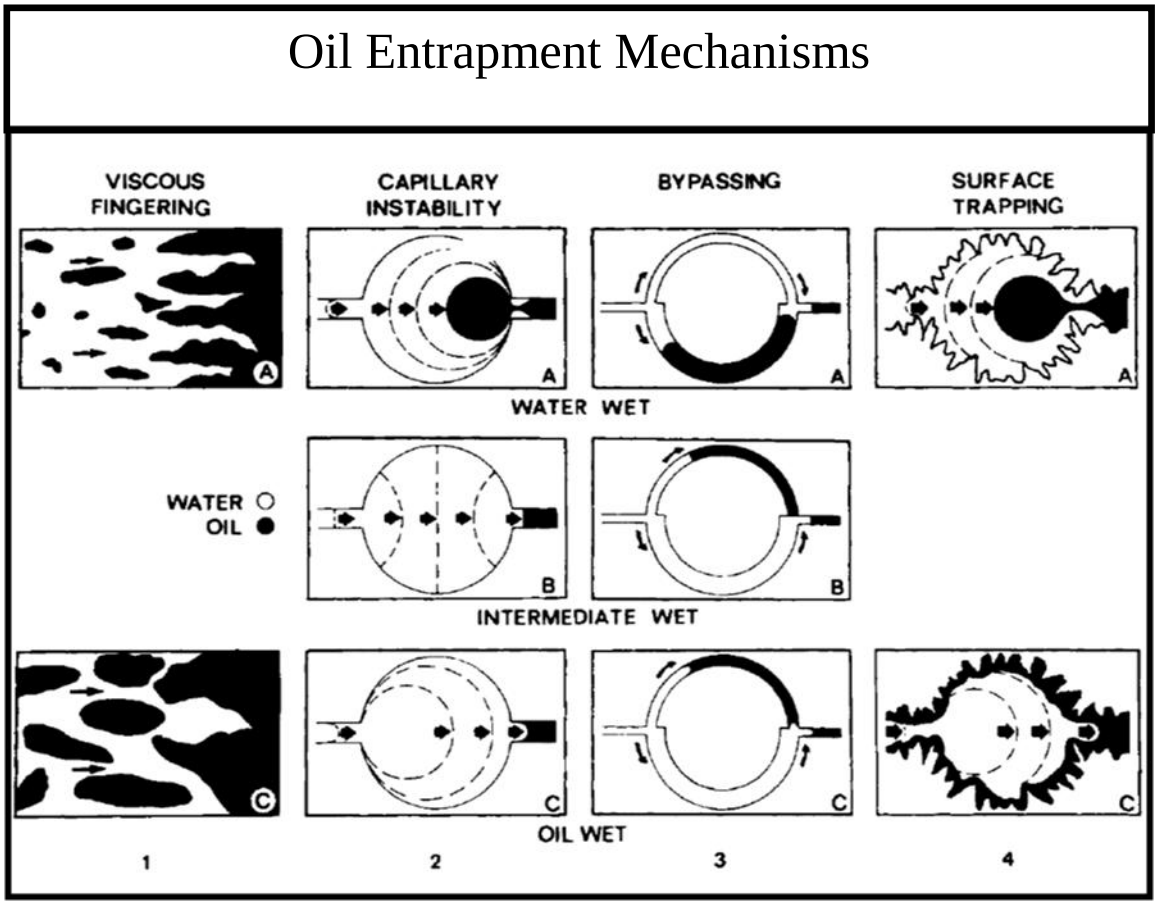

Figure 2-3: Four mechanisms of oil-trapping at pore scale for three wettability conditions (Wardlaw, 1996b).

Table 2-1 summarizes the relative importance of entrapment mechanisms at different wettability conditions. Viscous fingering is only dependent on the oil/water viscosity ratio and to a lesser extent on the frontal velocity; therefore, in a system with a moderate viscosity ratio of around one, the viscous fingering has little effect on oil entrapment. The effect of wettability on viscous fingering is also small. While the oil entrapment by viscous fingering is not dependent on the wettability of the system, the state of wettability has a large effect on oil entrapment by the other three trapping mechanisms.

The experimental studies of oil displacement from single model pores, has shown that oil trapping by a snap-off mechanism can be inhibited if the water-advancing contact angle exceeds approximately 70° (Li and Wardlaw, 1985a). Conversely, oil trapping by the surface trapping mechanism is directly related to the oil-wet tendency of pore walls. Therefore, a change from strongly water-wet to strongly oil-wet conditions increases oil

entrapment by a "surface trapping" mechanism, whereas it is expected to decrease immobilized oil due to capillary instabilities and bypassing (Wardlaw, 1996b).

However, the relationship between "bypassing" mechanism and state of wettability is more complicated. In a strongly oil-wet system, water begins to travel preferentially through the largest pores with only weak imbibition into smaller pores. This results in higher saturation of bypassed oil at breakthrough time in strongly oil-wet systems, compared to the case of strongly water-wet systems. Nevertheless, as water injection continues (because the residual oil is still connected) water opens new flowing channels and displaces a good fraction of the bypassed oil in oil-wet systems, whilst the bypassed oil remains unchanged in the strongly water-wet systems (Anderson, 1987; Craig, 1971). This causes lower saturation of bypassed oil in the strongly oil-wet systems, which is located in smaller pores and cervices, compared to the case of strongly water-wet systems where the residual bypassed oil is present in the larger pores (Wardlaw, 1996b).

Table 2-1: The relative importance of entrapment mechanisms and effect of wettability on trapping mechanisms in moderate oil/water viscosity ratio conditions (light oils).

Wettability Conditions	Viscous Fingering	Snap-off	By Passing	Surface Trapping
Strongly Water-Wet	S	L ↑	L ↓	S ↓
Intermediate Wet	S	S	M	M
Strongly Oil-Wet	S	S	M	L

L= Large trapping potential (trapping a significant fraction of oil)
M=Medium trapping potential (trapping some of oil)
S= Small trapping potential (trapping a negligible fraction of oil)
Arrows indicate increasing (↑) and decreasing (↓) potential for trapping by various mechanisms as a function of wettability.

The relationship between "bypassing" mechanism and state of wettability is however more complicated. In a strongly oil-wet system, water begins to travel preferentially through the largest pores with only weak imbibition into smaller pores. This results in higher saturation of bypassed oil at breakthrough time in strongly oil-wet systems compared to the case of strongly water-wet systems. Nevertheless, as water injection continues, because the residual oil is still connected, water opens new flowing channels and displaces a good fraction of the bypassed oil in oil-wet systems whilst the bypassed

oil remains unchanged in the strongly water-wet systems (Anderson, 1987; Craig, 1971). This causes lower saturation of bypassed oil in the strongly oil-wet systems which is located in smaller pores and cervices compared to the case of strongly water-wet systems where the residual bypassed oil is present in the larger pores (Wardlaw, 1996b).

2.3.4 Recovery Efficiency

There are three different oil saturations of interest in waterflooding: breakthrough saturations, practical (or economical) saturation and true residual saturation. The breakthrough saturation is calculated when water is first produced at the outlet of the system and final saturation is reached after many PVs of waterflood, when the oil production is eventually stopped. There is a time in between when the water-oil ratio is so high that waterflood is no longer economical, the system is at the practical or economical residual oil saturation. In this text, the term "recovery" is attributed to this saturation, unless specified otherwise. All three saturations are essentially equal in a strongly water-wet system with a moderate oil/water viscosity ratio, however, the saturations can differ greatly in intermediate and oil wet systems (Anderson, 1987). This is due to the fact that for strongly water-wet systems, oil behind the displacement front loses connectivity, so there is no further production of oil no matter how many pore volumes of water are injected; whilst for intermediate- or oil-wet systems, it appears that oil connectivity is never lost completely, thus oil recovery is greatly dependent on the volume of injected water (Morrow, 1991).

Several early examples of laboratory waterfloods show oil recovery decreasing with decreasing water-wetness (Donaldson and Thomas, 1971; KYTE et al., 1961; Lefebvre du Prey, 1973; Mungan, 1966; Newcombe et al., 1955). This is consistent with the intuitive notion that strong wetting preference of rock for water and associated strong capillary imbibition forces certainly aid in displacing oil and give the most efficient oil displacement. However in reality, the amount of oil that is trapped depends on the outcome of interface movement at the pore scale (displacement and entrapping mechanisms). An increasing number of examples of improved recovery with shift from strongly water-wet conditions are being reported for slightly water-wet or intermediate-wet conditions (Jadhunandan and Morrow, 1995; Morrow, 1990; Morrow and McCaffery, 1978; Tweheyo et al., 1999). Jadhunandan and Morrow (Jadhunandan and Morrow, 1995) investigated the relationship between wettability and waterflood oil

recovery in a series of Berea cores. They used crude oil as a wettability-altering agent and by varying the initial water saturation Swi and aging conditions, they reproduced different wettability conditions. From the results of over 50 waterfloods, a correlation was obtained between oil recovery and wettability defined by the Amott-Harvey wettability I_{w-o}. The results showed that oil recovery by waterflooding initially increased and then decreased as the wettability changed from strongly water-wet to oil-wet, with the oil recovery peaking at intermediate wettability conditions ("close but on the water-wet side of neutral-wet conditions"). The difference in recovery at different wettability conditions became increasingly definitive with continued flooding after water breakthrough. In the literature, it is generally accepted that intermediate-wet systems yield the largest amount of ultimate recovery (Amott, 1959; Anderson, 1987; Kennedy et al., 1955; Lorenz et al., 1974; Tweheyo et al., 1999). Figure 2-4 plots oil recovery and residual oil saturation data from Jadhunandan and Morrow (Jadhunandan and Morrow, 1995) at breakthrough, 3 and 20 PVs injected.

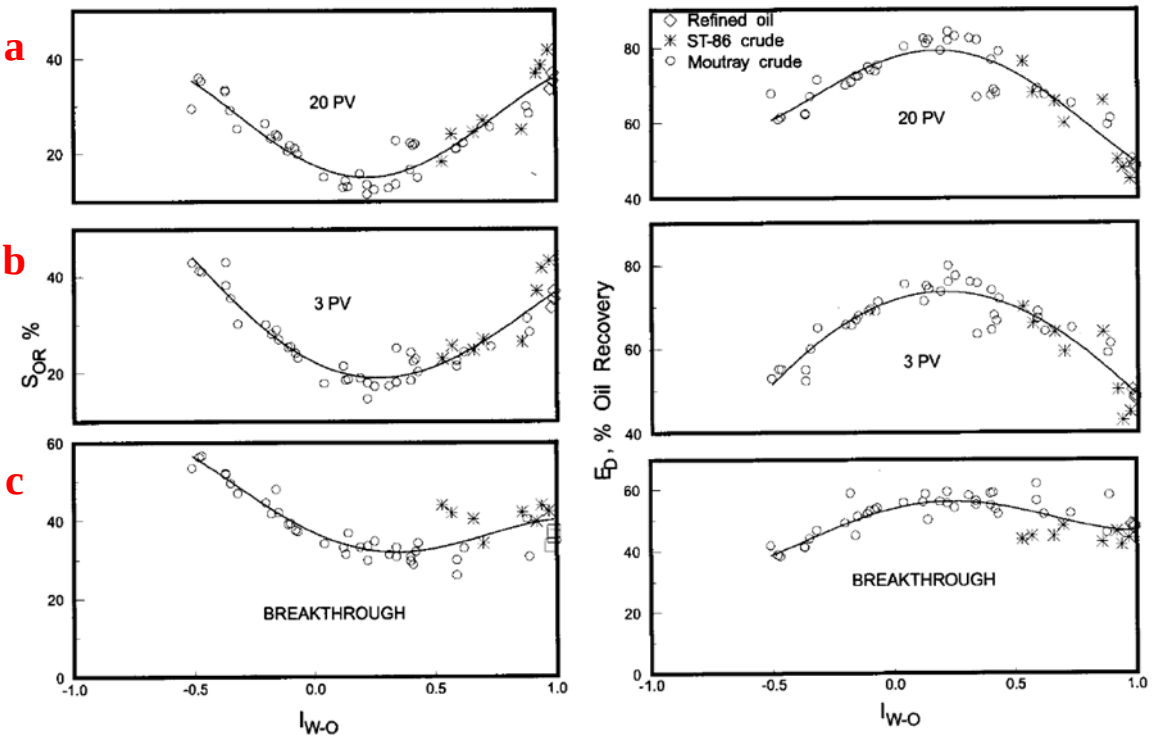

Figure 2-4: Oil breakthrough saturation (a), economical saturation (b) and, true residual saturation (c) and their corresponding recovery efficiency versus I_{w-o} for different wettability conditions during waterflooding of light oil samples (Jadhunandan and Morrow, 1995).

In summary, in a system with moderate oil/water viscosity ratio, waterflood in oil-wet systems is usually considered to be less efficient than waterflood in water-wet systems, because more water must be injected to recover a given amount of oil (Anderson, 1987); despite the fact that ultimate oil recovery might be similar if not higher in oil-wet systems (Amott, 1959; Jadhunandan and Morrow, 1995; Kennedy et al., 1955; Lorenz et al., 1974). However, the highest waterflood displacement efficiency is normally achieved in intermediate wet systems where the trapping by capillary forces is minimized.

2.4 CO2 FLOOD

An attractive solution for meeting the increasing demand for oil and simultaneously addressing environmental concerns in relation to thermal heavy oil production, could be injection of CO2 (produced from the steam generation process or other industrial sources) into the reservoir. Unlike water, CO2 dissolves in the heavy oil and improves the displacement process by reducing viscosity of the crude oil. Although heavy oil viscosity reduction, due to mixing with CO2, is not as high as the reduction achieved by thermal methods, viscosity reduction of two orders of magnitudes has been reported in the literature (Klins, 1984; Klins and Bardon, 1991). CO2 injection also provides a solution for recovery from heavy oil reservoirs in which thermal methods are impractical or uneconomical, especially for deeper reservoirs or those located in thin formations in which heat loss would be significant (Goyal and Kumar, 1989). Compared to thermal methods, CO2 injection can offer advantages on capital cost, energy consumption, environmental pollution, safety, and in-situ upgrading.

CO2 injection is a well-researched and established oil recovery method but it has been mainly applied to conventional (light) oil reservoirs where the main focus is on the miscible displacement of the oil by CO2 (Kovscek, 2002; Taber et al., 1997a; Taber et al., 1997b). This is very different from the application of CO2 in heavy oil reservoirs where due to the long-chain and heavy nature of the hydrocarbons the miscibility is very unlikely to happen and the main benefit of CO2 injection comes from the substantial drop in the viscosity of heavy oil. There has been some limited experience documented for CO2 injection in heavy oil reservoirs (Fulop et al., 1997; Issever and Topkaya, 1998; Khatib et al., 1981; Moffitt and Zornes, 1992; Saner and Patton, 1986; Spivak et al., 1990). The results show successful application of CO2 in heavy crude oils as low as 10 to 12 API using different injection strategies e.g. huff-and-puff and

drive process. Laboratory tests have shown that although miscibility cannot be reached, substantial additional recovery can be achieved by CO2 injection in heavy oil systems. The recovery improvement is mainly due to viscosity reduction and oil swelling and to a lesser extent due to oil swelling and IFT reduction and there is a direct relationship between pressure of the system and recovery improvement (Klins, 1984; Klins and Bardon, 1991; Matthews, 1989; Mayer et al., 1988; Miller, 1981; Sankur and Emanuel, 1983; Spivak et al., 1990; Srivastava et al., 1994).

2.4.1 Parameters Controlling CO2 Flood Performance

Reservoir pressure, temperature and crude oil composition are the primary parameters controlling the performance of CO2 flood. Unlike waterflood, the component exchange between crude oil and CO2 is an important part of the CO2 flood process, which leads to miscible or immiscible displacement types. Naturally, the most attractive scenario for recovery of oil by CO2 is miscible displacement. However, if miscibility is not attained other mechanisms driven from dissolution of CO2 into the oil phase and/or vaporization of hydrocarbon components into the CO2 phase can significantly improve oil recovery (Klins and Bardon, 1991). Klins (Klins, 1984) has classified the dominant displacement characteristics for a given CO2 displacement falling into one of five regions as shown in Figure 2-5a.

Region I: Low pressure applications (generally immiscible),
Region II: Intermediate pressure, high temperature applications (immiscible),
Region III: Intermediate pressure, low temperature applications (immiscible),
Region IV: High pressure application (miscible),
Region V: High pressure, low temperature liquid applications (immiscible).

In region I, the major effects of CO2 injection on oil recovery appear due to the solubility of CO2 in crude oil. The dissolution of CO2 improves recovery by a combination of various mechanisms including; oil swelling, reducing oil viscosity and, contributing to internal solution gas drive mechanism. Region II of this graph, shows conditions in which reservoir pressure is higher than those in Region I but still lower than MMP (minimum miscibility pressure). In this region, supplemental production mechanisms come into play and CO2 starts to extract oil in increasing amounts with increasing pressure. At pressures above MMP, miscibility is achieved between oil and

CO2 through first- or multiple-contact processes, as can be seen in Region IV. In miscible displacement processes, there is no interface between CO2 and oil and the capillary forces are removed. In the absence of the trapping capillary forces, the pore scale displacement process takes place very efficiently.

In specific reservoirs with exceptionally low temperature (e.g. reservoirs underlying permafrost) CO2 can be present in liquid state (region V). Liquid CO2 has high density comparable to that of crude oil and brine. This results in improved sweep efficiency through alleviating the gravitational segregation. The oil displacement by liquid CO2 is generally an immiscible process and takes place through recovery mechanisms similar to those in region II. Finally, in certain reservoir conditions, there is the possibility of formation of a third phase which is rich in CO2 and contains light and intermediate hydrocarbon components. The new phase generally appears at intermediate pressures and low temperature conditions as can be seen in region III of Figure 2-5a.

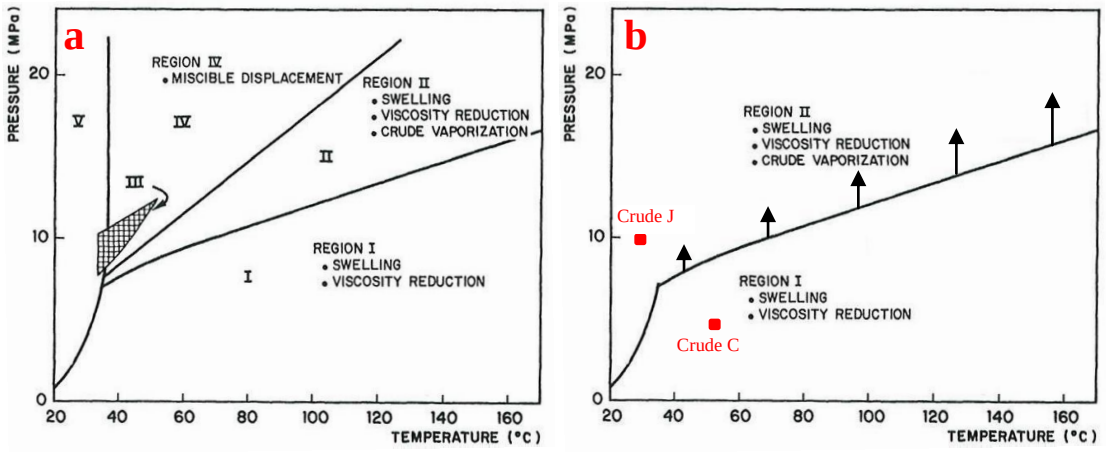

Figure 2-5: Picture (a) demonstrates the effect of reservoir temperature and pressure on CO2 recovery mechanisms in conventional oils (Klins, 1984). Picture (b) shows the same graph modified for heavy oils. The black arrows show elevation of the separating line as crude oils become heavier and more viscous.

Figure 2-5b illustrates the dominant displacement characteristics for CO2 in heavy oil systems. As shown, formation of the third phase and miscible displacement regions are removed and the graph is simplified to two regions of low pressure (region I) and high pressure displacement (region II). In region I, the major effects of CO2 injection on oil recovery appear due to the solubility of CO2 in heavy oil through mechanisms like viscosity reduction and swelling. In region II, the CO2 dissolution is still present in the

system; however, it is subsequently followed by an extraction mechanism. It should be noted that lines dividing the regions in Figure 2-5b are roughly generalized and will shift upward (requiring higher pressures) for heavier oil samples (Klins, 1984). The red square markers in Figure 2-5b show the reservoir pressure and temperature conditions of crude "C" and "J" which suggest that the process of oil recovery by CO2 injection take place in region I and region II respectively for crude "C" and crude "J". Due to the low reservoir pressure of crude "C", CO2 dissolution is the main mass transfer phenomenon between oil and CO2 which enhance oil recovery through viscosity reduction and oil swelling mechanisms. In the case of crude "J", the higher pressure of the reservoir causes greater CO2 dissolution in the oil (compared to crude "C") and at the same time extraction of hydrocarbon components into the liquid CO2.

In the process of oil recovery by immiscible CO2, direct displacement of oil by CO2 is the initial source of recovery improvement which takes place through drainage or double drainage mechanisms at the pore scale (these mechanisms are explained in the following section). However, the most important recovery mechanisms are related to the mixing and component exchange between oil and CO2. The recovery mechanisms related to mixing and compositional change in heavy oil and CO2 are as follows:

Viscosity Reduction: As CO2 saturates crude oil, a large reduction in the viscosity of the oil occurs. This reduction, like heating of oil in thermal recovery, can yield viscosities one-tenth to one-hundredth of the original oil viscosity. An example of this reduction in viscosity is illustrated in Figure 2-6 where two heavy oil samples are saturated with CO2 at 140 ^{o}F and different pressure conditions (Miller and Jones, 1981). Note that a larger percentage reduction occurs in the more viscous crude oil. For example, at a saturation pressure of 2000 psia and temperature of 140 °F, the more viscous crude sample (Cat Canyon oil) reduces its viscosity from 9000 cp to around 90 cp, a viscosity decrease of two orders of magnitude, while the less viscous crude sample (Wilmington Oil) undergoes a less pronounced viscosity reduction of twentyfold from 140 cp to 7 cp. Thus the viscosity reduction and its effect on mobility ratio is more significant in viscous oils and not as large in low viscosity oils (Klins, 1984).

To understand the process of oil viscosity reduction by CO2 dissolution, it is required to look into the type of the forces between hydrocarbon and CO2 molecules. Intermolecular forces are responsible for many of the physical properties of fluids,

including viscosity, diffusion, density, and surface tension (Zumdahl and Zumdahl, 2008). The attraction forces between hydrocarbon molecules in the oil phase are dependent on the length of carbon chain (carbon number) of the molecules. The inter-molecular forces will strengthen, if the carbon number increases as a result of increase in variations and polarity (both instantaneous and permanent) of the molecules (Olah and Molnar, 2003). However, CO2 molecules are small and non-polar; thus, attract other molecules by weak dispersion ("also called London") forces through formation of instantaneous dipoles. Therefore, when CO2 dissolves in the oil attraction forces between CO2-hydrocarbon molecules are not as strong as the original attraction forces between hydrocarbon molecules. Furthermore, positioning of the CO2 molecules in between hydrocarbon molecules increases the intermolecular distance and weakens the inter-molecular forces between hydrocarbon molecules. Weakening of the inter-molecular forces facilitates the molecular movement, reduces the resistance shear forces between flowing layers and eventually results in fall of viscosity (Sahoo, 2005).

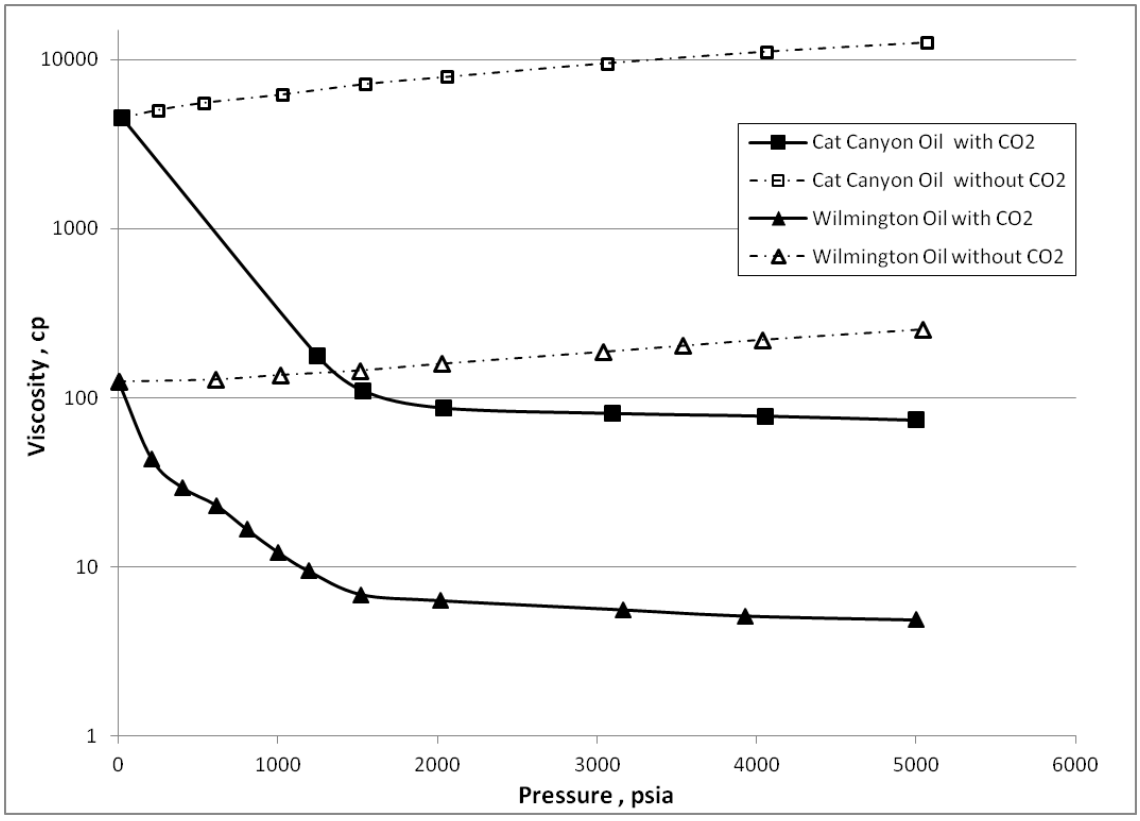

Figure 2-6: Viscosity of Wilmington oil with an API gravity of 17° and Cat Canyon Oil with an API gravity of 10° at 140 ºF and different pressure conditions with and without CO2 dissolution (Miller and Jones, 1981).

Swelling of Oil: The swelling of oil due to CO2 dissolution is important for two main reasons. Firstly, the residual oil left in the reservoir after flooding is inversely proportional to the swelling factor, i.e. the greater the swelling, the less stock tank oil abandoned in the reservoir. Secondly, separate oil blobs will become connected as the oil swells and forces water out of the pore space. This creates higher oil recovery and more favourable relative permeability curves at any given saturation condition (Klins, 1984).

Oil Extraction: At high pressure conditions, in addition to CO2 dissolution into the oil phase, light and intermediate hydrocarbon components may be vaporized into the CO2. When CO2 is added to the oil at low pressures, it dissolves in the oil and results in swelling of the oil phase. However, this swelling occurs only to a certain point. After a given pressure, oil begins to vaporize into the CO2 rich gas phase and its volume shrinks. This swelling and subsequent vaporization is shown by Holm and Josendal (Holm and Josendal, 1982) in Figure 2-7. As illustrated, at1000 psia the Mead-Strawn crude has swollen to 60 % of its original volume. Above 1000 psia, the oil phase begins to shrink significantly indicating hydrocarbon extraction. Note that there is an inverse relation between oil density and the strength of extraction mechanism. Therefore, despite a sizeable increase of oil recovery by this extraction mechanism in light crude oils, the contribution of this mechanism to oil recovery is less pronounced in the heavier crude oils.

Holm and Josendal (Holm and Josendal, 1982) report that this extraction of liquid hydrocarbons into a CO2 rich gaseous phase occurs when the density of CO2 is at least 0.25 to 0.35 gm/cc. The corresponding reservoir temperature-pressure pair that yield such densities for vaporization to occur is matched those presented as the lower limit of Region II, shown in Figure 2-5a and b. The vaporization process leads to gradation of fluids within the cross section of the reservoir, ranging from virgin reservoir oil to 100% CO2 vapour.

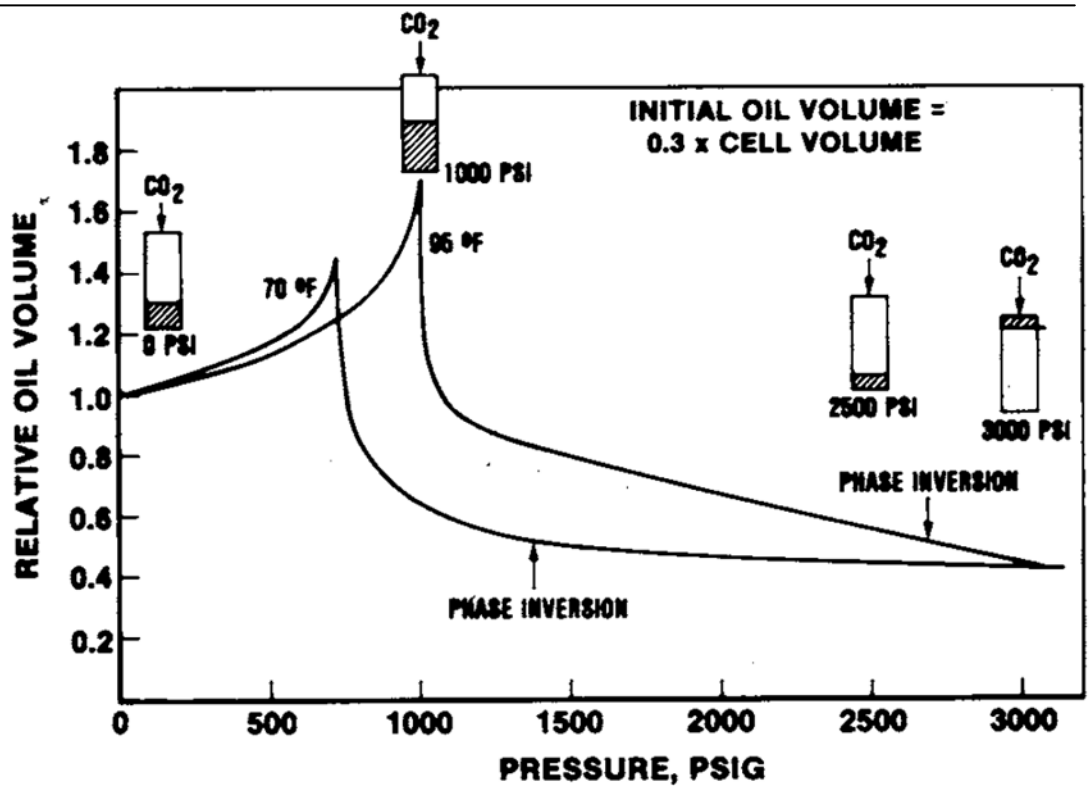

Figure 2-7: Change in volume of Cabin Creek stock-tank oil as CO2 was added at increasing pressure (Holm and Josendal, 1982).

Solution Gas Drive: Just as CO2 goes into the solution with an increase in reservoir pressure, after termination of the injection phase of a flood, gas will come out of solution and continue to drive oil into the wellbore (Klins, 1984). In high viscosity crudes, solution gas drive can lead to in situ formation of non-aqueous foam (foamy oil) which retards the formation of a continuous gas phase and dramatically increases the apparent trapped gas saturation. This provides the natural pressure maintenance mechanism and leads to much higher oil rates and recoveries of the original oil in place under solution gas drive(Maini et al., 1993).

2.4.2 Pore Scale Displacement Mechanisms

To analyze the process of oil recovery by direct displacement (without compositional exchange) and predict its efficiency during gas flood (CO2 in this study), a good knowledge of fluid distribution at the microscopic level is required. Rock wettability and spreading coefficient are considered to be principal parameters affecting flow characteristics and fluid distribution within the porous medium during three phase flow. Wettability is the ability of a fluid to spread on a solid to form wetting films (Hirasaki, 1991). In three phase conditions, gas generally tends to be the non-wetting phase, having least tendency to cover the surface of porous medium. Among water and oil,

one becomes wetting phase covering the rock surfaces and the other becomes intermediate-wetting phase. Intermediate-wetting phase is a non-wetting phase with respect to wetting phase but acts in a manner similar to that of a wetting phase with respect to gas (non-wetting phase).

The spreading coefficient is the ability of oil to form spreading film on water in the presence of gas (Adamson, 1960). The spreading coefficient is defined as a balance of the three interfacial tensions of the water-oil-gas system:

$S_{o/w}=\gamma_{wg}-\gamma_{og}-\gamma_{og}$

When $S_{o/w}>0$; the oil spontaneously forms spreading films between water and gas; these films maintain the hydraulic continuity of the oil phase. When $S<0$ the oil meets the water surface at a finite contact angle (Vizika et al., 1998).

Another important parameter is the saturation and distribution of fluids in porous media before starting gas injection. Gas might be injected in secondary mode (pre-waterflood) where water is present at its irreducible saturation (S_{wi})or in tertiary mode (post-waterflood) to recover the waterflood residual oil where water saturation is significant. All these parameters affect pore scale displacement mechanisms and their efficiency during a gas flood.

In a water-wet system with spreading behaviour, water is preferentially located in pore throats and forms continuous wetting films covering the rock surface. Gas is the non-wetting phase which occupies pore bodies and some of the interconnected pore throats. Oil occupies space that is intermediate between that occupied by the gas (central part) and the water (located primarily in the corners). Therefore, the bulk of the oil in a pore body is located at the throat entrances. In such a system, displacement of oil by gas proceeds by either: (1) "direct drainage" mechanism in which gas displaces oil by advancing a gas-oil interface, or (2) "double-drainage" mechanism, in which a gas-oil interface advance (first drainage event) is always associated with a corresponding oil-water interface movement (second drainage event). The second drainage event leads to the reconnection and recovery of residual oil blobs and water production at the outlet. A schematic of the double-drainage mechanism in water-wet systems with spreading behaviour is depicted in Figure 2-8. While recovery by "direct drainage" mechanism mostly takes place where the oil saturation is high and there are continuous paths of oil phase in porous medium; the latter mechanism (double-drainage) appears where the

water saturation is high and the oil phase is not connected throughout the porous medium. After gas breakthrough, oil production continues through thin oil films around the gas stream (Oren et al., 1992; Oren et al., 1994).

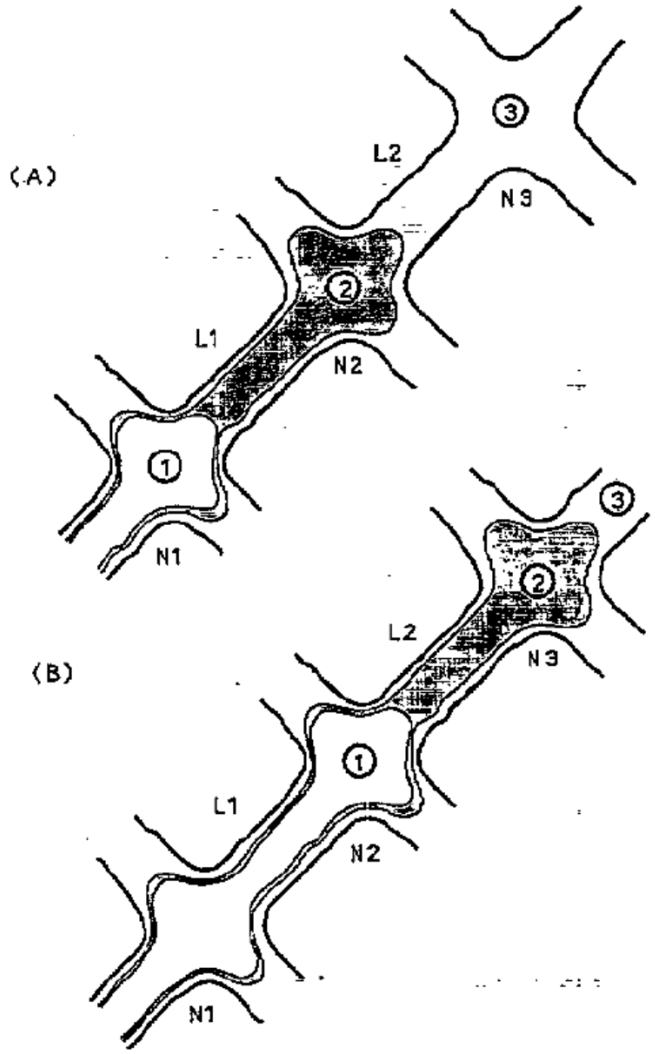

Figure 2-8: Double-drainage mechanism for a water-wet system with spreading behaviour (Oren et al., 1994).

In a water-wet system with non-spreading behaviour, the distribution of water and gas (wetting and non-wetting phases) remains similar to that for spreading systems discussed above. However, there are no oil spreading films separating gas and water with gas-water interfaces frequently observed. Oil (intermediate wetting phase) is located at the head of the advancing gas phase, where it is bound by a water-oil and gas-oil interface that intersect at a three phase contact line. The displacement of oil in the non-spreading system also proceeds by a "double-drainage" mechanism. However, gas does not invade the oil, since this leads to an increased gas-oil contact area and increase in system free energy. Therefore, the three phase contact line remains at the head of

advancing gas-oil interface during displacement. A schematic of the double-drainage mechanism in water-wet systems with non-spreading behaviour is depicted in Figure 2-9. Since continuous oil films are not created around the flowing gas, oil production stops after gas breakthrough (Oren et al., 1992; Oren et al., 1994).

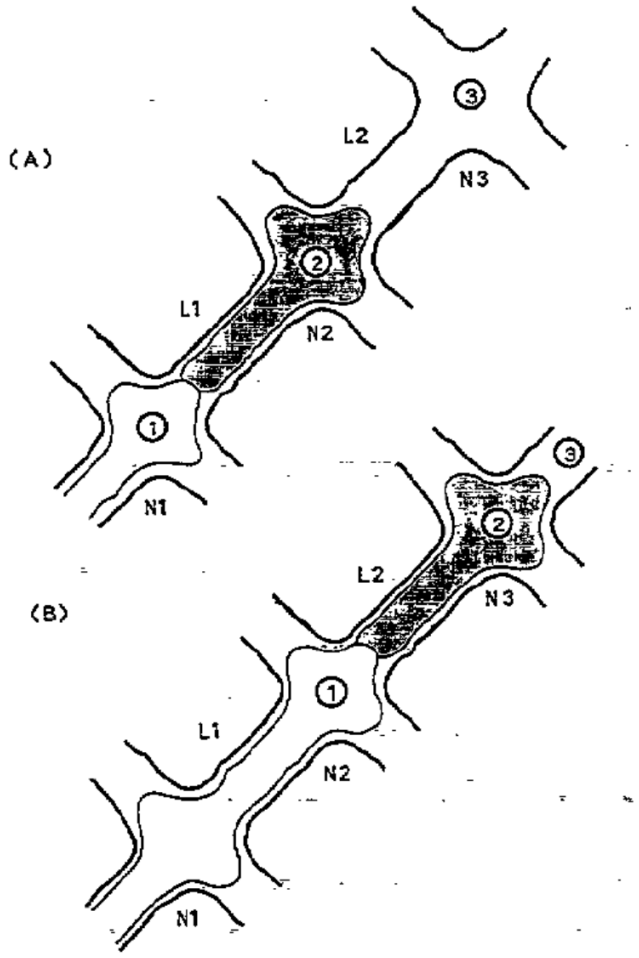

Figure 2-9: Double-drainage mechanism involving the movement of a three-phase contact line in a water-wet system with non-spreading behaviour (Oren et al., 1994).

In oil-wet systems, distribution of oil is similar to that for water in water-wet systems. Gas is the non-wet phase, which occupies pore bodies and some inter-connected pore throats. Water (intermediate-wetting phase) is also a non-wetting phase and is distributed in a manner similar to that of the gas phase. The only significant difference between non-spreading and spreading systems, is that for spreading systems the gas and water phases are separated by a thin but stable oil film, whilst for a non-spreading system the thin oil film is unstable and ruptures to form a small three-phase contact line. The pore-scale displacement mechanisms are very similar for spreading and non-spreading systems under oil-wet conditions. This is due to the fact that a localized oil

film or three-phase contact line has little effect on the displacement mechanism, because neither affects the continuity of the oil-wetting films. Displacement of oil by gas proceeds by either; (1) "direct drainage" mechanism in which gas displaces oil by advancing a gas-oil interface or (2) "double-drainage" similar to that previously described for water-wet systems. In the "double-drainage" mechanism, gas first displaces the intermediate-wetting phase (water), which then displaces oil (Oren and Pinczewski, 1994).

From a recovery improvement point of view, oil recovery is highest for oil-wet displacements (both spreading and non-spreading systems), which is attributed to the presence of highly conductive oil-wetting films. Recovery is lowest under strongly water-wet conditions for non-spreading systems, where there are no continuous oil films (Oren and Pinczewski, 1994).

2.5 FOAM FLOOD

While the displacement efficiency in gas injection processes can be high due to contribution of different recovery mechanisms which some of them explained in the previous section, the macroscopic sweep efficiency is generally low due to the combination of high mobility ratio, gravity segregation and heterogeneity in the real reservoirs. Despite the significant viscosity reduction as a result of CO2 dissolution, the same problem occurs in CO2 injection due to the viscosity and density contrast with the diluted-heavy crude oil. Injection of a viscous phase like foam simultaneously with CO2 or subsequently might be a viable way to displace the CO2-diluted oil out of the porous medium.

The definition of foam in porous media that we are using in this study is similar to that of Falls et al (Falls et al., 1988) which is a dispersion of gas in liquid such that the liquid phase is interconnected and at least some of the gas flow paths are blocked by lamellae. Figure 2-10 schematically illustrates a simple foam structure in porous media where the continuous gas stream has been dispersed into bubbles by surfactant-stabilized films (lamellae). Foam mobilities measured in porous media are many orders of magnitude smaller than that of the constituent gas and liquid. The mobility reduction is achieved primarily because the gas phase is dispersed into bubbles, which are generally about the size of the pore channels. Consequently, bubble interactions with pore walls dominate foam flow behaviour in porous media. For this reason, the pressure drop/flow rate

relationship of foam in porous media depends strongly on texture of the foam (Chambers and Radke, 1990).

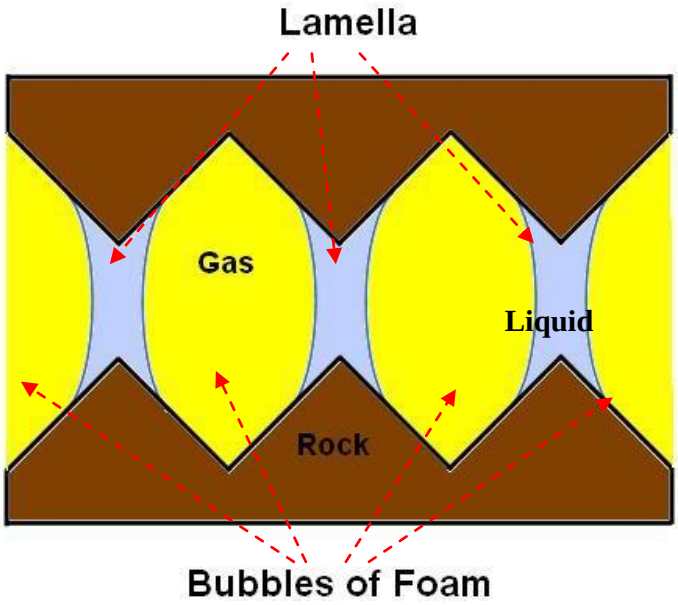

Figure 2-10: Schematic cross-section of foam in porous media.

Technically, there are two approaches to the application of foam in improved oil recovery (IOR). The simplest is to plug unwanted reservoir layers and regions near an injection or production well with relatively small volumes of foam. Oil saturation in near wellbore regions of injection wells is generally low as a result of higher velocities of fluids, therefore most of the laboratory experiments are performed without or at low oil saturations, if this approach to foam flood is considered. However, diverting flow in the near-well region may not affect flow patterns in the bulk of the reservoir. The more ambitious goal is "mobility control" throughout the entire formation. This latter approach requires creation of a foam-filled region spanning large distances over periods of months or years. It has potential to redirect flow patterns throughout the reservoir and greatly increase oil recovery (Rossen, 1995). Detailed studies of oil/foam interactions, displacement mechanisms and sweep efficiency are needed to evaluate foam performance in such processes.

A study of foam in porous media must account for three flow regimes encountered in field application: (1) surface facilities and the well itself, where inertial flow may create a bulk foam; (2) the rock face and the region near the wellbore where flow rates and ∇p are high; and (3) the formation farther from the injection well, where flow rates and ∇p rates much lower (Rossen, 1995). Each flow regime results in entirely different flow

behaviour and foam generation mechanisms. In this study we are focusing on the process of oil displacement at reservoir conditions (the third flow regime) where the shear forces are so low that the pore-scale events are prevailed by capillary, not viscous, forces.

2.5.1 Foam Generation Mechanisms

It is commonly accepted that lamellae are created by the following three mechanisms inside a realistic porous media:

1) "Leave behind" is creation of stabilized liquid films or lenses in pore throats as gas invades adjacent pore bodies through other throats e.g. as illustrated in Figure 2-11. Although sometimes cited as a source of "weak" or ineffective foam the leave behind mechanism can create a large number of lamellae. However if it is the only lamella creation mechanism, the gas will always have at least one continuous pathway for flow (Chen et al., 2006).

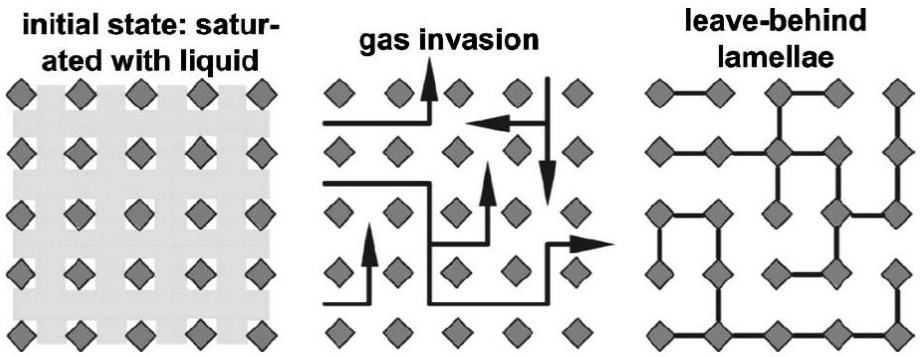

Figure 2-11: Schematic of lamella creation by the leave-behind mechanism. Gray diamonds represent sand grains; gap between them represent pore bodies and throats (Chen et al., 2006).

2) "Lamella division" denotes the event when two or more lamellae are created from a single one. Each time a mobilized lamella passes a pore body, with more than one pore throat unoccupied with liquid or another lamellae, this must either break or span both open throats, e.g. as illustrated in Figure 2-12.

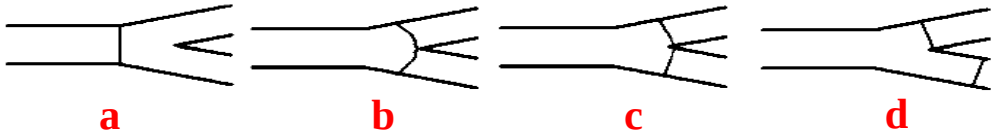

Figure 2-12: Schematic of a single lamellae-division event. In pictures "a" and "b", lamella enters branching point (pore body). In pictures "c" and "d", lamella divides in the two downstream throats, creating one additional lamella (Chen et al., 2006).

3) "Snap-off" is a third mechanism for lamella generation: lamellae are created in gas-filled pore throats (Figure 2-13) if the local capillary pressure falls to about half the capillary entry pressure of the throat while it depends on the geometry of the throat and the wettability of the medium, the value of one-half is a reasonable representative value for three dimensional (3D) pore geometries (Chen et al., 2006).

Figure 2-13: Schematic of snap-off in a pore throat. Black denotes pore-throat wall, gray water, and white gas (Chen et al., 2006).

2.5.2 Foam Termination Mechanisms

In the absence of oil, foam lamellae in porous media break by two mechanisms.

1) Capillary Suction Coalescence: Moving lamellae coalesce when they are rapidly stretched across large pore bodies. For a given gas flow rate and capillary pressure, pore-throat/pore body combinations with large aspect ratios, serve as termination sites. As the gas velocity and /or porous medium capillary pressure increases, more and more throat/body configurations become termination sites (Chambers and Radke, 1990).

2) Gas diffusion Coalescence: Trapped or static bubbles break by a second mechanism. Whenever two bubbles with different curvatures are in contact, gas diffuses from the more highly curved bubbles (smaller bubbles) to the less

curved bubbles (bigger bubbles) through the intervening lamellae. Eventually, the smaller bubbles disappear along with the common lamellae (Chambers and Radke, 1990).

Both mechanisms result in formation of one large bubble, instead of the two smaller bubbles that initially occupied the pore body. However, the former happens through a fast physical process, while the latter takes place through a slow diffusion process.

2.5.3 Foam Destabilization by Oil

There are several mechanisms by which oil can destabilize a foam; however, not all oils degrade all foams. Foaming surfactants may be absorbed by oil, causing depletion of the surfactant from the aqueous phase and gas/liquid interface; or surfactants from oil may be absorbed by the lamellae, producing a less favourable state for foaming. These phase-behaviour changes are usually negligible for the commercial foam forming surfactant/light crude oil combinations and conditions (Schramm and Novasad, 1992; Schramm et al., 1993). The oil may spontaneously spread on foam lamellae, displacing the elastic stabilizing interface; or oil may spontaneously emulsify, allowing drops to breach (enter) and rupture the stabilizing interface. These latter mechanisms, involving physical phase change, are usually considered to be the most important (Schramm and Novasad, 1990).

CHAPTER 3 EXPERIMENTAL FACILITIES AND FLUIDS

3.1 MICROMODEL RIG

A high-pressure micromodel rig, which can operate at maximum pressures and temperature of 5000 psia and 60 °C, was used in this study. Figure 3-1 and Figure 3-2 respectively show the actual photo and schematic diagram of the high-pressure high temperature micromodel rig, which consists of the following major components:

Fluid Storage Tank: A temperature-controlled oil bath is used to house injection fluids, lines and connections at constant temperature. In this part of the rig five fluid storage cells exist. Three of them are for injection of different fluids, e.g. crude oil, water, CO2, N2, and one cell is used to collect the effluent of the micromodel. One cell is filled with glycerol and is utilized to keep overburden pressure at a constant level during the test.

Micromodel Tank: This is another temperature-controlled oil bath, which is used to maintain the overburden and micromodel-housing chamber at constant temperature. The micromodel is loaded vertically in its housing chamber.

Low Rate Pumps: To inject fluids around the flow system (micromodel and overburden chamber) two low rate pumps were used. A third pump was used to pull back fluids and collect them into the retract cell. Deployment of two injection pumps allowed us to inject two fluids e.g. water and CO2 simultaneously through the micromodel. The

pumps are capable of working at pressures up to 6000 psia with a flow rate in the range of 0.0001 to 900 cm^3/hr.

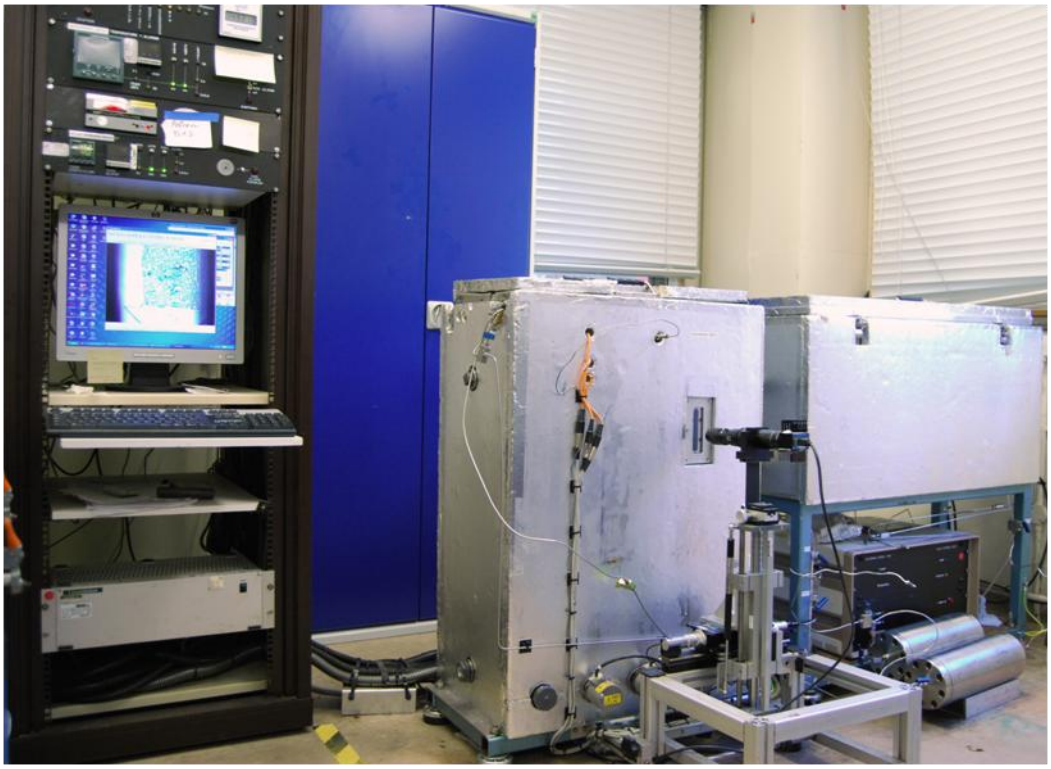

Figure 3-1: The high-pressure high-temperature micromodel rig used for the visualization tests in this study.

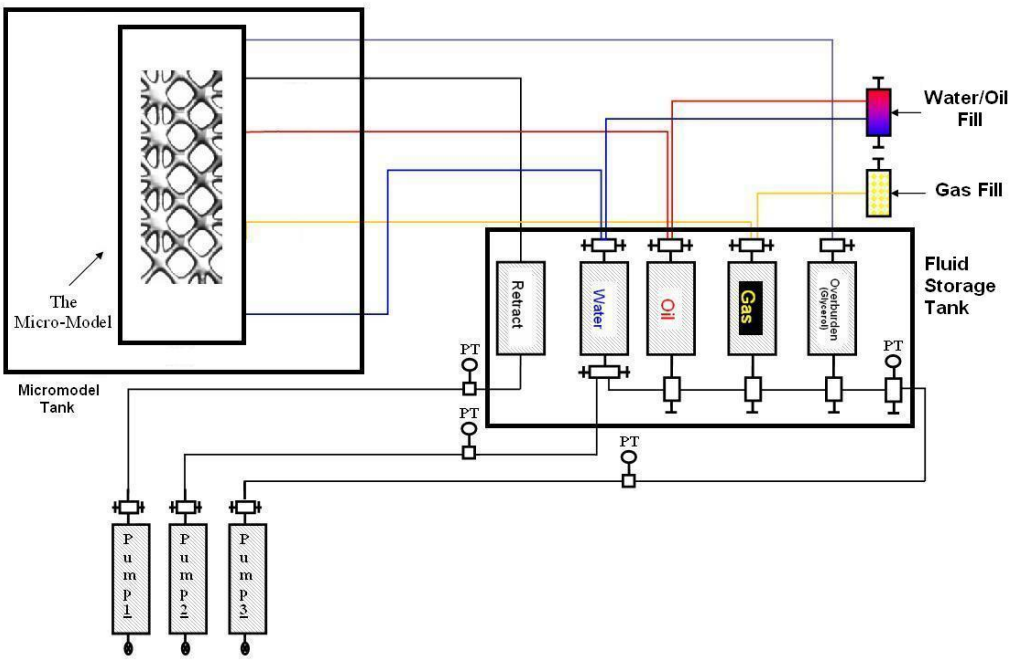

Figure 3-2: Schematic diagram of the micromodel rig.

Glass Micromodels: Micromodels are constructed from a two-dimensional pore structure that is etched onto the surface of a glass plate, which is otherwise completely flat. A second glass plate is then placed over the first, covering the etched pattern and thus creating an enclosed pore space. This second plate (the cover plate) has an inlet and outlet hole drilled at either end, allowing fluids to be displaced through the network of pores (Figure 3-3). Because the structure is only one pore deep and the containing walls are all glass, it is possible to observe the fluids as they flow along the pore channels and interact with each other. It is also possible to observe how the geometry of the pore network affects the patterns of flow and trapping.

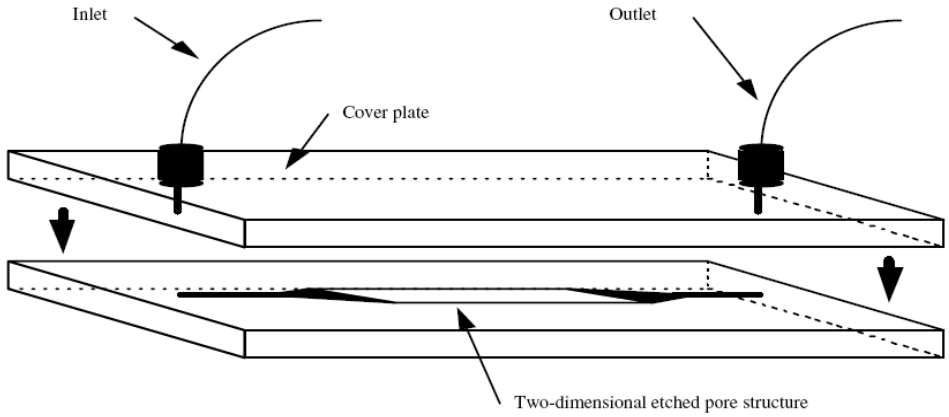

Figure 3-3: Schematics of a glass micromodel.

Various pore patterns including rock-look-alike and geometric can be designed and etched. The choice of pore pattern is normally made based on the objective of the study. If the objective of micromodel experiments is to generate data for mathematical modelling, geometric pore patterns (triangles, rectangular, or circles) are preferable as they have pores with definite shapes and sizes. Rock-look-alike pore patterns are derived from rock thin sections to better represent the reservoir rock structures and pore scale mechanisms (Sohrabi et al., 2008a; Sohrabi et al., 2000a; Sohrabi et al., 2001; Sohrabi et al., 2004; Sohrabi et al., 2008c). The rock structures are slightly modified and repeated a number of times to make the full length pattern of the micromodel.

In this study, two micromodels with different rock-look-alike patterns were used. The first pattern was originally taken from a thin section photograph of a Miller field core. Figure 3-4b shows the magnified section of the micromodel which has been repeated a number of times to make the full pattern as shown in Figure 3-4a. The red dotted line in Figure 3-4b shows a slide of the rock which has completely disconnected the vertical

flowing paths on the right hand side of this micromodel pattern. As a result, flow of fluids take place mostly from the continuous flow paths on the left hand side of the micromodel. Due to the existence of such difference in flow between the left hand side and right hand sides, this pattern is called "heterogeneous micromodel" in this thesis. The pore diameters are randomly distributed between 30 to 500 µm, providing a porosity of 55% and a permeability of around 3 Darcy. The dimensions of the micromodel and the pores are summarized in Table 3-1.

The second pattern was taken from a thin section photograph of a Clashach sandstone core. The permeability of the original core sample was measured to be around 0.8 Darcy. Figure 3-4 shows a magnified section and the full length picture of the micromodel. Since the vertical connectivity is almost equal between the pores on the left and right hand sides of the micromodel (as opposed to the first pattern), this pattern is named "homogenous micromodel" in this thesis. The pore diameters are randomly distributed between 40 to 500 µm, providing a porosity of 61% and a permeability of around 5 Darcy. The higher permeability of the this (homogenous) micromodel compared to the heterogeneous micromodel despite the similar range of pore diameter and porosity is believed to be due to better vertical connectivity of the pores on the right hand side of this micromodel pattern. The dimensions of the micromodel and the pores are summarized in Table 3-1

Table 3-1: Dimensions of the glass micromodels and their pore.

Micromodel Pattern	**Length cm**	**Width cm**	**MM PV cm^3**	**Ave. Pore depth μm**	**Pore dia. range μm**	**Porosity (%)**	**Perm. (Darcy)**
Rock Look alike (heterogeneous)	4	0.7	0.01	50	30-500	58	3
Rock Look alike (homogeneous)	4	0.7	0.01	50	40-500	61	5

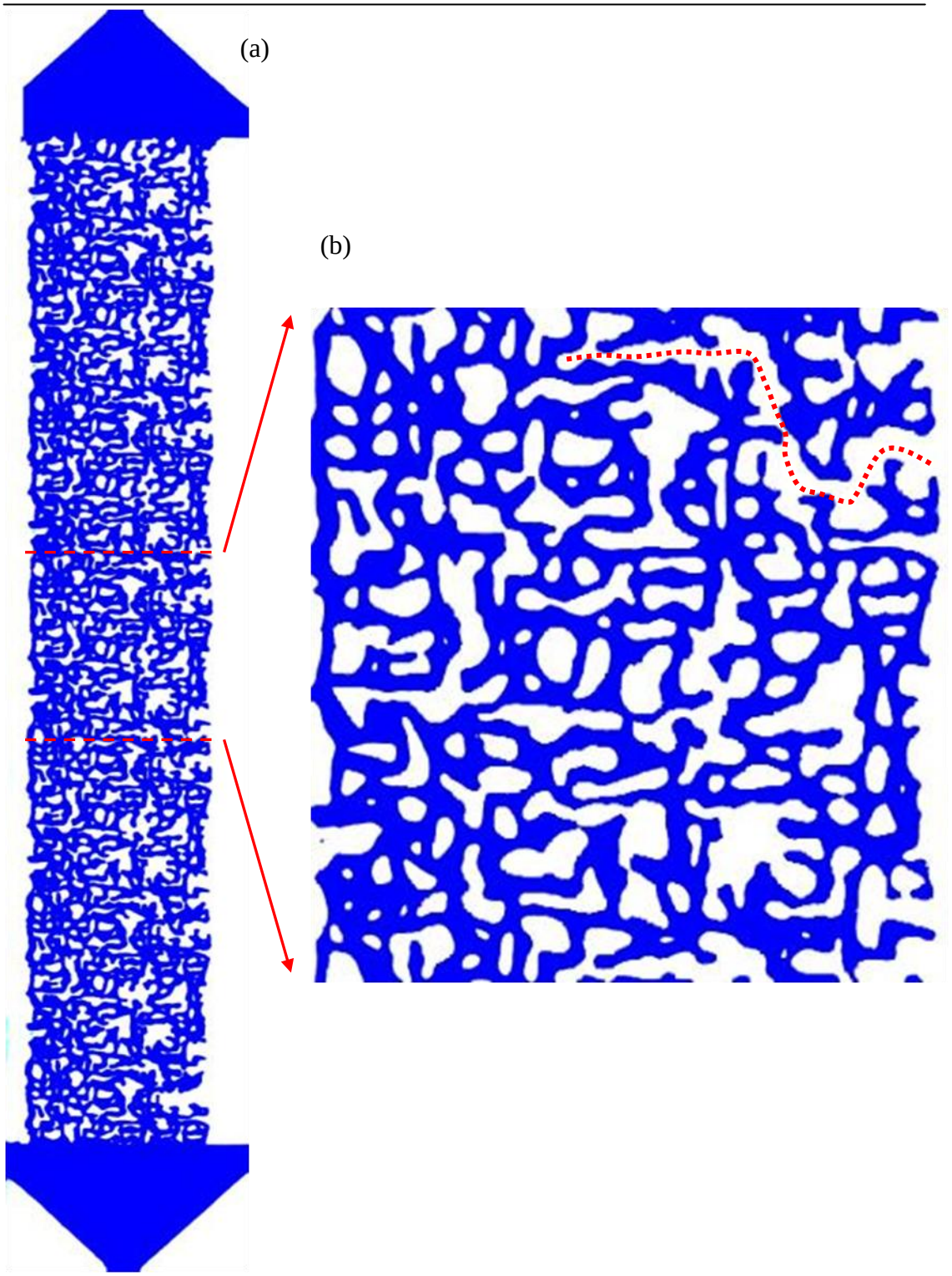

Figure 3-4: Pictures of the heterogeneous rock-look-alike micromodel which is fully saturated with blue-dyed water. Pores are shown in blue and unetched glass in white. A magnified section of the pore pattern (a) that has been repeated a few times to make the full length picture of the micromodel (b).

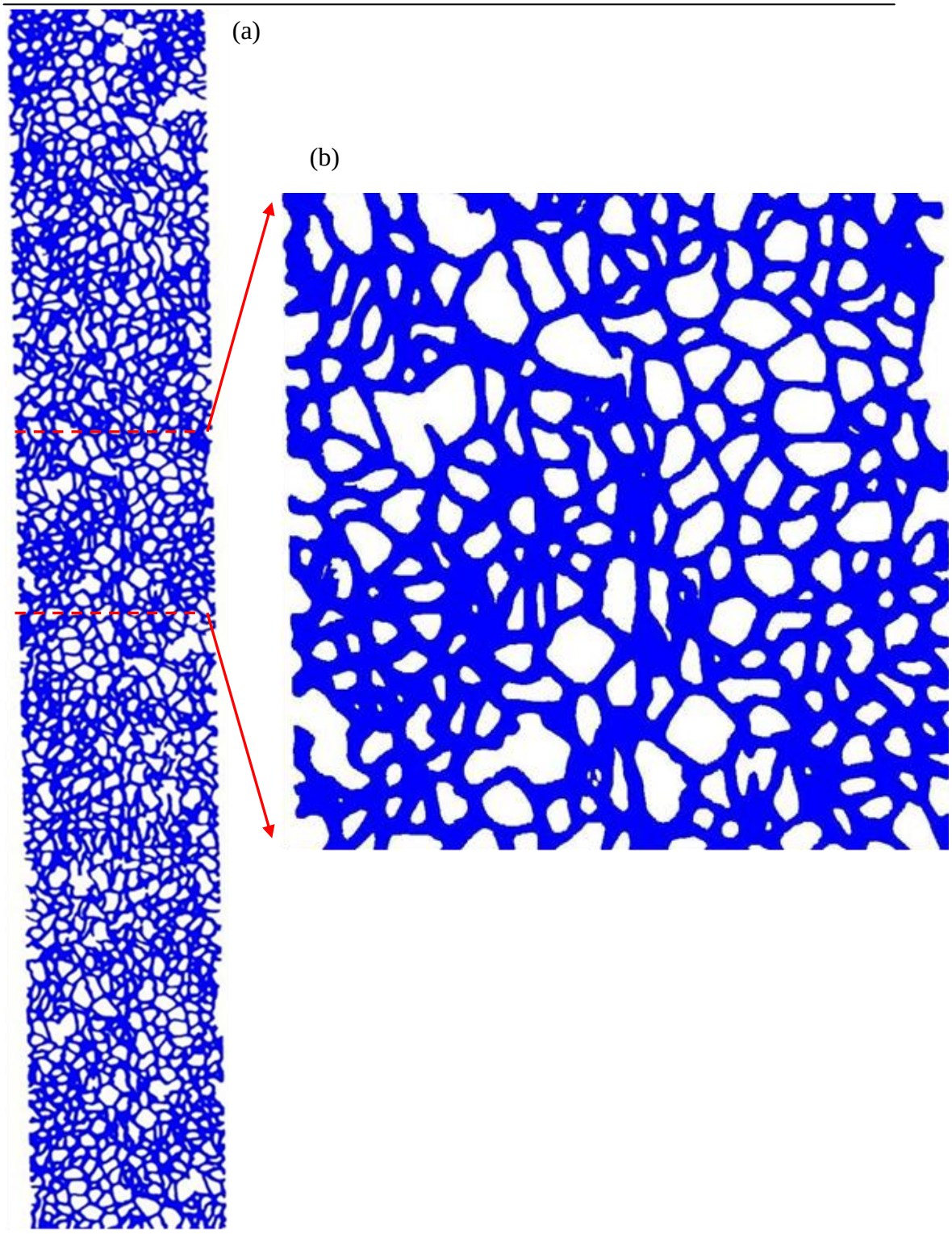

Figure 3-5: Pictures of the homogeneous rock-look-alike micromodel fully saturated with blue-dyed water. Pores are shown in blue and unetched glass in white. A magnified section of the pore pattern (a) that has been repeated a few times to make a half length picture of the micromodel (b).

Computer Controlled Linear Drive System: A computer controlled linear drive system is used in the tests, which allows a camera equipped with a magnifying lens to be positioned automatically at any part of the micromodel, or sequentially sweep the micromodel for digital recording. These digital records can then be used in image analysis to determine fluid saturation. The optical system can provide magnification up to 200 times. Figure 3-6 shows schematically the optical system of the micromodel rig.

Image Analysis System: To analyse the results of the micromodel experiments, it is necessary to detect and measure the changes in fluid saturations within the model. As the depth of the pores contained in the micromodel is relatively uniform, by measuring the area occupied by various fluids, saturation of fluids within the model can be determined. Using image analysis software, the areas with different colours can be measured to calculate the saturation of fluids in the micromodel and the swelling and shrinkage of different phases within the micromodel during experiments (Riazi et al., 2011; Sohrabi et al., 2000a; Sohrabi et al., 2001; Sohrabi et al., 2004). It should be noted that the full length pictures of the micromodel have been used for saturation measurement calculations which might be slightly different from the saturations in the magnified sections.

The colour of crude oil in the micromodel depends very much on the oil type and composition, which can vary from light brown to black. However, in general the heavier the crude oil, the darker its colour in the micromodel. Crude oil dilution due to the dissolution of CO2, can result in a colour change of crude to a much lighter colour. CO2 and water are both colourless in the micromodel. However, by adding blue dye to water or by digitally colouring the CO2 phase, it is possible to distinguish between these two fluid phases, which is essential for saturation calculations.

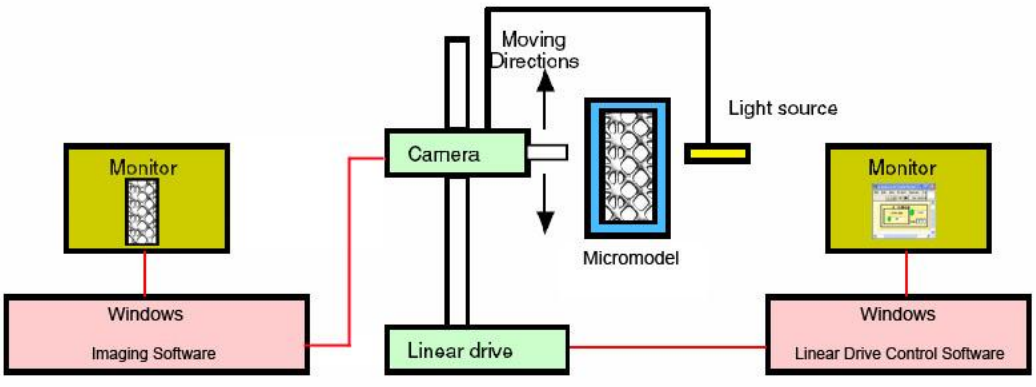

Figure 3-6: Schematic diagram of optical system of the micromodel rig.

3.2 COREFLOOD RIG

Figure 3-7 and Figure 3-8 respectively show the actual photo and schematic diagram of the high-pressure high temperature coreflood rig that was used in this study. The coreflood rig consists of the following major components:

High Pressure High Temperature Oven: A temperature-controlled air bath is used to house the core holder, injection fluids, back pressure regulator (BPR) lines, and connections at constant temperature (basically all equipment other than the injection pumps). The rig has five storage cells containing the injection fluids e.g. crude oil, water, CO2, and surfactant solutions.

Injection Pumps: Three pumps are used to move fluids around the system (core and bypass lines) in addition to applying overburden pressure on the core and supply pressure to the BPR. Deployment of three injection pumps also allows us to inject two fluids, i.e. surfactant solution and CO2, simultaneously through the micromodel, while the pressure at the back pressure regulator is maintained by the third pump.

Pressure Gauges: To evaluate and record the differential pressure across the core, two Quartz pressure transducers are connected to the inlet and outlet of the core.

The Back Pressure Regulator (BPR): A backpressure regulator (BPR) was used to maintain the pressure of the core outlet at 600 psia (test pressure) and delivered the core effluent at atmospheric pressure. The BPR used in these core tests is operated by compressed nitrogen and provides a relatively stable pressure at the outlet of the core.

Collecting Effluent: While running an experiment, the effluent from the BPR flows into a dual outlet separator, where the liquid would be collected in a graduated cylinder and the gas would go through a wet-test meter (GM) from the top of the separator. Both the liquid and gas are collected at atmospheric pressure and laboratory temperature.

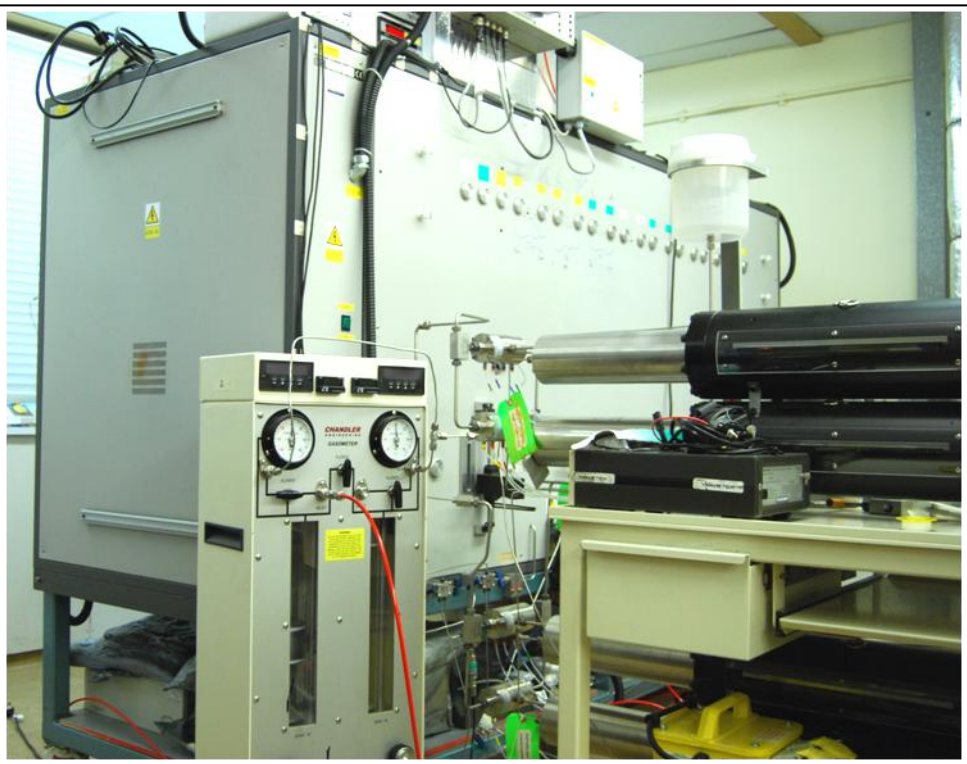

Figure 3-7: The high-pressure, high-temperature coreflood rig used in this study.

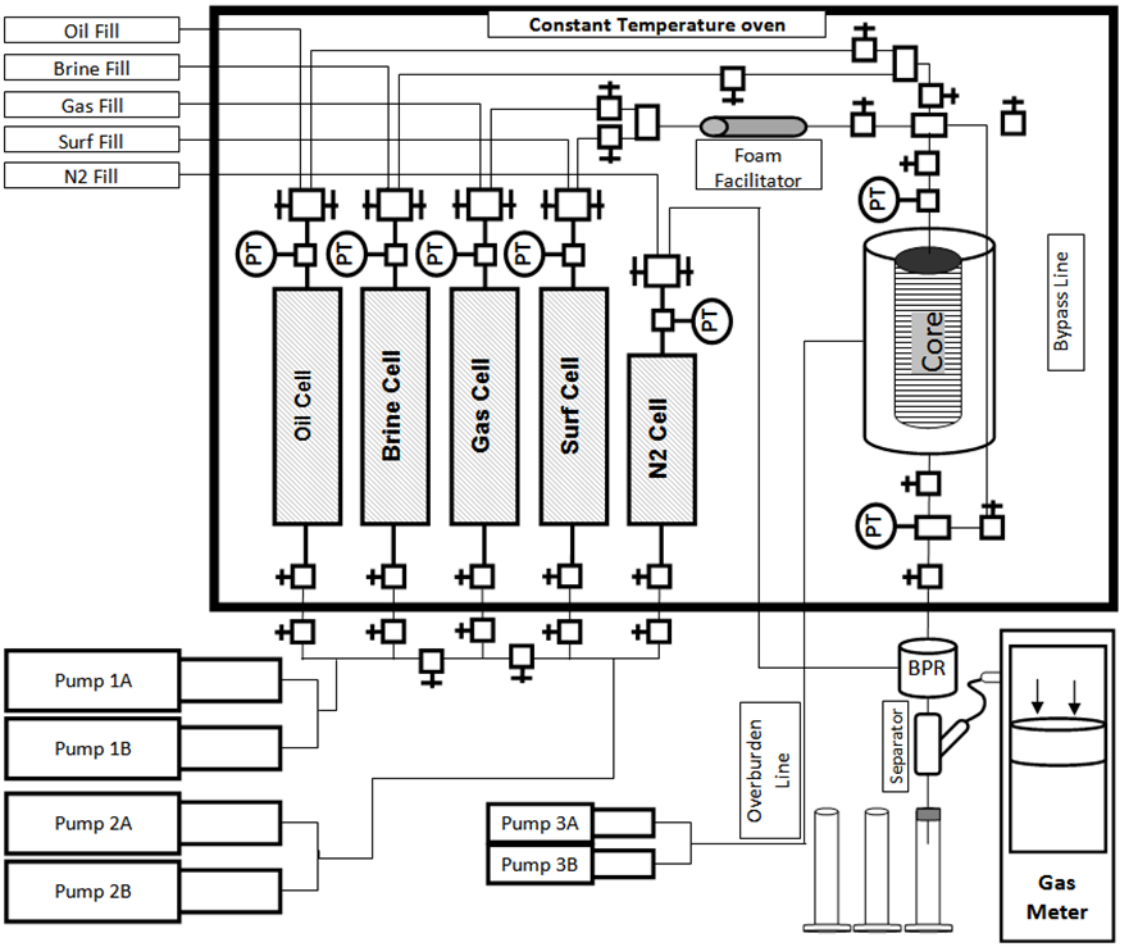

Figure 3-8: A simplified schematic diagram of the high pressure high temperature oven.

Sand Pack: A sand pack was used as the porous medium in these experiments. The reason for using a sand pack rather than a consolidated core was to perform the experiments in a porous medium that would resemble a typical heavy oil reservoir, which would usually be shallower than conventional oil reservoirs. Hence they are likely to be poorly consolidated with a relatively high permeability. To make the sand pack, a Teflon bar with a diameter of 5 cm and a length of 31.9 cm was used. An opening in the shape of a rectangle with a width of 3.7 cm and depth of 0.5 cm was created along the length of the bar, as shown schematically in Figure 3-9. Real sand particles were used to fill up the gap in the Teflon bar. The sand pack was then loaded in a high-pressure coreholder. The orientation of the sand pack was vertical with an injection port at the top and a production port at the bottom. A summary of sand pack properties is given in Table 3-2.

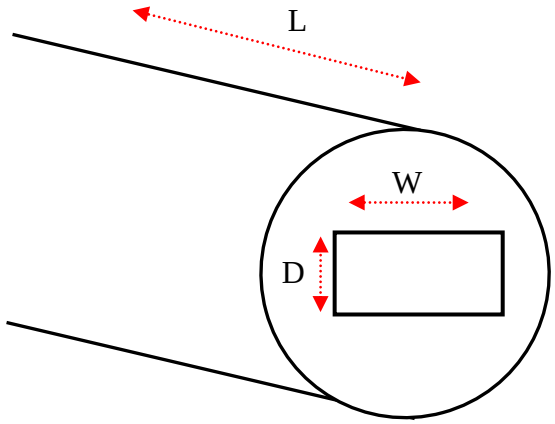

Figure 3-9: A schematic diagram of the sandpack used in the first series of coreflood tests.

Table 3-2: Basic properties of the core used in this study.

Parameter	**Size**	**Unit**
Depth (D)	0.502	cm
Width (W)	3.704	cm
Area (A)	1.8594	cm^2
Length (L)	31.9	cm
Core Pore Volume	23.5	cm^3
Porosity (ϕ)	40	%
Permeability to Brine (K)	1.4	Darcy

Core: To perform the new series of coreflood tests, the old sandpack was replaced with a consolidated core. The new core sample was a high permeability Fife silica-sand (carboniferous) sandstone taken from Burrowine Moor quarry in central Scotland. This high purity sandstone typically contains less than 2% feldspar and clay content. Due to its relatively high permeability, the core is ideally suited to represent heavy oil reservoirs, which are usually poorly consolidated with a relatively high permeability.

A thin section of core was cut from the same block that the core was taken from and was analysed using an environmental scanning electron microscope (ESEM) to identify the mineral content and pore structure of the rock sample. Figure 3-11 and Figure 3-12 present a series of micro-scale images of the rock sample and its mineral analysis. The results show that the rock is a high purity (Figure 3-11c), poorly cemented and friable quartz sandstone (Figure 3-11 a) with quartz overgrowth on the main quartz grains (Figure 3-11b). There are minor levels of feldspar and clay with Titanium (Figure 3-12). Open pore structures exist in the absence of cementing materials. To initially prepare the core for testing, the core was cleaned with copious amounts of toluene and methanol injected in succession, before drying and weighing the core. The core was then loaded in the core holder and core pore volume was measured. Subsequently, the core was fully saturated with brine and permeability measurement tests were performed on the sample. A summary of the core properties is given in Table 3-2.

Table 3-3: Basic properties of the core sample used in this reporting period.

Parameter	**Size**	**Unit**
Weight	1299.9	gr
Diameter	5.12	cm
Length	32	cm
Core Pore Volume (PV)	163.02	cm^3
Porosity (ϕ)	24.74	%
Permeability to Brine (K)	2.5	Darcy

Figure 3-10: The sandstone core which was used for the second series of coreflood tests.

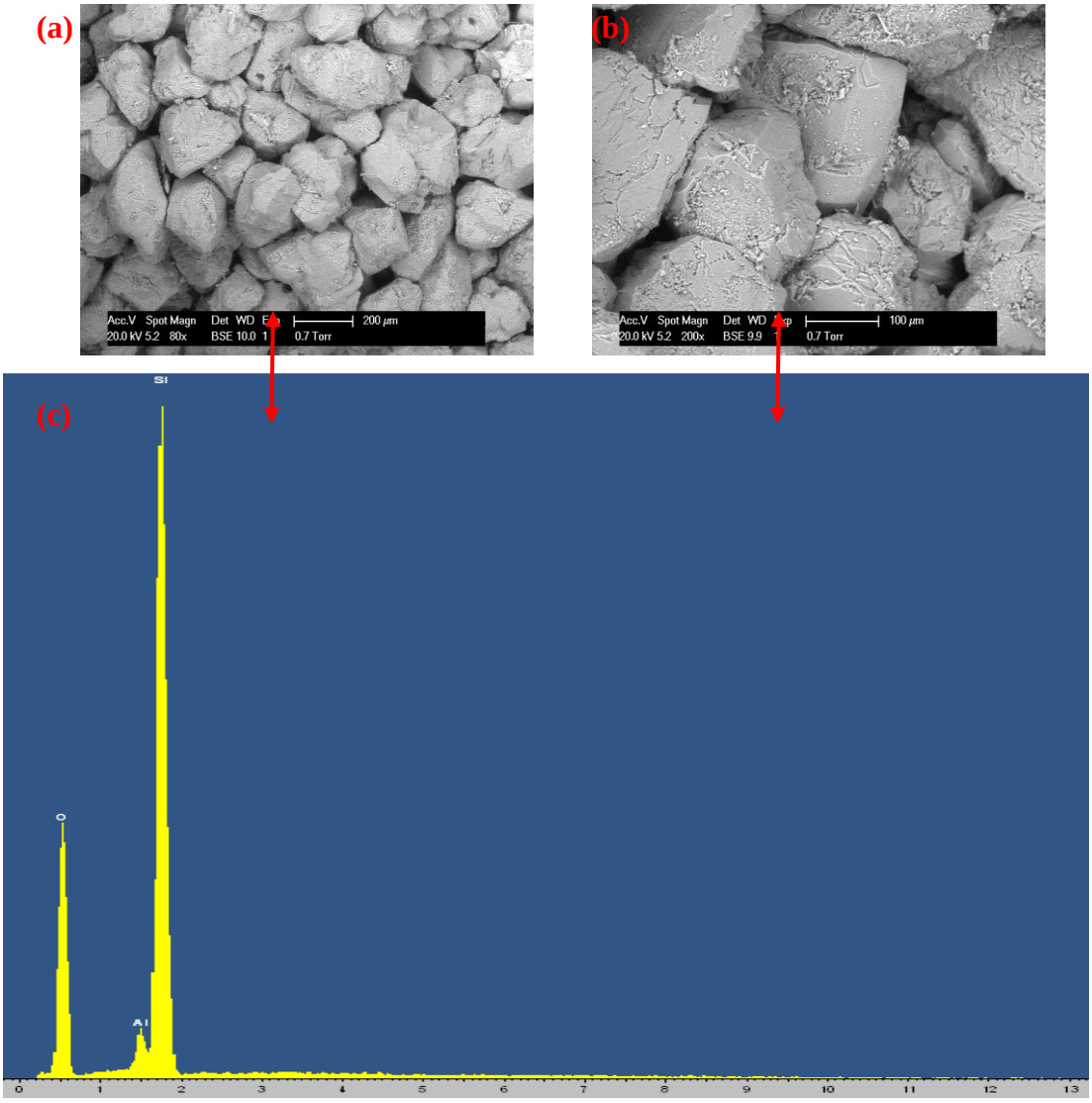

Figure 3-11: Pictures (a) and (b) present two highly magnified sections of the rock and picture (c) illustrates mineralogy of the rock in these two sections which shows clean quartz content with very low feldspar (Al) content.

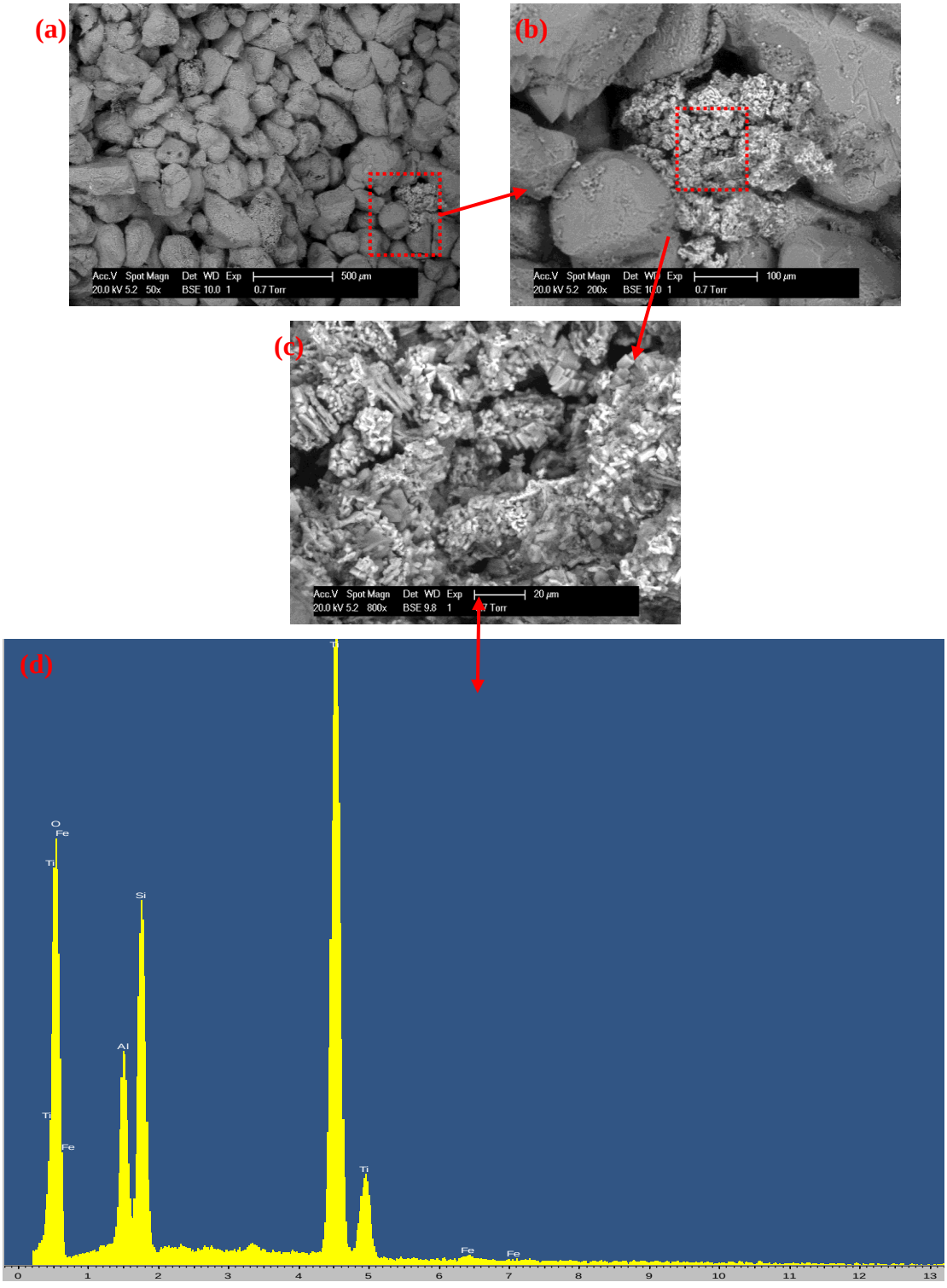

Figure 3-12: Pictures (a) to (c) show a clay particle in the rock sample and compare it to the surrounding sands grains. Picture (d) illustrates mineralogy analysis of this specific clay particle, which shows it contains a high Titanium (Ti) content.

3.3 VISCOSITY RIG

A high-pressure, high-temperature "capillary tube viscometer" rig was used for viscosity measurement tests in this study. In the capillary tube viscosity measurement technique, the pressure needed to force the fluid to flow at a specified rate through a narrow tube is measured. The viscosity is then calculated, based on the Poiseuille's Law of flow through a tube, which relates the pressure drop to flow rate, viscosity and resistivity of the tube. The main advantage of this technique is its simplicity of use, calibration and high accuracy compared to other methods of viscosity measurement. Figure 3-13 and Figure 3-14 show the actual photo and schematic diagram of the viscometer rig respectively, which consists of the following major components:

Constant Temperature Oven: A temperature-controlled air bath is used to house the capillary tube, injection and retractions cells, back pressure regulator (BPR), pressure transducers, lines and connections at constant temperature (basically all the equipment other than injection pumps).

Injection and Retraction Cells: Two vertical cells are used in the oven to contain the test sample. Having two cells allows us to circulate and further mix the fluid sample (usually mixtures of CO2 and oil) before being injected through the capillary tube.

Injection Pumps: Two pairs of pumps are used to pump fluids around the flow system (core and bypass lines) and also to apply overburden pressure on the core and supply pressure to the BPR (back pressure regulator).

Capillary Tube: The main part of the rig is the capillary tube, which is positioned horizontally and connected to the injection and retract cells on either side.

Pressure Gauges: To accurately measure and record differential pressure across the core, two Quartz pressure transducers are used with one connected to the inlet and the other to the outlet of the core.

The Back Pressure Regulator (BPR): A backpressure regulator (BPR) was used to maintain pressure of the system at a specific pressure. The BPR used in these tests was operated by compressed nitrogen and provides a relatively stable pressure at the outlet of the core.

Collecting Effluent: When running the experiment, effluent from the BPR flowed into a dual outlet separator, where the liquid was collected in a graduated cylinder and the produced gas passed through a wet-test (gas) meter (GM) from the top of the separator. Both the liquid and gas were collected at atmospheric pressure and laboratory temperature.

Before measurements could be taken, calibration of the rig was needed to ensure that results obtained were both accurate and reliable. To perform calibration, fluids of a known density and viscosity are loaded into the rig and used in the same way as explained in the experimental procedure. Each fluid was of the same standard (i.e. ISO17025) and a light (low viscosity) and heavy (high viscosity) fluid was used. This allowed the rig to be calibrated at both ends of the viscosity "spectrum".

Figure 3-13: The high pressure, high temperature viscosity measurement rig used in this study.

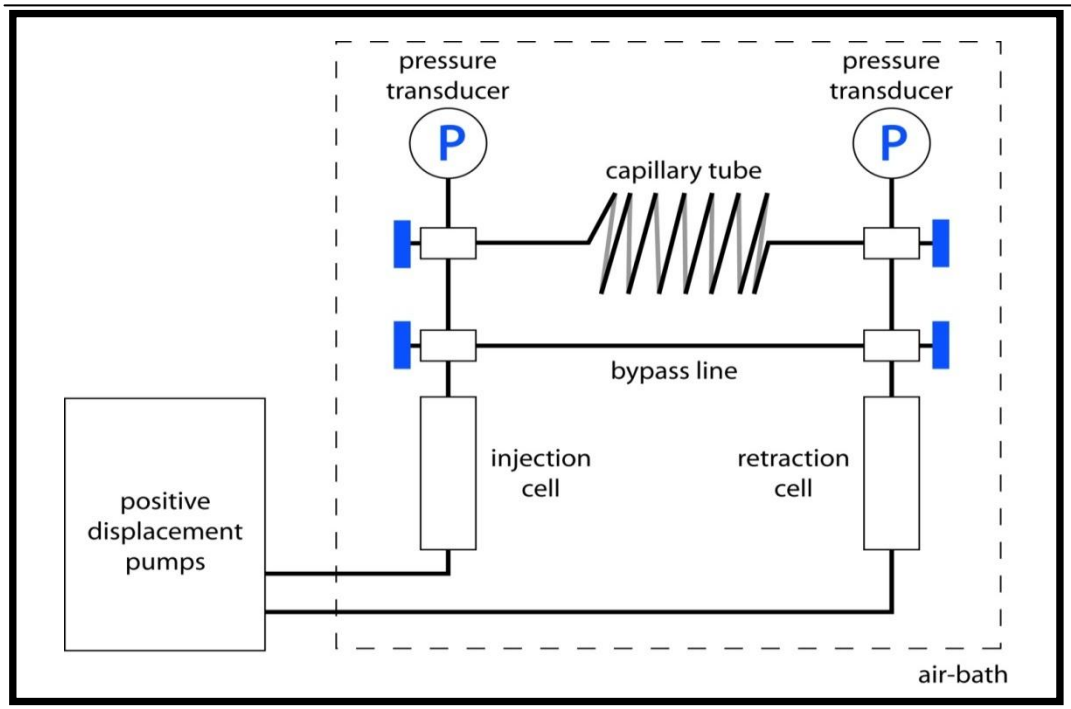

Figure 3-14: A schematic depiction of the apparatus used in this investigation for viscosity measurement of dead and CO2-saturated crude oil.

3.4 FLUIDS

Aqueous Phase: In the micromodel tests distilled water was used as the aqueous phase (both connate water and displacing fluid), however, in the coreflood tests a synthetic brine solution containing both NaCl and CaCl2 salts was prepared and used instead. This was due to the limitation of micromodel rig which could cause severe corrosion problems in some fittings if it was flooded with the brine solution. The brine solution had a total dissolved salt concentration of 10000 ppm consisting of 8000 ppm NaCl and 2000 ppm CaCl2. The brine was de-aired before injection into the storage cell.

Surfactant Solutions: The selection of surfactants was based on an extensive set of fluid characterization tests which are not reported here. The preliminary tests were performed using 30cc vials to investigate foam stability of different surfactants at ambient conditions with and without oil (Figure XXX). For final selection of surfactants, the surfactants which had better performance in the preliminary tests were examined in a visual cell at 10 bar pressure and lab temperature. Based on the results of the fluid characterization tests, Neodol 25-7 and AOS 14+ were used as the surfactant for foam generating purposes in this study. Neodol 25-7, a commercial product of Shell Chemical Co., is a C12-C15 alcohol ethoxylate with an average of approximately 7 moles of ethylene oxide per mole of alcohol. The "Neodol 25" family have been widely used for the study of foam properties at the lab scale. AOS 14-16 is a surfactant from Alpha Olefin Sulfonate family and was provided by Philips Chemical. AOS 14-16 has been widely used in the field for different EOR processes e.g. alkaline/surfactant/polymer injection and is the surfactant which was selected for the foam injection project in Snorre reservoir (Skauge et al., 2002). Table 3-4 presents the basic properties of the selected surfactants. The surfactant solutions were prepared by mixing an appropriate volume of the surfactant into the aqueous phase (distilled water in micromodel tests and brine solutions in coreflood tests).

Table 3-4: Basic properties of selected surfactants.

Surfactants	Type	Critical Micelle Conc.	Surface tension at CMC (dynes/cm)
Neodol 25-7	Non-Ionic	0.0016 vol.%	2
AOS 14-16	Anionic	-	-

Figure 3-15: Preliminary fluid characterization tests using crude "J" and different surfactant solutions.

Gas Phase: In most of the micromodel and core tests CO2 was used as the gas phase except MM Exp 11 where N2 was used as the gas phase. The gas samples were provided in a highly purified form of 99.8%. CO2 is present in vapour state at reservoir conditions of crude C" and in liquid state in reservoir conditions of crude "J". The basic properties of CO2 at different pressure and temperature conditions used in this study are listed in Table 3-5 and compared to that of water.

Table 3-5: Basic properties of CO2 at different pressures and temperatures.

	Temp. (°C)	Press. (psig)	State	Density (gr/ml)	Viscosity (cp)
CO2	50	600	Vapour	0.084	0.017
CO2	28	600	Vapour	0.1	0.016
CO2	28	1500	Liquid	0.82	0.075
Water	25	1500	Liquid	1.00	0.888

The crude oil samples used in this study have been provided by the sponsor companies and their basic properties are listed in Table 3-6. The heavy crude oil samples, crudes "C" and "J", were used for all coreflood tests and most of the micromodel tests. Based on the classification in the previous chapter and API gravity and viscosity data, crude "C" is classified as an Extra-Heavy Oil and crude "J" is classified as a (Medium-) Heavy Oil. The light crude oil sample, Crude "A", was only used for comparison purposes in the micromodel tests.

Table 3-6: Basic properties of the crude oil samples used in this study.

Crude Identification Name	API	Viscosity (cp)	Asphaltene Content (%)	Acid Number (mgKOH/gr)
"A"	39	< 1 @ 50 °C	0.53	-
"J"	16	674 @ 25 °C	2.60	0.94
"C"	10	8700 @ 50 °C	11.6	3.38

The following sections present part of the fluid characterization work in which the important properties of the oil samples were measured and quantified. The tests include density (API gravity) measurement, rheology identification, viscosity measurement using dead oil and CO2 diluted oil at various CO2 concentrations and, compositional analysis of the crudes.

3.4.1 Density Determination and Effect of Temperature

In the petroleum industry the classification system is generally based on the density of the crude samples. Density is also an extremely important parameter for the prediction of thermodynamic parameters (using empirical correlations) that are not experimentally measured. Therefore, determination of density is one of the basic tests which is regularly performed on the crude samples. In this series of tests the density of the crude samples was measured using "DM40" which is a 4 place digital density meter from Mettler-Toledo Company. In this equipment, the density is calculated based on the hydrostatic weighing technique in which the fluid is flowing through a U-tube that is pivoted on flexible end couplings. Based on the changes in the total weight of the tube, the density of the fluid can be calculated. The main advantage of this technique is that it needs a very small volume of the fluids (less than 2 cc) to perform the density measurement tests. The calibration (adjustment) process was carried out using standard water provided by Mettler-Toledo. Figure 3-16 plots the densities of crude "C" and "J" in 5°C intervals between 15°C to 60°C and Table 3-7 displays the measured density data and the corresponding API number of the crude oils.

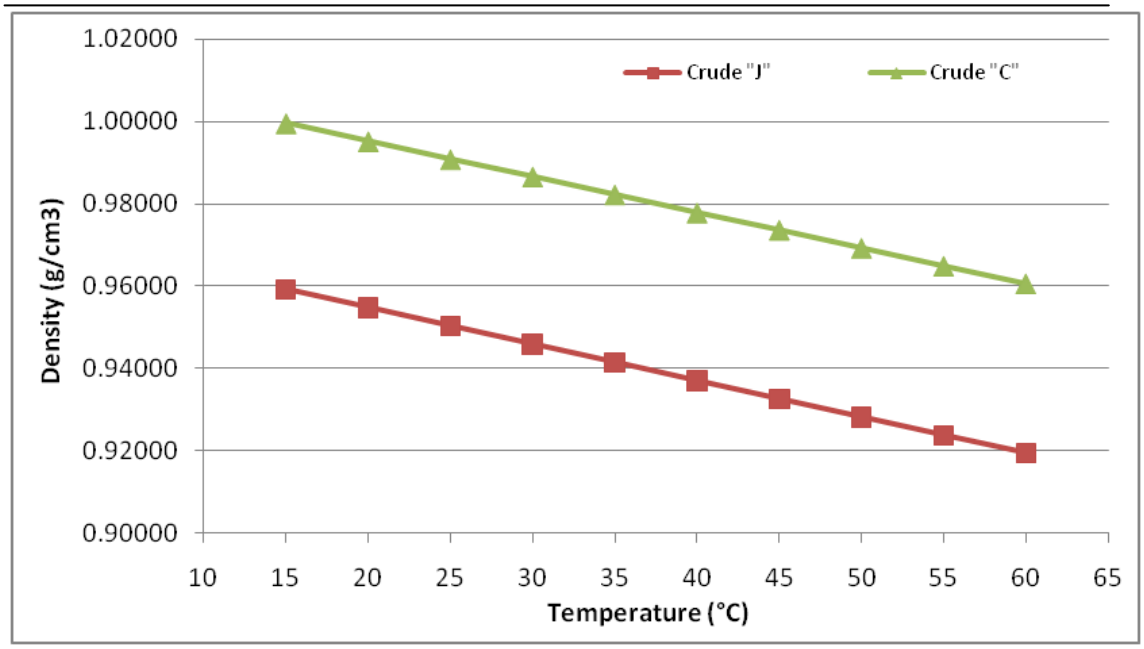

Figure 3-16: Measured density of crude "J" and "C" at 5°C intervals between 15°C to 60°C.

Table 3-7: Measured API number and density of crude "J" and "C" at 5°C intervals between 15°C to 60°C.

Crude "J"		Crude "C"	
Temp ('C)	Density (g/cm3)	Temp ('C)	Density (g/cm3)
15	0.95920	15	0.9996
20	0.95480	20	0.9952
25	0.95030	25	0.9908
30	0.94590	30	0.9866
35	0.94150	35	0.9822
40	0.93700	40	0.9778
45	0.93260	45	0.9736
50	0.92820	50	0.9692
55	0.92380	55	0.9648
60	0.91950	60	0.9605
°API	**15.9**	**°API**	**10.0**

Due to the very high viscosity of crude "C", a dilution technique was employed. In this method, crude "C" was initially diluted by toluene at a ratio of 1:1 wt% and then the diluted fluid was homogenized by shaking in a test tube. Based on the density measurement data of the mixture and pure toluene, the density of crude "C" at different temperatures was then calculated. The accuracy of the dilution method was checked by measuring the density of crude "J" and comparing that to data from the original measurement test, which showed a negligible difference between the measured data.

3.4.2 Rheology Analysis

Figure 3-17 and Figure 3-18 plot the viscosity data of crude "C" and "J" respectively, versus applied shear rate (rheology). Comparison of these two figures reveals that while the extra-heavy crude "C" is a non-Newtonian fluid with shear-thinning behaviour (oil viscosity decreases as shear rate increases), crude "J" is a Newtonian fluid with a viscosity independent from the applied shear rates.

The highly viscous crude oils are well recognized as having non-Newtonian rheology. These crude oils generally contain very high asphaltene content (e.g. above 10% in the case of crude "C"). At low shear rates asphaltenes can self assemble through physical interactions and form structural viscosity. Therefore, if higher shear rates are applied to the oil, more of these structures will break and crude oil will show lower viscosity (Saniere et al., 2004; Wang et al., 2006). If the asphaltene content is not high enough, these asphaltenic structures never form, hence the fluids show Newtonian flow characteristics, as observed in the case of crude "J" (Figure 3-18).

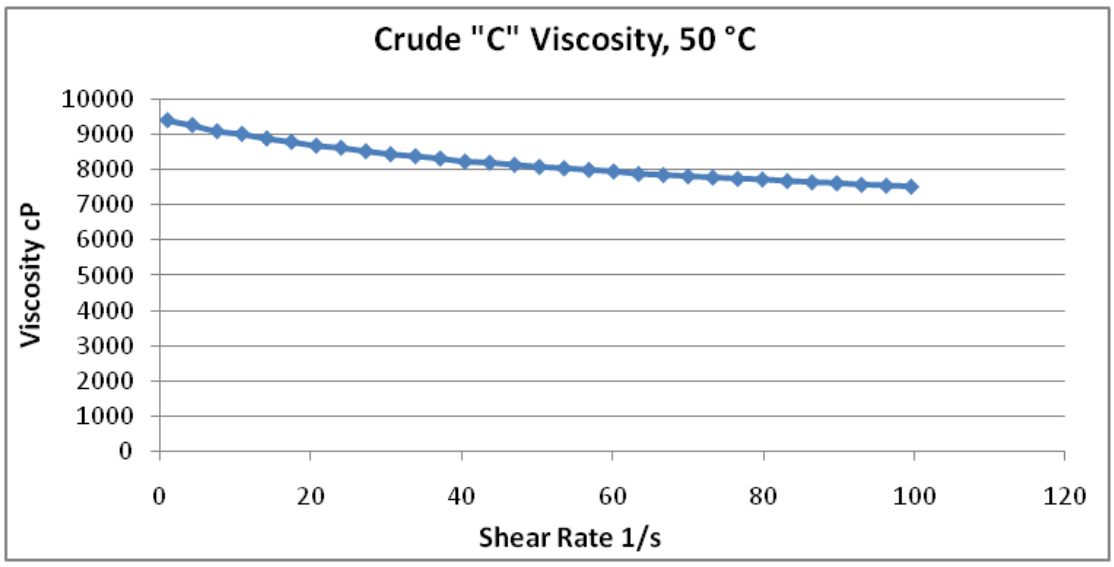

Figure 3-17: Viscosity of crude "C" versus shear rate at 50 °C and atmospheric pressure.

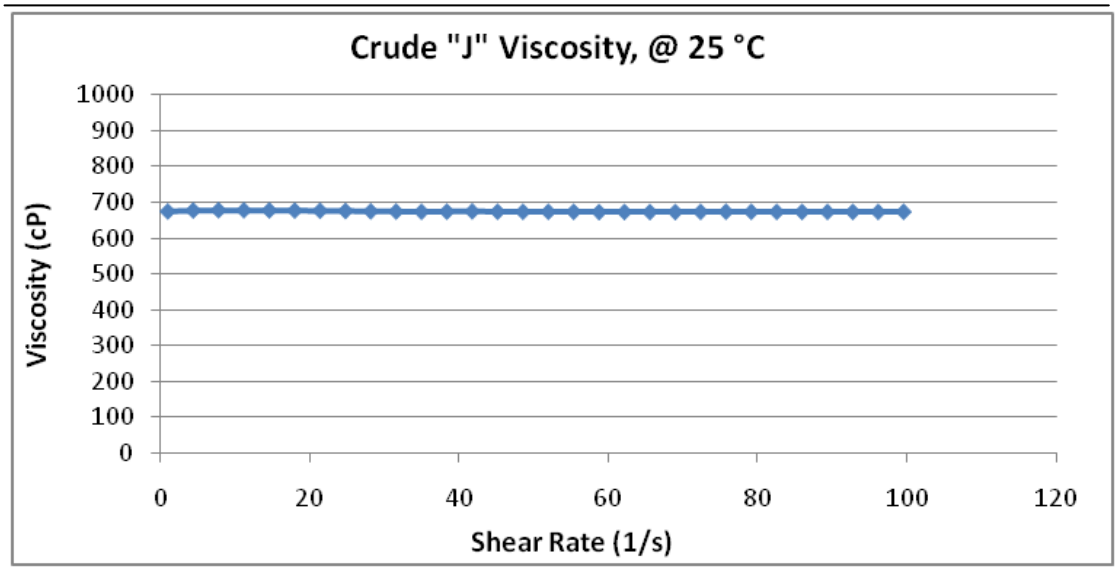

Figure 3-18: Viscosity of crude "J" versus shear rate at 25 °C and atmospheric pressure.

3.4.3 CO2 Solubility and Viscosity Measurement

As mentioned in the previous chapters, the main advantages of CO2 injection in heavy oil reservoirs (especially crude oil used in this study) is the significant reduction in oil viscosity that usually takes place upon the mixing of oil with injected CO2. In order to quantify the change of viscosity due to CO2 dissolution in the oil, a series of viscosity measurement tests were carried out using the capillary tube viscosity measurement rig explained in the previous chapter.

In the first series of the tests, the crude samples were fully saturated by CO2 at their reservoir conditions and their CO2 content and viscosity was measured. Table 3-8 summaries the measured viscosity and CO2 solubility data of the two crude samples used in this study. In the case of crude "C", viscosity dropped from 8670 cp to 660 cp (viscosity ratio of 7.6%) and; in the case of crude "J" viscosity dropped from 617 cp to 15.2 cp (viscosity ratio of 2.5%) when the crudes were fully saturated with CO2 at their corresponding reservoir condition. The larger viscosity reduction in the case of crude "J" is believed to be due to the higher solubility of CO2 in this oil compared to crude "C" (85 ccCO2/ccoil in crude "J" compared to only 27 ccCO2/ccoil in crude "C"). The larger fraction of light and intermediate components (Table 3-10), higher pressure and lower temperature of the reservoir (Klins, 1984) are all important parameters which promote dissolution of CO2 in crude "J" compared to crude "C".

Table 3-8: Dynamic viscosity and viscosity ratio for dead and CO2–saturated oils.

Crude sample	Reservoir press & temp (p,t)	CO2 solubility (ccCO2/ccoil)	Viscosity of dead oil (μ_{do})	Viscosity of CO2-saturated oil (μ_{cso})	Viscosity ratio (μ_{cso}/μ_{do})	Oil Swelling (B_o)
"C"	600 psig 50 °C	27 (ccCO2/ccoil)	8670 (cp)	660 (cp)	7.6%	5.5 %
"J"	1500 psig 28 °C	85 (ccCO2/ccoil)	617 (cp)	15.2 (cp)	2.5%	18.1 %

The second series of viscosity measurement tests were conducted, focusing on the effect of partial saturation of heavy oil by CO2. Figure 3-19 and Table 3-9 present the measured viscosity data of crude "C" partially saturated by CO2. The figure shows a linear relationship between CO2 content and viscosity of diluted oil samples up to a CO2 content of 60%. However, at higher CO2 contents, viscosity reduction continues at a lower rate. This data set reveals that even if the volume of CO2 is insufficient, or if there is a lack of time for complete mixing of the injected CO2 and the heavy crude oil, CO2 can still significantly drop the oil viscosity. It can be seen that viscosity of 50% (half) CO2 saturated crude oil is only a quarter of original dead oil in the case of crude "C".

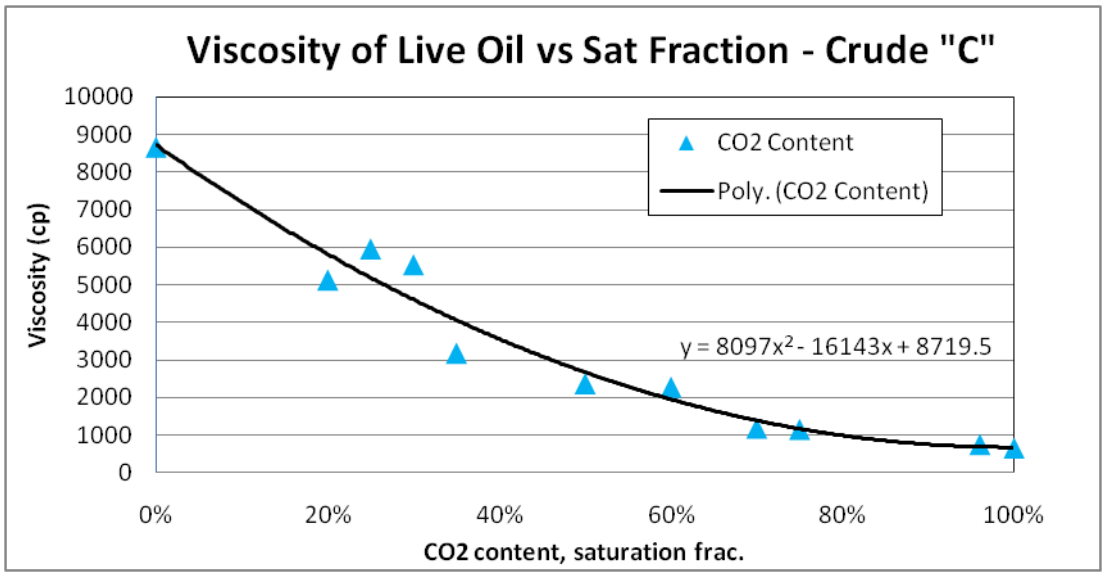

Figure 3-19: Dynamic viscosity of crude "C" versus the saturation fraction of CO2 at their reservoir conditions.

Table 3-9: Dynamic viscosity and viscosity ratio of crude "C" at different saturation fractions of CO2.

Pressure & Temperature	**CO2 Content**	**Viscosity(μ)**	**Viscosity ratio (μ_{cso}/ μ_{do})**
600 psig, 50 °C	0%	8670 (cP)	100.0%
600 psig, 50 °C	20%	5135 (cP)	59.2%
600 psig, 50 °C	25%	5962 (cP)	68.8%
600 psig, 50 °C	30%	5540 (cP)	63.9%
600 psig, 50 °C	35%	3187 (cP)	36.8%
600 psig, 50 °C	50%	2377 (cP)	27.4%
600 psig, 50 °C	60%	2283 (cP)	26.3%
600 psig, 50 °C	70%	1190 (cP)	13.7%
600 psig, 50 °C	75%	1160 (cP)	13.4%
600 psig, 50 °C	96%	760 (cP)	8.8%
600 psig, 50 °C	100%	660 (cP)	7.6%

3.4.4 Compositional Analysis

Table 3-10 presents the compositional analysis of crude "C" and crude "J" obtained by GC analysis. The results show that a large fraction of the hydrocarbon content is the C25+ group (77.59% in the case of crude "C" and 62.14% in the case of crude "J"). This suggests the compositional analysis of these heavy crude oils can be improved if performed using high temperature GC columns to allow heavier fractions of the crude sample to be analyzed. This information will be useful for numerical simulation of coreflood tests and tuning of EOS (equation of state), especially in the experiments using CO2.

Table 3-10: (a) Compositional analysis of crude "C" and (b) compositional analysis of crude "J".

(a)

Oil "C" Composition (Whitson's Generalised MWs)			
Comp	MWs	Weight%	Mole%
C1	16.04	0.00	0.00
C2	30.07	0.00	0.00
C3	44.10	0.00	0.00
iC4	58.12	0.00	0.00
nC4	58.12	0.00	0.00
iC5	72.15	0.00	0.00
nC5	72.15	0.00	0.00
C6s	84	0.01	0.09
C7s	96	0.02	0.09
C8s	107	0.09	0.46
C9s	121	0.12	0.52
C10s	134	0.23	0.94
C11s	147	0.40	1.48
C12s	161	0.68	2.30
C13s	175	1.01	3.13
C14s	190	1.14	3.24
C15s	206	1.46	3.85
C16s	222	1.66	4.06
C17s	237	1.54	3.53
C18s	251	1.81	3.90
C19s	263	1.79	3.68
C20s	275	1.85	3.64
C21s	291	1.80	3.35
C22s	300	1.67	3.02
C23s	312	1.79	3.11
C24s	324	1.71	2.86
C25s	337	1.63	2.62
C26+	839	77.59	50.12
NB MW measured by Cryette		100.00	100.00
		MW	542

(b)

Oil "J" Composition (Whitson's Generalised MWs)			
Comp	MWs	Weight%	Mole%
C1	16.04	0.00	0.00
C2	30.07	0.00	0.00
C3	44.10	0.00	0.00
iC4	58.12	0.00	0.00
nC4	58.12	0.00	0.02
iC5	72.15	0.02	0.10
nC5	72.15	0.01	0.06
C6s	84	0.07	0.32
C7s	96	0.14	0.56
C8s	107	0.37	1.29
C9s	121	0.72	2.23
C10s	134	1.12	3.13
C11s	147	1.39	3.54
C12s	161	1.87	4.37
C13s	175	2.23	4.78
C14s	190	2.28	4.50
C15s	206	2.89	5.27
C16s	222	2.92	4.93
C17s	237	2.61	4.13
C18s	251	2.87	4.29
C19s	263	2.68	3.81
C20s	275	2.74	3.73
C21s	291	2.27	2.92
C22s	300	2.36	2.95
C23s	312	2.26	2.71
C24s	324	2.05	2.37
C25s	337	1.98	2.21
C26+	652	62.14	35.76
NB MW measured by Cryette		100.00	100.00
		MW	375

3.4.5 Asphaltene Content and Precipitation Tests

Heavy oils generally contain a high content of asphaltenes. Indeed the main reason for high viscosity and shear thinning behaviour in most cases, is the presence of asphaltenes with their particles overlapping. Asphaltene content measurement was performed using n-Heptane (nC7) as the solvent and results are presented in Table 3-11. It can be seen that asphaltenes constitute a major part of these heavy crude oils, which reach a level higher than 10 % wt in the case of crude "C". Hence if precipitation of asphaltene particles takes place, it can significantly affect the recovery process.

Mixing of CO2 with oil is known to cause asphaltene precipitation, which is sometimes considered undesirable light oil reservoirs, due to the blockage of productive zones. However, in the case of heavy crude oils, due to the loss of asphaltenes, the upgraded oil should have a lower viscosity and higher mobility, in spite of deposited particles.

Furthermore, asphaltenes are known to be highly surface-active materials, promoting and stabilising foams and emulsions. If simultaneous injection of water and CO2 causes asphaltene flocculation and foam/emulsion formation, it can generate a viscous mixture suitable for displacing heavy oil.

A number of high pressure micromodel tests were designed and conducted to visually investigate asphaltene precipitation during CO2 injection. Different injection strategies, including continuous and slug CO2 injection, were considered at reservoir conditions of the heavy oil samples. Nonetheless, no evidence of major asphaltene precipitation or deposition was observed. Figure 3-20 displays a highly magnified section of the micromodel in one of the tests after 3 days of CO2 injection in crude "C". Water and oil are respectively colour-less and brown and CO2 is digitally coloured in yellow to better differentiate between water and CO2. Our previous visualization tests using light crude samples, has shown that if asphaltene flocculation and precipitation take place, the bottom of the pores occupied by oil will become darker and the system will lose its homogeneity of colour. However, in the case of these heavy oil samples, the uniform colour of the oil phase was never lost, which is a good indication of a lack of asphaltene precipitation in the system.

There are a large number of publications reporting results of studies on experimental and theoretical aspects of flocculation and dynamic deposition of asphaltenes by CO2 flood. Asphaltene separation and precipitation during CO2 injection is believed to be due to the reduction of solvency power of the crude oil e.g. by desorption of resins from asphaltene particles. However in the case of heavy crude oils, there is a high fraction of heavy hydrocarbon components (as can be seen in Table 3-10), which can stabilize asphaltene particles, even when crude oil is fully saturated with CO2.

Table 3-11: N-Heptane asphaltene content of crude "C" and crude "J".

Crude Name	Asphaltene Content
"C"	11.6 wt %
"J"	2.6 wt %

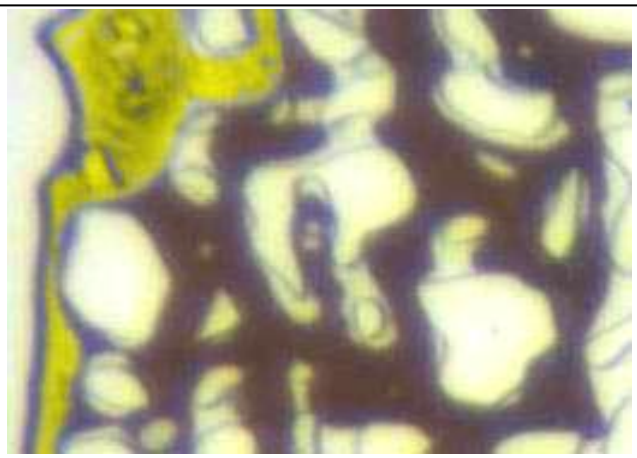

Figure 3-20: A magnified section of micromodel after CO2 injection (CO2 is digitally coloured in yellow) in crude "C" (brown) for an extended period of time (3 days). No evidence of major asphaltene precipitation can be seen in the oil phase.

3.4.6 Interfacial Tension Measurement

The interfacial tension between crude oil samples and distilled water was measured using the pendant drop technique and results are summarized in Table 3-12. The results show relatively low IFT for these heavy crude samples compared to conventional oils. IFT values of 17 and 23 dyne/cm were measured respectively in the case of crude "C" and crude "J", whilst in the case of light oils this value is normally around 30 dyne/cm. Low IFT values are typical behaviour in heavy oils, which is due to their high content of surface active materials (e.g. asphaltene and resin).

Table 3-12: Results of interfacial tension measurement tests between heavy crude samples and distilled water.

Crude Name	Interfacial Tension (Oil/DW,)
"C"	17 (dyne/cm) @ 50 °C
"J"	23 (dyne/cm) @ 20 °C

3.5 FLOW RATES AND DIRECTION

The injection of fluids through micromodels took place at a rate of 0.01 cm^3/hr equal to 1 MM pore volume (MM PV) per hour. This corresponds to a pore velocity of 3ft/day. In the tests where two fluids have been injected simultaneously the total injection rate maintained at 1 cm^3/hr. All the displacing fluids including CO2, water and foam were injected from top inlet and oil was injected through the micromodel from the inlet at the bottom of the vertically oriented micromodel.

In the coreflood experiments the injection rates have been designed to have pore velocity of 1 ft/day. In the sandpack the total injection rate was equal to 1 cm^3/hr and in the consolidated core this rate was equal to 7 cm^3/hr. In the experiments where two fluids have been injected simultaneously the total injection rate maintained at 1 cm^3/hr. All the fluids including CO2, water, foam and, heavy oil samples were injected from top of the vertically oriented core.

3.6 DIMENSIONLESS NUMBERS AND RATES OF INJECTION

It was explained in the theoretical chapter that phase trapping and mobilization of fluids in porous media is governed by the interplay between viscous, capillary and gravitational forces. Although the flow in porous media is driven by externally exposed viscous or gravitational forces, the flow at the pore scale is controlled by capillary forces. If viscous and gravitational forces increase and become comparable to capillary forces they might change the relative permeabilities and the effective parameters in multi-phase flow in porous media. Therefore, an understanding and appreciation of the magnitude of these forces is required to understand the mechanisms involved in the recovery processes (Green and Willhite, 1986).

In fluid dynamics, the capillary number (Na) represents the relative magnitude of viscous forces to the capillary forces acting across a particular interface between a liquid and gas phase or between two immiscible liquid phases (Dullien, 1992; Sahimi, 1995). In this text, the capillary number is defined similar to that of Green and Willhite (Green and Willhite, 1986) without considering the term of wettability (cos θ), as:

$$\mathrm{Nca} = \frac{v\mu_D}{\sigma}$$

Where; "μ_D" is the displacing phase viscosity, "v" is the pore velocity, and "σ" is the surface tension or IFT between the two fluid phases.

The Bond number (Bo) is a dimensionless number expressing the ratio of gravitational forces to capillary forces, as:

$$\mathrm{Bo} = \frac{\Delta\rho g K}{\sigma}$$

where "Δρ" is the density difference between two fluids, "g" is the acceleration due to gravity, "K" is permeability of the porous medium. As a rule of thumb, one can consider the fluid flow in porous medium to be dominated by capillary forces if the associated values of the capillary and bond numbers are equal or less than 10^{-5}.

Table 3-13 presents the rock and fluid data which have been used for calculation of dimensionless numbers for crude "C" and crude "J" at their reservoir temperature and pressure. The other data have either measured in the lab or provided by the sponsor companies. The interfacial tension between CO2 and heavy crude samples has been estimated using the literature data. The corresponding dimensionless numbers for different micromodel and coreflood experiments are then calculated in Table 3-14. The capillary numbers have been calculated for the waterflood scenarios since due to the higher viscosity of water compared to CO2 viscous dominant flow is more likely to happen. In the case of CO2 injection both capillary and bond numbers have been calculated.

The results show fully stable and capillary dominant flow in all micromodel and coreflood experiments with the capillary and bond number being less than 10E-5. However a comparison of the capillary number and bond number during CO2 injection periods shows that gravitational forces have significant effect on oil recovery being significantly larger than the corresponding capillary number. This difference between gravitational and viscous forces is more clear in the case of Crude "C" where the low density of vapour CO2 causes strengthening of gravitational forces. It should be noticed that the dimensionless numbers in Table 3-14 have been calculated using dead oil density. If the density of CO2 diluted crude samples is taken into account the calculated bond numbers might drop up to 10% .

Table 3-13: The rock and fluid data which have been used for calculation of dimensionless numbers.

General	Crude "C" (T= 50 °C, P = 600 psig)	Crude "J" (T= 28 °C, P = 1500 psig)
v = 3 ft/day MM v= 1 ft/day Core	σ_{ow} = 17 dyne/cm σ_{og} = 15 dyne/cm*	σ_{ow} = 23 dyne/cm σ_{og} = 5 dyne/cm*
K = 10 D MM K = 1.2 D sandpack K = 2.5 D core	ρ_{oil} = 0.969 g/cm^3 ρ_{co2} = 0.082 g/cm^3**	ρ_{oil} = 0.948 g/cm^3 ρ_{co2} = 0.798 g/cm^3**
	μ_w = 0.56 cp μ_{co2} = 0.017 cp**	μ_w = 0.85 cp μ_{co2} = 0.0703 cp**
* estimated from (Robinson, 1984; Yang and Gu, 2005) **(National Institute of Standards and Technology, 2011)		

Table 3-14: Dimensionless numbers calculated during micromodel and coreflood experiments using crude "C" and crude "J".

		Micromodel	Consolidated Core	Sandpack
Crude "C" T= 50 °C P = 600 psig	Waterflood	Nca= 3.7 E-7	Nca= 1.3 E-7	Nca= 1.3 E-7
	CO2 injection	Nca= 1.3 E-8 Bo= 5.7 E-6	Nca= 4.5 E-9 Bo= 1.4 E-6	Nca= 4.5 E-9 Bo= 6.9 E-7
Crude "J" T= 28 °C P = 1500 psig	Waterflood	Nca= 4.1 E-7	Nca= 1.5 E-7	-
	CO2 injection	Nca= 1.5 E-7 Bo= 1.3 E-6	Nca= 5.5 E-8 Bo= 7.27 E-6	-

CHAPTER 4 VISUAL INVESTIGATION OF HEAVY OIL RECOVERY BY WATERFLOOD

4.1 INTRODUCTION

In heavy oil waterflood, injected water displaces high viscosity crude oils thus, depending on the viscosity of the oil, the displacement phenomena might be partially or fully controlled by viscous forces. This changes the mechanisms of oil recovery and oil trapping at water breakthrough and subsequently alters the oil production performance after breakthrough time, in comparison to light oils. It is known that in the case of heavy oil waterflooding, due to the unfavourable oil/water viscosity ratio the injected water is moving faster than the oil ahead of the front. This results in relatively early water breakthrough and low displacement efficiency at breakthrough time. If water injection continues after breakthrough, the remaining oil can be recovered at low rates (Willhite, 1986). However, the effect of oil/water viscosity ratio on pore scale mechanisms of oil displacement and oil trapping is not fully understood.

A series of micromodel tests were designed and conducted to investigate the effect of oil viscosity and wettability of the system on displacement and trapping mechanisms at the pore scale. It was explained in the theoretical section that wettability and viscosity ratio are the prime parameters controlling the performance of waterflood at reservoir conditions. The results are then compared to light oil waterflood, and the differences in recovery mechanisms and their impact on production performance are highlighted. This study improves our understanding of the underlying physics of pore scale displacement of heavy oil and the key differences with light oil.

4.2 THE EFFECT OF OIL VISCOSITY

In the first case study, the effect of oil viscosity on the displacement process was investigated through three micromodel experiments using a light oil with viscosity of less than 1, a medium-heavy oil with viscosity of around 300 cp and an extra-heavy crude oil with viscosity of 8700 cp at test conditions. Generally, the condition of water-wetting is considered as the base case, against which the effects of other wetting conditions are compared. Therefore, all the tests are performed in the systems with water-wet preference.

A similar experimental procedure was followed in all micromodel tests reported here. The homogeneous rock-look-alike micromodel was first saturated with DW and pressurised to 600 psig at 44 °C. To resemble the initial migration of oil in a water-bearing reservoir and to establish an initial oil and water saturation, the crude oil was then injected from the bottom end of the micromodel and continued until the oil front reached the other end of the porous medium. To simulate waterflooding of an oil reservoir, the model was then flooded with water for an extended period of time (≥50 PV). Table 4-1 lists a summary of the fluids used and the pressure and temperature at which the MM Exp 1 to 3 were carried out.

Water was injected from the top end of the vertical micromodel at a very slow rate of 0.01 cm^3/hr (equal to 1 PV/day). This corresponds to a capillary number of 3.7E-7, which shows a capillary dominant displacement process. The effect of gravity forces on the recovery process was assumed to be negligible, as the density difference between the heavy crude oil and water is small.

Table 4-1: Fluids used and pressure and temperature conditions of MM Exp 1 to 3.

Porous Medium	Heterogeneous Rock-look-alike Micromodel
Crude Oil(s)	"A", "J" and "C" respectively for MM Exp 1, 2 and 3
Aqueous Phase	Distilled Water
Temperature	44 °C
Pressure	600 psig

4.2.1 MM Exp 1: Waterflooding a Conventional (light) Oil

The first micromodel test was a case of light oil (crude "A") waterflooding with an oil/water viscosity ratio of slightly less than 1. Initially, the micromodel was saturated

with DI water and then (to establish the initial saturation of oil in the micromodel) crude oil was injected (Figure 4-1). Relatively low oil saturation was achieved in the system at breakthrough of oil. However, to have a better comparison between the cases of different oil viscosities, injection continued and oil was circulated in the system until the oil saturation reached a level close to the tests using heavy and extra heavy crude oils (89%). Then, to simulate the process of waterflood, the micromodel was flooded with water. Figure 4-2 shows the same magnified section of the micromodel, after water breakthrough. The displacement process at the pore scale was observed to take place through corner filament flow, followed by either snap-off or piston type withdrawal. Comparison of Figure 4-1 with Figure 4-2, shows that during the water injection period most of the oil has been recovered and the remaining oil is in the form of disconnected oil blobs. These discontinuous pieces of oil were trapped and were not recoverable by continuation of water injection. The oil/water distribution in the micromodel remained unchanged after an extended period of waterflood (Figure 4-3).

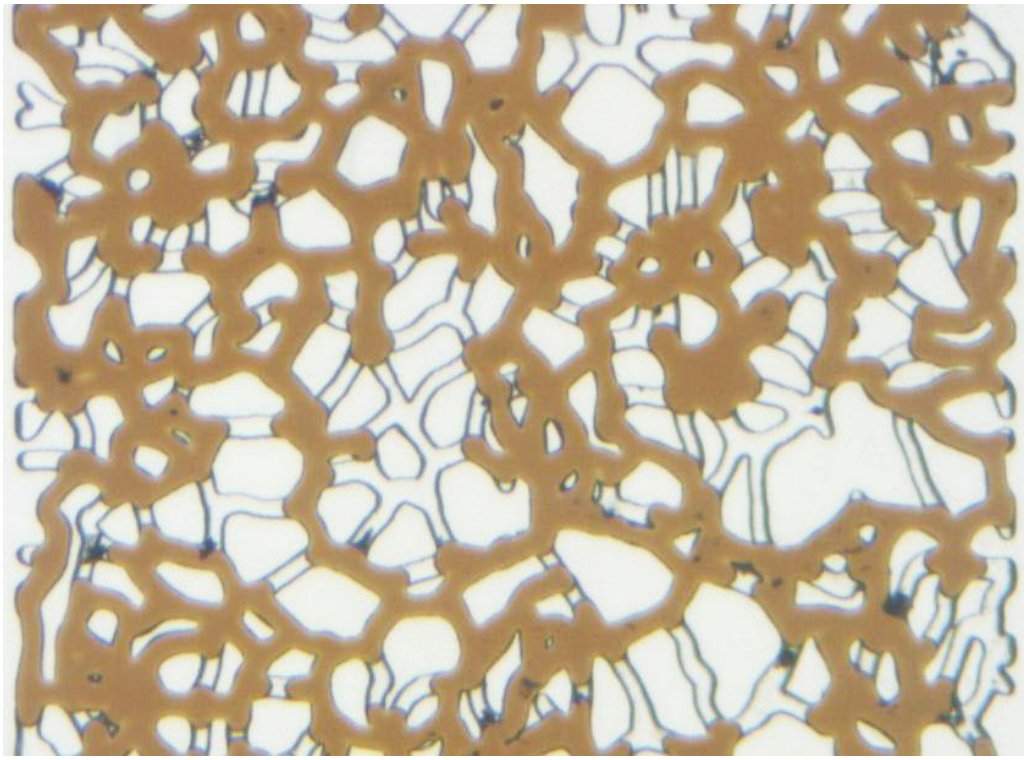

Figure 4-1: MM Exp 1; a magnified section of the micromodel at the end of the period of oil flood.

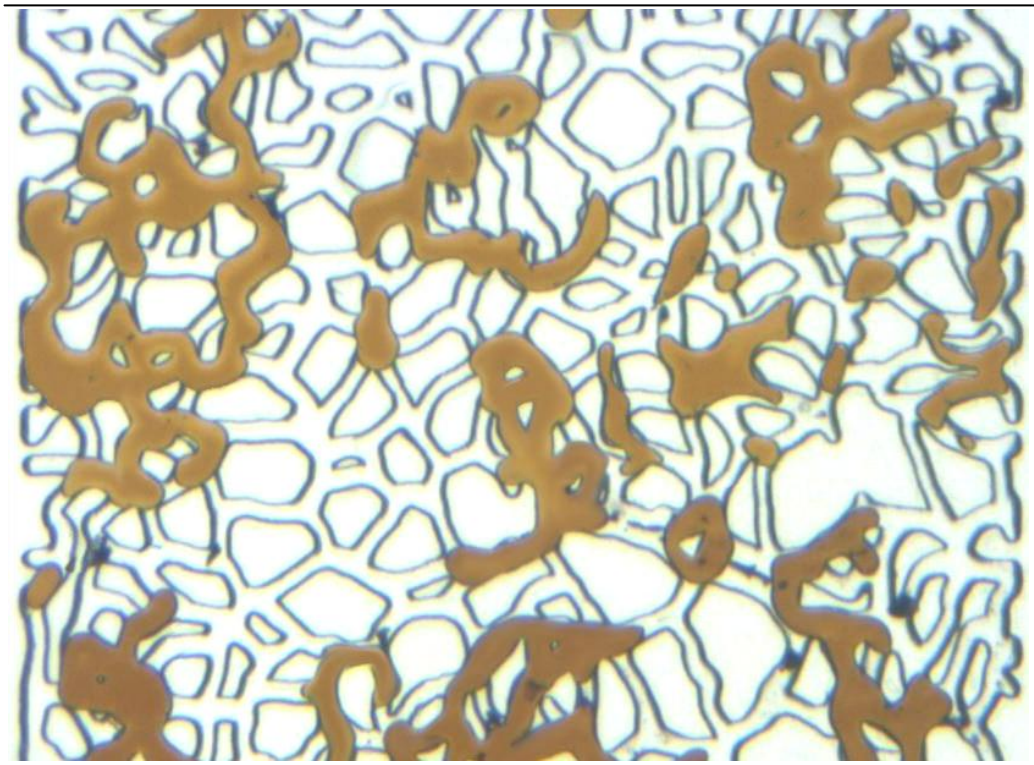

Figure 4-2: MM Exp 1; the same magnified section of the micromodel at breakthrough time during the period of waterflood.

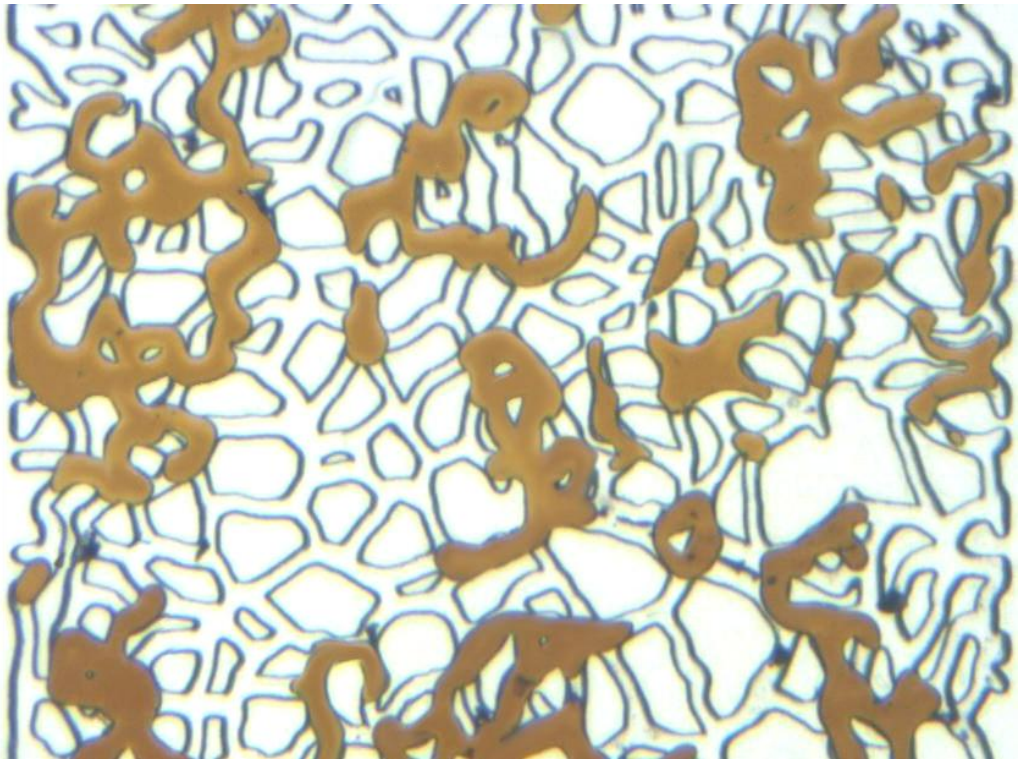

Figure 4-3: MM Exp 1; the magnified section of the micromodel at the end of the period of waterflood.

4.2.2 MM Exp 2: Waterflooding a Medium-Heavy Oil

The second micromodel test was performed to investigate the effect of increasing oil viscosity (by two orders of magnitude) on pore level displacement mechanisms using a medium-heavy crude oil (crude "E"). Using a similar procedure as the first test micromodel, it was initially saturated with distilled water and then crude oil was injected into the system. The oil injection continued until the oil reached the other end of the micromodel pattern. Having an oil/water viscosity ratio more than two orders of magnitude, a high oil saturation of 98% was achieved in the micromodel at the end of the oil flood period. Figure 4-4 shows the magnified section of the micromodel at the end of the oil injection period.

The micromodel was then flooded with water. Water was observed to displace oil in the same manner as the example of light oil, starting with flow of water on pore walls (corner filament flow) followed with snap-off process or piston type displacement. However, these pore level events occurred less frequently as water made a finger through the oil phase and did not reach a large fraction of pores that were fully occupied by oil. Figure 4-5 shows a section of the micromodel after the water breakthrough. Comparison of Figure 4-5 with Figure 4-4 shows that during the water injection period, some of the oil has been recovered, however, most of the resident oil has been left behind resulting in lower oil recovery compared to the example of light oil waterflood. The residual oil was in the form of large oil patches spread over a large number of pores that were connected through oil filaments, therefore, as waterflood continued after breakthrough oil was also observed to be produced.

As water injection continued, the injected water supported the water layers on the pore walls and these water layers became thicker. Subsequently, residual oil was forced to leave the pore and the connected filaments of oil became continuously thinner. In some pores, thickening of the water layer eventually resulted in rupture of these oil filaments (snap-off) or full recovery of the oil through piston type withdrawal. After a certain period of waterflood, the oil filaments which connected the large oil patches were ruptured and the remaining oil was fully surrounded by water. The complete rupture of these oil filaments took place after 10 PVs of waterflood and no more oil redistribution and production happened after that. Figure 4-6 illustrates the magnified section of the micromodel after an extended period of waterflood, where the red dotted circles show pore networks in which residual oil at breakthrough have been displaced later on.

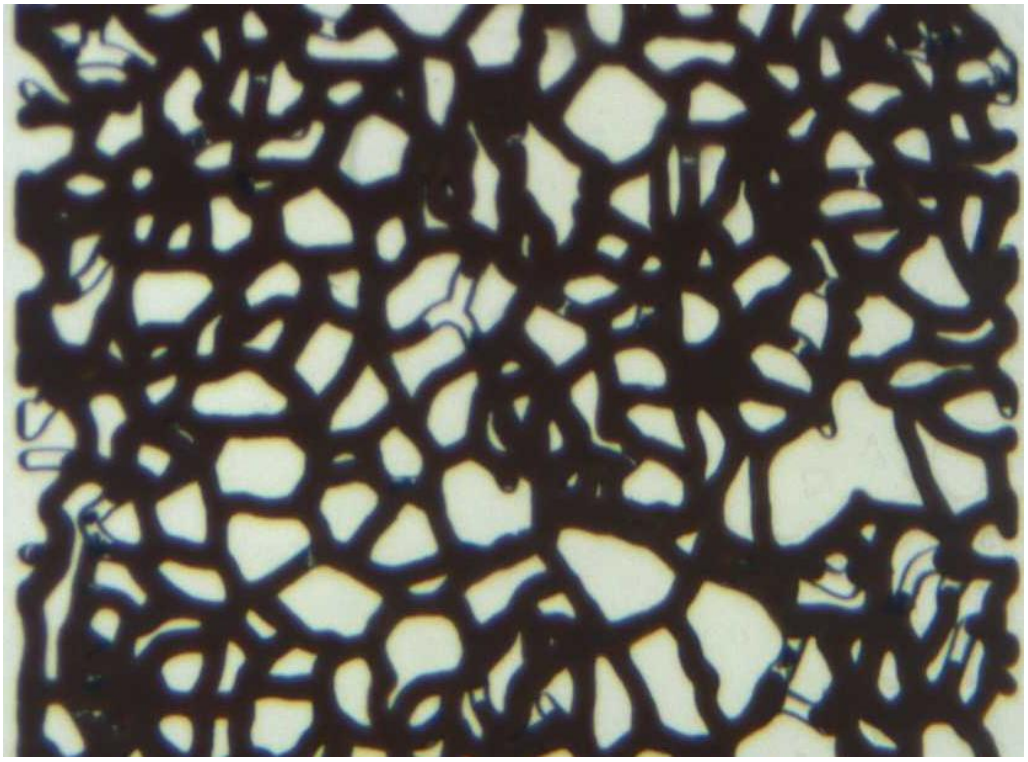

Figure 4-4: MM Exp 2; a magnified section of the micromodel at the end of the period of oil flood.

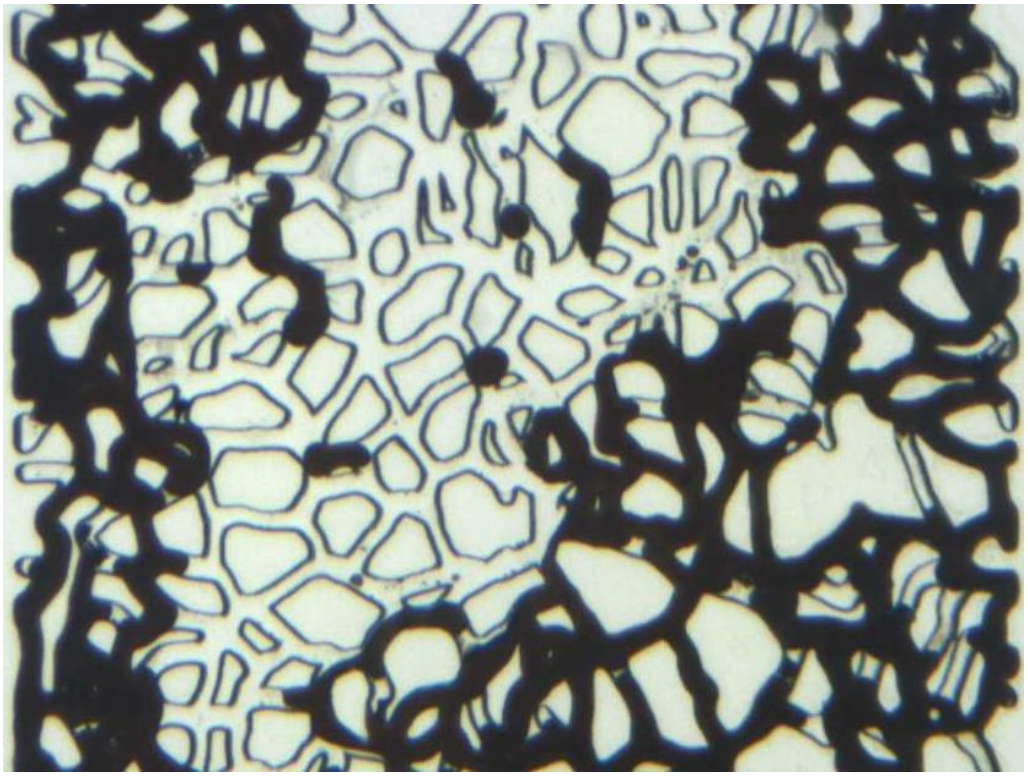

Figure 4-5: MM Exp 2; the same magnified section of the micromodel at breakthrough time during the period of waterflood.

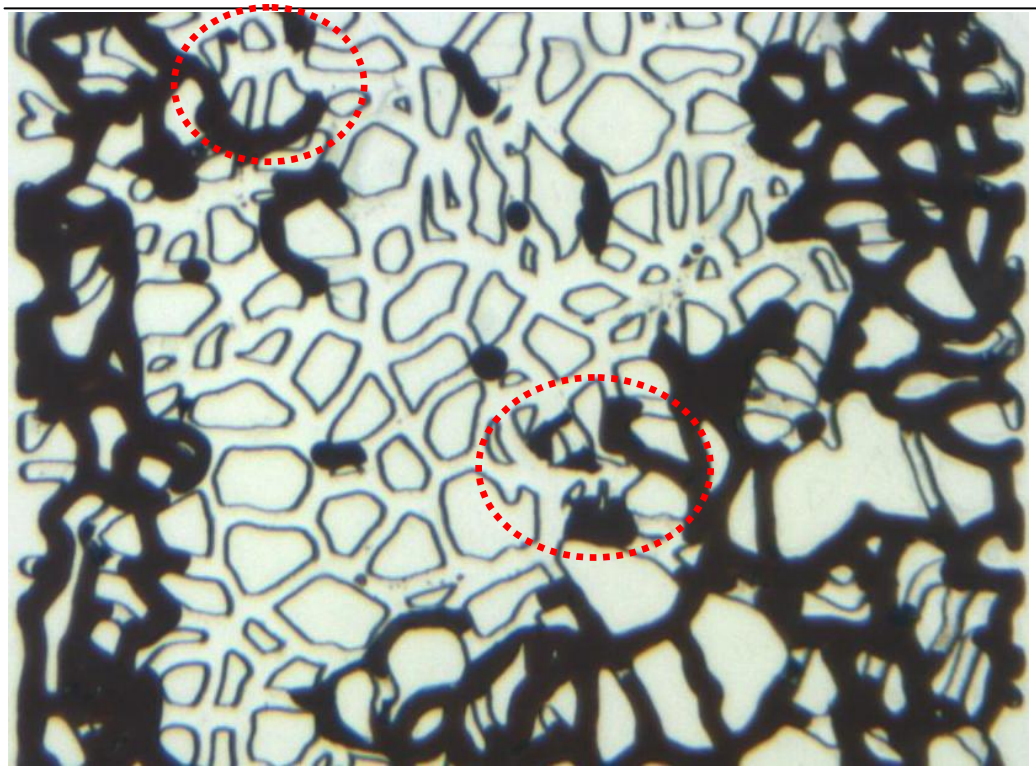

Figure 4-6: MM Exp 2; the magnified section of the micromodel at the end of the period of waterflood.

4.2.3 MM Exp 3: Waterflooding an Extra-Heavy Oil

The third micromodel test was performed using an extra-heavy crude oil (crude "C") with a viscosity more than 4 orders of magnitude greater than water. Similar preparation procedure as the previous tests were followed and the micromodel was then fully saturated with distilled water. Then, to establish the initial water/oil saturation, the extra-heavy crude oil was injected through the micromodel. Figure 4-7 presents the magnified section of the micromodel at the end of the period of oil injection, an oil saturation of 99% is achieved. The highly magnified images of the micromodel show there was still some water in the system, in the form of very thin films, attached to the pore walls.

The micromodel was then flooded with water for 50 PVs. At the early stages of water injection when breakthrough is yet to happen, water is displacing high viscosity heavy oil so the viscous forces are expected to be dominant over capillary forces (viscous dominant flow). Similar to the case of waterflood in medium-heavy oil (previous test), water was observed to open a narrow flowing path in the middle of the vertically positioned micromodel, while most of the pores were still fully saturated with oil. Figure 4-8 illustrates the same section of the micromodel at water breakthrough. It can

be seen that the width of this water finger is significantly smaller compared to the case of medium-heavy crude oil (Figure 4-5) corresponding to considerably lower oil recovery at breakthrough time. The pore scale displacement event took place only through piston type withdrawal, and oil trapping by capillary instability (snap-off) was not observed throughout the micromodel. The residual oil at this stage of the test was divided into two parts on the left and right side of the water finger, which were both continuous the entire length of the micromodel.

After the water breakthrough as the injected water became the continuous phase in the porous media, the pressure across the core dropped and the displacement was dominated by capillary forces. A progressively larger area of the micromodel was observed to be affected (flooded) with injected water, leading to a change of the original oil/water distribution and also producing more oil. The water was observed to initially support and thicken the existing water layers on the pore walls, which resulted in displacement of resident oil in the pores. As water injection continued, the pore level displacement event turned into either piston type withdrawal or snap-off in the pores, with low and high pore-throat aspect ratio respectively. Figure 4-9 presents the same section of the micromodel after an extended period of waterflood, which shows considerable additional recovery compared to the picture at breakthrough time (Figure 4-8).

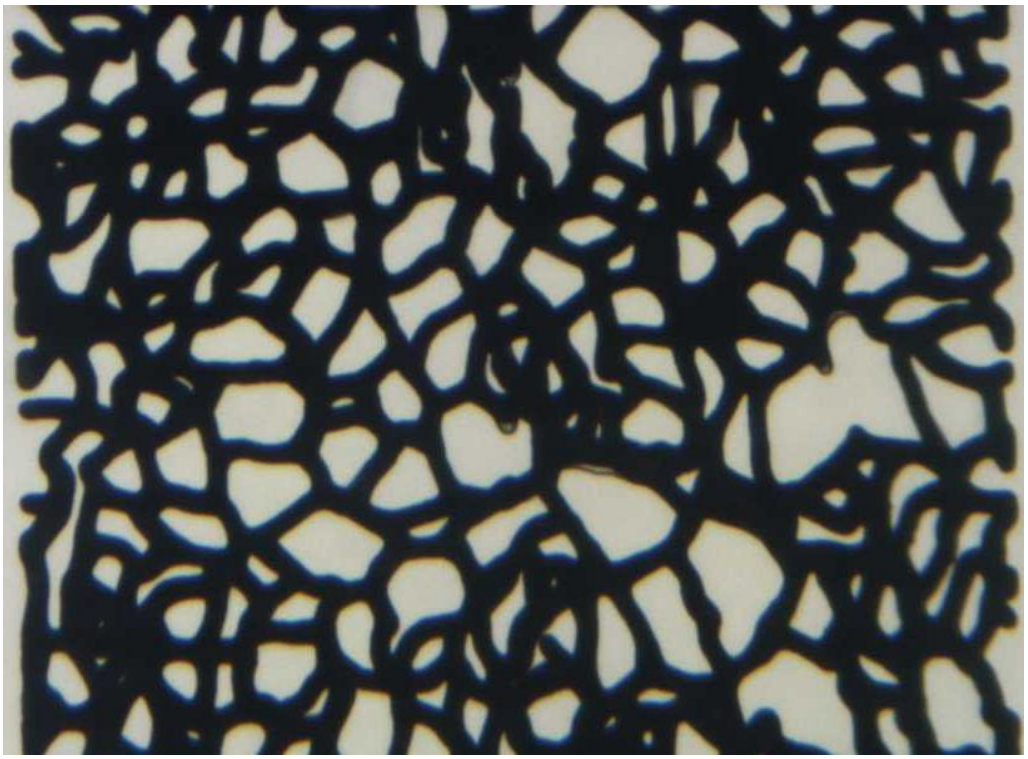

Figure 4-7: MM Exp 3; a magnified section of the micromodel at the end of the period of oil flood.

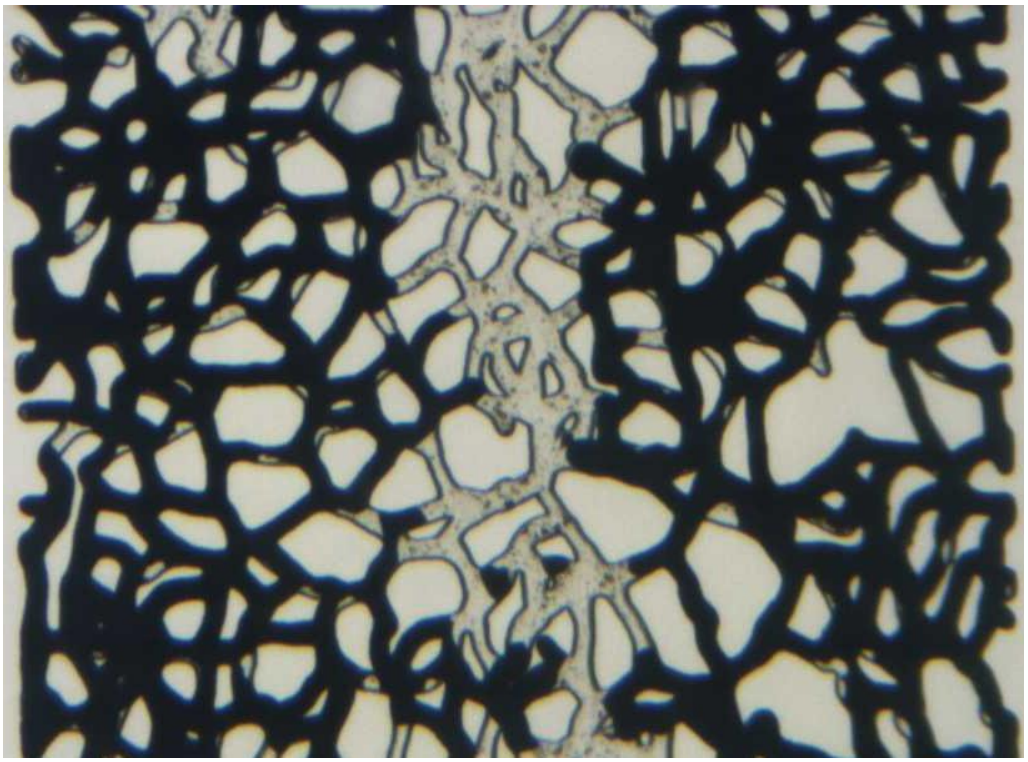

Figure 4-8: MM Exp 3; the same magnified section of the micromodel at breakthrough time during the period of waterflood.

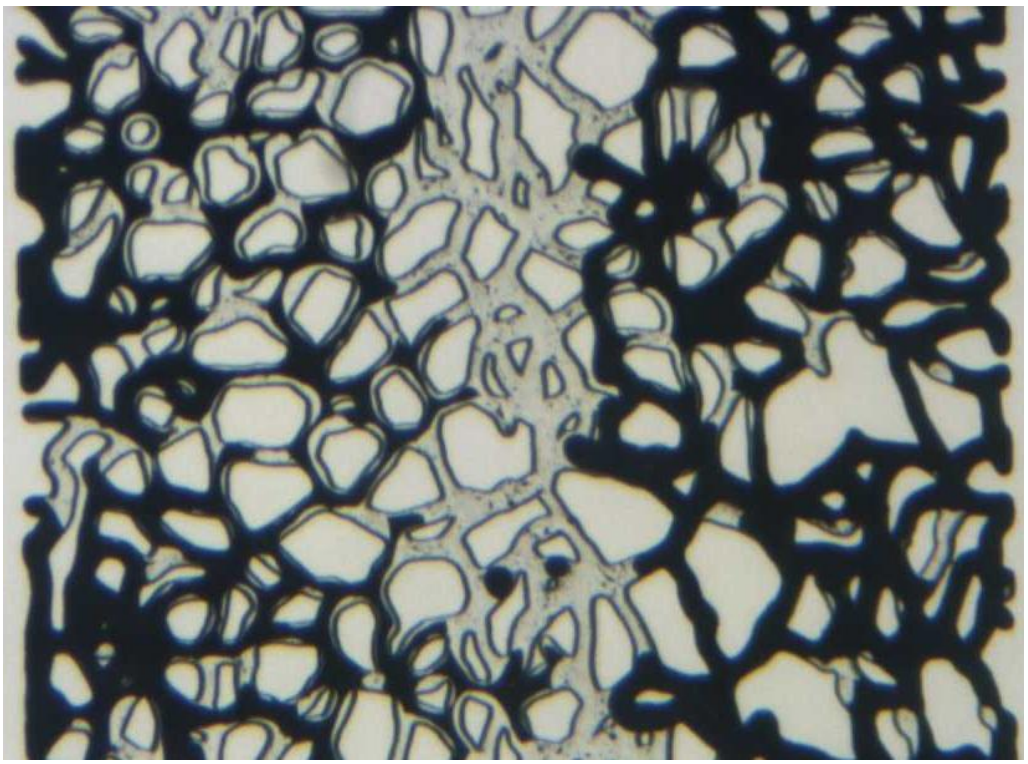

Figure 4-9: MM Exp 3; the magnified section of the micromodel at the end of the period of waterflood.

4.2.4 Discussions

Effect of Oil Viscosity on Displacement Efficiency

Our observations show that the displacement efficiency is a strong function of oil/water viscosity ratio and is inversely related to the viscosity of the oil phase. The increase in oil viscosity causes earlier water breakthrough (lower oil recovery) and longer period of simultaneous oil and water production, before the final residual oil saturation is reached. Figure 4-10 illustrates the oil recovery versus the pore volume of injected water in the previous experiments. The graph shows that the oil recovery at breakthrough time (the red markers) decreases as oil viscosity increases. A similar relationship also exists between ultimate oil recovery (after 50 PV's of water injection) and oil viscosity, however, the difference in recovery is less significant compared to breakthrough recovery. This is due to the persistence of oil recovery in heavier crudes where the residual oil remains connected after water breakthrough in as shown in Figure 4-3, Figure 4-6 and Figure 4-9.

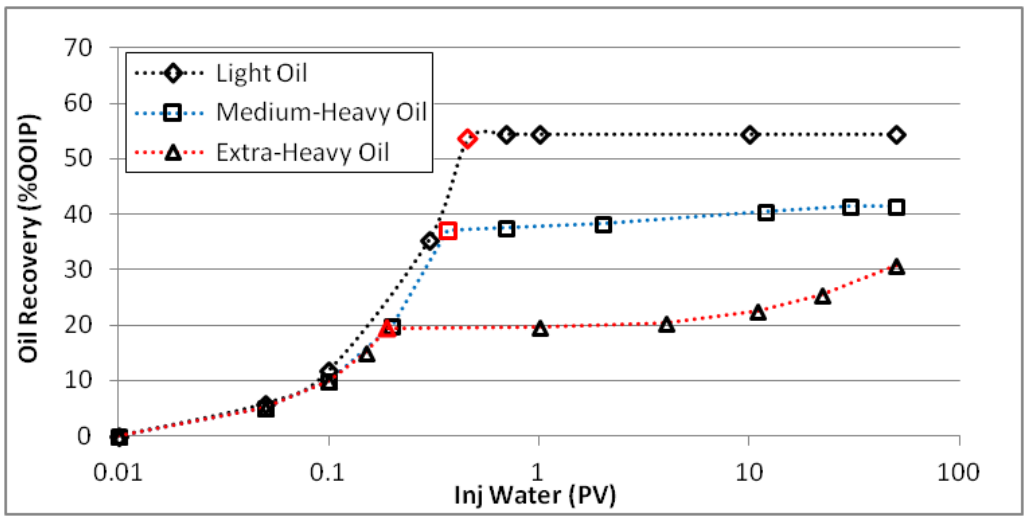

Figure 4-10: Oil recovery versus total PV of injected water using a light crude oil (MM Exp 1), a medium-heavy crude oil (MM Exp 2) and, an extra-heavy crude oil (MM Exp 3). The red markers define the water breakthrough time.

Effect of Oil Viscosity on Trapping Mechanisms

The micromodel tests revealed that the increase in oil viscosity and therefore the oil/water viscosity ratio modifies trapping mechanisms and the pore scale distribution of

trapped oil. As the contrast between oil and water viscosity increases, the viscous forces play a more important role in oil trapping (through viscous fingering mechanisms) and a smaller fraction of oil is trapped by capillary forces (through capillary instability and oil bypassing mechanisms).

In a water-wet system with moderate oil/water viscosity ratio, trapping of oil takes place due to the capillary forces, in which the residual oil remains in the porous media in the form of completely disconnected and scattered blobs (Figure 4-2). As the trapping viscous forces become stronger, due to the higher viscosity contrast between crude oil and water, the residual oil blobs become increasingly larger extending over a network of several pores. If the oil/water viscosity ratio is high enough the network of residual oil will remain continuous throughout the porous media. This type of trapping (due to viscous forces) was observed during waterflood of heavy crude oils (Figure 4-5 and Figure 4-8) where big patches of oil remained connected in the porous media, even after water breakthrough. Final trapping of oil takes place only when the remaining oil is completely surrounded by water after an extended period of waterflood.

Effect of Oil Viscosity on Pore Scale Displacement Mechanisms

Study of pore scale events shows that pore scale displacement mechanisms are independent from viscosity of oil phase and oil/water viscosity ratio, as long as the process remains *capillary dominant*. This means in such systems pore scale displacement mechanisms are only a function of wettability, similar to what was explained in the case of light oil waterflood in the previous chapters (corner filament flow followed by either snap-off or piston type withdrawal in water-wet systems, piston type withdrawal in intermediate-wet systems and water channelling in oil-wet systems). It's important to notice that while the increase in viscosity of oil phase does not alter the pore scale displacement mechanisms, it causes a significant decrease in the number of times these pore scale events occur. This is due to the fact that injected water finger through the porous medium and does not meet the resident oil in most of the pores.

However, if the increase in oil viscosity causes the displacement process to become *viscous dominant* it can greatly affect some of the displacement mechanisms. For instance in Exp 3, the viscous dominant flow before water breakthrough caused the corner filament flow and snap-off mechanisms to occur in fewer pores and the piston type withdrawal became the dominant displacement mechanism. The effect of oil

viscosity on displacement mechanisms will be explained in the following sections (Exp's 5, 6 and 7).

4.3 THE EFFECT OF WETTABILITY

The second set of micromodel experiments focused on the impact of state of wettability on displacement mechanisms and efficiency of heavy oil waterflood. The heterogeneous rock-look-alike pattern micromodel was used for this series of experiments, in which wettability conditions of strongly water-wet, intermediate wet (slightly water-wet and slightly oil-wet) and strongly oil-wet were simulated.

The micromodel which was used for this study initially showed strongly oil-wetting behaviour after being etched by Hydrofluoric acid. To shift wettability towards increased water-wet conditions the micromodel was soaked in the diluted solution of caustic soda. A very similar experimental procedure was followed in all micromodel tests reported here. The micromodel was first saturated with distilled water and pressurised to 600 psig at 44 °C. To resemble the initial migration of oil in a water-bearing reservoir and to establish an initial oil and water saturation, the crude oil was then injected from the bottom end of the micromodel and continued until the oil front reached the other end of the porous medium. Then injection stopped and oil was aged in the system for a period of 1or 2 day(s). To simulate waterflooding of an oil reservoir, the model was then flooded with water for an extended period of time (≥50 PVs). Table 4-2 lists a summary of the fluids used and the pressure and temperature at which the MM Exp 4 to 7 were carried out.

Table 4-2: Fluids used and pressure and temperature conditions of MM Exp 4 to 7.

Porous Medium	Heterogeneous Rock-look-alike Micromodel
Crude Oil	Crude "C" "C" (8700 cp @ 50 °C)
Aqueous Phase	Distilled Water
Temperature	44 °C
Pressure	600 psig

4.3.1 MM Exp 4: Strongly Water-Wet Conditions

The experiment began by saturating the micromodel with distilled water. Then, to establish the initial saturation, the crude oil was injected through the micromodel. Figure 4-11 shows a magnified section of the micromodel at the end of the period of oil

injection. Despite having dead end structures and an inverted cup-shape network of pores in this pattern, the oil saturation at the end of oil flood period reached value of 99.5%. This is believed to be a consequence of both high viscosity ratio between oil and water and strongly water-wet characteristics of the micromodel. Basically, in water-wetted porous media, oil injection results in very low connate water saturation. This is due to a counter-current displacement mechanism in which the injected oil invades pores from the centre of the pores and resident water leaves the pore space through layers of water attached to the rock surface. The positive capillary forces also help this displacement process in water-wet systems.

The micromodel was then flooded with distilled water. The injected water displaced the resident oil through film flow mechanism in most of the pores, however, oil displacement by piston type withdrawal was also observed in a few pores. Figure 4-12 illustrates the same section of the micromodel at water breakthrough. The fact that a continuous path of water flow did not form at breakthrough time is a good indication of strongly water-wet conditions of the system. Low oil recovery was observed to happen at breakthrough time, which was expected considering the very unfavourable viscosity ratio between resident oil and injected water.

The water injection after water breakthrough continued for 50 PVs. As the water injection continued more pores were observed to be gradually occupied by the injected water. The pore-scale mechanisms of oil displacement by water, were seen to start by a flow of water through the sharp corners of the pores that were still saturated with crude oil (corner filament flow). These water filaments were seen to thicken slowly pushing the oil away from the pores walls and towards the centre of pores, finally causing snap-off at some pore throats. In other pores with low pore to throat aspect ratio, the thickening of the water films eventually resulted in evacuation of oil from the pore body (piston type withdrawal). Figure 4-13 illustrates the same section of micromodel after the extended period of waterflood, which shows a significant fraction of waterflood residual oil at breakthrough time (Figure 4-12) has been produced after the extended period of waterflood.

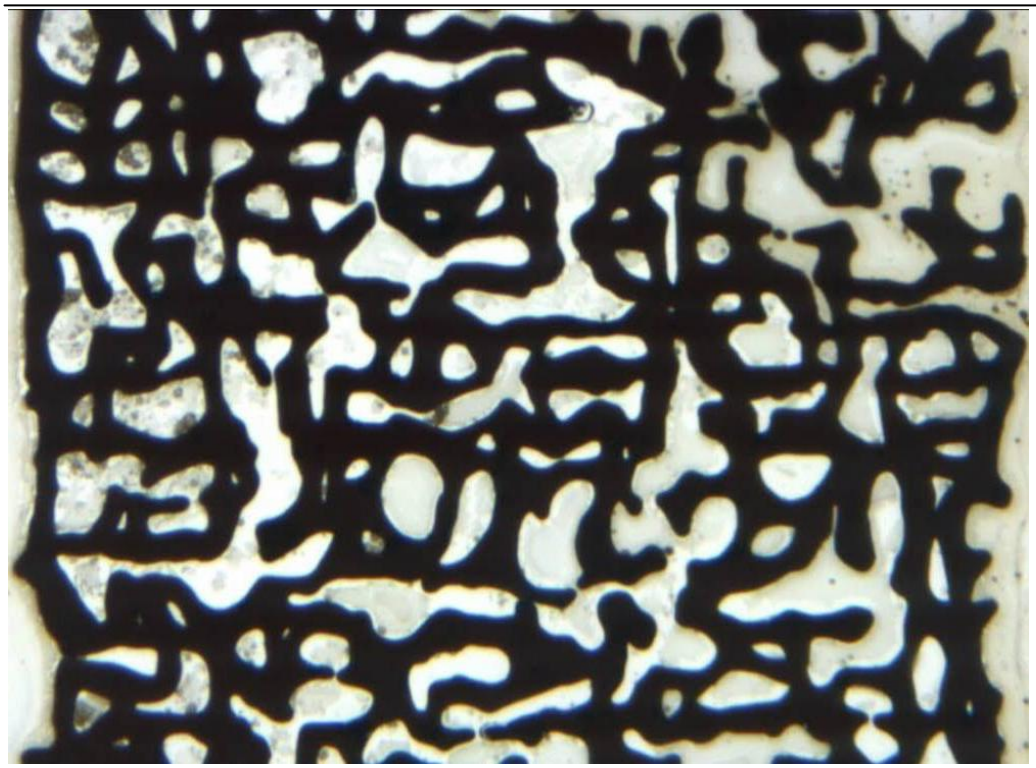

Figure 4-11: MM Exp 4; a magnified section of the micromodel at the end of the period of oil flood.

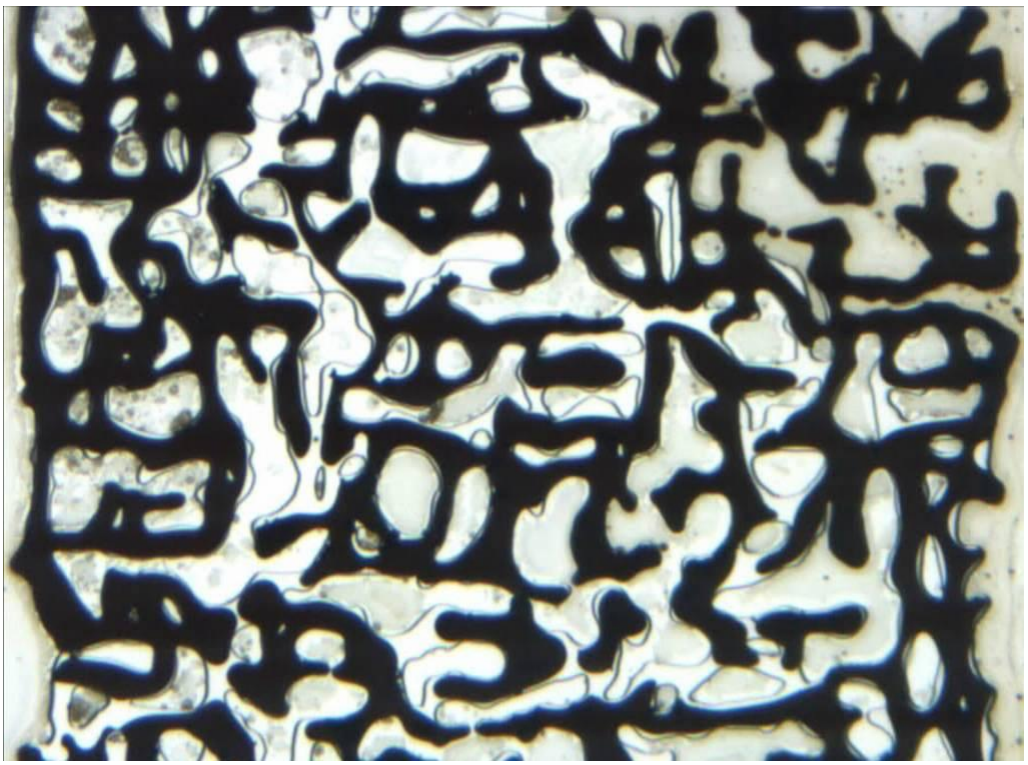

Figure 4-12: MM Exp 4; the same magnified section of the micromodel at breakthrough time during the period of waterflood.

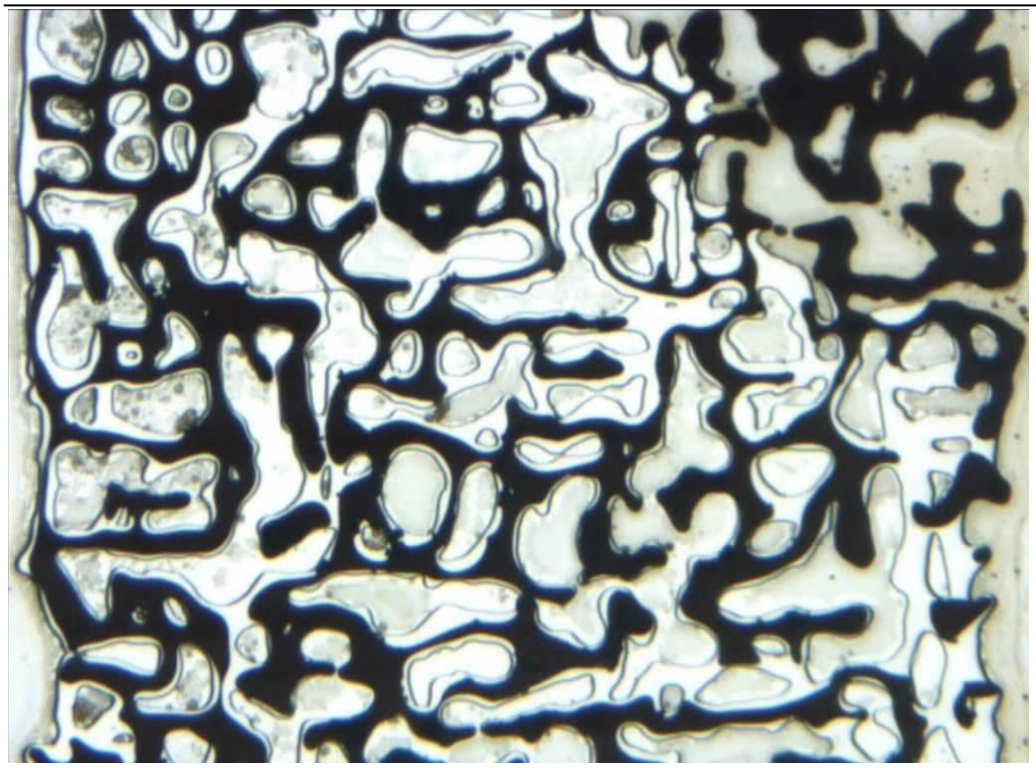

Figure 4-13: MM Exp 4; the magnified section of the micromodel at the end of the period of waterflood.

4.3.2 MM Exp 5: Intermediate-Wet Conditions (Slightly Water-Wet)

The second test was performed using the same micromodel and experimental procedure as the previous test, however, the wettability of micromodel in this test was weakly water-wet. Figure 4-14 shows a magnified section of micromodel at the end of the period of oil injection. As can be seen, similarly to the case of strongly water-wet conditions, the oil saturation attained at the end of oil flood period was very high (99% in this experiment). However, there are still pores in the micromodel which are not filled with oil. This is due to the fact that water layers on the glass surface are weak in some parts and cannot support flow of water, which results in trapping of water in some dead end pores during oil flood.

The micromodel was then flooded with water. The pore scale displacement took place first and foremost through piston type displacement mechanism. Channelling of water was also observed in a few pores in which water opened a flowing path in the middle of the pores, while layers of oil remained attached to the pores walls. Figure 4-15 illustrates the same section of the micromodel at the time of water breakthrough in this test. Low oil recovery was attained at breakthrough time, which was expected due to the very unfavourable viscosity ratio between the resident oil and injected water.

Unlike the example of a strongly water-wet system, a clear water flowing path can be seen in the middle of the micromodel.

The water injection continued for more than 50 PVs after the water breakthrough. Figure 4-16 shows the same section of the micromodel as in Figure 4-15 which reveals that incremental oil production after water breakthrough is significantly lower than the case of a strongly water-wet system. It can be seen that water layers on the pore surface have been thickened in pores near the flowing path of water during the extended period of waterflood, however, the water/oil distribution has remained unchanged in most of the pores.

Figure 4-14: MM Exp 5; a magnified section of the micromodel at the end of the period of oil flood.

Figure 4-15: MM Exp 5; the same magnified section of the micromodel at breakthrough time during the period of waterflood.

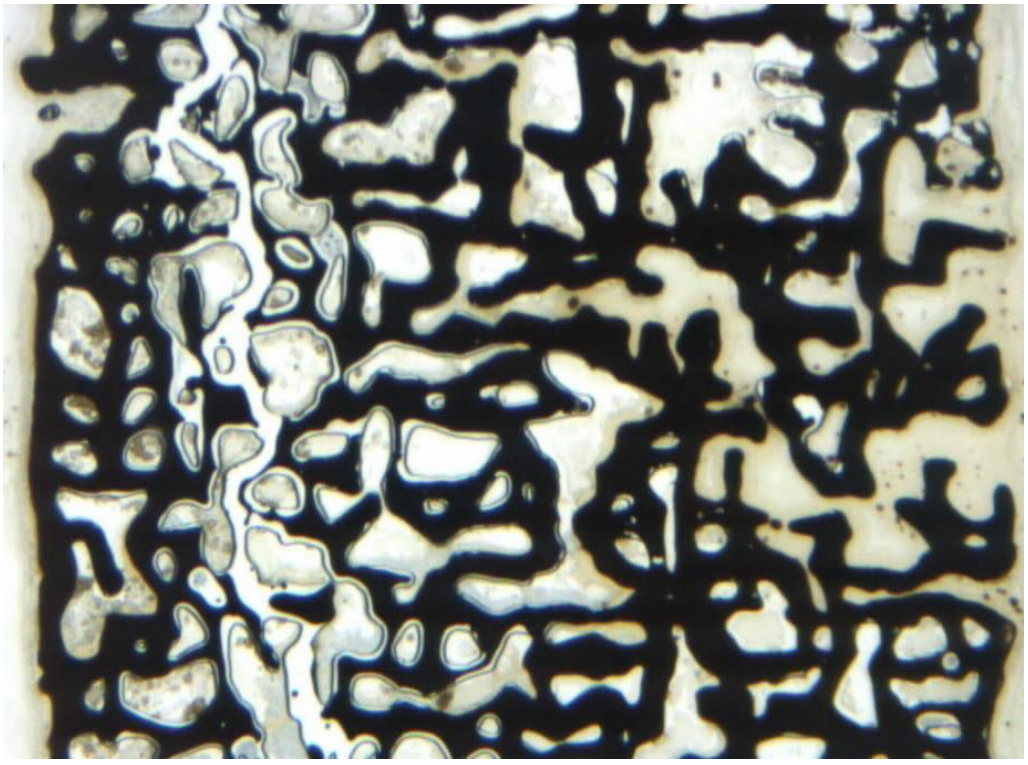

Figure 4-16: MM Exp 5; the magnified section of the micromodel at the end of the period of waterflood.

4.3.3 MM Exp 6: Intermediate-Wet Conditions (Slightly Oil-Wet)

In the third heavy oil waterflooding test the wettability condition of slightly oil-wet conditions was simulated. A new micromodel was used in this test, which in fact was a prototype of the heterogeneous rock look-a-like micromodel. The pore connectivity in this prototype was slightly lower than the original one that had been used for the first two tests.

The experiment began with saturating the micromodel with distilled water and then to establish the initial saturations, the heavy crude oil was injected through the micromodel. Figure 4-17 shows a magnified section of micromodel at the end of the period of oil injection. An oil saturation of 90% was achieved which was lower than the cases of water-wetted systems in the previous two tests, despite the fact that experimental conditions and fluids were not altered. It was explained earlier that high oil saturation in the case of strongly and slightly water-wet systems was due to a counter-current flow process at pore scale during oil flood period, where the injected oil enters the pore from the pore middle, however, the resident water leaves the pore through water layers on the glass surface. However, in the case of oil-wet systems the water layers are not continuous in most parts of the model that is being invaded by the injecting oil, therefore, the counter-current displacement process cannot take place. This results in trapping resident water in the dead-end pores and lower oil saturation (including slightly and strongly oil-wet conditions) compared to water-wetted systems.

The micromodel was then flooded with water. The displacement of resident oil by water was observed to take place mostly through channelling of water in the oil wetted pores. Oil displacement was also observed to take place through piston type mechanism in a few pores, where water layers remained connected on the surface of pore walls. Figure 4-18 illustrates the same section of micromodel at the time of water breakthrough. Low oil recovery was observed at the breakthrough time due to the very unfavourable viscosity ratio between the resident oil and injected water. The water injection continued for more than 50 PVs after the breakthrough. Despite very minor changes in oil/water distribution (red circles in Figure 4-19) the system remained largely unchanged and negligible additional oil was recovered. This behaviour was contrary to observation in the cases of water-wetted systems.

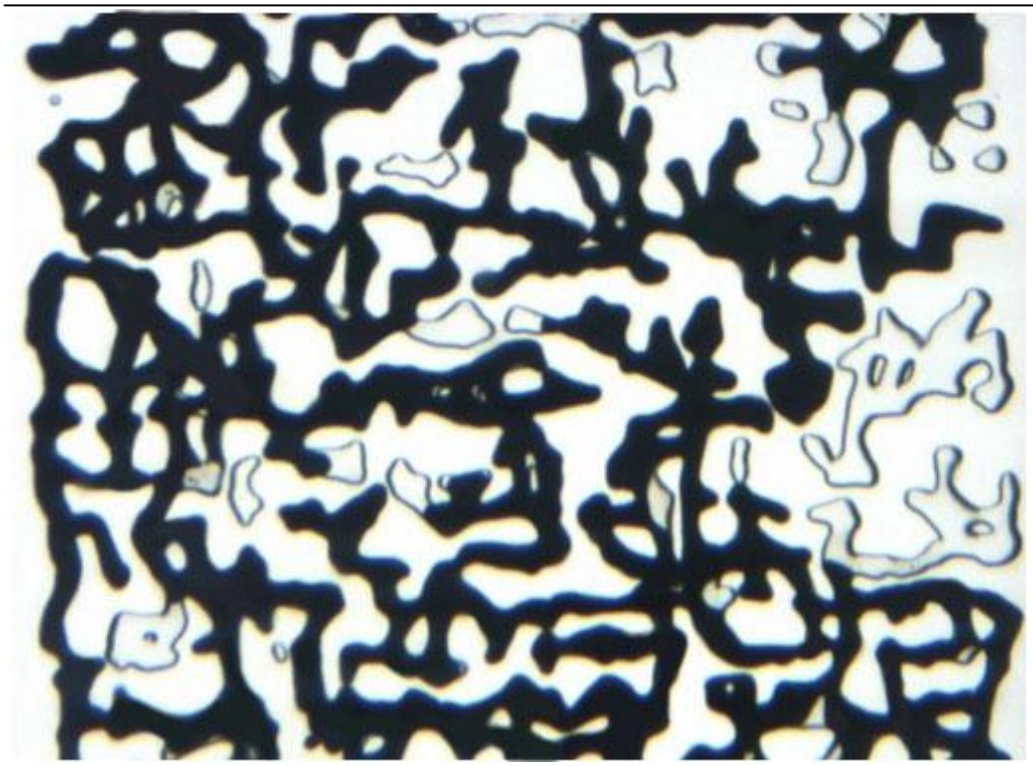

Figure 4-17: MM Exp 6; a magnified section of the micromodel at the end of the period of oil flood.

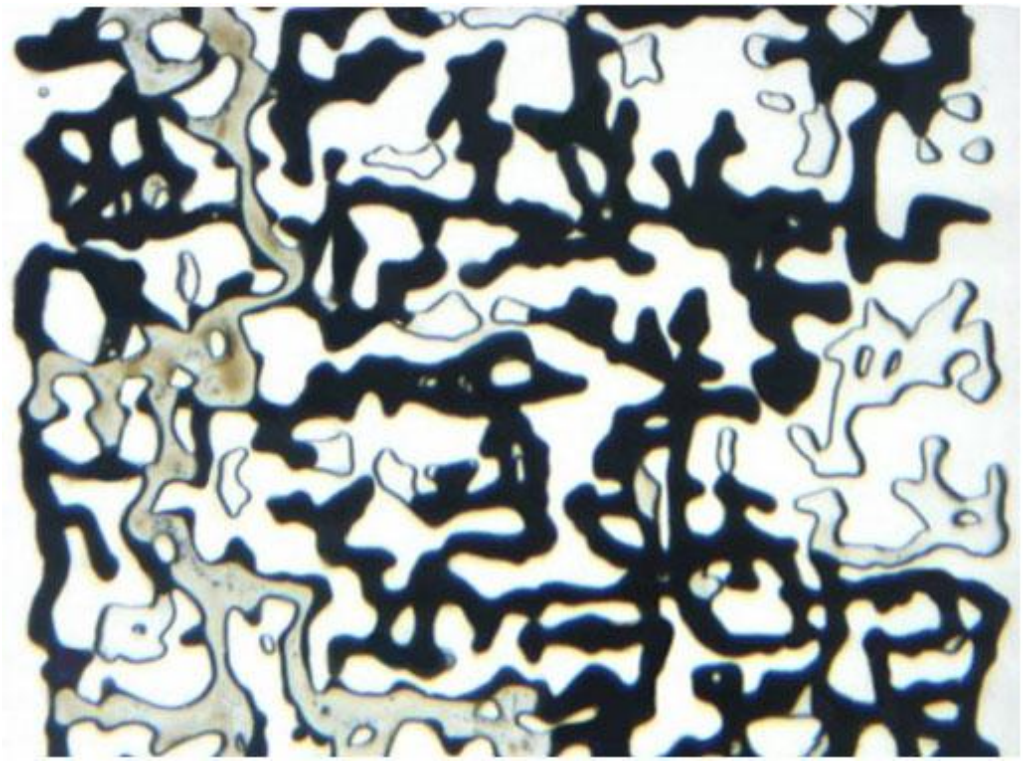

Figure 4-18: MM Exp 6; the same magnified section of the micromodel at breakthrough time during the period of waterflood.

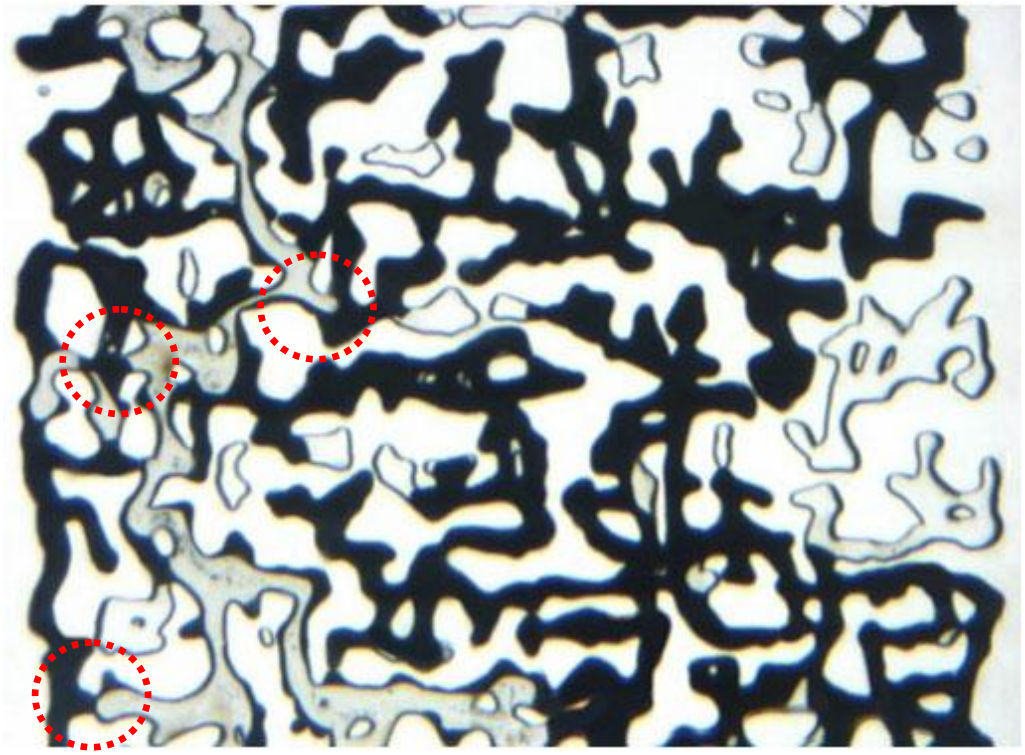

Figure 4-19: MM Exp 6; the magnified section of the micromodel at the end of the period of waterflood.

4.3.4 MM Exp 7: Strongly Oil-Wet Conditions

The last test was carried out with the intention of simulating process of waterflood in a strongly oil-wet system. The experiment began by saturating the micromodel with distilled water and then, to establish the initial saturations, the heavy crude oil was injected through the micromodel. Figure 4-20 shows a magnified section of micromodel at the end of the period of oil injection. An oil saturation of 78% was achieved which was even lower than the case of slightly oil-wet system in the previous experiment. This is believed to be due to the lack of water layers on pore walls that prevent displacement of water from dead-end pores, as was explained before.

The micromodel was then flooded with water. Water channelling was the dominant displacement mechanism at pore scale in which water displaced oil from larger pore bodies, whilst the stable layers of oil remained attached to the pore walls. Figure 4-21 illustrates the same section of micromodel as Figure 4-20 at the time of water breakthrough. The amount of oil recovered by water at breakthrough time in oil wetted systems (including this test and previous test) was similar to the cases of strongly water-wet and slightly water-wet conditions. However, if the recovery is calculated based on original saturation of oil in the micromodel this value would be higher in the oil wetted

systems, due to their lower saturation of original oil in place. The water injection continued for an extended period of time after water breakthrough. However, the extended period of waterflood did not result in further oil production and oil/water distribution remained unaffected in the micromodel (Figure 4-22).

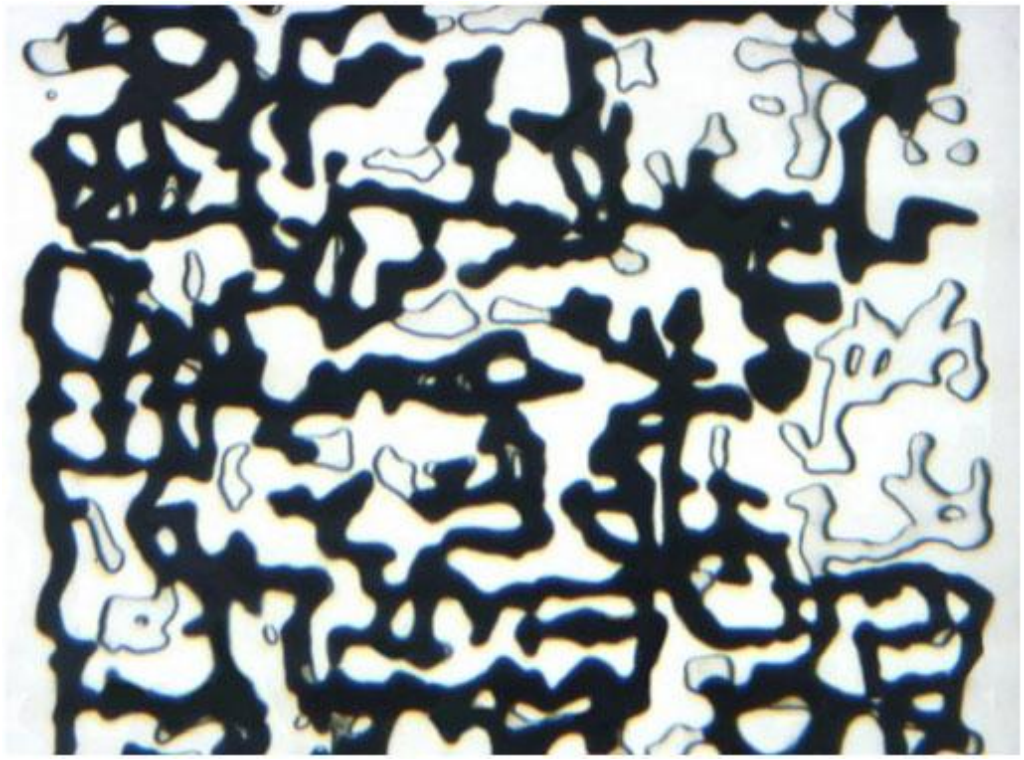

Figure 4-20: MM Exp 7; a magnified section of the micromodel at the end of the period of oil flood.

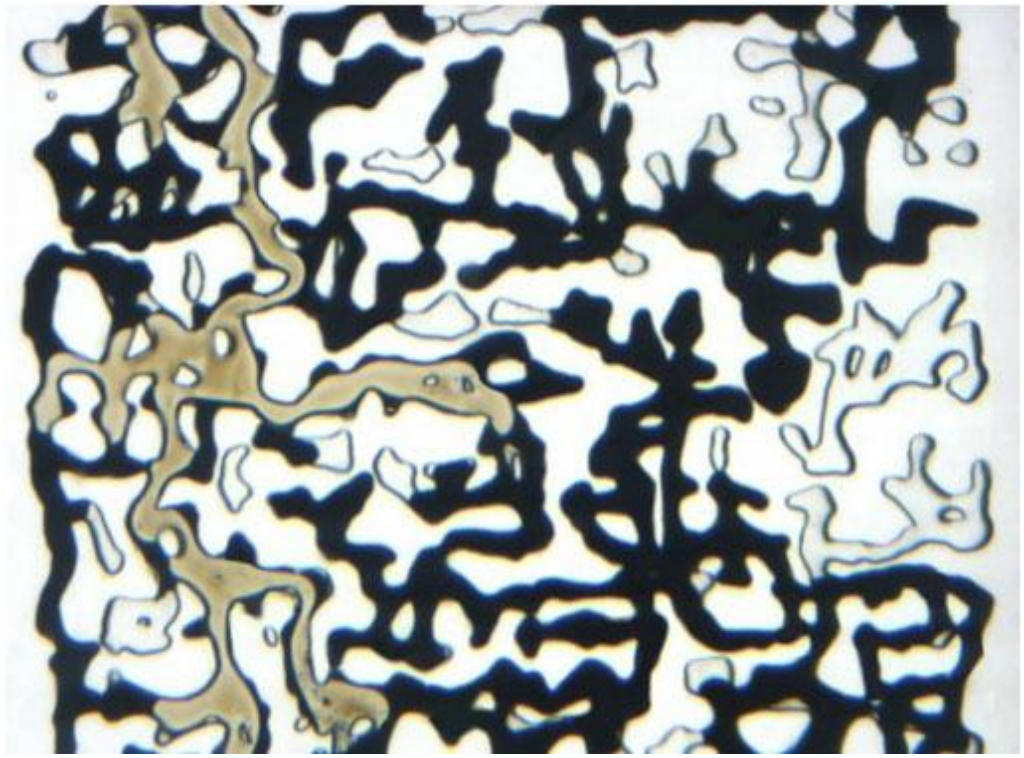

Figure 4-21: MM Exp 7; the same magnified section of the micromodel at breakthrough time during the period of waterflood.

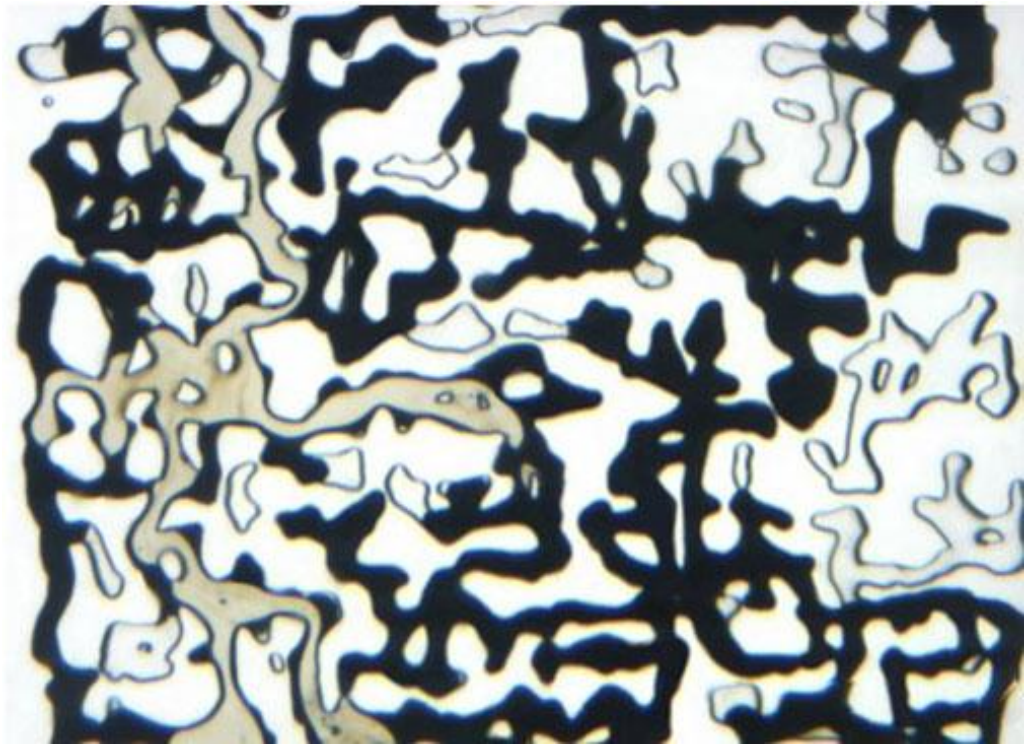

Figure 4-22: MM Exp 7; the magnified section of the micromodel at the end of the period of waterflood.

4.3.5 Discussions

Effect of Wettability on Displacement Efficiency

The observations from these series of micromodel tests show that as crude oil viscosity increases, the recovery at breakthrough becomes less dependent on the state of wettability of the system. This is due to the fact that in such systems most of the trapping takes place due to the viscous forces, and oil/water viscosity ratio becomes the prime parameter controlling recovery performance. Figure 4-23 plots the oil recovery versus the pore volume of injected water in the micromodel experiments presented in this section. The breakthrough recovery was 15, 13.9, 13.5 and 11.2 %OOIP respectively for the strongly water-wet, slightly water-wet, slightly oil-wet and strongly-oil-wet systems. A total number of 20 micromodel tests performed using the extra-heavy crude oil and micromodel pattern, which most of them are not reported here, all resulted in a recovery between 10 to 15 %OOIP at water breakthrough whilst the oil/water distribution could be different.

After water breakthrough, however, wettability significantly affected the rate of heavy oil recovery and final residual oil saturation. The oil recovery after water breakthrough was highest in the case strongly water-wet system and decreased as the system shifted towards increased oil-wet conditions. In the case of the strongly water-wet system the recovery dramatically improved to more than twice the recovery at breakthrough time (from 15 to 33%OOIP). The incremental recovery after water breakthrough was calculated to be 5.25 and 1.3 OOIP in the slightly water-wet and slightly oil-wet systems and no additional oil was recovered in the strongly oil-wet system after water breakthrough, as can be seen in Figure 4-23.

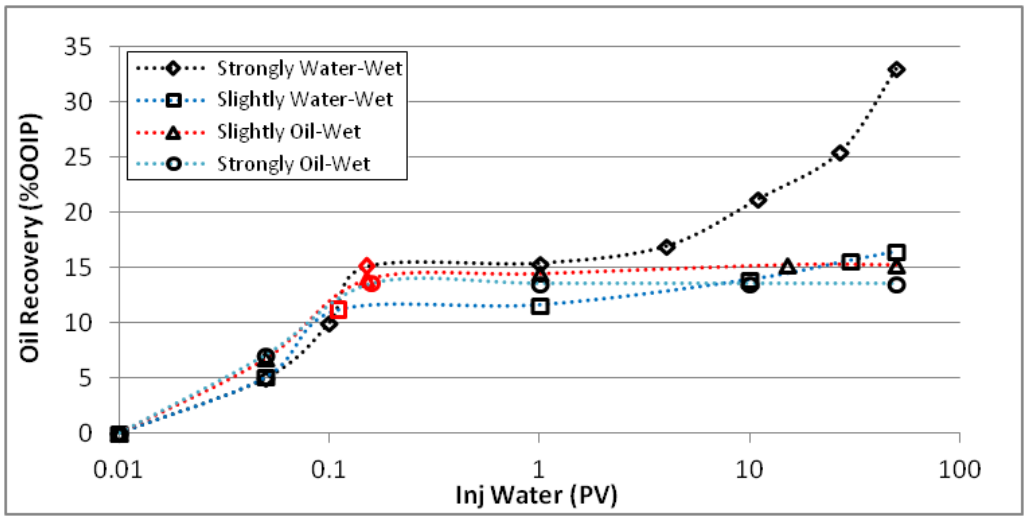

Figure 4-23: Oil recovery versus total PV of injected water using a strongly water-wet system (MM Exp 4), a slightly water-wet system (MM Exp 5), a slightly oil-wet system (MM Exp 6) and, an strongly oil-wet system (MM Exp 4). The red markers define the water breakthrough time.

Neutral and intermediate-wet conditions are generally considered as the most favourable conditions for recovery of light oils, due to the fact that in this wettability state trapping capillary forces will be minimized. However, based on our micromodel tests, it seems the optimum state of wettability can be a function of crude oil viscosity and as oil viscosity increases, the optimum state of wettability shifts towards more water-wet conditions. In the case of extra- heavy oil used in this study, waterflooding was observed to be most efficient in strongly water-wet conditions where the positive capillary forces (spontaneous imbibition process) are strongest.

Theoretically, production of oil phase in the porous media should continue as long as the residual oil is continuous and there is pressure difference across the porous medium. However, the fact that in these experiments oil recovery after water breakthrough was very much dependent on wettability of the system reveals that capillary forces also play an important role in recovery of heavy oil after water breakthrough.

In the systems where oil trapping takes place due to viscous forces (high oil viscosity and high oil/water viscosity ratio) the distribution of residual oil at breakthrough time is not stable from capillary forces considerations (test 2, 3, 4, 5 and 6). Therefore, as injection continues after water breakthrough, these forces attempt to mobilize a fraction of the residual oil and adjust distribution of oil and water in a capillary stable shape through "capillary imbibition" mechanism. The micromodel results presented above, show that in water-wet systems where positive capillary forces are present, this redistribution of oil and water does take place and it results in significant oil production (tests 2, 3, 4). However, in the tests with intermediate- or oil-wet tendency (tests 5 and 6 respectively) the redistribution process weakened and eventually stopped as the oil viscosity increased. There are two hypotheses for this distinctive behaviour of heavy oils under different wettability conditions.

(1) The heavy oils are well recognized to have non-Newtonian rheology due to their high asphaltene content (e.g. above 10% in this extra-heavy oil). When these

crude oils are in static conditions, asphaltenes can self assemble through physical interactions and form structural viscosity. Therefore, a certain amount of force has to be applied to the oil to break this structure and the crude oil flow in the porous media (Saniere et al., 2004; Wang et al., 2006). The driving force due to the pressure difference on both sides of the porous media is small after water breakthrough, which on its own might not be enough to displace the oil. In capillary dominant conditions the capillary forces are higher orders of magnitude than viscous forces, so if positive capillary forces can be present in the system (water-wet systems) they can assist the initial displacement of oil from the pores by overpowering the structural resistance. This explains why in systems where positive capillary forces are not present or are small, water cannot displace the residual oil after breakthrough or the production rate is lower than the case of water-wet systems.

(2) Another factor that causes weakening of heavy oil recovery process after water breakthrough compared to the case of light oils, is the fact that friction forces between oil and rock are significantly larger for heavy oils. In most areas of the reservoir the Reynolds number is considerably less than unity (Morrow and Heller, 1985) and flow is laminar. In laminar flow regime there is a direct relationship between viscosity and shear stress (Streeter et al., 1998). Existence of this resistance force can slow down or even stop flow of high viscous oils in narrow pores or deleteriously affect the process of oil production by oil film flow after water breakthrough.

Effect of Wettability on Trapping Mechanisms

It was mentioned in the previous section that an increase in oil viscosity increases the relative importance of viscous trapping mechanisms, compared to the other entrapment mechanisms that takes place in fewer pores. However, the strength of trapping mechanisms in different wettability conditions is a function of oil viscosity. The relationship between oil viscosity and entrapment mechanisms other than viscous fingering will be explained here.

In water-wet systems oil trapping takes place due to the capillary instability and bypassing mechanisms. Neither of these mechanisms are functions of oil viscosity and are only dependent on the wettability of the system. Therefore, the increase in oil

viscosity does not result in strengthening or weakening of these mechanisms as long as the displacement process remains capillary dominant.

In oil-wet systems, oil trapping is primarily due to surface trapping and by-passing mechanisms. The micromodel results showed that as oil viscosity increases, the thickness of oil films on oil-wet pore surfaces increase as well. Therefore, it is believed that an increase in oil viscosity enhances the surface trapping mechanism (despite the fact this mechanism occurs in a fewer number of pores compared to the case of light oils and therefore its relative importance on oil entrapment is reduced.

In the intermediate wet systems oil trapping take place mainly due to by-passing mechanism and partly due to capillary instability and surface trapping. While an increase in oil viscosity increases oil trapping by surface trapping the other two mechanisms remain unchanged. Table 4-3 summarizes the effect of viscosity increase on the trapping mechanisms under different wettability conditions.

Table 4-3: Effect of viscosity on trapping mechanisms.

Trapping Mechanisms	Viscous Fingering	Capillary Instability (Snap-off)	By Passing	Surface Trapping
Viscosity Ratio μ_o/μ_w ↑	↑	na	na	↑
Arrows indicate increasing (↑) and decreasing (↓) potential for trapping by various mechanisms as a function of viscosity.				

Effect of Wettability on Pore Scale displacement Mechanisms

In the previous section it was explained that in water-wet conditions the involved displacement mechanisms (corner filament flow and snap-off) are not dependent on oil viscosity. While similar behaviour was observed in the case of "channelling " and "piston type motion" mechanisms, the "oil film drainage" mechanism was observed to be largely dependent on viscosity of the oil phase in oil-wet and intermediate-wet conditions. In the experiment using this extra-heavy crude oil in oil-wetted conditions (Exp 6 and Exp 7) the oil recovery by oil film drainage mechanism was adversely affected by high oil viscosity and completely stopped. This is believed to be a

consequence of high frictional forces between the oil and pore surface, which prohibit film flow and production of the remaining oil.

4.4 FIELD APPLICATIONS

The results from the micromodel tests vividly show that the trapping forces involved and the distribution of residual oil are different in the case of heavy and light oils. In the case of light oils trapping forces are capillary type therefore, a reasonable option to enhance oil recovery is eliminating these forces. The rationale behind a wide use of surfactant and alkaline or their derivatives in EOR processes, is removing capillary forces by dropping interfacial tension by orders of magnitude. In the case of heavy oils most oil entrapment is induced by viscous forces, thus elimination of capillary forces by IFT reduction has no impact on this type of trapping on its own (this is a different scenario if IFT reduction results in other displacement mechanisms e.g. emulsification). On the other hand, injection of chemicals to drop IFT might adversely affect the process of oil recovery by a number of mechanisms. It was explained that in water-wet systems existence of positive capillary forces can assist process of oil recovery by "capillary imbibition" mechanism after water breakthrough; IFT reduction might negatively affect this recovery mechanism. Furthermore, flow of injected chemicals in water swept regions of the reservoir might reduce saturation of residual oil, which in turn eases off flow of water through existing fingers of water (increase relative permeability to water) and slow down development of these water fingers towards oil saturated regions of the reservoir.

It can also be recommended that performance of waterflood process in a heavy oil reservoir is enhanced by employing different techniques to shift wettability towards more water-wet conditions, e.g. injection of suitable alkaline solutions, surfactants or by changing composition of injected water. In heavy oil reservoirs that most oil production takes place after water breakthrough and at high water-cuts, even a slight improvement in water cut can make a significant contribution to final oil recovery. The other important point that should be taken into account is that wettability alteration from water-wet to oil-wet (which is known as an EOR technique) for increasing the recovery of conventional crude oils cannot be employed in heavy oil reservoirs. Even if the wettability alteration towards an oil-wet condition is a side effect of other operational activities in the field it needs careful consideration before being applied in the field as it can significantly reduce the rate of heavy oil recovery.

4.5 SUMMARY AND CONCLUSIONS

The main objective of this study was to investigate the pore scale mechanisms of displacement and entrapment during heavy oil waterflood and highlight the differences with the case of light oil waterflood under different wettability conditions. A total number of more than 100 micromodel tests were performed using light, medium-heavy and extra-heavy crude oils at different wettability conditions and the results of a few of them were presented here. The main conclusions drawn from these experiments are:

- The pore scale displacement mechanisms, during heavy oil waterflood, are not dependent on the viscosity of the oil phase as long as the process remains capillary dominant. The only exception is oil film drainage mechanism that might be significantly weakened and stop as oil viscosity increases.
- If viscosity increases cause conditions of viscous dominant flow, oil displacement mechanisms will be limited to piston type withdrawal and water channelling respectively in the water- and oil-wet systems. In the intermediate-wet systems a combination of these two recovery mechanisms exist.
- Oil entrapment in conventional (light) oils is due to the capillary forces that are in the form of separated pieces of oil completely surrounded by water, however, in heavy oils trapping is primarily due to the viscous forces (viscous fingering mechanism) and the residual oil remains continuous in the porous media. Therefore, to remobilize the trapped oil in heavy oil reservoirs a different approach from that of light oils is needed to improve oil recovery from heavy oil reservoirs.
- Heavy oil recovery before water breakthrough was observed to be principally controlled by the oil/water viscosity ratio and is not a strong function of wettability of the system.
- The capillary forces and state of wettability of the system play very important roles in determining heavy oil recovery after water breakthrough, which is different from the general assumption that capillary forces are not greatly involved in recovery process due to the high viscosity of these crudes.
- The highest recovery in the case of heavy oil waterflood was achieved in strongly water-wet system where the positive capillary forces were strongest. The recovery efficiency by waterflood dropped as the system shifted towards intermediate- and oil-wet conditions.

- It was concluded that the optimum conditions for oil recovery, shifts from intermediate-wet conditions for systems with moderate oil/water viscosity ratio towards increased water-wet conditions as the viscosity of the crude oil increases. This is due to the fact that capillary forces add to the driving force and enhance displacement of residual oil by "capillary imbibition" mechanism.
- Wettability modification toward increased water-wet conditions can promote the "capillary imbibition" mechanism and consequently improve performance of waterflood process in heavy oil reservoirs.

CHAPTER 5 VISUAL INVESTIGATION OF EXTRA-HEAVY OIL RECOVERY BY CO2 INJECTION IN CRUDE "C"

5.1 INTRODUCTION

This chapter presents the results of a series of visualisation experiments to investigate the performance of gravity-stable CO2 injection in crude "C" for recovery improvement and CO2 storage purposes. This study provides a better understanding of the pore scale mechanisms involved, during CO2 injection in this specific extra-heavy crude oil.

At reservoir conditions of crude "C" CO2 would be present in vapour state. Therefore, the CO2 dissolution and gravity forces are expected to play important role in recovery of this extra-heavy crude oil. All the micromodel experiments in this chapter were performed using the heterogeneous rock-look-alike pattern micromodel. The experiments using crude "C" show that system remains water-wet even after extended period of aging.

In the first part the effect of different injection strategies and combination with water (CO2 injection before, after or simultaneous with water injection) is investigated. The second part reports results of a series of novel micromodel experiments to investigate the effect of mobility control by CO2-foam flood and pore scale interactions between foam bubbles and heavy oil.

5.2 THE EFFECT OF INJECTION STRATEGY

In this section, three scenarios of CO2 injection are investigated using micromodel experiments. The first scenario simulates the case of CO2 injection and storage in a

mature heavy oil reservoir, which has already been flooded with water. The second scenario looks into the process of CO2 injection in a reservoir prior to waterflood, where the oil phase is still connected within the porous medium. Secondary injection of CO2 in heavy oil reservoirs is viable in the reservoirs where an adequate volume of CO2 is available (e.g. supply from power plants or steam generation plants). The third scenario was designed to investigate the performance of simultaneous injection of water and CO2 (CO2-SWAG) in this heavy crude oil. Water-alternating-gas (WAG) injection technology and its derivatives (including CO2-SWAG) are being increasingly applied in oil reservoirs, which may improve oil recovery efficiency by combining benefits of water and gas injection processes (Sohrabi et al., 2000b).

5.2.1 MM Exp 8: Tertiary (Post-Waterflood) CO2 Injection

The theoretical section explained that despite a highly unfavourable viscosity ratio between water and heavy oil, waterflooding is often employed in heavy oil reservoirs, both along or after primary recovery, in order to re-pressurize the reservoir and displace oil towards producing wells. The main advantages of waterflood are its low cost and widespread practise around the world. However, for heavy oil reservoirs (with oil viscosities above 1000 cp) primary production and waterflood can usually only recover up to 10% of the original oil in place. This means that at the end of waterflood there are still significant oil resources remaining as potential for EOR (enhanced oil recovery).

The first experiment was designed and carried out, with the main objective of simulating the process of immiscible CO2 injection after an initial waterflood. The main question in tertiary CO2 flood, is whether injected CO2 would displace the oil or merely finger through the continuous path of water created during the preceding waterflood. This is a very important point, because if injected CO2 does not contact residual oil, there will not be much oil displacement and recovery by CO2. Instead there will be a premature CO2 breakthrough (BT), with not much oil recovery after breakthrough through mechanisms like gravity drainage.

Procedure

1 *Initialization:* Micromodel was saturated with distilled water at T = 44 °C and P = 600 psig.

2 *Oil Flood:* Micromodel was flooded with crude oil "C" from bottom until the oil front reached the other end of the micromodel.

3 *1st Waterflood*: DW was injected in the micromodel for 3 days.

4 *CO2 Flood*: CO2 was injected in the micromodel for 2 days.

5 *2nd Waterflood*: DW was injected in the micromodel for 1 day.

Table 5-1 lists a summary of the fluids, the porous medium and the pressure and temperature setting used for this experiment.

Table 5-1: The fluids, porous medium and pressure and temperature setting used for MM Exp 8.

Porous Medium	Heterogeneous Rock-look-alike Micromodel
Crude Oil	"C" (8700 cp @ 50 °C)
Aqueous Phase	Distilled Water
Gas Phase	CO2
Temperature	44 °C
Pressure	600 psig

Results

Initialization and Oil Injection

The experiment began by saturating the micromodel with distilled water at 44 °C and 600 psig. To establish the initial saturation, crude oil C was injected through the micromodel. Since oil viscosity at experimental temperature was orders of magnitude higher than water viscosity, very high oil saturation was achieved at the end of the oil injection period; with water remaining mostly in dead end pores and in pores whose pore geometry would not allow displacement of water. Figure 5-1 and Figure 5-7a show the distribution of oil and connate water respectively, in a magnified section and the full length of micromodel at the end of oil injection period.

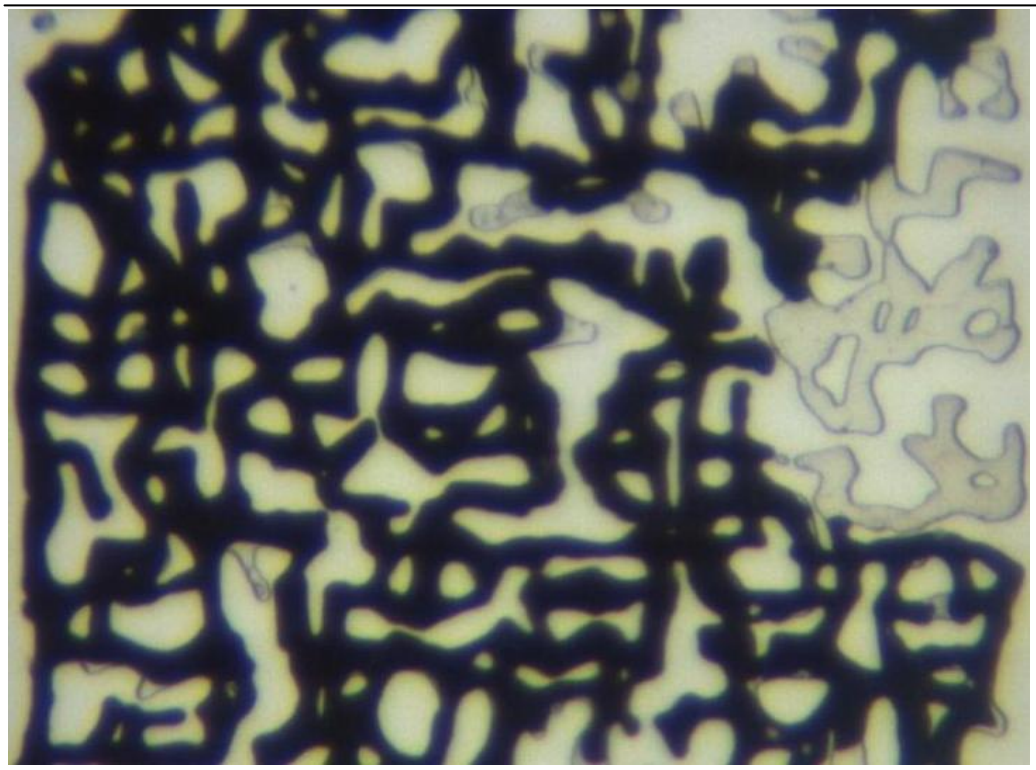

Figure 5-1: MM Exp 8; a magnified section of the micromodel at the end of the period of oil injection.

1st Water Injection

Having carried out the oil injection described above, the micromodel was then flooded with water. With the glass porous medium retaining its water-wet characteristics, the injected water was observed to flow and displace oil, mostly through corner filament flow mechanism and through piston type displacement mechanism in fewer pores. Figure 5-2 and Figure 5-7 illustrate the same magnified section and full length pictures of the micromodel respectively, after water breakthrough. Since vertical connectivity of the left side of the micromodel is considerably higher than its right side, the front of the water flowed originally in the left side of the micromodel. However, as water injection continued, oil recovery and change in water/oil distribution also continued and the flowing water affected a progressively larger area on the right side of the micromodel. Figure 5-3 and Figure 5-7 show the magnified section and full length pictures of the micromodel respectively, at the end of the period of waterflood. It can be seen that the originally narrow path of water continued to grow laterally from the left to right side of the micromodel, as a result of the capillary imbibitions mechanism explained in the previous chapter.

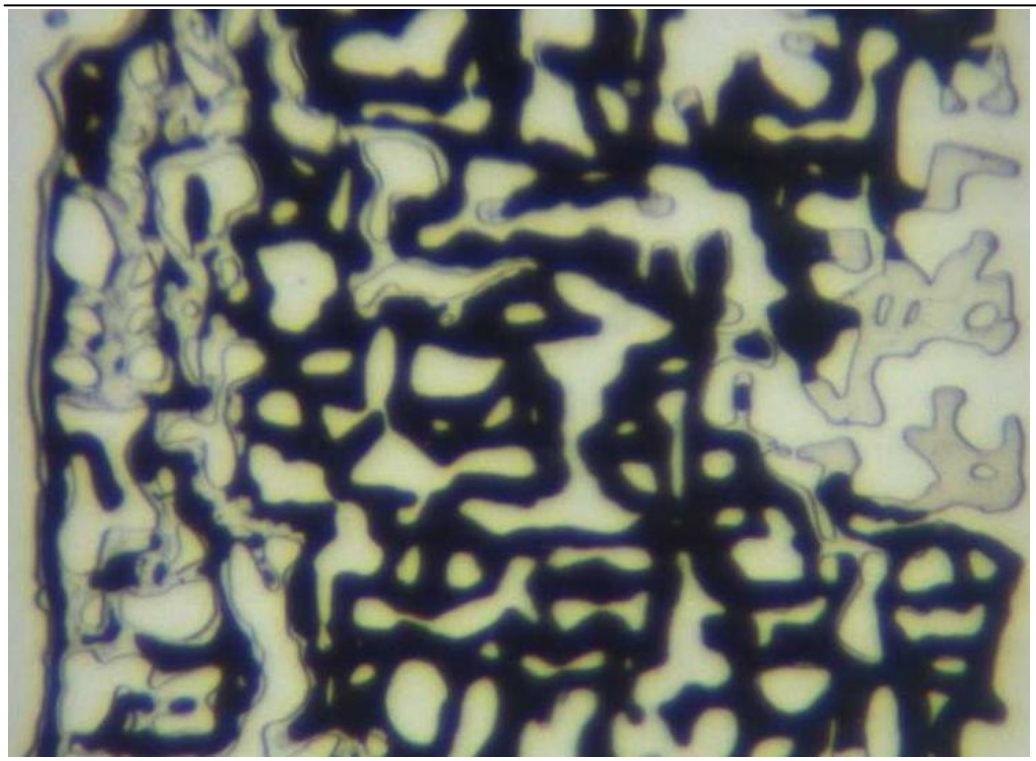

Figure 5-2: MM Exp 8; the same magnified section of the micromodel at breakthrough time during the 1st period of water injection.

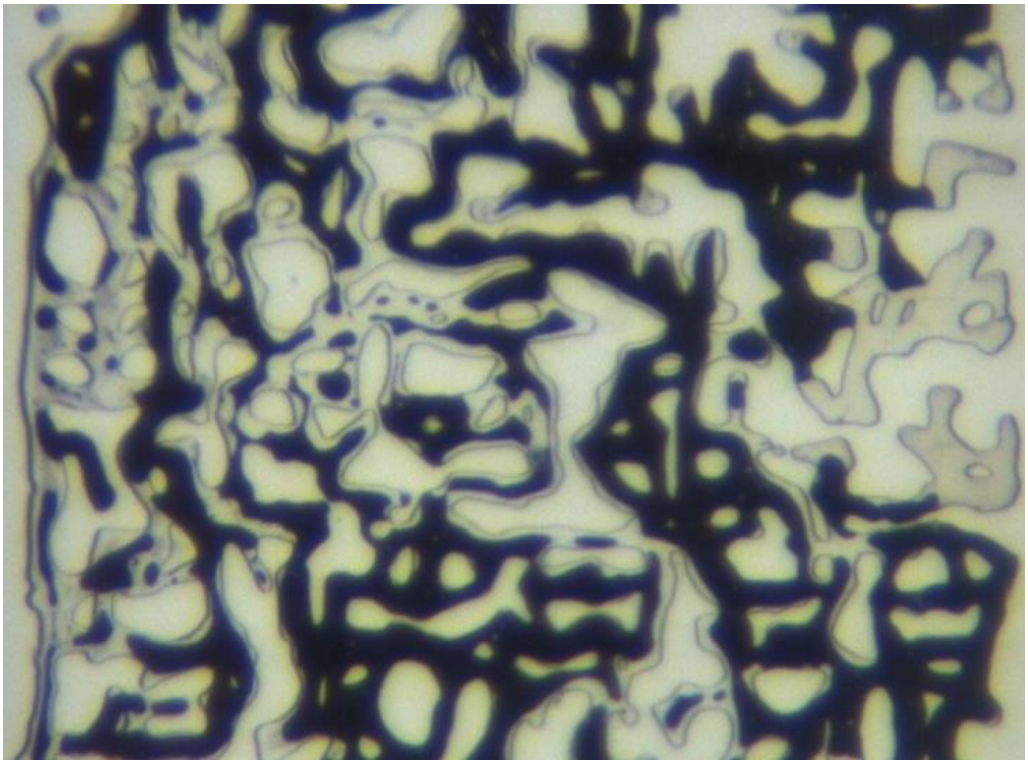

Figure 5-3: MM Exp 8; the magnified section of the micromodel at the end of the 1st period of water injection.

Tertiary CO2 Injection

After the initial water injection, CO2 injection commenced from top of the micromodel to simulate gravity stable displacement conditions. Being a non-wetting phase, the injected CO2 was observed to flow in the middle of the pores as opposed to water (wetting phase), which flowed in layers on the walls of micromodel pores in the preceding water injection period. During invasion of the porous medium by CO2, as the CO2 front advanced towards the producing end of the micromodel, crude oil was observed to spread between CO2 and water phases showing a positive oil spreading behaviour. In areas with relatively high oil saturation a small bank of oil was formed ahead of the CO2 front, which was displaced through a double-drainage displacement mechanism (Oren, 1994; Sohrabi et al., 2000b). Figure 5-4 and Figure 5-7 present the magnified section and full length picture of the micromodel respectively, after CO2 breakthrough.

As can be seen in these figures, the sweep efficiency as a result of direct displacement of heavy oil by CO2 was rather poor. There are two main reasons for this poor performance: firstly, *the viscosity contrast* between CO2 and crude oil, which resulted in a very unfavourable mobility ratio and hence injected CO2 fingered through the porous medium leaving behind most of the resident oil; and secondly, the *high water saturation* that disconnected the oil and further reduced its mobility.

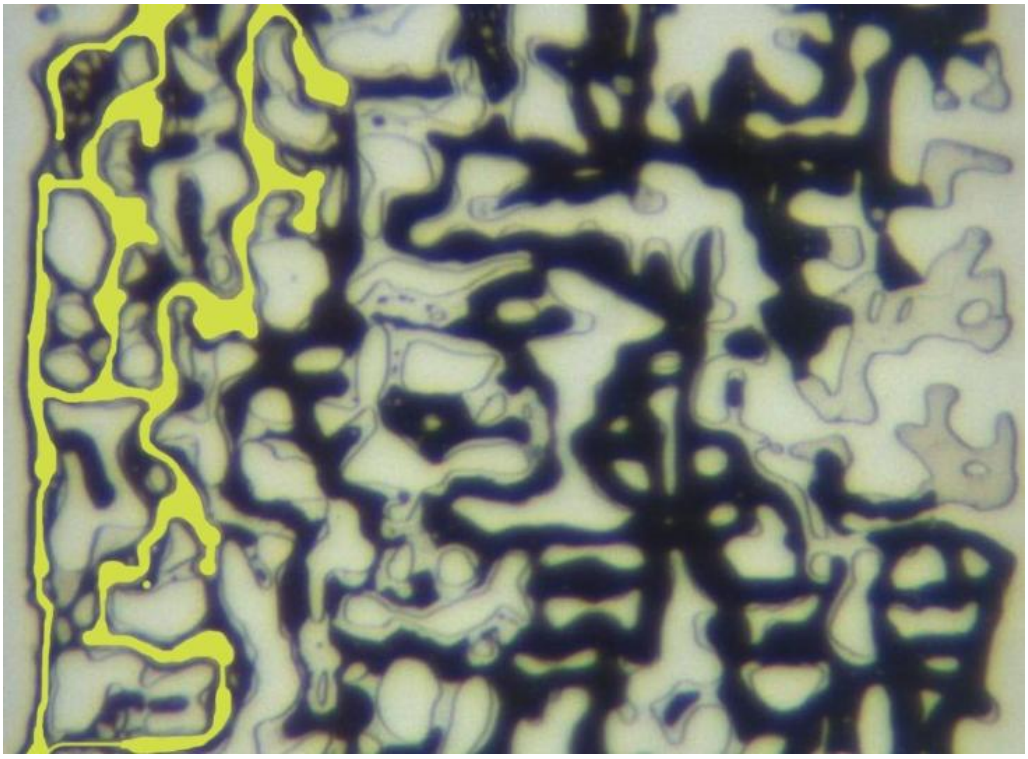

Figure 5-4: MM Exp 8; the magnified section of the micromodel at breakthrough time during the 1st period of water injection.

The injection of CO2 through the micromodel continued for two days, which resulted in significant dilution of the heavy crude oil. Figure 5-5 and Figure 5-7 show the magnified section and full length pictures of the micromodel respectively, after two days of CO2 injection. As shown, the colour of the area of crude oil, which is in direct contact with CO2, has changed from black to brown. This is a good indication of CO2 dissolution and dilution of the crude oil to a lighter mixture of oil and CO2. The fragmented red line in this picture demonstrates a layer of water in between the residence oil, which prohibits the injected CO2 from being in direct contact with oil on the right side of the micromodel. Although there is slight discolouring of oil on the right side of the micromodel, it is not comparable with the extent of colour change on the left side of the micromodel, which is in direct contact with CO2. This implies that secondary (pre-waterflooding) injection of CO2, in which the oil phase is mainly connected and continuous, would result in a more efficient process and hence higher oil recovery.

The dissolution of CO2 in the crude significantly reduced its viscosity and a small fraction of diluted oil was produced through layers of oil around the stream of CO2 during the extended period of CO2 injection; however, the overall recovery remained low.

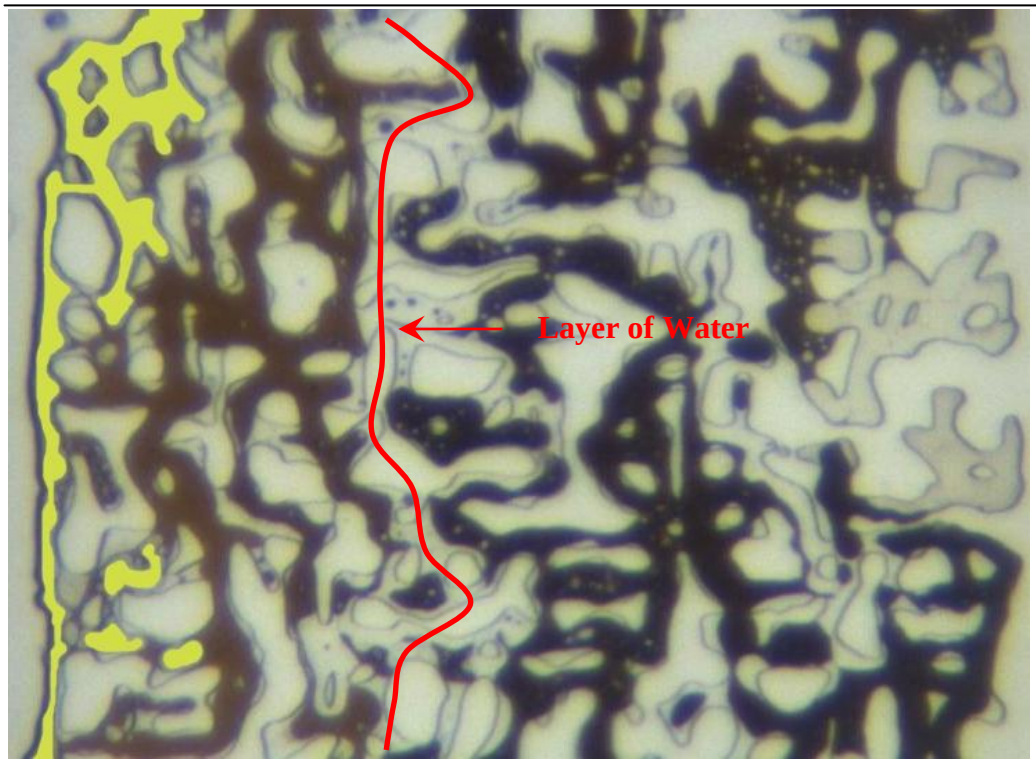

Figure 5-5: MM Exp 8; the magnified section of the micromodel at the end of the period of CO2 injection.

2nd Water Injection

The extended period of CO_2 injection was followed by the second period of water injection, which continued for a day. The flow of water caused fragmentation of CO2 phase in the micromodel and the continuous CO2 path became discontinuous and fragmented in the porous medium. Water was also observed to dissolve the CO2 and eventually all CO2 contained in the micromodel was dissolved in flood water at the end of the water injection period. Figure 5-6 and Figure 5-7 show the magnified section and full length pictures of the micromodel at the end of the second water injection period.

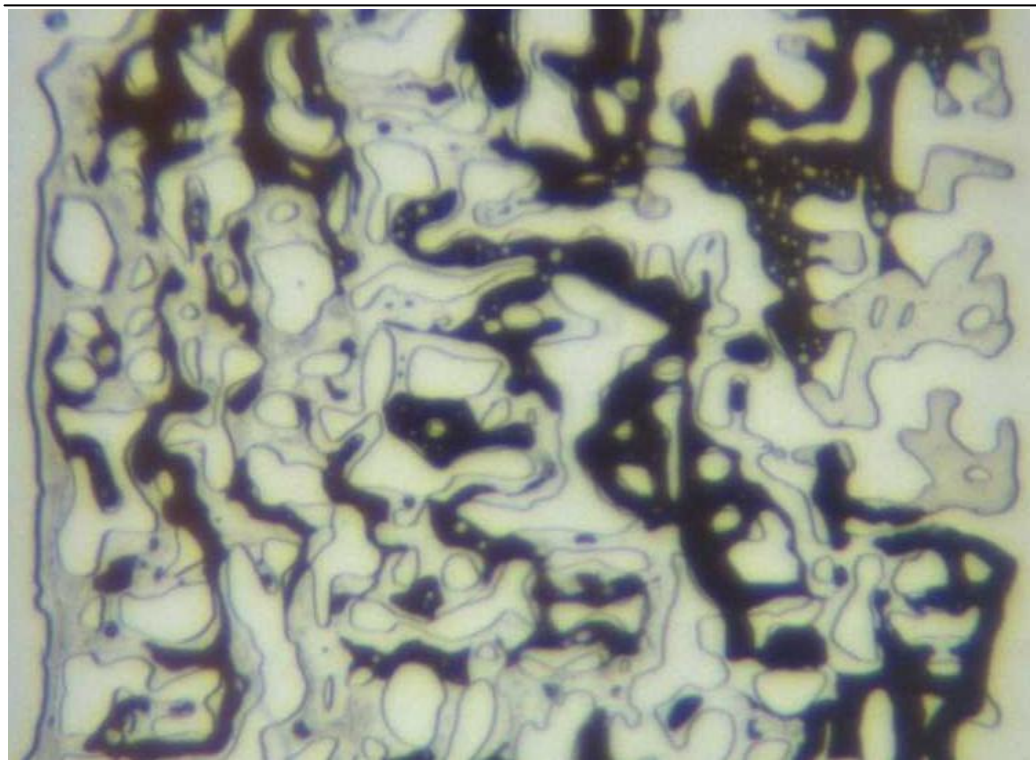

Figure 5-6: MM Exp 8; the magnified section of the micromodel at the end of the 2nd period of water injection.

Summary

Table 5-2 summarises the oil recovery data at breakthrough time and at the end of each stage of this experiment (MM Exp 8). A comparison of the recovery data shows that significant additional recovery has been obtained during the second period of water injection. The preceding CO2 injection significantly reduced viscosity of the oil and this diluted oil was readily mobilised and produced during the subsequent water injection period.

Table 5-2: MM Exp 8; Summary of the recovery data.

	Recovery @ BT (% OOIP)	Ultimate Recovery (% OOIP)	Cumulative Recovery (% OOIP)
1) 1st Waterflood	11	17	17
2) CO2 flood	6	8*	25
3) 2nd Waterflood	-	23	48
• A swelling factor of 5.5% has been considered for calculation of oil recovery.			

Figure 5-7: MM Exp 8; fluid distribution in the micromodel (a) after oil injection, (b) at breakthrough during 1st water injection, (c) after 1st water injection.

d **e** **f**

Figure 5-7 (continued): MM Exp 8; fluid distribution in the micromodel (d) at breakthrough time during CO2 injection, (e) after CO2 injection, (f) after 2nd water injection.

5.2.2 MM Exp 9: Secondary (Pre-Waterflood) CO2 Injection

The previous experiment (Exp 8) showed that water saturation and distribution in the porous medium had a very important impact on recovery of oil by immiscible CO2 injection. The presence of water can adversely affect dilution and recovery of that part of resident oil, which is not in direct contact with the CO2 stream and is separated by water layers. Furthermore, high water saturation significantly reduces the mobility of diluted oil in the system. A new micromodel experiment was designed and carried out to determine the level of additional oil recovery by immiscible CO2 injection in secondary mode (before waterflooding) and was compared with oil recovery by CO2 injection in tertiary mode (after waterflooding). The experiment consisted of an extended period of CO2 injection to simulate secondary injection of CO2.

Procedure

1 *Initialization:* Micromodel was saturated with distilled water at T = 44 °C and P = 600 psig.

2 *Oil Flood:* Micromodel was flooded with crude oil "C" from bottom until the oil front reached the other end of the micromodel.

3 *CO2 Flood*: CO2 was injected in the micromodel for 2 days.

Table 5-3 lists a summary of the fluids, the porous medium and the pressure and temperature setting used for this experiment.

Table 5-3: The fluids, porous medium and pressure and temperature setting used for.MM Exp 9.

Porous Medium	Heterogeneous Rock-look-alike Micromodel
Crude Oil	"C" (8700 cp @ 50 °C)
Aqueous Phase	Distilled Water
Gas Phase	CO2
Temperature	44 °C
Pressure	600 psig

Results

Initialization and Oil Injection

The experiment began by saturating the micromodel with distilled water at 44 °C and 600 psig. Then, to establish the initial oil saturation, the extra-heavy crude oil "C" was

injected through the micromodel. Injection of oil continued until oil reached the other end of the micromodel pattern. Due to high viscosity contrast between oil and water, a very high level of oil saturation was achieved at the end of the oil injection period. Figure 5-8 and Figure 5-14a show a magnified section and the full length pictures of the micromodel at the end of the oil injection period.

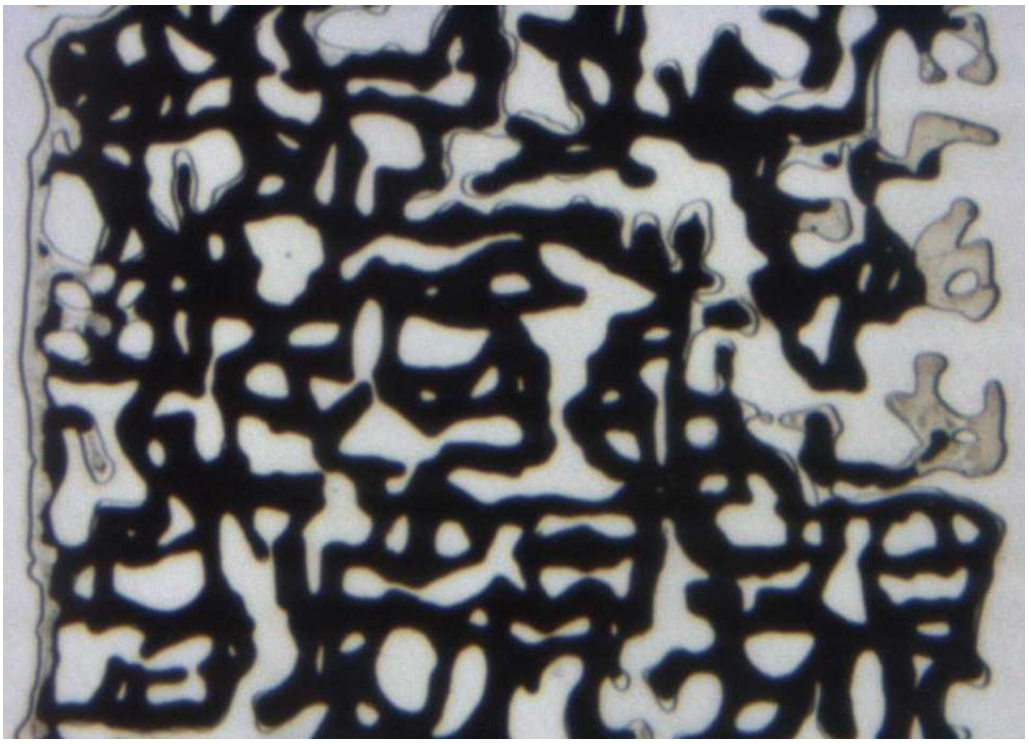

Figure 5-8: MM Exp 9; a magnified section of the micromodel at the end of the period of oil injection.

Secondary CO2 Injection

Having carried out the oil injection described above, the micromodel was then flooded with CO2. The injected CO2 opened a flowing path on the left side of the micromodel, where the vertical connectivity was higher. Figure 5-9 and Figure 5-14b show the magnified section and the full length pictures respectively of the micromodel after CO2 breakthrough. As shown, due to the high viscosity contrast between CO2 and heavy oil, the recovery at breakthrough time was low.

As the CO2 injection continued after the breakthrough, the CO2 stream readily widened towards the right side of the micromodel and accessed oil which was bypassed by CO2 in the low connectivity part (right side) of the micromodel. Figure 5-10 to Figure 5-13 show the sequence of magnified sections of micromodel respectively after 3 hours, 6

hours, 1 day and 2days of CO2 injection. The resident oil was initially diluted as a result of dissolution of CO2 (this can be identified from the change of oil colour in Figure 5-10 and Figure 5-11 compared to Figure 5-9) and then mobilized due to the gravitational force. This behaviour had not been observed in the first (tertiary) experiment due to the water shielding effect, which prevented the CO2 stream developing towards the right side of the micromodel, resulting in significant saturation of residual oil. Pictures (c) to (f) in Figure 5-14 show the full length picture of micromodel during the period of CO2 flood, in which recovery improvement as a result of widening the CO2 stream towards the right side of the micromodel can be clearly seen. Table 5-4 summarises the oil recovery data at different stages of this micromodel experiment (MM Exp 9).

Figure 5-9: MM Exp 9; the same magnified section of the micromodel at breakthrough time during the period of CO2 injection.

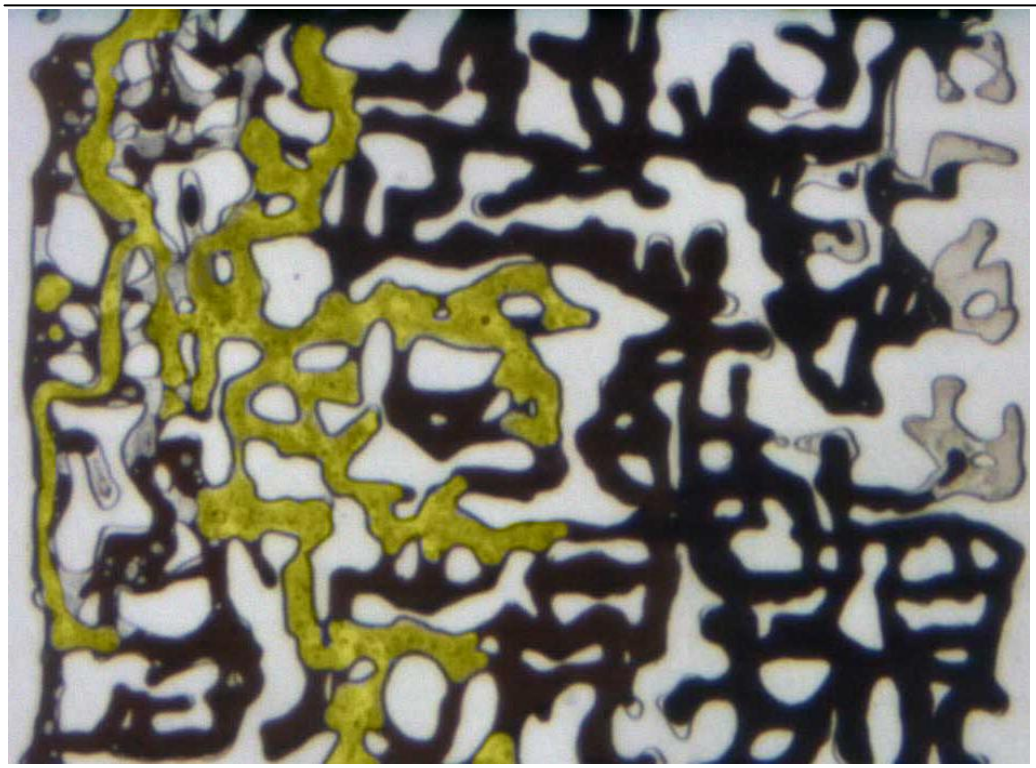

Figure 5-10: MM Exp 9; the magnified section of the micromodel after 3 hours of CO2 injection.

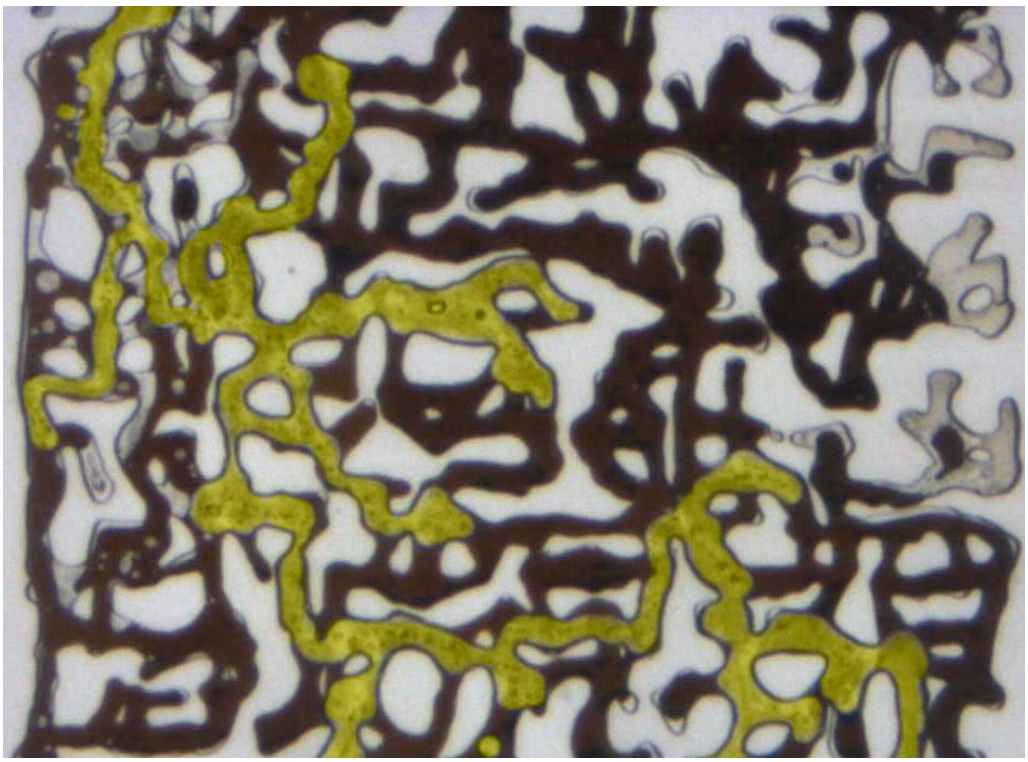

Figure 5-11: MM Exp 9; the magnified section of the micromodel after 6 hours of CO2 injection.

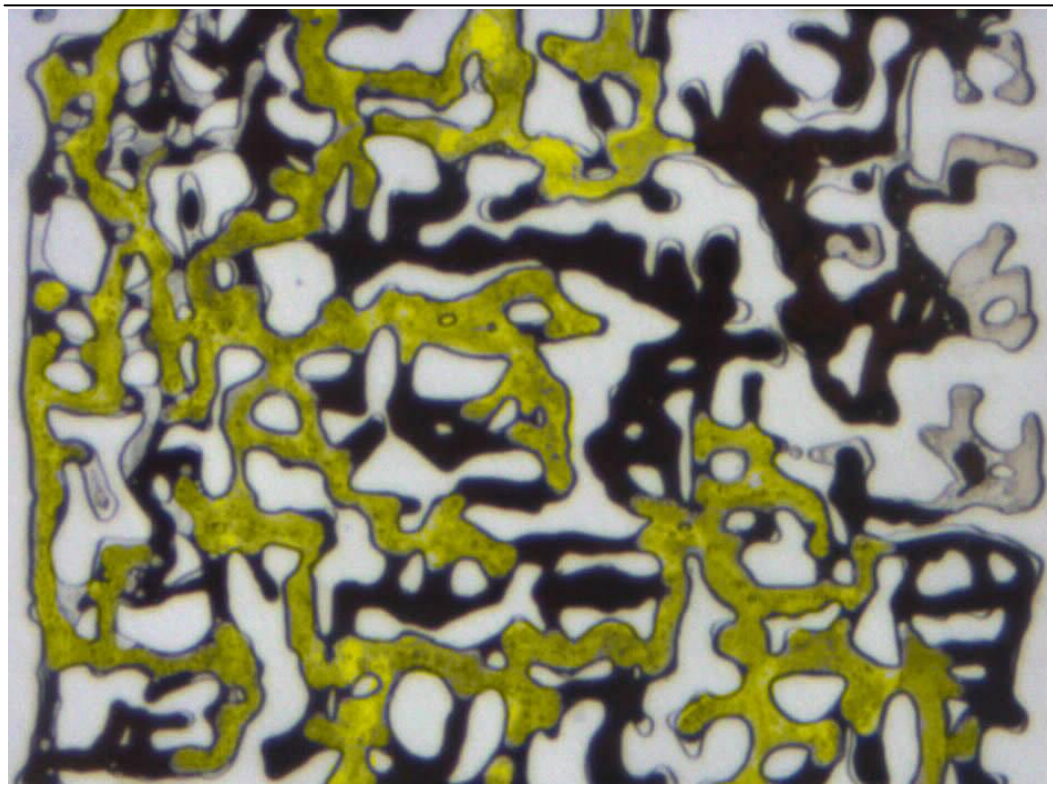

Figure 5-12: MM Exp 9; the magnified section of the micromodel after 1 day of CO2 injection.

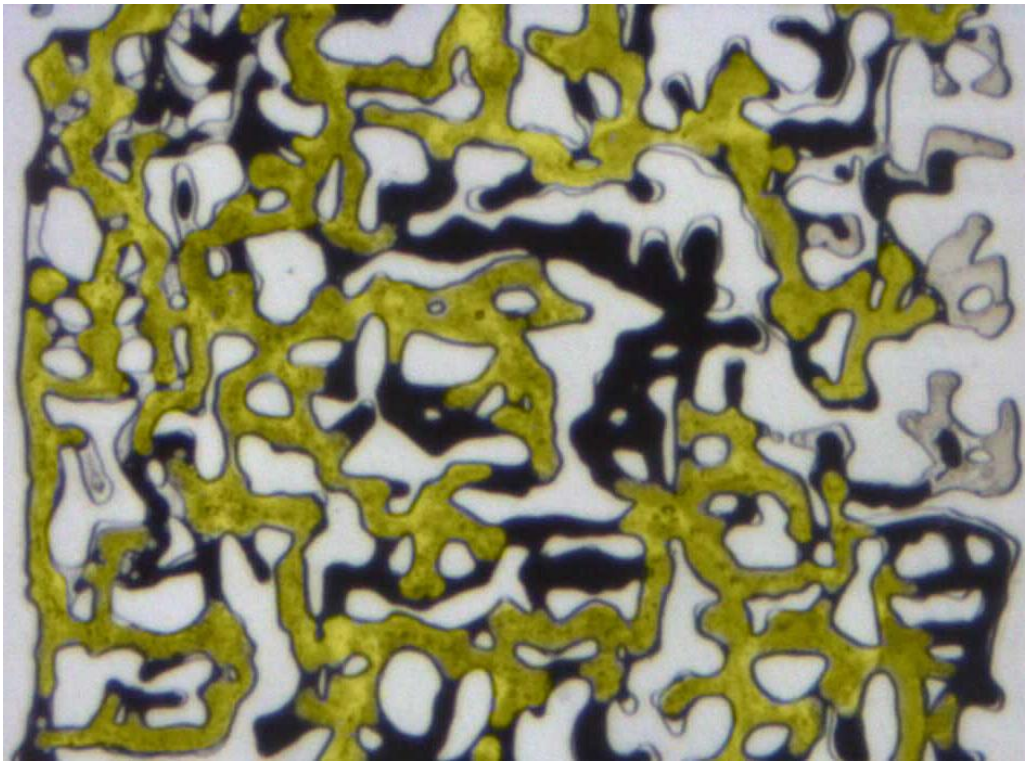

Figure 5-13: MM Exp 9; the magnified section of the micromodel at the end of the period of CO2 injection (2 days).

Table 5-4: MM Exp 9; Summary of the recovery data.

CO2 Injection	Recovery (% OOIP)
1) Breakthrough	13
2) 3 hours	23
3) 6 hours	36
4) 1 day	51*
5) 2 days	59*
A swelling factor of 5.5% has been considered for calculation of oil recovery.	

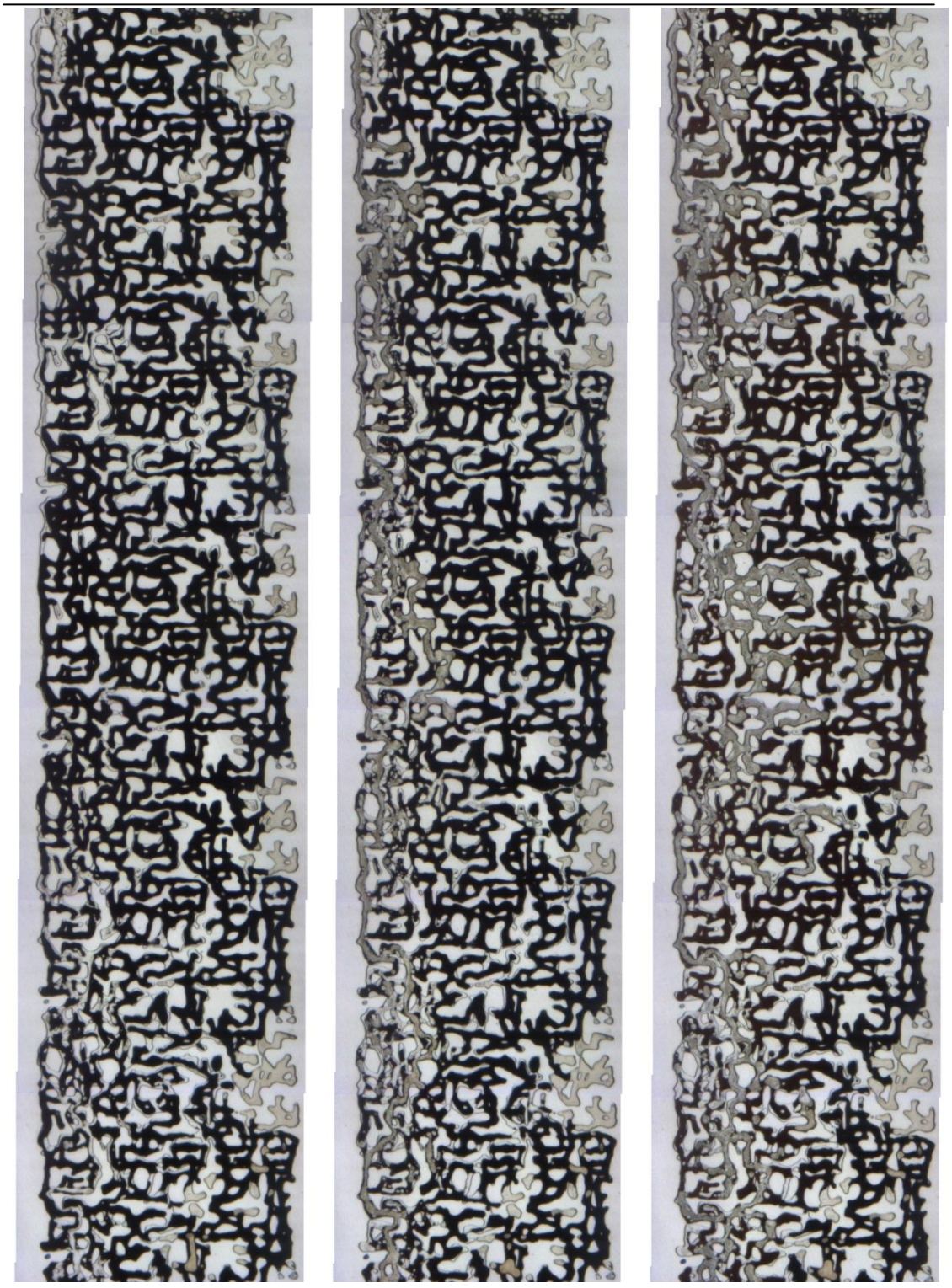

a **b** **c**

Figure 5-14: MM Exp 9; fluid distribution in the micromodel after (a) oil injection, (b) CO2 breakthrough and, (c) 3 hours of CO2 injection.

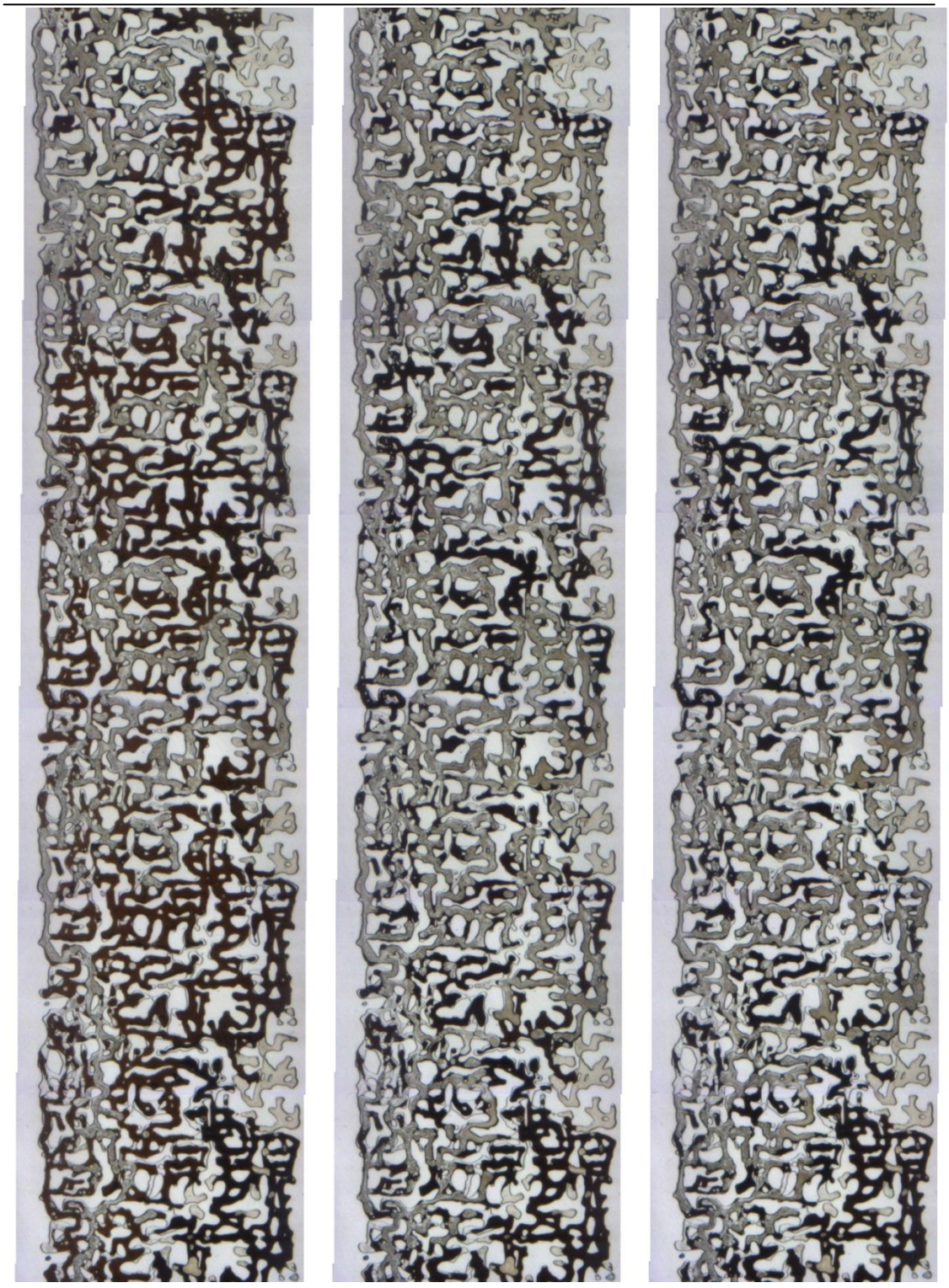

d **e** **f**

Figure 5-14 (continue): MM Exp 9; fluid distribution in the micromodel after (d) 6 hours, (e) 1 day and, (f) 2 days of CO2 injection.

5.2.3 MM Exp 10: CO2-SWAG Injection

Water-alternating-gas (WAG) injection technology and its derivatives (e.g. SWAG) are being increasingly applied as improved oil recovery methods (Sohrabi et al., 2000b). These techniques combine the effects of two traditional oil recovery methods: improved microscopic displacement efficiency of the gas flooding with an improved macroscopic sweep by injection of water. Additionally the oil recovery is also attributed to the contact of unswept zones, especially recovery of attic oil, as a result of gas rising towards the top and deposition of water towards the bottom of the reservoir. A number of micromodel tests were performed to investigate the impact of simultaneous injection of CO2 and water (CO2-SWAG) in this heavy oil, with one set of test results reported here.

It is worth mentioning that CO2-SWAG injection tests are generally conducted using pre-equilibrating fluids, to avoid dissolution of CO2 into the oil and water. However, dissolution of CO2 significantly reduces heavy oil viscosity, which makes the comparison of recovery at early times with other tests very difficult. Therefore, in this test, dead oil was used instead of a CO2-saturated heavy oil sample.

This experiment consisted of a period of water flood, which was then followed with an extended period of CO2-SWAG injection. The objective of the experiment was to visually investigate the pore scale events during CO2-SWAG injection in this heavy crude oil and at the same time investigate the possibility of spontaneous formation of foam and emulsion during the SWAG injection process. Crude oil "C" contains a high content of surface active materials and shows foamy behaviour during flow in porous media.

Procedure

1 *Initialization:* Micromodel was saturated with distilled water at T = 44 °C and P = 600 psig.

2 *Oil Flood:* Micromodel was flooded with crude oil "C" from bottom until the oil front reached the other end of the micromodel.

3 *CO2/water Co-Injection*: CO2 and water were simultaneously injected from the top of the micromodel at a volumetric ratio of 1:1 (maintaining the total injection rate of 0.01 cc/hr) for 2 days.

4 *Water Injection*: distilled water was injected in the micromodel for 1 day.

Table 5-5 lists a summary of the fluids used and the pressure and temperature at which the test was carried out.

Table 5-5: Fluids used and pressure and temperature conditions of MM Exp 10.

Porous Medium	Heterogeneous Rock-look-alike Micromodel
Crude Oil	"C" (8700 cp @ 50 °C)
Aqueous Phase	Distilled Water
Gas Phase	CO2
Temperature	44 °C
Pressure	600 psig

Results

Initialization and Oil Injection

The experiment began by saturating the micromodel with distilled water at 44 °C and 600 psig. Then, to establish initial oil and connate water saturation, crude "C" was injected through the micromodel. Injection of oil continued until oil reached the other end of the micromodel pattern. Figure 5-15 and Figure 5-22a show a magnified section and full length picture of the micromodel respectively, at the end of the oil injection period.

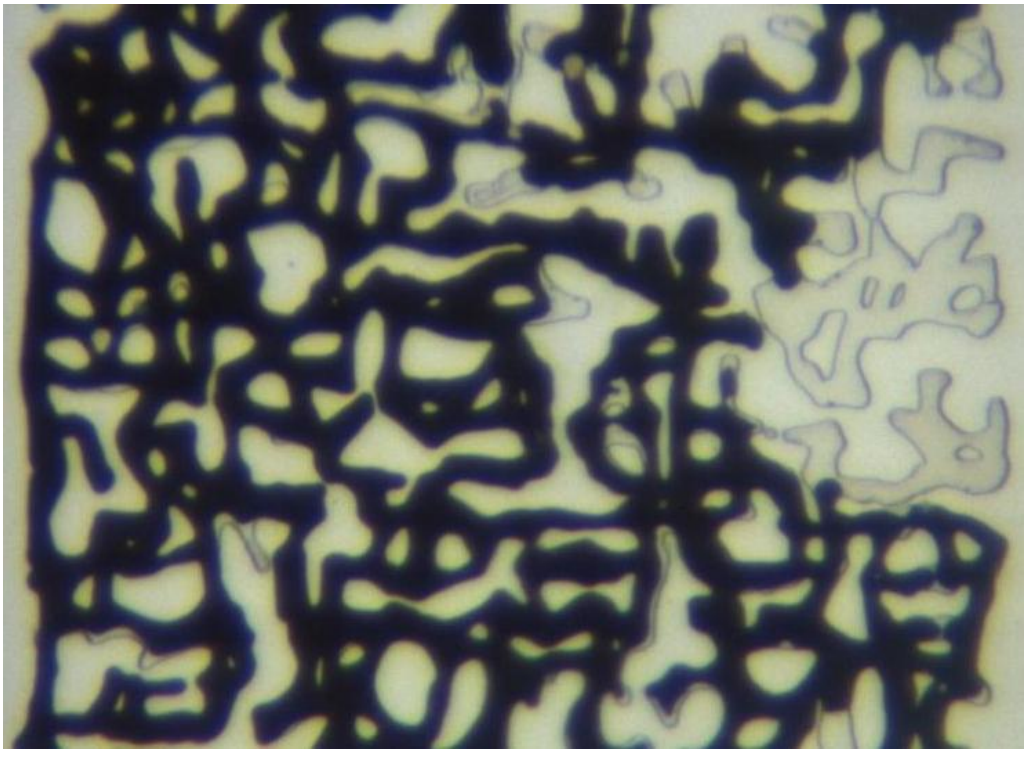

Figure 5-15: MM Exp 10; a magnified section of the micromodel at the end of the period of oil injection.

CO2/Water Co-Injection

Having carried out the oil injection described above, simultaneous injection of water and CO2 (CO2-SWAG) began and continued for two days. The sequence of images from Figure 5-16 to Figure 5-20 illustrates the distribution of fluids and oil recovery in the magnified section of micromodel at various times during the period of CO2-SWAG injection. The injected water/CO2 initially opened a flowing path on the left side of the micromodel, where the vertical connectivity was higher. This resulted in a low oil recovery at breakthrough time, as can be seen in Figure 5-16. However, as CO2-SWAG injection continued, CO2 and water gradually spread towards the low connectivity parts of the micromodel on the right side (Figure 5-17, Figure 5-18, Figure 5-19). During the CO2-SWAG injection period, water was observed to fragment CO2 by snap-off process and the fragmented pieces of CO2 spread over a larger area of the micromodel. Figure 5-20 shows the magnified section of micromodel at the end of CO2-SWAG injection period, when fragments of CO2 are scattered in a large area of the micromodel. The sequence of images from Figure 5-22b to Figure 5-22e also illustrate the distribution of fluids and oil recovery in the full length section of micromodel, at various times during the period of CO2-SWAG injection.

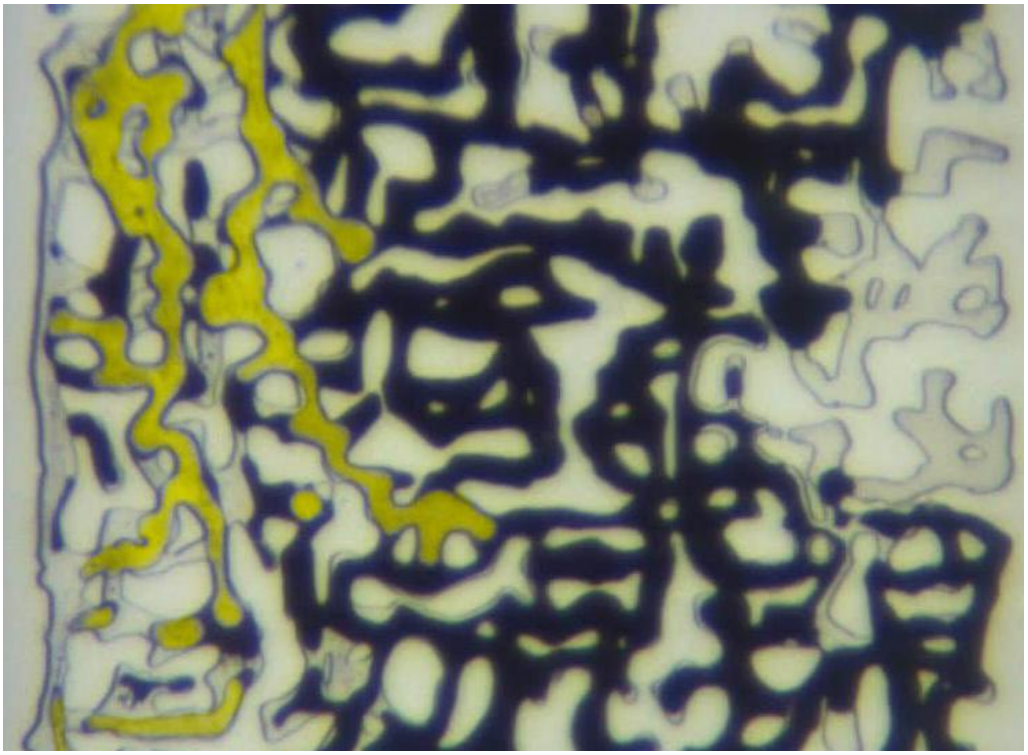

Figure 5-16: MM Exp 10; the same magnified section of the micromodel at breakthrough time during the period of CO2/water co-injection.

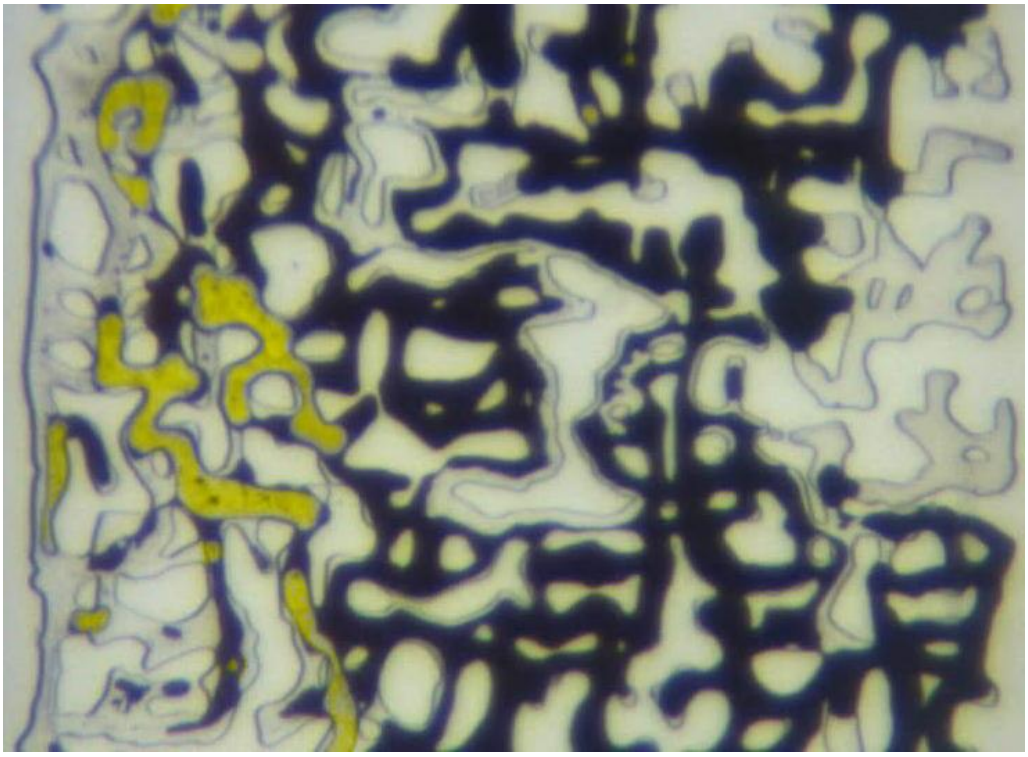

Figure 5-17: MM Exp 10; the magnified section of the micromodel after 6 hours of CO2/water co-injection.

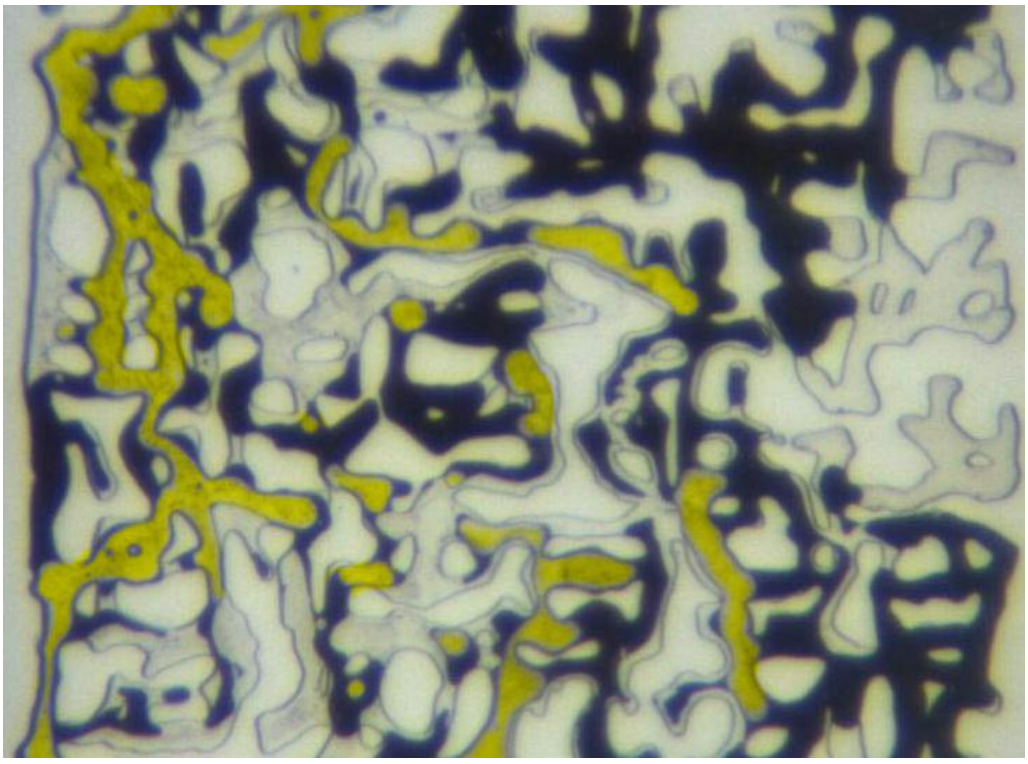

Figure 5-18: MM Exp 10; the magnified section of the micromodel after 12 hours of CO2/water co-injection.

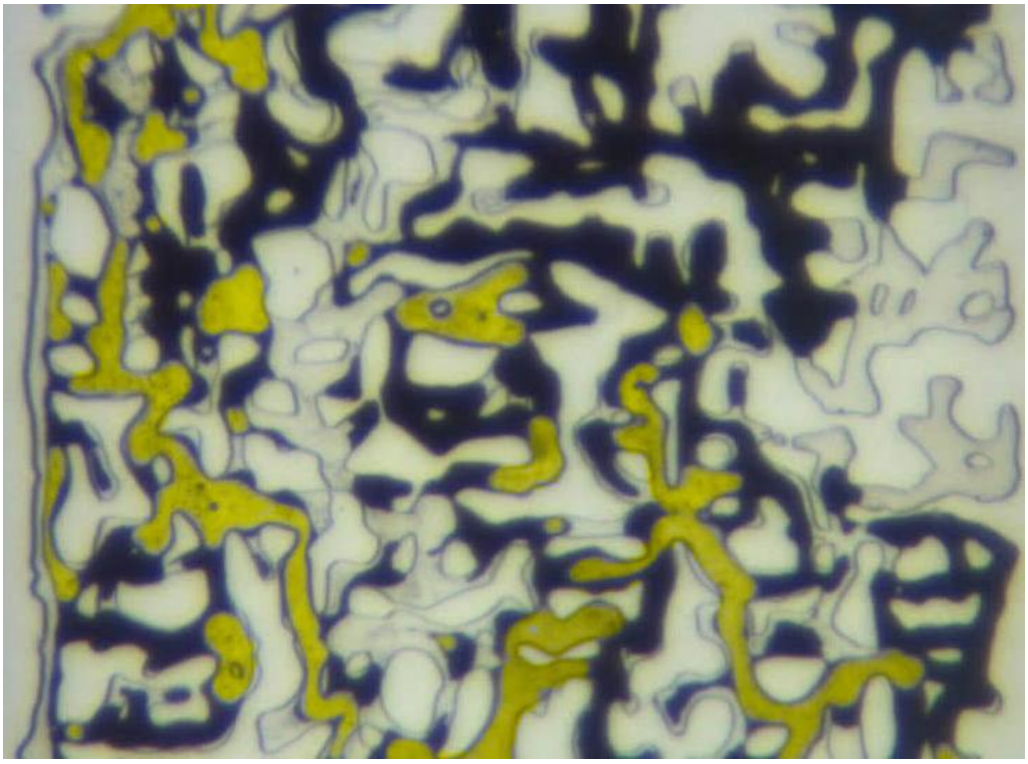

Figure 5-19: MM Exp 10; the magnified section of the micromodel after 1 day of CO2/water co-injection.

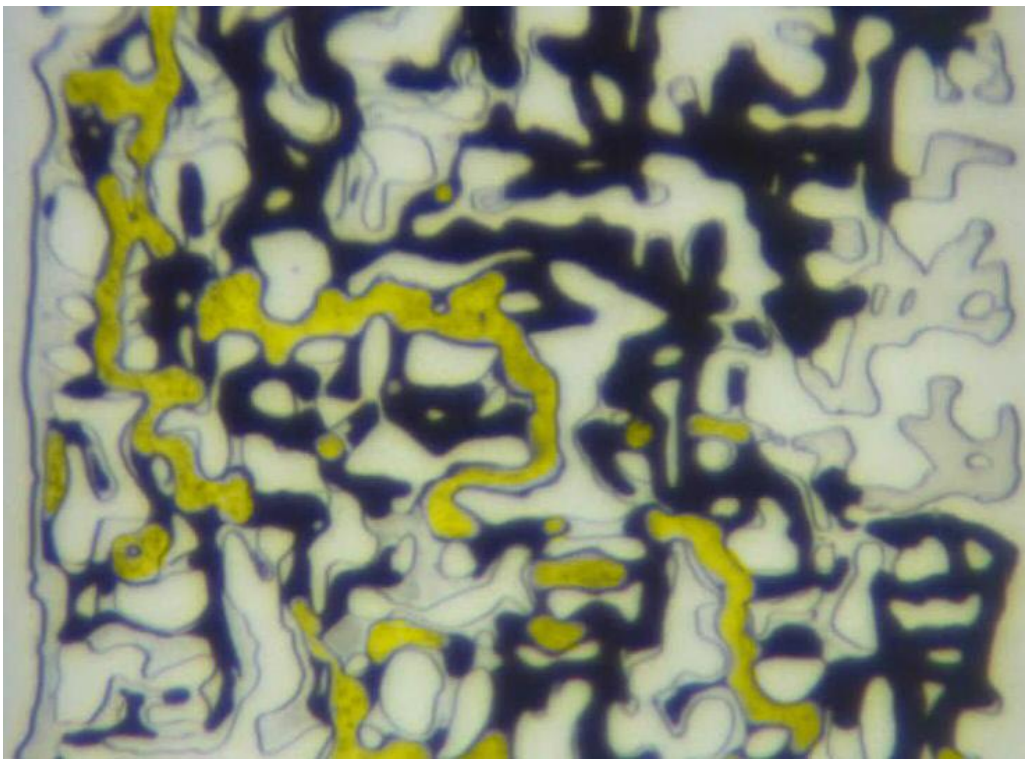

Figure 5-20: MM Exp 10; the magnified section of the micromodel at the end of the period of CO2/water co-injection (2 days).

Water Injection

After the period of CO2/water co-injection, a period of water injection commenced for 24 hours. Because residual oil at the end of the period of water/CO2 injection was in the form of disconnected oil ganglia, this period of water injection was unable to remobilize the residual oil and improve oil recovery; however, the main objective was to determine the dead oil volume of the residual oil. Figure 5-21 and Figure 5-22f show the magnified section and full length picture of the micromodel respectively at the end of this period of water injection. Comparison of Figure 5-21 with Figure 5-15 reveals that a significant part of extra-heavy crude oil has been recovered by the simultaneous injection of immiscible CO2 and water (since the period of water injection did not result in additional oil production the recovery improvement is only attributed to period of CO2/water co-injection).

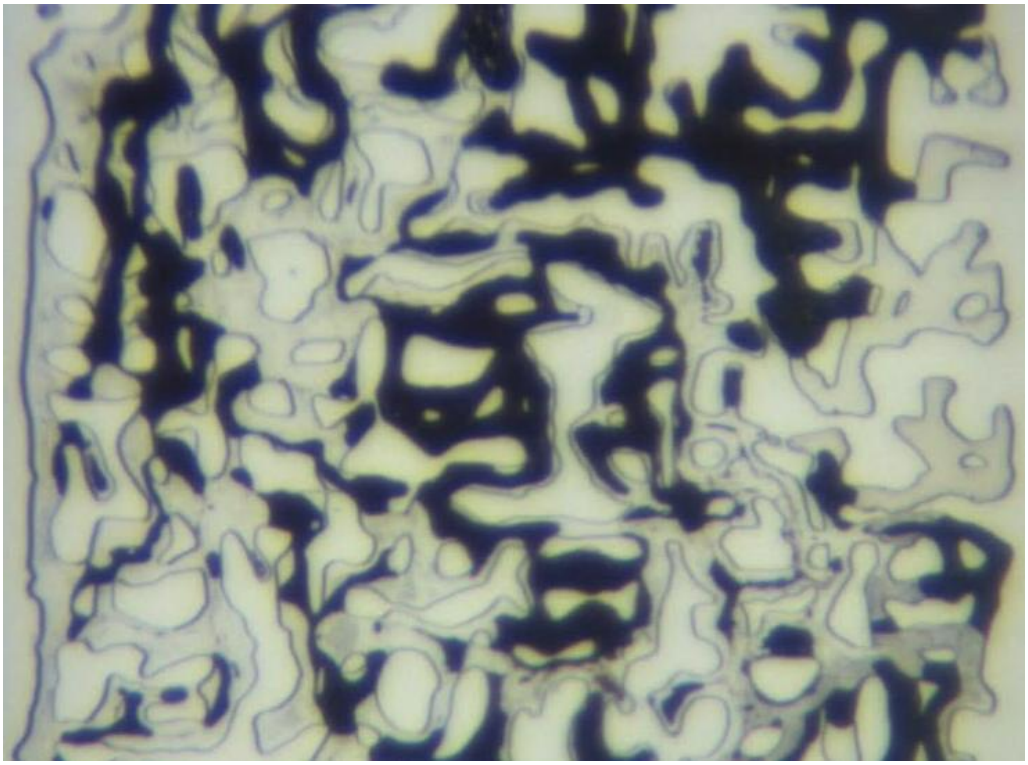

Figure 5-21: MM Exp 10; the magnified section of the micromodel at the end of the period of water injection (1 day).

Summary

Table 5-6 summarises the oil recovery data at different stages of this micromodel experiment (MM Exp 10). The final period of waterflood did not improve the oil recovery and an ultimate recovery of 43 %OOIP was achieved.

Table 5-6: MM Exp 10; Summary of the recovery data.

CO2/Water co-Injection	Recovery (% OOIP)
6) Breakthrough	17
7) 3 hours	26
8) 12 hours	35
9) 1 day	41*
10) 2 days	43*
A swelling factor of 5.5% has been considered for calculation of oil recovery.	

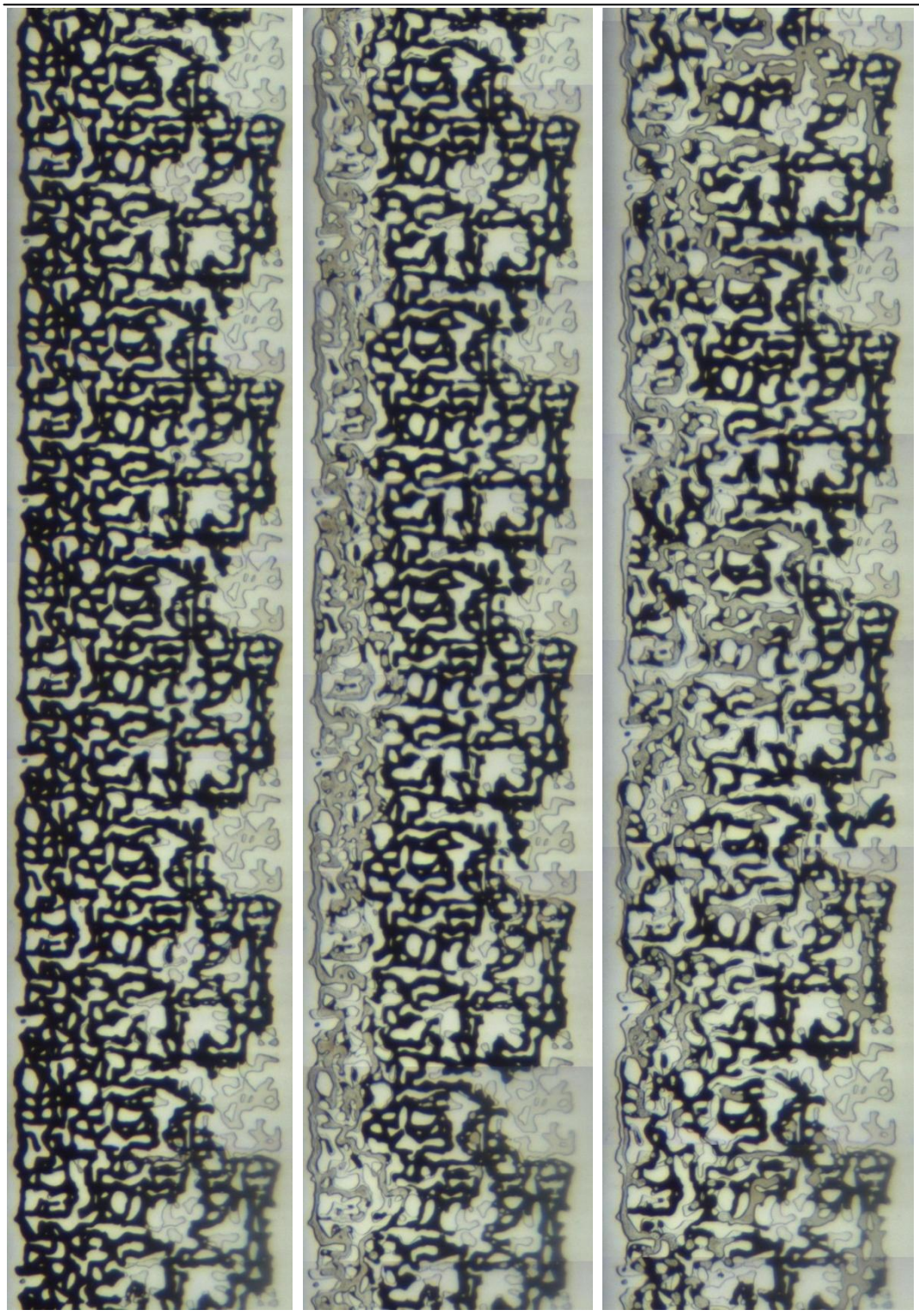

a **b** **c**

Figure 5-22: MM Exp 10; fluid distribution in the micromodel after (a) oil injection, (b) CO2 breakthrough and, (c) 6 hours of CO2/water co-injection.

d **e** **f**

Figure 5-22 (continue): MM Exp 10; fluid distribution in the micromodel after (d) 12 hours and, (e) 2 days of CO2/water co-injection and, (f) after the period of water injection.

5.2.4 Discussions

Recovery Efficiency of Different Injection Strategies

The presented micromodel results clearly show that injection of subcritical CO2 at the reservoir pressure and temperature of this extra-heavy crude oil, can significantly promote recovery performance; however, an extended period of injection is required. The highest recovery was achieved in the case of secondary CO2 injection (59% OOIP), followed by tertiary CO2 and water injection (48 %OOIP), CO2-SWAG (43 %OOIP) injection which significantly promoted oil recovery compared to the case of plain waterflood (17 %OOIP). This can be seen in Figure 5-23 and Figure 5-24, where oil recovery by CO2 injection under different injection scenarios is compared to the example of plain waterflood. Figure 5-23 compares residual oil saturation and fluid distribution in the magnified section of micromodel after (a) waterflood in Exp 8, (b) tertiary CO2 injection and the subsequent waterflood in Exp 8, (c) secondary CO2 injection in Exp 9, and (d) CO2-SWAG injection in Exp 10. Figure 5-24 presents similar comparisons, but using full length pictures of the micromodel.

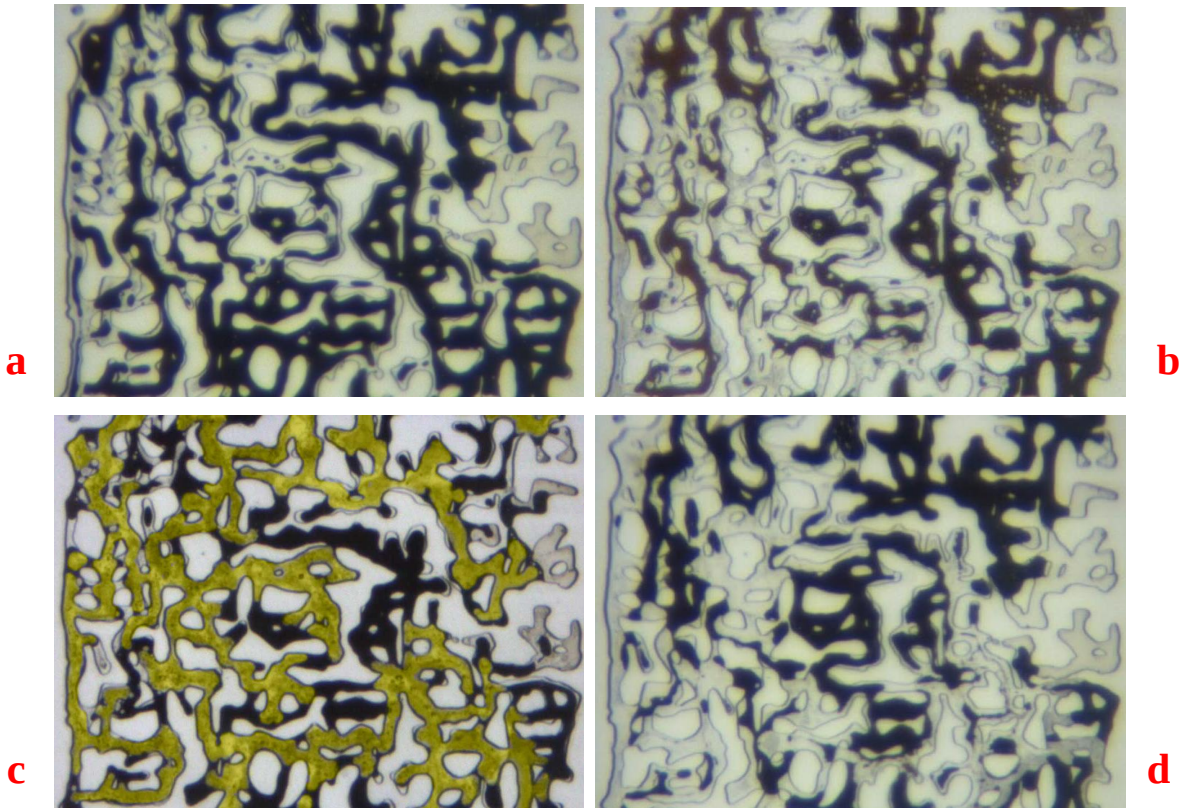

Figure 5-23: Comparison of recovery performance and oil saturation in the magnified section of the micromodel after a) waterflood in Exp 8, b) the tertiary CO2 injection and the subsequent waterflood in MM Exp 8, c) secondary CO2 injection in MM Exp 9 and, d) CO2-SWAG injection in Exp 10.

a **b** **c** **d**

Figure 5-24: Comparison of recovery performance and oil saturation in the length section of the micromodel after a) waterflood in Exp 8, b) tertiary CO2 injection and subsequent waterflood in MM Exp 8, c) secondary CO2 injection in MM Exp 9 and, d) CO2-SWAG injection in MM Exp 10.

Recovery Mechanisms

1) CO2 Dissolution: The theory section outlined that at sub-critical pressures, the main contribution of CO2 injection to recovery comes from CO2 dissolution and subsequent viscosity reduction in the heavy oil samples. This was confirmed by the fluid characterization experiments (chapter 2), where a viscosity reduction of around 92.4% was achieved when this extra-heavy crude oil was fully saturated with CO2 (viscosity reduction from 8700 cp to 617 cp). The diluted oil was then readily produced by a

number of pore scale displacement mechanisms, which will be explained in the following sections in the order they appeared in the micromodel.

2) Direct Displacement: in the early stages of injection, when CO2 is invading the pores that are partially or fully saturated with oil, displacement of oil is through direct displacement mechanisms. In the case of secondary injection mode, the displacement of oil is through a *direct-drainage mechanism* in which CO2, as the non-wetting phase, occupies the centre of the pores and displaces resident oil. In the case of tertiary injection mode, the displacement of oil is through a *double-drainage mechanism*, in which advancement of the CO2 front is associated with movement of oil-water interfaces ahead; this results in the modification of oil/water distribution and improvement in oil recovery (Oren, 1994; Sohrabi et al., 2000b). The fact that injected CO2 flowed through oil-occupied pores, rather than water-occupied pores, despite much higher viscosity of the crude oil compared to the water (more than 4 orders of magnitude), reveals the spreading behaviour of our oil/water/CO2 system.

3) Gravity Drainage: The density difference between the heavy oil and vapour CO2 resulted in a gravity drainage recovery mechanism that facilitated the flow of the CO2-diluted oil towards the production (bottom) end of the micromodel. This recovery process was more pronounced in the case of secondary CO2 flood, where the oil phase was connected in the porous medium and could easily flow towards the producing end of the micromodel.

Effect of CO2 Injection Strategy on Recovery Mechanisms

The dominant displacement mechanisms were observed to be dependent on injection strategy. In MM Exp 9, where CO2 was injected in a secondary mode, the extended period of CO2 injection successfully recovered the oil through gravity drainage without the need for a subsequent period of waterflood. In MM Exp 8, where CO2 was injected in tertiary mode, the existence of water layers resulted in reduced connectivity and mobility of the oil phase. Hence, whilst injection of CO2 significantly reduced oil viscosity, it was unable to improve oil recovery on its own and a subsequent period of water injection was required to displace the diluted heavy oil. In MM Exp 10, where CO2 and water were simultaneously injected, the gravity drainage mechanism was also ineffective, since the CO2 stream was scattered and a continuous stream of CO2 was not present throughout the micromodel (Figure 5-22c, d, e). Direct displacement of

diluted oil by water and CO2 was the main driving force for oil displacement and recovery.

Water Shielding Effect

As mentioned in the previous discussions, water shielding (or water blocking) adversely affected oil recovery performance during the extended period of tertiary CO2 injection. Figure 5-25a shows a magnified section of the micromodel at the end of the period of tertiary CO2 injection, where it can be clearly seen that injected CO2 has been unable to spread laterally in the porous medium towards the oil ganglia trapped on the right side of the porous medium. Moreover, diluted oil around the stream of CO2 is not efficiently produced, which is the opposite of the production performance in the case of secondary CO2 injection (Figure 5-25b). This is due to the fact that water shielding affects performance of CO2 injection in several ways. Firstly; the water layers dramatically reduce relative permeability of the oil phase and therefore the diluted oil around the CO2 stream is not displaced by gravity forces. Secondly; the injected CO2 is unable to meet some of the disconnected oil remaining after the initial water injection period, resulting in high residual oil saturation.

This behaviour is important for both oil recovery and storage purposes as CO2 can only be stored in these un-contacted oil ganglia by dissolution (not a free phase). This reduces availability of the reservoir pore volume and hence the volume of CO2 stored in the reservoir. From an EOR point of view, the presence of high water saturation that has disconnected the oil, reduces the sweep efficiency and amount of oil recovery.

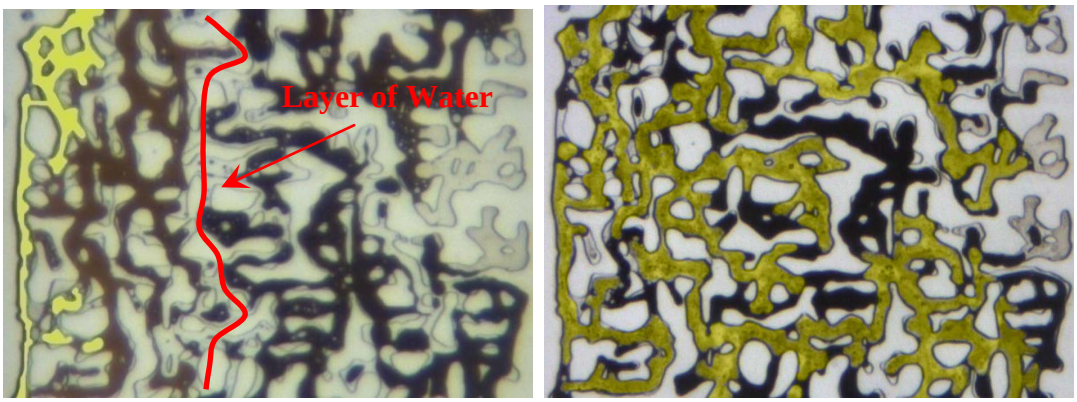

Figure 5-25: Comparison of the magnified section of the micromodel after 2 days of a) tertiary, and b) secondary CO2 injection.

5.3 THE EFFECT OF MOBILITY CONTROL BY CO2-FOAM

Foam is a means of mobility control, which improves the sweep efficiency of gas injections by reducing the negative effects of low gas viscosity and reservoir heterogeneity. Foam properties and interactions with oil, have mostly been characterized and studied by bulk foam and core flooding tests. In the former (typically), different variations of the common shake test are used, in which surfactant solution, air, and oil are mixed to produce foam, after which the decay of foam height is measured over time. The rate at which foam height decays, is thought to be a measure of the ability of the surfactant to produce and stabilize foam. Comparing results of foam formation and stability in the presence and absence of oil, can show the deleterious effect of the oil phase for that particular surfactant and solution. This result may indeed be valid for bulk foams; however, direct application of these experiments to foams in porous media is controversial. The type of foam present in a shake test may be radically different from that in porous media, especially with regard to foam structure, thickness of the lamellae, and the processes by which the foam collapses (Jimenez and Radke, 1989). The core flooding test is usually the only method used to study foam/oil interactions in porous media, and measures indirect properties of foam, such as pressure drops and foam-propagation rate across a core. Unfortunately, these secondary diagnoses have limited value for revealing the relevant interactions between foam and oil and displacement mechanisms in porous media (Jimenez and Radke, 1989; Nguyen et al., 2000).

Micromodels have proved to be useful in visualizing foam phenomena in porous media. Researchers have used micromodels to investigate the mechanisms by which foam is generated and destroyed, and the mechanisms that dominate bubble size distribution and rheological properties in porous media. Despite some upscaling limits regarding their dimensions, micromodel observations offer valid insights that can be extrapolated to coreflood studies (Nguyen et al., 2000). The available literature provides a valuable insight into the occurrence, properties, and propagation of foams in porous media using micro-scale visualization tests. These tests have mainly been carried out in clean micromodels (in the absence of oil) and very few have been reported in the presence of oil. The ones performed in the presence of oil, were first and foremost, focused on the deleterious effect of oils on foam propagation and stability; while the recovery mechanisms and efficiency of oil recovery by foam did not gain so much attention

(Kuhlman, 1990; Kulhman et al., 1994; Manlowe and Radke, 1990; Schramm and Novasad, 1990; Schramm and Novasad, 1992; Schramm et al., 1993).

In this section the author presents the results of two micromodel tests using CO2 and N2 foams to displace and recover an extra-heavy crude oil. The first test was designed to evaluate the potential of mobility control using CO2-foam and to visually investigate the interactions and displacement mechanisms between foam and this extra-heavy crude. The second test was designed to investigate the impact of gas type by using Nitrogen (N2) instead of CO2. N2 is more readily available than CO2; however, its dissolution in oil is considerably lower and hence a much less favourable modification in the oil's physical properties is expected.

Injection of surfactant solutions in these type of experiments changed the micromodel wettability to mixed-wet conditions. As a result the displacement pattern during the waterflood period in the following experiments is slightly different from those observed in the previous experiments. However, this difference does not affect the conclusions drawn from these experiment at the end of this section.

5.3.1 MM Exp 11: CO2-Foam Injection

The micromodel results from the previous section, showed that injection of CO2 can improve recovery of this extra-heavy crude sample if injection continues for an extended period of time. The main objective of this foam flood experiment was to investigate if mobility control by CO2-foam can effectively accelerate the process of oil displacement and shorten the period of injection.

Procedure and Conditions

1 *Initialization:* Micromodel was saturated with distilled water at T = 44 °C and P = 600 psig.

2 *Oil Flood:* Micromodel was flooded with crude oil "C" from bottom until the oil front reached the other end of the micromodel.

3 *Water Injection*: distilled water was injected in the micromodel for 1 day.

4 *Surfactant Injection*: The chemical solution was injected in the micromodel for 3 hours.

5 *CO2/Surfactant Co-Injection*: CO2 and surfactant solution were simultaneously injected in the micromodel at rates of 0.001 cm^3/hr and 0.01 cm^3/hr , respectively, (total of 0.011 cc/hr) for 2 days.

Table 5-7 lists a summary of the fluids used and the pressure and temperature at which the test was carried out.

Table 5-7: Fluids used and pressure and temperature conditions of MM Exp 11.

Porous Medium	Heterogeneous Rock-look-alike Micromodel
Crude Oil	"C" (8700 cp @ 50 °C)
Aqueous Phase	Distilled Water
Gas Phase	CO2
Chemical Solution	0.3 wt% NEODOL 25-7
Temperature	44 °C
Pressure	600 psig

Results

Initialization and Oil Injection Period

The experiment began by saturating the micromodel with distilled water at 44 °C and 600 psig. To establish initial oil and connate water saturation, crude "C" was then injected through the micromodel. Injection of oil continued until oil reached the other end of the micromodel pattern. Figure 5-26 and Figure 5-37a show a magnified section and the full length pictures of the micromodel at the end of the oil injection period.

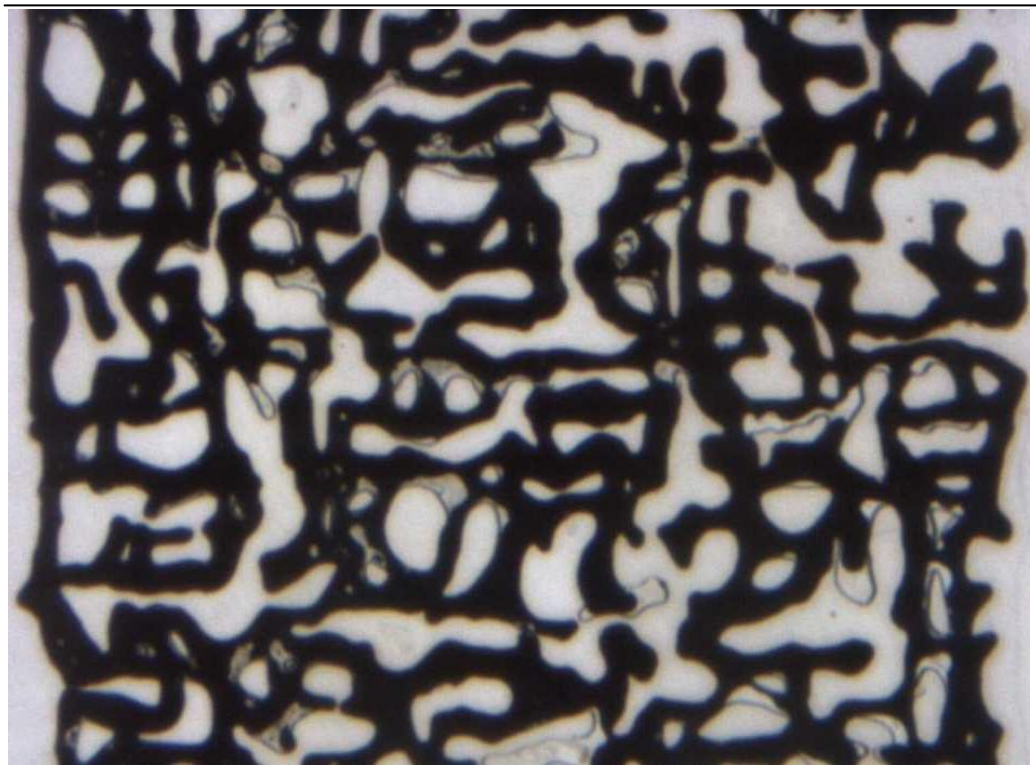

Figure 5-26: MM Exp 11; a magnified section of the micromodel at the end of the period of oil injection.

Water Injection

Having established the initial oil and water saturation, water injection started and continued for 1 day. Water was observed to finger through the high permeable region of the micromodel on the left hand side and leave behind (bypass) most of the oil. High saturation of oil at breakthrough is a well documented issue for heavy oils, which takes place as a result of the large viscosity contrast between the resident oil and the injected water. After the breakthrough, water injection continued, which resulted in additional oil recovery, albeit at very low rates. Figure 5-27 shows the same magnified section of the micromodel after 1 day of water injection. Comparison of this figure and Figure 5-26 shows that water has been unable to displace a large part of the oil. Figure 5-37(b) illustrates the full-length picture of the micromodel at the end of the water injection period.

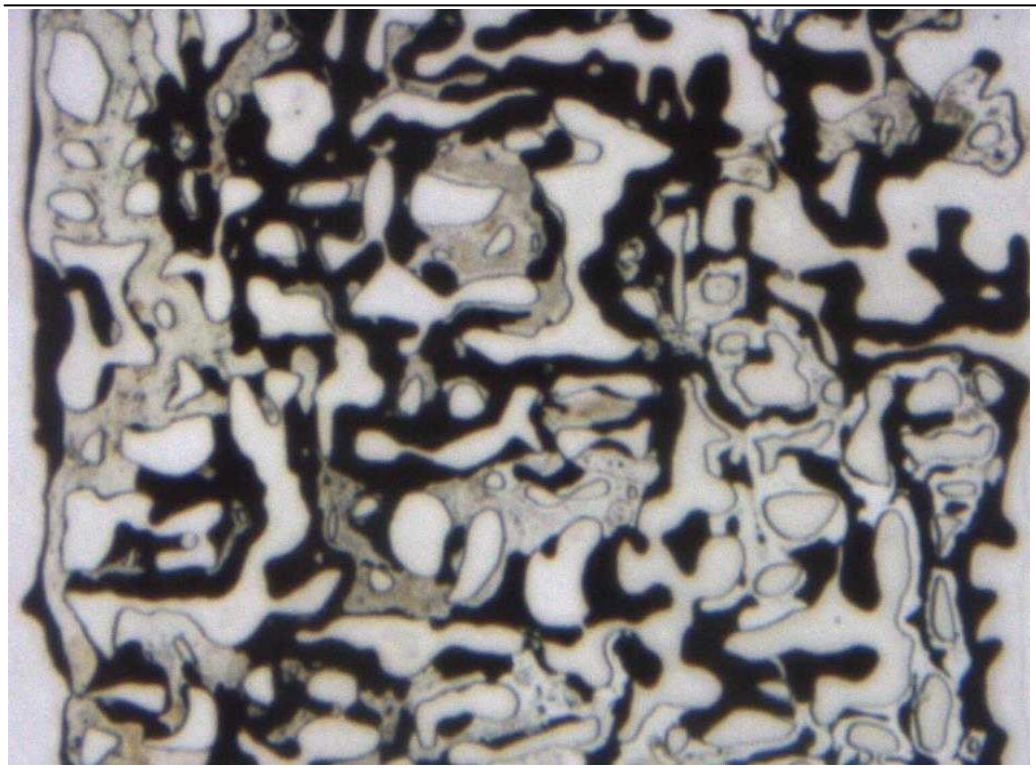

Figure 5-27: MM Exp 11; the same magnified section of the micromodel at the end of the period of water injection (1 day).

Surfactant Injection

After water flooding, the micromodel was flooded with the surfactant solution for 3 hours. Slight additional oil recovery was observed during the period of surfactant solution injection. The aim of this period of surfactant injection was to observe if any additional oil recovery would take place as a result of surfactant solution so that when surfactant is injected with gas, as part of the foam injection, the additional oil recovery will only be due to foam and not surfactant. Figure 5-28 and Figure 5-37c present the same selected magnified section of the micromodel and the full length picture of the micromodel after 3 hours of surfactant solution injection, respectively. The results showed very slight modification and negligible improvement in oil recovery.

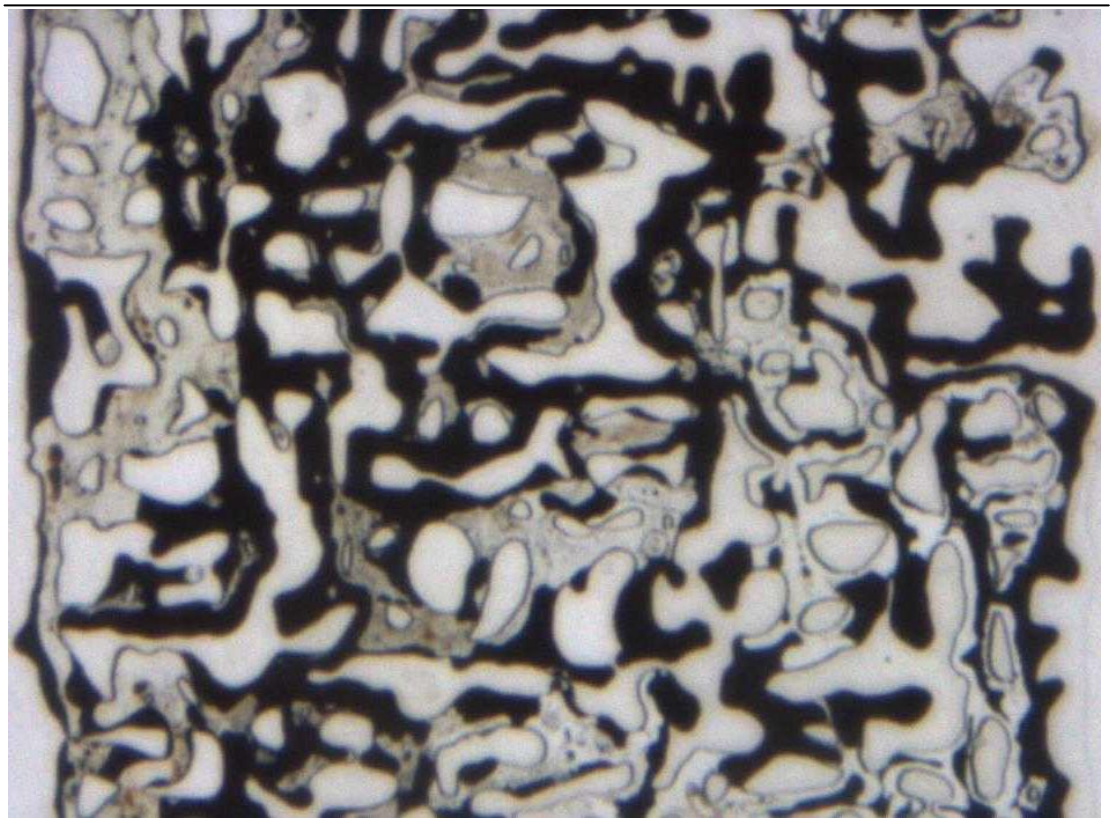

Figure 5-28: MM Exp 11; the magnified section of the micromodel at the end of the period of surfactant injection (3 hours).

CO2/Surfactant Co-Injection

Having carried out a short period of surfactant flooding, foam flood started and continued for 2 days. The arrival and progress of the front of the CO_2-foam in the micromodel was recorded using a digital camera and studied carefully. As bubbles of CO_2 contacted the waterflood residual oil in the micromodel, two processes took place simultaneously. The first process was direct displacement of the residual oil by CO_2 bubbles, which was much more efficient than the direct displacement process observed during tertiary CO_2 flood (Sohrabi et al., 2008b), as the number of moving interfaces between CO_2 and oil was significantly larger. The second process was destabilization of the foam bubbles by the surrounding oil. Therefore, despite having strong foam in the inlet of the micromodel (top), as foam front progressed towards the producing end of the micromodel, the CO_2 bubbles coalesced and joined each other making larger pieces of CO_2 in the lower sections (downstream) of the micromodel and at the outlet. As explained before, the spreading of oil over CO_2 bubbles causes weakening of the foam lamellae elasticity and consequently coalescence of the CO_2 bubbles as they flow through pores.

The advancement of the CO_2 foam was observed to be associated with the formation of a thick bank of oil ahead, which itself caused reconnection of the separated oil ganglia before the production of oil from the outlet of the micromodel. An important observation at this stage of the test was the formation of small droplets of water in oil (emulsification) just ahead of the CO_2 front. Figure 5-38 presents a highly magnified section of the micromodel during the flow of the CO_2-foam front in the model and the small droplets of water can be seen. The droplets of water were observed to form and coalesce repeatedly as the CO_2 front advanced, however, a constant number of droplets were almost always present ahead of the CO_2 front, which could increase the resistance to the flow of CO_2-foam through the porous medium and improve displacement efficiency of the process.

Figure 5-29 shows the same magnified section of the micromodel at the early stages of the foam injection period just after the breakthrough of the foam. Figure 5-37(d) presents the corresponding full picture of the micromodel after breakthrough, which shows bubbles of foam in the upper sections and larger pieces of CO_2 in the lower sections of the micromodel. After a certain period of foam (co-injection of CO_2 and surfactant solution) injection (e.g. 1 hour in the selected magnified section) the oil saturation decreased in the left side and upper sections of the model where the vertical connectivity was higher. In these regions of the micromodel, the oil was no longer spreading and the CO_2 bubbles were quite stable (Figure 5-30 and Figure 5-37e). At this stage, the oil displacement mechanism was observed to change from direct displacement to flow in the form of emulsions or small fragments of oil in between CO_2 bubbles and also through film flow over the pore walls.

As CO_2-foam became stable, the resistance to flow of foam increased and flow was diverted towards the low connectivity region on the right hand side of the micromodel, which was still holding high oil saturation. Initially, the high saturation of oil in this region caused the flow of CO_2 to be in the form of large pieces and fragments of CO_2. However, as injection continued, the saturation of oil decreased and CO_2-foam became increasingly more stable. After 10 hours of CO_2-foam flood, more than 90% of the waterflood-residual oil was displaced and recovered and the remaining oil was located mostly in the dead end pores. The residual oil in the dead end pores was also observed to be produced as CO_2-foam injection continued however through a much slower recovery mechanism. The sequence of pictures shown in Figure 5-29 to Figure 5-36

clearly illustrates the growth of CO_2-foam saturated region step by step in the magnified section of the micromodel. This displacement process demonstrates the CO_2-foam's remarkable ability to exhibit a lower mobility in high-permeable low oil-content regions compared to low-permeable high oil-content regions of porous media.

Figure 5-37 presents the images of the whole (full-length) micromodel during different stages of this micromodel test. A comparison of pictures (d) and (h) which have been taken during the period of CO_2-foam flood illustrates how effectively the extra heavy crude oil has been displaced and recovered. Pictures (e), (f) and (g) of Figure 5-37 reveal better sweep efficiency in the upper sections of the micromodel compared to the lower section. This is because, while the injected foam is displacing the resident oil in the lower sections, the mobilised oil from upstream (upper sections) sections reaches the lower section and increases the oil saturation in this region. In addition, the generated foam is more stable at upper sections as a result of contacting oil for a shorter period of time, therefore the displacement is more efficient at upper sections as well.

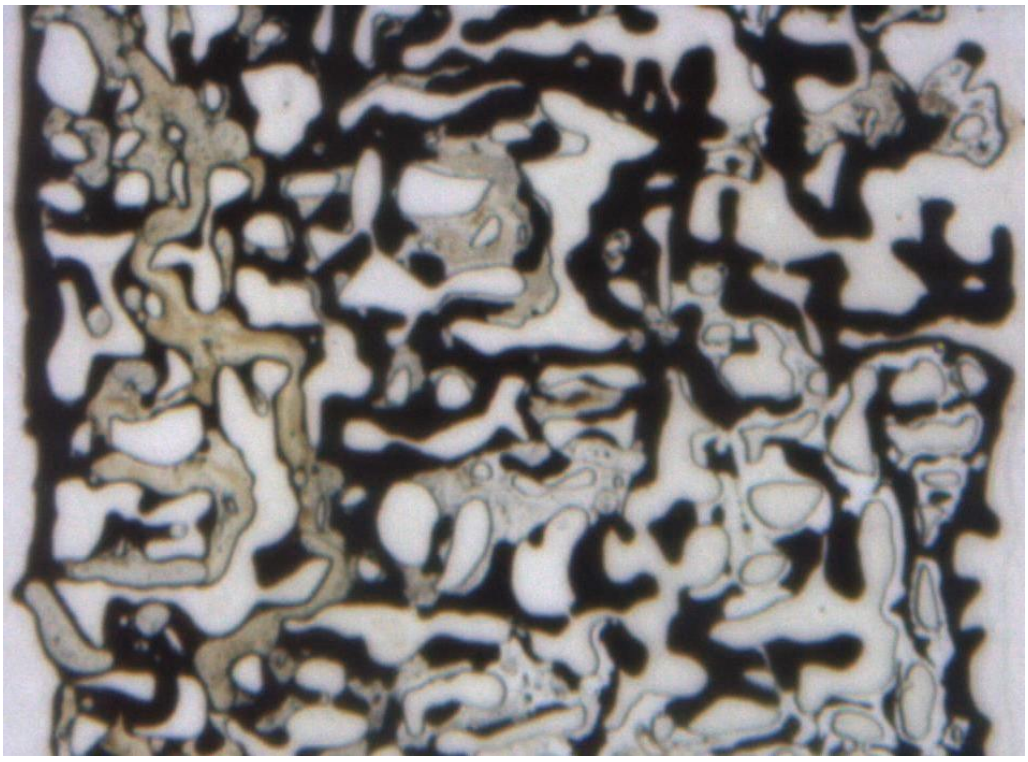

Figure 5-29: MM Exp 11; the magnified section of the micromodel at breakthrough time during the period of CO2/surfactant injection.

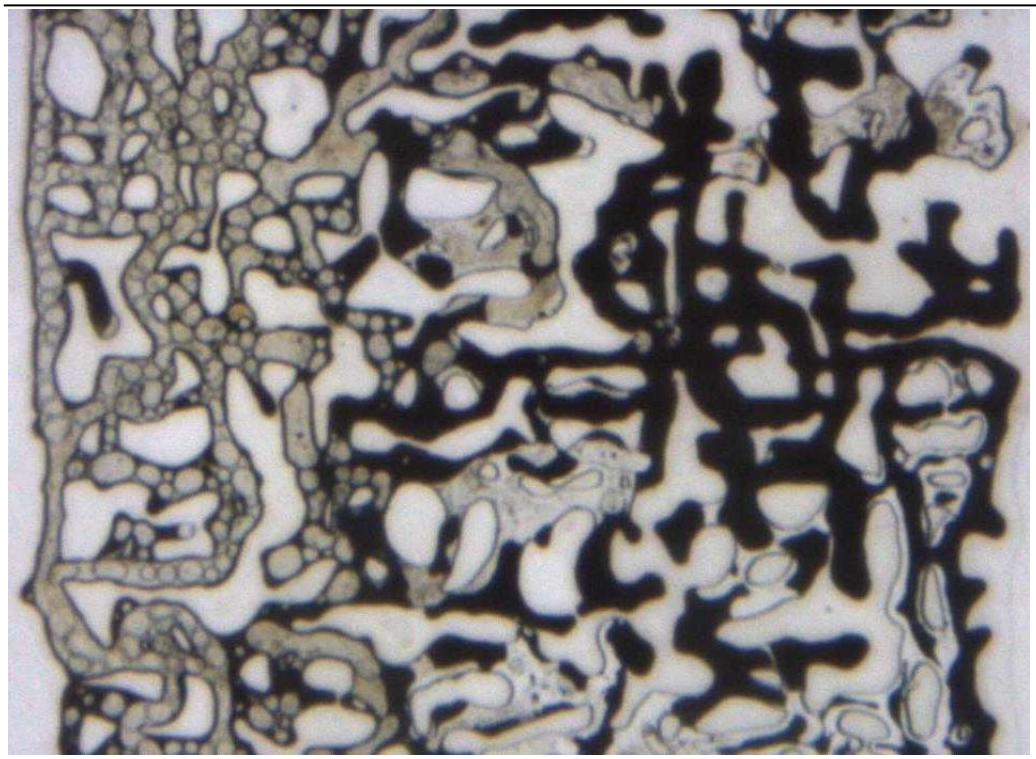

Figure 5-30: MM Exp 11; the magnified section of the micromodel after 1 hour of CO2/surfactant injection.

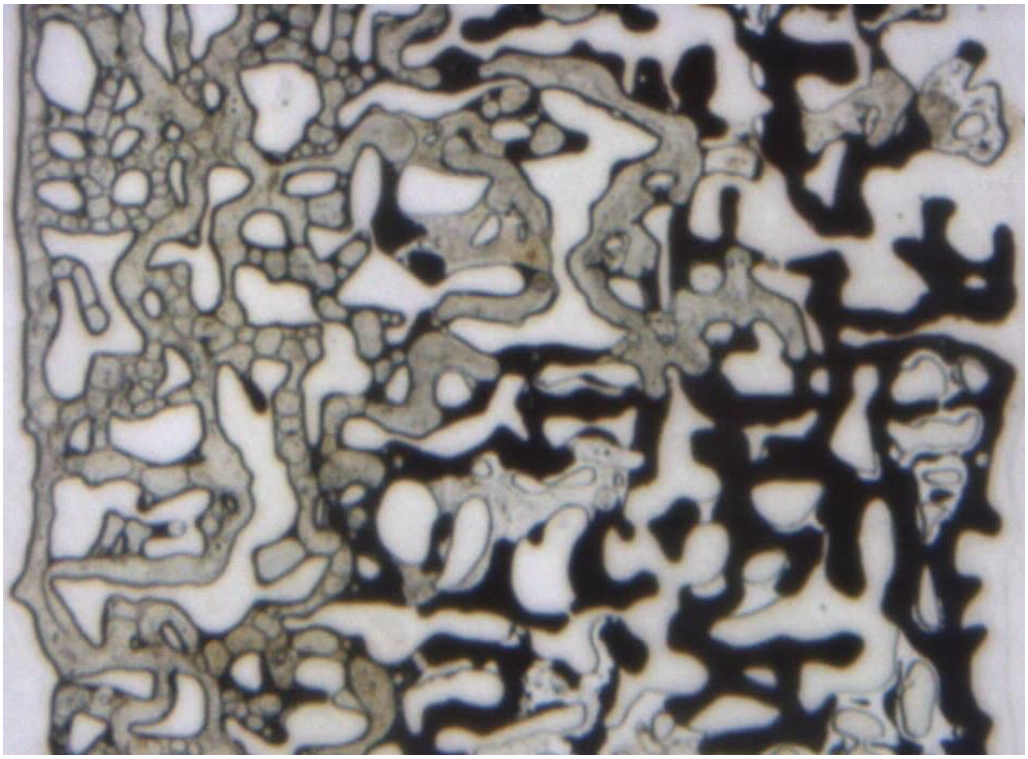

Figure 5-31: MM Exp 11; the magnified section of the micromodel after 2 hours of CO2/surfactant injection.

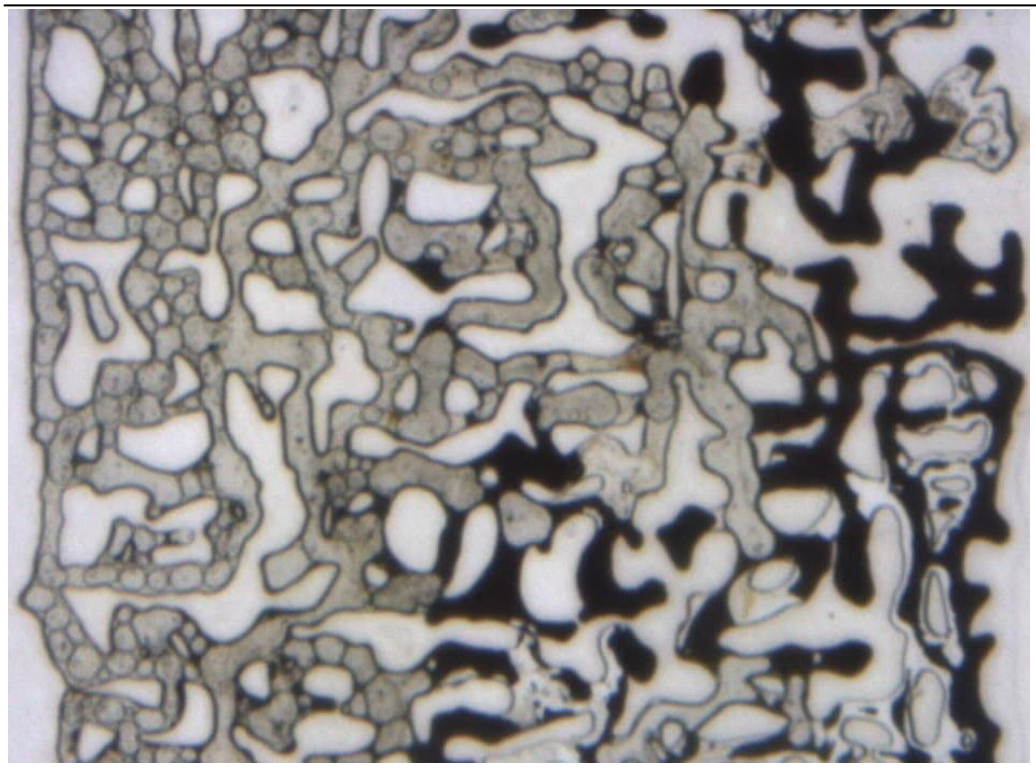

Figure 5-32: MM Exp 11; the magnified section of the micromodel after 5 hours of CO2/surfactant injection.

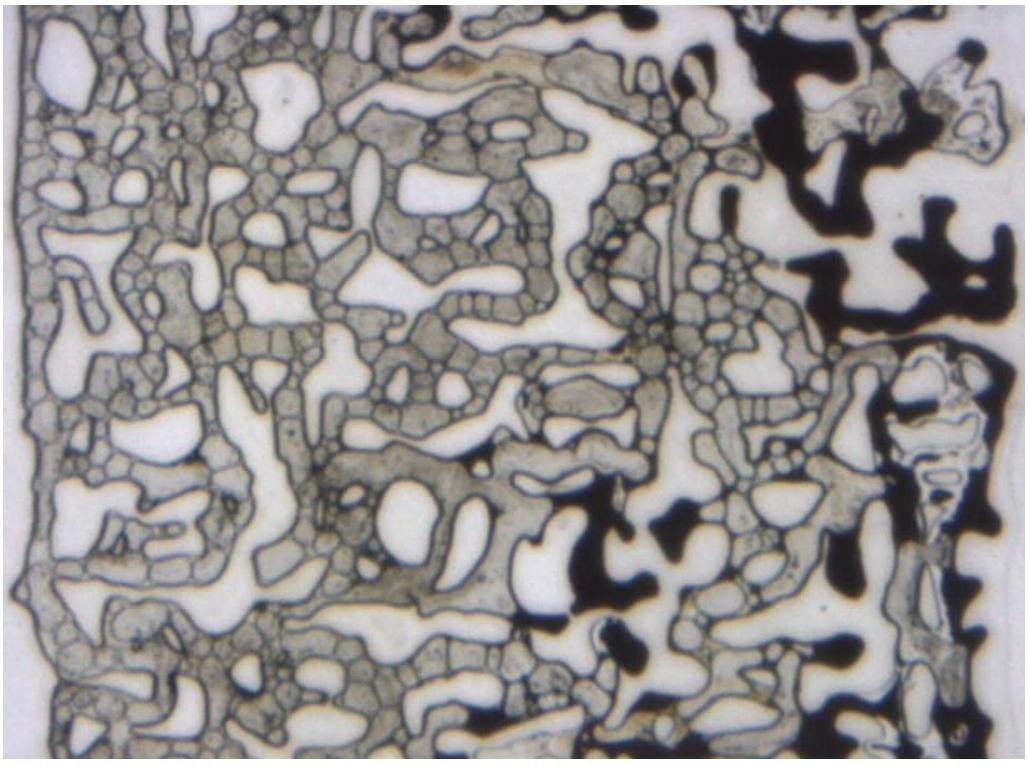

Figure 5-33: MM Exp 11; the magnified section of the micromodel after 10 hours of CO2/surfactant injection.

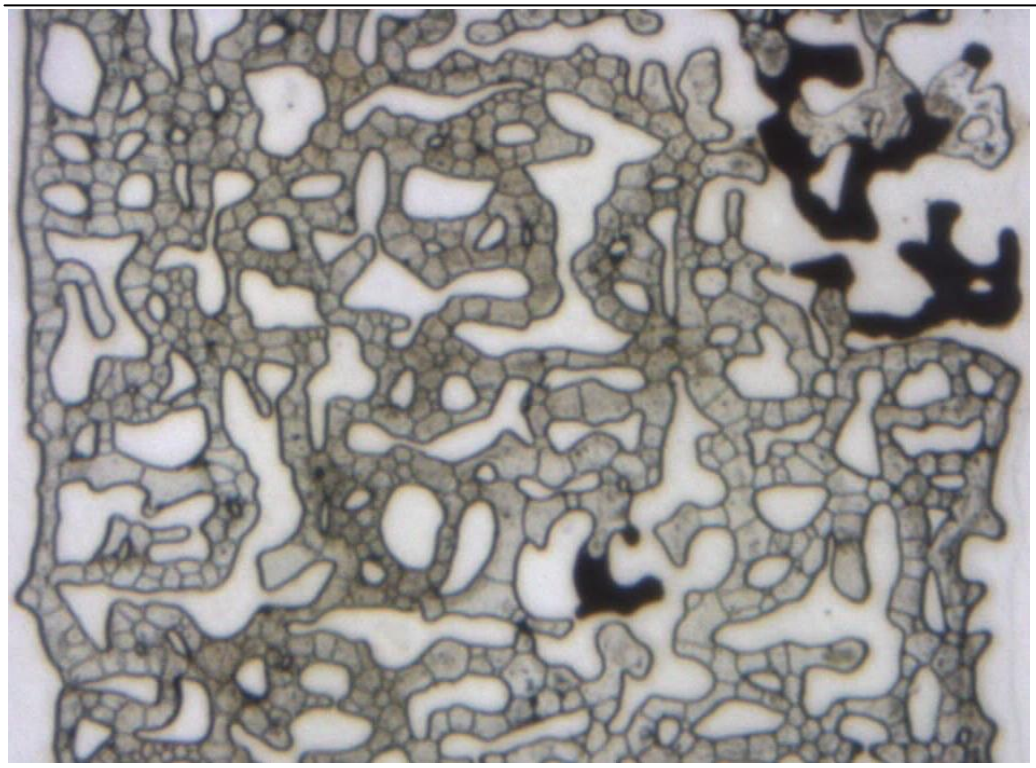

Figure 5-34: MM Exp 11; the magnified section of the micromodel after 15 hours of CO2/surfactant injection.

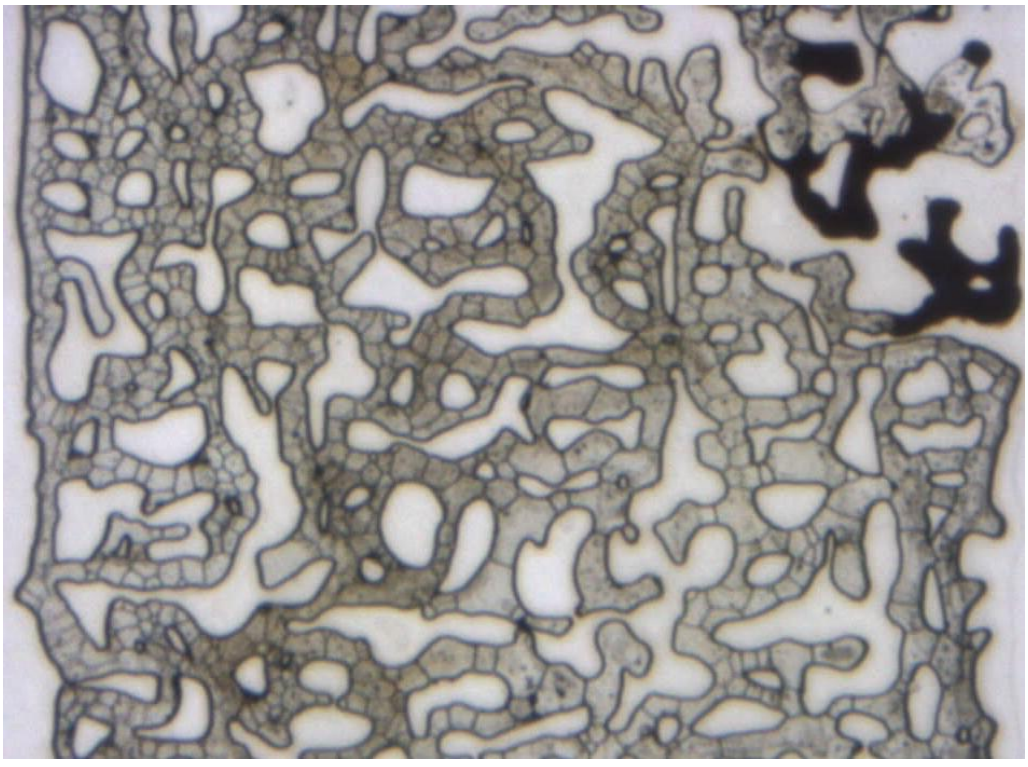

Figure 5-35: MM Exp 11; the magnified section of the micromodel after one day of CO2/surfactant injection.

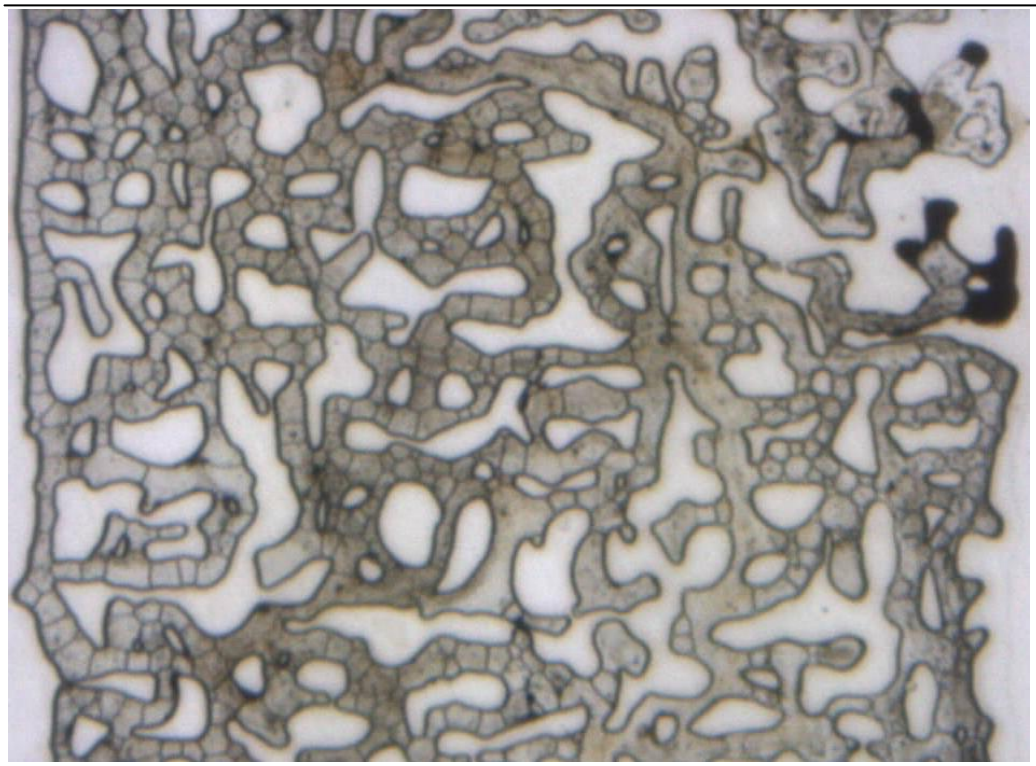

Figure 5-36: MM Exp 11; the magnified section of the micromodel after two days of CO2/surfactant injection.

Summary

Table 5-8 summarises the oil recovery data at different stages of this micromodel experiment (MM Exp 11). The results show that the process of CO2-foam flood has been very successful reaching a final recovery of 97%OOIP.

Table 5-8: MM Exp 11; Summary of the recovery data.

	Recovery @ BT (% OOIP)	Ultimate Recovery (% OOIP)	Cumulative Recovery (% OOIP)
1) Waterflood	19	28	28
2) Surfactant flood	0	1	29
3) CO2 surfactant co-Injection	9	68*	97
• A swelling factor of 5.5% has been considered for calculation of oil recovery.			

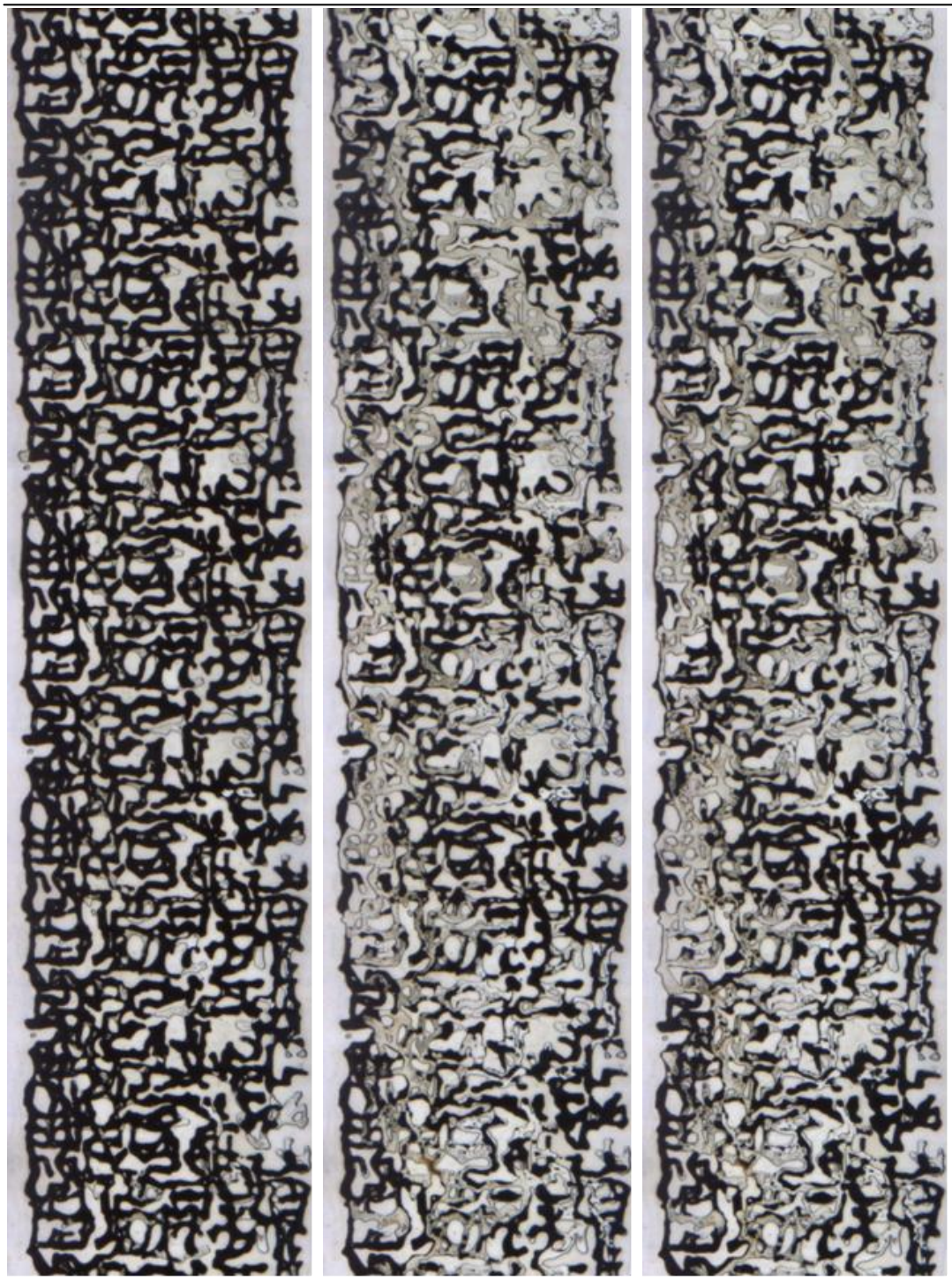

a **b** **c**

Figure 5-37: MM Exp 11; fluid distribution in the micromodel after (a) oil injection, (b) water injection and, (c) surfactant injection.

d **e** **f**

Figure 5-37 (continued): MM Exp 11; fluid distribution in the micromodel after (d) breakthrough, (e) one hour and, (f) 10 hours of CO2/surfactant injection.

g **h**

Figure 5-37 (continue): MM Exp 11; fluid distribution in the micromodel after (g) one day, and, (h) two days of CO2/surfactant injection.

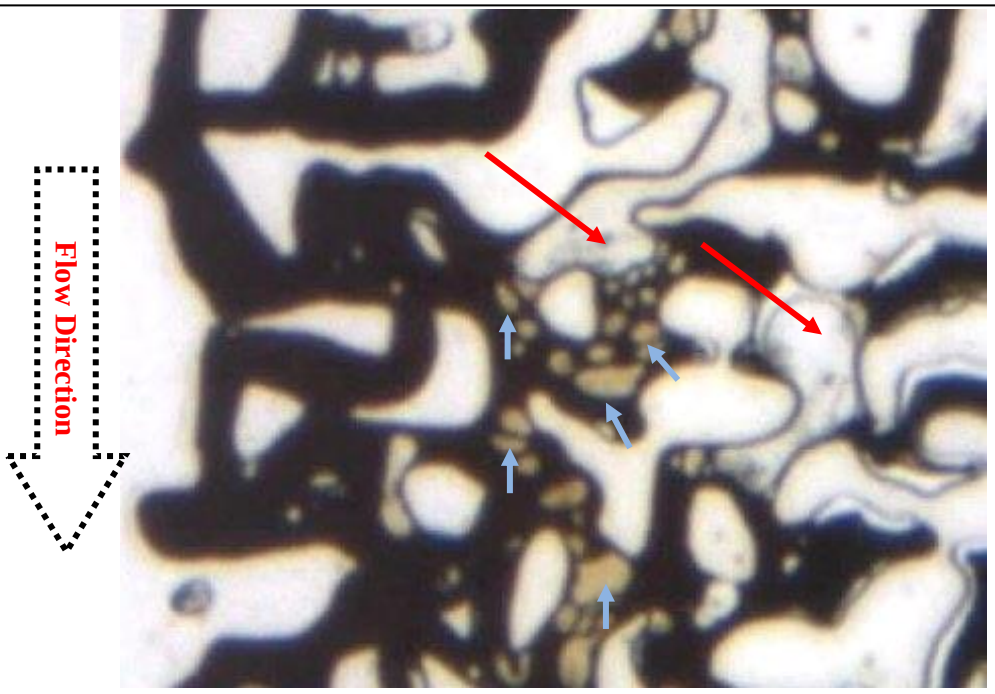

Figure 5-38: Formation of a thick bank of oil and generation of droplets of water in oil during the advancement of CO2-foam in a magnified section of the model. The red arrows show flowing CO2-foam and the blue arrows point at created droplets of water. As shown a large number of water droplets have been created and the droplets have higher density and lower size in places closer to the CO2 stream.

5.3.2 MM Exp 12: N2-Foam Injection

In the second foam flood experiment, effect of gas type was investigated using N2 instead of CO2. N2 is more readily available than CO2; however, its dissolution in oil is significantly less and hence considerably less modification in physical properties of the oil is expected. The same experimental procedure that had been followed in Exp 11 was followed here, with the only exception that the surfactant injection period was extended for 1 day. The surfactant solution, water and oil samples used in this test were exactly the same as the previous test.

Procedure and Conditions

1 *Initialization:* Micromodel was saturated with distilled water distilled water at T = 44 °C and P = 600 psig.

2 *Oil Flood:* Micromodel was flooded with crude oil "C" from bottom until the oil front reached the other end of the micromodel.

3 *Water Injection*: distilled water was injected in the micromodel for 1 day.

4 *Surfactant Injection*: The chemical solution was injected in the micromodel for 1 day.

5 *N2/Surfactant Co-Injection*: CO2 and surfactant solution were simultaneously injected in the micromodel at rates of 0.001 cm^3/hr and 0.01 cm^3/hr , respectively, (total of 0.011 cc/hr) for 3 days.

Table 5-9 lists a summary of the fluids used and the pressure and temperature at which the test was carried out.

Table 5-9: Fluids used and pressure and temperature conditions of MM Exp 12.

Porous Medium	Heterogeneous Rock-look-alike Micromodel
Crude Oil	"C" (8700 cp @ 50 °C)
Aqueous Phase	Distilled Water
Gas Phase	N2
Chemical Solution	0.3 wt% NEODOL 25-7
Temperature	44 °C
Pressure	600 psig

Results

Initialization and Oil Injection

The experiment began by saturating the micromodel with distilled water at 44 °C and 600 psig. Then to establish initial oil and connate water saturation, crude "C" was injected through the micromodel. Injection of oil continued until oil reached the other end of the micromodel pattern. Figure 5-39 and Figure 5-46a show a magnified section and full length pictures of the micromodel at the end of the oil injection period.

Figure 5-39: MM Exp 12; a magnified section of the micromodel at the end of the period of oil injection.

Water Injection

Having established the initial oil and water saturation, water injection started and continued for 1 day. Figure 5-40 and Figure 5-46b illustrate the same magnified section and full-length pictures of the micromodel respectively, at the end of the water injection period.

Figure 5-40: MM Exp 12; the same magnified section of the micromodel at the end of the period of water injection (1 day).

Surfactant Injection

Having flooded the micromodel with water; surfactant injection started and continued for 1 day (as opposed to the previous experiment in which surfactant was only injected for 3 hours). During surfactant flooding, some oil recovery was observed as a result of two main mechanisms: (1) wettability change to more water-wet conditions, and (2) reduction of interfacial tension between the oil and aqueous phase. These mechanisms had not been observed in the previous experiment, because of the short period of surfactant injection. Figure 5-41 and Figure 5-46c illustrate the selected magnified section and full length picture of the micromodel respectively, after 1 day of surfactant injection. As shown in these figures, the additional oil was mainly recovered from the left hand side of the heterogeneous micromodel, where the flowing path of water existed. This observation implies that for this heavy crude oil, injection of surfactant solution can only recover the oil nearby the path of the flowing surfactant and has no effect on residual oil in close vicinity of the water finger. This behaviour is dramatically different from the case of light oils, where the relatively similar viscosities of oil and water and trapping of oil due to capillary forces, result in high sweep efficiency by surfactant flood.

Figure 5-41: MM Exp 12; the magnified section of the micromodel at the end of the period of surfactant injection (1 day).

N2/Surfactant Co-Injection

At this point, simultaneous injection of N_2 and the surfactant solution began through the bypass line and was then diverted towards the micromodel. A distinct difference between this test and the CO_2-foam test (at arrival of the foam) was the non-spreading behaviour of the N_2/surfactant/oil system, which resulted in no additional oil recovery at breakthrough of foam. Unlike CO_2-foam, N_2-foam maintained its stability during flow through the micromodel with high oil saturation and even (as a result of the lamellae division process) the bubbles at the outlet of the micromodel were observed to be stronger and more stable than original foam at the entering port of the micromodel. Figure 5-47 presents a highly magnified section of the micromodel during the flow of the N_2-foam. The foam was observed to flow from the left hand side of the micromodel (the region with higher permeability) and through pores that were occupied by the aqueous phase. Comparison of Figure 5-38 and Figure 5-47 shows different flow behaviour for CO_2-foam and N_2-foam in the micromodel. While the former produced an oil spreading system, flowed through the oil-occupied pores and therefore mobilised a thick bank of oil in front of it; the latter showed a non-spreading behaviour, flowed mainly through the water-occupied pores and therefore did not produce a bank of oil as it advanced towards the producing end of the model.

Figure 5-42 presents the magnified image of the selected section of micromodel and Figure 5-46d shows the corresponding full-length picture of the micromodel after breakthrough of N_2. These figures show existence of stable foam in the left hand side of the image, just after the foam breakthrough.

The bubbles of foam gradually spread into the right side of the micromodel and displaced part of the bypassed oil as foam injection continued. However, after 4 days of N_2-foam injection, a significant fraction of the oil still remained unswept in the micromodel. The sequence of magnified pictures shown from Figure 5-43 to Figure 5-45, illustrates how the N_2-foam entered and displaced oil in the model during the 4 days of injection. Figure 5-46 (d), (e), (f) and (g) show full-length images of the micromodel during this period.

Figure 5-42: MM Exp 12; the magnified section of the micromodel at breakthrough time during the period of N2/surfactant injection.

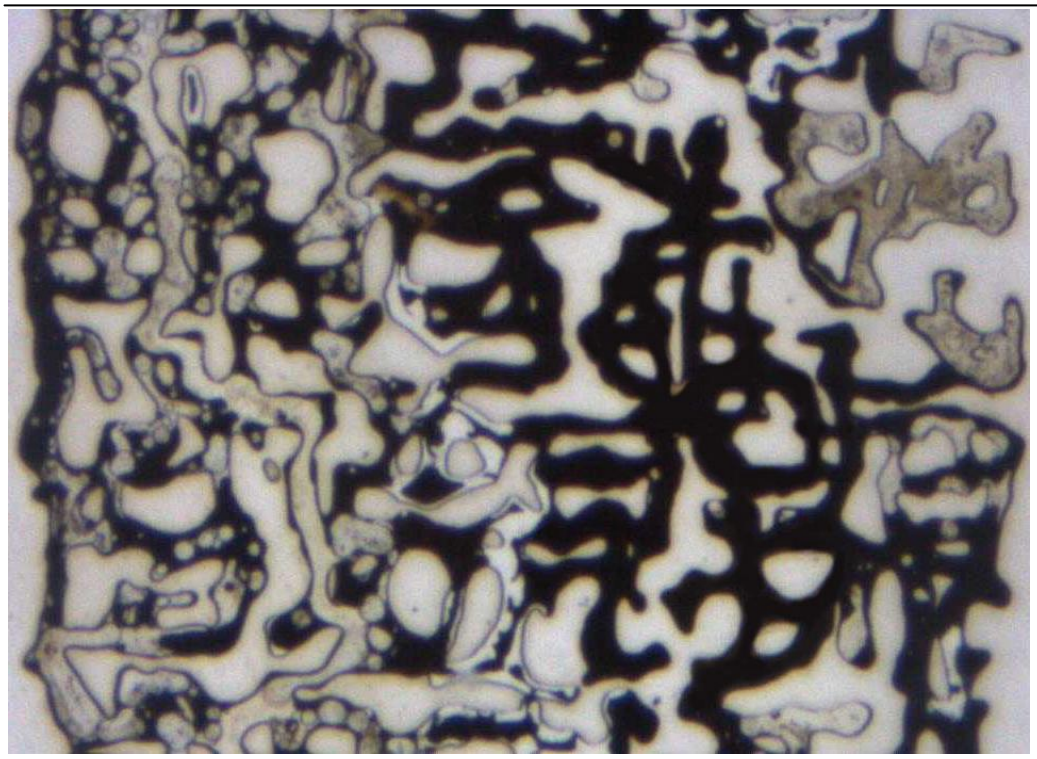

Figure 5-43: MM Exp 12; the magnified section of the micromodel after 1 hour of N2/surfactant injection.

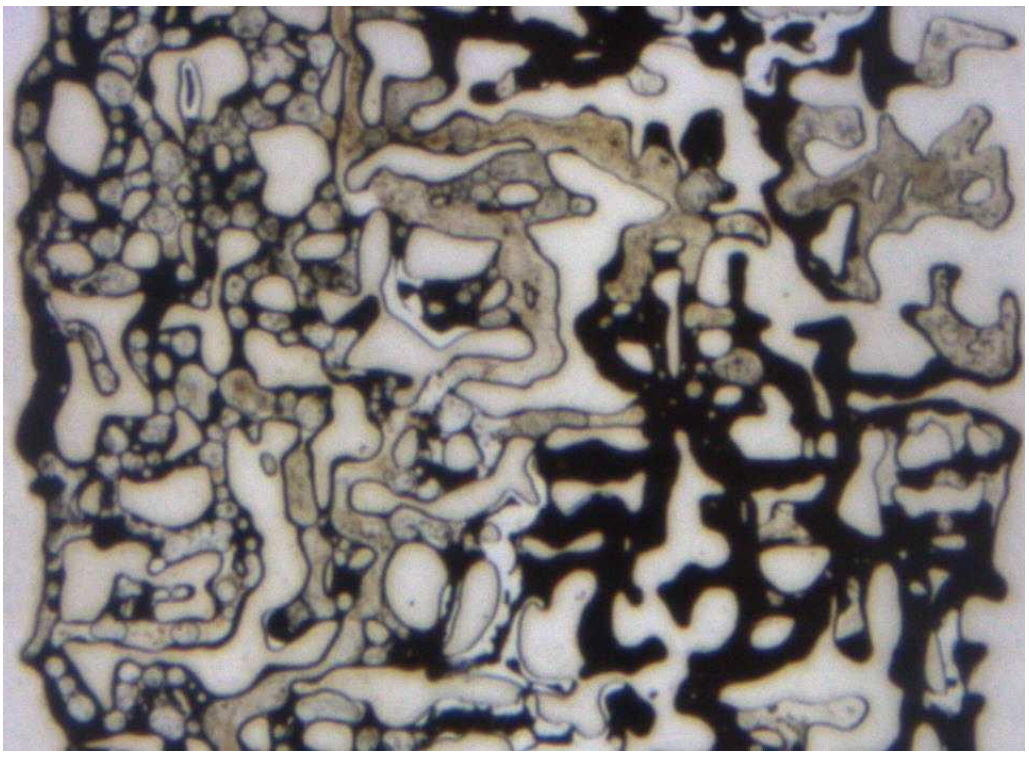

Figure 5-44: MM Exp 12; the magnified section of the micromodel after 1 day of N2/surfactant injection.

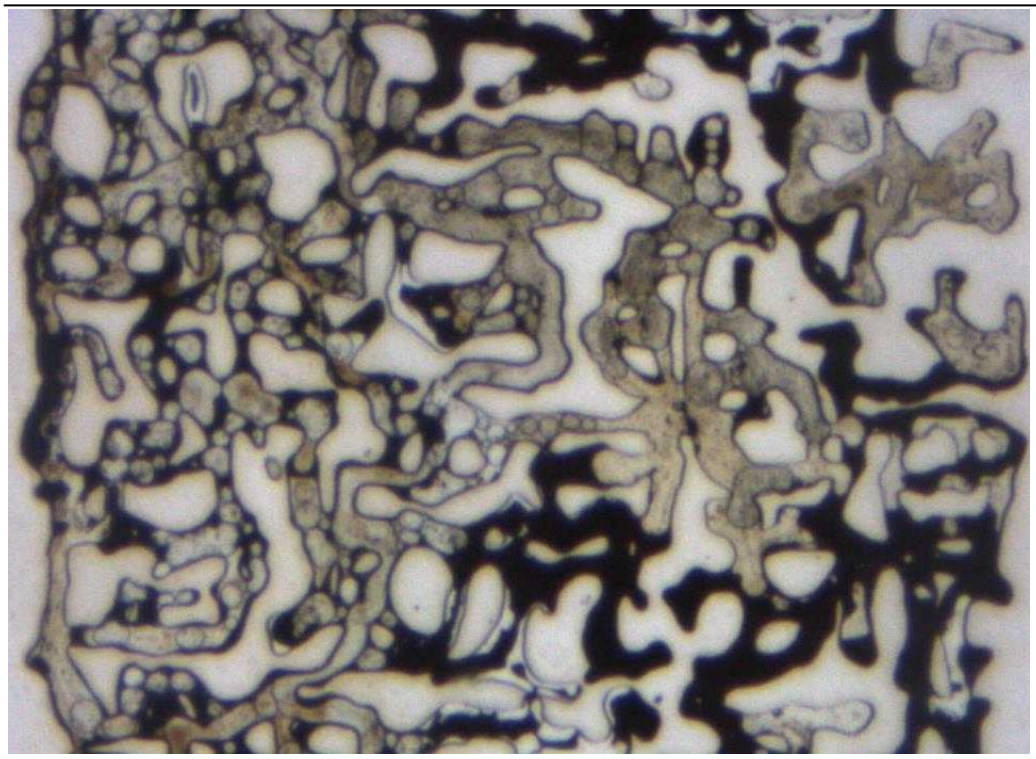

Figure 5-45: MM Exp 12; the magnified section of the micromodel after 4 days of N2/surfactant injection.

Summary

Table 5-10 summarises the oil recovery data at different stages of this micromodel experiment (MM Exp 12).

Table 5-10: MM Exp 12; Summary of the recovery data.

	Recovery @ BT (% OOIP)	Ultimate Recovery (% OOIP)	Cumulative Recovery (% OOIP)
4) Waterflood	11	13	13
5) Surfactant flood	0	16	29
6) CO2 surfactant co-Injection	4	19	48

a **b** **c**

Figure 5-46: MM Exp 12; fluid distribution in the micromodel after (a) oil injection, (b) water injection and, (c) surfactant injection.

d **e** **f**

Figure 5-46 (continue): MM Exp 12; fluid distribution in the micromodel after (d) breakthrough, (e) one hour and, (f) one day of N2/surfactant injection.

g

Figure 5-46 (continue): MM Exp 12; fluid distribution in the micromodel after (g) four days of days of N2/surfactant injection.

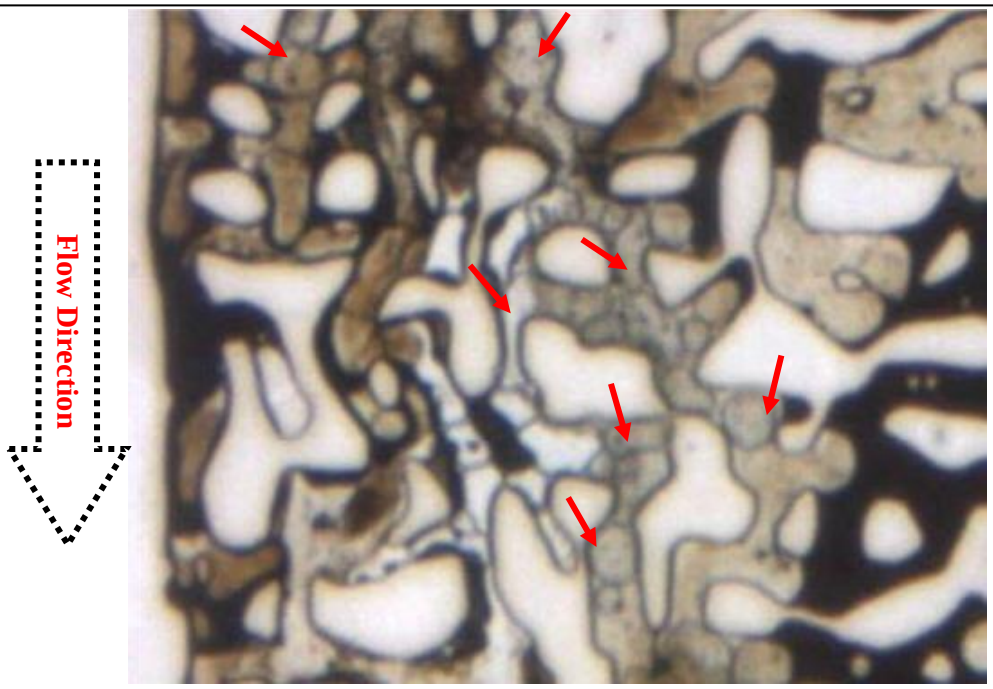

Figure 5-47: Flow of N_2-foam through water occupied pores without displacing the residual oil in the micromodel. The N_2-foam bubbles are quite stable in presence of oil and bank of oil has not been created in front.

5.3.3 Discussions

Foam Stability and Displacement Efficiency

For both CO_2 and N_2, foam bubbles generated exhibited a similar appearance, in terms of diameter and size distribution, as they reached the micromodel. However, the displacement mechanisms and final oil recovery efficiency of N_2-foam was notably different from that of CO_2-foam. Whilst N_2-foam was observed to be more stable after contacting the heavy oil, which was apparent from the smaller size of foam bubbles; oil recovery efficiency in CO_2-foam was significantly higher, displacing almost all the waterflood residual oil in a shorter period of time. The higher stability of N_2-foam is believed to be due to non-spreading behaviour of the system throughout the test, while in CO_2-foam, formation of layers of oil around CO_2 bubbles destabilized the bubbles at the early stages of injection.

Figure 5-48: Comparison of fluid distribution and remaining oil after 1 day of (a) CO_2 flood in MM Exp 8, (b) CO_2-foam flood in MM Exp 11 and, (c) N_2-foam flood in MM Exp 12.

Figure 5-48 compares the fluid distribution and remaining oil saturation after 1 day of CO_2 flood, CO_2-foam flood and N_2-foam flood. It is clear from the comparison of these figures that the CO_2-foam has been much more effective and efficient in enhancing the recovery of this extra-heavy crude oil, compared to plain CO_2 and N_2-foam. The results

reveal the essential role that gas type plays in overall performance of foam injection and clearly demonstrates that this role should not be underestimated. In N_2 foam injection, since solubility of N_2 in oil is very small (hence no improvement in oil flow and physical properties) additional oil recovery is only due to the improvement in mobility of N2. In CO_2 foam injection, however, the solubility of CO_2 in oil is significant and hence (in addition to mobility improvement) flow properties of the fluids (e.g. IFT and oil viscosity) are also favourably modified. Our viscosity measurement experiments (chapter 2) show that viscosity of this heavy crude oil can drop to 7.6% of its initial value, as a result of mixing with CO_2 under test conditions.

Pore Scale Recovery Mechanisms

In the reported micromodel experiments, foam bubbles were observed to initially displace residual oil in high-permeability regions of the micromodel. As saturation of oil decreased, foam became increasingly more stable showing higher viscosity. Thus flowing foam was gradually diverted towards low-permeability and dead end pores, which contained most of the waterflood residual oil. In addition to this, there are other mechanisms involved which contribute and enhance displacement of oil at single pore level. Our micromodel observations show four major displacement mechanisms, which are schematically demonstrated in Figure 5-53. These mechanisms are listed, based on the time they appeared in the micromodel, as follows:

Direct Displacement: The first displacement mechanism to appear in the model, was direct displacement of the bulk of oil from pore bodies by CO2 bubbles or the aqueous phase. After the first drainage event, oil recovery through direct displacement mechanism continued and remaining oil in the pore body was displaced in between CO2-foam bubbles (lamellae) as can be seen in the sequence of pictures in Figure 5-49. The two types of direct displacement mechanism are schematically illustrated in pictures (a) and (b) of Figure 5-53. Direct displacement of heavy oil by CO2 bubbles was more effective than direct displacement of oil by CO2 during tertiary CO2 flood in MM Exp 8, which took place through a double-drainage process. This is due to the fact that during foam flood, every single bubble of foam counts as a new CO2 front, which does not necessarily follow the other, leading to a more effective displacement of oil from the pores. Furthermore, blockage of pore bodies by foam bubbles not only decreases gas permeability, but also locally restricts the flowing path of the aqueous

phase. As a consequence, the surfactant solution starts flowing into new pore spaces that had initially been filled with the oil.

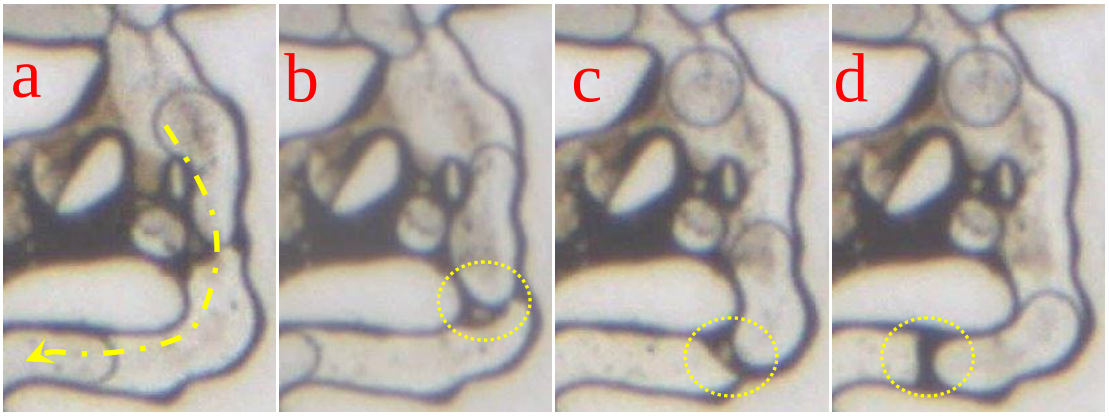

Figure 5-49: The process of direct displacement of oil in-between CO2-foam bubbles. The yellow arrow shows the flow direction of CO2-foam and the dotted yellow circles show formation and displacement of a thick oil film in front of the flowing CO2 bubble.

Emulsification of oil: The residual oil saturation after the initial direct displacement, was still significant. As CO2-foam injection continued, a large part of this residual oil was displaced and then flowed towards the production end of the micromodel, in the form of oil in water emulsions (droplets) in between the bubbles of CO2-foam. Due to existence of surfactant materials in the aqueous phase, these oil emulsions were observed to remain stable throughout the micromodel. The lower apparent viscosity of these oil-in-water emulsions, compared to that of heavy oil, significantly enhanced the displacement process. Figure 5-50 presents a highly magnified section of the micromodel, in which flow of oil emulsions in between CO2 bubbles can be clearly seen. The arrows in this figure are pointed towards the flowing oil emulsions. Formation of oil emulsion during (CO2-) foam flood is a well-known behaviour and has previously been reported in the literature (Kuhlman, 1990; Schramm and Novasad, 1990; Yang and Reed, 1989). Figure 5-53c schematically illustrates the mechanism of oil recovery by emulsification mechanism.

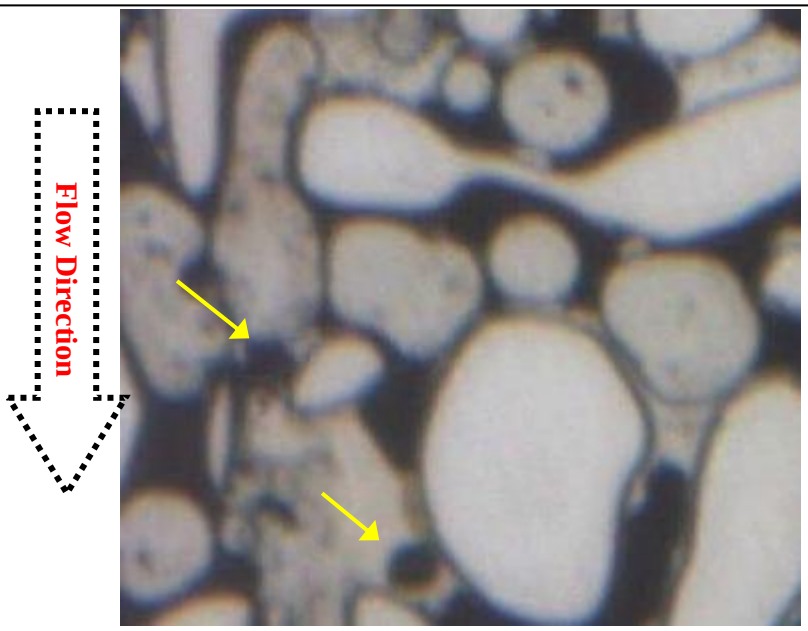

Figure 5-50: The process of oil recovery through oil emulsification mechanism in a highly magnified section of the micromodel in which flow of oil emulsions in between CO2-foam bubbles can be clearly seen (yellow arrows).

Co-current film flow: While the CO2 bubbles occupied the centre of the pore bodies, residual oil remained connected through films on the pore wall or in between foam bubbles. Therefore, as foam flow continued, the residual oil was produced through these oil films. The parameters such as: high viscosity of CO2-foam, its non-Newtonian nature of foam and large number of interfaces between CO2 bubbles, caused the film flow displacement mechanism to be significantly more effective than the example of CO2 flood (Exp 5). Figure 5-51 illustrates a highly magnified section of the micromodel, in which oil films on the pore walls and in between foam bubbles can be seen. These oil layers were displaced and mobilized in the same flowing direction as the CO2-foam. Figure 5-53d schematically illustrates the mechanism of oil recovery by co-current film flow mechanism.

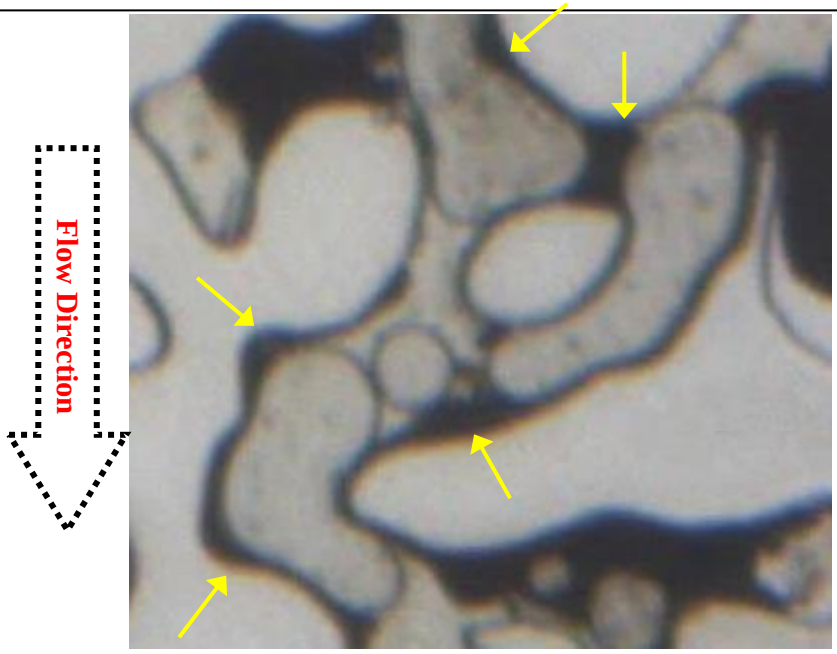

Figure 5-51: The process of oil recovery through co-current film flow mechanism in a highly magnified sections of the micromodel in which oil films (yellow arrows) in between CO2 bubbles and pore walls can be clearly seen.

Counter-current film flow: While the aforementioned film flow mechanism was observed to take place only in the interconnected pores, residual oil in the dead end pores was also displaced and recovered through oil films, but in a different manner. In this displacement mechanism, CO2 bubbles entered and occupied the centre of the pores forcing the resident oil out through oil layers around the CO2 bubble in the opposite direction. The displacement of oil from dead end pores through counter-current film flow mechanism, was observed to be significantly slower than the displacement of oil by co-current film flow and emulsification mechanisms from interconnected pores. Figure 5-52 presents a sequence of pictures that shows oil production from a dead-end pore through the counter-current film flow mechanism and Figure 5-53e schematically illustrates this mechanism.

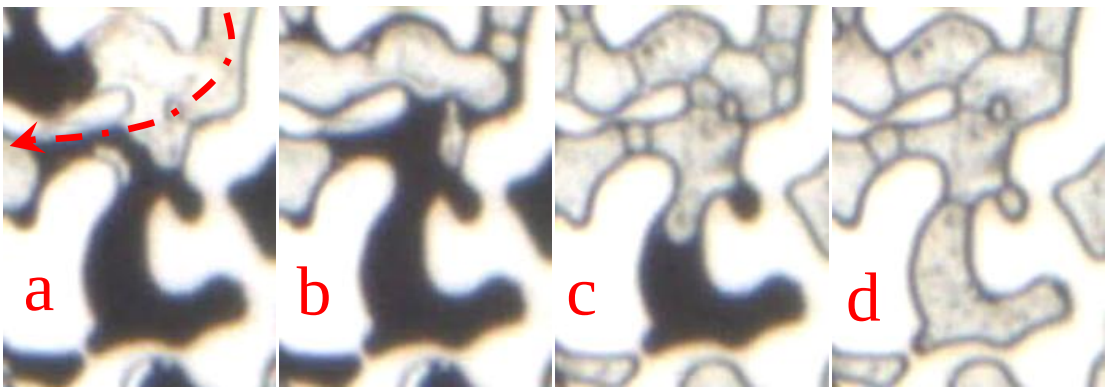

Figure 5-52: The process of oil recovery through counter-current film flow mechanism from a dead end pore. The red arrow in image (a) shows the flow direction of CO2-foam.

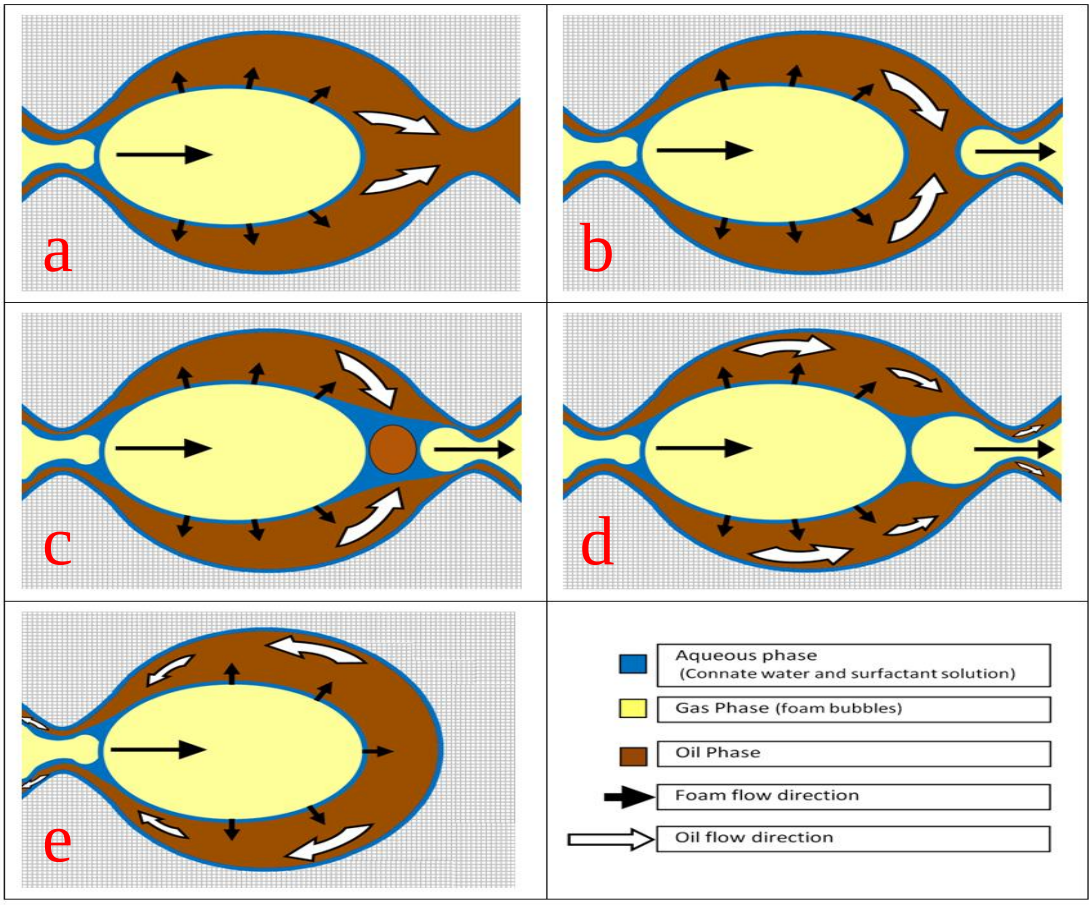

Figure 5-53: Schematic of the pore scale displacement mechanisms during foam-flood process. (a) Direct displacement of bulk oil, (b) direct displacement of oil in between foam bubbles, (c) emulsification, (d) co-current film flow and, (e) counter-current film flow mechanisms.

Foam Termination Mechanisms

The main foam destabilization mechanism was observed to be the spreading of the oil phase around the foam bubbles. This resulted in the formation of larger pieces of gas phase (either CO2 or N2) instead of small bubbles in that part of the micromodel, where the foam was in direct contact with the oil. This destabilization process can be clearly seen in Figure 5-31 and Figure 5-32 from Exp 11 and in Figure 5-44 from Exp 12 where the part of CO2/N2 foam, which is in a high oil saturation region (centre and right hand side of the micromodel) is larger in size compared to the flowing foam bubbles in the

left hand side of the micromodel. However, other mechanisms were also recognized as playing a role in the destabilization of foam, even in the absence of oil.

In the micromodel tests reported here, foam flood periods were initiated with a pre-flush of surfactant solution. Therefore, coalescence of foam bubbles by "capillary suction coalescence" mechanism never took place in the model. However, coalescence of foam bubbles by "diffusion coalescence" mechanism was frequently observed, where the relatively static neighbouring bubbles of foam (mostly in the right hand side of the micromodel) altered their sizes by diffusion from smaller to larger bubbles. The diffusion of CO2 through liquid lamella causes the smaller bubbles to become gradually smaller and eventually disappear, while the other bubbles grow bigger. Figure 5-54 presents a magnified image of the micromodel with a time difference of two hours. As can be seen, capillary diffusion mechanism has caused coalescence of a number of bubbles, which are shown by dotted circles in this figure.

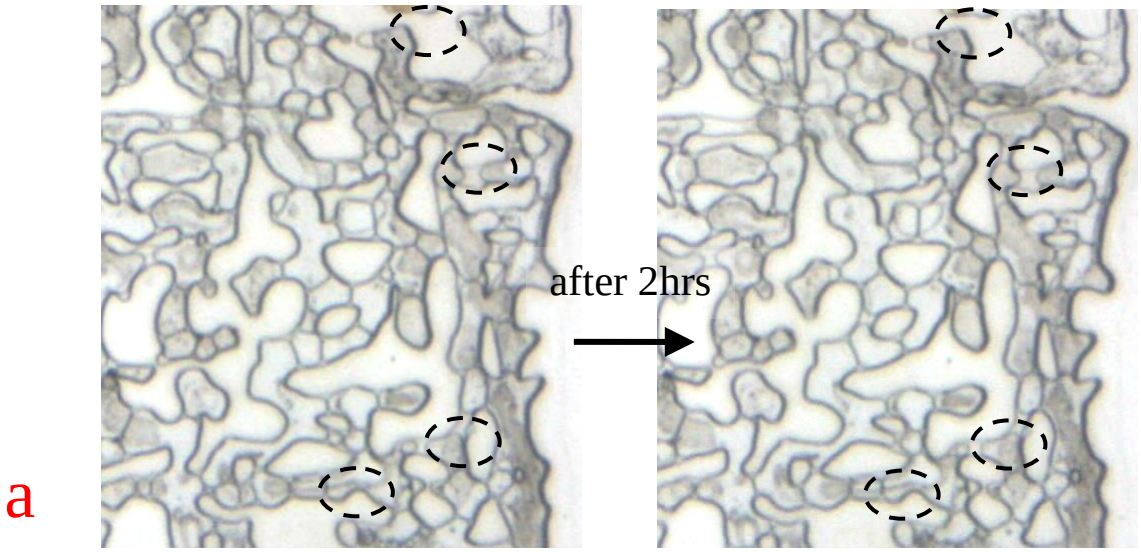

Figure 5-54: Pictures (a) and (b) compare the distribution of static foam in the right hand side of the micromodel, in a time difference of 2 hours in MM Exp 11. As can be seen a number of foam bubbles and lamellae have disappeared due to the gas diffusion coalescence mechanism (black dotted circles).

Oil Spreading Characteristics of the System

While a negative oil spreading system was apparent throughout the period of N_2-foam flood, identifying the spreading behaviour of the CO_2-foam was more complicated. At the beginning of the process of CO2-foam flood when the oil saturation was very high, the CO_2-oil-surfactant system exhibited oil spreading characteristics in which oil layers

spread between CO_2 and aqueous phases. However, the behaviour changed to a non-spreading behaviour after a short period of time, as CO_2-foam displaced oil and the oil saturation dropped significantly. This noticeable change in the spreading characteristics of the oil cannot be explained by the change in oil composition due to mixing with CO_2, as CO_2 dissolution is expected to shift the system towards increased oil spreading, not away from it, as was observed during the experiment.

While the change in the spreading behaviour of the system during the period of CO2-foam flood is not fully understood and requires further investigation, a direct relationship between oil saturation and its spreading behaviour was noticed. The CO2-oil/surfactant system remained oil-spreading, as long as oil saturation was high in the porous media. However, as the oil was displaced and its saturation decreased, this tendency of the oil to spread over the CO2 bubbles, decreased as well, and the system eventually became non-spreading. This caused the CO2-foam in the regions with high oil saturation to show less resistance to flow, compared to the regions where the oil was already displaced and hence assisted diversion of the CO2-foam flow towards high oil saturation regions and also improved displacement efficiency of the process.

5.4 SUMMARY AND CONCLUSIONS

The following conclusions can be drawn from the experiments in the first part of this chapter (injection strategies):

(1) The processes of oil recovery by waterflood, secondary and tertiary CO2 injection, and CO2-SWAG and CO2-foam injection were successfully simulated in the micromodel using an extra heavy crude oil (crude C). The oil recovery was significantly higher in all processes involving CO2 than that of plain waterflood. This is believed to be due to the major viscosity reduction in heavy oil due to mixing with CO2.

(2) From a recovery point of view, extended injection of CO2 in secondary mode showed the highest recovery efficiency, followed by CO2-SWAG and tertiary CO2 injection strategies.

(3) The main contributing mechanisms during secondary CO2 injection were observed to be dilution of crude oil followed by gravity drainage. Despite the initial poor sweep efficiency of the injected CO2, extended periods of injection resulted in a very high recovery efficiency.

(4) Unlike the secondary CO2 injection, tertiary CO2 injection showed a poor recovery efficiency as a result of the presence of water layers, which significantly disrupted the process of oil displacement and recovery by gravity drainage. The diluted oil was only recovered when the CO2 injection was followed with a period of waterflood.

(5) CO2-SWAG recovery was also promising due to dispersion of slugs of CO2 into the oil phase, which promoted direct displacement of oil by CO2 and water. In comparison to continuous CO2 injection, CO2-SWAG process also offers the advantage of utilizing less CO2.

The following conclusions are drawn from the experiments in the second part of this chapter (mobility control by foam):

(6) The results showed that when strong CO2-foam is formed in the porous media, the heavy crude oil can be displaced from the porous media very efficiently. In the case of N2-foam, despite formation of stronger foam in the system, the displacement process was observed to be less efficient. The better performance of CO2-foam process is attributed to the favourable reaction of the oil to CO2 (the viscosity reduction in the oil phase as a result of CO2 dissolution).

(7) N2-foam was observed to be more stable than CO2-foam even after contacting the heavy oil at early times of injection. The non-spreading characteristic of the oil during N2-foam injection compared to the oil spreading behaviour during CO2-foam injection is believed to be the main reason for this behaviour.

(8) Two main stages of oil recovery were observed and identified during the foam injection experiments. In the first stage, heavy oil was displaced from the well-connected pores and high permeability parts of the porous medium. As the main flowing path became partially blocked by foam, in the second stage, foam was gradually developed towards the low permeability parts and the dead-end pores and recovered the residual oil in those regions of the porous medium.

(9) Direct displacement of heavy oil by foam at the early times of injection was observed to be much more effective than the double-drainage displacement process during CO2 flood. At the later stages, after CO2-foam breakthrough, the

unswept oil in the previously flooded pores was displaced by two other mechanisms: "co-current film flow" and "oil emulsification". These mechanisms were observed in the interconnected pores and resulted in a high oil recovery of up to 90%.

(10) A new counter-current film flow mechanism was recognized, which improved the displacement of the residual oil trapped inside dead-end pores. Recovery of the residual oil from dead end pores by counter-current film flow mechanism, however, was significantly slower than displacement process in the inter-connected pores.

(11) Finally, CO2-foam injection performed much better compared to plain CO2 and N2-foam injection. However, it is believed that this process can be further improved by combining CO2 and N2 foam in an injection strategy in which N2-foam is used to provide more stable foam and thus better mobility control and CO2-foam is used to provide oil viscosity reduction and better displacement efficiency.

CHAPTER 6 VISUAL INVESTIGATION OF HEAVY OIL RECOVERY BY CO2 INJECTION IN CRUDE "J"

6.1 INTRODUCTION

This chapter presents the results of a series of visualisation experiments to investigate the performance of high pressure CO2 injection for improved recovery and storage purposes in crude "J". This study provides a better understanding of the pore scale mechanisms involved during high pressure CO2 injection and highlights the differences observed using low pressure CO2 injection.

The crude "J" reservoir has an exceptionally low temperature in which CO2 would be in liquid state. In liquid state, CO2 shows high densities comparable to those of oil and brine, which alleviate the well known issue of gravity segregation during CO2 injection. All the micromodel experiments in this chapter were performed using the homogeneous rock-look-alike pattern micromodel. Our experiments using crude "J", show that this crude sample has a tendency to make porous media oil-wet, therefore all the experiments in this chapter were performed in slightly oil-wet conditions.

In the first part of this chapter, the effect of injection pressure (low pressure and high pressure applications of CO2) and injection strategy (CO2 injection before or after water injection) has been investigated. The second part looks into the process of heavy oil recovery by CO2-emulsion and the pore scale interactions between foam and heavy oil.

6.2 THE EFFECT OF PRESSURE AND INJECTION STRATEGY

In this section, the effect of injection pressure (high pressure and low pressure applications of CO2) and injection strategy (scenarios of CO2 injection post and pre waterflood) are investigated through three micromodel experiments. The first two tests simulate the scenario of tertiary CO2 injection at a reduced pressure of 600 psig (where CO2 is present in vapour state) and at the real reservoir pressure of 1500 psig (where CO2 is present in liquid state). At reservoir pressure and temperature of crude "J", pure CO2 will be present in liquid state; however, the CO2 sources are very unlikely to be 100% pure and as a result the injected CO2-mixture can be a vapour at the reservoir pressure and temperature. Therefore, it is important to study the difference in oil recovery mechanisms and performance for both liquid and vapour CO2. If the benefits of having CO2 in liquid state are significant, the surface facilities could be installed to separate impurities from CO2 before injecting that into the reservoir. The third experiment looks into the process of CO2 injection in a reservoir, prior to waterflood, where the oil phase is still connected within the porous medium.

6.2.1 MM Exp 13: Tertiary Injection of Vapour CO2

To compare the performance of liquid and vapour CO2 under tertiary injection conditions, two micromodel tests were designed and conducted with similar procedure and materials, with the exception that one used vapour and the other used liquid CO2. The first micromodel experiment was carried out at a reduced pressure of 600 psig to ensure that the injected CO2 would be in vapour state. The performance of liquid CO2 injection under tertiary injection for crude oil "J" is investigated in the following experiment.

Procedure

1 *Initialization:* The micromodel was saturated with distilled water at T = 25 °C and P = 600 psig.

2 *Oil Flood:* The micromodel was flooded with crude oil "J" from the bottom until the oil front reached the other end of the micromodel.

3 *1st Waterflood*: distilled water was injected into the micromodel for 1 day.

4 *CO2 Flood*: Vapour CO2 was injected into the micromodel for 3 days.

5 *2nd Waterflood*: Distilled water was injected into the micromodel for 1 day.

Table 6-1 lists a summary of the fluids used and the pressure and temperature at test conditions.

Table 6-1: Fluids used and pressure and temperature conditions of MM Exp 13.

Porous Medium	Homogeneous Rock-look-alike Micromodel
Crude Oil	"J" (617 at 28 °C)
Aqueous Phase	Distilled Water
Gas Phase	Vapour CO2
Temperature	25 °C
Pressure	600 psig

Results

Initialization and Oil Injection

To begin the experiment, the micromodel was first saturated with distilled water. Subsequently, the crude oil (crude "J") was injected into the micromodel to establish the initial water/oil saturation. High oil saturation was achieved during the oil flood period due to the high oil/brine viscosity ratio. Figure 6-1 and Figure 6-7(a) show a magnified section and a full-length picture of the micromodel respectively, during this period of oil injection, in which the oil has a dark brown colour and connate water is colourless.

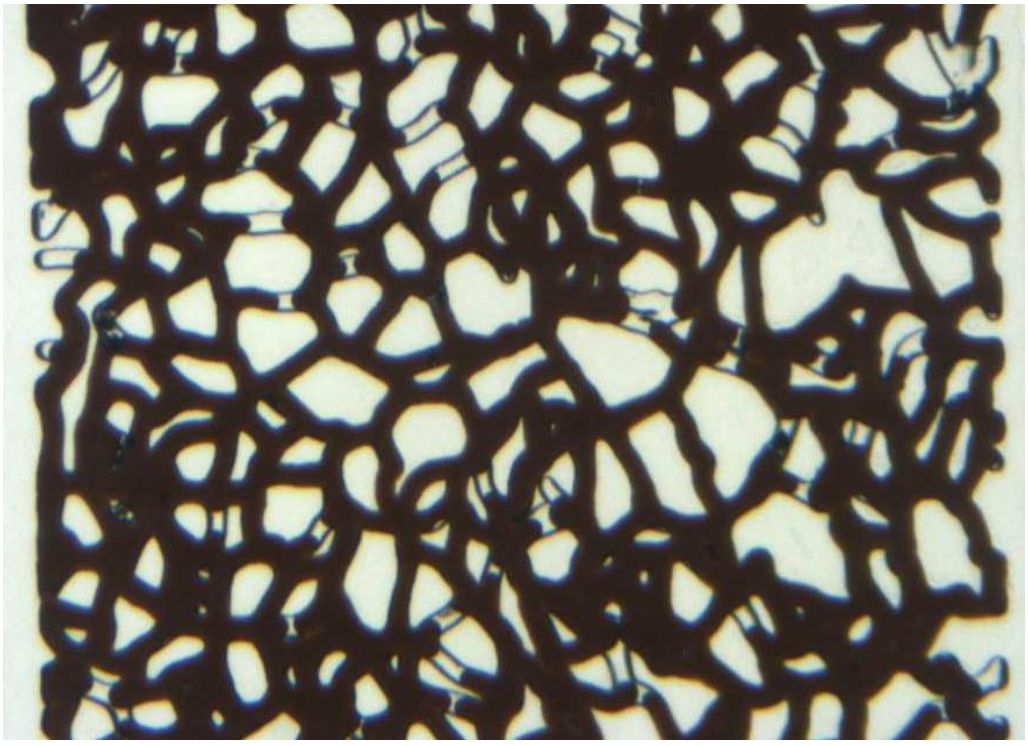

Figure 6-1: MM Exp 13; a magnified section of the micromodel at the end of the period of oil injection.

1st Water Injection

Having carried out the oil injection as described above, the micromodel was then flooded with water from the top end of the micromodel for a period of 1 day. The pore scale displacement of the oil by water was observed to be piston-type in the majority of pores. The system was recognized to have oil-wet tendency as the curvature of oil/water interfaces were mostly towards the oil phase. Additionally oil layers and stains could be easily spotted on pore wall and surfaces after displacement by water. and layers and stains of oil could be easily Good indications of the oil-wet tendency of the system are demonstrated by the curvature of oil/water interfaces being mostly towards the oil phase and the existence of layers and stains of oil on pore walls and surfaces. Figure 6-2 and Figure 6-7a illustrate the same magnified section and corresponding full-length picture of the micromodel respectively, at the end of this period of waterflood.

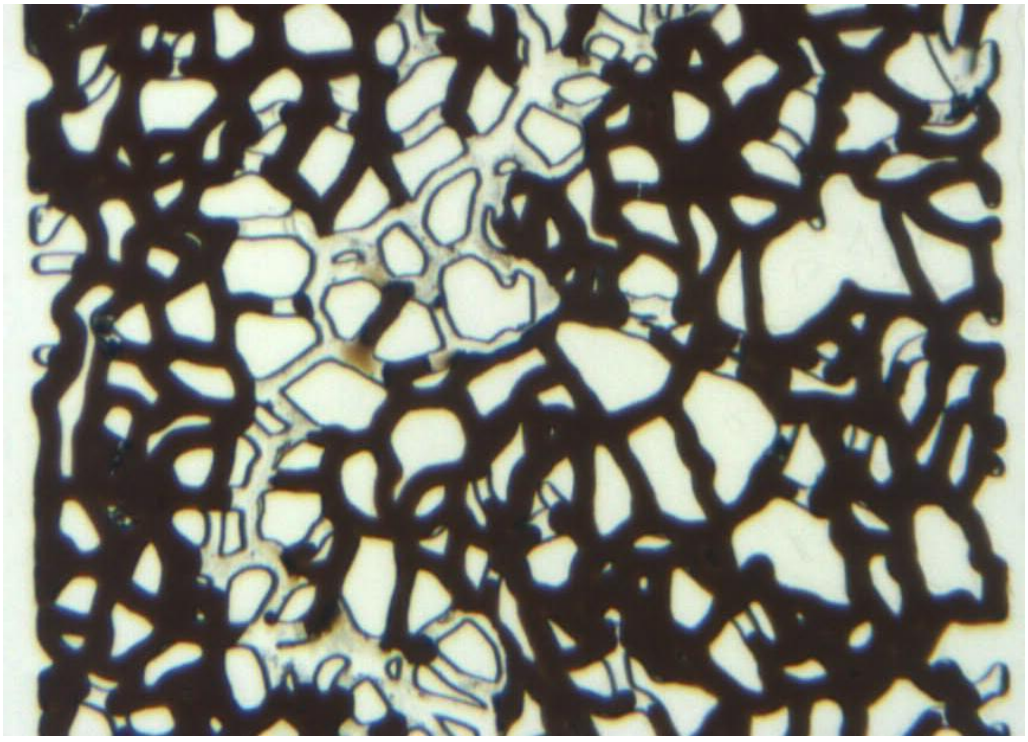

Figure 6-2: MM Exp 13; the same magnified section of micromodel at the end of the 1st period of water injection (1 day).

Tertiary Vapour CO2 Injection

After this water injection, injection of vapour CO2 started from the top end of the micromodel to benefit from gravity forces. The positive oil spreading nature of the system was evident in the micromodel, as the resident oil had a high tendency to spread over the flowing CO2, which caused the formation of thick visible layers of oil around the CO2 stream. Therefore, flowing CO2 could not come into direct contact with the water, and CO2 only invaded pores filled with heavy oil, rather than pores that were occupied with water (despite a much lower viscosity of water compared to the oil). Being a non-wetting phase, the injected CO2 was observed to flow in the middle of the pores and displace resident oil through a double-drainage mechanism. However, since viscosity of the vapour CO2 is much lower than the crude oil viscosity, CO2 was observed to finger through the porous medium bypassing a significant volume of oil. Figure 6-3 presents the magnified section of the micromodel at the breakthrough time of CO2.

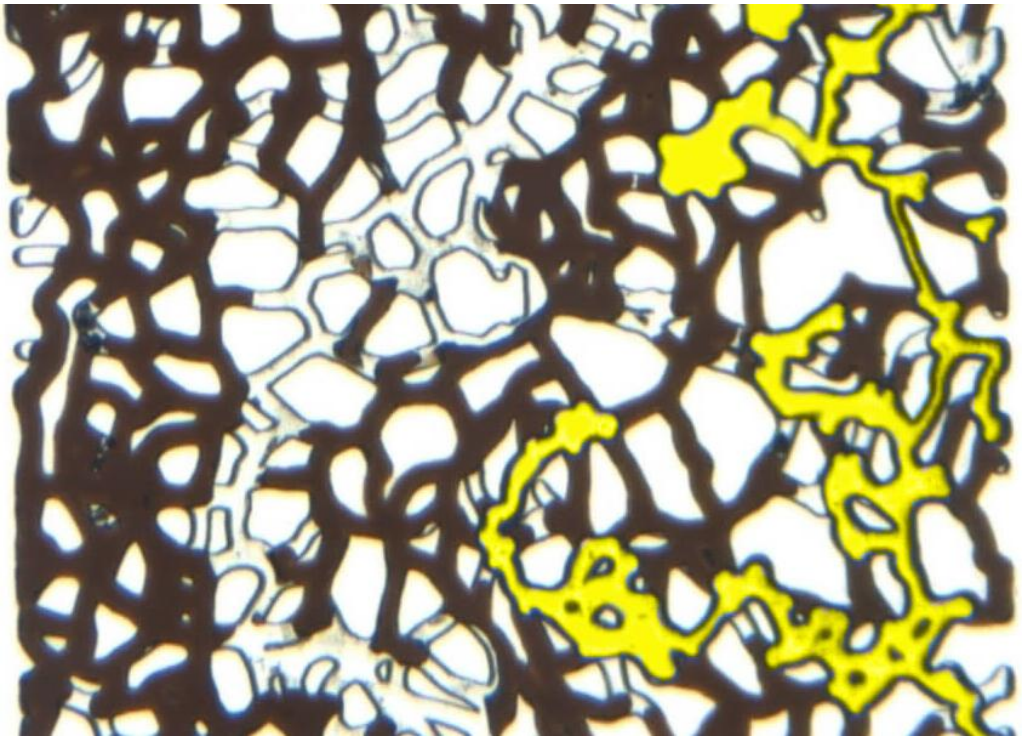

Figure 6-3: MM Exp 13; a magnified section of the micromodel at breakthrough time during the period of CO2 (vapour) injection.

After the CO2 breakthrough, injection of the vapour-CO2 continued for 3 days. During this time period the oil colour was observed to become brighter and isolated oil blobs were observed to swell slightly due to the CO2 dissolution. However, the extended period of vapour-CO2 injection did not result in additional oil recovery over what was

already produced at breakthrough. Figure 6-4 and Figure 6-7c show the magnified section and full-length pictures of the micromodel respectively, at the end of this period of CO2 injection. Comparison of Figure 6-3 and Figure 6-4 shows there are only minor changes in the fluid distribution in the micromodel, and no more oil has been recovered after the CO2 breakthrough. Furthermore, comparison of Figure 6-7c and Figure 6-7b reveals that the flow path of injected CO2 is only through oil filled pores on the right hand side of the micromodel, and pores in the middle of the micromodel (which are fully saturated with water) are not invaded by CO2 after 3 days of injection.

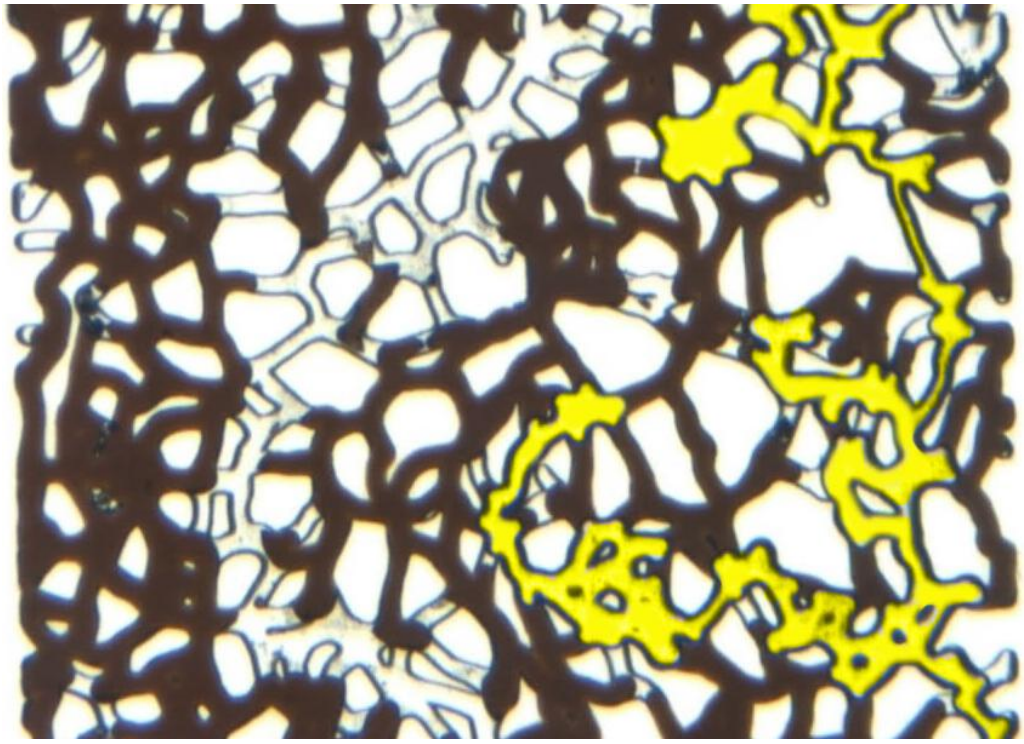

Figure 6-4: MM Exp 13; magnified section of the micromodel at the end of the period of CO2 (vapour) injection (3 days).

2nd Water Injection

The experiment was concluded with another period of water flooding to determine the recovery of the CO2 diluted oil by water flooding. In the early stages of this water injection period, the flow of water caused break up (snap off) of the continuous CO2 stream in the oil phase. Figure 6-5 shows the magnified section of the micromodel at water breakthrough time, when the CO2 phase is scattered and fragmented. Since the fragmented CO2 was not necessarily flowing from the previous CO2 path, this period of simultaneous flow of water and CO2, caused redistribution and improvement in oil recovery.

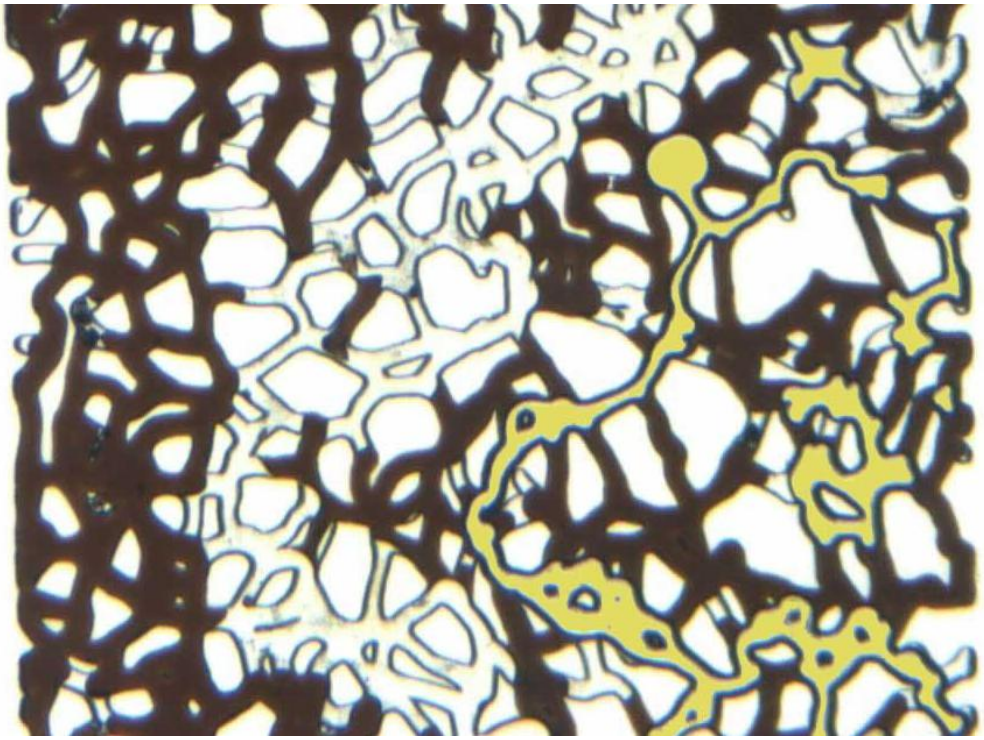

Figure 6-5: MM Exp 13; a magnified section of the micromodel at breakthrough time during the 2nd period of water injection.

As water injection continued, the isolated and broken pieces of CO2 were dissolved into the flowing water and no free CO2 phase was left in the porous medium (the injected water and CO2 were not pre-equilibrated). Figure 6-6 and Figure 6-7d display the same magnified section of the micromodel and corresponding full-length pictures of the micromodel respectively, at the end of the 2nd waterflood period. No free CO2 phase can be seen in these two images, due to the dissolution of CO2 in the injected water. Comparison of pictures (c) and (d) in Figure 6-7 shows slight improvement in oil recovery in regions where the oil has been connected to the CO2 stream (right hand side of the micromodel). However, no additional oil was recovered from regions where the oil was not directly connected to the CO2 stream and was fully covered with water (the red dotted circle on the left hand side of the micromodel).

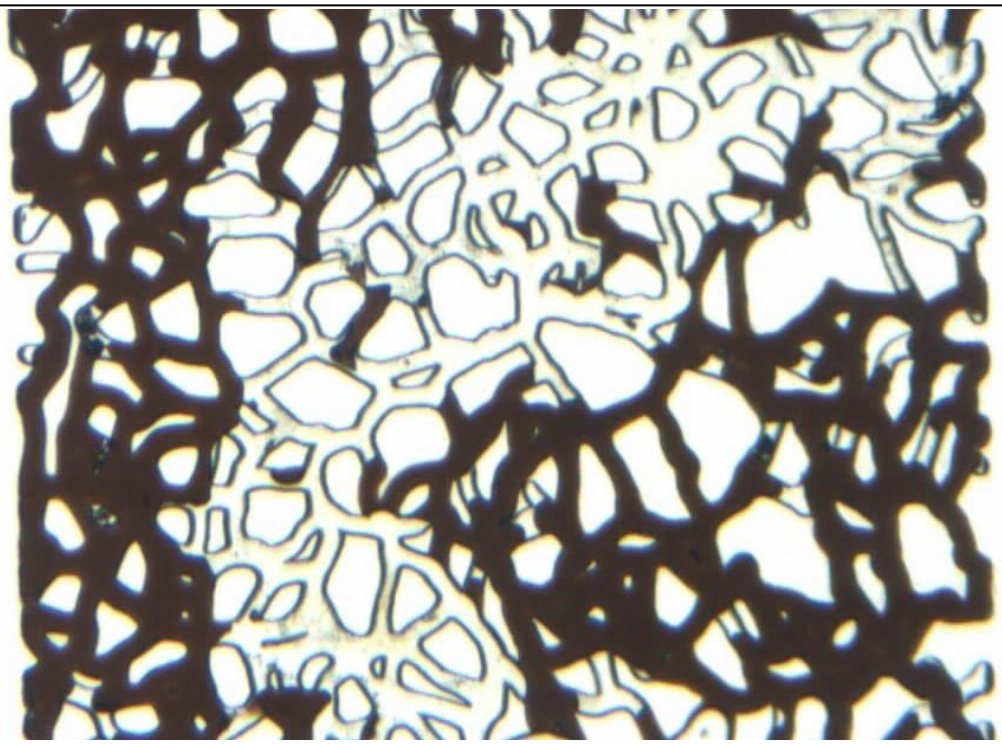

Figure 6-6: MM Exp 13; a magnified section of the micromodel at the end of the 2nd period of water injection (1 day).

Summary

Table 6-2 summarises the oil recovery data at different stages of this experiment (MM Exp 13). Overall, a good amount of oil recovery was observed during the period of vapour-CO2 injection (at breakthrough time of CO2). However, the extended period of CO2 injection after breakthrough time resulted in a small amount of incremental recovery. The subsequent period of water injection improved oil recovery in the regions where oil was connected to the main stream of CO2 (centre and right hand side of the micromodel); however, no redistribution and recovery was achieved from the oil blobs, which were separated from the CO2 stream by water layers.

Table 6-2: MM Exp 13; Summary of the recovery data.

	Recovery @ BT (% OOIP)	Ultimate Recovery (% OOIP)	Cumulative Recovery (% OOIP)
4) 1st Waterflood	-	17	17
5) CO2 flood	13	18*	35
6) 2nd Waterflood	2*	5	40
• A swelling factor of 8% has been considered for calculation of oil recovery.			

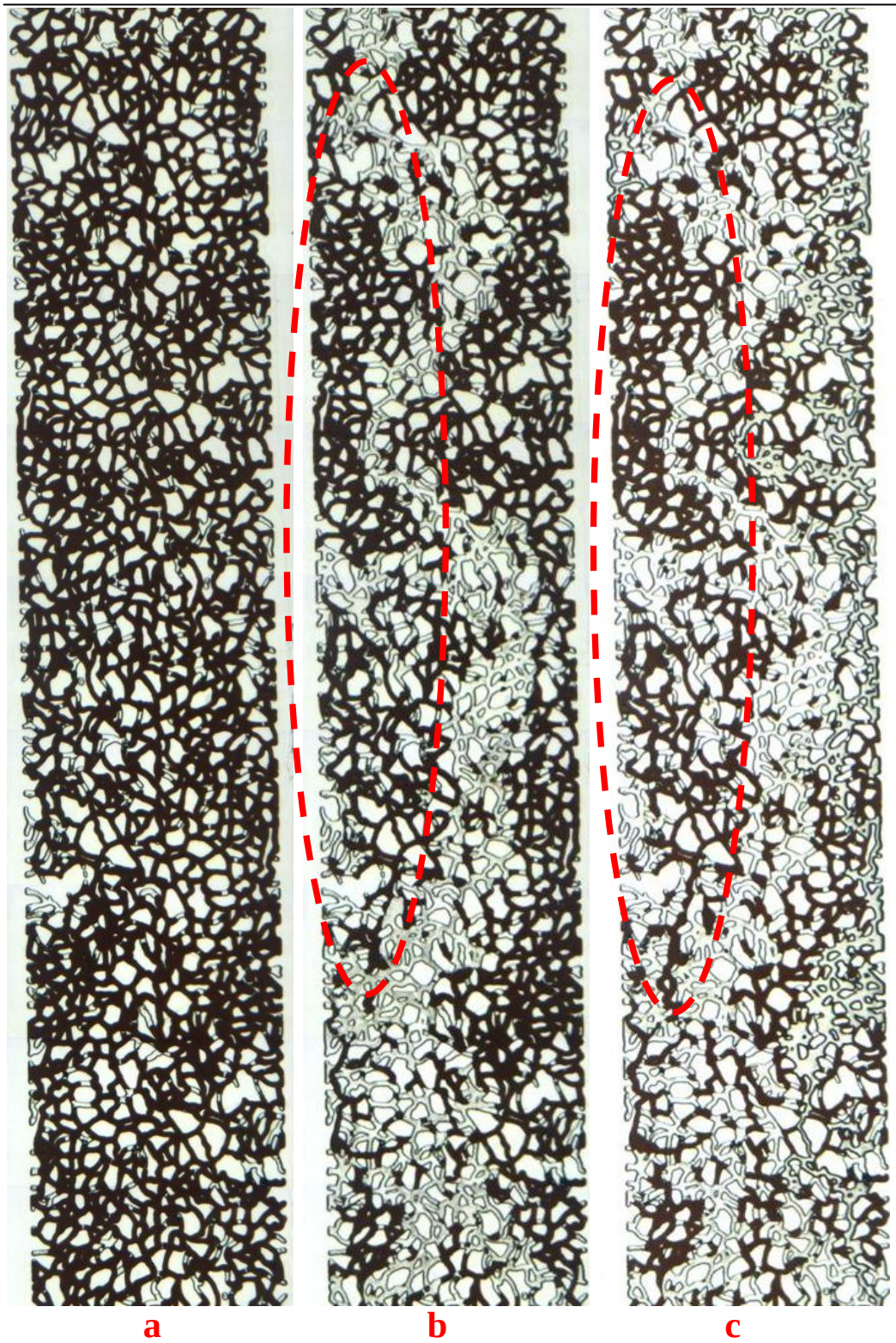

Figure 6-7: MM Exp 13; fluid distribution in the micromodel after (a) oil injection, (b) 1st water injection, and (c) vapour CO2 injection.

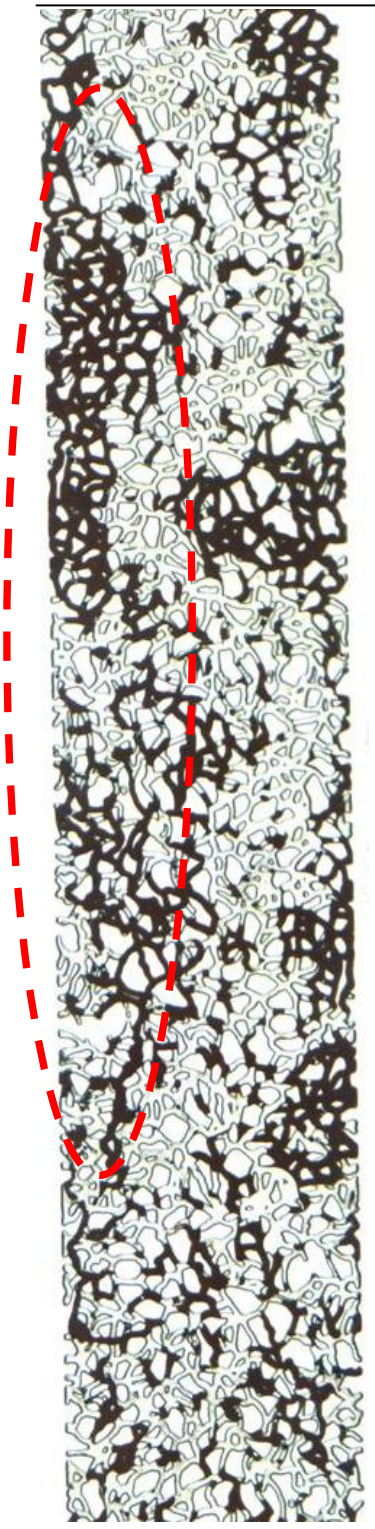

d

Figure 5-7 (continued): MM Exp 13; fluid distribution in the micromodel after (d) 2nd water injection.

6.2.2 MM Exp 14: Tertiary Injection of Liquid CO2

Having examined the performance of vapour CO2 injection at reduced reservoir pressure of 600 psig in the previous experiment, this test was designed and performed to evaluate the recovery mechanisms and displacement efficiency of liquid-CO2 injection at real reservoir conditions.

Procedure

1 *Initialization:* The micromodel was saturated with distilled water at T = 25 °C and P = 1500 psig.

2 *Oil Flood:* The micromodel was flooded with crude oil "J" from the bottom until the oil front reached the other end of the micromodel.

3 *1st Waterflood*: Distilled water was injected into the micromodel for 1 day.

4 *CO2 Flood*: Liquid CO2 was injected into the micromodel for 3 days.

5 *2nd Waterflood*: Distilled water was injected into the micromodel for 1 day.

Table 6-3 lists a summary of fluids used and the pressure and temperature at test conditions.

Table 6-3: Fluids used and pressure and temperature conditions of MM Exp 14.

Porous Medium	Homogeneous Rock-look-alike Micromodel
Crude Oil	"J" (617 at 28 °C)
Aqueous Phase	Distilled Water
Gas Phase	Liquid CO2
Temperature	25 °C
Pressure	1500 psig

Results

Initialization and Oil Injection

To begin the experiment, the micromodel was first saturated with distilled water. Subsequently, the crude oil (crude "J") was injected into the micromodel to establish initial water/oil saturation. High oil saturation was achieved during the oil flood period due to the high oil/brine viscosity ratio. Figure 6-8 and Figure 6-14a show a magnified section and full-length picture of the micromodel respectively, during this period of oil injection, in which the oil has a dark brown colour and the connate water is colourless.

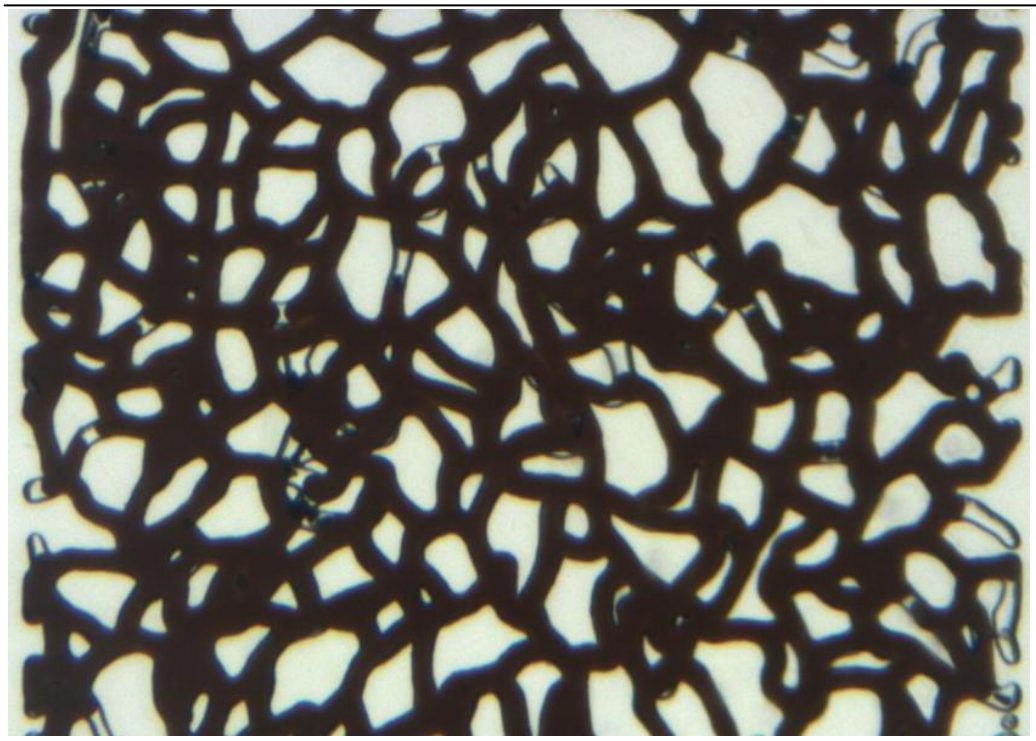

Figure 6-8: MM Exp 14; a magnified section of the micromodel at the end of the period of oil injection.

1st Water Injection

Having carried out the oil injection as described above, the micromodel was then flooded with water from the top end of the micromodel for a period of 1 day. Similarly to the previous test, water was observed to displace the resident oil in a piston-type manner. The type of displacement process and distribution of fluids after waterflood suggested slightly oil-wet conditions in the micromodel. Figure 6-9 and Figure 6-14a illustrate the same magnified section and corresponding full-length picture of the micromodel respectively, at the end of this period of waterflood.

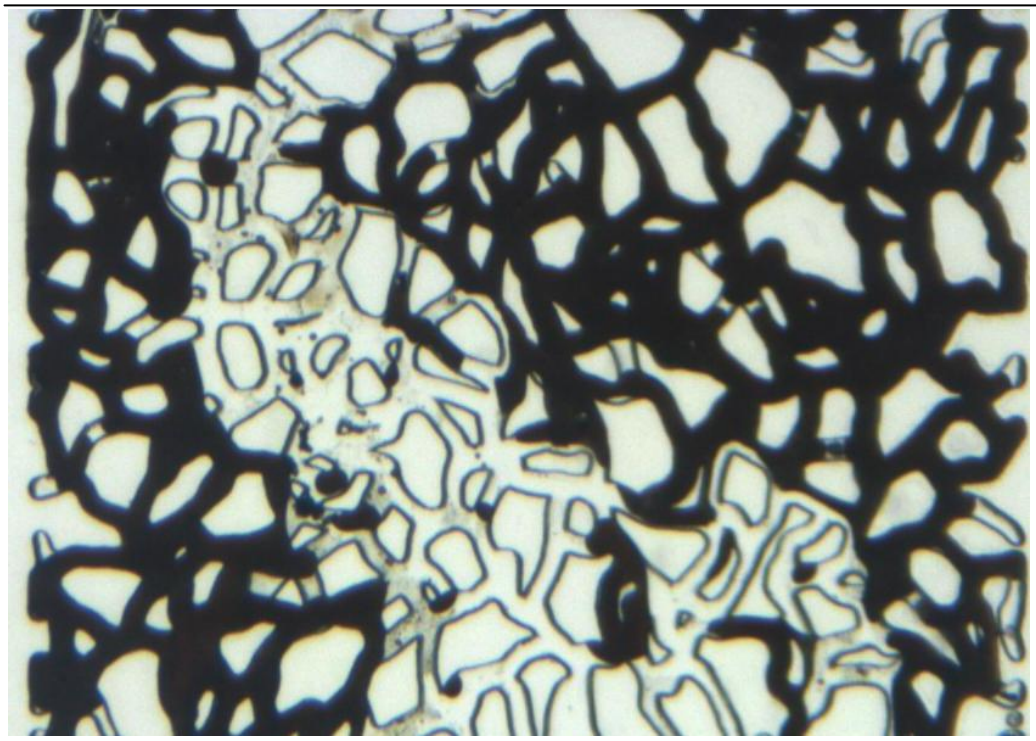

Figure 6-9: MM Exp 14; the same magnified section of the micromodel at the end of the 1st period of water injection (1 day).

Tertiary CO2 Injection

After this waterflood, injection of liquid-CO2 commenced from the top of the vertically oriented micromodel. The displacement process was observed to be very similar and comparable to that of vapour-CO2 at breakthrough time. Being the non-wetting phase, liquid-CO2 was observed to flow in the middle of the pores and displaced resident oil through a double-drainage mechanism. Also the resident oil was observed to have a high tendency to spread over the flowing CO2. Figure 6-10 and Figure 6-14c present the magnified section and the full-length picture of the micromodel respectively, after the breakthrough of CO2. As shown in Figure 6-14c, the injected liquid CO2 flowed through oil occupied pores in the right hand side of the micromodel and did not invade water filled pores in the centre, despite much lower viscosity of water compared to the heavy oil (similar to the example of vapour CO2 injection in the previous experiment).

One important observation at this stage of the test (at CO2 breakthrough) was that a similar oil recovery efficiency was observed in this test using liquid-CO2 and in the previous test using vapour-CO2, despite a higher viscosity of CO2 in liquid state (compare Figure 6-14c and Figure 6-7c). This behaviour might be due to the fact that even the viscosity of liquid CO2 is significantly lower than the viscosity of crude "J" (4 orders of magnitudes). Furthermore, liquid CO2 has a far greater density in comparison

to vapour-CO2; thus the positive effect of the higher viscosity of liquid CO2 was counterbalanced with weakening of gravity forces, considering that these two experiments injected CO2 from the top of the micromodel

Figure 6-10: MM Exp 14; the magnified section of the micromodel at breakthrough time during the period of CO2 (liquid) injection.

Despite the liquid and vapour CO2 flood having similar recovery mechanisms and efficiencies at breakthrough time, the performance of vapour and liquid CO2 was observed to be very different when CO2 injection continued after breakthrough. After breakthrough, as liquid-CO2 injection continued, swelling and discolouring of the oil was observed due to CO2 dissolution in the oil. However, after the first 20 minutes, the liquid CO2 was observed to extract the lighter components of those parts of the oil that were in direct contact with the CO2 stream, and therefore this oil became gradually darker and its volume also reduced. Simultaneously, that portion of oil, which was not directly in contact with the flowing CO2 (separated from CO2 by water), continued to swell as CO2 dissolution continued and it consequently became brighter in colour. Figure 6-11 and Figure 6-14d show the same selected section of the micromodel and full-length picture of the micromodel respectively, after 3 days of liquid-CO2 injection. Comparison of Figure 6-14c and Figure 6-14d shows oil recovery has significantly increased in the regions where the oil has been in direct contact with CO2 due to the extraction process.

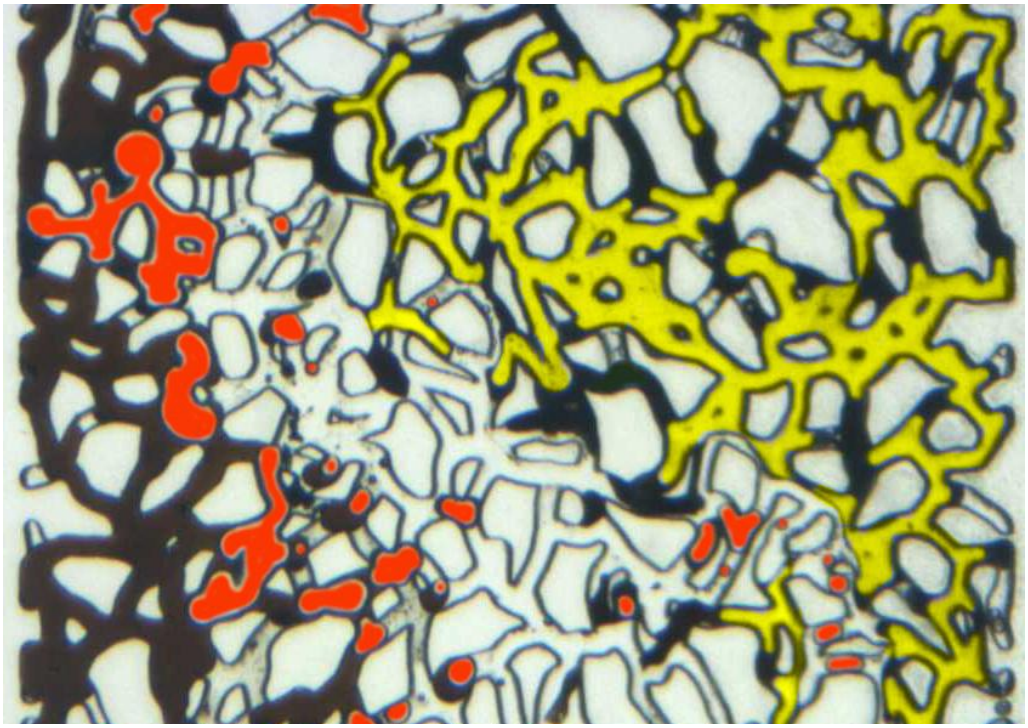

Figure 6-11: MM Exp 14; the magnified section of the micromodel at the end of the period of CO2 (liquid) injection which continued for 3 days.

Another important observation was the formation of a new phase in parts of the oil, which were not directly connected to the CO2. This new phase initially nucleated at the oil-water interface of the smaller oil blobs (in the middle of the micromodel) and as they grew bigger moved to the centre of the oil blobs, where they were fully covered with a layer of oil (in very few cases nucleation of these bubbles was also observed to occur in the middle of oil blobs). As the droplets (or bubbles) of the new phase grew bigger, they appeared to extract light components of the oil blob, which was evident from the darkening colour of the oil phase. In the later stages, these droplets also appeared in the bigger oil ganglia at the left hand side of the micromodel, with similar nucleation process. The bubbles which are digitally coloured red in Figure 6-11 are new phase bubbles at the end of the period of CO2 injection. The new phase was colourless in the micromodel and when it came into contact with the main stream of liquid-CO2, the mixing process was without formation of any interface, which suggests that the new phase is miscible with CO2.

2nd water injection

The CO2 injection period continued for one day and then followed with a second period of water injection for one day. Very similar to the previous test with vapour CO2, the flow of water caused break up (snap off) of the continuous CO2 stream. Since the fragmented CO2 was not necessarily flowing from the previous CO2 path, this period of simultaneous flow of water and CO2 caused redistribution and improvement in oil recovery. Figure 6-12 shows the selected section of the micromodel at water breakthrough time, when the CO2 phase is no longer continuous in the micromodel. The bubbles of new phase and CO2 are both coloured yellow in this figure.

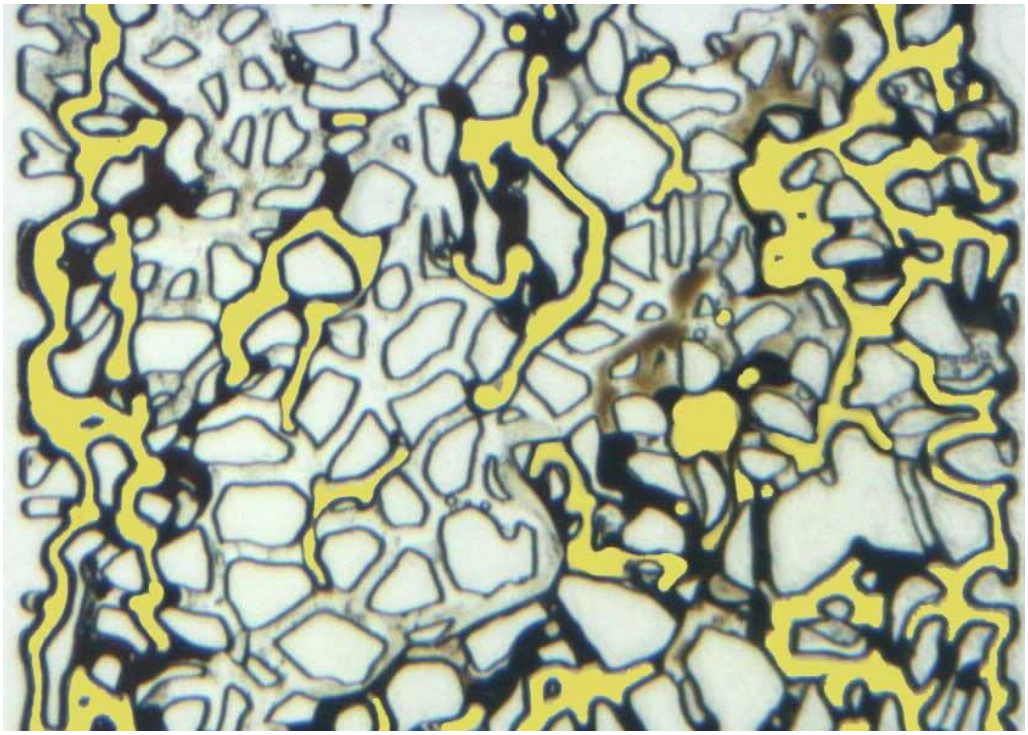

Figure 6-12: MM Exp 14; the magnified section of the micromodel at breakthrough time during the 2nd period of water injection.

As water injection continued, the isolated and broken ganglia of CO2 were dissolved into the flowing water and no free CO2 phase was left in the porous medium. Figure 6-13 and Figure 6-14e display the same magnified section of the micromodel and corresponding full-length picture of the micromodel respectively, at the end of the 2nd waterflood period. No free CO2 phase can be seen in these two images.

One important observation at this stage of the test was the more pronounced redistribution and recovery improvement compared to the example of vapour-CO2 (previous test). In the example of vapour CO2, the redistribution of fluids caused by the 2nd waterflood only had minor effects on the portion of oil connected to the main stream

of CO2. However, in the case of liquid-CO2 (current test) the 2nd period of waterflood caused a much higher redistribution and recovery, mostly from that part of the oil that was separated from the main stream of CO2 with layers of water. Comparison of Figure 6-13 and Figure 6-11 shows that the bypassed oil in the left hand side of the micromodel during 1st waterflood and CO2-Flood is displaced during the 2nd waterflood period. The full length pictures (Figure 6-14d and Figure 6-14e) also confirm this recovery improvement during this period of waterflood. The red circle in Figure 6-14d identifies a large piece of oil, which was bypassed by water during the 1st waterflood and again was not produced during the liquid-CO2 injection period. Figure 6-14e reveals that this part of the oil is fully displaced and recovered during the 2nd waterflood. However, oil recovery has not significantly improved on the right hand side of the micromodel, where oil has been in direct contact with liquid-CO2. This is as a result of the extraction process, which has caused the remaining oil to become more viscous.

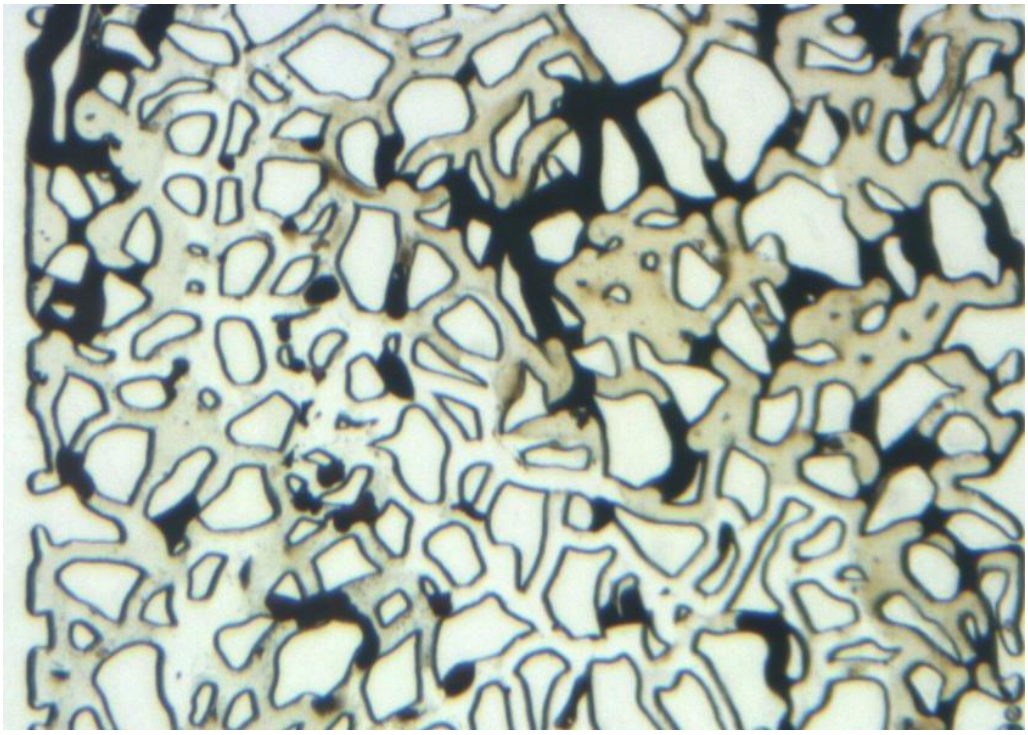

Figure 6-13: MM Exp 14; the magnified section of the micromodel at the end of the 2nd period of water injection (1 day).

Summary

Table 6-4 summarises the oil recovery data at different stages of this experiment (MM Exp 14). The results from this micromodel test (using liquid-CO2) show the recovery

mechanisms and efficiency were quite similar to the previous test during the first period of waterflood and the subsequent period of CO2 injection until CO2 breakthrough (29 and 28 %OOIP recovery in the previous and current experiments, respectively). However, after the CO2 breakthrough, oil production continued in this experiment as opposed to the previous experiment by an extraction mechanism in which CO2 stripped out the lighter hydrocarbons from the oil. The subsequent period of waterflood enhanced oil recovery, especially in the regions where oil was not connected to the main stream of CO2 (during CO2 flood). Comparison of Figure 6-14e and Figure 6-7d shows that the oil recovery was significantly (31 %OOIP) higher in the current test using CO2 in liquid state, compared to the previous test using CO2 in vapour state.

Table 6-4: MM Exp 14; Summary of the recovery data.

	Recovery @ BT (% OOIP)	Ultimate Recovery (% OOIP)	Cumulative Recovery (% OOIP)
7) 1st Waterflood	-	18	18
8) CO2 flood	10	34*	52
9) 2nd Waterflood	15*	19	71
• A swelling factor of 18.1% has been considered for calculation of oil recovery.			

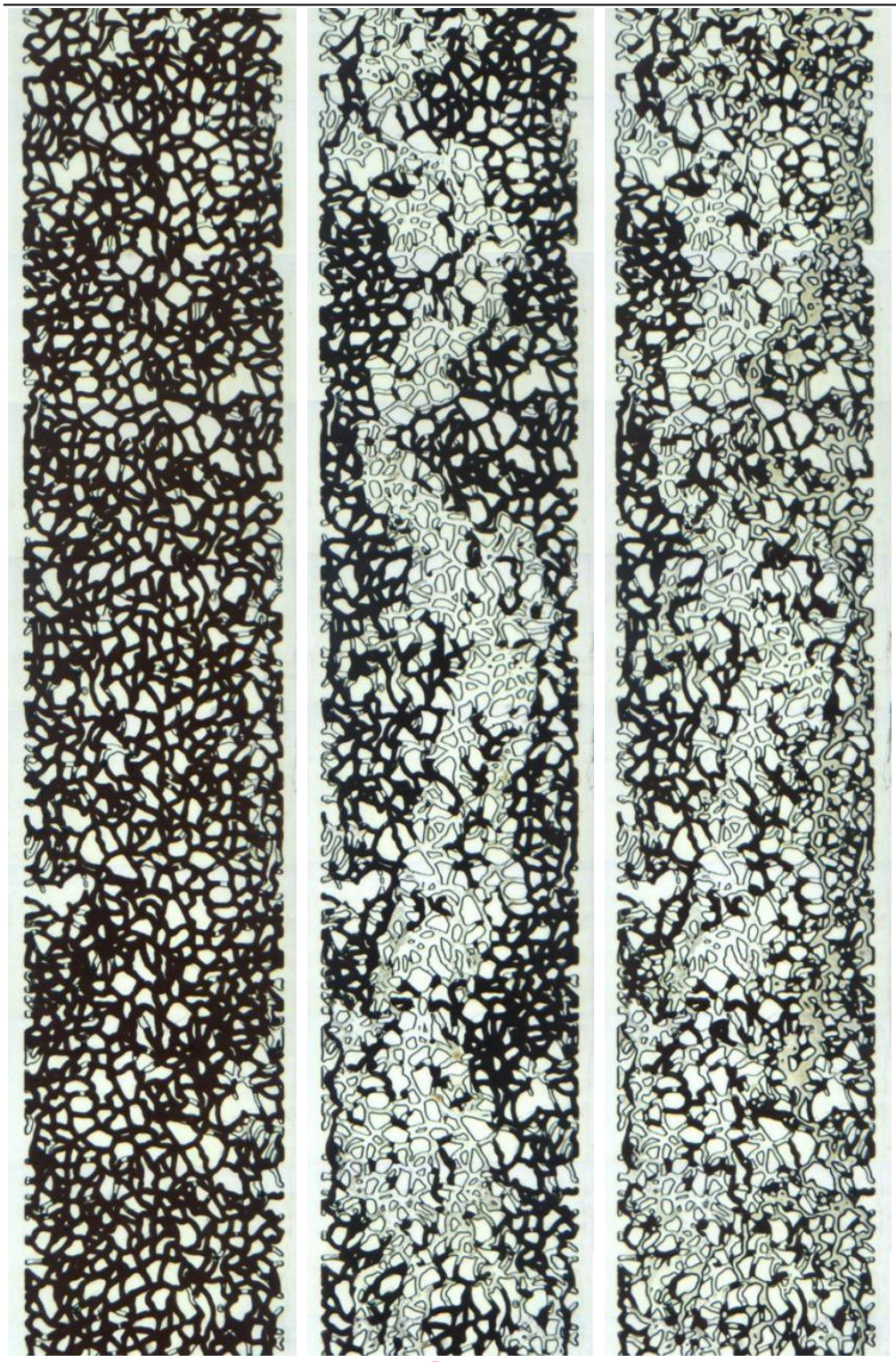

Figure 6-14: MM Exp 14; fluid distribution in the micromodel after (a) oil injection, (b) 1st water injection, (c) at breakthrough during liquid CO2 injection.

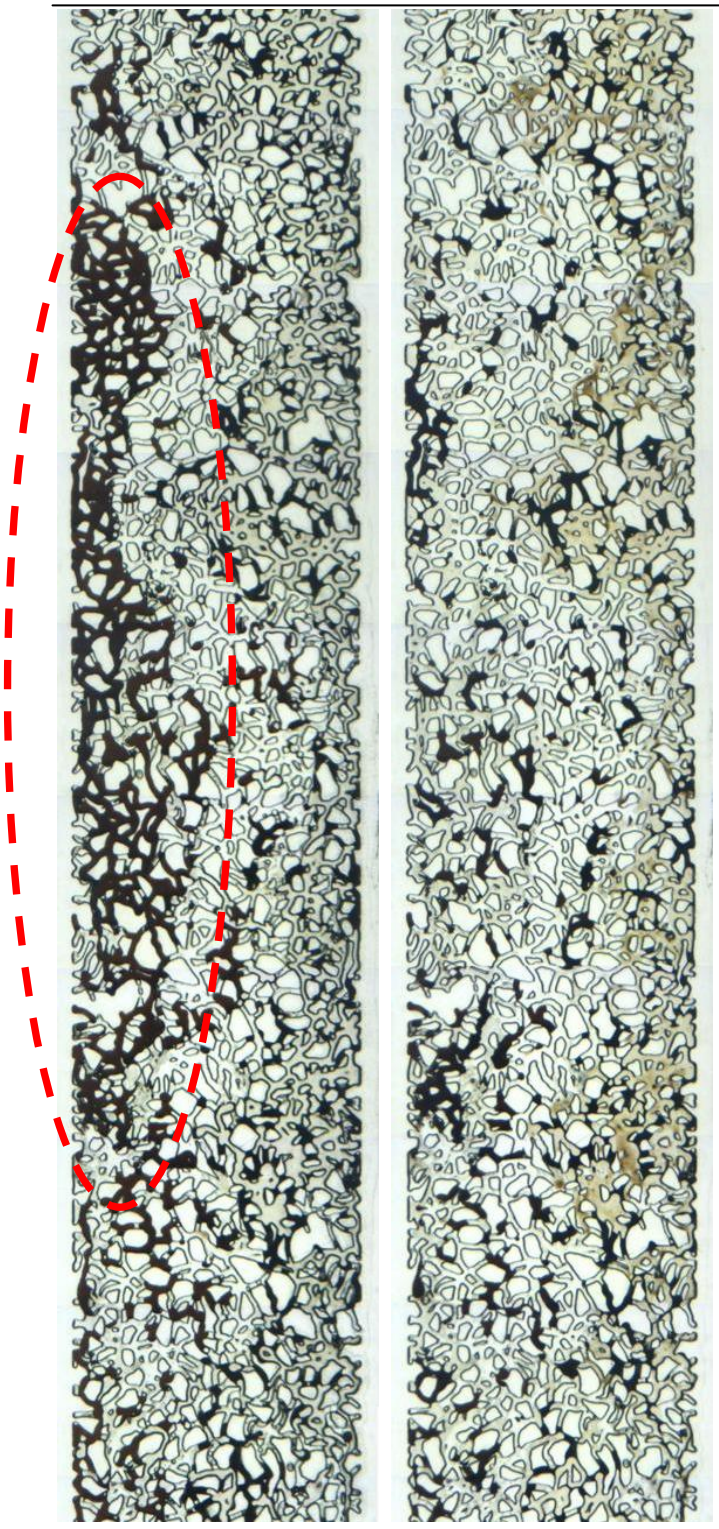

Figure 5-7 (continued): MM Exp 14; fluid distribution in the micromodel after (d) liquid CO2 injection and, (e) 2nd water injection.

6.2.3 MM Exp 15: Secondary Injection of Liquid CO2

The last experiment in the first part of this chapter looks into the process of secondary liquid CO2 injection at reservoir conditions, for enhanced recovery of crude "J". The comparison of results of this experiment with the previous experiment, can assist in selecting the most appropriate injection strategy of CO2 (pre- or post-waterflood injection of CO2).

Procedure

1 *Initialization:* The micromodel was saturated with distilled water at T = 25 °C and P = 1500 psig.

2 *Oil Flood:* The micromodel was flooded with crude oil "J" from the bottom until the oil front reached the other end of the micromodel.

3 *CO2 Flood*: Liquid CO2 was injected into the micromodel for 1 day.

Table 6-5 lists a summary of fluids used and the pressure and temperature at test conditions.

Table 6-5: Fluids used and pressure and temperature conditions of MM Exp 15.

Porous Medium	Homogeneous Rock-look-alike Micromodel
Crude Oil	"J" (617 at 28 °C)
Aqueous Phase	Distilled Water
Displacing Phase	Liquid CO2
Temperature	25 °C
Pressure	1500 psig

Results

Initialization and Oil Injection

To begin the experiment, the micromodel was first saturated with distilled water. Subsequently, crude "J" was injected into the micromodel to establish the initial water/oil saturation. Figure 6-15 and

Figure 6-21a show a magnified section and full-length picture of the micromodel respectively, at the end of this period of oil injection, in which the oil has a dark brown colour and the connate water is colourless. A high oil saturation was achieved during the oil flood period, due to the high oil/brine viscosity ratio.

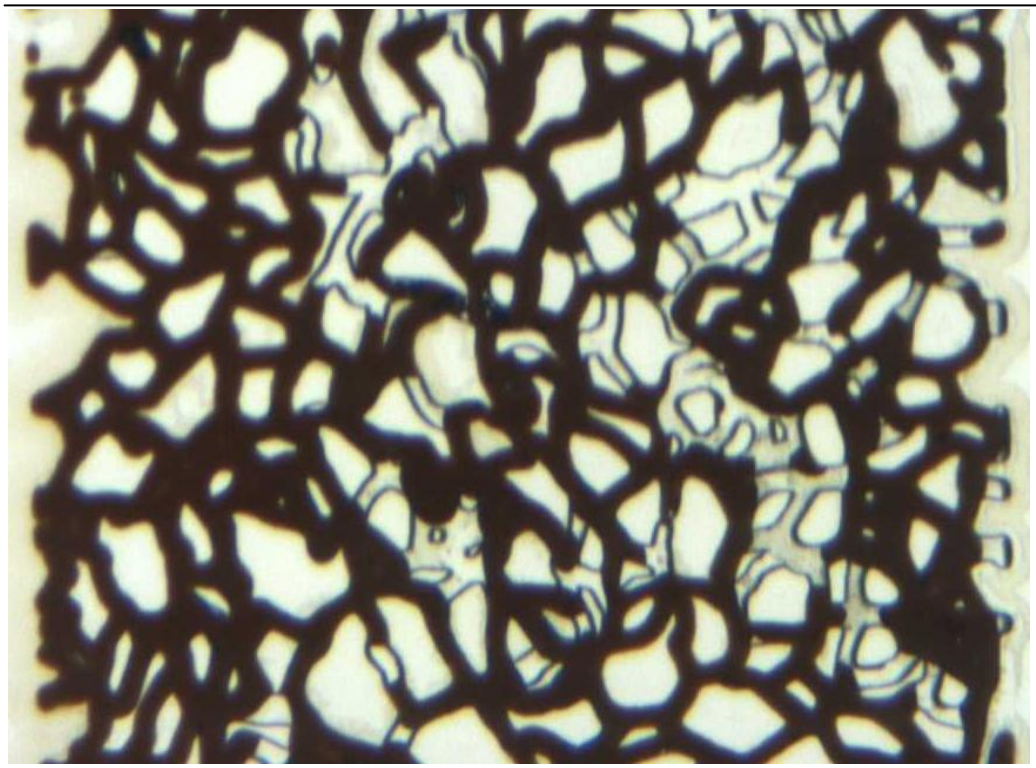

Figure 6-15: MM Exp 15; a magnified section of the micromodel at the end of the period of oil injection.

Secondary CO2 Injection

CO2 was initially circulated through the bypass lines for an extended period of time, to ensure all the lines and connections were filled with liquid CO2 and CO2 injection had reached steady state conditions, then liquid CO2 was diverted towards the micromodel. Being a non-wetting phase, injected CO2 was observed to flow in the middle of the pores and displace resident oil towards the producing end of the micromodel. Figure 6-16 and

Figure 6-21b show the same magnified section and full length picture of the micromodel at CO2 breakthrough time. Having a much lower viscosity compared to the crude oil, injected CO2 was observed to finger through the porous medium and bypass some oil in the middle and right hand side of the micromodel.

Just after the first contact between the injected liquid CO2 and crude oil, two physical phenomena appeared simultaneously. While the CO2 molecules dissolved and diffused into the oil phase, the lighter hydrocarbons from the oil phase were extracted by the continuous stream of flowing liquid CO2. The detailed study of the video clips at the early stages of the CO2 injection, shows that the CO2 dissolution process was stronger at the early stages of liquid CO2 injection; however, as the injection continues, the

extraction process predominant the pore scale interaction between the oil and liquid CO2. Figure 6-17 and Figure 6-18 show the same magnified section of the micromodel after 3 and 5 hours of liquid CO2 injection respectively. The lighter colour of oil and swelling of the oil blobs are good indications of the CO2 dissolution process in the first 3 hours of liquid CO2 injection. It is important to notice that even at later stages, while resident oil in the regions close to the main stream of CO2 is being produced by extraction process (which can be recognized from the darker colour of oil in Figure 6-18), resident oil further away from the CO2 is still gaining more CO2 and swells. This mechanism can be distinguished from the lighter colour of oil in the right hand side of the micromodel and the swelling of the oil that is not in direct contact with CO2. An example of locations of such behaviour has been highlighted by the red dotted circles in Figure 6-17 and Figure 6-18. As injection of CO2 continued, CO2 opened new flow paths and displaced resident diluted oil on the right hand side of the micromodel, as shown in Figure 6-19.

After the first 10 hours of CO2 injection, extraction of light hydrocarbons in the oil phase became the dominant recovery mechanism in the micromodel. This could be recognized from the darkening of oil colour and the redistribution pattern of fluids in the micromodel. The oil recovery by extraction mechanism resulted in widening of the available CO2 paths and new branches of CO2 formation to nearby oil saturated pores at very slow rates. This was completely different from the pattern of oil displacement by direct displacement at the early stages of injection, when CO2 was developing new flowing paths through the interconnected oil occupied pores. Figure 6-20 and Figure 6-21c shows the magnified section and full length picture of the micromodel respectively, after 1 day of continuous liquid CO2 injection, in which oil colour is significantly darker than the original colour of crude "J". As shown, very high oil recovery has been achieved by a combination of CO2 dissolution and extraction mechanisms. Table 7-2 summarises the oil recovery data at different stages of this experiment (MM Exp 15).

During the extended period of liquid CO2 injection in this experiment and previous experiment (tertiary CO2 injection), the injected CO2 was fully covered by oil phase. Therefore, even though CO2 injection continued for an extended time period, dissolution of water in the liquid CO2 and reduction of water saturation (sometimes called water dry-up process) was never observed.

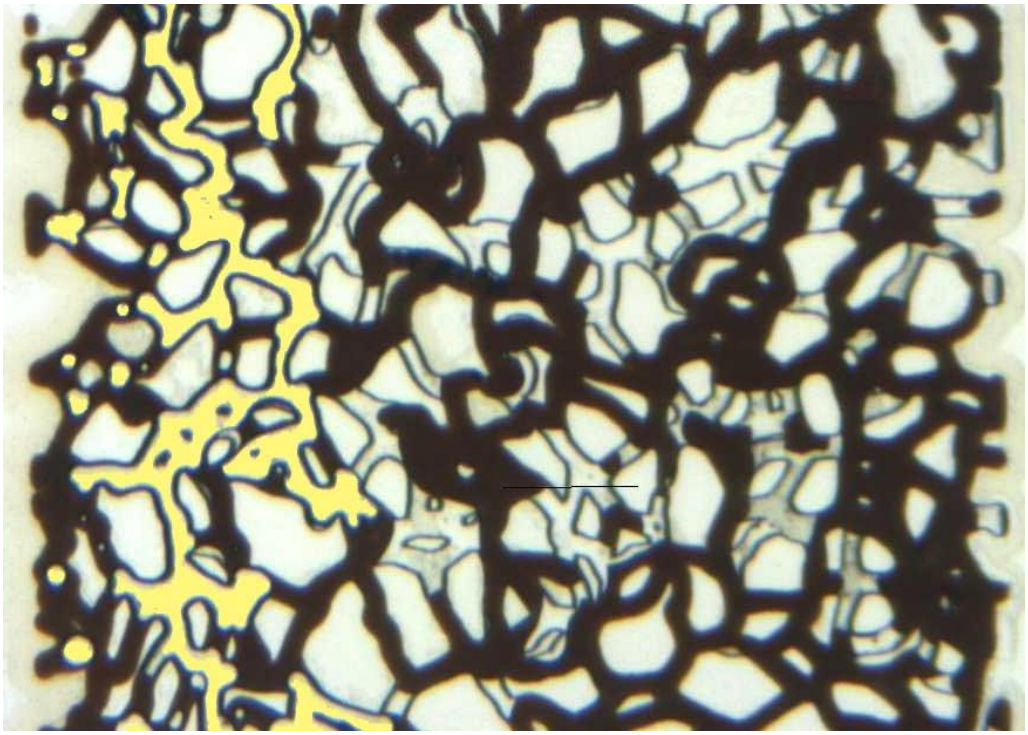

Figure 6-16: MM Exp 15; the same magnified section of the micromodel at breakthrough time during the period of liquid-CO2 injection.

Figure 6-17: MM Exp 15: a magnified section of the micromodel after 3 hours of liquid-CO2 injection.

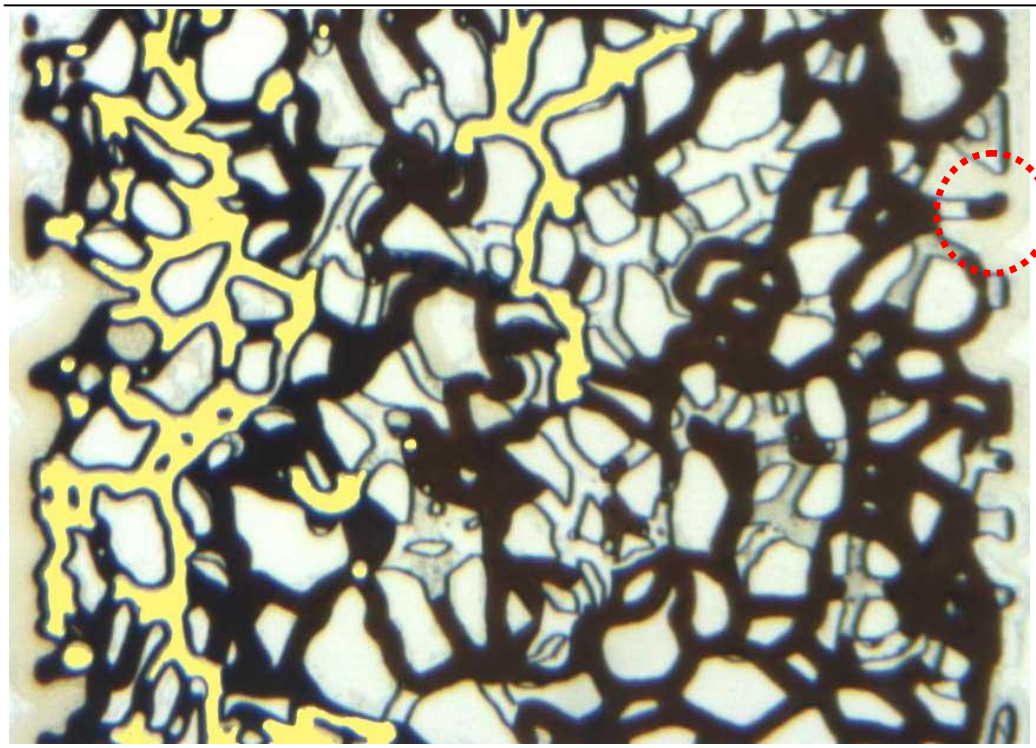

Figure 6-18: MM Exp 15: a magnified section of the micromodel after 5 hours of liquid-CO2 injection.

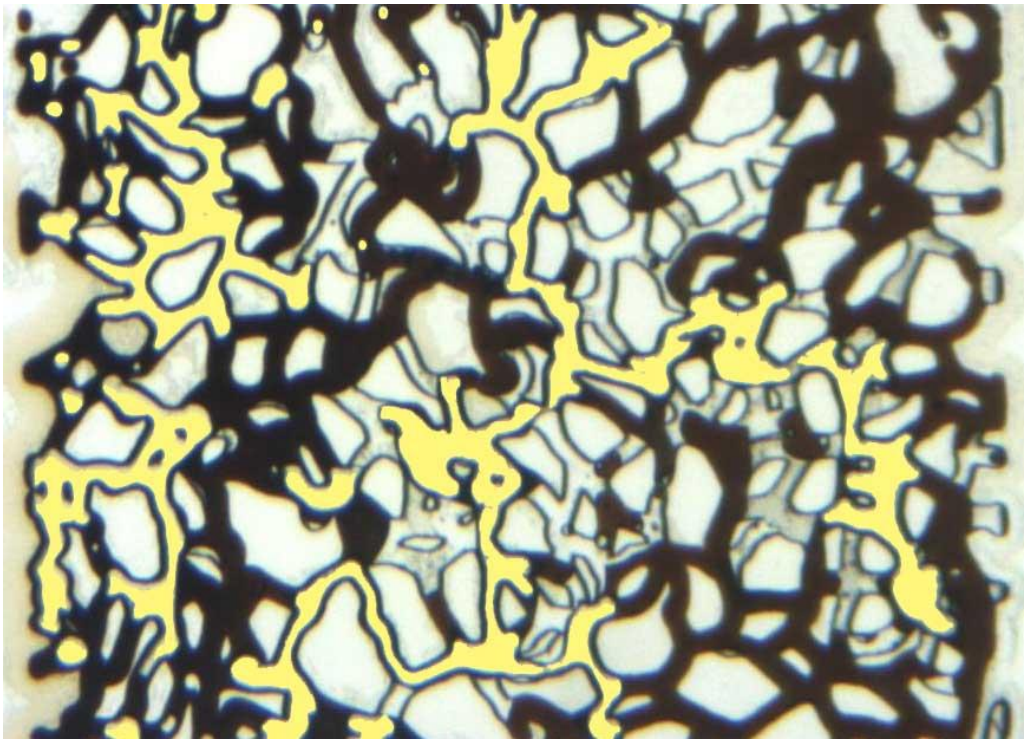

Figure 6-19 MM Exp 15: a magnified section of the micromodel after 10 hours of liquid-CO2 injection.

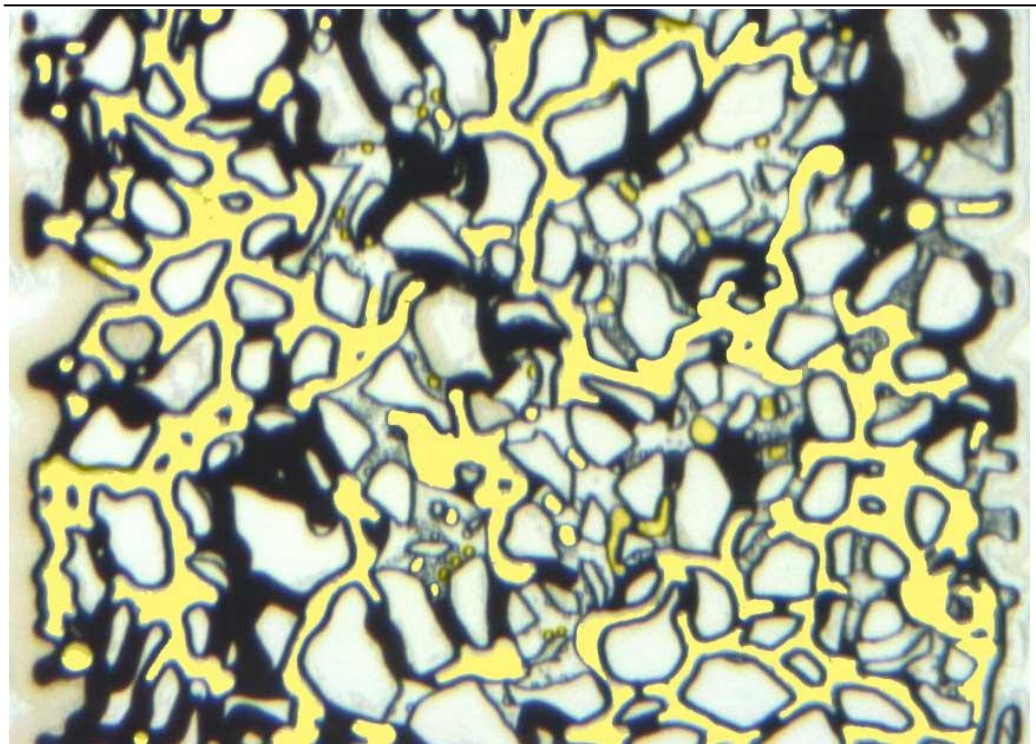

Figure 6-20: MM Exp 15: a magnified section of the micromodel after 1 day of liquid-CO2 injection.

Table 6-6: MM Exp 15; Summary of the recovery data.

CO2 Injection	Recovery (% OOIP)
11) Breakthrough	23
12) 3 hours	33
13) 5 hours	40
14) 10 hours	56
15) 1 day	69
A swelling factor of 18.1% has been considered for calculation of oil recovery.	

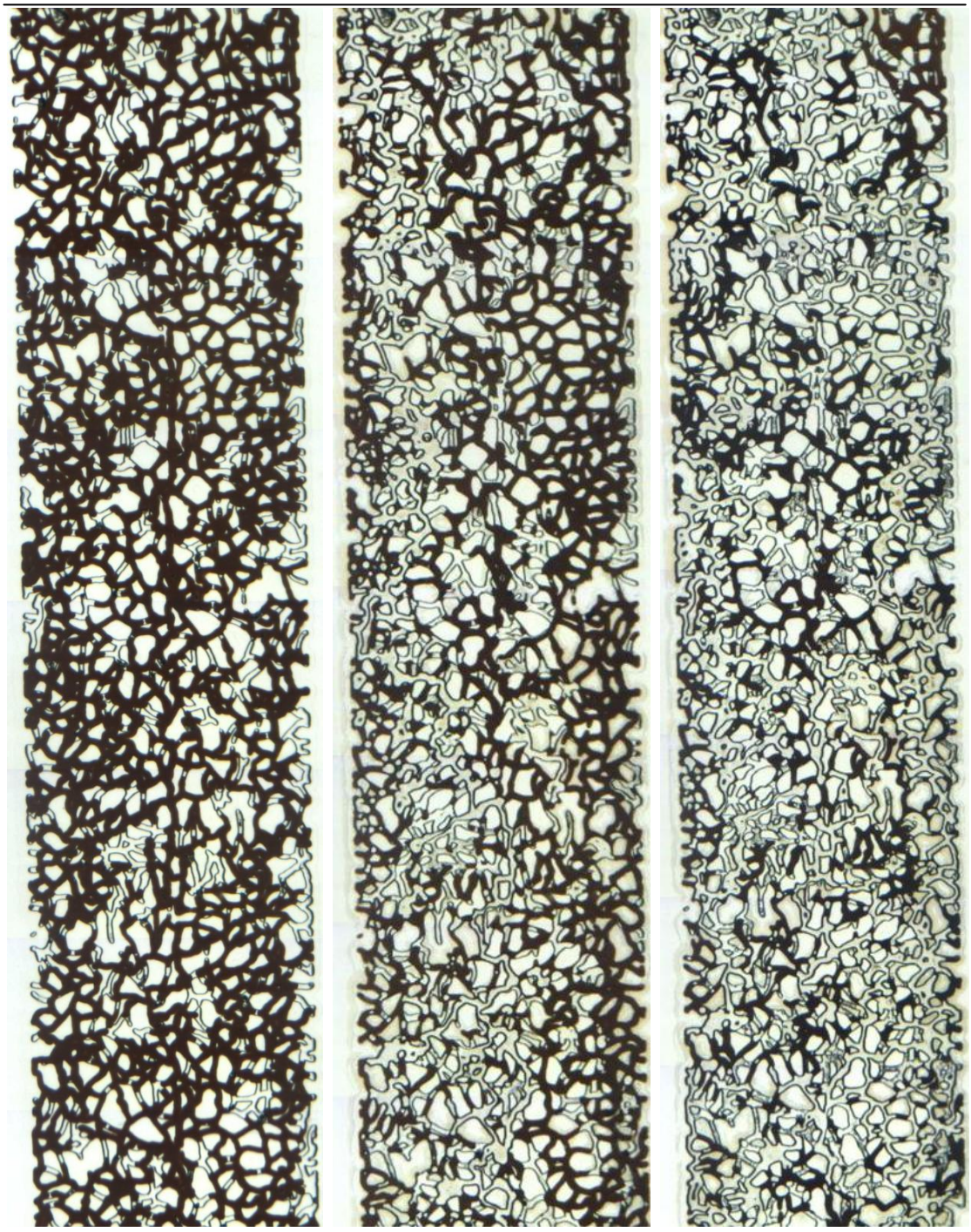

Figure 6-21: MM Exp 15; fluid distribution in the micromodel after (a) oil injection, (b) CO2 breakthrough and, (c) after 1 day of liquid-CO2 injection.

6.2.4 Discussion

Recovery Mechanisms and Efficiency during Low Pressure and High Pressure Application of CO2

Comparison of the processes of heavy oil recovery by vapour CO2 in Exp 13 (low pressure application of CO2) and by liquid CO2 in Exp 14 (high pressure application of CO2) reveals that the recovery efficiency and involved mechanisms were quite similar, until breakthrough of CO2. The system had an oil spreading tendency in both cases, forming a layer of oil around the stream of injected CO2. Before breakthrough, direct displacement of oil by injected CO2 was the main recovery process, which took place through a double-drainage mechanism (the flowing CO2 displaced an oil bank in front, which in turn displaced water).

However, after CO2 breakthrough, the recovery process was very different in the liquid and vapour CO2 cases. In the example of *vapour CO2 injection* (Exp 13), the recovery of oil almost stopped after CO2 breakthrough, despite having an extended period of CO2 injection. A very minor redistribution of the oil was seen and a negligible amount of oil was recovered by the oil film flow mechanism, through oil layers around the flowing stream of CO2. The dominant interaction between the oil and vapour-CO2 was CO2 dissolution, which was evident from the swelling and colour change (to a brighter colour) of the oil phase. The recovery mechanisms in the example of vapour CO2 were very similar to the recovery mechanisms observed during CO2 injection in crude "C" (Exp 8), which was carried out using vapour CO2 at a similar pressure, but higher temperature.

However, in the example of *liquid CO2 injection* (Exp 14), the oil recovery and redistribution continued after the CO2 breakthrough through two recovery mechanisms. CO2 dissolution and viscosity reduction was higher at an elevated pressure of 1500 psig and recovery was also assisted by the extraction mechanism, in which the lighter hydrocarbon components were stripped into CO2. The extraction mechanism was evident from the darkening colour of the oil connected to the flowing stream of CO2. Another mechanism, which for the first time was observed and reported here, is formation of a new phase in the separated oil blobs (oil not connected to CO2). Formation of this new phase assisted oil recovery, by increasing the volume of the isolated oil blobs and connecting them to the main stream of CO2. This resulted in recovery of the oil through extraction mechanism or diversion of the flowing path of

CO2. Formation of the new phase also assisted the displacement of oil during the subsequent period of water injection, which will be discussed in the following section.

Displacement of the Diluted Oil during the Subsequent Period of Waterflood

The period of water injection subsequent to the CO2 injection period (2nd period of water injection) showed different recovery performance in the examples of vapour and liquid CO2. The results showed that whilst the 2nd period of water flood resulted in poor recovery in the test performed using vapour CO2 (Exp 13), the recovery improved significantly in the test performed using liquid CO2 (Exp 14). Furthermore, the slight improvement in the example of vapour CO2 was from the region where oil was in direct contact with CO2 and the oil, which was separated with a layer of water, showed only minor redistribution. In the example of liquid CO2, most of the additional oil recovery was from the part of oil that was not in direct contact with CO2.

At the early stages of waterflood: CO2, oil, and the injected water flow simultaneously through the porous medium with water (the wetting phase) continuously breaking up oil and CO2, until a certain saturation level of water is achieved in the model. In Exp 13, vapour CO2 and water had significantly lower viscosity compared to oil, which (combined with having an existing flowing path for CO2 and water) resulted in poor oil recovery during the 2nd period of waterflood. In Exp 14, there are a number of mechanisms that improved the waterflood, subsequent to injection of liquid CO2 (compared to the case of vapour-CO2) as described below:

1- *Formation of droplets of a new phase and blockage of the flow path of water*: Formation of the new phase in oil blobs during the liquid-CO2 flood caused the existing path for the flow of water to be partially blocked. Hence the injected water was diverted towards other parts of the micromodel, where oil saturation was higher. Figure 6-22 presents a sequence of pictures during the liquid CO2 injection period, in which the role of formation of a new phase on blockage of an existing water flow path can be vividly seen. At breakthrough time, while liquid CO2 is flowing in the right hand side of the micromodel, the presence of a network of pores saturated with water in the middle of the micromodel separates the remaining oil in the left hand side from the liquid CO2. However, as the injection of liquid CO2 continues, the new phase appears in oil blobs in the middle of the micromodel (as highlighted by the red circles in Figure 6-22).

Formation of this new phase in blobs of the oil eventually results in partial blockage of the flowing path of water, at the end of the period of liquid CO2 flood. Therefore, during the subsequent period of water injection, the injected water was diverted towards the regions that had not been flooded with water before e.g. the diluted oil on the left side of the micromodel.

2- *Higher CO2 dissolution and Viscosity reduction:* To inject CO2 in liquid state the pressure of the system should be higher than the pressure of vapour CO2. Increasing the test pressure allows more CO2 dissolution in the oil, which in-turn results in a further viscosity drop. Therefore, the water injected subsequent to the liquid-CO2 flood is displacing less viscous oil, compared to the example of waterflood subsequent to the vapour-CO2 injection. However, it should be noted that this is not the case for the oil blobs that have been connected to the flowing stream of liquid-CO2, as the extraction process is the dominant mechanism and reduces the CO2 saturation in oil.

3- *Oil Viscosity Gradient as a result of the Extraction Process:* The combination of the extraction process from the portion of oil connected to the flowing stream of liquid CO2 and CO2 dissolution in oil blobs shielded with a layer of water, results in formation of a viscosity gradient at the end of the period of liquid CO2 injection. Therefore, during the subsequent period of waterflood, CO2-diluted oil would be displaced by water much easier than the residual oil after extraction process, which has a much higher viscosity.

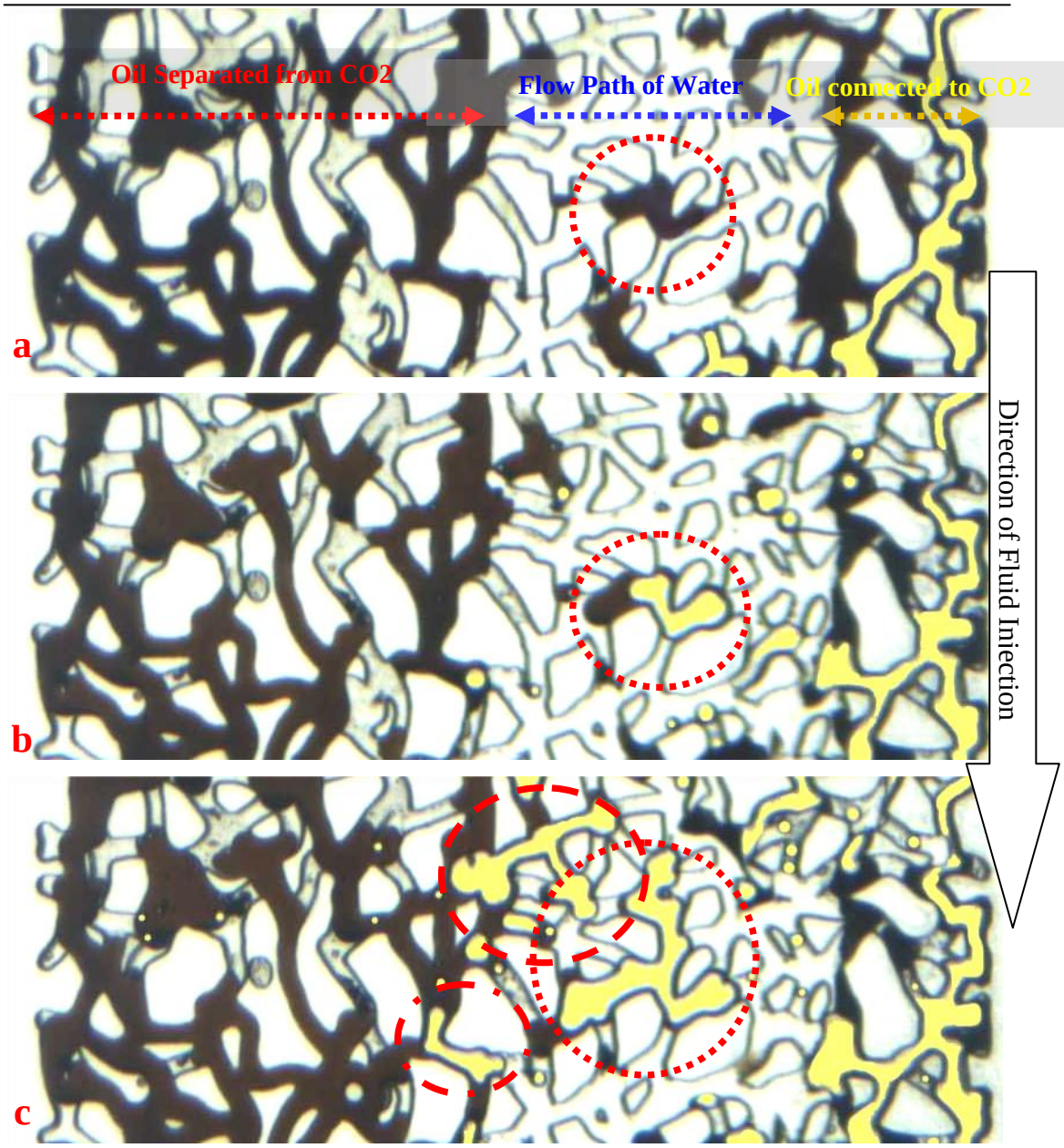

Figure 6-22: A magnified section of the micromodel during the liquid-CO2 flood after (a) CO2 BT, (b) 12 hours and, (c) 1 day of liquid CO2 flood. The circles highlight separated blobs of oil, which have been enlarged as a result of the formation of a new phase and which blocked the flowing path of water.

Formation of a New Phase during Liquid CO2 Injection

In Exp 14, a novel observation was reported during the extended period of liquid CO2 injection, in which a new phase was formed inside the oil blobs that were separated from the flowing CO2 by layers of water. This new phase was observed to be colourless in the micromodel and miscible with CO2, in the cases it came in contact with the flowing stream of liquid CO2. It is worth mentioning that formation of a third phase which is rich in CO2 during CO2 injection, is well documented in the literature of

CO2 EOR, however, it is different from the observations reported here. The author's observations show the new phase is formed in oil blobs not directly connected to the stream of flowing CO2 and is miscible with CO2; whereas, what is reported in the literature is for direct contact between CO2 and the oil and there are interfaces between new phase and CO2 (they are immiscible).

Additionally, the author's observation of a new phase formation can take place in a wider range of pressure and temperature compared to the previous reports of formation of an immiscible phase between oil and CO2 in the literature. Region III in the Figure 6-23 is the pressure and temperature range in which formation of a third immiscible phase is reported when CO2 comes in direct contact with crude oil (Klins, 1984). The red circles in this figure show the fluid characterization experiments in which formation of the new phase has been detected in the oil blobs surrounded by water layers. The red squares present the experiments in which formation of the new phase has not observed. It should be noted that since formation of this new phase has only been observed in the oil blobs which are separated from main stream of CO2 by water layers, normal PVT tests cells cannot be used for characterization of this phenomenon and micromodel experiments are the only developed technique which can be used to visually detect the pressure and temperature limits of formation of this new phase.

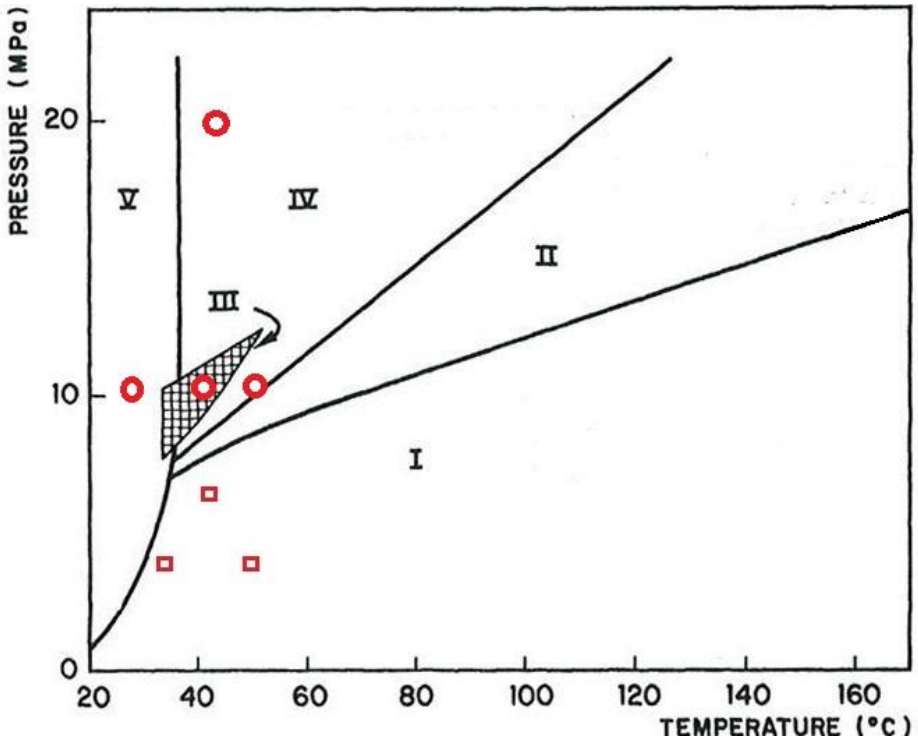

Figure 6-23: The effect of reservoir temperature and pressure on CO2 recovery mechanisms and formation of new phase (Klins, 1984). The red circles in this figure show the fluid characterization experiments by the author in which formation of the new phase has been detected in the oil blobs surrounded by water layers and the red squares are the experiments in which formation of the new phase has not observed.

While the understanding of the thermodynamic phenomena that results in formation of this new phase requires further investigation, the current hypothesis is that CO2 is dissolved in the oil phase through the water surrounding the oil; however, as soon as it reaches a certain high concentration level it forms a CO2-reach phase. Therefore, it is very probable that the new phase mostly consists of CO2 plus light hydrocarbons from the crude oil.

The droplets of the new phase nucleated in the oil phase near oil/water interfaces, and as they grew bigger they moved to the centre of the oil blobs. It should be noted that in tests (not discussed here) with non-spreading systems (water spreading) the new phase droplets formed and remained at the oil/brine interface. The new phase nucleates and grows in the smaller oil blobs much faster than bigger ganglia of oil and it extracts lighter components of oil when it becomes larger. This is evident by the darkening of oil around the droplets of the new phase. To further investigate this pore scale observation, a number of complementary tests were designed and conducted using different crude oils under different pressure and temperature conditions. The results showed the new phase only forms in the conditions where CO2 exist, either in the super-critical or in the liquid states, and formation of this phase was never seen in the experiments using vapour CO2 (e.g. Exp 8 and Exp 12 in this study). Furthermore, formation of the new phase was faster and more extensive in the lighter crude oils.

Formation of the new phase might improve oil recovery during the period of CO2 injection or during the subsequent period of water injection:

1. *During liquid-CO2 (or SC-CO2)* injection: Formation of these droplets can enlarge the separated oil blobs (as these droplets form in the middle of the oil phase), which can result in reconnection of the disconnected oil blobs and additional oil recovery. This level of enlargement of the oil, achieved by

formation of the new phase, is much higher than swelling due to CO2-dissolution.

2. *During the subsequent waterflood:* Droplets of the new phase have shown a tendency to nucleate primarily in the smaller oil blobs. Therefore, they initially appear in that part of the porous media that has already been flooded with water and as a result, the oil blobs are smaller. Formation of these droplets can block the flowing path of water (or at least significantly reduce the relative permeability to water) and divert injected water towards un-swept regions of the porous media during the second period of waterflood.

Effect of Injection Strategy on Recovery Mechanisms and Efficiency of Liquid CO2

Figure 6-24 and Figure 6-25 compare the oil recovery by plain water injection to the examples of oil recovery by tertiary and secondary injection of liquid CO2 in the magnified section and full length pictures of the micromodel respectively As shown, significant improvement in oil recovery was achieved in both scenarios of secondary and tertiary injection of liquid CO2. However, the dominant mechanisms were observed to be different in the tertiary and secondary injection of CO2 resulting in different recovery performance.

In the example of secondary injection of liquid CO2, the direct displacement of oil by injected CO2 was enhanced as a result of CO2 dissolution and viscosity reduction in the oil phase. Being assisted by gravity forces, the recovery of diluted oil continued after CO2 breakthrough and was later followed by the extraction mechanism. The combination of these mechanisms resulted in an improved recovery performance, as shown in Figure 6-24d and Figure 6-25d.

In the example of tertiary injection of liquid CO2, the part of residual oil that was in direct contact with injected CO2 was recovered through direct displacement, which was assisted by CO2 dissolution and viscosity reduction in the oil phase. After breakthrough, extraction of light hydrocarbon components was the dominant mechanism and due to the reduced mobility of oil (high water saturation) the gravity drainage mechanism did not play a major role in recovery. The part of residual oil that was not in direct contact with liquid CO2 (due to a water shielding effect) was successfully recovered when the period of CO2 injection was followed with a period of

waterflood, as shown in Figure 6-24c and Figure 6-25c. This process was assisted by formation of a new phase in the small separated oil blobs, which extensively restricted the flowing path of water and diverted it towards the oil occupied pores.

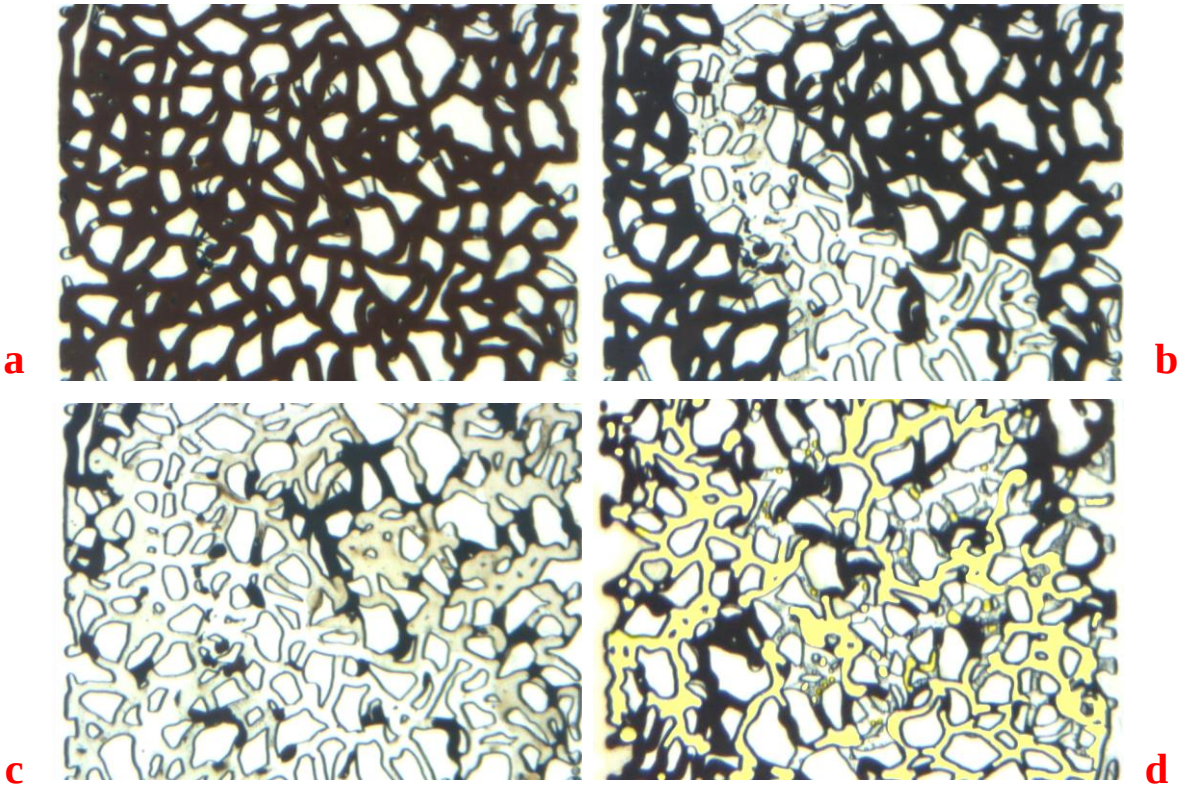

Figure 6-24: Comparison of the recovery performance and oil saturation in a magnified section of the micromodel after a) oil injection, b) the initial water injection in Exp 14, c) the second period of water injection that was carried out subsequently to a period of CO2 injection in Exp 14 and, d) CO2 injection in Exp 15.

a **b** **c** **d**

Figure 6-25: Comparison of the recovery performance and oil saturation in the full length section of the micromodel after a) oil injection, b)the initial water injection in Exp 14, b) the second period of water injection that was carried out subsequently to the period of tertiary CO2 injection in Exp 14 and, c) CO2 injection in Exp 15.

6.3 THE EFFECT OF MOBILITY CONTROL BY CO2-EMULSION

This section presents the results of the micromodel experiments investigating the application of CO2-emulsion as a mobility control technique for improved recovery of crude "J". Since at reservoir conditions of crude "J" CO2 is in liquid state, technically speaking, dispersion of CO2 in water results in CO2-emulsion rather than CO2-foam.

6.3.1 MM Exp 16: CO2-Emulsion Injection

Procedure and Conditions

1 *Initialization:* The micromodel was saturated with distilled water at T = 25 °C and P = 1500 psig.

2 *Oil Flood:* The micromodel was flooded with crude oil "J" from the bottom until the oil front reached the other end of the micromodel.

3 *Water Injection*: Distilled water was injected into the micromodel for 2 hours.

4 *Surfactant Injection*: The chemical solution was injected into the micromodel for 1 hour.

5 *CO2/Surfactant Co-Injection*: Surfactant solution and liquid CO2 were simultaneously injected into the micromodel at a volumetric ratio of 1:9 for 1 hour.

Table 6-7 lists a summary of the fluids used and the pressure and temperature at test conditions.

Table 6-7: Fluids used and pressure and temperature conditions of MM Exp 16.

Porous Medium	Homogeneous Rock-look-alike Micromodel
Crude Oil	"J" (617 at 28 °C)
Aqueous Phase	Distilled Water
Displacing Phase	Liquid CO2
Chemical Solution	0.3 wt % AOS 14
Temperature	25 °C
Pressure	1500 psig

Results

Initialization and Oil Injection

To begin the experiment, the micromodel was first saturated with distilled water. Subsequently, the oil was injected into the micromodel to establish the initial water saturation. Oil injection continued until oil reached the other end of the micromodel. As expected, high oil saturation was achieved at the end of the oil flood period due to the high oil/brine viscosity ratio. Figure 6-26 and Figure 6-36(a) show a magnified picture of the micromodel and full-length picture of the micromodel respectively, after the oil injection period in which the oil has dark brown colour and the connate water is colourless.

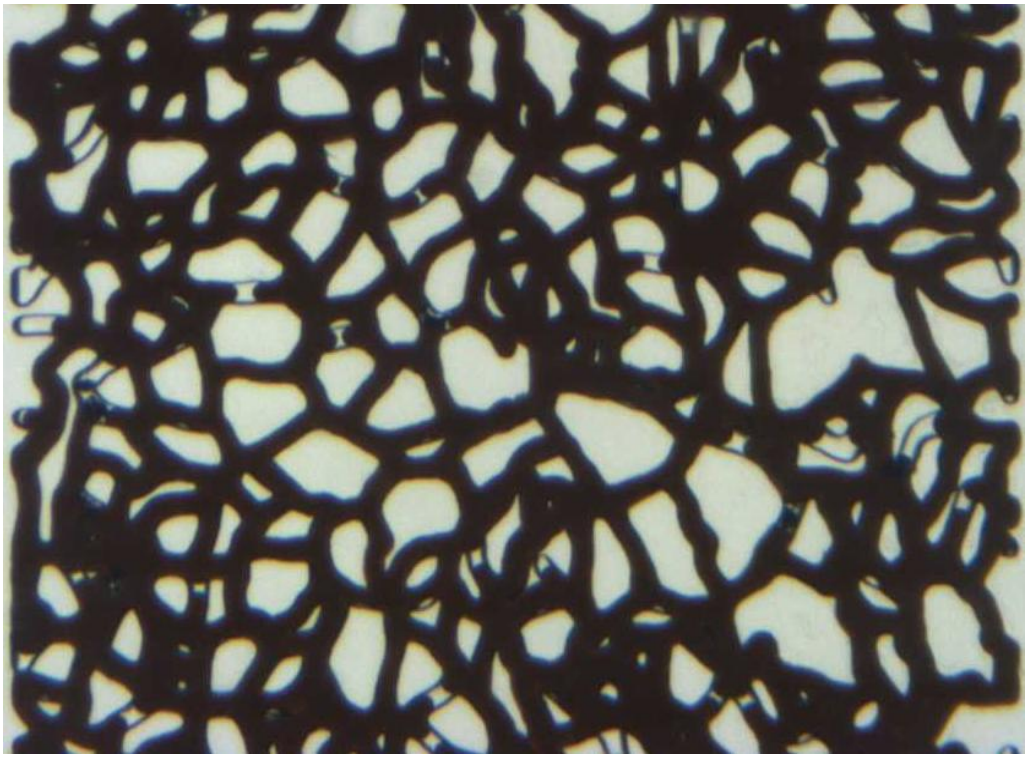

Figure 6-26: MM Exp 16; a magnified section of the micromodel at the end of the period of oil injection.

Water Injection

Having established the initial oil and water saturations in the micromodel, a period of water injection started, which was continued for 1 day. Figure 6-27 shows the selected magnified section of the micromodel after 1 day of waterflood. Comparison of Figure 6-27 and Figure 6-26 shows that during water flooding, some of the crude oil was displaced from the porous medium but a large part of the oil remained in the micromodel.

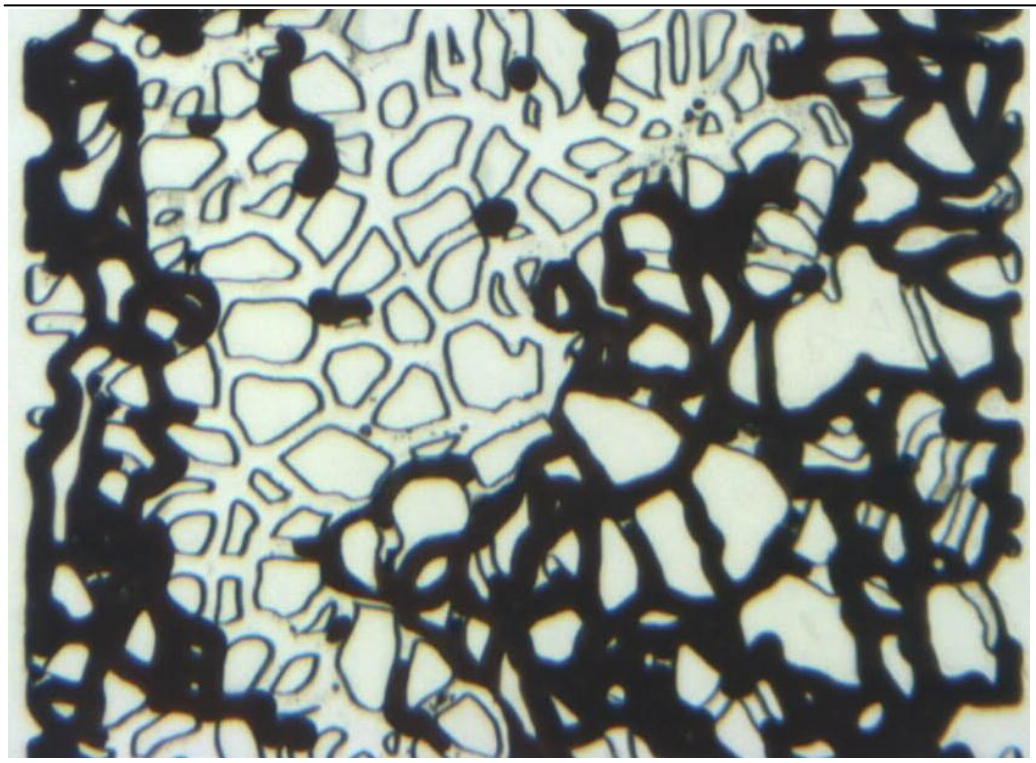

Figure 6-27: MM Exp 16; the same magnified section of the micromodel at the end of the period of water injection (1 hour).

Surfactant Injection

After water flooding, the micromodel was flooded with the surfactant solution for 1 hour. A slight increase in additional oil recovery was observed during the surfactant solution injection period. This was performed so that when foam was injected the observed additional oil recovery could be attributed to foam, rather than the positive effects of surfactant injection. Figure 6-28 and Figure 6-36b present the same selected magnified section and full length picture of the micromodel respectively, at the end of the period of surfactant solution injection.

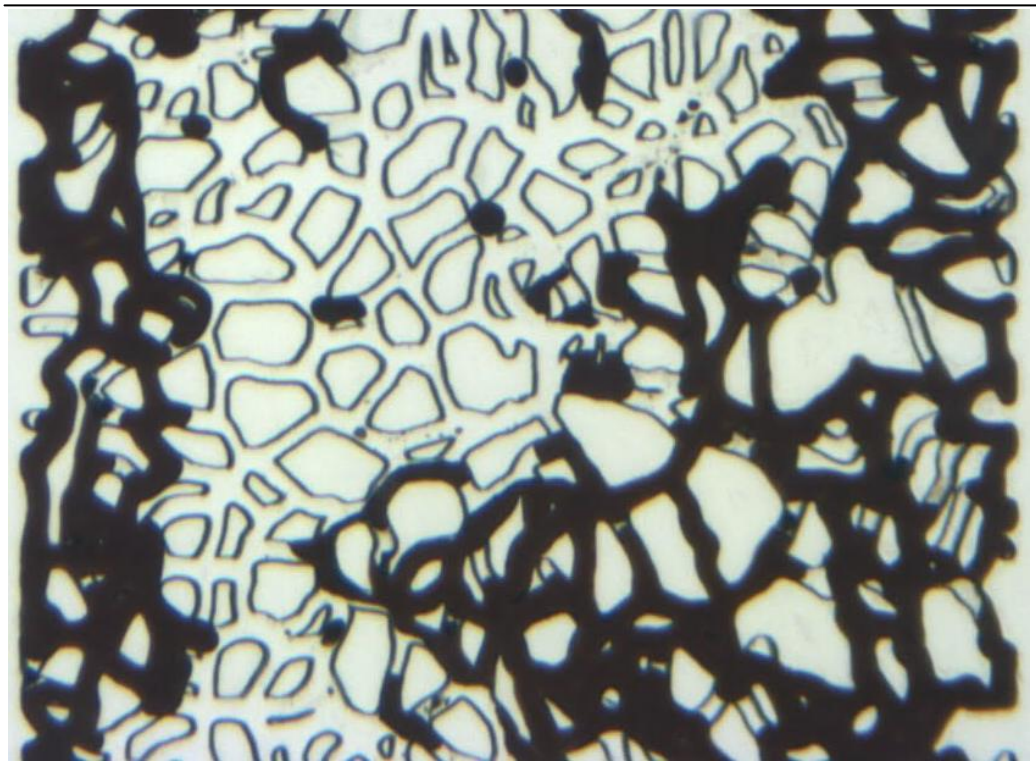

Figure 6-28: MM Exp 16; a magnified section of the micromodel at the end of the period of surfactant injection (3 hours).

CO2/Surfactant Co-Injection

Having carried out a period of surfactant flooding, the simultaneous injection of liquid CO2 and surfactant solution started and continued for 1 hour. Initially, the surfactant solution and liquid-CO2 were simultaneously injected and circulated through the bypass line for a relatively long period of time. During this period, the pressure of injection, retract cells and the connecting lines were precisely monitored to ensure that steady state flow had been attained in the system. Subsequently, the flow of CO2 and surfactant solution was diverted into the micromodel.

The mixture of CO2 and surfactant solution entered the micromodel in the form of large pieces of CO2 in surfactant solution. However, as CO2 pieces flowed in the porous medium they turned into smaller droplets of CO2 by lamella (or bubble) division mechanism. When these droplets of CO2 came into contact with residual oil in the micromodel, the oil was displaced in the form of oil in water emulsion. The in-situ generated oil emulsion was observed to be stable in the presence of surfactant solution, which resulted in formation of a relatively large bank of oil emulsion ahead of the CO2 emulsion front. Having a higher viscosity compared to the aqueous phase, the oil emulsion bank in turn displaced and formed a bank of oil. Figure 6-29 shows the

magnified section of the micromodel during this stage of the test. Comparison of this figure with Figure 6-28, before CO2/surfactant flood, shows that oil saturation in this section of the micromodel has dramatically increased due to formation of the bank of oil.

The observations in the magnified section of the micromodel show that as the CO2/surfactant co-injection continued, the bank of oil was displaced by the bank of oil emulsion (Figure 6-30), which itself was pushed forward by the injected CO2 emulsion (Figure 6-32). The CO2 emulsion became increasingly more stable, as injection of fluids continued and more oil was produced from the micromodel. The gradual strengthening of the CO2 emulsion is evident in the sequence of images shown from Figure 6-31 to Figure 6-35. The type of interfaces between the oil and CO2 in these figures suggests the presence of a non-spreading system in the micromodel. This means that interfaces between CO2 and the aqueous phase were observed in the system, as well as interfaces between CO2 and heavy oil. The occurrence of a non-spreading coefficient can be attributed to a very low IFT between the liquid CO2 and aqueous phase, as a result of surfactant injection.

Pictures (c) to (i) in Figure 6-36 show the full length picture of the micromodel at different time steps during the period of CO2/surfactant injection. The red dashed lines in these pictures show the approximate location of the above mentioned phases (the CO2 emulsion, bank of oil emulsion and oil bank). It should be noted that these lines only show the approximate location of boundaries as the change from one phase to another is very gradual. This means that the CO2 emulsion phase and oil emulsion phase exist throughout the micromodel. In the CO2 emulsion region, oil droplets can be seen, both in the CO2 emulsion region and similarly in the oil emulsion bank CO2 phase (albeit a lower number of droplets). As the CO2/surfactant injection continued, this bank of oil and oil emulsion continued to be displaced by CO2 emulsion towards the producing end of the micromodel. The breakthrough of the oil emulsion and the CO2 emulsion took place after 15 minutes (Figure 6-36e) and 35 minutes (Figure 6-36f) of CO2/surfactant co-injection respectively. Injection of CO2/surfactant continued for 1 hour. Figure 6-36i shows the full length picture of the micromodel at the end of the period of CO2/surfactant injection. A very high oil recovery was achieved and almost all of the waterflood residual oil was produced after this period of CO2/surfactant injection.

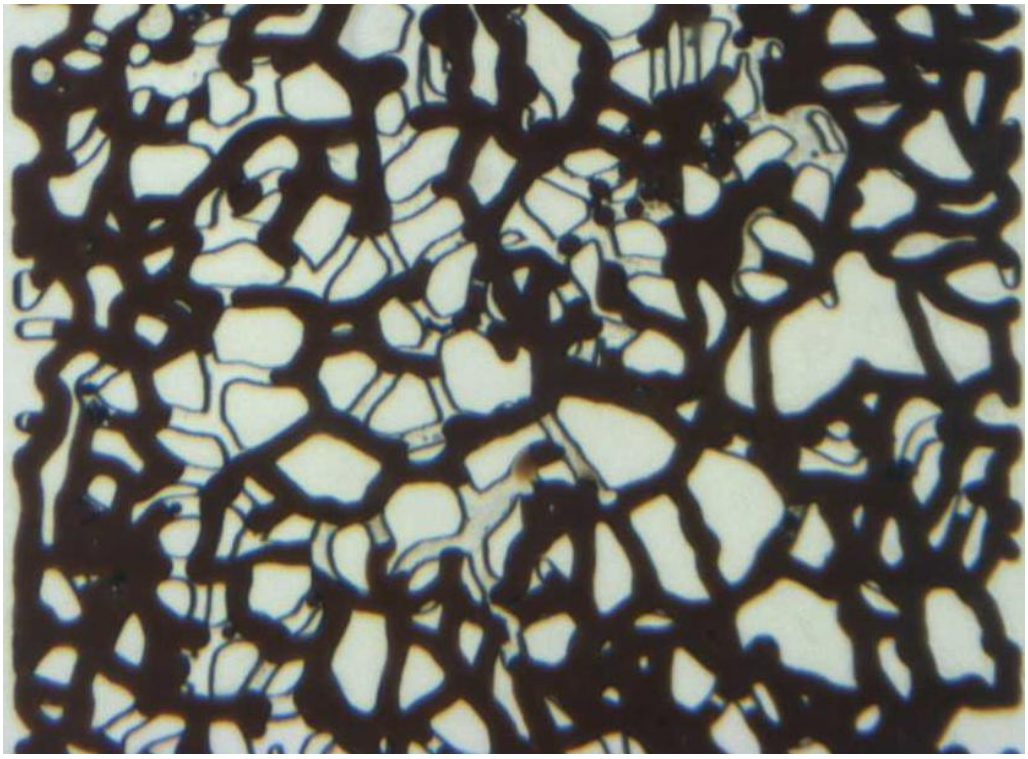

Figure 6-29: MM Exp 16; a magnified section of the micromodel at arrival of oil bank after 5 minutes of CO2/surfactant injection.

Figure 6-30: MM Exp 16; a magnified section of the micromodel at arrival of the oil emulsion bank after 10 minutes of CO2/surfactant injection.

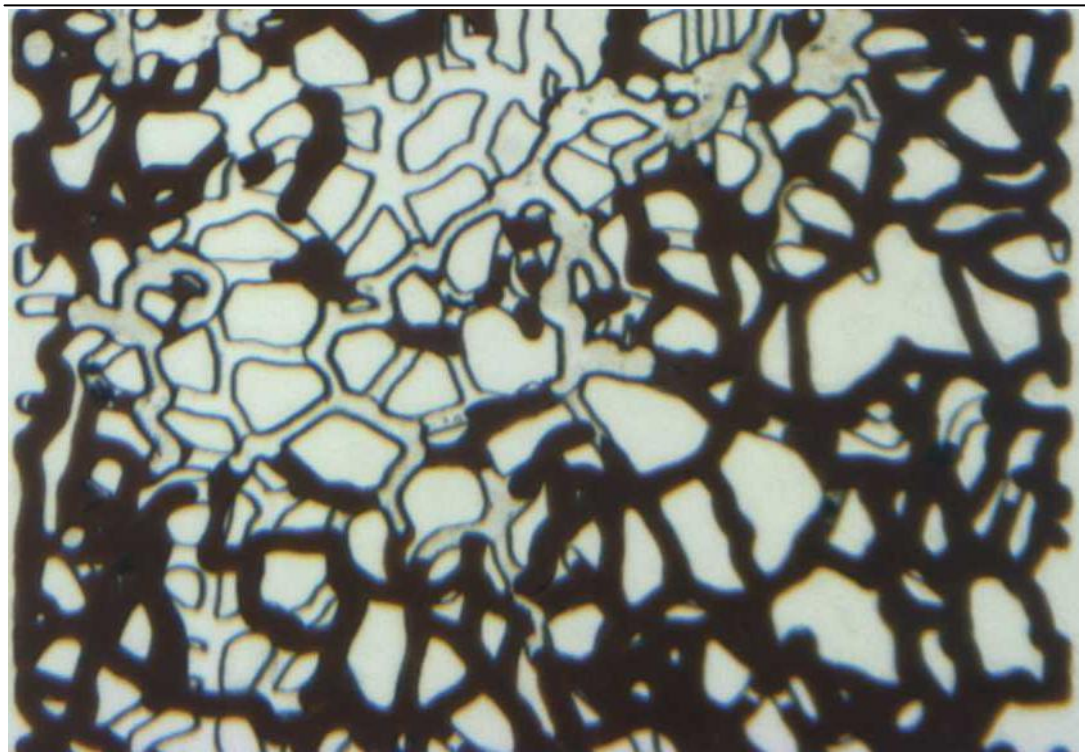

Figure 6-31: MM Exp 16; a magnified section of the micromodel after 15 minutes of CO2/surfactant injection.

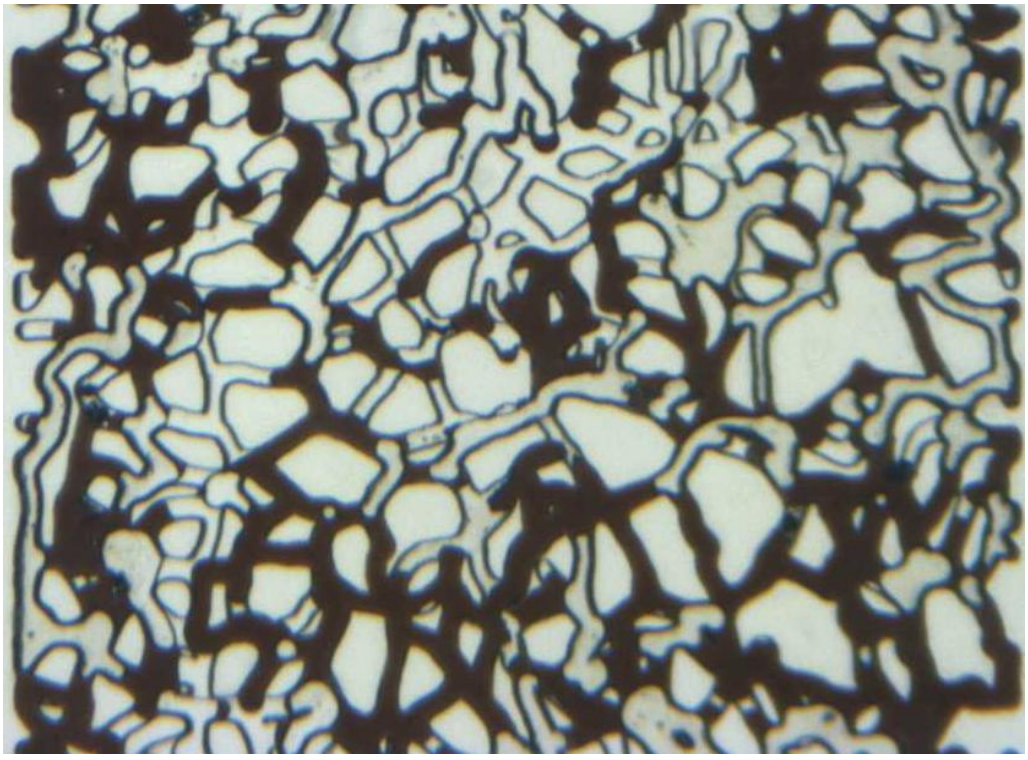

Figure 6-32: MM Exp 16; a magnified section of the micromodel after 25 minutes of CO2/surfactant injection.

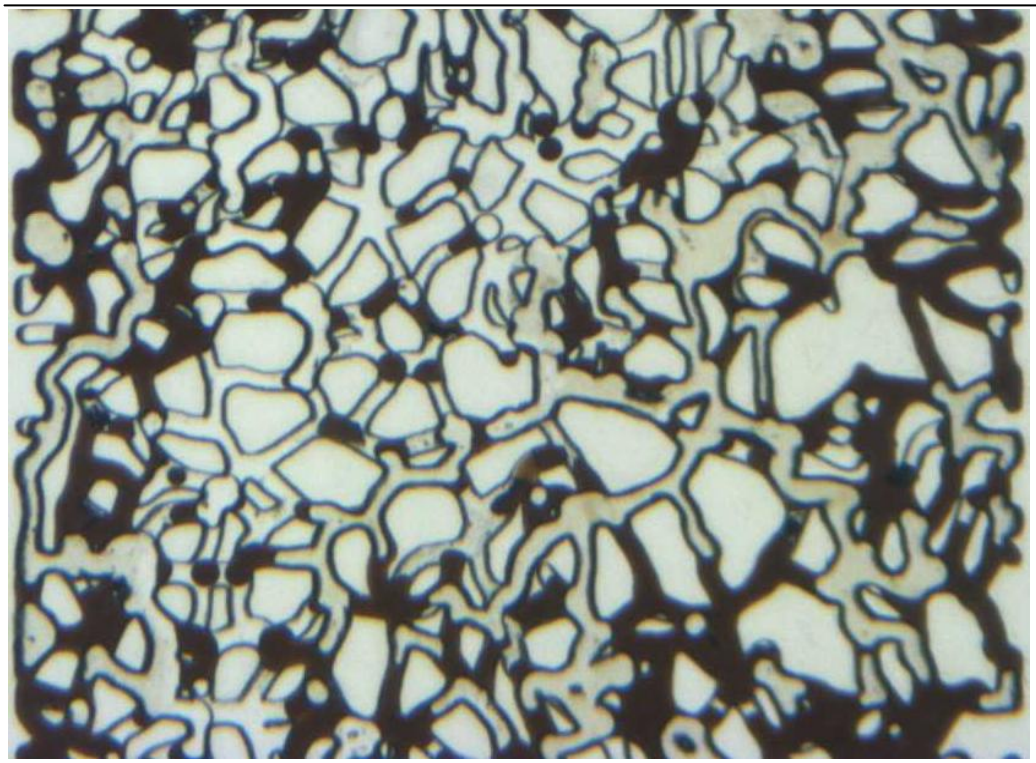

Figure 6-33: MM Exp 16; a magnified section of the micromodel after 35 minutes of CO2/surfactant injection.

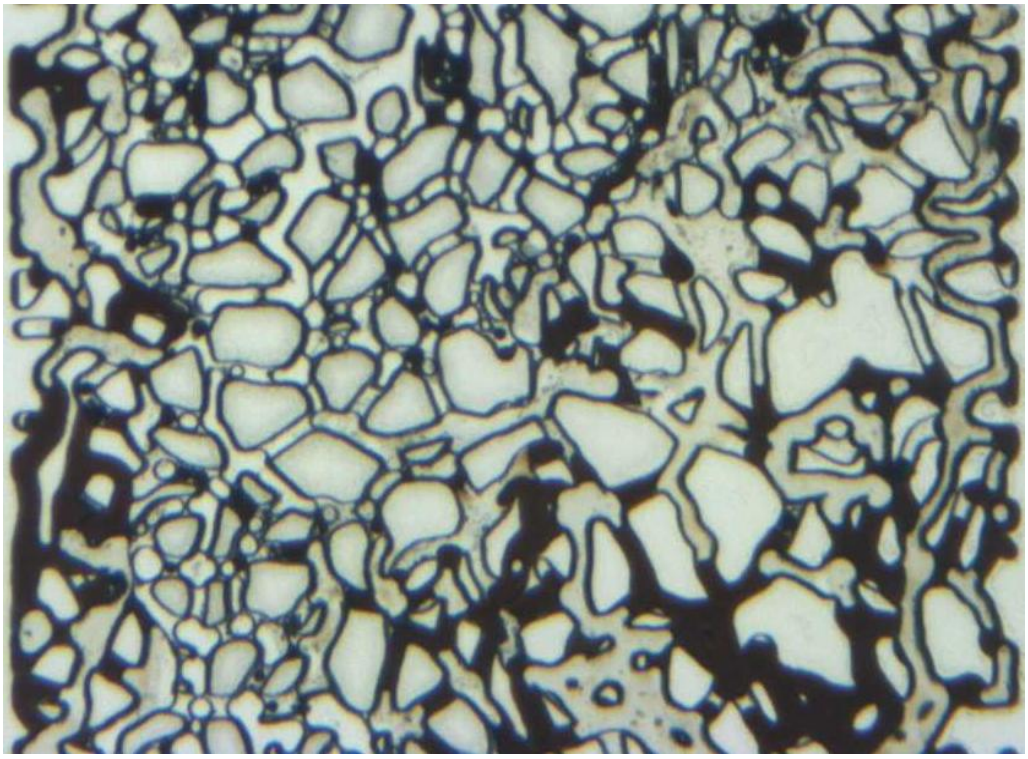

Figure 6-34: MM Exp 16; a magnified section of the micromodel after 45 minutes of CO2/surfactant injection.

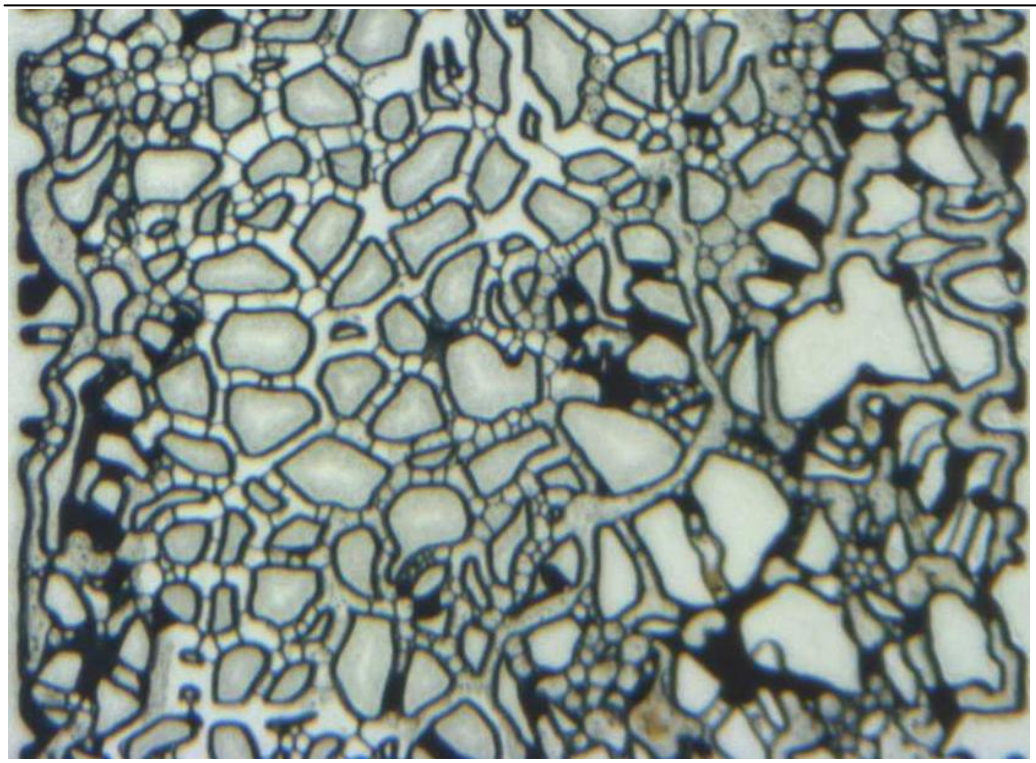

Figure 6-35: MM Exp 16; a magnified section of the micromodel after 1 hour of CO2/surfactant injection.

Summary

Table 6-8 summarises the oil recovery data at different stages of this micromodel experiment (MM Exp 16). The results show that the process of CO2-emulsion flood has been very successful reaching a final recovery of 85%OOIP after 1 hour of CO2/surfactant co-injection. The combination of a large viscosity reduction in the oil phase (due to CO2 dissolution) and mobility control for the CO2 phase (due to formation of emulsions) is the main reason for the observed oil recovery improvement.

Table 6-8: MM Exp 16; Summary of the recovery data.

	Recovery @ BT (% OOIP)	Ultimate Recovery (% OOIP)	Cumulative Recovery (% OOIP)
1) Waterflood	17	24	24
2) Surfactant flood	0	4	28
3) CO2 surfactant co-Injection	14	68*	85
• A swelling factor of 18.1% has been considered for calculation of oil recovery.			

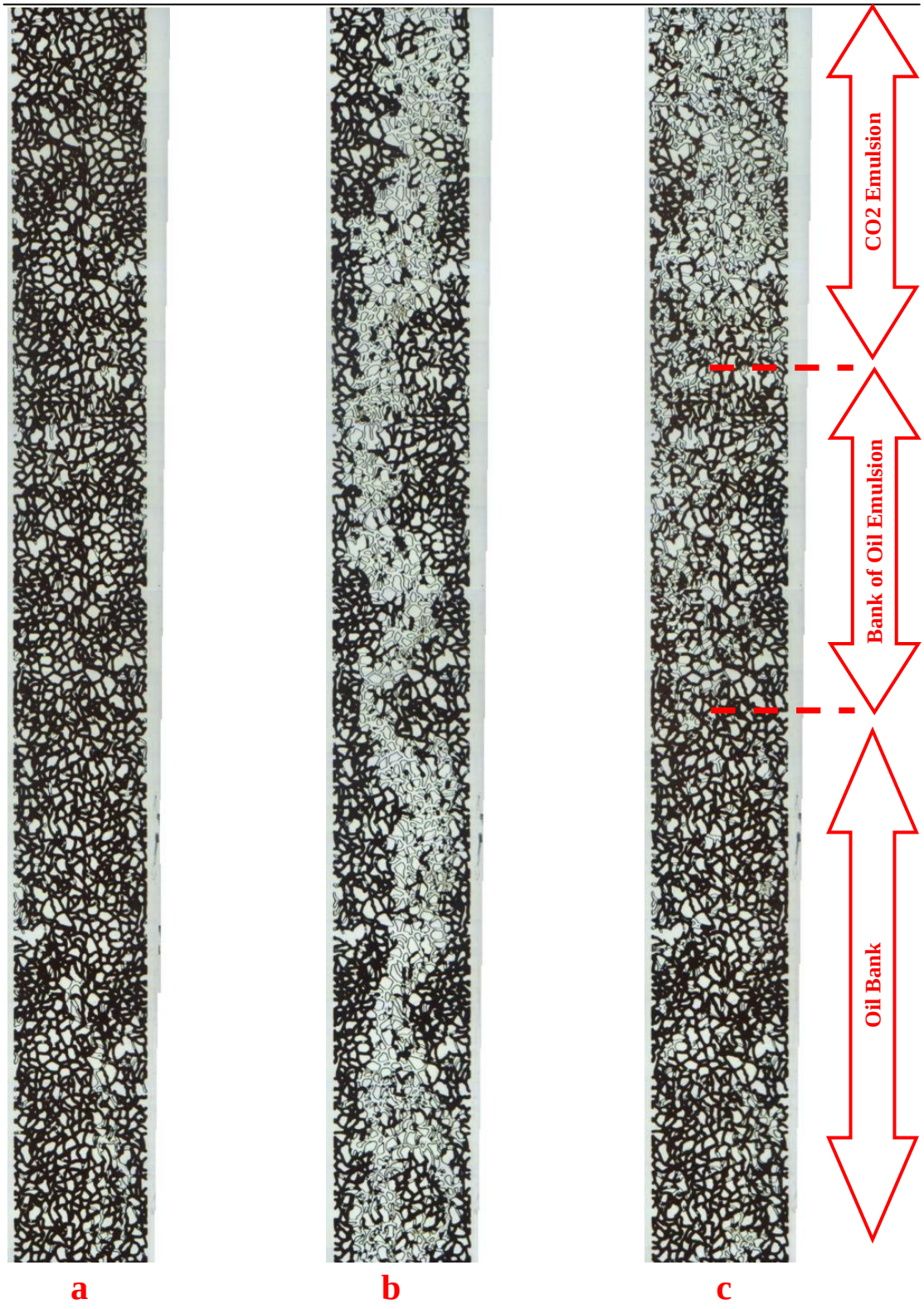

Figure 6-36: MM Exp 16; fluid distribution in the micromodel after (a) oil injection, (b) water and surfactant injection and, (c) 5 minutes of liquid CO2/surfactant injection.

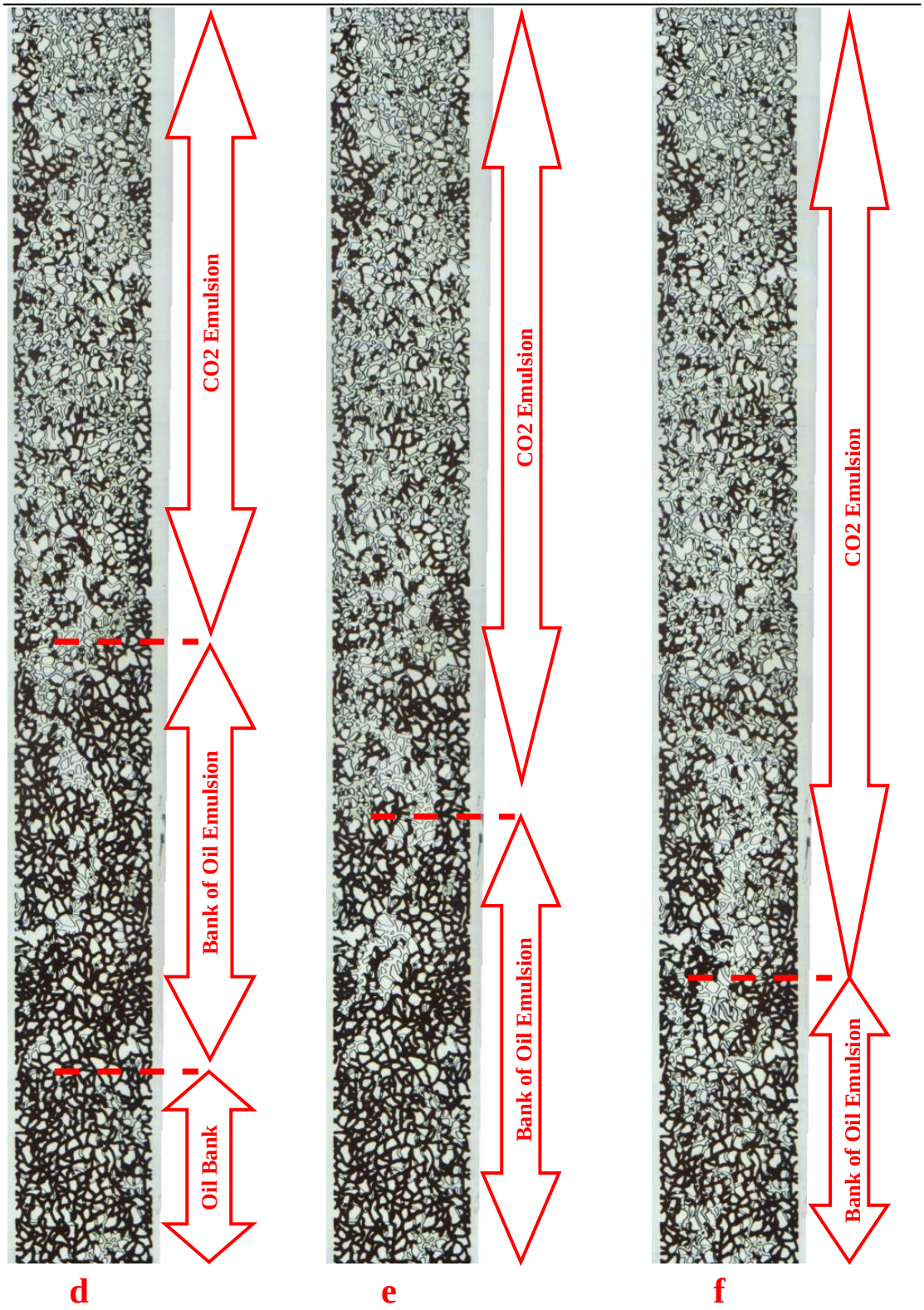

Figure 6-36 (continued): MM Exp 16; fluid distribution in the micromodel after (d) 10 minutes, (e) 15 minutes and, (f) 25 minutes of liquid CO2/surfactant injection.

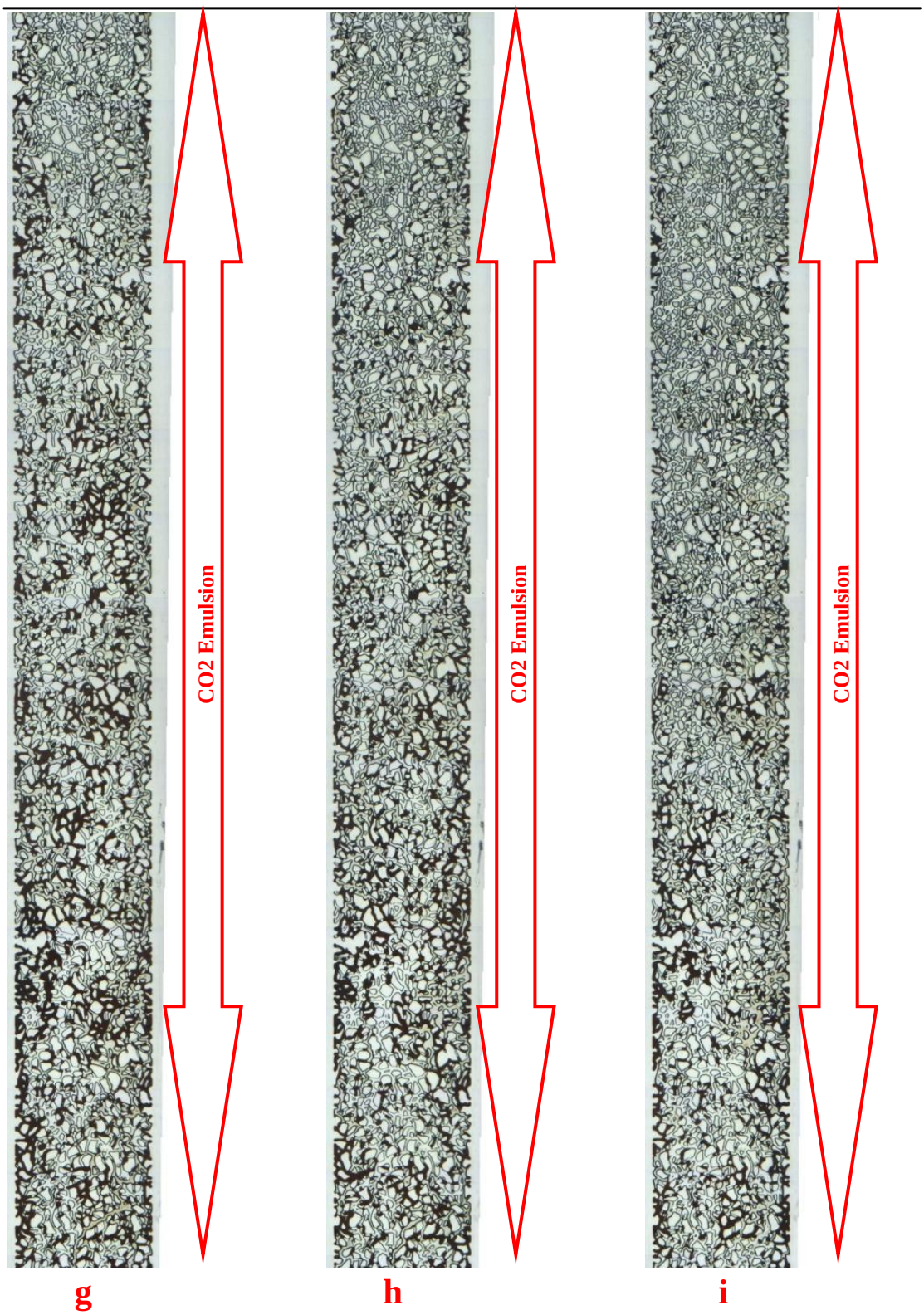

Figure 6-36 (continued): MM Exp 16; fluid distribution in the micromodel after (g) 35 minutes, (h) 45 minutes and, (i) 1 hour of liquid CO2/surfactant injection.

6.3.2 Discussions

CO2 Emulsion Stability and Displacement Efficiency

A comparison of generated CO2 bubbles in the example of CO2-foam (Exp 11) and CO2-emulsion (Exp 16) show similar appearance, in terms of diameter and size distribution, as they arrived at the micromodel. However, as the CO2-foam and CO2-emulsion phases entered the micromodel pattern, the flow of bubbles of CO2-emulsion caused the formation of new and smaller CO2-bubbles through lamellae division mechanism, which did not take place to the same extent in the example of CO2-foam. Furthermore, the CO2-emulsion bubbles were much more stable when they came into contact with the oil phase. The higher stability of CO2-emulsion bubbles, compared to CO2-foam bubbles, is believed to be due to the strong non-spreading behaviour of the CO2-emulsion system.

A combination of the high viscosity of generated CO2-emulsion and the significant viscosity reduction in the oil phase, as a result of CO2 dissolution, resulted in a very efficient displacement process, in which all the resident oil in the micromodel was recovered in 1 hour of CO2/surfactant injection (1 pore volume). **Figure 5-48** compares the fluid distribution and remaining oil saturation after 1 hour of liquid CO_2 flood in Exp 14 and CO_2 emulsion flood in this experiment. As shown, the CO_2-emulsion has been much more effective and efficient in enhancing the recovery of this heavy crude oil compared to plain CO_2.

Figure 6-37: Comparison of fluid distribution and the remaining oil after 1 hour of (a) tertiary liquid-CO_2 injection in Exp 14 and, (b) CO2/surfactant co-injection in Exp 16.

Differences in Displacement Process in CO2-Foam and CO2-Emulsion

The benefits of CO2-emulsion (or foam) flood arise from three sources: first; the mechanisms related to interactions between CO2 and crude oil e.g. CO2 dissolution and

extraction, second; the huge reduction in the mobility of CO2, which causes diversion of CO2 flow towards the unswept regions of the porous media and improves the sweep efficiency and third; the displacement mechanisms that improve the displacement efficiency at pore level. In the previous chapter, four displacement mechanisms were introduced that contributed to oil recovery at the pore scale during CO2-foam flood in crude "C" (Exp 11), as follows:

(1) Direct Displacement.
(2) Emulsification of oil.
(3) Co-current film flow.
(4) Counter-current film flow.

Our observations show that while the same recovery mechanisms exist in the case of CO2-emulsion flood, the strength and role these mechanisms play in oil recovery varies significantly. Being more stable against oil, oil recovery during the CO2 emulsion flood was mainly by direct displacement and emulsification mechanisms (MM Exp 14) compared to the example of CO2 foam flood, where the film flow mechanism was responsible for a major fraction of oil recovery (MM Exp 11). This explains why a large bank of oil in water emulsion was formed ahead of the injected CO2-emulsion and while such a bank never formed during CO2 foam injection. Figure 6-38 illustrates a highly magnified section of the micromodel in which the flow of oil in water emulsions can be clearly seen.

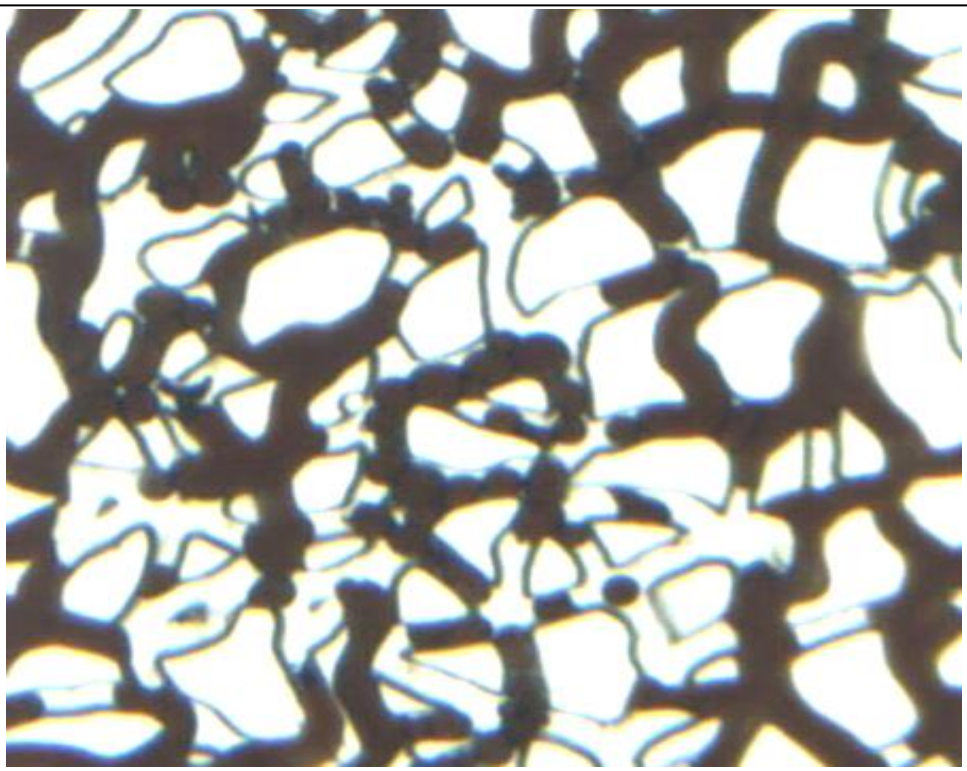

Figure 6-38: A highly magnified section of the micromodel, showing displacement of the oil phase by formation of a bank of liquid-CO2 and oil in water emulsions.

6.4 SUMMARY AND CONCLUSIONS

The following conclusions can be drawn from the experiments in the first part of this chapter (effect of CO2 state and strategies of injection):

- The process of tertiary liquid-CO2 injection resulted in higher recovery than tertiary vapour-CO2 injection. While similar recovery performance was observed at breakthrough time, after BT, the injection of liquid CO2 improved oil recovery by extraction mechanism in that part of the remaining oil that was in direct contact with the main stream of CO2. The recovery of that part of the remaining oil that was fully covered by water layers and separated from the flowing stream of CO2, was also improved by formation of a new phase.
- Formation of a new phase in the oil blobs that were not in contact with the injected liquid CO2 was observed and reported here, which helped oil recovery during the period of liquid-CO2 flood and during the subsequent period of water injection. However, the mechanism behind formation of this phase is not fully understood yet and needs further investigation.
- During the subsequent period of waterflood, oil recovery was also higher in the test performed using liquid-CO2 due to: blockage of the flowing path of water with

droplets of the new phase, higher viscosity reduction and viscosity gradient in the remaining oil.

The following conclusions can be drawn from the experiments in the second part of this chapter (Effect of CO2 states and strategies of injection):

- A strong CO2-emulsion was formed in the micromodel that efficiently displaced crude "J" from the micromodel
- A large bank of oil in water emulsion was formed ahead of the generated CO2-emulsion, which displaced the oil bank towards the producing end of the micromodel.
- Direct displacement and oil emulsification mechanisms were observed to be the main displacement mechanisms contributing to oil recovery. Nevertheless, the film flow mechanisms that played an important role in oil recovery by CO2-foam, were observed to be less efficient due to the strong negative tendency of the system.

CHAPTER 7 COREFLOOD INVESTIGATION OF EXTRA-HEAVY OIL RECOVERY BY CO2 INJECTION IN CRUDE "C"

7.1 INTRODUCTION

This chapter presents the results of 5 coreflood experiments to investigate performance of CO2 injection in crude "C". In the first part of this chapter, the effect of the CO2 injection strategy on recovery performance of crude "C" is investigated through three coreflood experiments. The second part of this chapter is focused on the effect of mobility control by CO2-foam injection. The first group of the experiments (injection strategy) were performed using a sandpack and the remainder of the experiments were conducted using a high permeable consolidated sandstone core. The properties of the sand pack and consolidated core are explained in Chapter 3 of this text.

7.2 THE EFFECT OF INJECTION STRATEGY

The objective of this series of coreflood experiments was to verify and quantify visual observations made in the micromodel experiments using the same crude oil, CO2 and water as in Chapter 5. The first two tests investigate the effect of CO2 injection after and before conventional water flooding (tertiary and secondary CO2 injection mode) and the following experiment simulates the processes of CO2-SWAG injection. All experiments in this section were performed using a sandpack.

7.2.1 Core Exp 1: Tertiary CO2 Flood

This experiment was carried out to investigate the performance of tertiary (post water flood) CO2 injection in crude oil "C" and to then compare the results of this core test with the corresponding micromodel test (MM Exp 8).

Experimental Procedure and Conditions

In the core flood experiment a procedure similar to the MM Exp 8 was followed. However, the aqueous phase used was a brine solution, rather than distilled water, which was used in the micromodel test. The results of the core flood experiment verified many of the observations made during the direct flow visualisation experiments. All fluid injections were performed from the top of the vertically oriented core.

1. *Initialization:* Sandpack was saturated with brine at T = 50 °C and P = 600 psig
2. *Oil Flood:* Sandpack was flooded with crude oil "C" and an oil saturation of 97% was achieved.
3. *1st Waterflood*: Brine injected into the sandpack for 1.7 PVs.
4. *CO2 Flood*: CO2 injected into the sandpack from the top with an injection rate of 1 (cm^3hr^{-1}) for 6.9 core Pore Volumes.
5. *2nd Waterflood*: Brine injected into the sandpack from the top with an injection rate of 1 (cm^3hr^{-1}) for 3.1 core Pore Volumes.

Table 7-1 lists a summary of fluids used and the pressure and temperature at which the test was carried out.

Table 7-1: Core Exp 1; Fluids used and pressure and temperature conditions.

Porous Medium	Sandpack
Crude Oil	"C" (8700 cp @ 50 °C)
Aqueous Phase	Brine 10000 ppm (8/2 ratio between NaCl/$CaCl_2$)
Gas Phase	Vapour CO_2
Temperature	50 °C
Pressure	600 psig

Results

Oil Flood and Initialization

The sandpack was initially saturated with brine. Then the crude oil was injected through the core for an extended period of time to ensure that the core was uniformly saturated with the oil. The oil saturation obtained at the end of the oil injection period was 97% due to the very high viscosity of Crude "C".

1st Waterflood

The core was then flooded with water to simulate secondary waterflooding of an oil reservoir. As expected, due to a very large viscosity contrast between the flood water and extra-heavy oil, an early water breakthrough was observed. The first droplets of water were observed at the outlet after 0.13 PV of brine injection, when the recovered oil in the collecting cylinder was only 9.9 % OOIP. After the water breakthrough, oil recovery continued, as shown by the gradual change in the slope of the oil recovery curve after the breakthrough (deviation from straight line) in Figure 7-1. Water injection continued for a relatively long period of time and more than 1.7 PVs of water were injected through the core. Significant additional oil recovery was achieved after water breakthrough and oil recovery increased to 16.4 % OOIP at the end of the period of waterflood. Most of the recovery took place during the 1st pore volume of brine injection (~16 % OOIP).

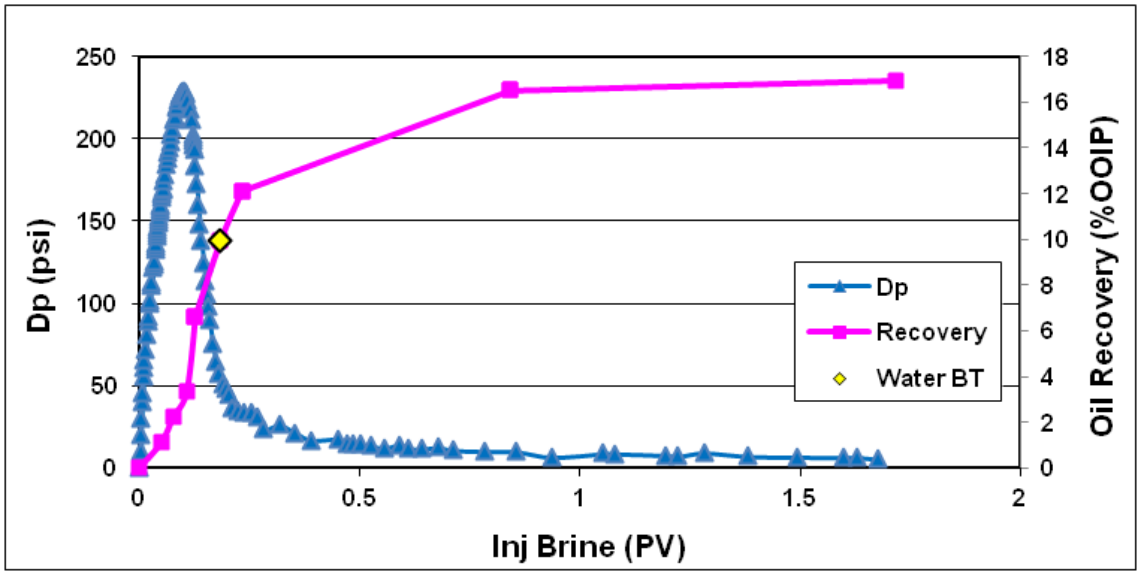

Figure 7-1: Core Exp 1; Oil recovery and differential pressure across the core versus PV of injected brine during 1st period of waterflood.

Figure 7-1 shows that the differential pressure across the core increased as water injection began and subsequently peaked at 225 psi before dropping back. Differential pressure across the core at water breakthrough was still high at 52 psi, compared to the stabilized pressure at the end of this waterflood period of approximately 5 psi. Given the very high viscosity contrast between the oil and flood water (oil viscosity of 8700 cp compared to less than 1 cp for the brine at test conditions), it was expected that after

water breakthroughdifferential pressure across the core would drop sharply and would quickly stabilise around a minimum value. However, as oil was still being produced after the water breakthrough, differential pressure remained high.

Tertiary CO2 Flood

After the initial waterflood period, CO2 injection commenced from the top end of the vertically oriented core. As CO2 injection progressed, initially, only brine was observed to be produced from the core until most of the injected brine was displaced from the core. The brine production was followed by production of a small bank of crude oil (1 % OOIP) before CO2 breakthrough. The injection of CO2 continued after breakthrough for 6.9 PVs. During the extended period of CO2 injection, oil was continuously produced from the sandpack at low rates. Figure 7-2 schematically illustrates the sequence of fluid production from the core during this period of CO2 injection.

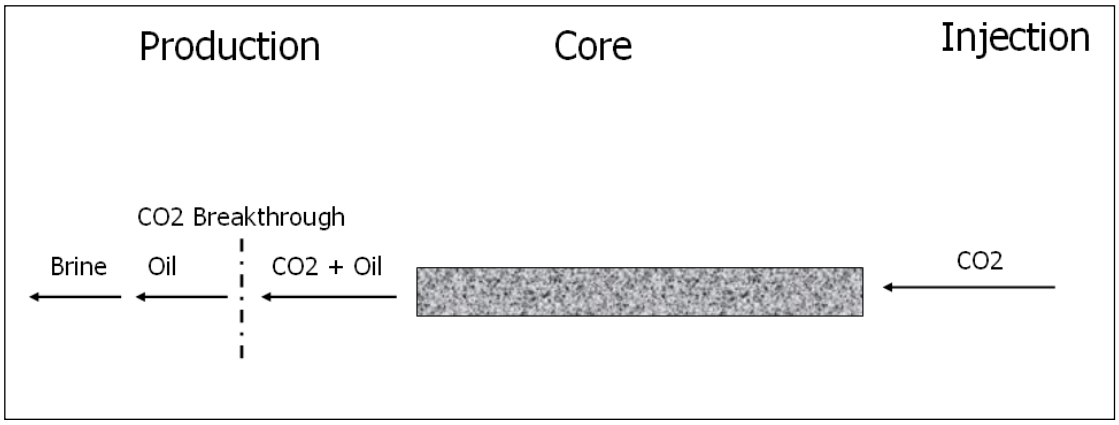

Figure 7-2: Core Exp 1; sequence of fluid production from the core before and after CO2 breakthrough during the period of CO2 flood.

The fact that a bank of oil was produced before the CO2 breakthrough is a strong indication of the positive oil spreading behaviour in the CO2/oil/water system. It means that the CO2 had been invading the oil-filled pores, rather than water. Due to the viscosity difference between the oil and brine, the bank of oil would in turn displace water and that explains why initially only water was produced before the oil bank. These observations are consistent with those made during the corresponding visualisation (micromodel) experiments using the same oil where oil spreading behaviour was observed.

Figure 7-3 displays the rate of oil production and oil recovery versus the volume of the injected CO2 during this period of CO2 injection. The important point that should be noted at this stage of the test is that despite a low oil recovery at the CO2 breakthrough, (only 1% of the initial oil in the core) the oil recovery has continued after breakthrough during the extended period of CO2 injection and eventually 10 % OOIP (original oil in place) was recovered from the core. The unfavourable viscosity ratio between the injected CO2 and resident heavy oil is believed to be the main reason for low oil recovery by the direct displacement mechanism before CO2 breakthrough. However, after CO2 breakthrough, oil production was prolonged due to some indirect recovery mechanisms. The viscosity reduction and swelling mechanisms (both oil and brine) as a result of CO2 dissolution, along with gravity forces caused by density difference between the oil and CO2, make major contributions to the oil recovery after CO2 breakthrough.

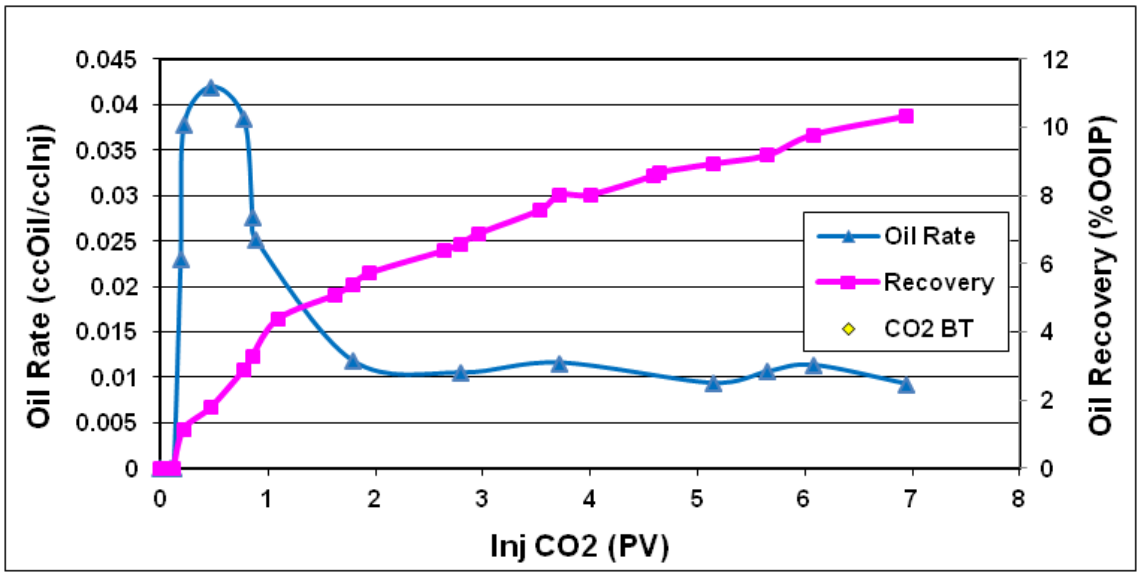

Figure 7-3: Core Exp 1; Oil production rate and oil recovery versus PV of injected CO2 during the period of CO2 flood.

2nd Water Injection

After the CO2 injection period, a 2nd water injection was carried out to examine the potential of water to recover the CO2 diluted oil. 3.1 PVs of water were injected during the 2nd water injection period. 2 % OOIP incremental oil recovery at the breakthrough of water (at 0.26 PV of water injection) was recorded, which then increased to 5.1 % OOIP as waterflood continued.

Summary

Table 7-2 summarises the oil recovery at breakthrough time and at the end of each stage of this experiment (tertiary CO2 injection). Figure 7-4 demonstrates the cumulative oil recovery curve (for the whole test) versus the total PV of injected fluids. Over 16 % OOIP of the oil was recovered during the initial extended water flooding period. The subsequent immiscible CO2 injections recovered 10.6 % OOIP of the oil in addition to what had been recovered during the preceding water flooding period. A second water injection period recovered another 5.1 % OOIP of the CO2 diluted oil. The additional oil recovery of 15.7 % OOIP during CO2 flood and subsequent waterflood, reveals the high potential of CO2 to improve the recovery of this heavy crude oil after conventional water flooding. However, an extended period of around 7 PVs was required for CO2 to achieve this recovery improvement. Figure 7-5 depicts the saturation of fluids inside the core at different stages of the experiment. It should be noted that the estimated saturation of CO2 includes the free CO2 and those fractions of CO2 which are dissolved in the oil and brine. It can be seen that a CO2 saturation of 23% was achieved at the end of the tertiary CO2 flood period, which is more than twice as much as the volume of recovered oil. The difference is the CO2 stored in the core through displacement of the resident brine.

Table 7-2: Core Exp 1; Summary of the results.

	Recovery @ BT (% OOIP)	Ultimate Recovery (% OOIP)
16) 1st Waterflood	9.9%	16.4 %
17) CO2 flood	1%	10.6 %
18) 2nd Waterflood	2.0%	5.1 %
Total	**-**	**32.1%**

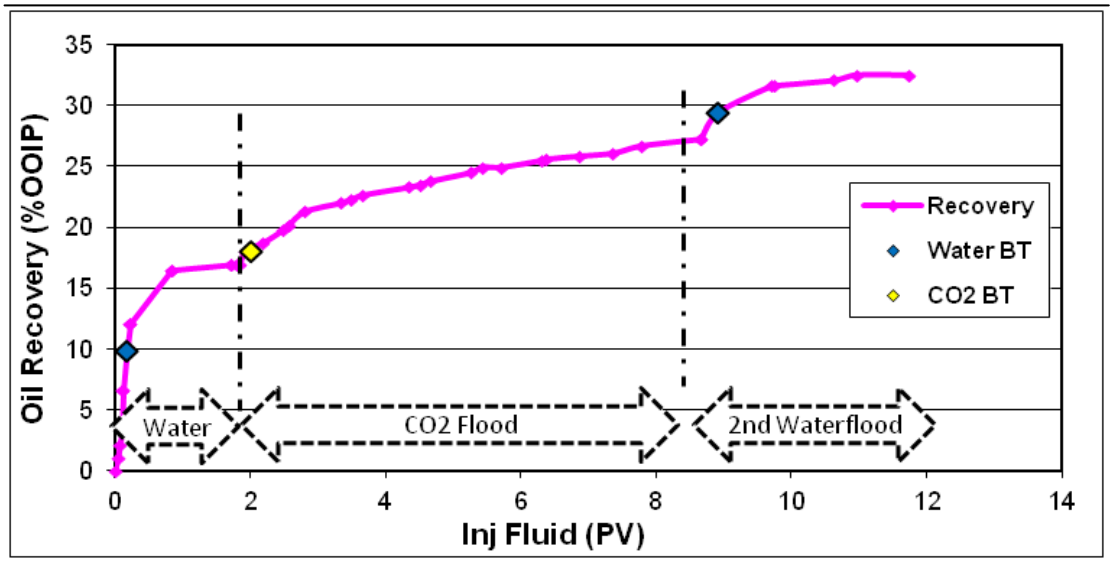

Figure 7-4: Core Exp 1; Recovery curve at different stages of the test.

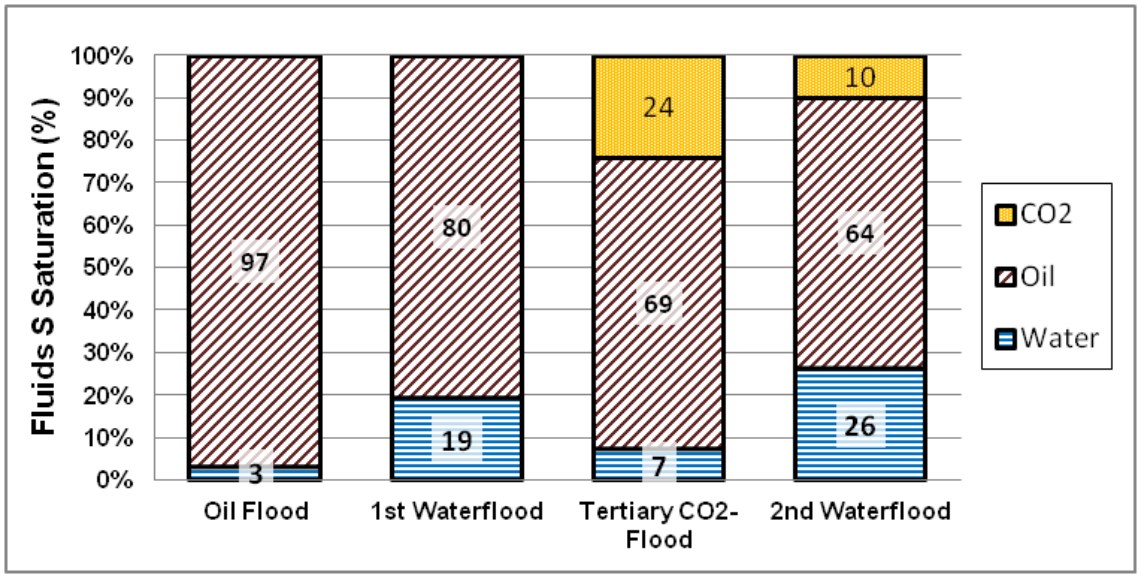

Figure 7-5: Core Exp 1; Saturation of fluids in the core during different stages of the experiment.

7.2.2 Core Exp 2: Secondary CO2 Injection

In the previous section, the performance of CO2 injection in tertiary mode (post waterflood) was examined. The second coreflood experiment was performed to simulate the process of secondary (pre-waterflood) immiscible CO2 flood in crude "C" and to confirm the observations made in the corresponding micromodel test (MM Exp 9).

Procedure and Conditions

In this coreflood experiment a procedure similar to the MM Exp 9 was followed, with the only difference being that a brine solution was used as the aqueous phase, instead of distilled water, as used in the micromodel test. All fluid injections were performed from the top of the vertically oriented core.

1. *Initialization:* The sandpack was saturated with brine at T = 50 °C and P = 600 psig
2. *Oil Flood:* The core was flooded with crude oil "J" and an oil saturation of 97 %OOIP was achieved.
3. *CO2 Injection*: 7 PVs of CO2 were injected through the core
4. *Water Injecting*: 1.9 PVs of brine were injected through the core.

Table 7-3 lists a summary of fluids used and the pressure and temperature at test conditions.

Table 7-3: Core Exp 2; Fluids used and pressure and temperature conditions.

Porous Medium	Sandpack
Crude Oil	"C" (8700 cp @ 50 °C)
Aqueous Phase	Brine 10000 ppm (8/2 ratio between NaCl/CaCl2)
Gas Phase	Vapour CO2
Temperature	50 °C
Pressure	600 psig

Results

Oil Flood and Initialization

The sandpack was initially saturated with brine. Subsequently, crude oil was injected through the core for an extended period of time to ensure the core was uniformly saturated with the oil. The oil saturation obtained at the end of the oil injection period was 97% due to the very high viscosity of Crude "C".

Secondary CO2 Injection

Having established the initial oil saturation and distribution in the core, CO2 was injected through the core from the top end of the vertically positioned core. During the CO2 injection, initially, only oil was produced from the core outlet; however, as the CO2 injection continued the effluent changed to foamy oil (mixture of CO2 and oil).

Production of foamy oil was observed shortly before the CO2 breakthrough took place. The CO2 breakthrough took place after injection of 0.35 PV of CO2 and resulted in an oil recovery of 11 % OOIP. Similarly to the previous core test, oil production continued after the CO2 breakthrough at low rates due to the combination of CO2 dissolution and gravity drainage mechanisms, which resulted in a significant final oil recovery of 22.3 %OOIP at the end of the CO2 flooding period. Figure 7-6 displays the rate of oil production and oil recovery versus the volume of injected CO2 during this period of CO2 flood.

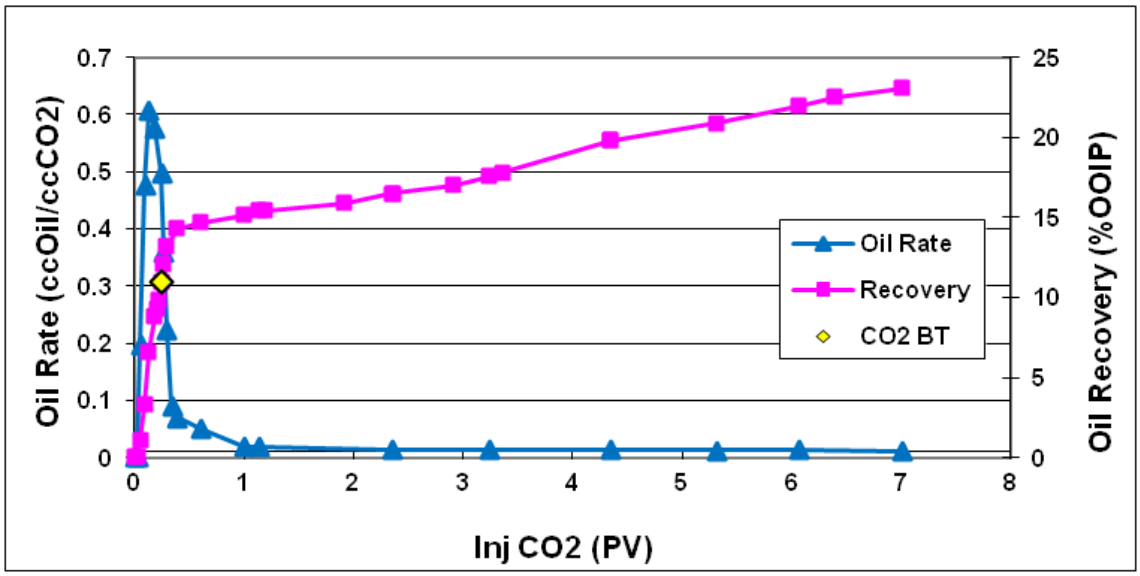

Figure 7-6: Core Exp 2; Oil production rate and oil recovery versus PV of injected CO2 during the period of CO2 flood.

Figure 7-7 plots the oil production rate versus the pore volume of injected CO2 in this test and compares that to the tertiary CO2 injection in Core Exp 1. The early recovery data after CO2 breakthrough (2 PVs of CO2 injection) have not been considered in this graph as it seems that in this time period oil/brine swelling (as a result of CO2 dissolution) is the main mechanism of oil displacement and production. The higher rate of oil recovery during the secondary CO2 injection, compared to the tertiary CO2 injection, is apparent in this graph. Based on the results from micromodel experiments, the difference in recovery rate is attributed to the presence of layers of water separating the injected CO2 and oil in the case of tertiary CO2 flood. These layers restrict the flow path of the diluted oil and reduce its relative permeability. Hence, the oil recovery process, which mainly takes place due to gravity forces, slows down.

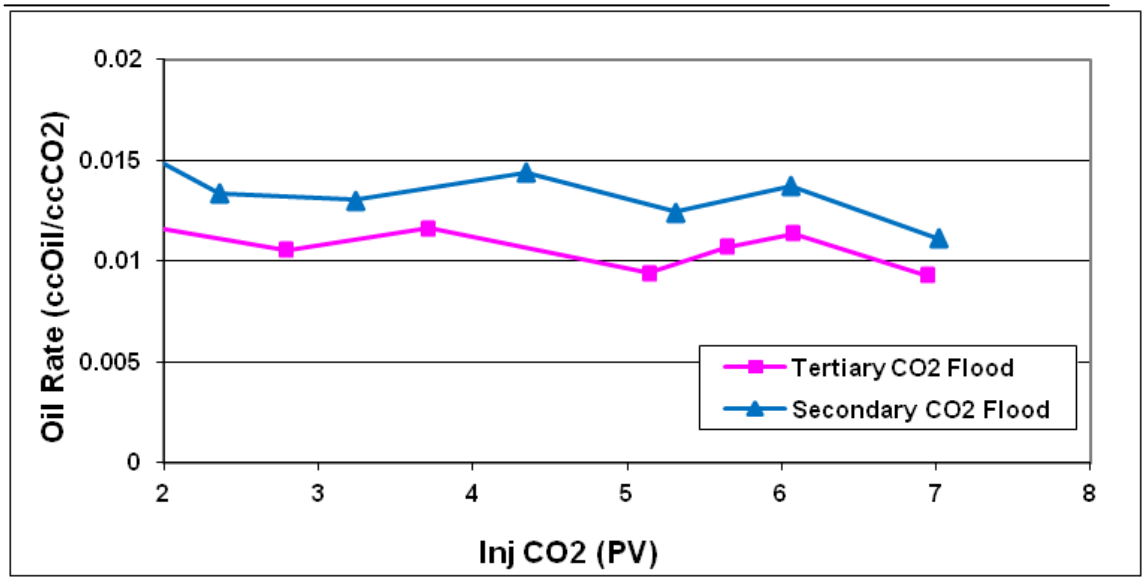

Figure 7-7: Comparison of oil production rate during secondary (Core Exp 2) and tertiary (Core Exp 1) CO2 injection in Crude "C".

Waterflood Period

After the extended period of CO2 injection, water injection commenced, to examine the potential of water to displace and recover the CO2-diluted oil. The water breakthrough occurred after injection of 0.28 pore volumes of water. An incremental oil recovery of 5.3 % OOIP was observed at the water breakthrough, which increased to 6.8 % OOIP as waterflood continued for 1.9 PVs.

Summary

Table 7-4 summarises the oil recovery at breakthrough time and at the end of each stage of this experiment (secondary CO2 injection).Figure 7-8 demonstrates the cumulative oil recovery curve (for the whole test) versus the total PV of injected fluids. 22.3 % OOIP of the heavy oil was recovered during the initial extended CO2 flooding period, which was performed under immiscible and gravity stable conditions. The subsequent water injection recovered 6.8 % OOIP additional oil, supplementary to what had been recovered during the CO2 injection. Figure 7-9 depicts the fluid saturations (CO2, oil and water) in the core at the end of each stage of this coreflood experiment.

Table 7-4: Core Exp 2; Summary of the results.

	Recovery @ BT (% OOIP)	Ultimate Recovery (% OOIP)
1) CO2 flood	11%	22.3 %
2) Waterflood	5.3 %	6.8 %
Total	-	**29.1%**

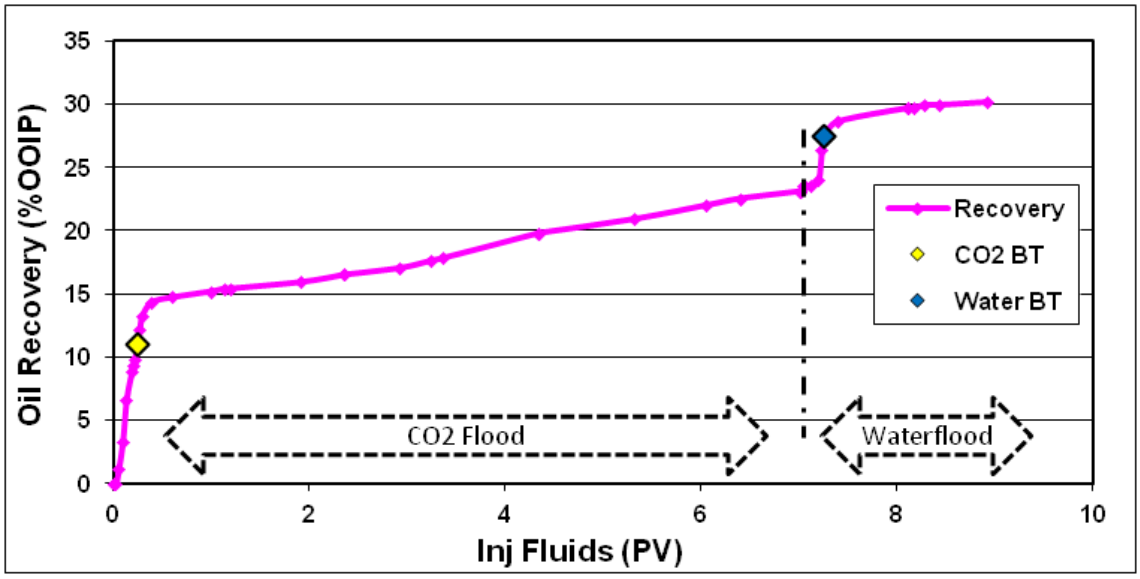

Figure 7-8: Core Exp 2; Recovery curve at different stages of the test.

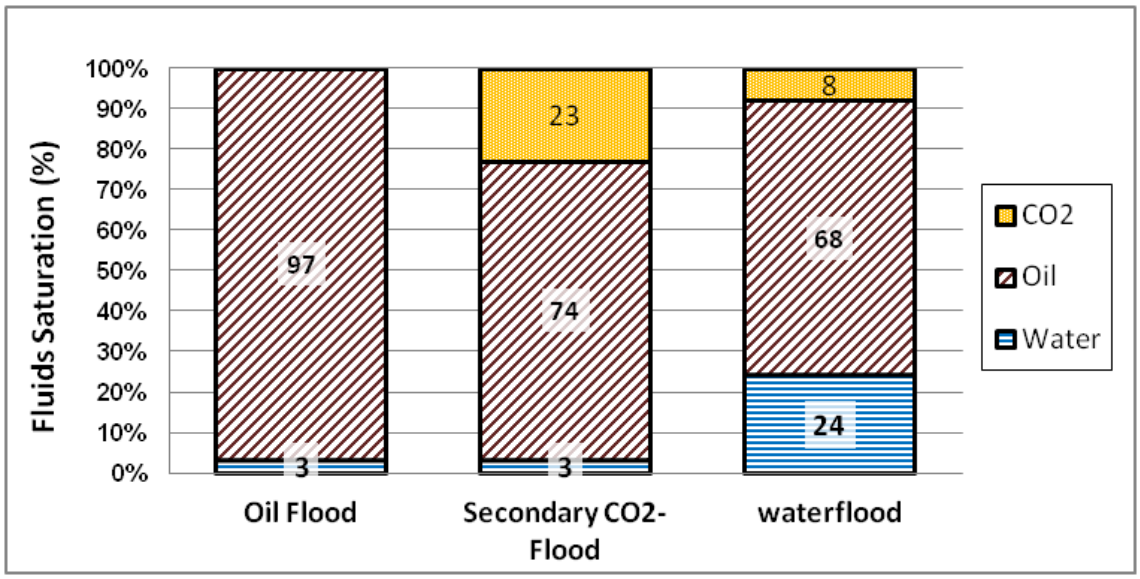

Figure 7-9: Core Exp 2; Saturation of fluids in the core during different stages of the test.

7.2.3 Core Exp 3: CO2-SWAG Injection

The third coreflood experiment was carried out to simulate the process of CO2-SWAG injection in crude "C".

Procedure and Conditions

In this coreflood experiment a procedure similar to MM Exp 10 was followed with the only difference that a brine solution was used (instead of distilled water) as the connate and displacing water. All fluid injections were performed from the top of the vertically oriented core.

1. *Initialization:* The sand pack was saturated with brine at T = 50 °C and P = 600 psig.
2. *Oil Flood:* The core was flooded with crude oil "J", achieving an oil saturation of 97 % OOIP.
3. *Waterflood*: 1.9 PVs of brine were injected through the core.
4. *CO2/Water Co-injection*: 6 PVs of CO2 and water were simultaneously injected through the core at a volumetric ratio of 1:1 (maintaining the total injection rate of 1 cm^3hr^{-1}).

Table 7-5 lists a summary of fluids used and the pressure and temperature at test conditions.

Table 7-5: Core Exp 3; Fluids used and pressure and temperature conditions.

Porous Medium	Sandpack
Crude Oil	"C" (8700 cp @ 50 °C)
Brine	10000 ppm (8/2 ratio between NaCl/CaCl2)
Gas Phase	VapourCO2
Temperature	50 °C
Pressure	600 psig

Results

Oil Flood and Initialization

The sandpack was initially saturated with brine. Subsequently, crude oil was injected through the core for an extended period of time to ensure the core was uniformly saturated with the oil. An oil saturation of 97% was achieved at the end of this period of oil injection.

Water Injection

The core was then flooded with brine for 1.5 PVs. As expected, due to a very large viscosity contrast between the flood water and crude oil, an early water breakthrough after 0.15 PV of water injection was observed. The oil recovery at water breakthrough was recorded to be 10.5 % OOIP, which increased to 18 % OOIP at the end of the period of waterflood

CO2/Water Co-Injection

After the initial period of waterflood, simultaneous injection of CO2 and water started. At this stage, both fluids were injected at the same rate of 0.5 cc/ hr through the core. Since brine and CO2 were injected at a very slow rate, it is believed that they reached equilibrium conditions in the injection lines before entering the core and contacting residual oil. During the early injection period only water was recovered from the core. The rate of water production was even slightly higher than the rate of water injection, which similarly to the previous tertiary CO2-injection test, implies displacement of the resident water in the core by CO2 (as observed in the micromodel tests). This resulted in an oil recovery of 3.7 % OOIP at breakthrough time. CO2-SWAG injection continued until a total volume of 6 PVs of CO2 and water were injected. SWAG injection ultimately resulted in 12.75 % OOIP incremental oil recovery, in addition to what had been produced by the initial waterflood. Figure 7-10 shows the rate of oil production and oil recovery during this period of simultaneous injection of CO2 and water.

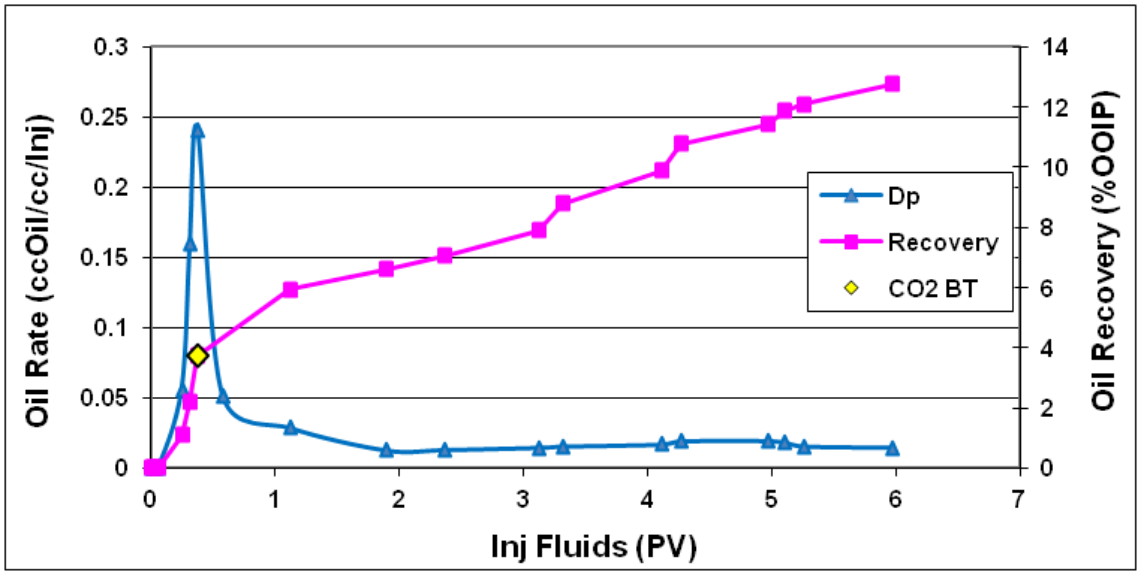

Figure 7-10: Core Exp 3; Oil production rate and oil recovery versus total PV of injected fluids during the period of CO2/water injection.

Figure 7-7 plots the oil production rate versus the pore volume of injected CO2 in this test and compares it to that of tertiary CO2 injection in Core Exp 1. The early recovery data after CO2 breakthrough (2 PVs of injection) have not been considered in this graph as it seems that in that time period, oil/brine swelling (as a result of CO2 dissolution), was the main mechanism of oil displacement and production. The higher rate of oil recovery during the CO2-SWAG injection compared to the tertiary CO2 injection is apparent in this graph. The better performance of CO2-SWAG is believed to be due to two reasons. First, mobility reduction in the injected CO2 and second, the improvement in pore scale displacement efficiency as previously explained in the corresponding micromodel experiment.

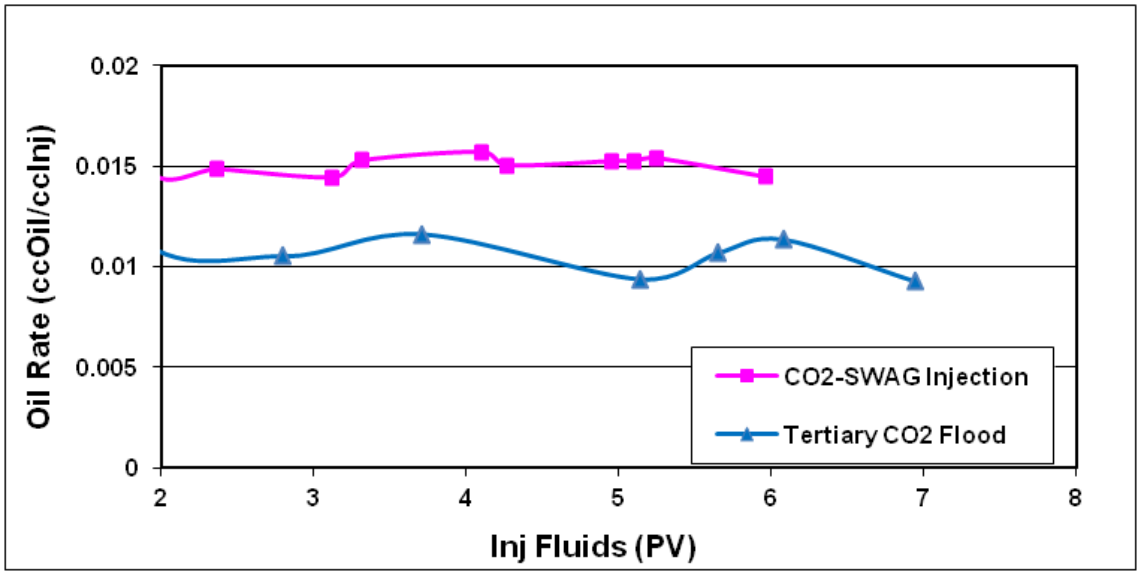

Figure 7-11: Comparison of oil recovery rate data during CO2-SWAG injection (Core Exp 3) and tertiary CO2 flood (Core Exp 1).

Summary

Table 7-6 summarises the oil recovery at breakthrough time and at the end of each stage of this experiment (CO2-SWAG injection). Figure 7-12 demonstrates the cumulative oil recovery curve (for the whole test) versus the total PV of injected fluids. 18 % OOIP of the heavy oil was recovered during the initial water flooding period, which was performed for 1.9 PVs. Oil recovery was improved by 3.7 % OOIP at breakthrough time, after the subsequent period of water co-injection, and 12.75 % OOIP at the end of the test. Figure 7-13 depicts the fluid saturations (CO2, oil and water) in the core at the end of each stage of this coreflood experiment.

Table 7-6: Core Exp 3; Summary of the results.

	Recovery @ BT (% OOIP)	Ultimate Recovery (% OOIP)
1) CO2 flood	10.5%	18 %
2) Waterflood	3.7 %	12.75 %
Total	-	**30.75%**

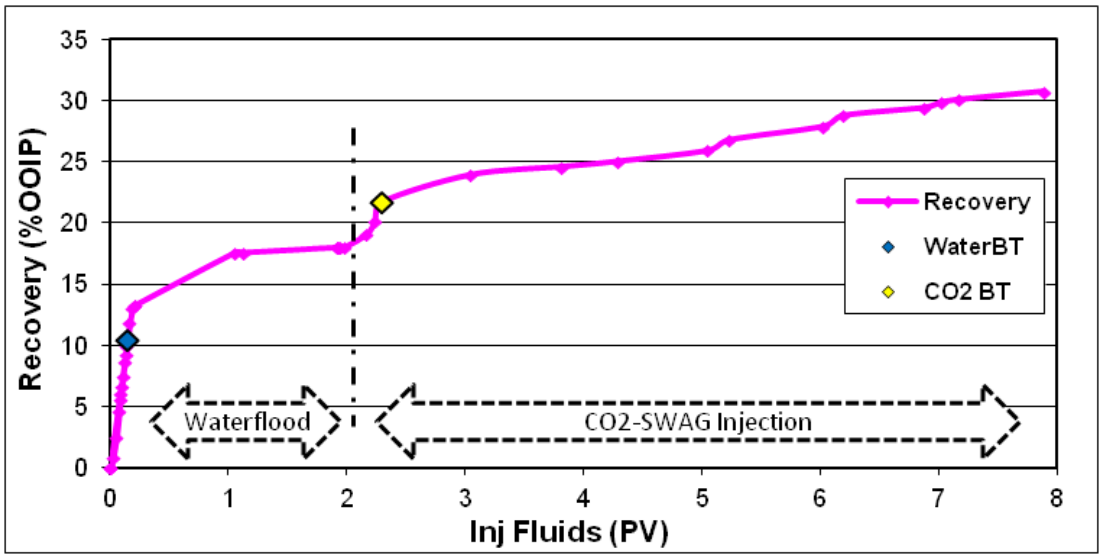

Figure 7-12: Core Exp 3; Recovery curve at different stages of the test.

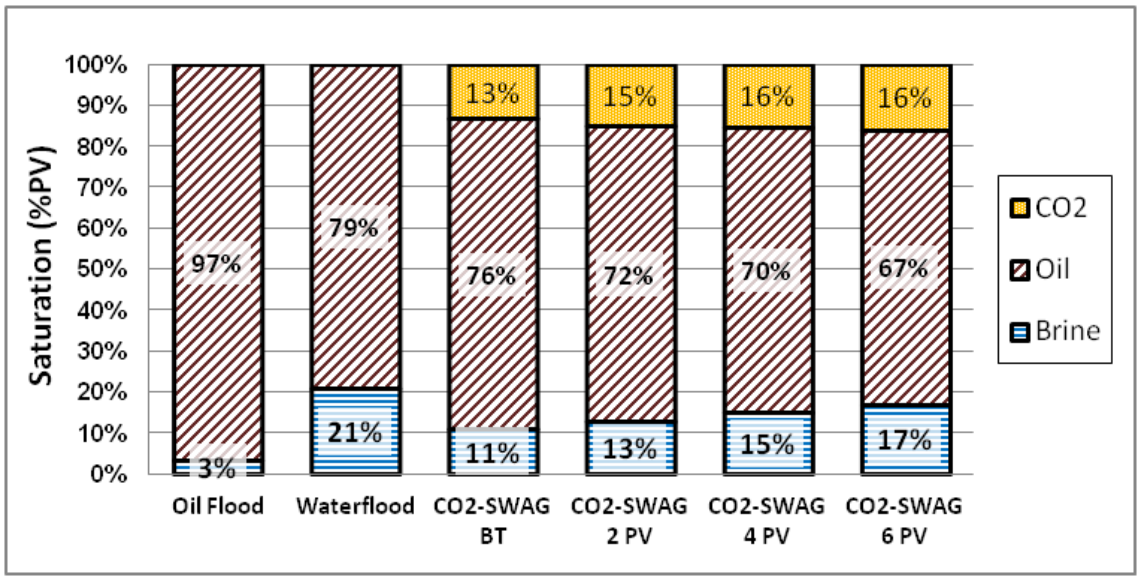

Figure 7-13: Core Exp 3; Saturation of fluids in the core during different stages of the test.

7.2.4 Discussions

Recovery Efficiency of Different Injection Strategies

In the three core flood experiments reported here, an average ultimate oil recovery of 30 % OOIP was achieved as a result of water and CO2 injection under different injection strategies. This is almost twice the recovery achieved during plain waterflood (16.4 % OOIP, Core Exp 1). Considering the very high viscosity of the heavy crude oil this is a good recovery efficiency which was mainly due to a significant reduction in the viscosity of the heavy oil due (as a consequence of CO2 injection. However, it should be noted that this recovery was achieved after an extended period of injection.

A comparison of oil recovery efficiency during the first 9 PVs of CO2 and water injection in Core Exp 1, 2 and 3 reveals that the oil production is highest in the case of CO2-SWAG injection, where the simultaneous injection of CO2 and water caused reduced mobility. The ultimate recovery using this method was 30.75 % OOIP, which was respectively 1.65 and 2.75 % OOIP higher than secondary and tertiary injection methods respectively, despite a lower volume of injected CO2 (7 PVs of CO2 in tertiary and secondary CO2 injection methods versus 3 PVs of CO2 in the CO2-SWAG injection method).

A comparison of the secondary and tertiary CO2 injection methods show that the recovery is slightly higher in the case of tertiary CO2 injection at early stages of water injection; however, the final recovery is higher in the case of secondary CO2 injection. While the secondary injection of CO2 recovered 29.1 % OOIP, the tertiary injection of CO2 resulted in recovery of 28 % OOIP. One reason for this difference in recovery is continuity of the oil phase in the example of secondary CO2 injection, which promotes the oil recovery process by gravity drainage as previously explained. The other reason is that in the secondary CO2 injection, water injection is conducted following the CO2 injection period and therefore it would be displacing the CO2-diluted oil with a much lower viscosity than the original oil, which would be the case in the example of tertiary (post water flood) CO2 injection.

A comparison of the recovery data from these 3 coreflood experiments with those from micromodel experiments, shows that the oil recovery is typically lower in the coreflood tests and extended periods of injection are required to obtain good recoveries. This difference in recovery is attributed to the high viscosity of this heavy crude oil (crude

"C"), which causes more severe fingering problems and higher residual oil saturation in porous media with larger scales (like core) compared to small porous media (like micromodel) with limited flowing paths.

Recovery Mechanisms

The results from the flow visualization experiments (micromodel) showed that at early injection times direct displacement of oil by CO2 is the dominant mechanism. After CO2 breakthrough, oil recovery continues as a result of a combination of CO2 dissolution and viscosity reduction, oil/water swelling and gravity drainage. In the following paragraphs the impact of these recovery mechanisms to oil recovery is discussed. However initially, to investigate the possibility of compositional changes in the oil phase as a result of hydrocarbon vaporization, the oil samples from the period of CO2 injection in Core Exp 2 were tested using a density meter. The samples with significant difference in oil density would then be analyzed using gas chromatography for precise compositional analysis. The results from density measurement tests are illustrated in Figure 7-14, which shows no significant change in density of produced oil as a result of compositional change. This is a valued characteristic of the low pressure application of CO2; the recovery mechanisms driven from CO2 dissolution in the oil phase, e.g. viscosity reduction and oil/water swelling are the dominant recovery improvement mechanisms. This observation is in line with theoretical work and micromodel observations presented in the previous chapter.

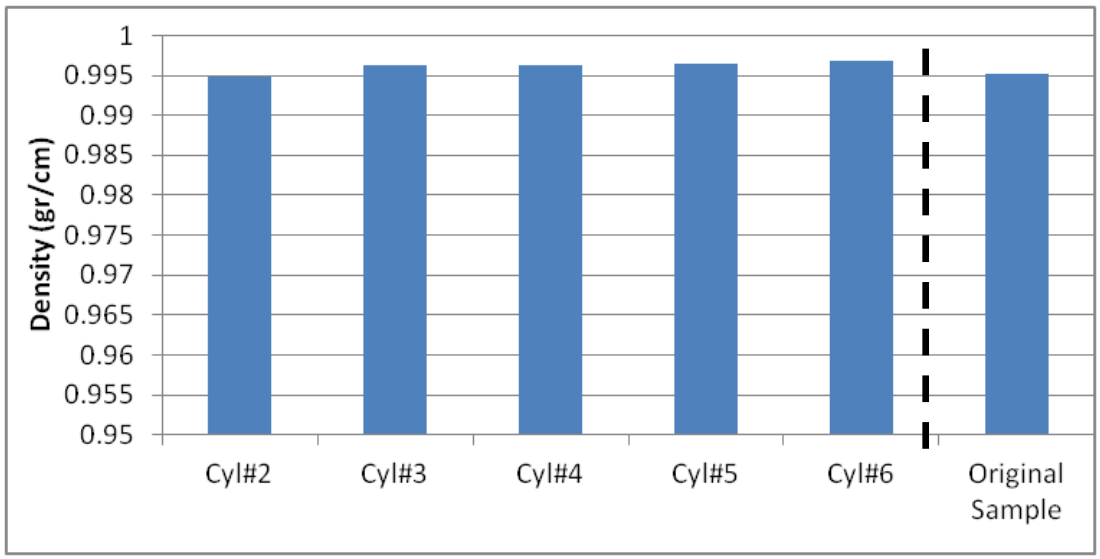

Figure 7-14: Analysis of the oil produced during secondary CO2 injection in Core Exp 2 using density measurement tests.

1) Direct Displacement: the author's observations show, in spite of the very unfavourable viscosity ratio between CO2 and heavy oil, if CO2 is injected in gravity stable conditions, high oil recovery by direct displacement can be obtained. The oil recovery at CO2 breakthrough was equal to 11 % OOIP when CO2 was injected in secondary mode (Core Exp 2). This was slightly higher (1 % OOIP) than the oil recovery at breakthrough time during secondary waterflood in Core Exp 1. This additional recovery is attributed to the contributions of other mechanisms like CO2 dissolution and effect of gravitational forces, despite lower viscosity of CO2 compared to water at test conditions. Nevertheless, direct displacement of oil by CO2 was not effective when CO2 was injected in tertiary mode (Core Exp 1). The poor performance of the direct displacement mechanism resulted in only a 1 % OOIP recovery improvement at CO2 breakthrough in this experiment. This is attributed to high water saturation in the core and an unfavourable viscosity ratio between the water and oil. This resulted in a double-drainage mechanism in which the small bank of oil ahead of the CO2 front displaced the resident water in the core instead of the residual oil.

2) Oil/Brine Swelling: Figure 7-10 shows the rate of oil production during the period of CO2 injection in Core Exp's 1, 2 and 3. A close look at the rate of oil production shows the oil production remains relatively high, even after CO2 breakthrough, for a short period of time before stabilizing at a constant rate. The higher rate of oil recovery at early periods of injection after CO2 breakthrough (first 2 pore volumes of CO2 injection) is attributed to the CO2 dissolution and subsequent swelling in oil and connate water.

3) Viscosity reduction: CO2 dissolution in heavy oil diluted the oil and significantly decreased the oil viscosity. This significantly improved oil mobilization and recovery. The diluted oil was then readily mobilized either by gravity drainage forces in Core Exps 1 and 2 or by the pressure gradient across the core as a result of viscous forces in Core Exp 3.

4) Gravity drainage: In the experiments where CO2 was injected continuously (CO2 Exp 1 and 2) the diluted oil was then mobilized as a result of gravity forces. Mobilization of the diluted oil by gravity drainage contributed to oil recovery from the beginning of the process of CO2 injection; however, it became the dominant recovery mechanism only after 2 PVs of CO2 injection, when oil production was stabilized at a

relatively constant rate. It should be noted that this recovery mechanism was more pronounced in the case of secondary CO2 injection, where the oil phase was connected in the porous medium. Existence of layers of water limited the mobility of oil and therefore reduced recovery of diluted oil by gravity forces, as can be seen in Figure 7-7. The gravity drainage mechanism was not believed to be as effective in Core Exp 3, where CO2 and water were simultaneously injected into the core. The micromodel observation showed that during CO2-SWAG injection, CO2 is scattered in porous media and not continuous like the example of secondary and tertiary injection of CO2. Therefore, the gravity drainage mechanism does not play an important role in the oil recovery of this process.

CO2 Storage by Different Injection Strategies

To compare the volume of stored CO2 in the core by different injection strategies, the saturation of fluids after the period of CO2 flood is analyzed (consequently the final period of waterflood in Core Exp 2 was overlooked). Figure 7-15 compares the volume of CO2 stored in the core at the end of the period of CO2 injection for different injection scenarios. As shown, due to the high saturation of oil in the core and also very low density of the vapour CO2 at reservoir conditions of crude "C", most of the stored CO2 (more than 50%) is dissolved in the heavy crude oil. In real field conditions, extended injection periods and low injection rates would be required to saturate the heavy crude oil with CO2. This is as a result of the high viscosity of the crude oil and very low diffusion rates in such systems.

From a CO2 storage point of view, while injection of CO2 in both secondary and tertiary injection scenarios shows a similar performance, the volume of stored CO2 is slightly lower in the scenario of a CO2-SWAG injection. This shows good potential for a CO2-SWAG injection scenario for both enhanced oil recovery and CO2 storage purposes, considering the volume of injected CO2 in the CO2-SWAG injection experiment was almost half the volume of injected CO2 during the secondary and tertiary injection experiments. A comparison between the secondary and tertiary CO2 injection scenarios reveals that: while early injection of CO2 (prior to waterflood) in heavy oil reservoirs would be beneficial from an oil recovery point of view, it would offer similar storage capacity as that of tertiary CO2 flood.

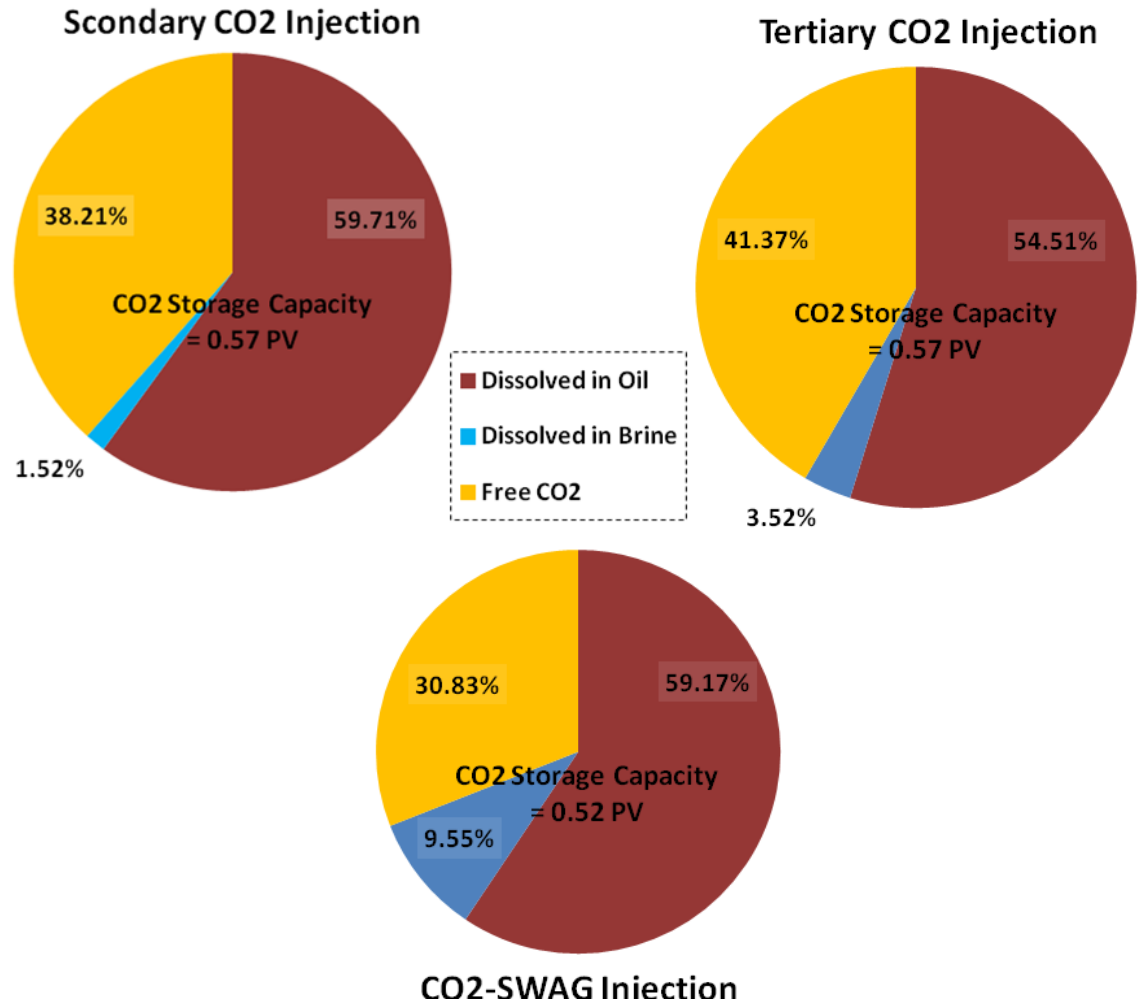

Figure 7-15: Comparison of the amount of stored CO2 in the core for different scenarios of CO2 injection.

7.3 THE EFFECT OF MOBILITY CONTROL BY CO2-FOAM

Based on observations from the micromodel tests (MM Exp 11), in which good recovery performance was achieved as a result of CO2-foam injection, a series of experiments were designed to investigate and quantify the performance of CO2-foam flood at core scale.

In the second series of coreflood tests, the sandpack was replaced with a new consolidated sandstone core. This was to avoid the difficulties and uncertainties due to the migration of sand particles, which is a common issue in sandpacks. Also due to the larger volume of the new consolidated core sample, compared to the sandpack, analyzing the data would be easier and more reliable. The new core was high permeable clean silica sand with very low shale and feldspar content.

The first experiment reported here is an example of tertiary CO2 flood at reservoir conditions of crude "C". This test is considered as the base case with which to compare the results of CO2-foam injection. The second experiment is a preliminary test to measure the viscosity of CO2-foam in the clean core (without oil), and finally the last test in this section simulates the process of heavy oil displacement by CO2-foam.

7.3.1 Core Exp 4: Tertiary CO2 Flood (Using Consolidated Core)

Procedure and Conditions

All fluid injections were performed from the top of the core at a constant rate of 7 cm^3hr^{-1}, equivalent to a frontal velocity of 1ft/ day.

1. *Initialization:* The core was saturated with brine at T = 50 °C and P = 600 psig.
2. *Oil Flood:* The core was flooded with crude oil "C".
3. *Aging:* The oil was left in the core for 1 day.
4. *Waterflood:* Two PVs of brine were injected through the core.
5. *CO2 Flood:* Extended period of CO2 injection in the core for 5.5 PVs.

Table 7-7 lists a summary of fluids used and the pressure and temperature at test conditions.

Table 7-7: Core Exp 4; Fluids used and pressure and temperature conditions.

Porous Medium	Consolidated Sandstone Core
Crude Oil	"C" (8700 cp @ 50 °C)
Brine	10000 ppm (8/2 ratio between NaCl/CaCl2)
Gas Phase	Vapour CO2
Surfactant Solution	0.3 wt % AOS 14+ dissolved in brine solution
Temperature	50 °C

Results

Oil Flood and Initialization

The core was first thoroughly cleaned by toluene and methanol, and then saturated with the brine solution and a brine permeability measurement performed. The crude oil was injected through the core for an extended period of time to establish uniform initial oil and water saturations in the core. Due to the high viscosity of crude "C", the brine was displaced from the core in a piston type manner and production of brine was stopped shortly after oil breakthrough. This resulted in a relatively high initial oil saturation of 89%. Figure 7-16 shows the volume of brine produced and the differential pressure across the core versus the PV of injected oil during the oil injection period. The lower saturation of oil at the end of the period of oil flood, compared to Core Exp 1 where the sandpack was used, is attributed to the existence of dead end pores and networks of pores in the consolidated core (as opposed to artificial sandpacks).

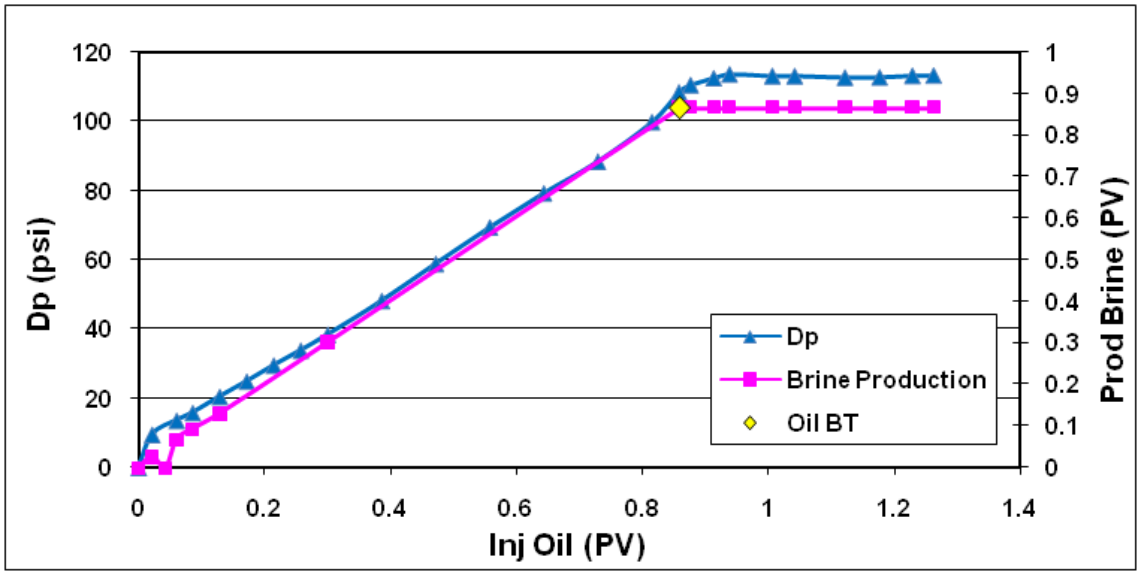

Figure 7-16: Core Exp 4; brine displacement and differential pressure across the core versus PV of injected extra-heavy oil during the period of oil flood.

Aging

At the end of the oil flood period, the inlet and outlet valves of the core were closed and the core remained at that condition for a day to allow the core to age briefly. The micromodel tests we carried out on this oil have shown that this crude oil does not have a strong tendency to alter wettability compared to other heavy crudes, and that the porous medium remains mostly water-wet in the presence of oil C. However, those tests were performed using only a monovalent salt (NaCl) and there is a possibility of wettability alteration in the presence of divalent salts (e.g. $CaCl_2$), which are present in the brine solution used in the core tests.

Water Injection

After establishing the initial oil and connate water saturations, the core was flooded with the brine. As expected, due to a very large viscosity contrast between the flood water and the crude oil, an early water breakthrough was observed. The first droplets of water were observed at the outlet after only 0.08 PV of brine injection, which resulted in a recovery of 9 % OOIP. After brine breakthrough, brine injection continued for a relatively long period of time and more than 2 PVs of brine were injected through the core. The oil recovery increased from 10 % OOIP at breakthrough to 18 % OOIP and 20 % OOIP, after 1 and 2 PVs of brine injection respectively. Most oil recovery after the breakthrough took place during the 1st PV of brine injection, after which time recovery of the oil continued but at a lower and fairly constant rate. Figure 7-17 shows the oil recovery and the differential pressure across the core during this water injection period.

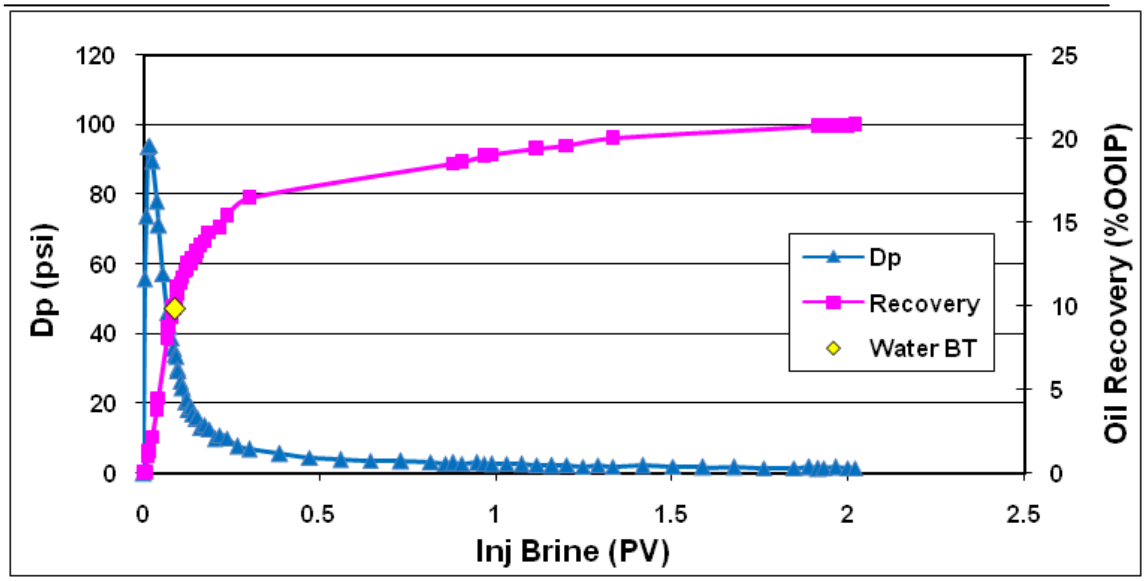

Figure 7-17: Core Exp 4, Oil recovery and differential pressure across the core versus PV of injected brine during the period of waterflood.

Tertiary CO2 Injection

After the initial period of waterflood, CO2 injection commenced, again from the top of the vertically oriented core. At the initial stages of CO2 injection (before the CO2 breakthrough), the core effluent consisted of brine and oil at very high water cuts. As the CO2 injection progressed, brine production continued and a significant volume of brine in the core was displaced. The brine production was followed by production of a small bank of crude oil (0.5 % OOIP) before CO2 breakthrough. The CO2 breakthrough happened after injection of 0.31 PV of CO2. The oil recovery continued after CO2 breakthrough, which resulted in recovery of 3 % OOIP, 9 % OOIP and 17 % OOIP after 1, 3 and 5.5 PVs of CO2 injection respectively. This volume of oil was produced in addition to what had already been produced during the preceding waterflood. Figure 7-18 displays the oil recovery and the differential pressure across the core, during this period of CO2 injection.

Figure 7-19 compares the rate of oil production (cc of produced oil per cc of injected CO2) during this period of CO2 flood, with the stabilized rate of oil production at the end of the preceding period of waterflood. As shown, oil production rate dropped to around 0.027 cc oil/cc inj after the CO2 breakthrough and remained unchanged at that rate, even after 5.5 PVs of CO2 injection. This rate is around 4 times higher than the rate of oil production by plain waterflood, which was 0.007 cc oil/cc inj. GOR also

showed similar behaviour and remained relatively constant after CO2 breakthrough, at values of around 1800 cc CO2/cc oil.

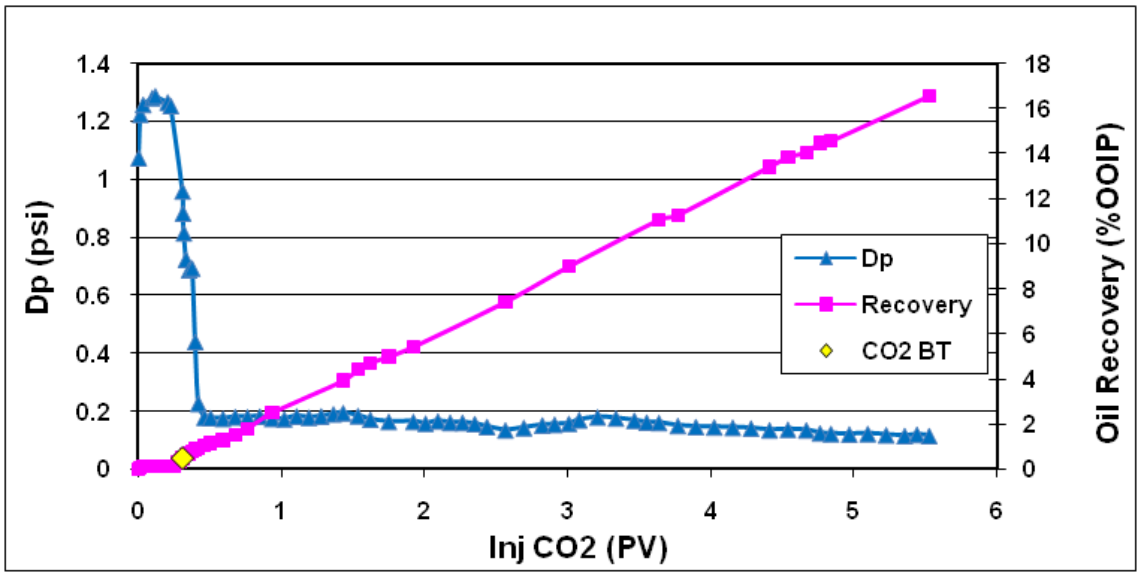

Figure 7-18: Core Exp 4; Oil recovery and differential pressure across the core versus PV of injected CO2 during the period of CO2 flood.

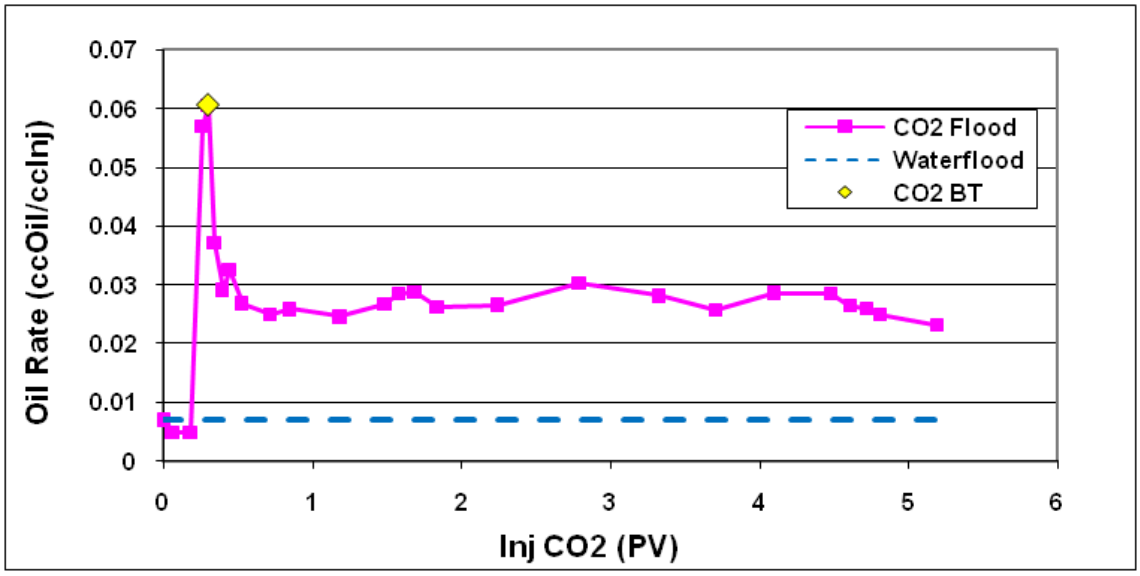

Figure 7-19: Core Exp 4; Comparison of oil production rate during CO2 flood and waterflood periods.

Measuring Saturation of Fluids inside the Core

At the end of this tertiary CO2 flood test, the saturation of fluids in the core was measured. Good consistency was achieved between the results from the main test and the saturation measurement test, in which the saturation of residual oil in the core was calculated as 55% and 54% respectively.

Summary

Table 7-8 summarises the amount of incremental oil recovery and cumulative oil production achieved at each stage of this experiment. Figure 7-20 demonstrates the cumulative oil recovery curve (for the whole test) versus the total PV of injected fluids. Figure 7-21 depicts the fluid saturations inside the core at different stages of the experiment and compares final saturations with those obtained from the saturation measurement test.

Table 7-8: Core Exp 5; Summary of the results of tertiary CO2 injection in crude "C" at 600 psig and 50 °C.

Recovery							
Water Flood				CO2-Foam Flood			
	Inj (PV)	Recovery	Cum Rec		Inj (PV)	Recovery	Cum Rec
BT	0.08	9%	9%	BT	0.31	0.5%	20%
1 PV	0.98	18%	18%	1 PV	0.93	3%	22%
2 PV	2.01	20%	20%	3 PV	3.01	9%	29%
				5.5 PV	5.53	17%	37%

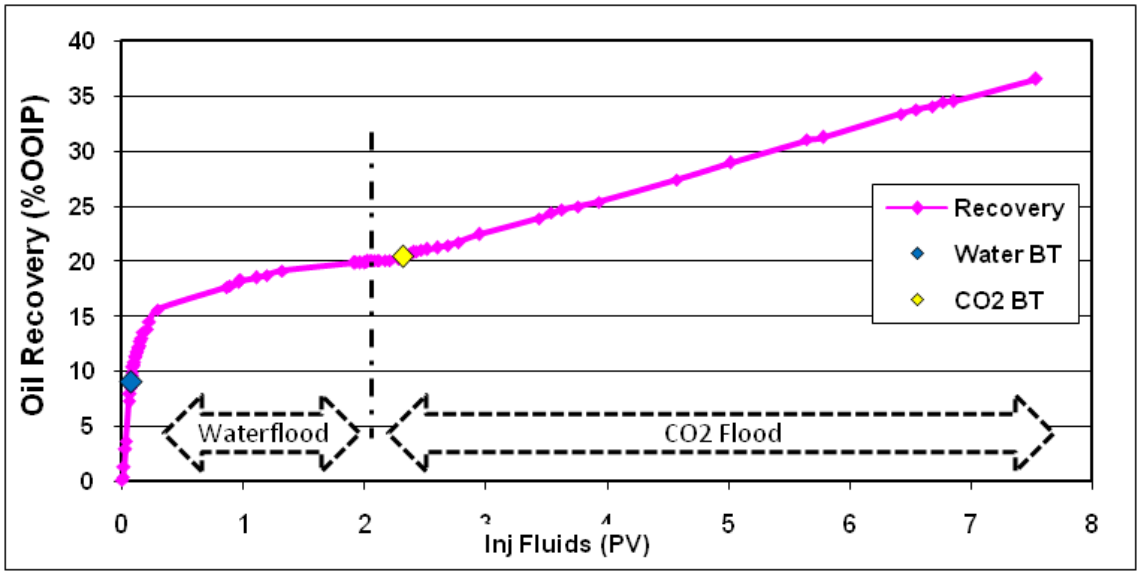

Figure 7-20: Core Exp 4; Recovery curve at different stages of Experiment 4 (tertiary CO2 injection in crude "C" at 600 psig and 50 °C).

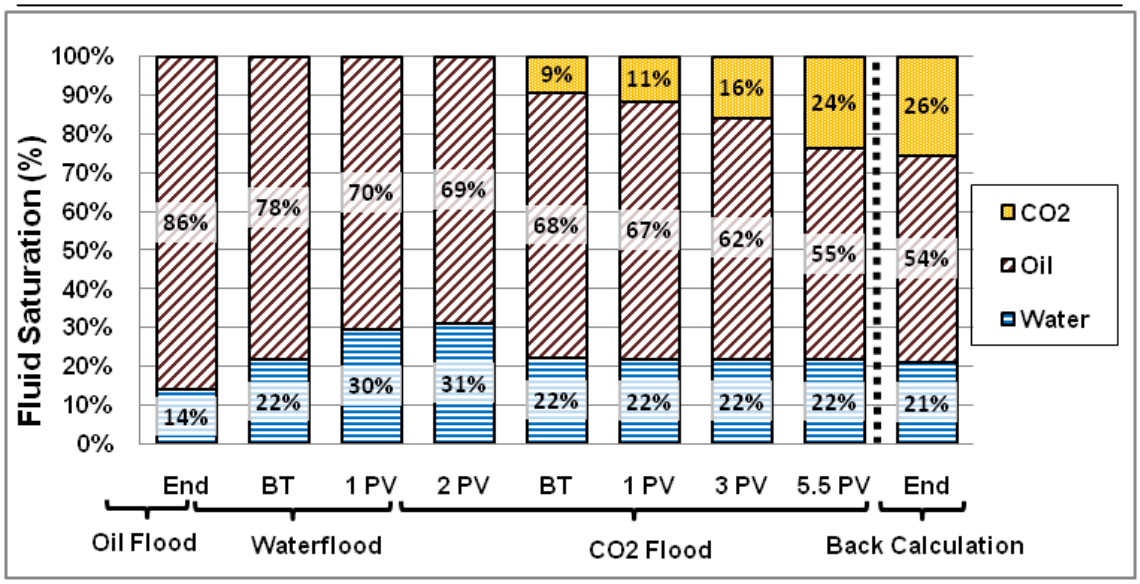

Figure 7-21: Core Exp 5; Saturation of fluids in the core during different stages of the Experiment (tertiary CO2 injection in crude "C" at 600 psig and 50 °C).

7.3.2 Core Exp 5 (Preliminary): CO2-Foam Viscosity Measurement

This coreflood experiment was performed in order to measure the viscosity of CO2-foam at reservoir conditions of crude "C" in a clean core. The viscosity data from this experiment will be useful for a better understanding of the recovery data in Core Exp 6. Table 7-9 shows the pressure and temperature at which the test was performed, as well as the fluids used in the test.

Table 7-9: Core Exp 6 (Preliminary); Fluids used and pressure and temperature conditions.

Porous Medium	Consolidated Sandstone Core
CO2	Vapour CO2
Surfactant Solution	0.3 wt % AOS 14+ dissolved in a brine solution of 10000 ppm (8:2 ratio between NaCl:CaCl2)
Temperature	50 °C
Pressure	600 psig

To perform the test, the core was initially saturated with the surfactant solution and then the CO2 and surfactant were simultaneously injected through the core at rates of 4.5 cc/ hr and 2.5 cc/ hr respectively, corresponding to a frontal velocity of 1 ft/ day. Figure 7-22 presents the differential pressure across the core and the apparent viscosity of the CO2-foam during this period of CO2/surfactant injection. As shown, the differential pressure across the core increased at a constant rate during the first 6 PVs of CO2/surfactant injection and then stabilized at a differential pressure of around 10 psi, equal to an apparent viscosity of 550 cp. This value was approximately one order of magnitude less than the viscosity of the dead crude oil (8700 cp), yet was at the same range as the oil that is fully saturated with CO2 (660 cp). Comparison of the CO2-foam viscosity in this test with that of vapour CO2 at the same test conditions (0.017 cp) shows a resistance factor (CO2 viscosity increase) of 32000 times, as a result of the formation of CO2-foam in the core.

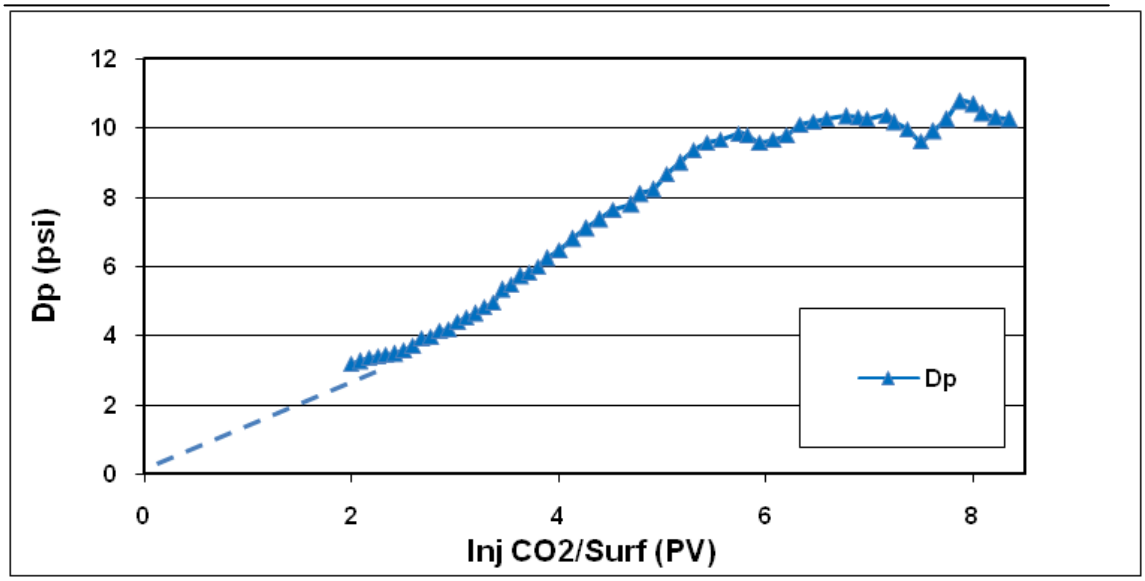

Figure 7-22: Core Exp 5 (Preliminary): Foam apparent viscosity and differential pressure across the core during CO2-foam flood. The fragmented line shows that the data in that injection period is estimated.

7.3.3 Core Exp 5: CO2-Foam Flood

The main objective of this core flood experiment was to investigate the potential of enhancing the displacement and recovery of crude "C" by formation of CO2-foam at reservoir conditions of this crude oil.

Procedure and Conditions

All fluid injections were performed from the top of the core at a constant rate of 7 cm^3 hr^{-1}; equivalent to a frontal velocity of 1ft/ day. In the example of co-injection of CO2 and surfactant solution the total injection rate was equal to 7 cm^3 hr^{-1}.

1. *Initialization:* The core was saturated with brine at T = 50 °C and P = 600 psig.
2. *Oil Flood:* The core was flooded with crude oil "C".
3. *Aging:* The oil was left in the core for 1 day.
4. *Waterflood:* One PV of brine was injected through the core.
5. *CO2-Foam Flood:* Six PVs of surfactant solution and vapour CO2 were injected simultaneously through the core with the ratio of 4.5:2.5 respectively for CO2 and surfactant solution.

Table 7-10 lists a summary of fluids used and the pressure and temperature at test conditions.

Table 7-10: Core Exp 5; Fluids used and pressure and temperature conditions.

Porous Medium	Consolidated Sandstone Core
Crude Oil	"C" (8700 cp @ 50 °C)
Brine	10000 ppm (8:2 ratio between NaCl:CaCl2)
Gas Phase	Vapour CO2
Surfactant Solution	0.3 wt % AOS 14+ dissolved in brine solution
Temperature	50 °C
Pressure	600 psig

Results

Oil Flood and Initialization

The core was first thoroughly cleaned by toluene and methanol, and then saturated with the brine solution and a brine permeability measurement performed. Then, the crude oil was injected through the core to establish an initial oil and water saturation. Oil was observed to displace water in a piston type manner, which resulted in an initial oil saturation of 89%. After the oil injection period, the inlet and outlet of the core were closed and the core remained at that condition for a day for aging purposes.

Water Injection Period

The core was then flooded with brine from the top of the vertically mounted core. Brine breakthrough took place after 0.09 PV of brine injection, which resulted in recovery of 10 % OOIP. Brine injection continued for one PV in which the oil recovery increased from 10 % OOIP (at the breakthrough) to 19 % OOIP.

CO2/Surfactant Co-Injection

After the period of waterflood, co-injection of CO2 and surfactant commenced, again from the top of the core. At the initial stages of CO2/surfactant injection, before the CO2 breakthrough, the core effluent mostly consisted of brine and oil at high water cuts. Brine production was followed by production of a relatively large bank of crude oil that recovered 11.2 % OOIP before CO2 broke through (after 0.49 PV of CO2/surfactant co-injection). Oil recovery continued after CO2 breakthrough, which resulted in 19, 28, 43 and 56 % OOIP additional oil recovery, after 1 , 2 , 4 and 6 PVs of CO2/surfactant injection respectively. This additional oil recovery was supplementary to what had been recovered during the preceding water injection period.

Figure 8-21 displays differential pressure across the core and the oil recovery data during this period of CO2/surfactant injection. When the CO2/surfactant injection starts, there was an increase in differential pressure before the CO2 breakthrough, which is believed to be due to the formation in the core of an oil bank (ahead of the CO2-foam). After the CO2 breakthrough, differential pressure gradually decreases and reaches its minimum of 3 psig at around 1.5 PVs of CO2/surfactant injection. As more CO2 and surfactant was injected through the core, differential pressure gradually increased. This is due to formation of CO2-foam in the core at a later stage. It is important to note that the formation of foam, which resulted in a differential pressure increase, took place while the core still contained a high residual oil saturation of 0.47%. This behaviour is different from the observations from a light oil reservoir, where an oil saturation of between 10 to 20% can deleteriously affect the process of foam flood and prevent formation of strong foam.

Figure 8-23 illustrates the rate of oil production (cm^3 of produced oil versus cm^3 of injected CO2) and gas oil ratio of the effluent during the period of CO2/surfactant injection. As shown, in the early stages of injection and before CO2 breakthrough, the rate of oil production is very low; however just before CO2 breakthrough there is a jump in oil recovery rate when the oil rate reached a maximum value of 0.3 cc oil/cc Inj. Oil rate gradually drops after the CO2 breakthrough and continues at a relatively constant rate of 0.08 cc oil/cc inj until 5 PVs of injection. A second drop in the oil production rate was then observed and oil production stopped at around 6 PVs of CO2/surfactant injection. At the same time the GOR sharply increases from the relatively constant rate of 2000 cc oil/cc CO2 to values of approximately 5000 cc oil/cc CO2.

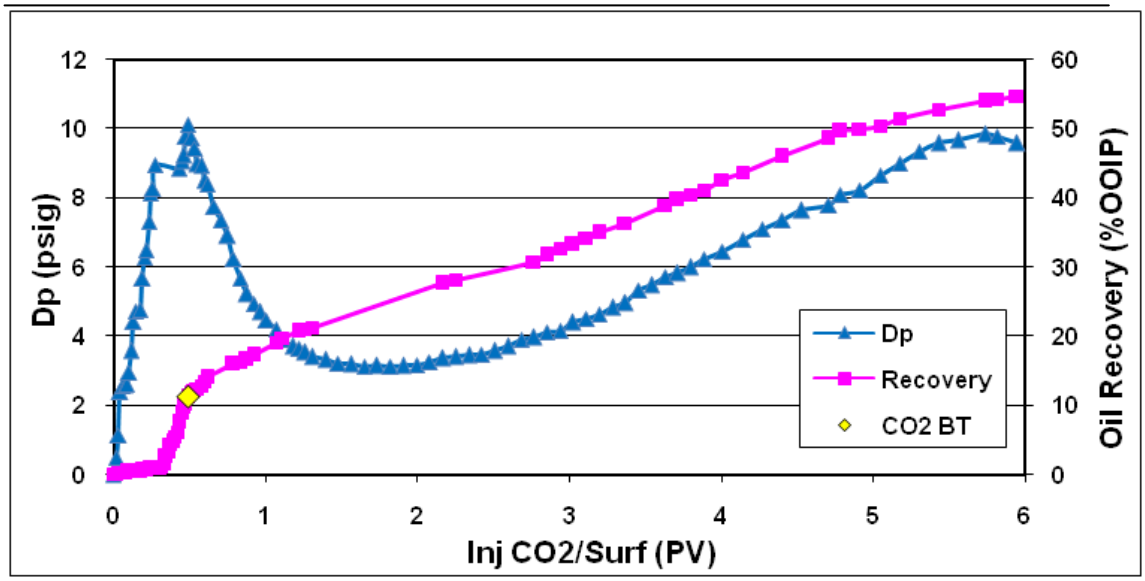

Figure 7-23: Core Exp 5; Oil recovery and differential pressure across the core versus total PV of injected fluids during the period of CO2/surfactant flood.

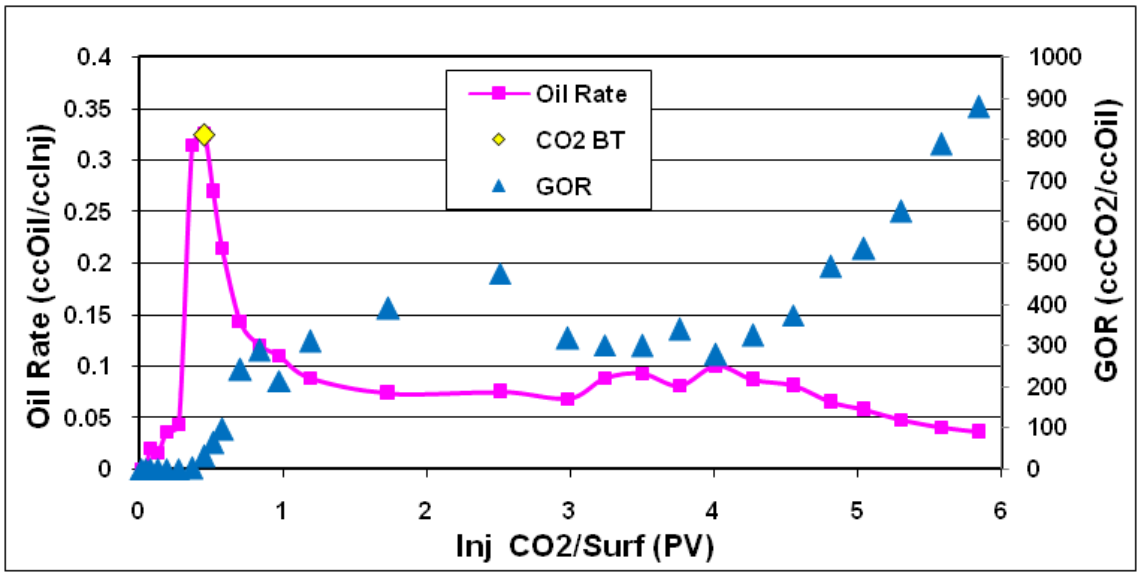

Figure 7-24: Core Exp 5; Oil production rate and oil recovery versus total PV of injected fluids during the period of CO2/surfactant flood.

Measuring Saturation of Fluids inside the Core

At the end of this foam flood test, the saturation of fluids in the core was measured. Good consistency was achieved between the results from the main test and saturation measurement test in which saturation of residual oil in the core was calculated as 22.5% and 21% respectively.

Summary

Table 7-11 summarises the amount of incremental oil recovery and cumulative oil production achieved at each stage of this experiment. Figure 7-25 demonstrates the cumulative oil recovery curve (whole test) versus total PV of injected fluids. As shown, oil recovery has increased by a factor of 4 from 19 % OOIP at the end of waterflood period to 75 % OOIP after 6 PVs of CO2-foam flood.

Table 7-11: Core Exp 7; Summary of results of the CO2-foam flood in crude "C" at 600 psig and 50 °C.

Recovery							
Water Flood				CO2-Foam Flood			
	Inj (PV)	Recovery	Cum Rec		Inj (PV)	Recovery	Cum Rec
BT	0.09	10%	10%	BT	0.49	11.2%	31%
1 PV	1.08	19%	19%	1 PV	1.07	19%	39%
				2 PV	2.17	28%	48%
				4 PV	4.01	43%	63%
				6 PV	5.94	55%	75%

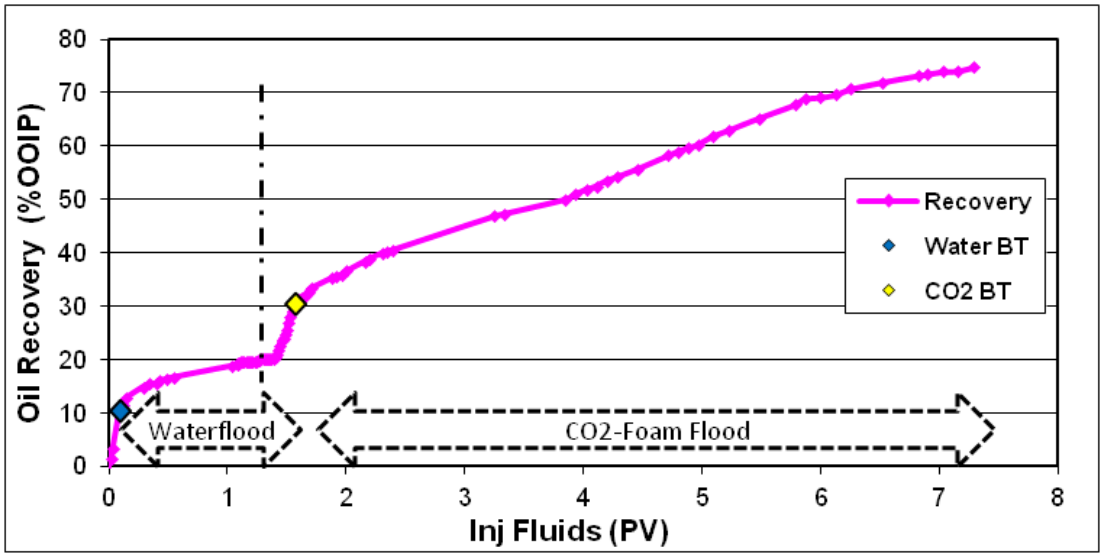

Figure 7-25: Core Exp 5; Recovery curve at different stages of CO2-foam flood in crude "C" at 600 psig and 50 °C.

7.3.4 Discussions

Comparison of Tertiary CO2 and CO2-Foam Flood

Figure 7-26 compares differential pressure across the core during CO2-foam flood and tertiary CO2 flood in crude C, at its reservoir conditions of 600 psig and 50 °C. As shown in this figure, injection of CO2-foam has successfully pressurized the core and increased the differential pressure across the core by a factor of 170 (10.2 psi differential pressure during the CO2-foam flood, compared to 0.06 psi during the CO2 flood) during the later stages of injection. This differential pressure across the core corresponds to an apparent foam viscosity of around 550 cp, which is very close to the viscosity of crude "C" when fully saturated with CO2 (660 cp). This means that CO2-foam can make a stable front and displace the diluted oil efficiently.

Figure 7-27 compares the incremental oil recovery (based on waterflood remaining oil) obtained in the CO2-foam test, with that obtained in the tertiary CO2 flood test. This graph shows that formation of foam in the core has dramatically increased both breakthrough and ultimate recovery from the core. The difference in oil recovery is more significant at breakthrough time, where 16 % of waterflood residual oil (S_{wro}) oil was recovered during CO2 foam injectin, while only 1 % S_{wro} oil was recovered during tertiary CO2 injection. Comparison of ultimate recoveries, show that an incremental oil recovery of 68 % S_{wro} of waterflood residual oil (S_{wro}) was attained after 6 PVs of CO2/surfactant injection, whilst during the tertiary CO2 flood, the incremental recovery reached only 21 %S_{wro} in the same time period. This shows a recovery improvement of more than 3 times, as a result of mobility control by CO2-foam.

In addition to recovery improvement, injection of CO2-foam significantly reduced the volume of gas produced at the early stages of injection. Figure 7-28 compares GOR obtained during the CO2-foam and CO2 flood tests. During the first 4 PVs of injection, when most of the oil was recovered, a GOR of around 350 cc CO2/cc Oil was recorded during the CO2-foam flood test, which was 5 times lower than the GOR achieved during tertiary CO2 flood (1800 cc CO2/cc Oil).

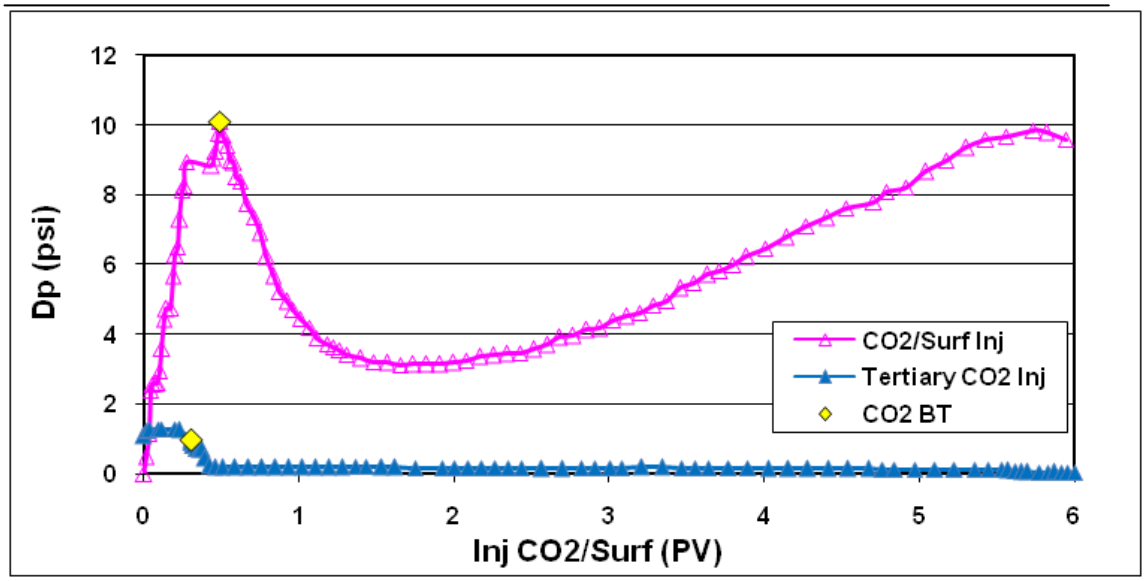

Figure 7-26: Comparison of the differential pressure across the core during CO2-foam flood (Core Exp 5) and tertiary CO2 flood (Core Exp 4).

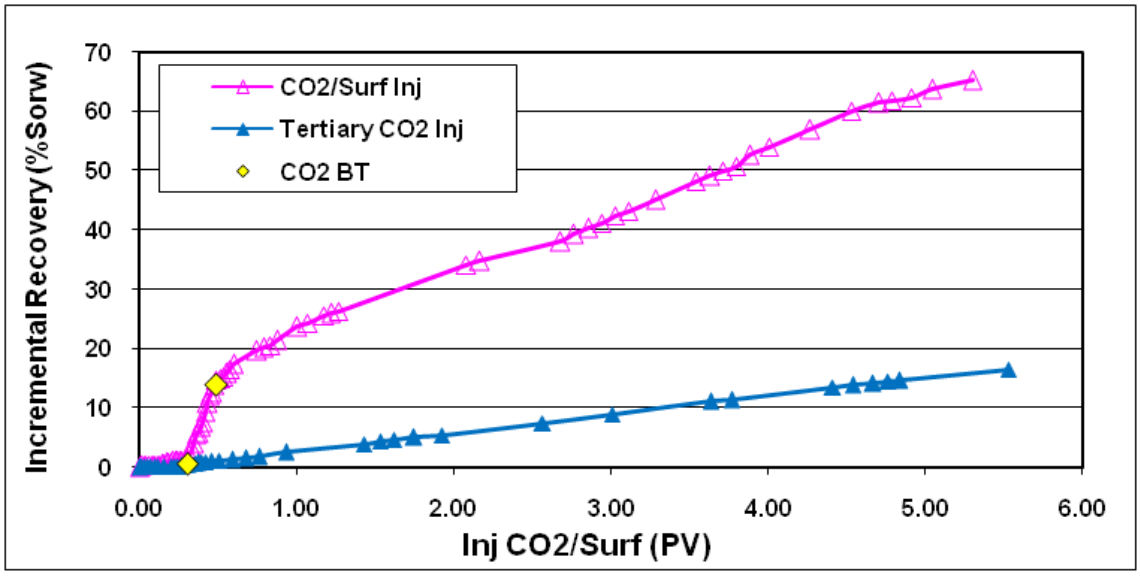

Figure 7-27: Comparison of the incremental oil recovery (based on waterflood remaining oil saturation) during CO2-foam (Core Exp 5) and tertiary CO2 flood (Core Exp 4) tests at 600 psig.

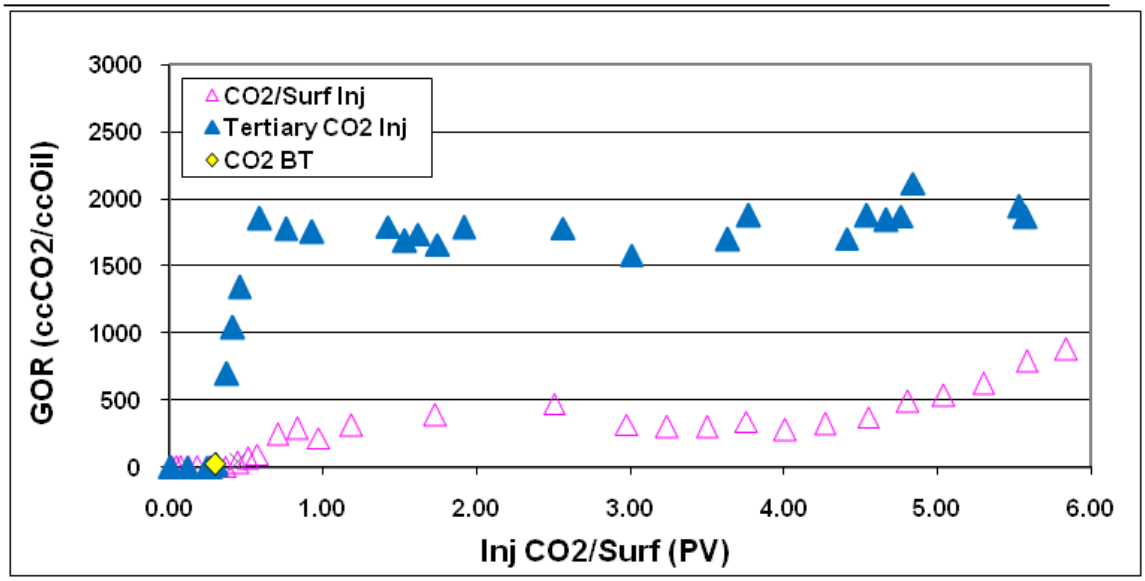

Figure 7-28: Comparison of the differential pressure across the core during CO2-foam flood (Core Exp 5) and tertiary CO2 flood (Core Exp 4).

Effect of Oil Saturation on Foam Stability

The adverse effect of oil on foam stability has been repeatedly documented in the literature. The experiments using hydrocarbon foams has shown a steep decrease in the apparent viscosity of foam at oil saturations higher than 13 to 15%. However, our coreflood test shows that CO2-foam can form and pressurize the system even at heavy oil saturations of up to 50%. In Core Exp No 5, pressurization of the core due to in-situ generation of CO2-foam started after 1.5 PVs of CO2/surfactant injection, when the oil saturation was as high as 48% and showing an apparent foam viscosity around 180 cp.

The reason for stability of CO2-foam at higher oil saturations compared to the example of light oils is believed to be due to the pattern of oil displacement during initial waterflood. The unstable nature of viscous oil displacement by water causes the formation of continuous but narrow fingers of water through the heavy oil phase. Due to the lower resistance to flow, the injected CO2-foam naturally flows through narrow fingers that are formed and occupied by water during the initial period of waterflood. After a short period of surfactant and CO2 injection, the oil saturation in these regions drops to very low values suitable for CO2-foam propagation. Therefore, pressurization starts in the system even though most of the porous media is still fully saturated with heavy oil. As the CO2-foam forms in these narrow water fingers and blocks these flowing paths, the flow diverts towards high oil saturation regions and displaces the residual oil in other parts of the porous media containing high oil saturation.

Furthermore, it was mentioned in the literature review chapter that foam is generally more stable against heavier hydrocarbons.

Recovery Mechanisms

During the period of CO2-foam injection, in addition to CO2 dissolution and the subsequent recovery mechanisms (e.g. swelling and viscosity reduction), the oil recovery is improved by mobility control and pore scale displacement mechanisms explained in the previous chapters (direct displacement, emulsification, co-current and counter-current film flow). Mobility control and pressurization of the core, as a result of strong foam formation in the core, can be clearly seen in Figure 7-26. However, the gravity drainage mechanism is not expected to play an important role in recovery of heavy oil during CO2-foam injection. This is due to the fact that the CO2 phase is not a continuous phase in the porous media and is in the form of small bubbles of foam. Additionally, due to the high viscosity of CO2-, the viscous forces are significantly higher than the example of CO2 injection and the effect of gravity forces can be overlooked in comparison to viscous forces.

7.4 SUMMARY AND CONCLUSIONS

The following conclusions were drawn from first part of this chapter (effect of injection strategy):

1. The results of this study demonstrate that in addition to the CO2 disposal benefits, there is a huge potential for heavy oil recovery improvement by CO2 injection in these reservoirs. The ultimate oil recovery for all scenarios of secondary, tertiary and SWAG CO2 injection was almost twice the recovery during plain waterflood.
2. The highest oil recovery was achieved in the case of CO2-SWAG injection. Tertiary injection of CO2 showed the lowest recovery compared to secondary CO2 and CO2-SWAG injection strategies.
3. From a CO2-storage point of view, however, the same amount of CO2 storage was almost achieved in secondary and tertiary CO2 injection, which was considerably higher than the CO2 stored in the case of CO2 SWAG injection.

The following conclusions were drawn from the second part of this chapter (effect of mobility control):

4. Very high potential was observed for CO2-foam to enhance the recovery of crude oil "C" at its reservoir conditions (600 psi and 50 C). The injected CO2-foam dramatically improved the displacement efficiency from 20% Srow in tertiary CO2 flood, to approximately 69% Srow after 6 PVs of CO2/surfactant (CO2 foam) injection.
5. At the same time, mobility ratio between the displacing phase and crude oil process was enhanced, as a result of the increase in viscosity of the displacing phase from 0.016 cp for vapour CO2 to 550 cp for CO2-foam. The lower mobility ratio can result in better sweep efficiency at the reservoir scale.
6. CO2-foam caused substantial reduction of the mobility of injected CO2, even at high oil saturations of approximately 50%, where other researchers have reported that foam cannot be formed in the case of light oils. This behaviour is attributed to the formation of water fingers in heavy oil with low oil saturation, which facilitates the formation of CO2 foam/emulsion even at the early stages of injection.

CHAPTER 8 COREFLOOD INVESTIGATION OF HEAVY OIL RECOVERY BY CO2 INJECTION IN CRUDE "J"

8.1 INTRODUCTION

This chapter presents the results of 3 coreflood experiments that investigated the performance of CO2 injection in crude "J" at reservoir conditions of this crude oil. Coreflood experiments in this chapter were designed, based on the results of the micromodel experiments, using this crude oil, and were presented in chapter 6. In the first part of this chapter, the effect of CO2 injection strategy on recovery performance of crude "J" is investigated through two coreflood experiments. The second part of this chapter is focused on the effect of mobility control by CO2/surfactant co-injection and formation of CO2-emulsion in the core. While wettability tests have not been performed for this specific crude oil and rock sample, the previously presented micromodel observations showed that this crude sample has a high tendency to make porous media oil-wet, therefore it is believed that all the experiments in this chapter are performed in slightly oil-wet conditions.

8.2 THE EFFECT OF INJECTION STRATEGY

The micromodel observations showed that injection of CO2 can dramatically improve recovery of crude "J" in secondary and tertiary injection modes. The objective of this series of coreflood experiments is to verify and quantify the visual observations made in the micromodel experiments. In this section, the performance of CO2 injection in pre-waterflood and post-waterflood modes is investigated and the results are compared to the case of plain waterflood.

8.2.1 Core Exp 6: Tertiary Injection of Liquid CO2

Despite its unfavourable mobility ratio, water is normally injected in heavy oil reservoirs for both pressure maintenance and oil displacement purposes. Therefore, secondary waterflood is generally considered as the base case for heavy oil recovery. This coreflood experiment was started with a waterflood period, subsequently followed by a period of CO2 injection to investigate the performance of tertiary CO2 injection in this crude oil. The experiment concluded with a second waterflood period to displace the CO2 diluted heavy oil. The oil recovery results obtained from this experiment show a significant additional oil recovery of 33 %OOIP, as a result of CO2 injection.

Procedure and Conditions

All fluid injections were performed at a constant rate of 7 cm^3hr^{-1} (equivalent to a frontal velocity of 1ft/ day) and from the top end of the vertically oriented core.

1. *Initialization:* Core was saturated with brine at T = 28 °C and P = 1500 psig.
2. *Oil Flood:* Core was flooded with crude oil "J".
3. *Aging:* The oil was left in the core for a period of 2 days.
4. *1st Waterflood:* Two PVs of brine were injected through the core.
5. *CO2 Flood:* Three PVs of CO2 were injected through the core.
6. *2nd Waterflood:* Two PVs of brine were injected through the core.

Table 8-1 shows the pressure and temperature at which the test was carried out, as well as fluids used in the test.

Table 8-1: Core Exp 6; Fluids used and pressure and temperature conditions.

Porous Medium	Consolidated Sandstone Core
Crude Oil	"J" (617 @ 28 °C)
Aqueous Phase	10000 ppm (8/2 ratio between NaCl/CaCl2)
Gas Phase	Liquid CO2
Temperature	28 °C
Pressure	1500 psig

Results

Oil Flood and Initialization

Initially, the core was thoroughly cleaned with toluene and methanol and then saturated with the brine solution, after which a brine permeability measurement was performed. The crude oil (crude J) was then injected through the core for an extended period of time to ensure that the core was completely and uniformly saturated with the oil. The resident brine was observed to be displaced by oil in a piston type manner (brine production stopped shortly after oil breakthrough), and a relatively high oil saturation of 83% was obtained at the end of the oil injection period, due to the large viscosity contrast (3 orders of magnitude) between displaced brine and the displacing oil. Figure 8-1 shows the volume of brine produced and differential pressure across the core versus the PVs of injected oil during the oil flood period. The piston type displacement of brine by the heavy crude oil can be inferred from the flat part of the brine production curve after the oil breakthrough.

At the end of the oil flood period, the inlet and outlet valves of the core were closed, and the core remained at that condition for a period of two days to allow the core to age. The micromodel tests that we carried out on this oil, have shown that crude "J" has a tendency to alter wettability of the system from water-wet towards more oil-wet conditions.

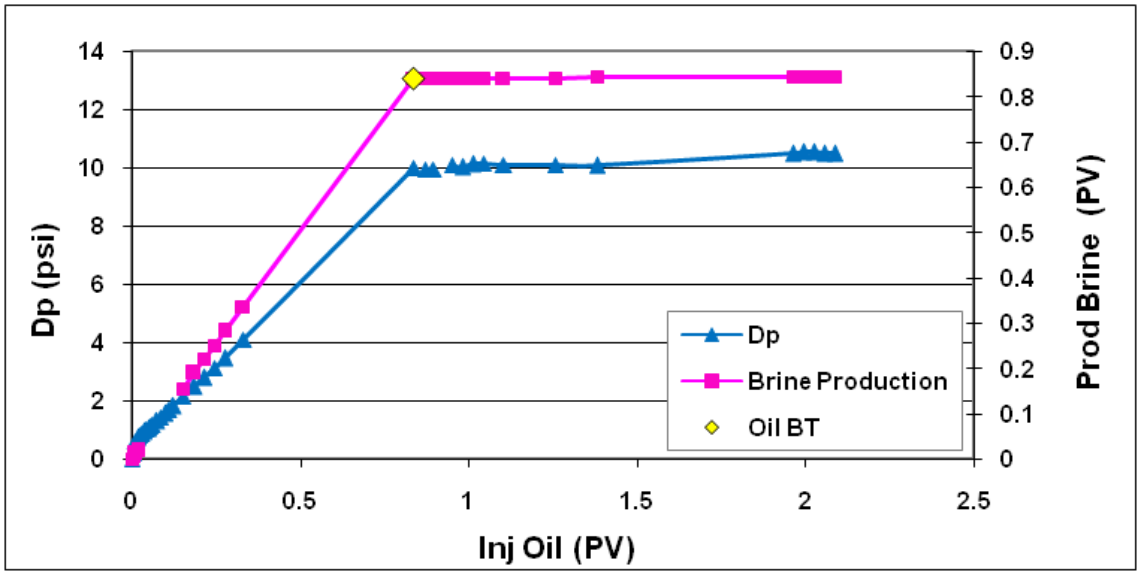

Figure 8-1: Core Exp 6; brine displacement and differential pressure across the core versus PVs of injected heavy oil during the period of oil flood.

1st Water Injection

The core was then flooded with brine. As expected, due to a very large viscosity contrast between the flood water and crude oil, an early water breakthrough was observed. The first droplets of water were observed at the outlet only after 0.16 PV of brine injection, which resulted in a recovery of 20% of original oil in place (20 %OOIP). After the breakthrough, brine injection continued for a relatively long period of time and more than 2 PVs of water were injected through the core. Significant additional oil was recovered after the water breakthrough and the recovery increased from 20 %OOIP at breakthrough, to 32 %OOIP and 36 %OOIP after 1.09 V and 2.21 PVs of brine injection, respectively. Most of the oil recovery after the breakthrough, took place during the 1st PV of brine injection. Figure 8-2 shows the oil recovery and differential pressure across the core during this water injection period. Figure 8-3 demonstrates the rate of oil production and water-cut of the core effluent during the period of waterflood. As shown, after the first PV of water injection, the recovery of oil continued at a low and constant rate. At breakthrough time, water cut of the core effluent jumped from 0 to 0.9 cc water/cc total and was then gradually raised to 0.96 cc water/cc total after one PV of water injection. The oil rate remained unchanged at that rate for the rest of the water flood period.

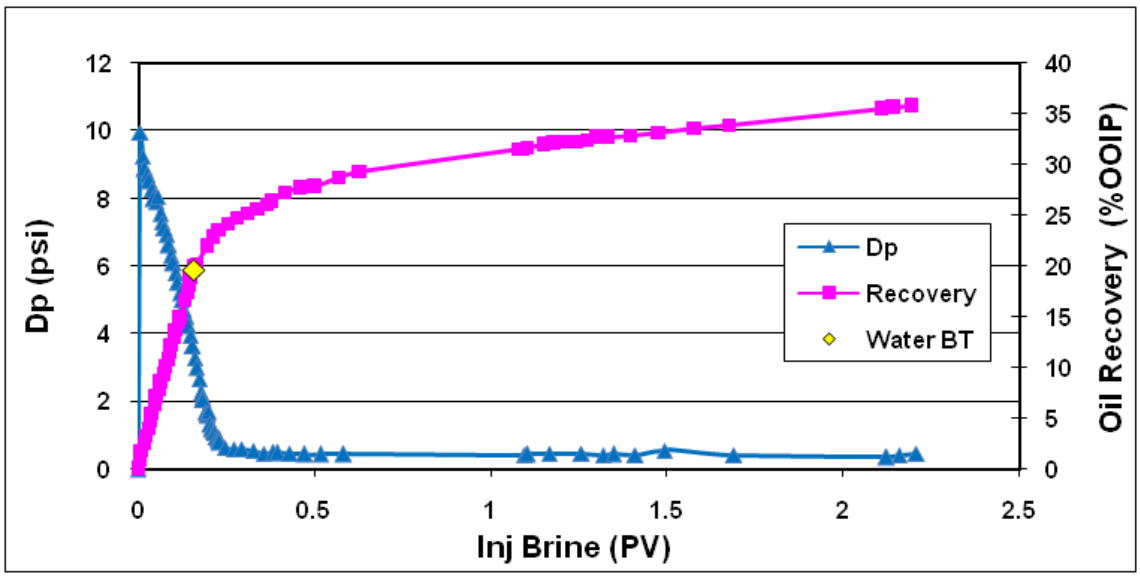

Figure 8-2: Core Exp 6; Oil recovery and differential pressure across the core versus PV of injected brine during 1st period of waterflood.

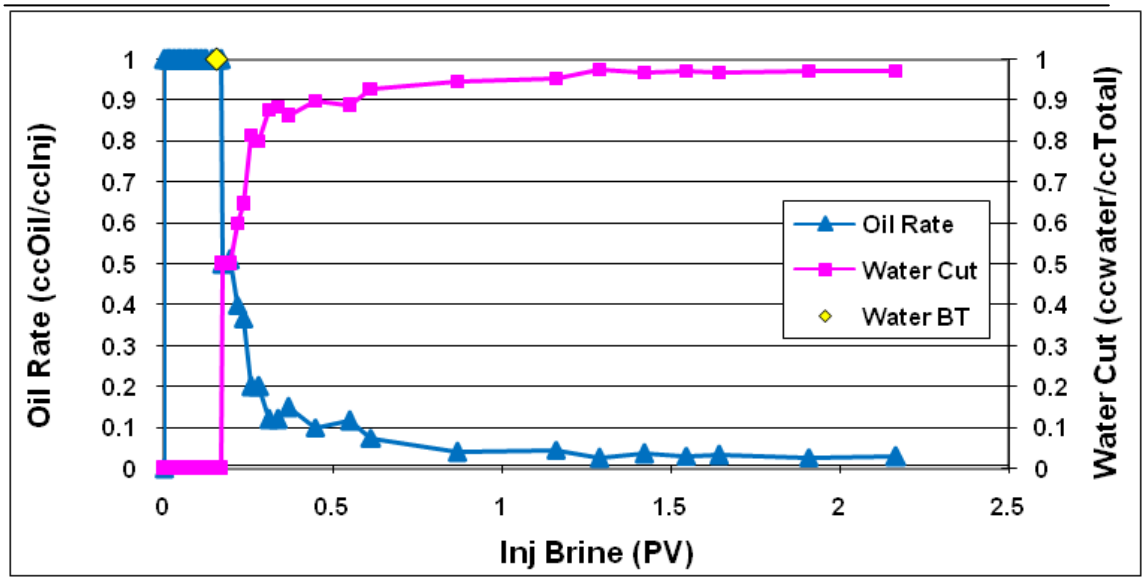

Figure 8-3: Core Exp 6, Oil production rate and water cut of the effluent versus PV of injected brine during the first period of waterflood.

Tertiary CO2 Injection

After an extended period of waterflood, CO2 injection commenced again from the top end of the vertically oriented core. During the early stages of CO2 injection, before CO2 breakthrough, the core effluent consisted mostly of brine at very high water cuts (0.96). As the CO2 injection progressed, brine production continued until most brine in the core (above 60%) was displaced. The brine production was followed by production of a small bank of crude oil (around 3 %OOIP), before CO2 broke through. The CO2 breakthrough happened after injection of 0.21 PV of CO2. The injection of CO2 continued for an extended period of time, until 3 PVs of CO2 was injected through the core. The CO2 flood resulted in 19 %OOIP, 30 %OOIP and 33 %OOIP additional recovery after 1, 2.02 and 3.01 PVs of CO2 injection respectively. This volume of oil was produced in addition to what had already been produced during the preceding waterflood. Figure 8-4 displays the differential pressure across the core and the oil recovery data versus pore volume of the injected CO2. As shown, most oil recovery occurred after the CO2 breakthrough and during the first and second PV of CO2 injection.

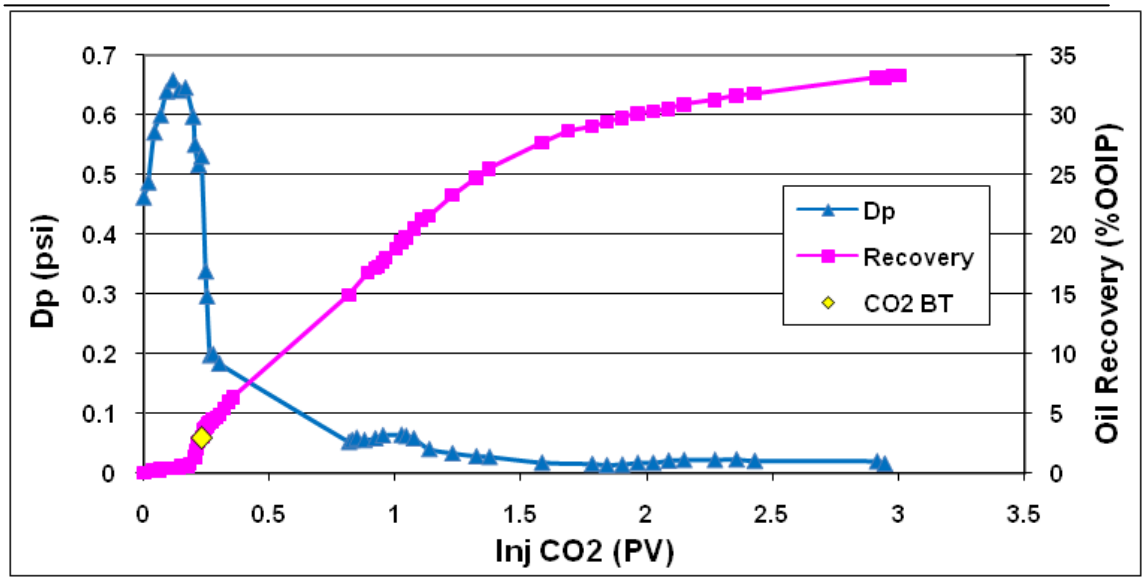

Figure 8-4: Core Exp 6; Oil recovery and differential pressure across the core versus PV of injected CO2 during the period of CO2 flood.

The unfavourable viscosity ratio between injected CO2 and resident heavy oil is believed to be the main reason for the low oil recovery by the direct displacement mechanism (before the CO2 breakthrough). However, after the breakthrough, oil production continues due to the CO2 dissolution and subsequent viscosity reduction and swelling at the early stages. In the later stages, gravity drainage and oil extraction mechanisms are believed to be the dominant mechanisms.

Figure 8-5 depicts the rate of oil production (cc of produced oil versus cc of injected CO2) and gas oil ratio of effluent produced (cc of produced CO2 versus cc of produced oil at lab conditions) versus CO2 injection. It can be seen that for a relatively long period of time (1.5 PVs) after the CO2 breakthrough, the oil was recovered at a constant rate of 0.2 cc oil/cc inj. However, the oil rate dropped steadily thereafter and reached a very low value of 0.02 cc/cc at the end of 3 PVs of CO2 injection. It can be seen that the gas oil ratio followed a similar trend and remained constant at values around 200 cc CO2/cc oil during the first 1.5 PVs of CO2 injection after breakthrough, and then raised to values around 17000 and remained constant.

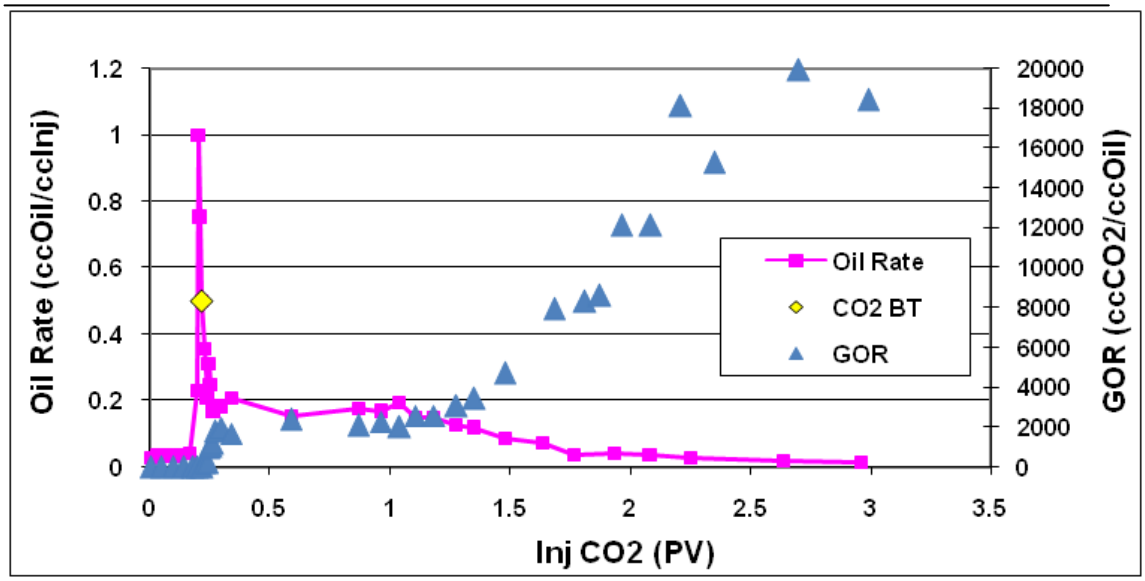

Figure 8-5: Core Exp 6; Oil production rate and gas oil ratio versus PV of injected CO2 during the period of CO2 flood.

2nd Water Injection

After the CO2 injection period, a 2nd water injection was carried out to examine the potential of water to recover the CO2 diluted oil. Two PVs of water were injected during the 2nd water injection period. 0.5 % OOIP incremental oil recovery at the breakthrough of water (at 0.18 PV of water injection) was recorded, which then increased to 2 % OOIP as the waterflood continued. Figure 8-6 shows the oil recovery and differential pressure across the core during this water injection period. The gradual decrease in differential pressure in this figure is due to dissolution of CO2 in the injected brine and a subsequent increase in water relative permeability.

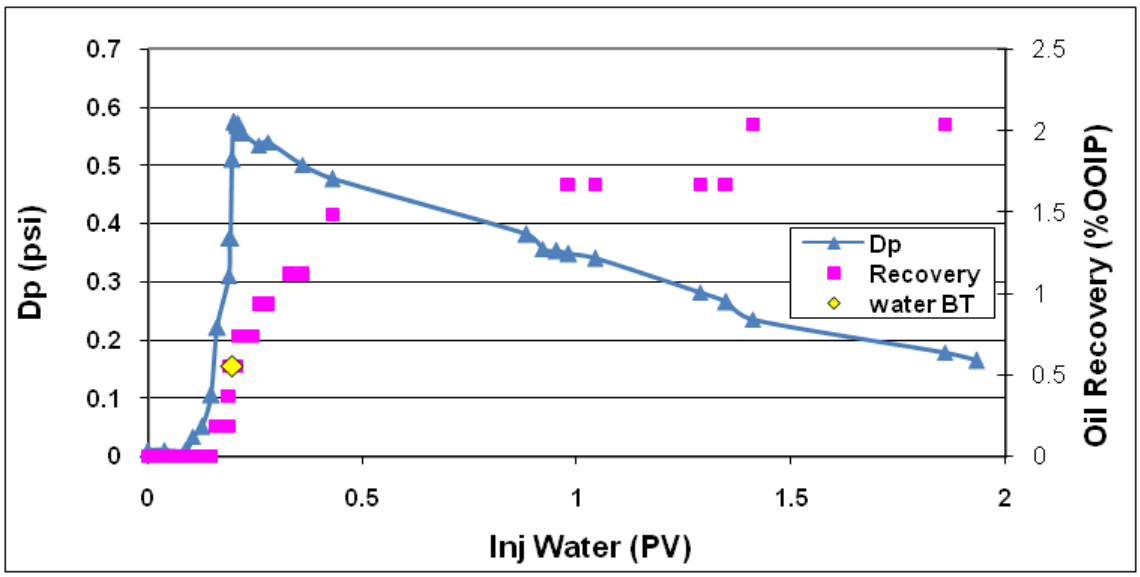

Figure 8-6: Core Exp 6; Oil recovery and differential pressure across the core versus PV of injected brine during 2nd period of waterflood.

Summary

Table 8-2 summarises the amount of incremental oil recovery and cumulative oil production achieved at each stage of this experiment. Figure 8-8 demonstrates the cumulative oil recovery curve (for the whole test) versus the total PV of injected fluids. Over 36 % OOIP of the oil was recovered during the initial extended water injection period. The subsequent immiscible CO2 injections recovered another 33 %OOIP on top of that. The second period of waterflood recovered an extra 2 %OOIP of oil from the core. The significant additional oil recovery (33 %OOIP) during the tertiary CO2 injection reveals the huge potential of CO2 to improve the recovery of this heavy crude oil after conventional water flood. The results also reveal that oil recovery at breakthrough of CO2 is not significant and to instigate a significant level of additional oil recovery, CO2 injection should continue after the CO2 breakthrough for at least 1 or 2 PVs. As can be seen, due to an excellent performance achieved with the tertiary CO2 injection, a very high ultimate oil recovery of 71 %OOIP was achieved in this experiment, despite the relatively high viscosity of the oil. Figure 8-8 depicts the saturation of fluids inside the core, at different stages of the experiment.

Table 8-2: Core Exp 6; Summary of the results.

Recovery										
		1st Water Flood			CO2 Flood			2nd Water Flood		
Recovery		Inj (PV)	Recovery	Cum Rec	Inj (PV)	Recovery	Cum Rec	Inj (PV)	Recovery	Cum Rec
	BT	0.16	20%	20%	0.22	3%	39%	0.18	0.5%	69%
	1 PV	1.09	32%	32%	1.00	19%	54%	1.04	2%	71%
	2 PV	2.21	36%	36%	2.02	30%	66%	1.93	2%	71%
	3 PV				3.01	33%	69%			

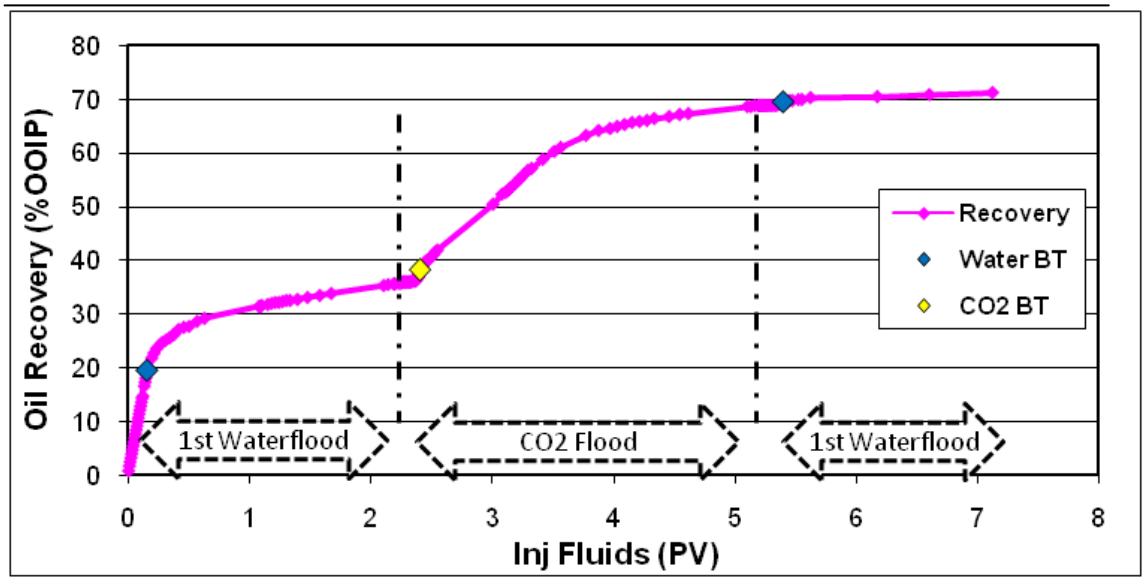

Figure 8-7: Core Exp 6; Recovery curve at different stages of the test.

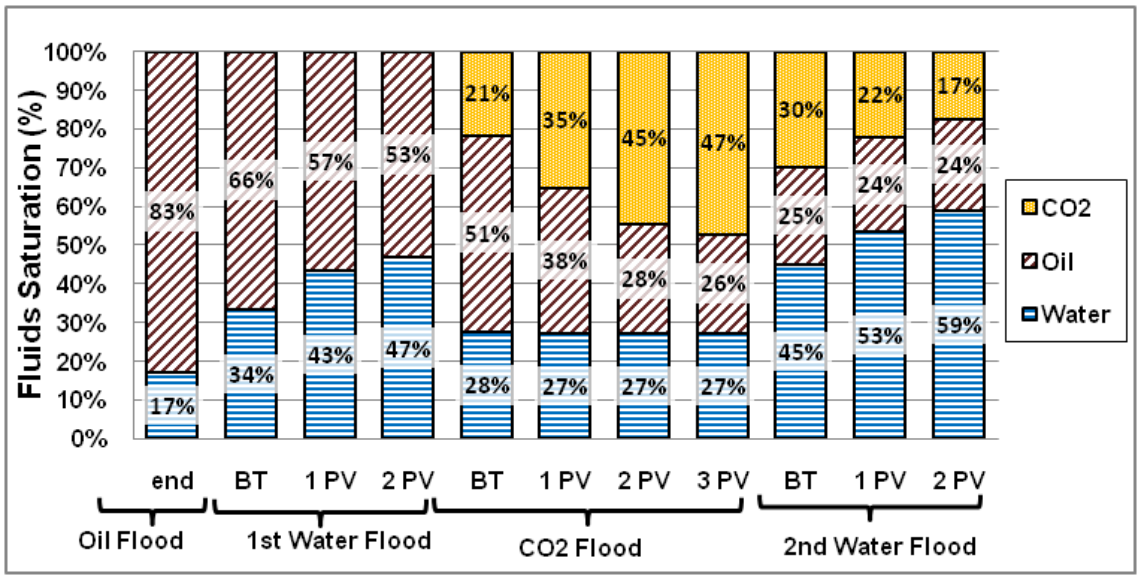

Figure 8-8: Core Exp 6; Saturation of fluids in the core during different stages of the test.

8.2.2 Core Exp 7: Secondary CO2 Flood at Elevated Pressure

The previous experiment examined the performance of tertiary CO2 injection in crude "J". However, the main objective of this core experiment was to investigate the performance of CO2 injection in the same crude oil before waterflood (as a secondary oil recovery method).

Procedure and Conditions

All fluid injections were performed at a constant rate of 7 cm^3hr^{-1} (equivalent to frontal velocity of 1ft/ day) and from the top end of the core.

1. *Initialization:* Core was saturated with brine at T = 28 °C and P = 1500 psig.
2. *Oil Flood:* Core was flooded with crude oil "J".
3. *Aging:* The oil was left in the core for a period of 2 days.
4. *CO2 Flood:* Three PVs of CO2 were injected through the core.
5. *Waterflood:* Two PVs of brine were injected through the core after CO2 injection.

Table 8-3 shows the pressure and temperature at which the test was carried out, as well as the fluids used in the test.

Table 8-3: Core Exp 7; Fluids used and pressure and temperature conditions.

Porous Medium	Consolidated Sandstone Core
Crude Oil	"J" (617 @ 28 °C)
Brine	10000 ppm (8/2 ratio between NaCl/CaCl2)
CO2	Liquid CO2
Temperature	28 °C
Pressure	1500 psig

Results

Initialization and Oil Flood

The core was initially saturated with brine. Subsequently, the crude oil (crude "J") was injected through the core for an extended period of time to establish the initial oil, as well as connate water saturation. The resident brine was observed to be displaced by the oil in a piston type manner and a relatively high oil saturation of 85% was obtained

at the end of the oil injection period. After the oil flood, the inlet and outlet valves of the core were closed and the core was allowed to age for a period of two days.

Secondary CO2 Injection

After establishing initial oil saturation, the core was directly flooded with CO2 (without undergoing water flood) from the top end of the vertically mounted core. Similarly to the case of the secondary waterflood (previous test), due to a very large viscosity contrast between the displacing fluid (CO2 here) and the crude oil, an early breakthrough was observed. CO2 broke through the core only after 0.12 PV of CO2 injection, which resulted in a recovery of 13 %OOIP. After the breakthrough, CO2 injection continued for 3 PVs. Significant additional oil recovery was observed after the CO2 breakthrough and oil recovery increased from 13 %OOIP at breakthrough time to 39 %OOIP, 56 %OOIP and 61 %OOIP respectively, after the injection of 1.00, 2.01 and 3.22 PVs of CO2 through the core. Similarly to the case of the tertiary CO2 injection (previous test), most of the oil recovery took place during the 1st and the 2nd PV of CO2 injection and the recovery process significantly decelerated during the 3rd PV of injected CO2. Figure 8-9 shows the recovery of oil and the differential pressure measured across the core during this secondary CO2 injection period.

Figure 8-10 depicts the rate of oil production (cc of produced oil versus cc of injected CO2) and gas oil ratio of effluent produced (cc of produced CO2 versus cc of produced oil at lab conditions) versus CO2 injection. After the CO2 breakthrough, the oil rate dropped from 1 cc oil/ cc inj to around 0.18 cc oil/ cc inj and remained constant at that rate for almost 1 PV of CO2 injection (the plateau between 0.5 to 1.5 PVs in Figure 8-10). At later stages, oil production rate dropped again and reached values of less than 0.03 after 3 PVs of injection. Formation of the plateau in production rate is believed to be due to the change of the dominant oil recovery mechanism by CO2 from dissolution to extraction.

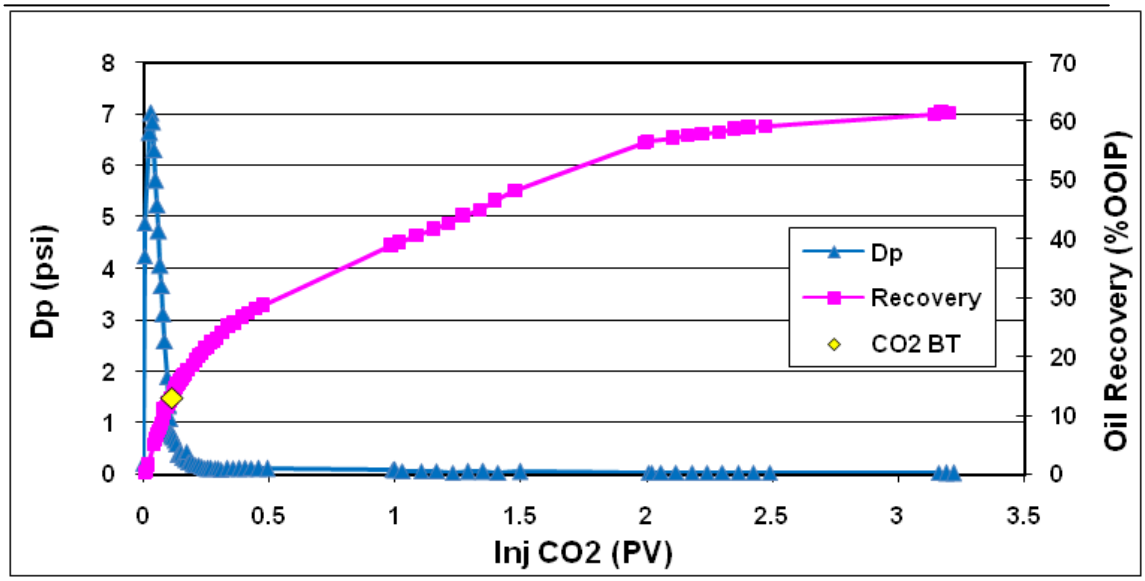

Figure 8-9: Core Exp 7; Oil recovery and differential pressure across the core versus PV of injected CO2 during the period of CO2 flood.

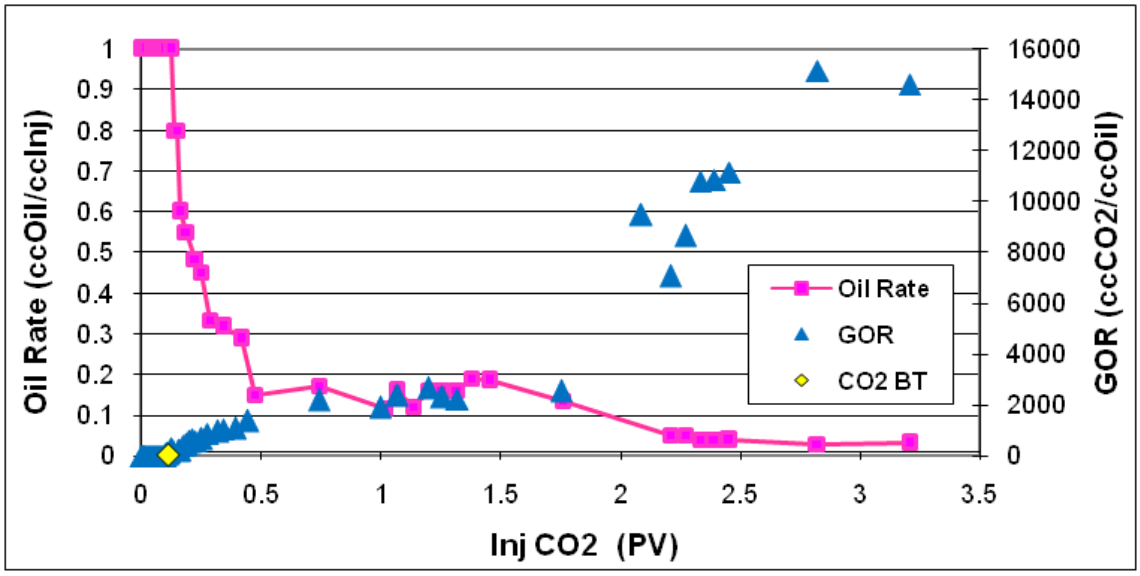

Figure 8-10: Core Exp 7; Oil production rate and gas oil ratio versus PV of injected CO2 during the period of CO2 flood.

Waterflood Period

After the extended period of CO2 injection, water injection commenced to examine the potential of water to displace and recover the CO2-diluted oil. Figure 8-11 shows the oil recovery and differential pressure across the core during the waterflood period carried out subsequent to CO2 injection. The water breakthrough occurred after the injection of 0.29 PV of brine in the core, which resulted in additional oil recovery of 2.03 %OOIP. The additional oil recovery increased to 7.36 % and 7.96 % after 1.00 and 2.02 PVs of brine injection respectively. As can be seen in Figure 8-11, most of the

additional oil recovery took place in the first PV of brine injection and subsequently oil recovery slowed down. The jump in oil recovery suggests formation of a bank of diluted oil in front of the injected water.

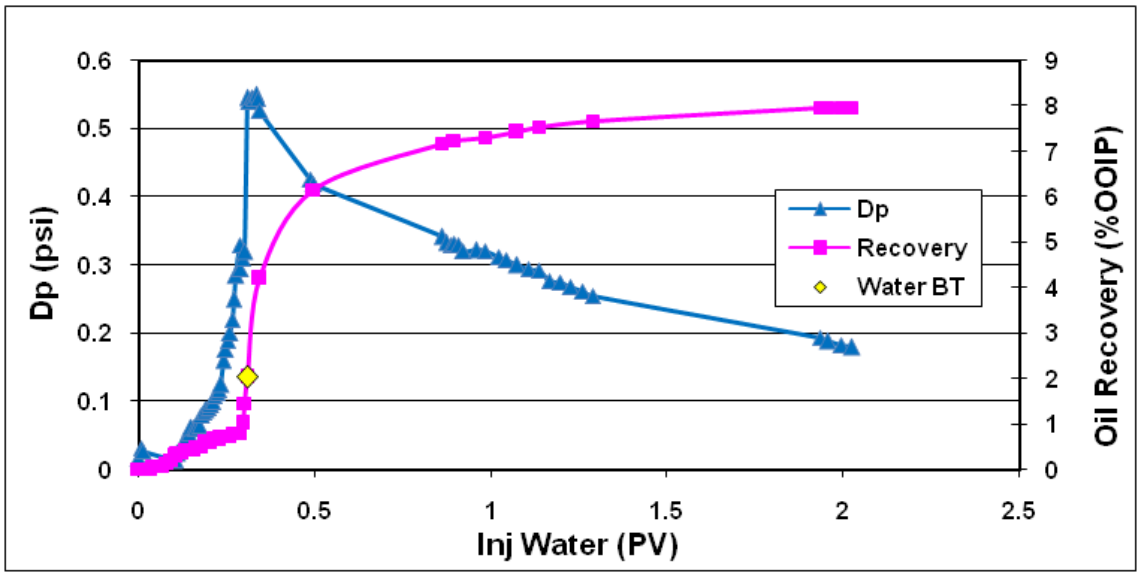

Figure 8-11: Core Exp 7; Oil recovery and differential pressure across the core versus PV of injected brine during the period of waterflood.

Summary

Table 8-4 summarises oil recovery, as well as cumulative oil production, achieved at each stage of this experiment (secondary CO2 injection). Figure 8-12 demonstrates the cumulative oil recovery curve (for the whole test) versus the total PV of injected fluids. 61 % OOIP of the oil was recovered during the initial extended (3 PVs) period of CO2 flood with 56% recovered in the first 2 PVs of CO2 injection. Comparison of the oil recovery during this secondary CO2 injection (61 %OOIP) with the secondary waterflood in the previous test (36 % OOIP), clearly demonstrates the huge potential of CO2 injection. The subsequent waterflood period recovered an additional 8 %OOIP of the oil, which makes a massive ultimate oil recovery of 69% in this experiment. Figure 8-13 depicts the saturation of fluids inside the core at different stages of the experiment.

Table 8-4: Core Exp 7; Summary of the results.

Recovery							
		CO2 Flood			Water Flood		
Recovery		Inj (PV)	Recovery	Cum Rec	Inj (PV)	Recovery	Cum Rec
	BT	0.12	13%	13%	0.29	2%	64%
	1 PV	1.00	39%	39%	1.00	7%	69%
	2 PV	2.01	56%	56%	2.02	8%	69%
	3 PV	3.22	61%	61%			

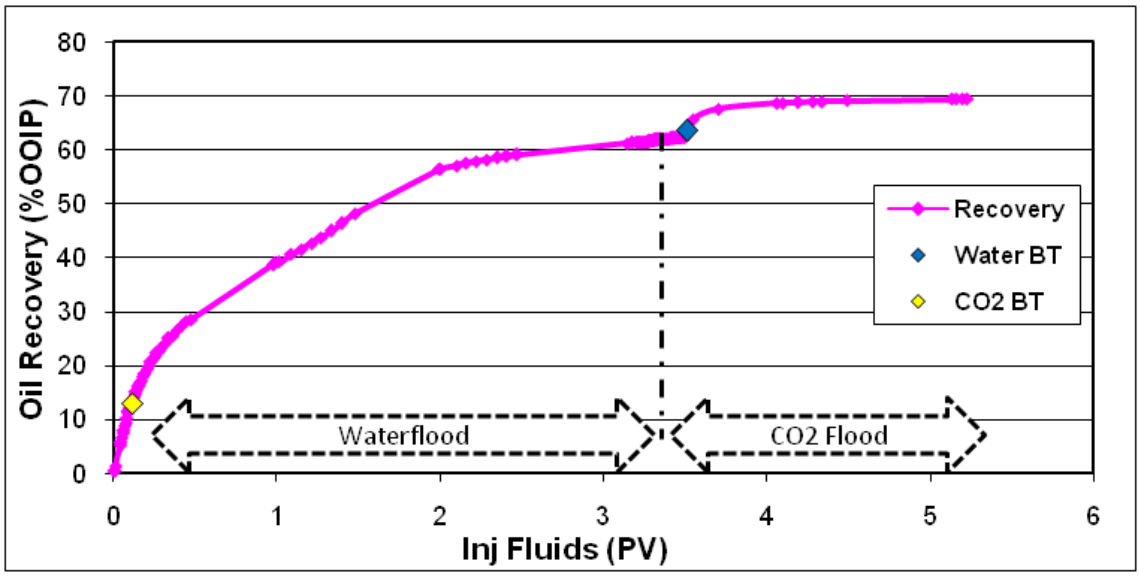

Figure 8-12: Core Exp 7; Recovery curve at different stages of the test.

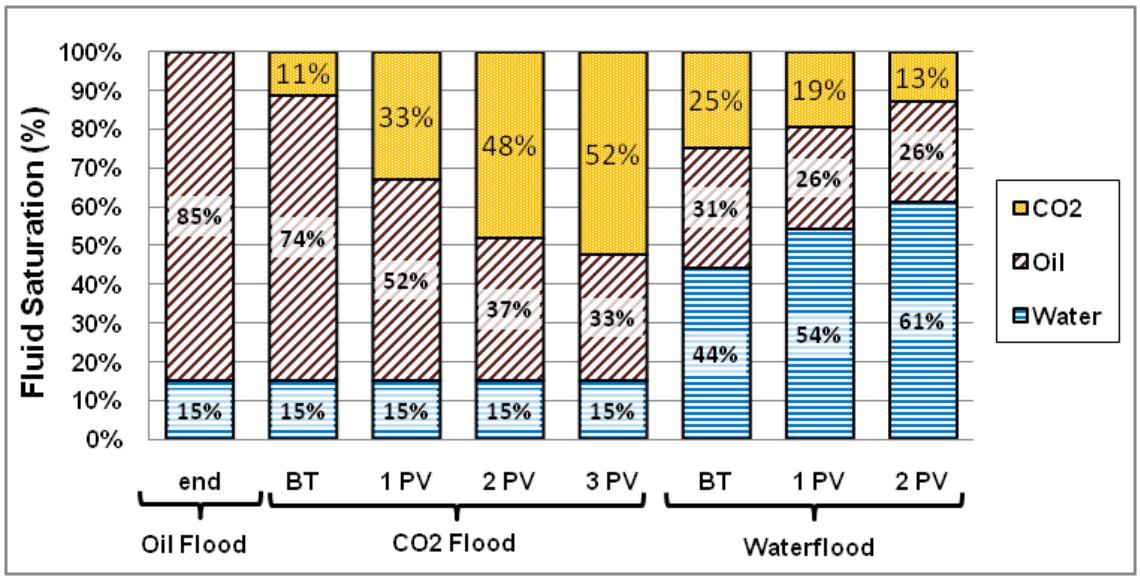

Figure 8-13: Core Exp 7; Saturation of fluids in the core during different stages of the test.

8.2.3 Discussions

Comparison of different Scenarios of CO2 Injection and Waterflood

A comparison of recovery data during the period of waterflood and the periods of tertiary and secondary CO2 flood in crude "J" shows significant improvement in oil recovery, as a result of CO2 injection. In Core Exp 6, where CO2 was injected after an initial period of waterflood, final recovery was almost twice the oil recovery during the initial period of plain waterflood. In Core Exp 7, where CO2 was injected in secondary mode (pre-waterflood), the oil recovery by liquid CO2 flood was observed to be significantly higher than the case of plain waterflood. Figure 8-14 compares oil recovery curves during the secondary waterflood (Core Exp 8) and secondary CO2 flood (Core Exp 9). This comparison reveals that: whilst waterflood shows a slightly better recovery performance at breakthrough time, after breakthrough, the secondary CO2 flood results in significantly higher oil recovery. As shown in Figure 8-14, after two PVs of injection, oil recovery of OOIP is 24 % higher in the case of secondary CO2 flood compared with water flood.

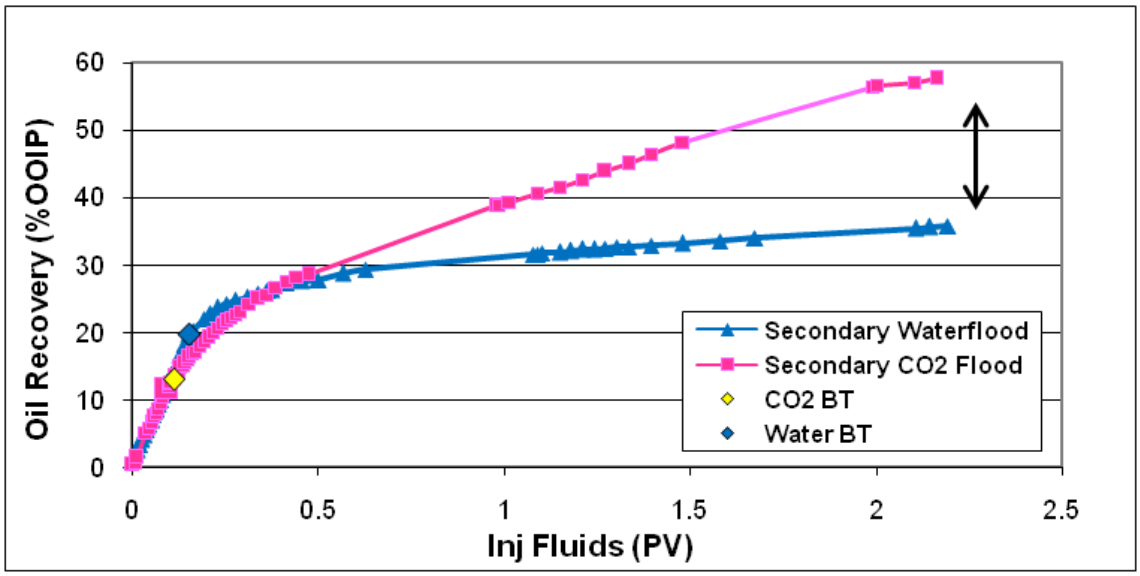

Figure 8-14: Comparison of oil recovery during secondary waterflood (Core Exp 6) and secondary CO2 flood (Core Exp 7).

The slightly higher oil recovery by waterflood at water breakthrough time (compared to oil recovery at CO2 breakthrough in the secondary CO2 injection test) is believed to be due to two factors. Firstly, the higher viscosity of water compared to CO2; and secondly, the fact that water is the wetting phase and scatters in the network of water layers provided by Swi. This effect reduces the adverse effect of high mobility ratio and

water fingering effects. The higher rate of oil recovery after breakthrough in the CO2 injection test, is due to the effects of CO2 dissolution in the oil and subsequent favourable changes that take place in the porous medium.

The overall comparison of oil recovery during the secondary and tertiary CO2 injection tests in Figure 8-15 reveals that, while both scenarios offer an incremental recovery of around 100% (compared to the case of plain waterflood), the secondary CO2 flood scenario offers much higher oil recovery at the early stages of injection compared to tertiary CO2 injection (black arrow in Figure 8-15).

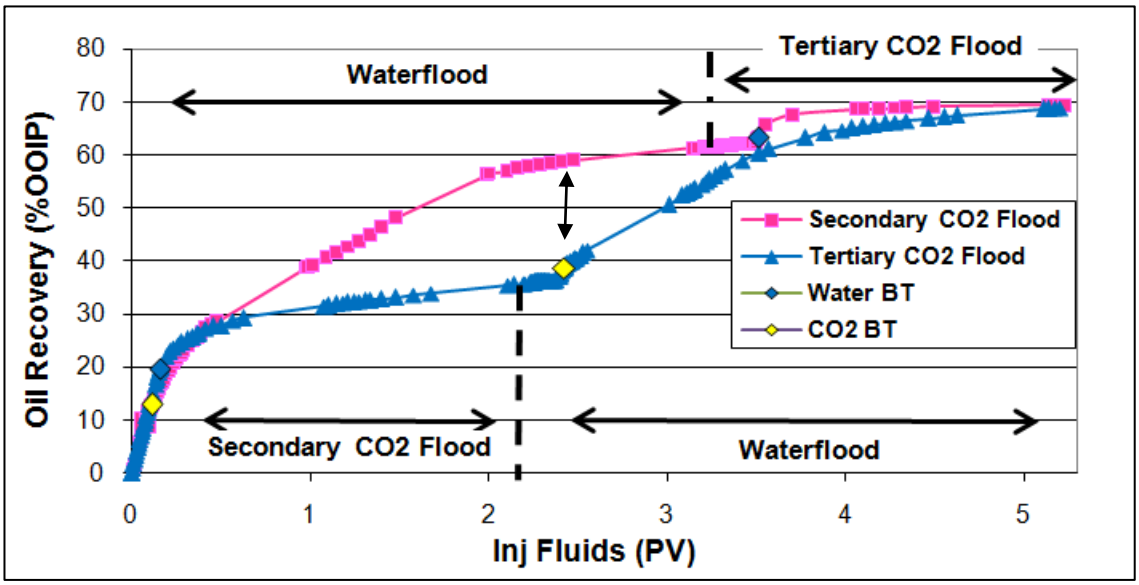

Figure 8-15: Comparison of the overall oil recovery during tertiary (Core Exp 6), secondary (Core Exp 7), and CO2 flood tests. The better performance of the secondary CO2 injection scenario at early times (e.g. 2 PVs) is clear in this plot.

Recovery Mechanisms

Figure 8-16 compares oil recovery rates for the tertiary and secondary CO2 injection experiments. As shown, despite the higher oil recovery rate in the secondary CO2 flood at early stages (before CO2 breakthrough and shortly after), the oil recovery rate in the intermediate stage (between 0.5 and 1.5 PVs of CO2 injection) and very late stages (after 2 PVs of CO2 injection) are very similar. To understand this behaviour and the similarities and differences in oil recovery rate, it is necessary to look into the mechanisms involved at different stage of the CO2 flood.

The displacement of the resident oil by CO2 takes place due to viscous displacement and swelling mechanisms at early stages of injection (before breakthrough and a short time after that). Being the non-wet phase, CO2 displaces the resident oil through a drainage mechanism in the case of secondary CO2 injection and through a double-drainage mechanism in the case of tertiary CO2 injection at pore level. In the former, CO2 displaces and produces the resident oil. However, in the latter the flowing CO2 displaces an oil bank at the front, which in turn displaces and produces water. Additionally, higher saturation of oil in the core (in the case of secondary CO2 injection) results in higher oil production due to a swelling mechanism. A combination of these two processes causes higher oil recovery during the early stages of CO2 injection in the case of secondary CO2 flood, compared to the case of tertiary CO2 flood, as seen in Figure 8-16.

As CO2 injection continues after breakthrough, the oil is gradually saturated by CO2, which itself initiates two new phenomena. Firstly, the viscous displacement (due to existence of differential pressure across the core) and gravity drainage mechanisms are boosted as a result of the viscosity reduction in the oil phase and secondly the swelling mechanism slows down and is replaced by the extraction mechanism. The micromodel observations in Chapter 6 showed that oil recovery by extraction mechanism is a slow process, due to the existence of heavy components in the crude oil. In order to identify the role of different mechanisms, 4 samples of the produced oil from the case of secondary CO2 flood (Core Exp 7) were collected and analysed by a gas chromatograph (GC). The results are shown in Figure 8-17.

The compositional analysis shows that in cyl#1 and cyl#2 the oil composition is quite similar, which means at this stage (up to 1 PVs of CO2 injection) oil production by extraction mechanisms is insignificant. However, there is slight up-gradation in cyl#3 and significant up-gradation in cyl#4 (higher weight percent of intermediate components e.g. C15 and lower weight percent of C20+ component), which means that while CO2 extraction mechanism is partly contributing to oil recovery in cyl#3 it is the governing mechanism in cyl#4. Based on the compositional analysis, it can be concluded that the first plateau of similar oil production rates between 0.5 and 1.5 PVs of CO2 injection, is majorly due to the viscous displacement and gravity drainage mechanisms that are assisted by CO2 dissolution and viscosity reduction. However, the

second plateau of similar oil production rates after 2 PVs of CO2 injection is chiefly due to the extraction of lighter components of the residual oil by high pressure CO2.

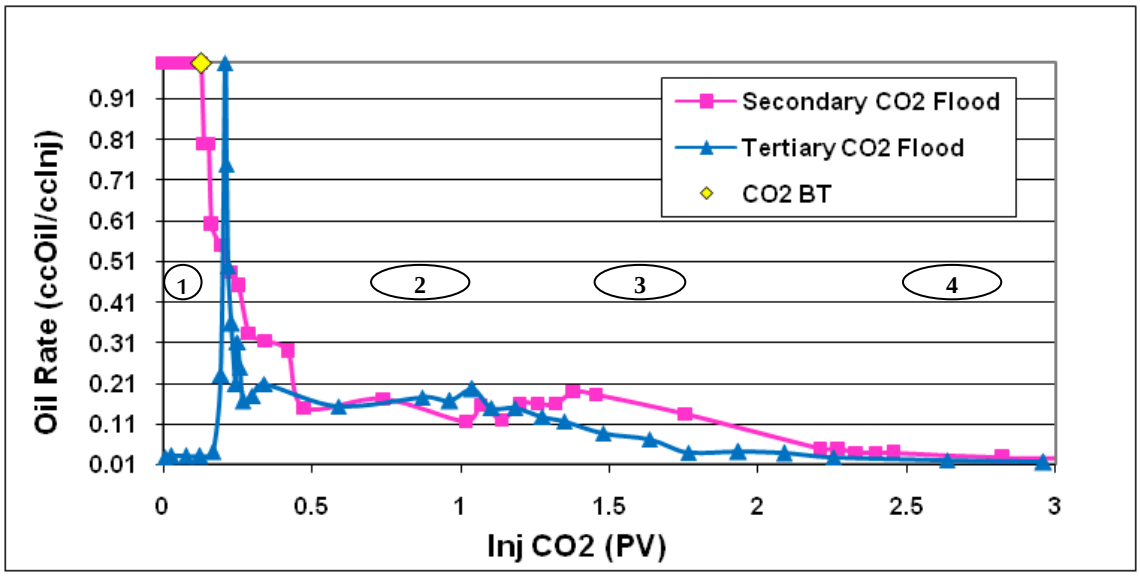

Figure 8-16: Comparison of the oil production rate during secondary (Core Exp 7) and tertiary (Core Exp 6) CO2 injection.

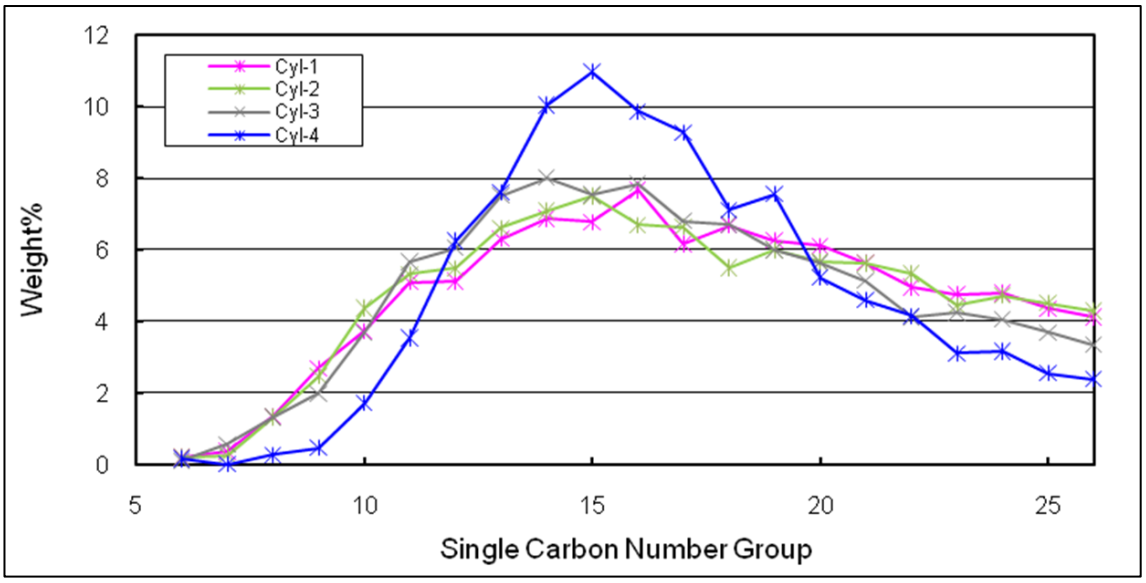

Figure 8-17: Comparison of the composition of produced oil at different stages of secondary CO2 flood experiment (Core Exp 7).

CO2 Storage by Different Injection Strategies

To compare the volume of stored CO2 in the core by different injection strategies, saturation of fluids after the period of CO2 flood is considered (this means the final water injection in both experiments can be avoided). Figure 7-15 compares the total volume of CO2 stored in the core, including free CO2 and dissolved CO2 in the water

and oil phase, at the end of three PVs of CO2 injection in secondary and tertiary modes. As shown in the scenario of secondary CO2 injection, a total volume of 0.52 PV of CO2 was stored in the core after three PVs of CO2 injection; while for the same injection period, a total volume of 0.47 PV of CO2 was stored in the core when CO2 was injected in tertiary mode. This reveals that secondary injection of CO2 not only offers better recovery efficiency at early injection times, it also provides better capacity for CO2 storage in reservoir conditions of crude "J".

One important observation is that most stored CO2 in the core (around 90%) is in the form of free CO2. This is very different from the case of CO2 storage in crude "C", where most of the stored CO2 was dissolved in the oil phase. This is due to low oil saturation in the core at the end of the period of CO2 injection in crude "J" and also high density of liquid CO2, which could increase storage capacity of free CO2 compared to the other forms of storage. It should be noted that despite lower volumetric storage capacity at reservoir conditions, crude "J" provides much higher CO2 storage compared to crude "C" if the calculation is based on the volume of CO2 in standard conditions. For example, the storage capacity of 0.52 for secondary CO2 injection in crude "J", which is calculated at reservoir conditions of crude "J", would be equal to 244 PVs at standard conditions; while the storage capacity of 0.57, which was achieved during secondary CO2 injection at reservoir conditions of crude "C", would be equal to 53 PVs at reservoir condition. This shows that if CO2 injection is performed at the corresponding reservoir conditions, the actual storage capacity would be around 5 times higher in the case of CO2 injection in crude "J" compared to CO2 injection in crude "C".

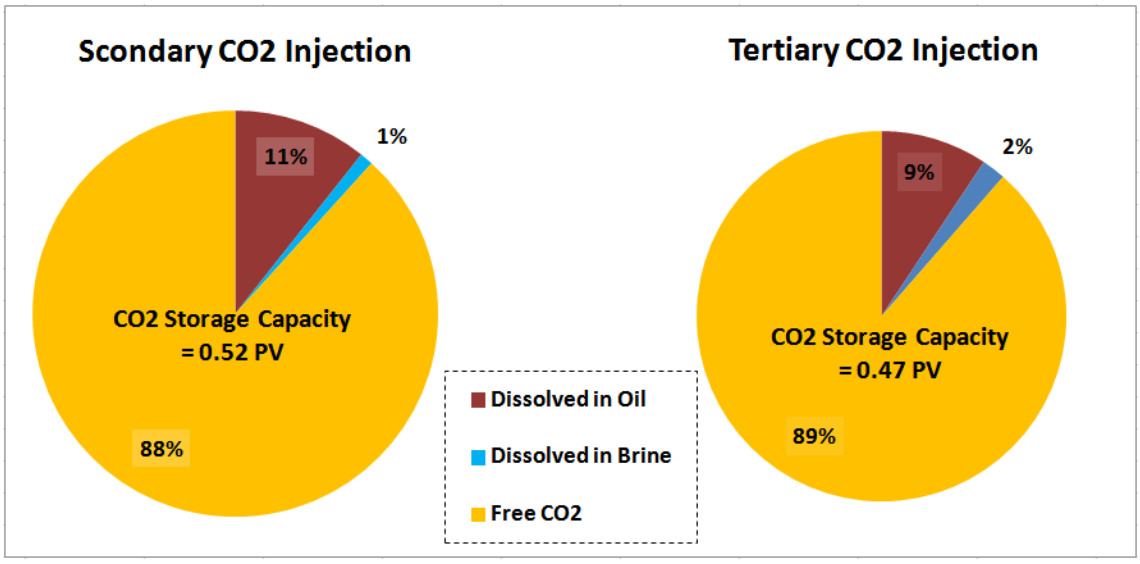

Figure 8-18: Comparison of the amount of stored CO2 in the core in different scenarios of CO2 injection.

Comparison of Performance of CO2 Injection in Crude "C" and Crude "J"

To study the performance of CO2 flood in heavy oils, both displacement and sweep efficiencies should be taken into account. The displacement efficiency can be evaluated using core recovery data and the sweep efficiency can be roughly estimated using the mobility ratio between displacing and displaced fluids. Comparison of the recovery data shows that while in the case of crude "C", injected CO2 was unable to efficiently displace most of the waterflood residual oil, the injection of CO2 successfully displaced and recovered the residual oil in the case of crude "J". Figure 8-19 compares the additional oil recovery, as a result of tertiary CO2 flood in crudes "C" and "J" at their corresponding reservoir conditions. An incremental oil recovery of over 50 % Sorw was achieved after 3 PVs of CO2 injection in crude "J", whilst the additional recovery, in the same injection period, was less than 10 % Sorw for crude "C" and only 17.5 % Sorw after 5.5 PVs of CO2 injection. It is believed that the better performance in the case of crude "J" is due to the considerably lower viscosity of CO2 diluted oil (15 cp). The viscosity of CO2 diluted oil in the case of crude "C" was 670 cp, which was still significantly higher than the corresponding viscosity for CO2 and water at test conditions. This comparison highlights the importance of oil characteristics and reservoir conditions on the performance of CO2 injection.

It should be noted that even in the case of crude "J", where a good displacement efficiency was achieved in the core tests, the mobility ratio needs to be improved for a successful recovery process at larger scales; otherwise, the fingering of CO2 due to the unfavourable mobility ratio between the CO2 and heavy oil can adversely affect the recovery performance.

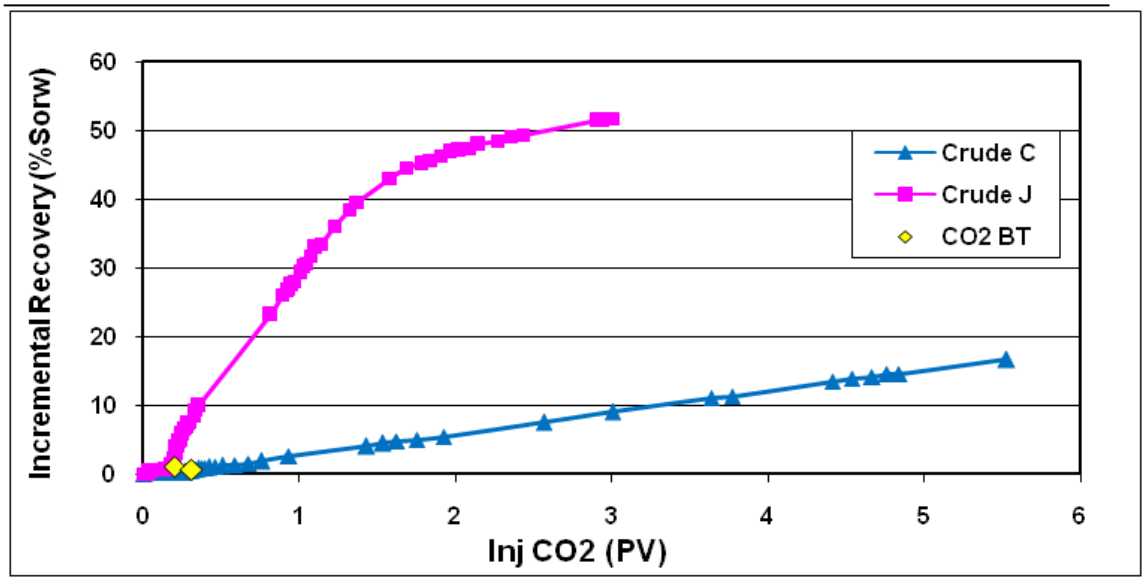

Figure 8-19: Comparison of the incremental oil recovery (based on waterflood remaining oil saturation) during tertiary CO2 injection in crudes "C" (Core Exp 4) and "J" (Core Exp 6) at their reservoir conditions.

8.3 THE EFFECT OF MOBILITY CONTROL BY CO2-EMULSION

It was mentioned in the previous section that despite good recovery performance during CO2 injection in crude "J", to apply the CO2 injection process at larger scales, mobility control techniques should be employed to reduce viscous fingering of injected CO2. Dissolution of CO2 in the oil phase reduces viscosity of the oil and enhances its flow and mobility in porous media. However, even viscosity of the diluted oil is significantly higher than viscosity of CO2. Therefore at the field scale, the fingering effect will reduce efficiency of the CO2 flood process. One promising solution would be to increase viscosity of the CO2 phase by in situ formation of CO2 foam/emulsion.

Based on the observations from the micromodel experiments (MM Exp 16) in which good recovery performance was achieved as a result of CO2-emulsion injection, a series of experiments were designed to investigate and quantify the performance of CO2-emulsion flood at core scale. The experiments, which are reported here, consisted of a preliminary test in the clean core (without oil) to measure viscosity of CO2-emulsion in the core and a second test to simulate the process of heavy oil displacement by CO2-emulsion. In the coreflood tests using CO2-emulsion, due to the high stability of emulsion generated, the foam facilitator filter (which was used in the previous tests to simulate conditions of mixing and flow at near wellbore conditions) was removed.

8.3.1 Core Exp 8 (Preliminary): CO2-Emulsion Viscosity Measurement

The coreflood experiment was performed in an attempt to measure viscosity of the CO2-emulsion at reservoir conditions of crude "J" in a clean core. Table 8-5 shows the pressure and temperature at which the test was carried out, as well as fluids used in the test.

Table 8-5: Core Exp 8 (Preliminary); Fluids used and pressure and temperature conditions.

Porous Medium	Consolidated Sandstone Core
CO2	Liquid CO2
Surfactant Solution	0.3 wt % AOS 14+ dissolved in a brine solution of 10000 ppm (8/2 ratio between NaCl/CaCl2)
Temperature	25 °C
Pressure	1500 psig

To perform the test, the core was initially saturated with surfactant solution and then the CO2 and surfactant were simultaneously injected through the core at a rate of 3.5 cc/hr (total of 7 cc/hr) for both CO2 and surfactant solution, corresponding to a frontal velocity of 1 ft/day. Figure 8-20 presents the differential pressure across the core and the apparent viscosity of the CO2-emulsion during this period of CO2/surfactant injection. As can be seen, the differential pressure across the core increased at a constant rate during the first 2.5 PVs of the injection and then was stabilized at around 50 psig. This differential pressure was used to back calculate the apparent viscosity of the emulsion generated in the core, which was equal to 2800 cp. Comparison of the CO2 emulsion viscosity achieved in this test, with that of pure CO2 under the same conditions (0.075 cp) shows a resistance factor of around 40000 times, as a result of the formation of CO2 emulsion in the core. The CO2 breakthrough took place after injection of 1.5 PVs of CO2/surfactant (equal to 0.75 PV of CO2); however, the CO2 break through did not have a significant effect on the trend of pressure increase in the core, as can be seen in Figure 8-20.

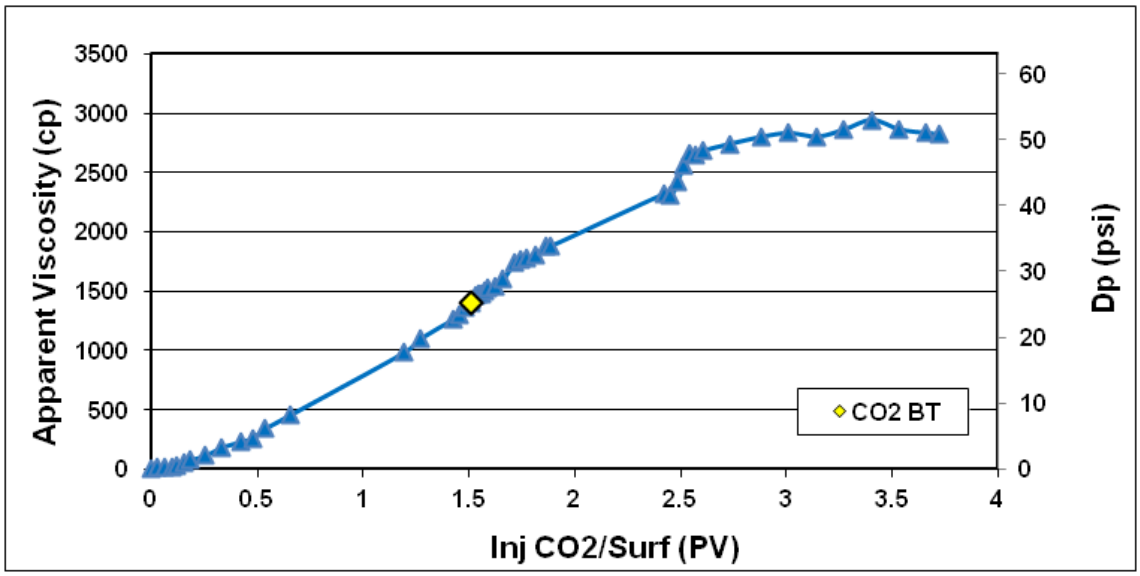

Figure 8-20: Core Exp 8 (preliminary); apparent viscosity of CO2-emulsion and differential pressure across the core during co-injection of CO2/surfactant.

8.3.2 Core Exp 8: CO2-Emulsion Flood

The main objective of this core flood test was to investigate the potential of enhancing oil displacement by CO2/surfactant co-injection and formation of CO2-emulsion in the core.

Procedure and Conditions

All fluid injections were performed from the top of the core at a constant rate of 7 cm^3hr^{-1}, equivalent to a frontal velocity of 1ft/day. In the case of co-injection of CO2 and surfactant solution, total injection rate was equal to 7 cm^3hr^{-1}.

1. *Initialization:* Core was saturated with brine at T = 28 °C and P = 1500 psig.
2. *Oil Flood:* Core was flooded with crude oil "J".
3. *Aging:* The oil was left in the core for 2 days.
4. *Waterflood:* Two PVs of brine were injected through the core.
5. *CO2-Foam Flood:* Three PVs of surfactant solution and liquid CO2 were injected simultaneously through the core with the ratio of 4.5/2.5 respectively for CO2 and surfactant solution.

Table 8-6 lists a summary of fluids used and the pressure and temperature at which the test was carried out.

Table 8-6: Core Exp 8; Fluids used and pressure and temperature conditions.

Porous Medium	Consolidated Sandstone Core
Crude Oil	"J" (617 @ 28 °C)
Brine	10000 ppm (8/2 ratio between NaCl/CaCl2)
Gas Phase	Liquid CO2
Surfactant Solution	0.3 wt % AOS 14+ dissolved in brine solution
Temperature	28 °C
Pressure	1500 psig

Results

Oil Flood and Initialization

The core was initially saturated with brine. Subsequently, the crude oil (crude J) was injected through the core to establish an initial oil and water saturation. An oil saturation of 83% was obtained at the end of the oil injection period. After this period of oil injection the inlet and outlet of the core was closed and the core remained at that condition for a period of 2 days for aging purposes.

Water Injection

The core was then flooded with brine from the top end of the vertically mounted core. As expected, due to a very large viscosity contrast between the flood water and crude oil, an early water breakthrough was observed. The first droplets of water were observed at the outlet only after 0.13 PV of brine injection, which resulted in recovery of 16 %OOIP of oil in the core. After the breakthrough, brine injection continued for a relatively long period of time and a total of two PVs of water were injected through the core. The oil recovery increased from 16% at breakthrough to 25 % and 28 % after 0.92 and 1.91 PVs of brine injection respectively. Most of the recovery after breakthrough took place within the 1st PV of brine injection. The recovery of oil continued after the first PV of water injection at a low, but stable rate.

CO2/Surfactant Co-Injection

After an extended period of waterflood, co-injection of CO2 and surfactant commenced, again from the top end of the core. At the early stages of CO2/surfactant injection, before the CO2 breakthrough, the core effluent mostly consisted of brine and oil at high water cut (around 0.95). Brine production was followed by production of a small bank of crude oil before CO2 broke through. Figure 8-21 displays the differential pressure across the core and the oil recovery data versus injected pore volume of CO2/surfactant. Figure 8-22 illustrates the same data, but in a shorter period of time (the first 1.5 PVs of CO2 and surfactant injection) for a better view of the differential pressure change at the early stages. The CO2 breakthrough occurred after 0.21 PV of CO2/surfactant co-injection, which resulted in a recovery of 3 %OOIP. The oil production rate peaked just before CO2 breakthrough, at an oil production rate of 1 cc oil/cc inj and then gradually dropped to 0.5 cc oil/cc inj during the next 0.21 PV of CO2/surfactant injection.

This period of oil production at 0.5 cc oil/cc inj continued for 0.21 PV of CO2/surfactant injection after CO2 breakthrough, at which point a bank of oil emulsion broke through the core. The effluent produced was observed to be a very stable emulsion, which was formed as a result of mixing between the crude oil and injected surfactant solution. The oil recovery at breakthrough time of the oil emulsion was recorded to be 16 %OOIP. The breakthrough of the emulsion bank was associated with a drop in oil production rate from 0.5 cc oil/cc inj to 0.2 cc oil/cc inj.

The injection of CO2/surfactant continued for an extended period of time, until 3 PVs of CO2/surfactant was injected through the core. This resulted in 3, 16, 27, 40 and 50%

additional oil recovery at/after CO2 breakthrough (0.21 PV), oil emulsion breakthrough (0.42 PV), 1.01, 2.00 and 3.00 PVs of co-injection of CO2 and surfactant respectively This additional oil recovery was over and above what had been recovered during the preceding water injection period. Figure 8-21 shows that as CO2/surfactant injection starts, there is an increase in differential pressure just before the CO2 breakthrough, which is believed to be due to the formation of a large oil bank in the core. After CO2 breakthrough, differential pressure gradually decreased and reached its minimum at the breakthrough of the oil-emulsion. However, when CO2 and surfactant injection continued, the differential pressure gradually increased again, which this time, is thought to be due to the formation of a CO2-surfactant emulsion in the core at a later stage.

Figure 8-23 illustrates the rate of oil production and the gas oil ratio of the produced effluent versus PV of injected CO2 and surfactant. It can be seen that the rate of oil production reaches a maximum of 1 cc oil/cc inj just before CO2 breakthrough, and then drops to values around 0.5 cc oil/cc inj until the breakthrough of oil emulsion, when it stabilizes at values around 0.2 cc oil/cc inj for the rest of the period of CO2/surfactant co-injection.

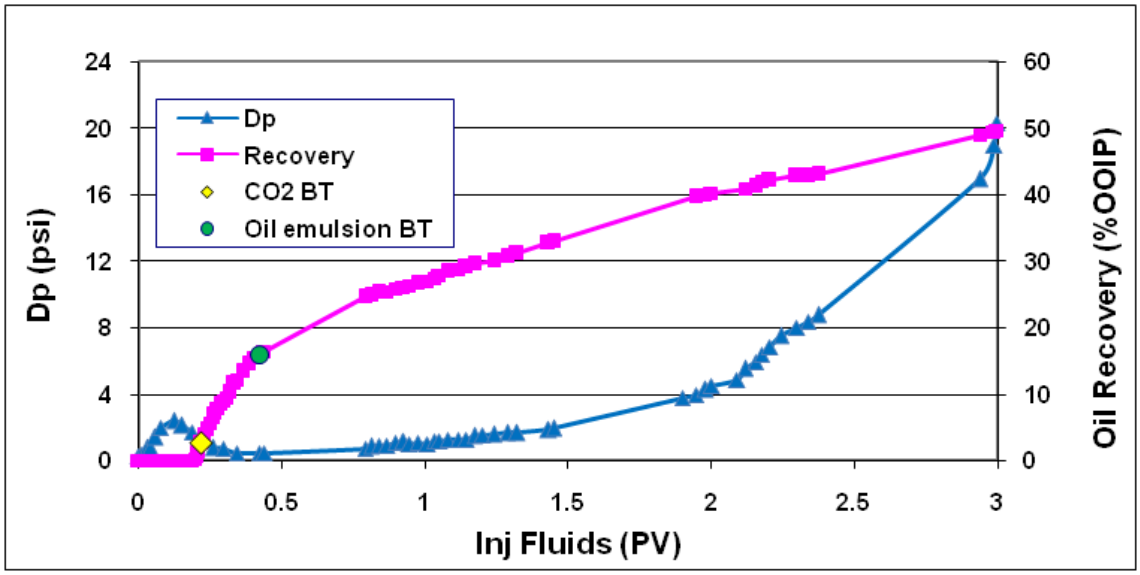

Figure 8-21: Core Exp 8; oil recovery and differential pressure across the core versus PV of injected fluids during the period of CO2/surfactant co-injection.

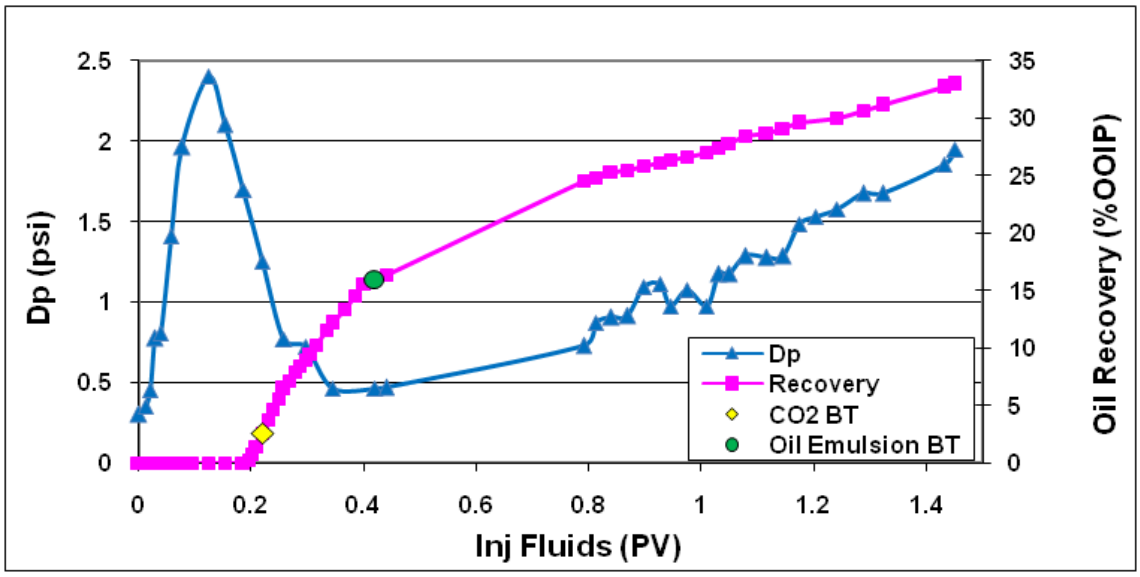

Figure 8-22: Core Exp 8; oil recovery and differential pressure across the core versus PV of injected fluids at early injection stage during the period of CO2/surfactant co-injection.

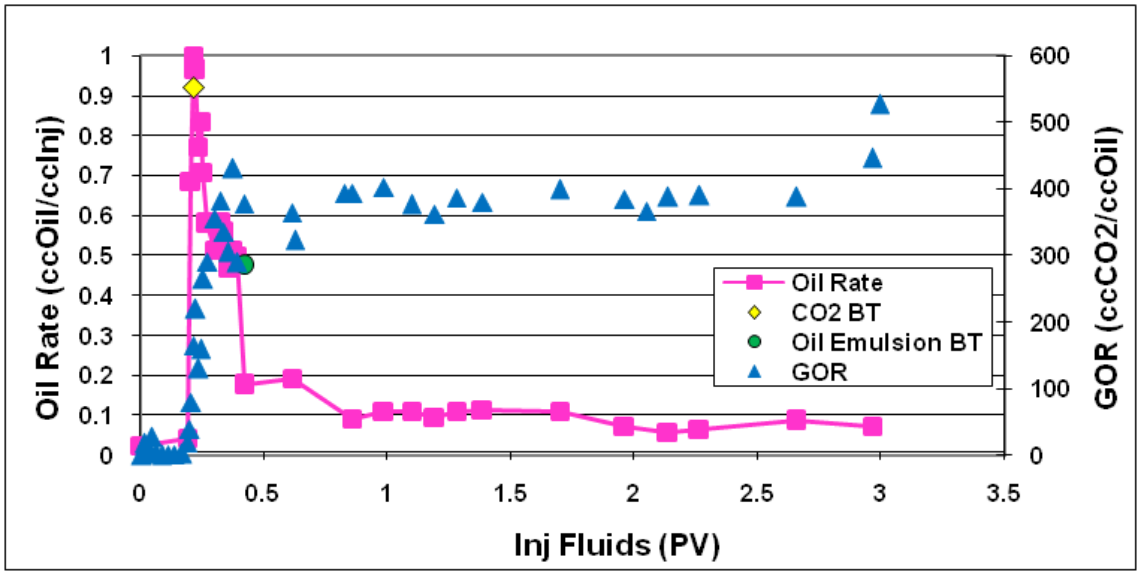

Figure 8-23: Core Exp 8; oil production rate and gas oil ratio of the effluent versus PV of injected fluids during the period of CO2/surfactant co-injection.

Summary

Table 8-7 summarises the amount of incremental oil recovery and cumulative oil production achieved at each stage of this experiment. Figure 8-24 demonstrates the cumulative oil recovery curve (for the whole test) versus the total PV of injected fluids. 28 %OOIP of the oil was recovered during the initial extended waterflood period. The subsequent period of co-injection of the CO2 and surfactant (CO2 emulsion) recovered

an additional 50 %OOIP of the oil. These results reveal the huge potential of CO2 emulsion injections for improving recovery of this heavy crude oil. Figure 8-25 demonstrates the fluid's saturation inside the core at different stages of the experiment.

Table 8-7: Core Exp 8; summary of the results.

Recovery							
1st Water Flood				CO2-Emulsion Flood			
	Inj (PV)	Recovery	Cum Rec		Inj (PV)	Recovery	Cum Rec
BT	0.13	16%	16%	CO2 BT	0.21	3%	31%
1 PV	0.92	25%	25%	Oil Emulsi	0.42	16%	44%
2 PV	1.91	28%	28%	1 PV	1.01	27%	55%
				2 PV	2.00	40%	69%
				3 PV	3.00	50%	78%

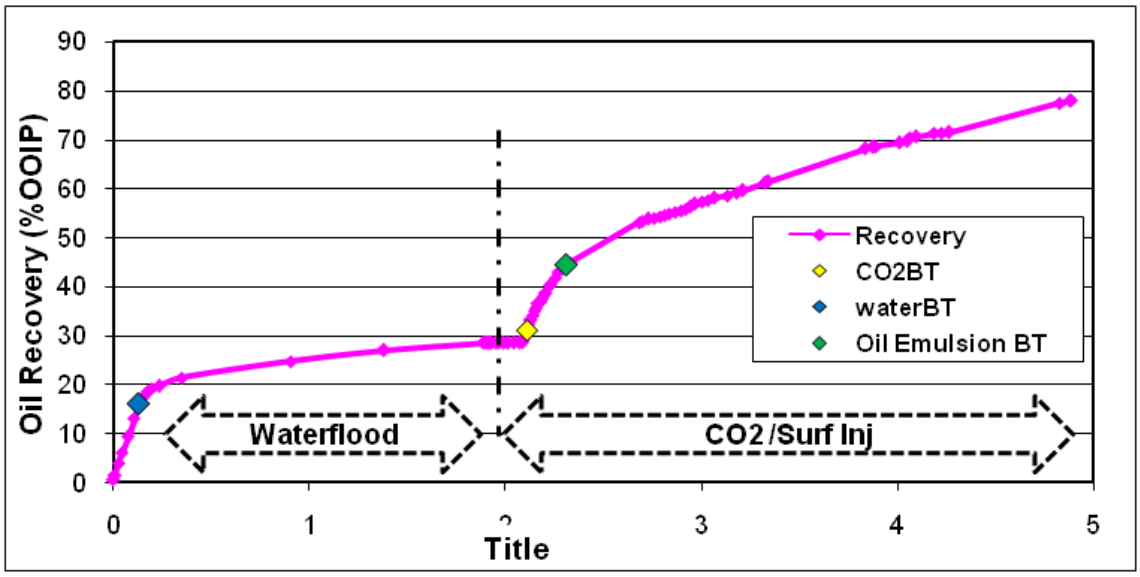

Figure 8-24: Core Exp 8; recovery curve at different stages of the test.

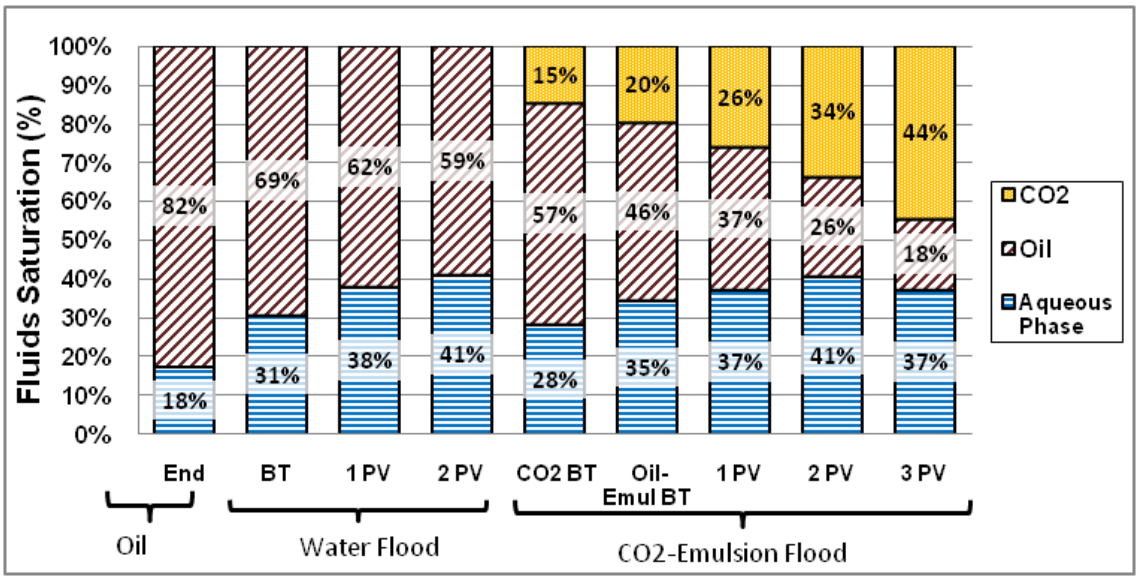

Figure 8-25: Core Exp 8; saturation of fluids in the core at different stages of the test.

8.3.3 Discussions

Comparison of Tertiary CO2 flood and CO2-Emulsion Flood

Figure 8-26 compares differential pressure across the core during the CO2/surfactant co-injection in Core Exp 8 and tertiary CO2 injection in Core Exp 6, at reservoir conditions of crude "J" (1500 psig and 28 °C). As shown in this figure, in-situ formation of CO2-emulsion has successfully pressurized the core and increased differential pressure across the core by 3 orders of magnitude (20 psi differential pressure during CO2/surfactant co-injection compared to 0.02 psi during tertiary CO2 injection) after three PVs of injection. This differential pressure across the core corresponds to an apparent emulsion viscosity of around 2800 cp. This means that in-situ generated CO2-emulsion can displace the heavy crude oil with viscosity of 674 in stable conditions.

Figure 8-27 compares the incremental oil recovery (based on waterflood remaining oil saturation) during the CO2/surfactant co-injection in Core Exp 8 and tertiary CO2 injection in Core Exp 6. This graph shows an ultimate incremental oil recovery of 70 % S_{wro} for the CO2/surfactant co-injection against 50% S_{wro} obtained by tertiary CO2 injection. The superior performance of the former is believed to be primarily due to the mobility control and pressurization of the system. The recovery mechanisms contributing to oil recovery during CO2/surfactant co-injection will be explained in the following sections.

In addition to recovery improvement, the generation of CO2-emulsion significantly reduced the volume of the produced gas. Figure 8-28 compares GOR obtained during the CO2/surfactant co-injection in Core Exp 8 and tertiary CO2 injection in Core Exp 6. The difference in GOR of effluent produced, is more apparent after the first PV of injection. After 3 PVs of injection the GOR is around 3000 cc CO2/cc Oil during CO2/surfactant co-injection, while at the same time period the GOR is around 18000 cc CO2/cc Oil during tertiary CO2 injection. Taking into account that the rate of CO2 injection in CO2/surfactant co-injection experiment is two-third of the rate during tertiary CO2 injection, a 4 times improvement in GOR has been achieved as a result of formation of strong CO2 emulsion in the core.

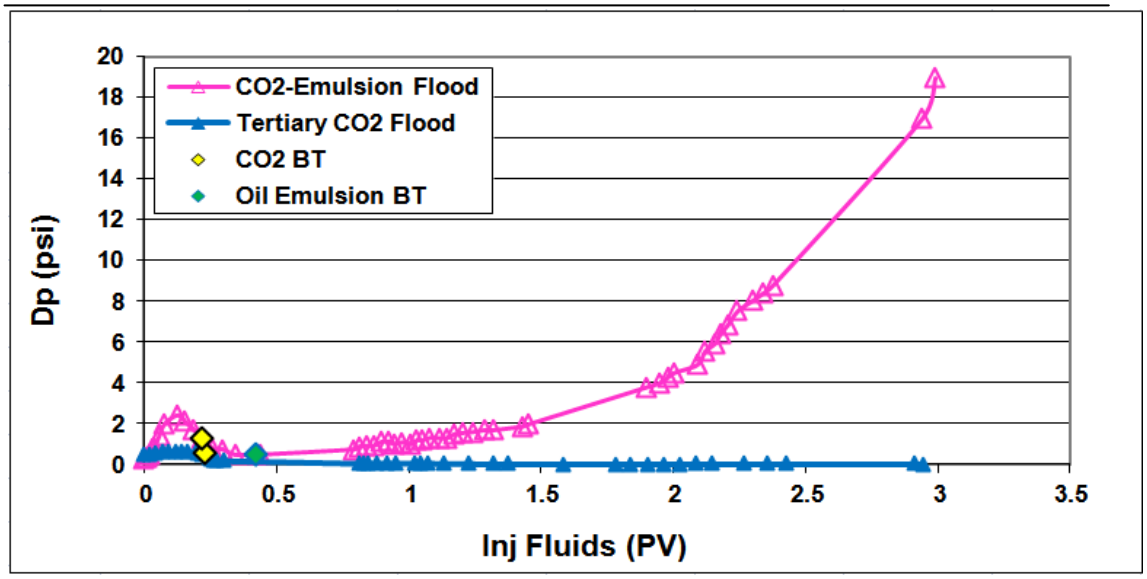

Figure 8-26: Comparison of differential pressure across the core during CO2/surfactant co-injection in Core Exp 8 and tertiary CO2 injection in Core Exp 6.

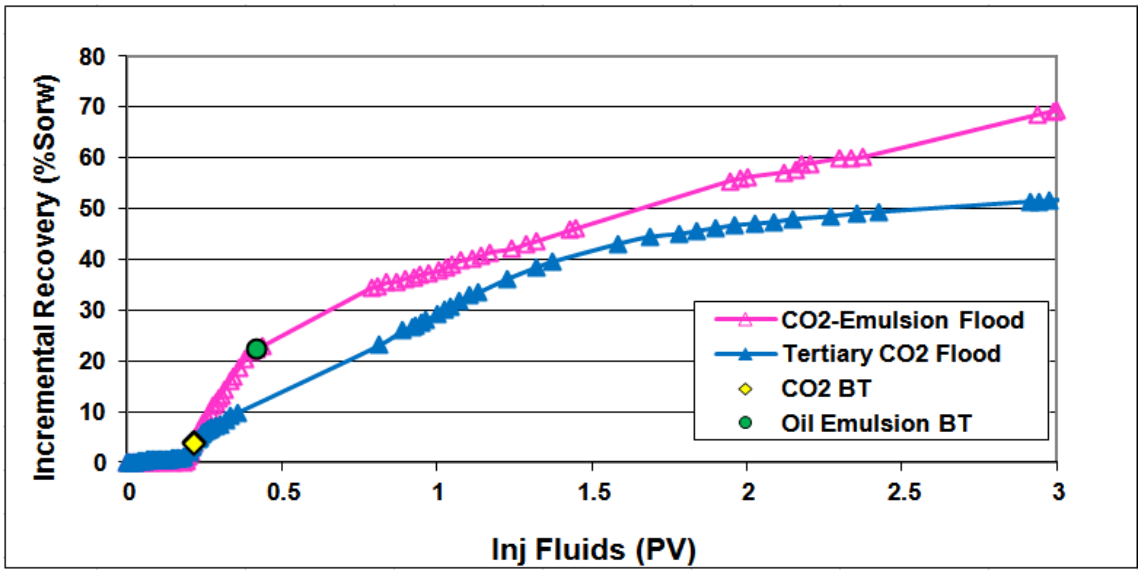

Figure 8-27: Comparison of the incremental oil recovery (based on waterflood remaining oil saturation) during CO2/surfactant co-injection in Core Exp 8 and tertiary CO2 injection in Core Exp 6.

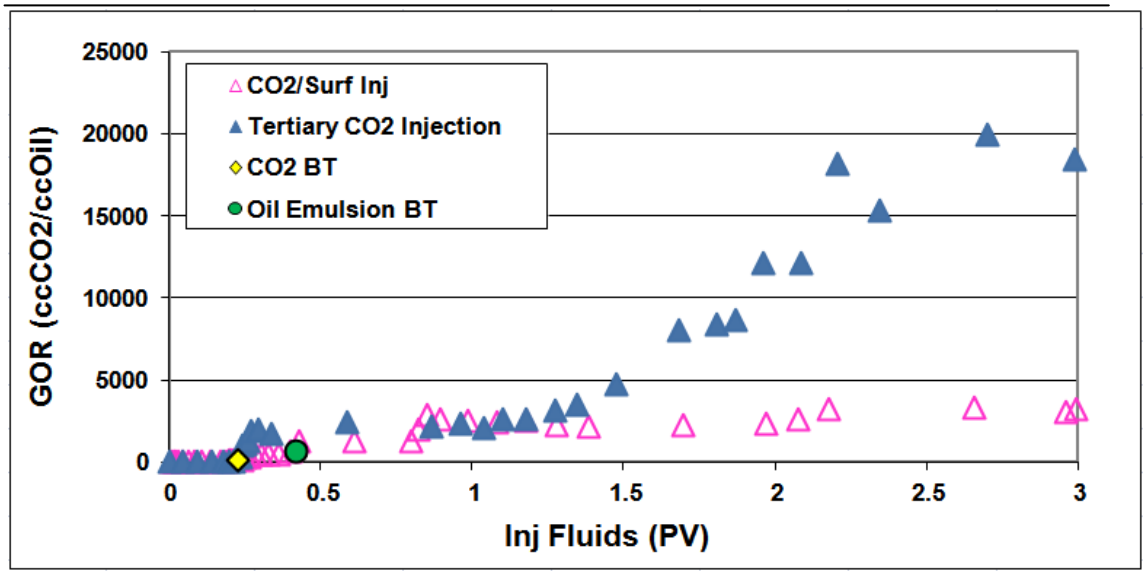

Figure 8-28: Comparison of gas oil ratio of the effluent during CO2/surfactant co-injection in Core Exp 8 and tertiary CO2 injection in Core Exp 6.

Effect of Oil Saturation on Foam Stability

Similarly to the case of CO2/surfactant co-injection in Core Exp 5, in this experiment the in-situ generation of CO2-emulsion and pressurization of the system started at oil saturation of around 50%. The pressurization of the core due to generation of CO2-emulsion started only after 0.4 PV of CO2/surfactant injection, when the oil saturation was as high as 47% showing an apparent foam viscosity around 60 cp.

Oil Recovery Mechanisms during CO2/Surfactant Co-Injection

In order to understand and describe the mechanisms involved in oil recovery by CO2 emulsion produced in situ by co-injection of CO2 and surfactant, we used oil recovery data obtained from the coreflood test in conjunction with observations made in the micromodel tests. Based on the micromodel test reported in Chapter 6, three groups of mechanisms have been identified for improved oil recovery during CO2/surfactant co-injection. These are:

1) Mechanisms associated with CO2 injection: All the oil recovery mechanisms involved in CO2 flood (explained in the previous section) are also operating in oil recovery during co-injection of CO2 and surfactant. Direct displacement of oil by CO2, viscosity reduction and swelling due to CO2 dissolution all contribute to oil recovery and improve the displacement process. However, it is believed that the extraction mechanism is less effective compared to the case of continuous CO2 injection in tertiary and secondary modes. This is a result of

the spreading characteristics of the system changing to non-spreading, as a result of very low interactional tension between CO2 and surfactant solution. In non-spreading conditions. existence of interfaces between CO2 and surfactant solution results in limited interfaces between oil and CO2 and therefore weakening of extraction mechanism.

2) Mobility Control: formation of CO2-emulsion, as a result of co-injection of CO2/surfactant, is believed to be the main reason for recovery improvement in this experiment. The best indication for existence of this recovery mechanism is the gradual increase in differential pressure across the core during CO2/surfactant co-injection (Figure 8-26). The effect of mobility control on oil recovery will be more pronounced on a larger scale and in heterogeneous systems.

3) Pore scale displacement mechanisms: Four pore scale mechanisms were identified in the micromodel experiments which contributed to oil displacement at pore scale (direct displacement, emulsification, co-current and counter-current film flow mechanisms). The micromodel observations showed that direct displacement and emulsification mechanisms are the main contributing mechanisms in reservoir conditions of crude "J". The coreflood data also confirm this observation and show that formation of a bank of oil emulsion is the dominant oil recovery mechanism after 0.4 PV of CO2 and surfactant injection (oil emulsion breakthrough). This O/W (oil-in-water) emulsion has a higher apparent viscosity than the injected surfactant solution and a lower viscosity than the oil phase. As a result of this mechanism, the residual oil (remaining after waterflood) can be displaced easier in the form of emulsion and at the same time the higher viscosity of this emulsion causes better sweep and displacement efficiency compared to surfactant solution. Additionally, the non-uniform nature of the emulsions causes frequent blockage of the flow path of the aqueous phase and therefore flow path modification, which in turn causes the displacement and recovery of the residual oil in unswept areas.

The gravity drainage mechanism, which was an important contributing recovery mechanism during tertiary and secondary injection of CO2, is not expected to play an important role in recovery of heavy oil during CO2-foam injection. This is due to the

fact that the CO2 phase is not a continuous phase in porous media and is in the form of small bubbles of foam. Additionally, due to the high viscosity of CO2-foam, the viscous forces are significantly stronger than the case of continuous CO2 injection and the effect of gravity forces can be neglected in comparison to viscous forces.

Oil/Water Emulsions and Mechanisms of Formation

Our observations during micromodel tests show that oil emulsions form in the porous media due to two essential contributing factors during injection of CO2 and surfactant. The first factor is the existence of a low IFT between the oil and aqueous phase (due to the presence of surfactant) and the second is the large amount of mixing in the system due to the flow of CO2 bubbles. Therefore, if any of these two factors are missing in a system (e.g. simple CO2 flood or simple surfactant flood), the bank of oil emulsion (observed in our experiments) is either weak with negligible impact or does not form at all.. Formation of the oil-in-water emulsion enhances oil recovery by reducing viscosity of the oil, increasing apparent viscosity of the aqueous phase, blockage of the flowing paths and modification of oil distribution ahead of the CO2 emulsion front.

While in the micromodel tests only O/W emulsion was observed to form during CO2/surfactant injection, in the core tests produced effluent was observed to be a complex W/O/W emulsion. This was recognized from the lower viscosity of effluent compared to the original oil, which is a good indication of O/W (oil in water) emulsion, and also the shrinkage of oil volume with time (indicative of water content in oil). While the O/W emulsion was observed to break up quickly after production at lab conditions, the remaining W/O emulsion was very stable and was separated only using physical and chemical techniques. The sample was originally centrifuged at 400 rpm and a temperature of 40 ^{o}C for 5 hours. The separated water was removed and the rest of the effluent was diluted with toluene. Then, the sample was rested in a high temperature oven for a day and the procedure was repeated until no more water was separated. Figure 8-29 illustrates two pictures of a sample of core effluent (water in oil emulsion) just after production (left) and after two days resting in a high temperature oven. In the second picture, shrinkage of oil (the phase due to segregation of the water content) is evident.

(a)

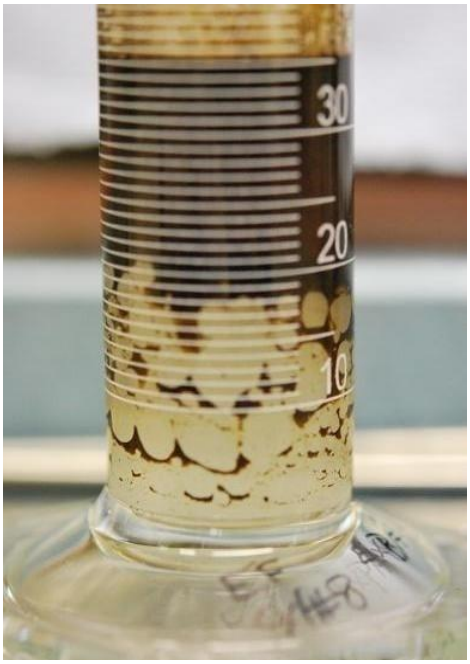

(b)

Figure 8-29: Comparison of the recovered effluent just after disconnection of the cylinder (a) and after resting for a couple of days in high temperature oven (b). The shrinkage of oil volume due to segregation of water content of W/O emulsion is evident.

Performance of CO2/Surfactant Co-Injection in Crude "C" and Crude "J"

The objective of co-injection of CO2/surfactant in Crude "J", was only to improve the mobility ratio through increasing viscosity of the injected CO2. Due to the positive performance of tertiary CO2 injection in this crude oil, improvement of displacement efficiency was not required. However, due to the poor performance of CO2 injection in crude "C" (only 17 % Srow after 5.5 PVs of CO2 injection), CO2/surfactant co-injection was expected to improve the displacement efficiency as well as the mobility ratio.

Figure 8-30 depicts the incremental oil recovery (Sorw) as a result of the CO2-foam/emulsion injection in crudes "C" and "J" and Table 8-8 presents the details of the displacement process. In the case of crude "J", formation of CO2-emulsion has significantly improved the mobility ratio ($\mu o/\mu_D$) of the system to values less than one (0.24), which means a very stable displacement process, good sweep efficiency and a piston type displacement. Additionally, injection of CO2-foam has improved displacement efficiency of the recovery process from 51 % Srow in the case of tertiary CO2 flood to 69 % Srow.

In the case of crude "C", the CO2-foam dramatically improved the displacement efficiency of this extra-heavy crude oil from 17 % Srow (by tertiary CO2 flood) to 68 % Srow. The mobility ratio between the CO2-foam and dead oil reached the value of 18.8, and approximately one (1.2) between the diluted oil and injected foam. While this mobility is orders of magnitude lower than that of water and CO2, which offers much better sweep efficiency in the real reservoir, the mobility ratio of more than one means the displacement of this oil by CO2-foam requires a longer period of injection to permit CO2 to dissolve in the oil, and the subsequent viscosity reduction improves the displacement process.

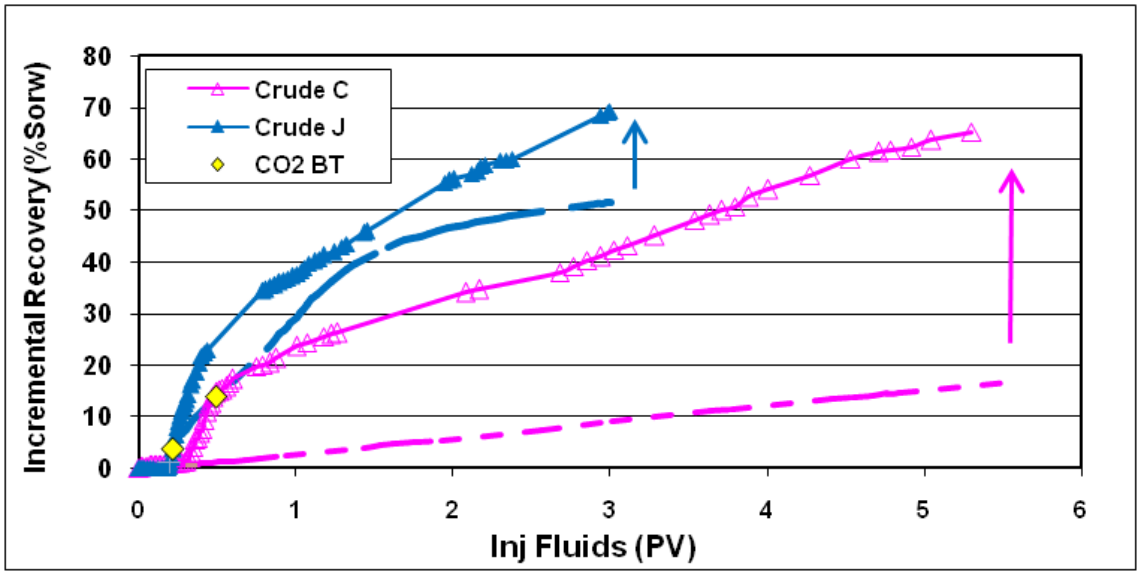

Figure 8-30: Comparison of the incremental oil recovery (based on waterflood remaining oil saturation) during co-injection of CO2/surfactant in crude "C" (Experiment 5) and in crude "J" (Experiment 8) and additional comparison to the incremental recovery during tertiary CO2 injection (dotted lines).

Table 8-8: Comparison of recovery performance of CO2-Foam/Emulsion injection in Crude "C" and crude "J".

Crude Oil	Test Conditions (T, P)	Oil Viscosity at test conditions (μ)	Displacing Phase, its Viscosity at test conditions (μ)	Viscosity Ratio ($\mu o/ \mu_D$)	Recovery Efficiency (Sorw)
"C"	50 C 600 psig	Dead Oil, 8700 cp CO2 Sat = 660 cp	CO2-Foam, 550	18.8 (dead oil) 1.2 (CO2 Sat)	68 % 6PVs Inj
"J"	28 C 1500 psig	Dead Oil =617 cp CO2 Sat = 15 cp	CO2-Emulsion 2800 cp	0.24 (dead oil) 0.01<(CO2 Sat)	69 % 3PVs Inj

8.4 SUMMARY AND CONCLUSIONS

Conclusions drawn from the first part of this chapter:

- Performance of CO2 flood and CO2 emulsion/foam flood was successfully investigated for crude "J" at 1500 psig and 28 °C in a series of core flood tests.
- Very good consistency between the MM and core results was obtained. This significantly assisted understanding of the active mechanisms involved in the recovery process.
- Tertiary injection of CO2 doubled recovery during the initial period of waterflood, by increasing oil recovery from 36 %OOIP at the end of the period of waterflood to 69 %OOIP after 3 PVs of CO2 injection.
- Secondary CO2 flood also showed huge potential for recovery improvement of crude "J", especially after CO2 breakthrough. An additional recovery of up to 25% was obtained after 2 PVs of CO2 injection, compared to oil recovery by waterflood in the same oil.
- From a CO2 storage perspective, secondary injection of CO2 showed higher potential with a storage capacity of 0.52 PV compared to 0.47 PV storage capacity during tertiary injection of CO2. It should be noted that this CO2 storage capacity was calculated after 3 PVs of CO2 injection.

Conclusions drawn from the second part of this chapter:

- Under the reservoir conditions of crude "J", where CO2 is in liquid state, co-injection of CO2 and surfactant solution resulted in the formation of a very strong CO2-emulsion in the core with a viscosity of up to 2800 cp. This is around 4 times higher than the dead-oil viscosity of crude J and it resulted in a very efficient displacement process.
- In addition to enhancing the mobility ratio, CO2-emulsion also slightly improved the displacement efficiency of crude "J" from 51 % Srow (during tertiary CO2 flood) to 69 % Srow.
- CO2-foam/emulsion caused substantial reduction of the mobility of injected CO2 even at high oil saturations of near 50%, where other researchers have reported that in the case of light oils no foam is formed. This behaviour is attributed to the formation of water fingers in the heavy oil with low oil

saturation, which facilitates the formation of CO2 foam/emulsion even at the early stages of injection.

- The main contribution to oil recovery at the pore scale came from the direct displacement mechanism and emulsification of oil.

CHAPTER 9 SUMMARY, CONCLUSIONS AND RECOMMENDATIONS

9.1 SUMMARY

The main objective of the work presented in this thesis was to investigate application of CO2 and water to enhance heavy oil recovery. The idea was that dissolution of CO2 would reduce viscosity of the heavy crude oil in a manner similar to thermal recovery techniques and the diluted oil would be displaced by water or other displacing fluids. Two specific heavy crude oils were assigned to this work with noticeably different thermodynamic properties and reservoir conditions. The first oil sample was crude "C", an extra-heavy crude oil with a viscosity of 8700 cp at reservoir pressure and temperature of 50 °C and 600 psia. The second oil sample was crude "J", a (medium-) heavy crude oil with a viscosity of 600 cp at reservoir pressure and temperature of 28 °C and 1500 psia. CO2 is present in vapour form at the relatively low reservoir pressure and temperature of crude "C" and in liquid form at high reservoir pressure and an exceptionally low reservoir temperature of crude "J". Since CO2 provides different recovery mechanisms at the reservoir conditions of these two crude samples, separate sets of experiments were required for each crude oil. In this work, the research objectives were achieved by conducting a comprehensive set of fluid characterization, flow visualization and coreflood experiments. The Results of the reported experiments are summarized as follows.

9.1.1 Flow Characterization Experiments

The fluid characterization experiments were performed with the main objective of providing basic properties of oil samples and their mixtures with CO2. These data were

later used for interpreting the micromodel and coreflood results and to better understand the contributing mechanisms during CO2 flood. Some of the important results from fluid characterization experiments are summarized below.

- The rheology experiments showed that while Crude "J" is a Newtonian fluid having a viscosity independent from shear rate, crude "C" is a non-Newtonian fluid with a shear thinning behaviour in which the viscosity of oil decreased as the shear rate increased.
- One important observation was the magnitude of viscosity reduction in the crude samples when they were exposed to CO2. The viscosity of crude "J" and crude "C" reduced to 15.2 cp (2.5% of the initial viscosity) and 660 cp (7.6% of the initial viscosity) respectively when they were fully saturated with CO2 at their reservoir conditions. While the viscosity of CO2 diluted crude "C" was still significantly higher than CO2 and water viscosity, in the case of crude "J", the viscosity of diluted oil was in a range that is generally considered as a good candidate for waterflood.
- Results also showed that in reservoir conditions (pressure and temperature) of crude "C" the component exchange between oil and CO2 is limited to CO2 dissolution in the oil phase, while at higher pressures of crude "J" reservoir, there is also mass transfer from oil into the CO2. This means that while in crude "C", oil viscosity reduction and swelling are the only contributing mechanisms; in crude "J", the recovery is also assisted by oil extraction mechanism.
- In the experiments with both crude oils, no precipitation of asphaltene particles was observed in the oil phase when crude oils were diluted with CO2.

9.1.2 Flow Visualization (Micromodel) Experiments

The main objective of the flow visualization experiments was to investigate the pore scale recovery and entrapment mechanisms during heavy oil displacement by water and CO2 and highlight the differences with the case of light crude oils.

Heavy Oil Recovery by Water Injection

- The pore scale displacement mechanisms, during heavy oil waterflood, are not dependent on the viscosity of the oil phase as long as the process remains capillary dominant. The only exception is the oil film drainage mechanism that might be significantly weakened and stop as oil viscosity increases.

- If the viscosity increase causes viscous dominant flow conditions, oil displacement mechanisms will be limited to piston type withdrawal and water channelling in the water- and oil-wet systems respectively. In the intermediate-wet systems, a combination of these two recovery mechanisms might be observed.
- The increase in viscosity of the crude oil strengthens oil entrapment by viscous fingering and surface trapping mechanisms.
- Oil entrapment in conventional (light) oils is due to capillary forces and residual oil is in the form of separated pieces of oil completely surrounded by water. However, in heavy oils trapping is primarily due to viscous forces and the residual oil remains continuous in the porous media. Being trapped by different type of forces, remobilization of the residual oil in heavy oil reservoirs requires a different approach from that of light oils. For instance, IFT reduction by surfactant was observed to be inefficient in such systems.
- The heavy oil recovery before water breakthrough was observed to be principally controlled by the oil/water viscosity ratio, which was not affected by wettability.
- The capillary forces and state of wettability were observed to play a very important role in determining heavy oil recovery after water breakthrough, which differs from the general assumption that capillary forces are not greatly involved in the recovery process due to the high viscosity of these crudes.
- The highest recovery in the case of heavy oil waterflood was achieved in a strongly water-wet system, where the positive capillary forces were strongest. The recovery efficiency by waterflood dropped as the system shifted towards intermediate- and oil-wet conditions.
- It was concluded that optimum conditions for oil recovery shifts from intermediate-wet conditions (for systems with moderate oil/water viscosity ratio) towards increased water-wet conditions, as the viscosity of the crude oil increases.
- Two parameters were recognized for better recovery performance in water-wet systems. Firstly, capillary forces add to the driving viscous force and enhance displacement of residual oil at the pore scale by "capillary imbibition" mechanism. Secondly, in oil-wet and intermediate-wet systems, a large fraction of oil is trapped by surface trapping forces, while in water-wetted systems this type of trapping is minimized.

Heavy Oil Recovery by CO2 Injection

- The processes of oil recovery by secondary and tertiary CO2 injection, CO_2-SWAG and CO2-foam injection were successfully simulated in the micromodel using our heavy crude samples. The oil recovery was significantly higher in all processes involving CO2 than that of plain waterflood and crude "J" showed better recovery performance compared to crude "C".
- The main contributing mechanisms during secondary CO2 injection in crude "C", were observed to be dilution of crude oil and gravity drainage. Despite the initial poor sweep efficiency of injected CO2, an extended period of injection resulted in a very high recovery efficiency.
- Unlike the secondary CO2 injection, the gravity drainage mechanism was not effective in recovery of crude "C" when CO2 was injected in tertiary mode. This was a result of the presence of water layers, which significantly reduced mobility of diluted oil and disrupted the process of oil recovery by the gravity drainage mechanism. The diluted oil was only recovered when the CO2 injection was followed with a period of waterflood.
- CO2-SWAG recovery was also promising, due to dispersion of CO2 slugs into the oil phase, which promoted direct displacement of oil by CO2 and water. Because the CO2 phase was not continuous in the micromodel, during the period of CO2-SWAG injection, gravity drainage is not believed to play an important role in this injection scenario.
- The main contributing mechanisms during secondary injection of high pressure (liquid) CO2 in crude "J", were observed to be: dilution of crude and gravity drainage, followed by extraction mechanisms in later stages.
- The process of tertiary liquid CO2 injection resulted in higher recovery than tertiary vapour-CO2 injection. While similar recovery performance was observed at breakthrough time; after breakthrough, the injection of liquid CO2 improved oil recovery by extraction mechanism from the remaining oil which was in direct contact with the main stream of CO2. Recovery of the part of the remaining oil that was fully covered by water layers and separated from the flowing stream of CO2, was also slightly improved by formation of a new phase, which caused reconnection of some of the separated oil blobs in the flowing stream of CO2.

- During the subsequent period of waterflood, the oil recovery was also higher in the test performed using liquid-CO2 rather than vapour CO2. It was the result of a combination of parameters including: blockage of the flowing path of water with bubbles of the new phase, higher viscosity reduction, and the viscosity gradient in the remaining oil.
- Formation of the new phase in oil blobs, which were not in contact with the injected liquid CO2, was observed and reported here for the first time. This helped oil recovery during the period of liquid-CO2 flood and during the subsequent period of water injection. However, the mechanism behind formation of this phase is not yet fully understood and needs further investigation.

Heavy Oil Recovery by CO2 Foam/Emulsion Injection

- The results showed that when strong CO2-foam/emulsion is formed in porous media, heavy crude oil can be displaced from the porous media very efficiently. When liquid CO2 was used (in the case of crude "J") the generated CO2-emulsion was more stable, compared to the example of CO2-foam using vapour CO2 (in the case of crude "C").
- At the reservoir conditions of crude "C", N2-foam was observed to be more stable than CO2-foam, even after contacting the heavy oil at early times of injection. The non-spreading behaviour of the oil during N2-foam injection, compared to the oil spreading behaviour during CO2-foam injection, is believed to be the main reason for this stability. However, the N2-foam was observed to be less efficient in terms of recovery improvement. The superior performance of the CO2-foam process is attributed to the favourable modification of oil properties by CO2 (e.g. viscosity reduction in the oil phase as a result of CO2 dissolution).
- Two main stages of oil recovery were observed and identified during the foam injection experiments. In the first stage, heavy oil was displaced from the well-connected pores and high permeability parts of the porous medium. As the main flowing path became partially blocked by foam (in the second stage), the foam gradually developed towards the low permeability parts and dead-end pores, thus recovering residual oil in those regions of the porous medium.
- In CO2 foam/emulsion injection experiments, four displacement mechanisms were identified from video and magnified pictures and introduced into the

literature, some of which, for the first time. These mechanisms include direct displacement of oil by CO2 bubbles, emulsification, co-current film flow, and counter current film flow mechanisms.

- Direct displacement of heavy oil by foam at the early stages of injection, was observed to be much more effective than the double-drainage displacement process during tertiary CO2 flood. During the later stages, after CO2-foam breakthrough, the +
- Oil in previously flooded pores was displaced by two other mechanisms: "co-current film flow" and "oil emulsification". These mechanisms were observed in the interconnected pores and resulted in a high oil recovery of up to 90%.
- A new counter-current film flow mechanism was recognized that improved the displacement of residual oil trapped inside the dead-end pores. However, recovery of the residual oil from the dead end pores by counter-current film flow mechanism was significantly slower than the displacement process in the inter-connected pores.
- The emulsification mechanism was observed to be more efficient at the reservoir conditions of crude "J", where the oil had much less tendency to spread over the CO2-emulsion bubbles, compared to the case of CO2-foam at reservoir conditions of crude "C". This resulted in formation of a large bank of oil in water emulsion, (which formed ahead of the generated CO2-emulsion) that displaced the oil bank towards the producing end of the micromodel.
- While CO2-foam injection performed considerably better, compared to N2-foam injection at the reservoir conditions of crude "C", it is believed that this process can be further improved. This would involve combining CO2 and N2 foam in an injection strategy, in which N2-foam is used to provide more stable foam and thus better mobility control, and CO2-foam is used to provide oil viscosity reduction and better displacement efficiency. Furthermore, it can solve the problem of CO2 availability, if there is a limited volume of CO2.

9.1.3 Coreflood Experiments

Based on the micromodel observations, coreflood experiments in the second part of this work were designed to evaluate and quantify the potential of different recovery processes, for improved recovery of these heavy crude oils.

Heavy Oil Recovery by CO2 Injection

- CO2 injection potential was evaluated by performing coreflood experiments with two viscous crude samples, under their reservoir conditions. The ultimate oil recovery for all scenarios of secondary, tertiary and SWAG-CO2 injection, was almost twice the recovery during plain waterflood for both crude samples. In addition to recovery improvement benefits, a huge potential was observed for CO2 disposal in these heavy oil reservoirs.
- In the case of crude "C", the highest oil recovery was achieved when CO2 and water were co-injected (CO2-SWAG) and tertiary injection of CO2 resulted in the lowest level of recovery compared to other injection scenarios. From a CO2-storage point of view however, almost the same amount of CO2 storage was achieved in secondary and tertiary CO2 injection, which was higher than the CO2 stored in the case of CO2 SWAG injection.
- Comparison of secondary and tertiary injection of CO2 in crude "J" reveals that secondary CO2 injection offers better recovery efficiency at early injection times. An additional recovery of up to 25% was obtained after 2 PVs of secondary CO2 injection, compared to oil recovery by waterflood. The CO2 storage capacity was also slightly higher when CO2 was injected in secondary mode.
- Better recovery performance was observed during the CO2 injection processes in crude "J" compared to crude "C". This superior performance is believed to be primarily due to the higher reservoir pressure, which resulted in higher CO2 dissolution and viscosity reduction (15.2 cp). The other reason was the contribution of the extraction mechanism to oil recovery, which prompted oil recovery during the later stage of the injection. However, the impact of the latter mechanism is believed to be less significant, since the extraction mechanism is a very slow process in heavy crude oils.
- The lower recovery efficiency in the case of crude "C", was due to the fact that the diluted oil had a viscosity of around 660 cp, which was significantly higher than the corresponding viscosity of water and CO2 under test conditions. This resulted in a very poor mobility ratio between displacing and displaced phases. To improve recovery efficiency, it is necessary to further decrease the mobility ratio; either by enriching CO2 with hydrocarbon solvents, or by viscosifying the CO2 using foam.

- Due to the higher density of liquid CO2 and its superior displacement performance (higher CO2 saturation) in reservoir conditions of crude "J" compared to vapour CO2 at reservoir conditions of crude "C", larger volume of CO2 was stored in the experiments that crude "J" was used.

Heavy Oil Recovery by CO2 Foam/Emulsion Injection

- The process of co-injection of CO2 and surfactant, resulted in formation of strong foam and emulsion in the core, and successfully improved both oil recovery efficiency and mobility ratio of the displacement process.
- Co-injection of CO2 and surfactant at reservoir conditions of crude "C" resulted in formation of a strong CO2-foam in the core with an apparent viscosity of 550 cp. While foam viscosity was still more than one order of magnitude lower than that of dead crude oil, it was within the same range as the diluted oil viscosity. This means if the oil is already diluted with CO2, it can be efficiently displaced by injected CO2-foam.
- Co-injection of CO2 and surfactant at reservoir conditions of crude "J", resulted in the formation of a strong CO2-emulsion in the core with an apparent viscosity of 2500 cp, which was 4 times higher than the viscosity of the dead crude oil.
- The impact of co-injection of CO2 and surfactant on oil recovery was more apparent in the case of crude "C", where the oil recovery by CO2 injection was not very efficient. In the case of crude "C", the displacement efficiency dramatically improved from 20%Srow in tertiary CO2 flood to near to 69%Srow after 6 PVs of CO2/surfactant (CO2 foam) injection. In the case of crude "J", the displacement efficiency improved from 50%Srow in tertiary CO2 flood to near to 70%Srow after 3 PVs of CO2/surfactant (CO2-emulsion) injection.
- CO2-foam/emulsion caused a substantial reduction in mobility of the injected CO2, even at high oil saturations of near 50%, where other researchers have reported that, in the case of light oils, foam cannot be formed. This behaviour is attributed to the formation of water fingers in heavy oil, with low oil saturation during the initial period of waterflood that facilitates the formation of CO2 foam/emulsion, even at the early stages of injection.

9.2 CONCLUSIONS

- Heavy oil recovery by waterflood is more efficient in water-wet systems where the positive capillary forces assist displacement of oil at the pore scale. Heavy

oil entrapment by "surface trapping" mechanism is another contributing factor that significantly reduces efficiency of waterflood in intermediate- and oil-wet systems.

- Being trapped by different type of forces, remobilization of the residual oil in heavy oil reservoirs requires a different approach from that of light oils. For instance, IFT reduction by surfactant was observed to be inefficient for enhanced heavy oil recovery. To have good recovery performance in heavy oil systems, it is required to promote the mobility ratio of the displacement process either through reducing viscosity of heavy oil (e.g. using CO2 and solvents) or by increasing viscosity of displacing fluids (e.g. using foam).
- The results of this study demonstrate that there is huge potential for recovery improvement and CO2 storage by CO2 injection in heavy oil reservoirs.
- In the case of crude "C", the highest oil recovery was achieved by CO2-SWAG injection and tertiary injection of CO2 resulted in lowest recovery compared to the other injection scenarios. From CO2-storage point of view, however, almost the same amount of CO2 storage was achieved in secondary and tertiary CO2 injection which was higher than the CO2 stored in the case of CO2 SWAG injection.
- Considering the very high viscosity of crude "C" and the poor performance of waterflood in this crude oil, injection of CO2 successfully improved oil recovery to twice the recovery by plain waterflood. However, it is believed that the CO2 recovery performance in this crude oil can be further improved by addition of hydrocarbon solvents to CO2 or by increasing viscosity of CO2 to provide better mobility ratio in the displacement process.
- Comparison of secondary and tertiary injection of CO2 in crude "J" reveals that secondary CO2 injection provides much better recovery efficiency at early injection times and offer higher potential for CO2 storage purposes.
- Formation of the new phase in the oil blobs which were not in contact with the injected high pressure CO2 was observed and reported here for the first time which helped oil recovery during the period of CO2 flood and during the subsequent period of water injection. However the mechanisms behind formation of this phase are not fully understood yet and need further investigation.
- The process of co-injection of CO2 and surfactant resulted in formation of strong foam and emulsion in the core and successfully improved both oil

recovery efficiency and mobility ratio of the displacement process. The generated CO2-foam/emulsion showed viscosities of 550 cp and 2500 cp respectively at reservoir conditions of crude "C" and crude "J".

- The impact of co-injection of CO2 and surfactant on oil recovery was more apparent in the case of crude "C" where an improvement of more than 3 folds was observed in recovery efficiency compared to tertiary CO2 injection.
- CO2-foam/emulsion caused substantial reduction of the mobility of the injected CO2 even at high oil saturations of near 50% where other researchers have reported that no foam can be formed in the case of light oils.
- Four displacement mechanisms were identified from video and magnified pictures and which improved oil recovery at micro-scale during CO2 foam/emulsion flood. These mechanisms include direct displacement of oil by CO2 bubbles, emulsification, co-current film flow, and counter current film flow mechanisms.

9.3 RECOMMENDATIONS

In this work all the flow visualization and coreflood experiments were performed at gravity stable conditions. To investigate the effect of gravity forces on recovery performance it is required to repeat few of these experiments in horizontal cores where the gravity forces might adversely influence the recovery performance.

In the case of crude "J" further core experiments might be needed to evaluate the process of CO2-SWAG injection and also investigate the effect of impurities in CO2 (e.g. N2) on recovery performance of this crude oil.

In early experiments the effect of enriching CO2 by hydrocarbon solvents was investigated through limited micromodel experiments in crude "C". It would be recommended to perform further flow visualization and coreflood experiments to understand the impact of hydrocarbon solvents on recovery performance of this crude oil. Formation of multiple phases and their impact on recovery performance should be considered in this study.

In the case of co-injection of CO2 and surfactant and formation of foam and emulsion, screening experiments would be suggested to investigate effect of alkali materials, different surfactants and surfactant concentration. Further core tests can be designed to

find the optimum strategy for CO2/surfactant injection and the ratio of injection. It is also recommended that the effect of pressure and temperature on foam/emulsion formation, propagation, viscosity and stability is investigated in comprehensive set of experiments.

Formation of a new phase in the oil blobs which are not in direct contact with CO2 was reported in this work which can improve oil recovery through several mechanisms during CO2 injection and the subsequent period of waterflood. It would be recommended to perform a comprehensive set of micromodel and fluid characterization experiments to investigate the mechanism behind formation of this phase and magnitude of its contribution to oil recovery.

Simulation studies would be needed to investigate whether the commercial simulators can reliably simulate the process of oil recovery by water and CO2 injection in heavy oil systems using pressure and recovery data from coreflood experiments reported in this thesis. Simulation of the process of oil recovery by CO2-foam/emulsion also can be considered in the future works.

APPENDIX A: REPEATABILITY INVESTIGATION

The main objective of this appendix is to investigate the repeatability of the micromodel experiments which were reported in chapters 4, 5 and, 6. Most of the micromodel experiments in this thesis have been repeated at least once to make sure about reproducibility of the observations. Two of these experiments are selected here to cover the main recovery processes (waterflood, CO2 and CO2-foam injection) explained in this work. In the first part, the displacement pattern and recovery efficiency during the periods of water and CO2 injection in MM Exp 8 are compared to those of a repeated test. In the second part, similar comparison has been made to investigate the repeatability of the results during CO2-foam injection in MM Exp 11. The similarity of the displacement patterns and recovery efficiencies are good indications of accuracy and reproducibility of the results obtained from these micromodel experiments.

A.1 MM EXP 17: REPLICATE OF MM EXP 8

In MM Exp 8 the process of tertiary CO2 flood in crude "C" was investigated. In this experiment heavy oil was displaced by vapour CO2 after an initial period of waterflood. Since MM Exp 8 contains both waterflood and CO2 flood periods, by comparing its results with a replicate experiment, reproducibility of both waterflood and CO2 flood process can be investigated. MM Exp 17 was carried out using a procedure similar to MM Exp 8 without the final period of waterflood. The fluids and pressure and temperature conditions were also remained the same as MM Exp 8.

Procedure

1 *Initialization:* Micromodel was saturated with distilled water at T = 44 °C and P = 600 psig.

2 *Oil Flood:* Micromodel was flooded with crude oil "C" from bottom until the oil front reached the other end of the micromodel.

3 *Waterflood*: DW was injected in the micromodel for 3 days.

4 *CO2 Flood*: CO2 was injected in the micromodel for 2 days.

Table A-1 lists a summary of the fluids, the porous medium and the pressure and temperature setting used for this experiment.

Table A-1: The fluids, porous medium and pressure and temperature setting used for MM Exp 17.

Porous Medium	Heterogeneous Rock-look-alike Micromodel
Crude Oil	"C" (8700 cp @ 50 °C)
Aqueous Phase	Distilled Water
Gas Phase	CO2
Temperature	44 °C
Pressure	600 psig

Results

The experiment began by saturating the micromodel with distilled water at 44 °C and 600 psig. To establish the initial saturation, crude oil C was then injected through the micromodel. Figure A-1 and Figure A-4 respectively show a magnified section and the full length of micromodel and compare the distribution of oil and connate water, in MM Exp 8 and in this experiment at the end of oil injection period. It can be seen that , similar to MM Exp 8, very high oil saturation has been achieved due to the high viscosity contrast between oil and water.

Water was then injected through the micromodel. Figure A-2 and Figure A-5 respectively show the magnified section and the full length picture of t he micromodel and compare water/oil distribution in MM Exp 8 and in this experiment during the period of waterflood. Water was observed to finger through the left side of the micromodel where the vertical connectivity was high in both experiments.

Having the micromodel flooded with water for 3 days, the period of CO2 injection started. Figure A-3 and Figure A-6 respectively show the magnified section and the full length picture of the micromodel and compare the fluids distribution in MM Exp 8 and in this experiment during the period of tertiary CO2 injection. As can be seen, CO2 opened a flowing path through the left side of the micromodel and displaced most of the water in that region of the micromodel. However, layers of water remained continuous in the middle of the micromodel and interrupted continuity of oil throughout the micromodel. Existence of these water layers resulted in "water shielding effect" and reduced performance of CO2 injection compared to the case of secondary CO2 injection.

Summary

The comparison of the micromodel pictures in this experiment (MM Exp 17) and MM Exp 8 show very good match between the results in terms of mechanisms and patterns of displacement. Table A-2 summarises the oil recovery data at breakthrough time and at the end of each stage of this experiment (MM Exp 17) and compare it to the recovery data of MM Exp 8. The recovery data show very similar performance for the initial period of waterflood and the following period of tertiary CO2 injection in these two experiments.

Table A-2: Summary of the recovery data in MM Exp 17 and comparison to MM Exp 8.

		Recovery @ BT (% OOIP)	Ultimate Recovery (% OOIP)	Cumulative Recovery (% OOIP)
MM Exp 17	Waterflood	11	17	17
	CO2 flood	6	8*	25
MM Exp 8	Waterflood	10	15	15
	CO2 flood	6	8*	23
* A swelling factor of 5.5% has been considered for recovery calculations.				

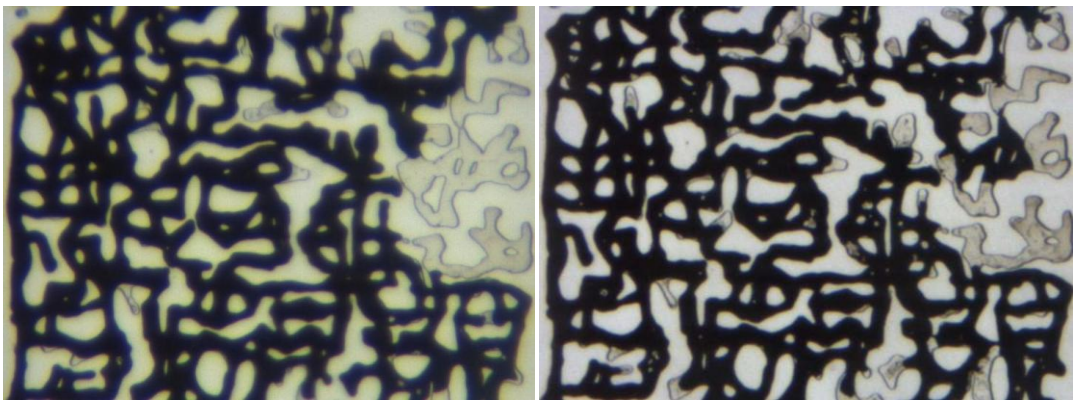

a **b**

Figure A-1: Fluid distribution in a magnified section of the micromodel after oil injection, (a) in MM Exp 8 and, (b) in this experiment (MM Exp 17).

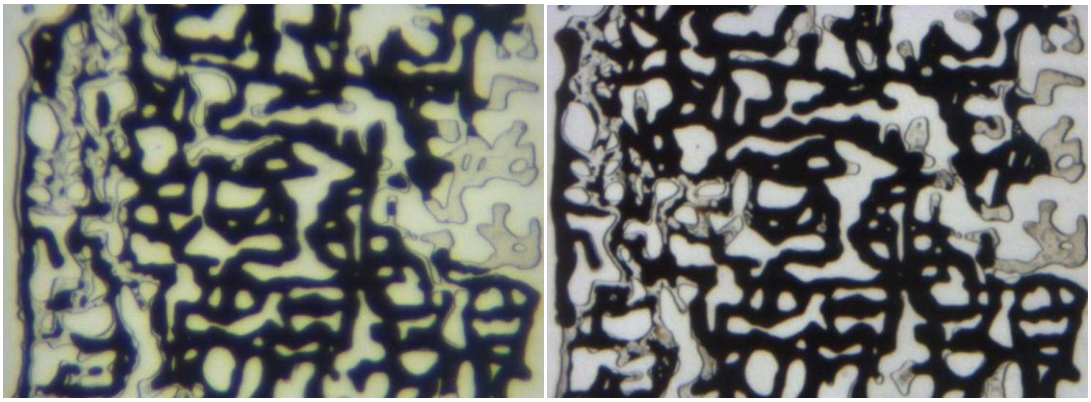

a **b**

Figure A-2: Fluid distribution in the magnified section of the micromodel after waterflood, (a) in MM Exp 8 and, (b) in this experiment (MM Exp 17).

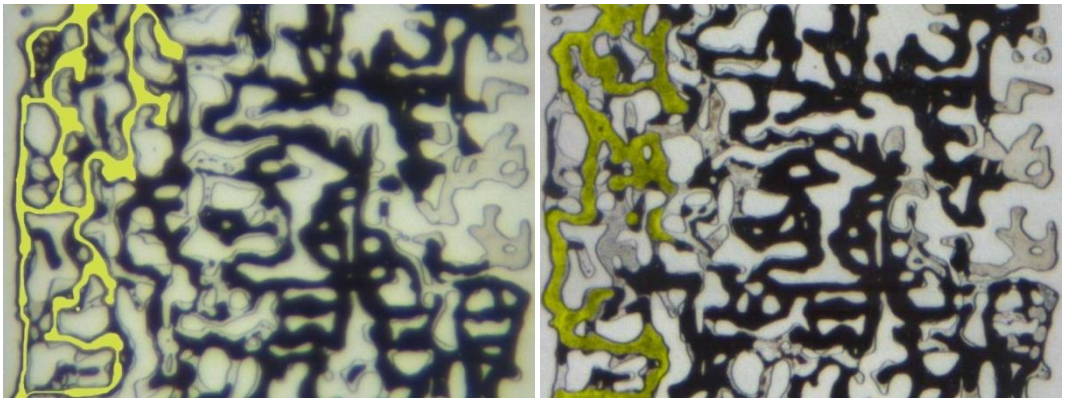

a **b**

Figure A-3: Fluid distribution in the magnified section of the micromodel after tertiary CO2 injection, (a) in MM Exp 8 and, (b) in this experiment (MM Exp 17).

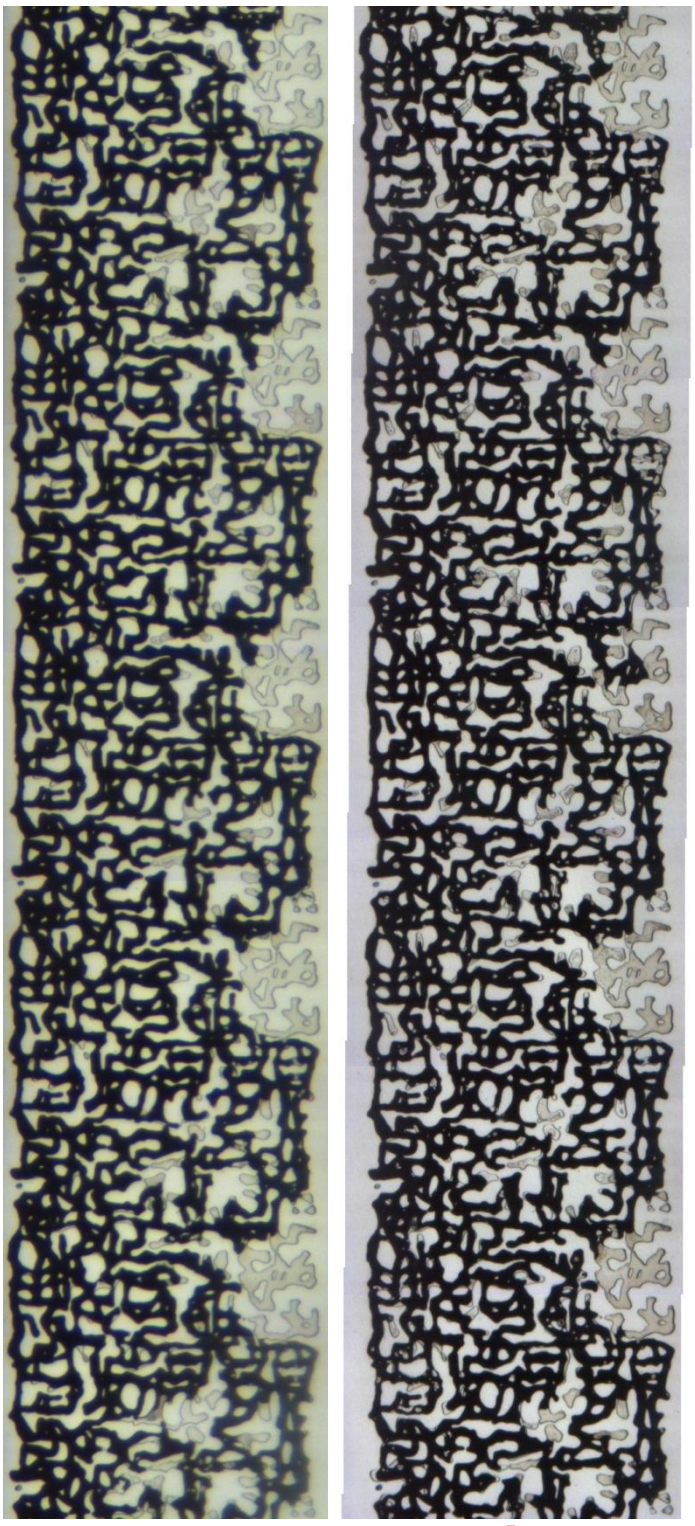

Figure A-4: Fluid distribution in the micromodel after oil injection, (a) in MM Exp 8 and, (b) in this experiment (MM Exp 17).

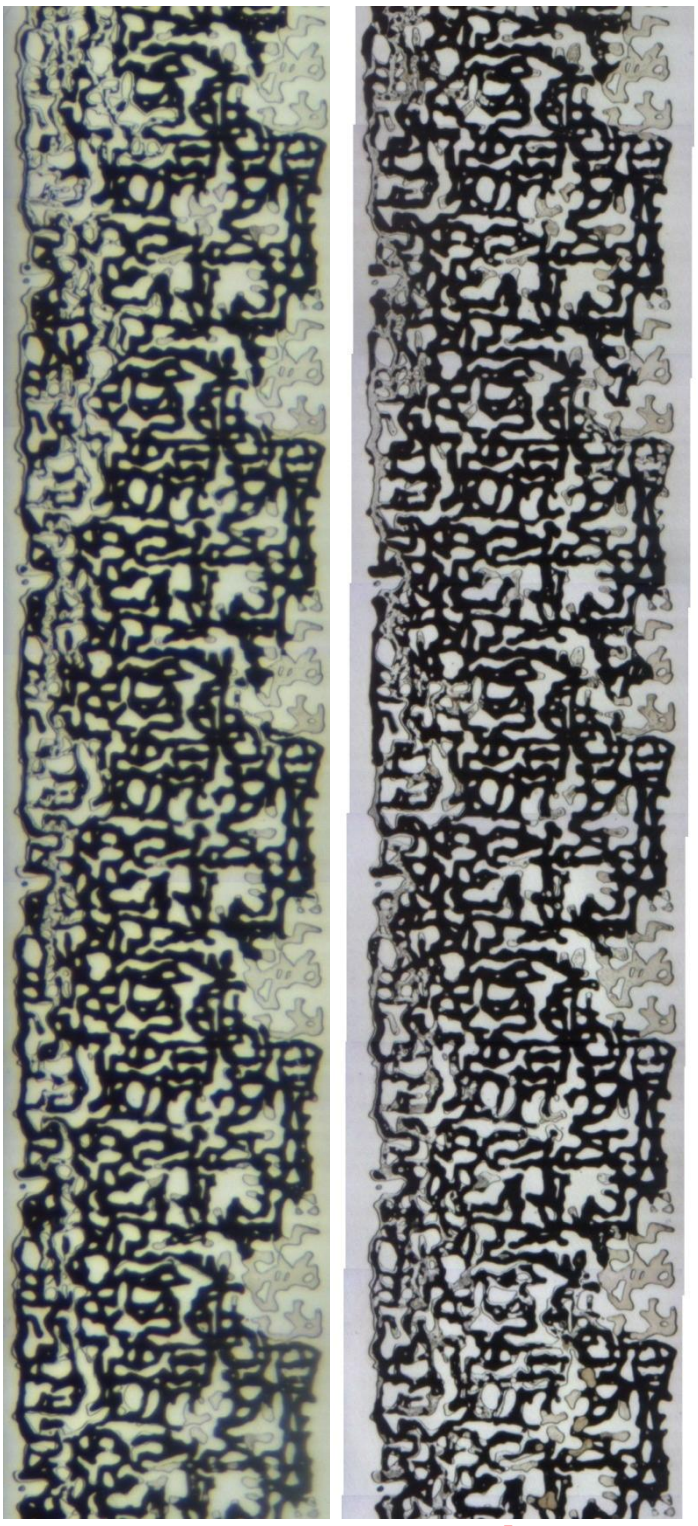

Figure A-5: Fluid distribution in the micromodel after waterflood, (a) in MM Exp 8 and, (b) in this experiment (MM Exp 17).

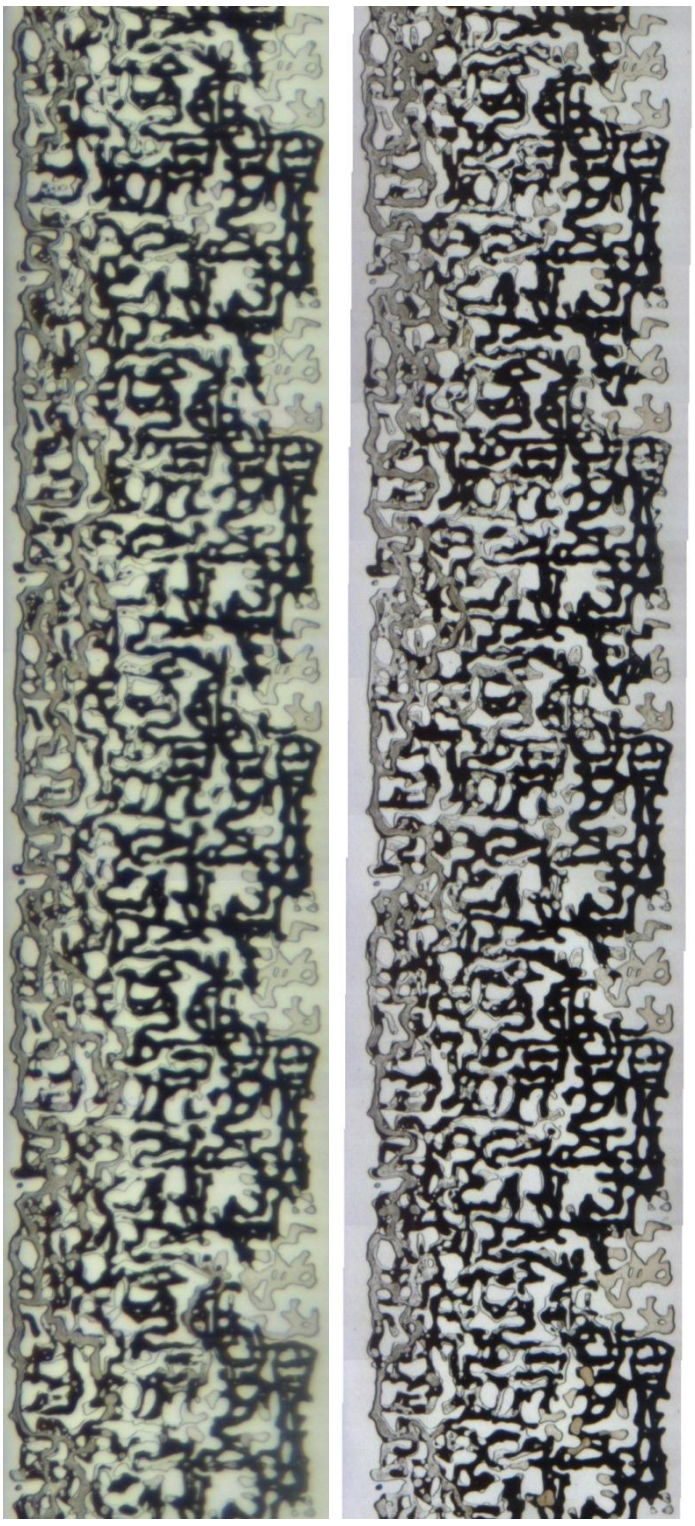

a **b**

Figure A-6: Fluid distribution in the micromodel after tertiary CO2 injection, (a) in MM Exp 8 and, (b) in this experiment (MM Exp 17).

A.2 MM EXP 18: REPLICATE OF MM EXP 11

In MM Exp 18 the reproducibility of the results during CO2-foam flood process in MM Exp 11 was investigated. The experiment was carried out using a procedure similar to MM Exp 11 with the only exception that initial waterflood period continued for a short time period (1 hour of waterflood in this experiment instead of 1 day waterflood in MM Exp 11). The fluids and pressure and temperature conditions were also remained the same as MM Exp 11.

Procedure and Conditions

1 *Initialization:* Micromodel was saturated with distilled water at T = 44 °C and P = 600 psig.

2 *Oil Flood:* Micromodel was flooded with crude oil "C" from bottom until the oil front reached the other end of the micromodel.

3 *Water Injection*: distilled water was injected in the micromodel for 1 hour.

4 *Surfactant Injection*: The chemical solution was injected in the micromodel for 3 hours.

5 *CO2/Surfactant Co-Injection*: CO2 and surfactant solution were simultaneously injected in the micromodel at rates of 0.001 cm^3/hr and 0.01 cm^3/hr , respectively, (total of 0.011 cc/hr) for 2 days.

Table A-3 lists a summary of the fluids used and the pressure and temperature at which the test was carried out.

Table A-3: Fluids used and pressure and temperature conditions of MM Exp 11.

Porous Medium	Heterogeneous Rock-look-alike Micromodel
Crude Oil	"C" (8700 cp @ 50 °C)
Aqueous Phase	Distilled Water
Gas Phase	CO2
Chemical Solution	0.3 wt% NEODOL 25-7
Temperature	44 °C
Pressure	600 psig

Results

The experiment began by saturating the micromodel with distilled water at 44 °C and 600 psig. To establish the initial saturation, crude oil C was then injected through the

micromodel. Figure A-7 and Figure A-14 respectively show a magnified section and the full length picture of the micromodel and compare the distribution of oil and connate water, in MM Exp 11 and in this experiment at the end of the oil injection period. It can be seen that , similar to MM Exp 11, very high oil saturation has been achieved due to the high viscosity contrast between oil and water.

Having established the initial oil and water saturation, water injection started and continued for 1 hour. The short period of waterflood was followed with surfactant injection for 3 hours. Figure A-8 and Figure A-15 respectively show the magnified section and the full length picture of the micromodel and compare distribution of fluids in MM Exp 11 and in this experiment (MM Exp 18) during the period of surfactant injection. The higher saturation of oil in MM Exp 18 is due to the shorter period of waterflood prior to surfactant injection in this experiment.

Having the micromodel saturated with surfactant solution, the period of CO2/surfactant co-injection started and continued for 2 days. Figure A-9 and Figure A-16 respectively show the magnified section and the full length picture of the micromodel and compare the fluids distribution in MM Exp 11 and in this experiment (MM Exp 18) at CO2 breakthrough time. At breakthrough time, CO2 opened a narrow flowing path on the left side of the micromodel. As injection continued and strong foam formed in the micromodel, initially the oil on the left side of the micromodel (high vertical connectivity region) was displaced by CO2-foam and then the foam was gradually developed towards the right side of the micromodel where most of the waterflood residual oil was located. The last stage was recovery of the oil in the dead end pores which took place very slowly through counter-current film flow mechanism. The sequence of pictures from Figure A-9 to Figure A-13 show the magnified section of the micromodel and compare the oil saturation in MM Exp 11 and this experiment at different times during the period of CO2/surfactant co-injection. The sequence of pictures from Figure A-16 to Figure A-20 also provides similar comparison between MM Exp 11 and MM Exp 18, however, using the full length pictures of the micromodel.

Summary

The comparison of the pictures of the micromodel in this experiment (MM Exp 18) and MM Exp 11 show very good match between the results in terms of mechanisms and

patterns of displacement. Table A-4 summarises the oil recovery data at different times during the period of CO2/surfactant co-injection in this experiment (MM Exp 18) and compares to the recovery data of MM Exp 11. The recovery data show very similar performance for CO2-foam injection in these two experiments.

Table A-4: Summary of the recovery data in MM Exp 18 and comparison to MM Exp 11.

	Recovery @ BT ($\%\ S_{orw}$)	Recovery 1 hour of CO2/Surf Inj ($\%\ S_{orw}$)	Recovery 10 hours of CO2/Surf Inj ($\%\ S_{orw}$)	Recovery 1 day of CO2/Surf Inj ($\%\ S_{orw}$)	Recovery 2 days of CO2/Surf Inj ($\%\ S_{orw}$)
MM Exp 18	7.5	20.7	57.3*	91.0*	97.6*
MM Exp 11	11.2	22.5	52.5*	88.6*	95.8*
• A swelling factor of 5.5% has been considered for calculation of oil recovery.					

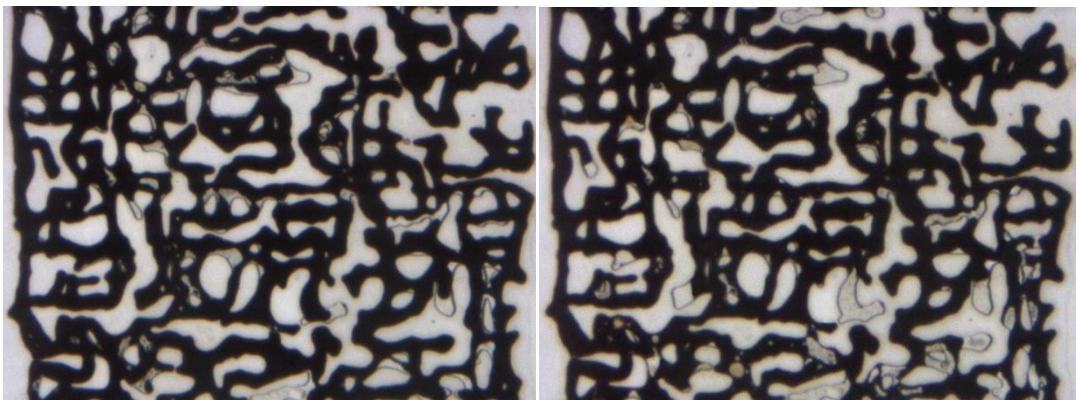

a **b**

Figure A-7: Fluid distribution in a magnified section of the micromodel after oil injection in, (a) MM Exp 11 and, (b) this experiment (MM Exp 18).

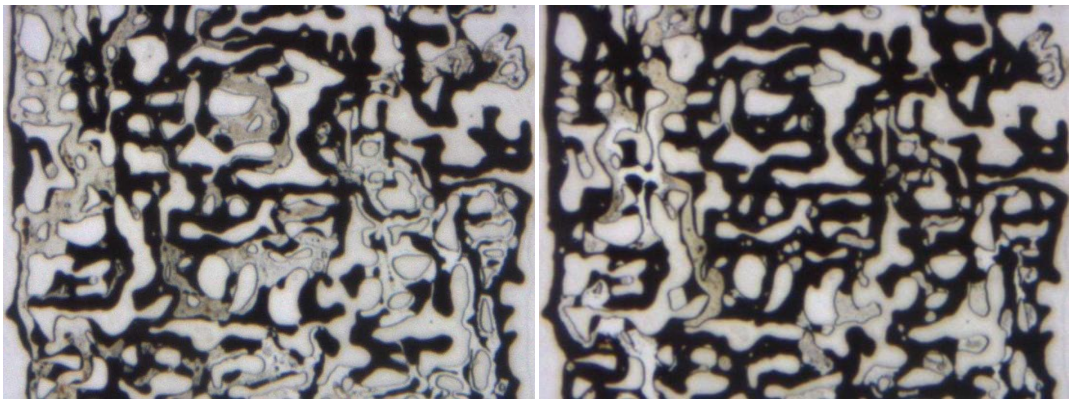

a **b**

Figure A-8: Fluid distribution in the magnified section of the micromodel after surfactant injection in, (a) MM Exp 11 and, (b) this experiment (MM Exp 18).

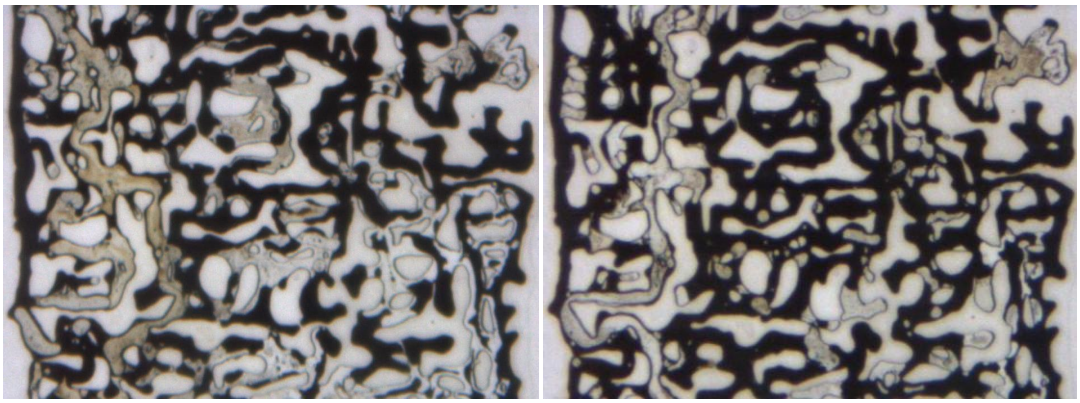

a **b**

Figure A-9: Fluid distribution in the magnified section of the micromodel at breakthrough time during the period of CO2/surfactant co-injection in, (a) MM Exp 11 and, (b) this experiment (MM Exp 18).

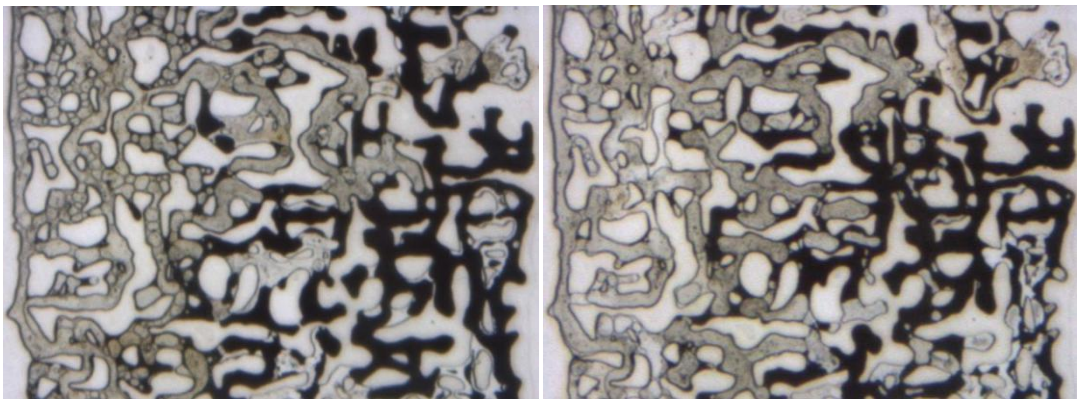

a **b**

Figure A-10: Fluid distribution in the magnified section of the micromodel after 2 hours of CO2/surfactant co-injection in, (a) MM Exp 11 and, (b) this experiment (MM Exp 18).

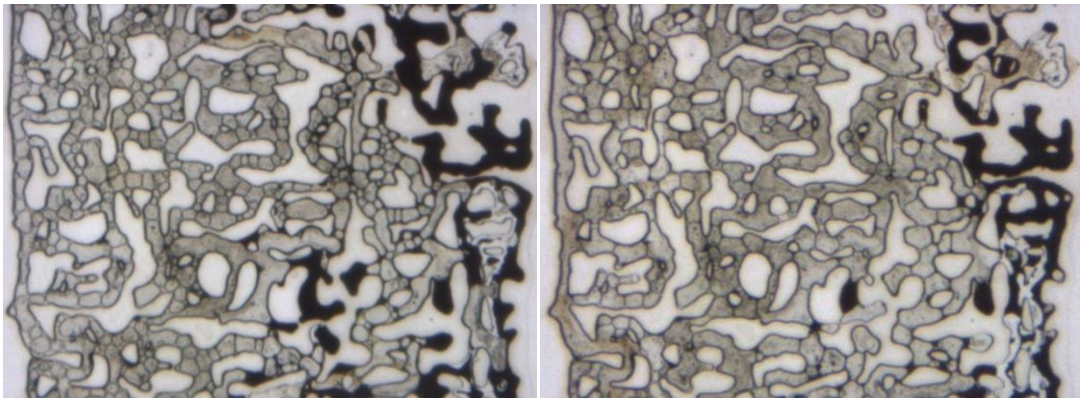

a **b**

Figure A-11: Fluid distribution in the magnified section of the micromodel 10 hours of CO2/surfactant co-injection in, (a) MM Exp 11 and, (b) this experiment (MM Exp 18).

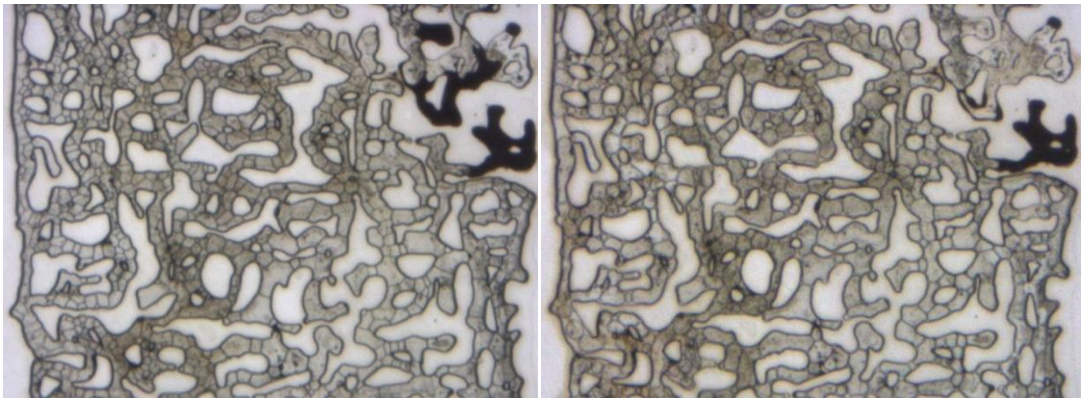

a **b**

Figure A-12: Fluid distribution in the magnified section of the micromodel after 1 day of CO2/surfactant co-injection, (a) in MM Exp 11 and, (b) in this experiment (MM Exp 18).

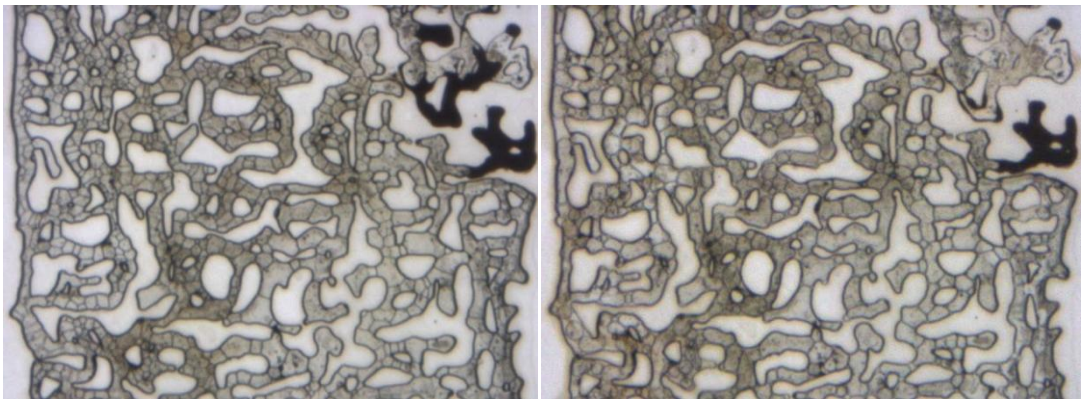

a **b**

Figure A-13: Fluid distribution in the magnified section of the micromodel after 2 days of CO2/surfactant co-injection in, (a) MM Exp 11 and, (b) this experiment (MM Exp 18).

a **b**

Figure A-14: Fluid distribution in the micromodel after oil injection, (a) in MM Exp 11 and, (b) in this experiment (MM Exp 18).

a **b**

Figure A-15: Fluid distribution in the micromodel after surfactant injection, (a) in MM Exp 11 and, (b) in this experiment (MM Exp 18).

a **b**

Figure A-16: Fluid distribution in the micromodel at breakthrough time during the period of CO2/surfactant co-injection, (a) in MM Exp 11 and, (b) in this experiment (MM Exp 18).

a **b**

Figure A-17: Fluid distribution in the micromodel after 2 hours of CO2/surfactant co-injection, (a) in MM Exp 11 and, (b) in this experiment (MM Exp 18).

a **b**

Figure A-18: Fluid distribution in the micromodel after 10 hours of CO2/surfactant co-injection, (a) in MM Exp 11 and, (b) in this experiment (MM Exp 18).

Figure A-19: Fluid distribution in the micromodel after 1 day of CO2/surfactant co-injection, (a) in MM Exp 11 and, (b) in this experiment (MM Exp 18).

Figure A-20: Fluid distribution in the micromodel after 2 days of CO2/surfactant co-injection, (a) in MM Exp 11 and, (b) in this experiment (MM Exp 18).

APPENDIX B: RELATIVE PERMEABILITY CALCULATIONS

The main objective of the coreflood experiments reported in this thesis was to quantitatively evaluate potential of different processes and develop new techniques to improve recovery of two specific heavy crude oil samples. However, as was explained in the introduction chapter (Figure 1-1), the coreflood data are also used to extract the relative permeability data for up-scaling and field simulation purposes. In "Enhanced Heavy Oil Recovery JIP" this part of the work has been assigned to other members of the group[1] and reported in the project steering meetings (Sohrabi et al., 2010). It should be noted that among coreflood experiments reported in this thesis only the waterflood experiments can be used for estimation of relative permeability data. Since CO2 and oil were not pre-equilibrated there was significant mass transfer during displacement of oil by CO2, therefore the relative permeability curves cannot be drawn from the pressure and recovery data of such experiments.

The results of two core flood experiments (Core Exp 4 and Core Exp 6) were used to obtain relative permeability (kr) data of waterflood process in crude "C" and crude "J". Sendra, a two phase coreflood simulator, was used to determine relative permeability curves by history matching the production and differential pressure data of water flood experiments. Sendra is based on a 1D black oil simulation model to history match the core flood experimental data. The unknown relative permeability curve is approximated by a mathematical function (e.g. Corey, Burdine, etc) with end-point relative permeability and exponents as history matching parameters. This history matching is an

[1] Mr Olufemi Saliu performed the relative permeability calculations for the tests reported here.

optimization process, where the difference between the simulation results and the experimental data is minimised (Sohrabi et al., 2010).

B.1 MODEL DESCRIPTION AND PVT DATA

A 1-D model was constructed in Sendra which consisted of a single well producer and an injector with 100x1x1. In a grid sensitivity exercise it was confirmed that the results are independent of grid size (Sohrabi et al., 2010). The model parameters are similar to the properties of the silica-sand core used in this study (Table 3-2). The PVT data of crude oil samples were prepared by fluid characterization experiments explained in Chapter 3 of this thesis and the PVT data for brine and CO2 were taken from "Fluid Thermodynamic and Transport Properties Database" (National Institute of Standards and Technology, 2011). Table B-1 lists the PVT data used in this Model.

Table B-1: The PVT data used in the Sendra model.

Fluid	P (psig)	T (ºC)	ρ (gr/cm^3)	μ (cp)	B (rcc/scc)
Crude "C"	600	50	0.9692	8700	1
Crude "J"	1500	28	0.9459	617	1.03
Brine	600	50	0.9898	0.5476	1.00
Brine	1500	28	1.0008	0.8312	1.02
CO2	600	50	0.0822	0.0169	0.0024
CO2	1500	28	0.7976	0.0703	0.0192

B.2 RESULTS

The history match results for the secondary waterflood processes of crude "C" and crude "J" are respectively shown in Figure B-1 and Figure B-2 and the corresponding relative permeability curves are shown in Figure B-3 and Figure B-4.

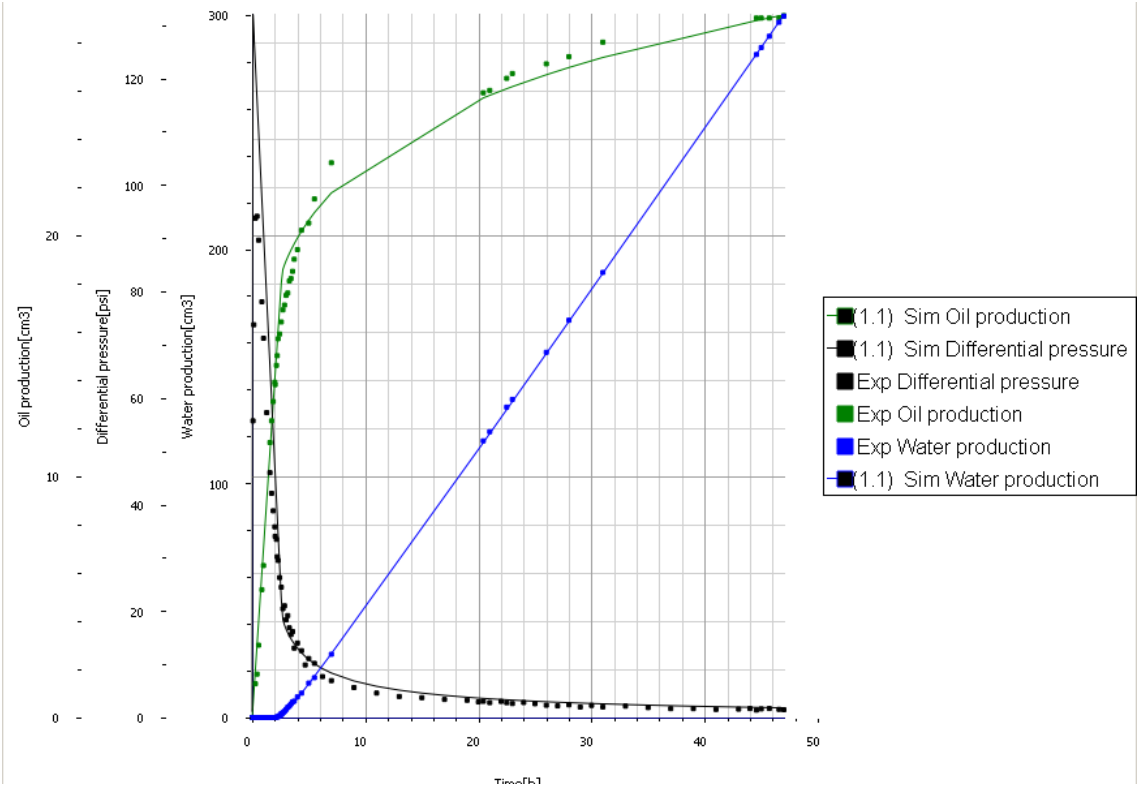

Figure B-1: Experimental and simulated recovery and pressure data of the waterflood process in crude "C" (Sohrabi et al., 2010).

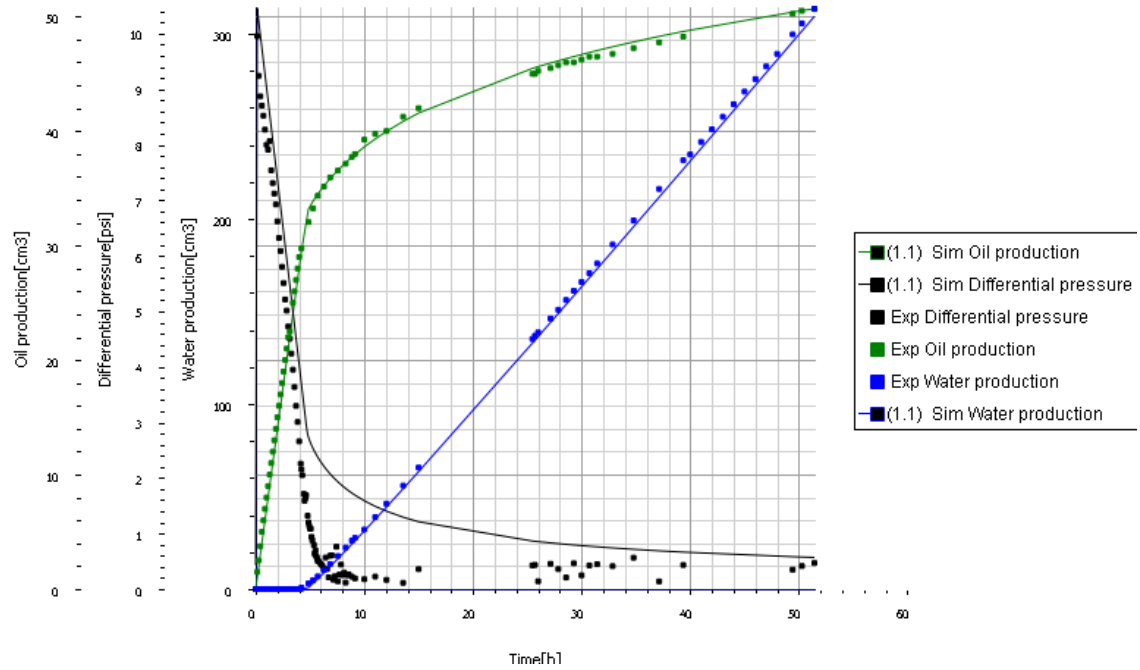

Figure B-2: Experimental and simulated recovery and pressure data of the waterflood process in crude "J" (Sohrabi et al., 2010).

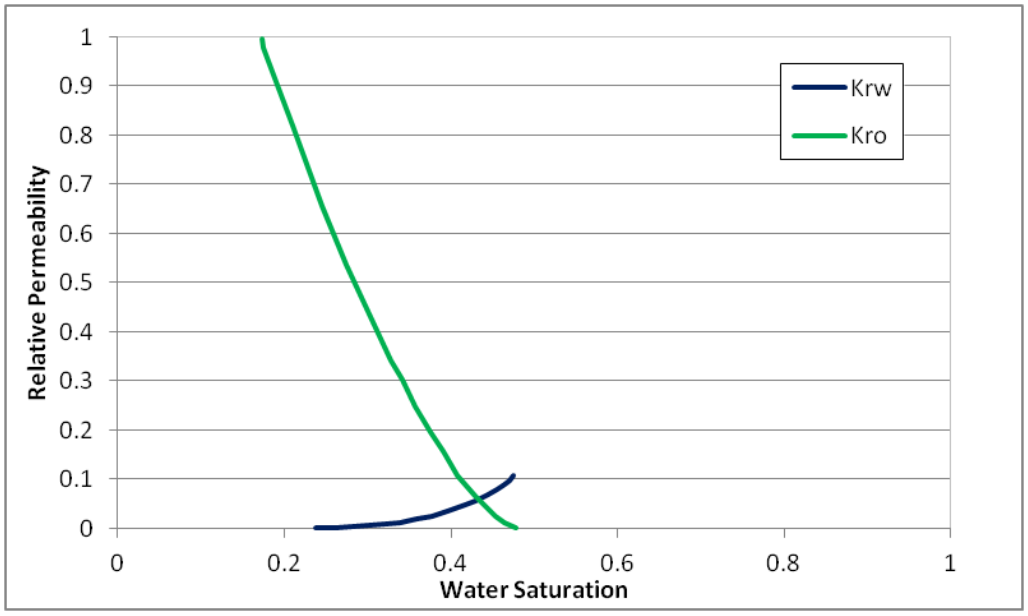

Figure B-3: Sendra-generated relative permeability curves for crude "C" and water (Sohrabi et al., 2010).

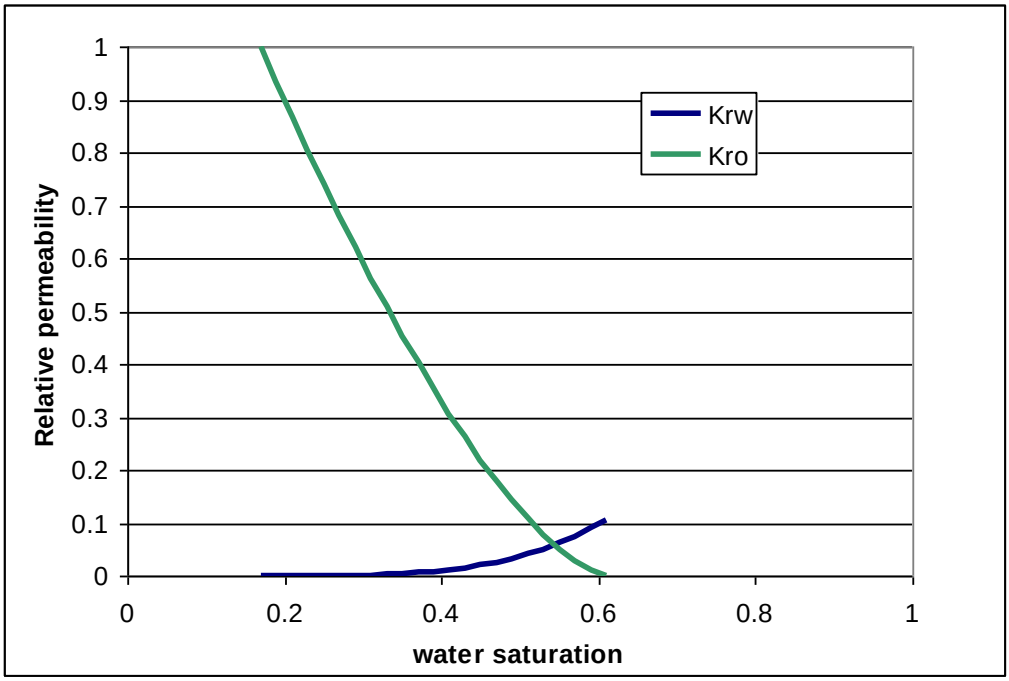

Figure B-4: Sendra-generated relative permeability curves for crude "J" and water (Sohrabi et al., 2010).

B.3 DISCUSSIONS

The relative permeability curves drawn from the recovery and pressure data during the period of waterflood in crude "C" and crude "J" show very high Kro at low water saturation and low Krw values at water saturations as high as 0.5 and 0.6. This trend which is a typical behaviour in heavy oil systems is believed to be due to the high

viscosity difference between oil and water. Generally there are two approaches regarding the impact of oil viscosity on oil/water relative permeability. First one is that the relative permeabilities are independent from the fluids viscosity; therefore the measured values for light oil systems can be applied to heavy oil systems. This approach is supported by experimental data provided by Geffen et al. (1951), Richardson (1957) and Sandberg et al (1958). However, the experimental results which support this approach do not include wide range of oil/water viscosity ratios. More recent experimental results show that the relative permeabilities might be affected by change in oil viscosity.

The results reported by Odeh (1959) and Danis and Jacquin (1983)) showed that the oil relative permeability can be very high at low water saturation and oil effective permeability shows an increasing trend with increasing oil/water viscosity ratio. This is due to the lubricating effect of the water film on pore surface as was experimentally observed by Templeton and Rushing (1956).

The variation of residual oil and irreducible water saturation with increasing oil viscosity also reveals the influence of fluid viscosity on relative permeabilities. Abrams (1975) conducted waterflood experiments on sandstone and limestone cores and his results showed residual oil saturation is larger for a higher oil/water viscosity ratio. Tzimas et al. (1997) studied the role of viscosity ratio during forced imbibitions in porous media using tow layered glass micromodels. The results indicated that for the same capillary number the residual oil saturation increases with increasing oil viscosity.

Lo and Mugan (1973) measured oil water relative permeability using the steady state technique. Their results showed that that with increasing in temperature residual oil saturation decreased, irreducible water saturation increased, and oil relative permeability increased. They attributed the change in oil relative permeability to the variation of oil viscosity and viscosity ratio.

The investigation by Wang et al. (2006) on heavy oil with viscosity ranging from 430 - 13,550 cp, showed that The results show that the increase in oil viscosity can systematically change the relative permeability curves. As oil viscosity increased, the relative permeability to water and oil decreased and that this decrease is greater at higher saturations. The effective oil permeability at irreducible water saturation was

greater than the absolute permeability measured by single water phase which was attributed to lubricating effect. The irreducible water saturation decreased and the residual oil saturation increased as the viscosity increased. The variation of irreducible water saturation with increasing oil viscosity was similar to that of Lo and Mugan (1973). It was also noted that the increase in residual oil saturation was linear with a logarithmic value of oil viscosity.

It should be noted that since the period of waterflood continued for a short time period (2 PV's) in both experiments the recovery and pressure data cover a short range of water and oil saturation in the relative permeability curve. As a result, the estimation of the water and oil end points are not accurate in Figure B-3 and Figure B-4 and need to be measured using specifically designed experiments with extended periods of waterflood to measure the end point saturations and the relative permeabilities.

REFERENCES

ABRAMS, A., 1975. Influence of Fluid Viscosity, Interfacial Tension, and Flow Velocity on Residual Oil Saturation Left by Waterflood. *SPE Journal*, **Vol 15**.

ADAMSON, A.W., 1960. Physical Chemistry of Surfaces. New York, Interscience.

AHMADLOO, F., ASGHARI, K. and RENOUF, G., 2010. Performance Prediction of Waterflooding in Western Canadian Heavy Oil Reservoirs Using Artificial Neural Network. *Energy & Fuels*, **Vol. 24**.

ALBOUDWAREJ, H., FELIX, J., TAYLOR, S., BAKER, A., PALMER, D., PATTISON, K., BESHRY, M., KRAWCHUK, P., BROWN, B., CALVO, R. and TRIANA, J.A.C., 2006. Highlighting Heavy Oil. *Oilfield Review*, **Vol. 18,** 34-53.

AMOTT, E., 1959. Observations Relating to the Wettability of Porous Rock *Petroleum Transactions*, **Vol 216,** 156-162.

ANDERSON, W.G., 1987. Wettability Literature Survey - Part 6: The Effects of Wettability on Waterflooding. *Journal of Petroleum Technology*, **Vol. 39**.

BELIVEAU, D., 2009. Waterflooding Viscous Oil Reservoirs. *SPE Reservoir Evaluation & Engineering*, **Vol 12**.

BOBERG, T.C., 1988. Thermal Methods of Oil Recovery. Wiley.

BRICE, B.W. and RENOUF, G., 2008. Increasing Oil Recovery from Heavy Oil Waterfloods. In: SPE/PS/CHOA International Operations and Heavy Oil Recovery.

BURGER, J., SOURIEAU, P. and COMBARNOUS, M., 1985. Thermal Methods of Oil Recovery. Paris, Technip.

CENTURY, J.R., 2008. Tar Sands: Key Geological Risks and Opportunities. *The Leading Edge*, **27,** 1202-1204.

CHAMBERS, K.T. and RADKE, C.J., 1990. Capillary Phenomena In Foam Flow Through Porous Media. In: MORROW, N.R.s (Ed.): Interfacial Phenomena in Oil Recovery. *Surfactant Science Series*, 191-256.

CHATZIS, I., MORROW, N.R. and LIM, H.T., 1983. Magnitude and Detailes Structure of Residual Oil Saturation. *Society of Petroleum Engineers Journal*, **Vol 23**.

CHEN, M., YORTSOS, Y.C. and ROSSEN, W.R., 2006. Pore-Network Study of the Mechanisms of Foam Generation In Porous Media. *Physical Review E*, **vol. 73,** 181-189.

CLARK, B., GRAVES, G., LOPEZ-DE-CARDENAS, J.E., GURFINKEL, M.E. and PEATS, A.W., 2007. Heavy oil, Extra-Heavy Oil and Bitumen - Unconventional Oil. In: CLARK, B.s (Ed.): Facing the Hard Truth about Energy.

CRAIG, F.F., 1971. The reservoir engineering aspects of waterflooding. New Tork, Society of Petroelum Engineers.

CUPCIC, F., 2003. Extra Heavy Oil and Bitument, Impact of Technologies on Recovery Factor - The challenges of Enhanced Recovery. In: Association for the Study of Peak Oi and Gas (ASPO) Annual Meeting.

DANIS, M. and JACQUIN, C., 1983. Influence du Contraste de Viscosités sur les Perméabilités Relatives lors du Drainage. Expérimentation et Modélisation. *Revue de l'Institut Français du Pétrole*, **Vol 38**.

DOE, 2006. U.S. Heavy Oil Resources Potential. *DOE Fact Sheet*.

DONALDSON, E.C. and THOMAS, R.D., 1971. Microscopic Observations of Oil Displacement in Water-Wet and Oil-Wet Systems. In: Fall Meeting of the Society of Petroleum Engineers of AIME.

DULLIEN, F.A.L., 1992. Porous Media, Fluid Transport and Pore Structure. New York, Academic Press.

FALLS, A.H., HIRASAKI, G.J., PATZEK, T.W., GAUGLITZ, D.A., MILLER, D.D. and RATULOWSKI, T., 1988. Development of a Mechanistic Foam Simulator: The Population Balance and Generation by Snap-off. *SPE Reservoir Engineering*, **Vol. 3**.

FULOP, R., BIRO, Z., GOMBOS, Z., PAPAY, J. and TRAMBOCZKY, S., 1997. Enhanced Oil Recovery by CO2 Flooding. In: 15th World Petroleum Congress.

GOYAL, K.L. and KUMAR, S., 1989. Steamflooding for Enhanced Oil Recovery. In: DONALDSON, E.C., CHILINGARIAN, G.V. and YEN, T.F.s (Eds.): Enhanced Oil Recovery: Processes and Operations. *Developments in Petroleum Science*.

GREEN, D.W. and WILLHITE, G.P., 1986. Enhanced Oil Recovery. Society of Petroleum Engineers.

HIRASAKI, G. and ZHANG, D.L., 2004. Surface Chemistry of Oil Recovery from Fractured, Oil-Wet, Carbonated Formations. *SPE Journal*, **Vol. 9**.

HIRASAKI, G.J., 1991. Wettability: Fundamentals and Surface Forces. *SPE Formation Evaluation*, **Vol 6**.

HOLM, L.W. and JOSENDAL, V.A., 1982. Effect of Oil Composition on Miscible-Type Displacement by Carbon Dioxide *SPE Journal*, **Vol 22**.

ISSEVER, K. and TOPKAYA, I., 1998. Use of Carbon Dioxide to Enhanced Heavy Oil Recovery. In: 7th UNITAR International Conferenceon Heavy Crude and Tar Sands.

JADHUNANDAN, P.P. and MORROW, N.R., 1995. Effect of Wettability on Waterflood Recovery for Crude-Oil/Brine/Rock Systems. *SPE Reservoir Engineering*, **Vol 10,** 40-46.

JENNING, H.Y., 1965. Waterflood Behaviour of High Viscosity Crude in Preserved Soft and Unconsolidated Cores. *Annual Society of Petroleum Engineers of AIME fall meeting*. Denver, CO, USA.

JIMENEZ, A.I. and RADKE, C.J., 1989. Dynamic Stability of Foam Lamellae Flowing Through a Periodically Constricted Pore. Washington DC, American Chemical Society.

KENNEDY, H.T., BURJA, E.O. and BOYKIN, R.S., 1955. An Investigation of the Effects of Wettability on Oil Recovery by Water flooding. *The Journal of Physical Chemistry*, **59,** 867-869.

KHATIB, A.K., EARLOUGHER, R.C., GODSEY-EARLOUGHER and KANTAR, K., 1981. CO2 Injection as an Immiscible Application for Enhanced Recovery in Heavy Oil Reservoirs. In: SPE California Regional Meeting.

KLINS, M.A., 1984. Carbon Dioxide Flooding: Basic Mechanisms and Project Design. D. Reidel Publishing Company.

KLINS, M.A. and BARDON, C.P., 1991. Carbon Dioxide Flooding. In: BAVIERE, M.s (Ed.): Basic Concepts in Enhanced Oil Recovery Process.

KOVSCEK, A.R., 2002. Screening Criteria for CO2 Storage in Oil Reservoir. *Petroleum Science and Technology*, **Vol 20**.

KUHLMAN, M.I., 1990. Visualizing the Effect of Light Oil on CO2 Foams. *Journal of Petroleum Technology*, **SPE 17356, vol. 42,** 902-908.

KULHMAN, M.I., FALLS, A.H. and WELLINGTON, S.L., 1994. Gas/Oil Lamellae and Surfactant Propagation in Carbon Dioxide Foam. *SPE 27788, SPE/DOE Improved Oil Recovery Symposium*. Tulsa, OK, USA.

KUMAR, M., HOANG, V.T., SATIK, C. and ROJAS, D.H., 2008. High-Mobility-Ratio Waterflood Performance Prediction: Challenges and New Insights. *SPE Reservoir Evaluation & Engineering*, **Vol. 11**.

KYTE, J.R., NAUMANN, V.O. and MATTAX, C.C., 1961. Effect of Reservoir Environment on Water-Oil Displacements *Journal of Petroleum Technology*, **Vol 13**.

LATIL, M., 1980. Enhanced Oil Recovery. Paris, France, Technip.

LEFEBVRE DU PREY, E.J., 1973. Factors Affecting Liquid-Liquid Relative Permeabilities of a Consolidated Porous Medium *SPE Journal*, **Vol 13**.

LI, Y. and WARDLAW, N.C., 1985a. The Influence of Wettability and Critical Pore-Throat Size Ratio on Snap-off. *Journal of Colloid and Interface Science*, **Vol. 109,** 461-472.

LI, Y. and WARDLAW, N.C., 1985b. Mechanism of Nonwetting Phase Trapping during Imbibition at Slow Rates. *Journal of Colloid and Interface Science*, **vol. 109,** 473-486.

LO, H.Y. and MUNGAN, N., 1973. Effect of Temperature on Water-Oil Relative Permeabilities in Oil-Wet and Water-Wet Systems. In.

LORENZ, P.B., DONALDSON, E.C. and THOMAS, R.D., 1974. Use of Centrifugal Measurments of Wettability to Predict Oil Recovery. In.

MAI, A. and KANTZAS, A., 2008. Mechanisms Heavy Oil Recovery by Low Rate Waterflooding. *Canadian International Petroleum Conference*. Calgary, Alberta, Canada.

MAI, A. and KANTZAS, A., 2009a. Heavy Oil Waterflooding: Effect of Flow Rate and Oil Viscosity. *Journal of Canadian Petroleum Technology*, **Vol. 48**.

MAI, A. and KANTZAS, A., 2009b. Insights Into Non-Thermal Recovery of Heavy Oil Reservoirs. *Journal of Canadian Petroleum Technology*, **Vol. 48**.

MAI, A. and KANTZAS, A., 2010. Mechanisms of Heavy Oil Recovery by Low Rate Waterflooding. *Journal of Canadian Petroleum Technology*, **Vol. 49,** 44-50.

MAINI, B.B., SARMA, H.K. and GEORGE, A.E., 1993. Significance of Foamy-oil Behaviour In Primary Production of Heavy Oils. *Journal of Canadian Petroleum Technology*, **Vol. 32**.

MANLOWE, D.J. and RADKE, C.J., 1990. A Pore-Level Investigation of Foam/Oil Interactions in Porous Media. *SPE Reservoir Engineering*, **SPE 18069, vol. 5** 495-502.

MARTINEZ, A.R., DESORCY, G.J., DEKKER, H., SMITH, S. and ION, D.C., 1987. Classification and Nomenclature Systems for Petroleum and Petroleum and Petroleum Reserves In: 12th World Petroleum Congress.

MATTHEWS, C.S., 1989. Carbon Dioxide Flooding. In: DONALDSON, E.C., CHILINGARIAN, G.V. and YEN, T.F.s (Eds.): Enhanced Oil Recovery: Processes and Operations. *Developments in Petroleum Science*.

MAYER, E.H., EARLOUGHER SR., R.C. and SPIVAK, A., 1988. Analysis of Heavy-Oil Immiscible CO2 Tertiary Coreflood Data. *SPE Reservoir Engineering*, **Vol 3**.

MILLER, J.S., 1981. A laboratory Study to Determine Physical Characteristics of Heavy Oil After CO2 Saturation. In: SPE/DOE Second Joint Symposium on Enhanced Oil Recovery.

MILLER, J.S. and JONES, R.A., 1981. A Laboratory Study to Determine Physical Characteristics of Heavy Oil after CO2 Saturation, In: SPE/DOE Enhanced Oil Recovery Symposium.

MILLER, K.A., 2006. Improving the State of the Art of Western Canadian Heavy Oil Waterflood Technology. *Journal of Canadian Petroleum Technology*, **Vol. 45**.

MOFFITT, P.D. and ZORNES, D.R., 1992. Postmortem Analysis: Lick Creek Meakin Sand Unit Immiscible CO2 Waterflood Project In: SPE Annual Technical Conference and Exhibition.

MOORE, T.F. and SLOBOD, R.L., 1956. Displacement of Oil by Water-effect of Wettability, Rate, and Viscosity on Recovery. In: 30th Fall Meeting of the Petroleum Branch of the American Institute of Mining and Metallurgical Engineers.

MORROW, N.R., 1990. Wettability and Its Effect on Oil Recovery. *Journal of Petroleum Technology*, **Vol 42**.

MORROW, N.R., 1991. Introduction to Interfacial Phenomena in Oil Recovery. In: MORROW, N.R.s (Ed.): Interfacial Phenomena in Petroleum Rrecovery. Vol. 36 of Surfactant Science Series.

MORROW, N.R. and HELLER, J.P., 1985. Fundamentals of Enhanced Recovery. In: DONALDSON, E.C., CHILINGARIAN, G.V. and YEN, T.F.s (Eds.): Enhanced Oil Recovery, I: Fundamentals and Analysis.

MORROW, N.R. and MCCAFFERY, F.G., 1978. Displacement Studies in Uniformly Wetted Porous Media. In: PADDAY, G.F.s (Ed.): Wetting, Spreading, and Adhesion. 289-319.

MUNGAN, N., 1966. Interfacial Effects in Immiscible Liquid-Liquid Displacement in Porous Media *SPE Journal*, **Vol 6**.

NATIONAL INSTITUTE OF STANDARDS AND TECHNOLOGY, 2011. Fluid Thermodynamic and Transport Properties Database (REFPROP) In.

NEWCOMBE, J., MCGHEE, J. and RZASA, M.J., 1955. Wettability Versus Displacement in Water Flooding in Unconsolidated Sand Columns. *Petroleum Transactions, AIME*, **Vol 204**.

NGUYEN, Q.P., ALEXANDROV, A.V., ZITHA, P.L. and CURRIE, P.K., 2000. Experimental and Modeling Studies on Foam in Porous Media A Review. *SPE International Symposium on Formation Damage Control*. USA.

ODEH, A.S., 1959. Effect of Viscosity Ratio on Relative Permeability. *Petroleum Transactions, AIME*, **Vol 216**.

OECD/IEA, 2005. Resources to Reserves - Oil and Gas Technologies for the Energy Markets of the Future. In.

OLAH, G.A. and MOLNAR, A., 2003. Hydrocarbon Chemistry. Wiley-Interscience.

OREN, P.E., 1994. Pore-Scale Network Modelling of Waterflood Residual oil Recovery by Immiscible Gas Flooding. In: SPE/DOE Ninth Symposium on Oil Recovery.

OREN, P.E., BILLIOTTE, J. and PINCZEWSKI, W.V., 1992. Mobilization of Waterflood Residual Oil by Gas Injection for Water-Wet Conditions *SPE Formation Evaluation*, **Vol 7**.

OREN, P.E., 1994. Pore-Scale Network Modelling of Waterflood Residual Oil Recovery by Immiscible Gas Flooding. In: Ninth Symposium on Improved Oil Recovery.

OREN, P.E. and PINCZEWSKI, W.V., 1994. The Effect of Wettability and Spreading Coefficients on the Recovery of Waterflood Residual Oil by Miscible Gasflooding. *SPE Formation Evaluation*, **Vol 9**.

PLOUCHARD, G., 2001. Évaluation des Émissions de CO2 Des Filières Énergétiques Conventionnelles et Non Conventionnelles de Production de Carburants À Partir des Ressources Fossiles. In., K2300083.

RENOUF, G., 2007. Do Heavy and Medium Oil Waterfoods Differ? In: Petroleum Society's 8th Canadian International Petroleum Conference.

RIAZI, M., SOHRABI, M., BERNSTONE, C., JAMIOLAHMADY, M. and IRELAND, S., 2011. Visualisation of mechanisms involved in Co2 injection and storage in hydrocarbon reservoirsand water-bearing aquifers. *Chemical Engineering Research and Design*, **Vol 89,** 1827-1840.

RICHARD F. MEYER and ATTANASI, E.D., 2003. Heavy Oil and Natural Bitumen - Strategic Petroleum Resources. *USGS Fact Sheet*.

RICHARDSON, J.G., 1957. The Calculation of Waterflood Recoveryfrom Steady-StateRelative Permeability Data. *Journal of Petroleum Technology*, **Vol 9**.

ROBINSON, D.B., 1984. The Thermodynamic and Transport Properties of Bitumens Heavy Oils. Edmonton, Alberta Oil Sands Technology and Research Authority.

ROMM, J.J., 2006. Hell and High Water: The Global Warming Solution. HarperCollins.

ROOF, J.G., 1970. Snap-Off of Oil Droplets in Water-Wer Pores. *SPE Journal*, **Vol. 10**.

ROSE, W. and WITHERSPOON, P.A., 1956. Studies of Waterflood Performance; II. Trapping Oil in a Pore Doublet. In: FRYE, J.C.s (Ed.): Illinois State Geological Survey.

ROSSEN, W.R., 1995. Foams in Enhanced Oil Recovery. In: PRUD'HOMME, R.K. and KHAN, S.A.s (Eds.): Foams: theory, measurements, and applications. 596.

SAHIMI, M., 1995. Flow and Transport in Porous Media and Fractured Rock. Amsterdam, The Netherlands, Elsevier.

SAHOO, P., 2005. Engineering Tribology. PHI Learning Pvt. Ltd.

SALATHIEL, R.A., 1973. Oil Recovery by Surface Film Drainage In Mixed-Wettability Rocks *Journal of Petroleum Technology*, **Vol 25**.

SANDBERG, C.R., GOURNAY, L.S. and SIPPEL, R.F., 1958. The Effect of Fluid-Flow Rate and Viscosity on Laboratory Determinations of Oil-Water Relative Permeabilities. *Petroleum Transactions, AIME,* **Vol 213**.

SANER, W.B. and PATTON, J.T., 1986. CO2 Recovery of Heavy Oil: Wilmington Field Test *Journal of Petroleum Technology,* **Vol. 38**.

SANIERE, A., HENAUT, I. and ARGILLIER, J., F., 2004. Pipeline Transportation of Heavy Oils, a Strategic, Economic and Technological Challenge *Oil & Gas Science and Technology*, **Vol 59,** 455-466.

SANKUR, V. and EMANUEL, A.S., 1983. A laboratory Study of Heavy Oil Recovery with CO2Injection. In: California Regional Meeting

SCHRAMM, L.L. and NOVASAD, J.J., 1990. Micro-Visualization of Foam Interactions with a Crude Oil. *Colloids and Surfaces*, **vol. 46,** 21-43

SCHRAMM, L.L., 1992. The Destabilization of Foams for Improved Oil Recovery by Crude Oils : Effect of the Nature of the Oil. *Journal of petroleum science & engineering* **vol. 7,** 77-90

SCHRAMM, L.L., TURTA, T. and NOVASAD, J.J., 1993. Microvisual and Coreflooding Studies of Foam Interactions with a Light Crude Oil. *SPE Reservoir Engineering*, **SPE 20197, vol. 8** 201-206

SKAUGE, A., AARRA, M.G., SURGUCHEV, L., MARTINSEN, H.A. and RASMUSSEN, L., 2002. Foam-Assisted WAG: Experience from the Snorre Field. In: SPE/DOE Improved Oil Recovery Symposium.

SOHRABI, M., DANESH, A. and MAHMOUD, J., 2008a. Visualisation of Residual Oil Recovery by Near-miscible Gas and SWAG Injection Using High-pressure Micromodels. *Transport in porous media,* **Vol 74,** 239-257.

SOHRABI, M., EMADI, A., JAMIOLAHMADY, M., IRELAND, S. and BROWN, C., 2008b. Mechanisms of Extra-Heavy Oil Recovery by Gravity-Stable CO2 Injection. *International Symposium of the Society of Core Analysts*, 12. Abu Dhabi, UAE.

SOHRABI, M., EMADI, A., SALIU, O. and FARZANEH, A., 2010. Enhanced Heavy Oil Recovery, Phase II, December 2010. In: SOHRABI, M. and JAMI, M.s (Eds.): Enhanced Heavy Oil Recovery

SOHRABI, M., HENDERSON, G.D., TEHRANI, D.H. and DANESH, A., 2000a. Visualisation of Oil Recovery by Water Alternating Gas (WAG) Injection Using High Pressure Micromodels - Water-Wet System. *SPE Annual Technical Conference and Exhibition*. Dallas, Texas, USA.

SOHRABI, M., TEHRANI, D.H., DANESH, A. and HENDERSON, G.D., 2001. Visualisation of Oil Recovery by Water Alternating Gas (WAG) Injection Using High Pressure Micromodels - Oil-Wet & Mixed-Wet Systems. *SPE Annual Technical Conference and Exhibition*. New Orleans, Louisiana, USA.

SOHRABI, M., TEHRANI, D.H., DANESH, A. and HENDERSON, G.D., 2004. Visualisation of Oil Recovery by Water Alternating Gas (WAG) Injection Using High Pressure Micromodels. *SPE Journal*, **Vol 9**.

SOHRABI, M., TEHRANI, D.H., DANESH, A. and MAHMOUD, J., 2008c. Microscopic Mechanisms of Oil Recovery By Near-Miscible Gas Injection. *Transport in porous media*, **Vol 74,** 351-367.

SPIVAK, A., GARRISON, W.H. and NGUYEN, J.P., 1990. Review of an Immiscible CO2 Project, Tar Zone, Fault Block V, Wilmington Field, California. *SPE Reservoir Engineering*, **Vol 5**.

SRIVASTAVA, R.K., HUANG, S.S., DYER, S.B. and MOURITS, F.M., 1994. Heavy Oil Recovery by Subcritical Carbon Dioxide Flooding. In: Latin American/Carbbean Petroleum Engineering Conference.

STREETER, V.L., WYLIE, E.B. and BEDFORD, K.W., 1998. Fluid Mechanics. WCB/McGraw Hill.

SUTTON, E., 1968. Waterflood Performance in a High Viscosity Oil Reservoir. *SPE Fall Meeting*. New Orleans, USA.

TABER, J.J., MARTIN, F.D. and SERIGHT, R.S., 1997a. EOR-Screening Criteria Revisited - Part 1: Introduction to Screening Criteria and Enhanced Recovery Field Projects. *SPE Reservoir Engineering*, **Vol 12**.

TABER, J.J., MARTIN, F.D. and SERIGHT, R.S., 1997b. EOR-Screening Criteria Revisited - Part 2: Application and Impact of Oil Prices. *SPE Reservoir Engineering*, **Vol 12**.

TEMPLETON, C.C. and S.S., R.J., 1956. Oil-Water Displacements in Microscopic Capillaries. *Journal of Petroleum Technology*, **Vol 8**.

THOMAS, S., 2007. Enhanced Oil Recovery - An Overview. *Oil & Gas Science and Technology*, **Vol 63**.

TWEHEYO, M.T., HOLT, T. and TORSÆTER, O., 1999. An experimental study of the relationship between wettability and oil production characteristics. *Journal of Petroleum Science and Engineering*, **24,** 179-188.

TZIMAS, G.C., MATSUURA, T., AVRAAM, D.G., BRUGGHEN, V.D., W., C. and G. N., P., A. C, 1997. The Combined Effect of the Viscosity Ratio and the Wettability during Forced Imbibition through Nonplanar Porous Media. *Journal of Fluid and Interface Science*, **Vol 189**.

VITTORATOS, E., 2010. Optimal Heavy Oil Waterflood Management May Differ from that of Light Oils. In: SPE EOR Conference at Oil & Gas West Asia.

VIZIKA, O., ROSENBERG, E. and KALAYDJIAN, F., 1998. Study of Wettability and Spreading Impact in Three-Phase Gas Injection by Cryo-Scanning Electron Microscopy. *Journal of Petroleum Sience and Technology*, **Vol 20,** 189-202.

WANG, J., DONG,M. AND ASGHARI, K., 2006. Effect of Oil Viscosity on Heavy-Oil/Water Relative Permeability Curves. In: SPE/DOE Symposium on Improved Oil recovery.

WANG, S., HUANG, Y. and CIVAN, F., 2006. Experimental and theoretical investigation of the Zaoyuan field heavy oil flow through porous media. *Journal of Petroleum Science and Engineering*, **50,** 83-101.

WARDLAW, N.C., 1982. The Effects of Geometry, Wettability, Viscosity and Interfacial Tension on Trapping in Single Pre-Throat Pairs. *The Journal of Canadian Petroleum*, **vol. 21**.

WARDLAW, N.C., 1996a. Factors Affecting Oil Recovery From Carbonate Reservoirs and Prediction of Recovery. In: MORROW, N.R.s (Ed.): Interfacial Phenomena in Petroleum Rrecovery. Vol. 36 of Surfactant Science Series.

WARDLAW, N.C., 1996b. Factors affecting oil recovery from carbonate reservoirs and prediction of recovery. In: CHILINGARIAN, G.V., MAZZULLO, S.J. and RIEKE, H.H.s (Eds.): Carbonate reservoir characterization: a geologic, engineering analysis, part II. Developments in Petroleum Science, 867-903.

WILLHITE, G.P., 1986. Waterflooding. Society of Petroleum Engineers.

YANG, C. and GU, Y., 2005. Effects of Heavy-Oil/Solvent Interfacial Tension on Gravity Drainage in the Vapor Extraction (Vapex) Process. In: SPE International Thermal Operations and Heavy Oil Symposium.

YANG, S.H. and REED, R.L., 1989. Mobility control using CO_2 foams. *64th Annual Technical. Conference*.

ZUMDAHL, S.S. and ZUMDAHL, S.A., 2008. Chemistry. Cengage Learning.